

Sustainable Strategies for the Upgrading of Natural Gas: Fundamentals, Challenges, and Opportunities

Edited by

Eric G. Derouane, Valentin Parmon,
Francisco Lemos and Fernando Ramôa Ribeiro

NATO Science Series

Sustainable Strategies for the Upgrading of Natural Gas: Fundamentals, Challenges, and Opportunities

NATO Science Series

A Series presenting the results of scientific meetings supported under the NATO Science Programme.

The Series is published by IOS Press, Amsterdam, and Springer (formerly Kluwer Academic Publishers) in conjunction with the NATO Public Diplomacy Division.

Sub-Series

I. Life and Behavioural Sciences	IOS Press
II. Mathematics, Physics and Chemistry	Springer (formerly Kluwer Academic Publishers)
III. Computer and Systems Science	IOS Press
IV. Earth and Environmental Sciences	Springer (formerly Kluwer Academic Publishers)

The NATO Science Series continues the series of books published formerly as the NATO ASI Series.

The NATO Science Programme offers support for collaboration in civil science between scientists of countries of the Euro-Atlantic Partnership Council. The types of scientific meeting generally supported are “Advanced Study Institutes” and “Advanced Research Workshops”, and the NATO Science Series collects together the results of these meetings. The meetings are co-organized by scientists from NATO countries and scientists from NATO’s Partner countries — countries of the CIS and Central and Eastern Europe.

Advanced Study Institutes are high-level tutorial courses offering in-depth study of latest advances in a field.

Advanced Research Workshops are expert meetings aimed at critical assessment of a field, and identification of directions for future action.

As a consequence of the restructuring of the NATO Science Programme in 1999, the NATO Science Series was re-organized to the four sub-series noted above. Please consult the following web sites for information on previous volumes published in the Series.

<http://www.nato.int/science>

<http://www.springeronline.com>

<http://www.iospress.nl>



Sustainable Strategies for the Upgrading of Natural Gas: Fundamentals, Challenges, and Opportunities

edited by

Eric G. Derouane

Universidade do Algarve,
Faro, Portugal

Valentin Parmon

Boreskov Institute of Catalysis,
Novosibirsk, Russia

Francisco Lemos

Instituto Superior Técnico,
Universidade Técnica de Lisboa,
Portugal

and

Fernando Ramôa Ribeiro

Instituto Superior Técnico,
Universidade Técnica de Lisboa,
Portugal

 **Springer**

Published in cooperation with NATO Public Diplomacy Division

Proceedings of the NATO Advanced Study Institute on
Sustainable Strategies for the Upgrading of Natural Gas:
Fundamentals, Challenges, and Opportunities
Vilamoura, Portugal
6–18 July 2003

A C.I.P. Catalogue record for this book is available from the Library of Congress.

ISBN-10 1-4020-3309-5 (PB) Springer Dordrecht, Berlin, Heidelberg, New York
ISBN-13 978-1-4020-3309-4 (PB) Springer Dordrecht, Berlin, Heidelberg, New York
ISBN-10 1-4020-3308-7 (HB) Springer Dordrecht, Berlin, Heidelberg, New York
ISBN-10 1-4020-3310-9 (e-book) Springer Dordrecht, Berlin, Heidelberg, New York
ISBN-13 978-1-4020-3308-7 (HB) Springer Dordrecht, Berlin, Heidelberg, New York
ISBN-13 978-1-4020-3310-0 (e-book) Springer Dordrecht, Berlin, Heidelberg, New York

Published by Springer,
P.O. Box 17, 3300 AA Dordrecht, The Netherlands.

Printed on acid-free paper

All Rights Reserved
© 2005 Springer

No part of this work may be reproduced, stored in a retrieval system, or transmitted in any form or by any means, electronic, mechanical, photocopying, microfilming, recording or otherwise, without written permission from the Publisher, with the exception of any material supplied specifically for the purpose of being entered and executed on a computer system, for exclusive use by the purchaser of the work.

Printed in the Netherlands.

TABLE OF CONTENTS

Preface	ix
Lectures	1
Natural Gas: Fuel or Feedstock? Jens R. Rostrup-Nielsen	3
Molecular Chemistry of Alkane Activation Frigyes Solymosi	25
Economics of Alkane Conversion Jean-Paul Lange	51
Theoretical Basis of the Activation of Light Alkanes M. Witko, R. Tokarz-Sobieraj, R. Gryboś	85
Surface Organometallic Chemistry of Tantalum: Application to the Metathesis of Alkanes Catalyzed by a Tantalum Hydride Supported on Silica J. Thivolle-Cazat, C. Coperet, S. Soignier, M. Taoufik, J.M. Basset	107
The Challenges in Converting Remote Natural Gas to Valuable Products David Trimm	125
Alternative Routes to Synfuel from Natural Gas David Trimm	137
New Technologies for Light Alkane Upgrading Jorge Gascon, Carlos Tellez, Javier Herguido, Miguel Menendez	149
Fundamentals of the Fischer-Tropsch Synthesis A.L. Lapidus	173
Reactor Technology for Syngas and Hydrogen E.H. Stitt	185
Engineering Alkanes to Olefins and Higher Value Chemicals Domenico Sanfilippo, Ivano Miracca, Marco Di Girolamo	217
Membrane Reactors for the Fischer-Tropsch Synthesis Alexander A. Khassin	249
Sources of Methane for Sustainable Development V.N. Parmon	273
Communications	285
CO ₂ Separation by Membranes in Natural Gas Processing G. Clarizia, E. Drioli	287

Structural and Textural Properties of MCM-41 Mesoporous Molecular Sieves Containing Nb, V, Mo – Alternative Catalysts for Hydrocarbons Oxidation	293
I. Nowak, B. Kilos, M. Ziolek, J.C. Volta	
Acidic and Catalytic Properties of Dealuminated BEA Zeolites	301
J.P. Marques, I. Gener, P. Ayrault, J.C. Bordado, J.M. Lopes, F. Ramôa Ribeiro, M. Guisnet	
Influence of the H-Ferrierite Sample on the Selectivity of Skeletal n-Butene Isomerization	305
B. De Menorval, N.S. Gnep, M. Guisnet	
Study on the Lattice Defects in the Mixed Oxides of Neodymium and Alkaline Earth Elements and their Role on the Oxidative Coupling of Methane	309
D. Filkova, R. Edreva-Kardjieva, N. Dragan, D. Crisan, L. Petrov	
Molecular Mechanism of the Methane Dissociation on the Vanadium Oxides Clusters. DFT Calculations	317
Witold Piskorz, Ewa Broclawik	
Acidity, Activity and Micro-Kinetics Studies in an H-ZSM5	321
P. Borges, R. Ramos Pinto, M.A.N.D.A. Lemos, J. Védrine, E.G. Derouane, F. Lemos, F. Ramôa Ribeiro	
Microkinetic Model for Propane Activation over H-ZSM5	327
X. Wang, H. Carabineiro, M.A.N.D.A. Lemos, F. Lemos, F. Ramôa Ribeiro	
¹³ C MAS NMR Mechanistic Study of the Initial Stages of Propane Activation over Zn/H-MFI Catalyst	333
Yu.G. Kolyagin, J. Quartararo, E.G. Derouane, F. Fajula, I.I. Ivanova	
Dehydrogenation of Propane over Chromium-Based Catalysts	339
P. Michorczyk, J. Ogonowski, D. Ralowicz	
Catalytic Oxidation of Methanol to Formaldehyde	345
A.H. Yılmaz, F.S. Atalay, S. Atalay	
Conversion of Gas Condensate over Metal-Containing MFI Catalysts	351
A.G. Popov, A.V. Smirnov, J. Krysciak, M. Derewinski, O.V. Barsukov, E.G. Derouane, F. Lemos, F. Fajula, I.I. Ivanova	
Coke Formation on Alumina and Alumina Supported Platinum Catalysts	359
Zenon Sarbak	
Activation Studies of the Cs-Doped Cu/ZnO Catalyst for the Higher Alcohol Synthesis	365
L. Nowicki, T. Olewski, T. Bedyk, S. Ledakowicz	

Development of High Temperature Catalytic Reactors for Oxidative Conversion of Natural Gas	377
S. Cimino, F. Donsì, R. Pirone, G. Russo	
The Effect of Process Conditions on Product Formation in Fischer- Tropsch Synthesis	383
Sh.S. Itkulova	
Mathematical Modeling of Steam Reforming Tubes with Shaped Particles	389
A.P. Kagyrmanova, I.A. Zolotarskii, N.V. Vernikovskaya, E.I. Smirnov, V.A. Kuzmin	
Application of NMR Microimaging for the Investigation of the Heterogeneous Catalytic Reactions inside Catalyst Pellets and Fixed Catalyst Bed	395
A.A. Lysova, I.V. Koptuyug, A.V. Kulikov, V.A. Kirillov, R.Z. Sagdeev, V.N. Parmon	
Conclusions	401
Natural Gas as Feedstock	403
Jacques C. Védrine	
Sustainable Strategies for the Upgrading of Natural Gas	413
Eric G. Derouane	
Participants	421
Subject Index	435
Author Index	441

PREFACE

Energy and feedstock materials for the chemical industry are in increasing demand and, with constraints related to the availability and use of oil, the energy and chemical industry is undergoing considerable changes. In the recent years, major restructuring has occurred in the oil, petrochemical, and chemical industry, with increasing attention devoted to the use of natural gas, methane in particular, as a chemical feedstock rather than just as a fuel. The conversion of remote natural gas into liquid fuels or other transportable chemicals is a challenge to industrial catalysis. Few processes exist so far with the major ones involving the conversion of natural gas to synthesis gas by steam reforming, CO_2 reforming, or partial oxidation, followed by the syntheses of methanol, hydrocarbons (Fischer-Tropsch synthesis), or ammonia. The development of new processes for the conversion of natural gas has suffered from the price differential between the product and natural gas being too small. However, this situation is now changing: (i) as synthetic fuels have a premium value because they are sulphur-free and may also have high cetane and octane numbers and (ii) as new routes appear to synthesize higher value products.

The need for the use of cheaper and widely available feedstocks, and the development of sustainable and environmentally friendly chemical processes is rapidly growing under both economical and public pressures. Obviously, adding value to light ($\text{C}_1\text{-C}_4$) hydrocarbons, i.e., the use of natural gas whose major component is methane, as a chemical feedstock, has become of increasing importance as natural gas reserves appear to exceed oil reserves. However, the upgrading and functionalization of natural gas components will only be a reality if it is demonstrated that there is a fundamental basis and a tangible advantage into making selectively C-C bonds (from light hydrocarbons) and high value oxygenates, rather than breaking C-C bonds (cracking of oil) or generating carbon oxides. Promising new uses of methane which exclude the production of synthesis gas and its utilization, and the oxidative coupling of methane, are the high temperature pyrolysis of $\text{C}_1\text{-C}_3$ alkanes with short residence time in a hot zone leading to polycyclic aromatics, the conversion of methane to aromatic compounds using molybdenum-modified zeolites as catalysts, the direct and selective conversion of methane to methanol or formaldehyde (homogeneous gas phase process or homogeneous and heterogeneous catalytic processes), the oxidative methylation of hydrocarbons with methane, and the carbonylation of methane by CO to acetic acid. Other interesting reactions are the direct conversion of ethane to ethanol or acetic acid, and that of

propane to isopropanol, acrolein, and acrylic acid. Heterogeneous catalysis should not be viewed as the preferred choice for such conversions, and either homogeneous catalysis or biomimetic alkane activation should also be considered.

Advances in the development of new sustainable routes for the conversion of natural gas will be strongly promoted by increasing integration of efforts and expertise comprising all the areas of knowledge involved. Catalysts and processes cannot be addressed separately. They must be developed continuously and interactively by academic and industrial teams. Academic programs often study reactions and catalysts under conditions that are convenient, but not necessarily relevant to potential application, while industrial laboratories devote much less effort to mechanistic studies that are often central to understanding and progress. To counter this splitting of effort that may hinder progress in this area, research programmes aimed at addressing future research targets in this field should involve multidisciplinary teams comprising chemists from the heterogeneous and homogeneous catalysis communities, materials scientists, theoretical scientists and (reaction and reactor) chemical engineers. In addition, it is essential that strong collaborations should be established between the industrial and academic communities. These collaborations should be established at the project design stage to ensure that both viable targets and timescales are agreed and achieved.

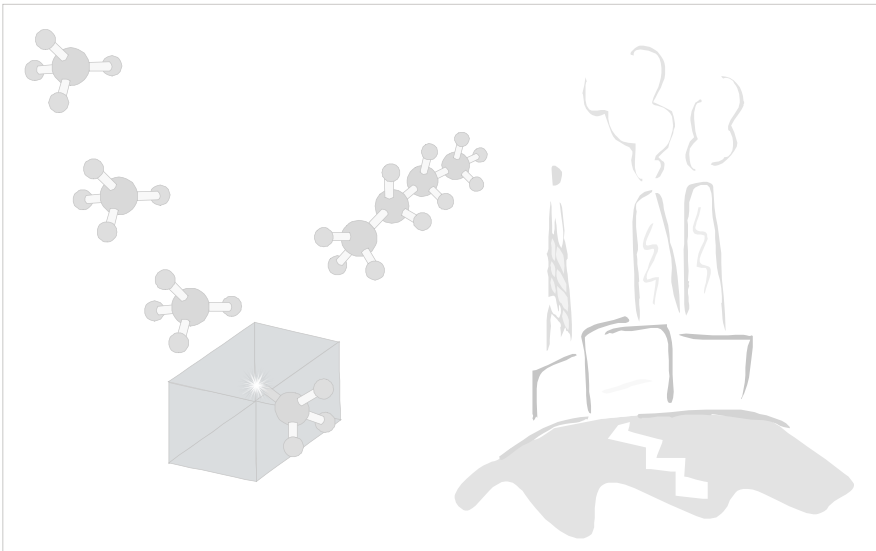
The aim of the ASI that took place in Portugal in July 2003 was to gather a multidisciplinary group of people involved in the field, experts, practitioners, and students, in the discussion of this important issue for the energy and chemical industry. One of the outcomes of this ASI is the present book which comprises all the written contributions that were presented, either as lectures by the invited speakers or by communications from other participants, as well as the discussions that took place during the lectures, the workshops and the poster sessions. The book is divided into three sections. The first one contains the lectures presented at the meeting, the second one comprises the communications contributed during the discussion periods, and the third one covers the conclusions of the NATO ASI.

The editors wish to thank all attendees of the meeting, in particular the lecturers who promoted the discussions by their lively and superb presentations as well as the other active and dedicated participants. Special thanks are due to the people involved in the organisation of the ASI, in particular to the local organising committee, Hugo Carabineiro, Ricardo Ramos Pinto, Pedro Borges, Maria Amélia Lemos, Filipe Freire, José Manuel Lopes, Carla Pinheiro, Isabel Fonseca, and to Pat Gibbs for her efficient secretarial help. Sponsorship of the meeting by the NATO Science Programme, the Technical University of Lisbon, Finibanco, Fundação para a Ciência e Tecnologia, Taguspark Society, BP, Total, the British Council, the

French Embassy in Portugal and Sociedade do Ar Líquido is also acknowledged.

Eric Derouane
Valentin Parmon
Francisco Lemos
Fernando Ramôa Ribeiro

SECTION 1



LECTURES

Chapter 1

NATURAL GAS: FUEL OR FEEDSTOCK?

Jens R. Rostrup-Nielsen

Haldor Topsøe A/S, Nymøllevvej 55, DK-2800 Lyngby, Denmark

Abstract: Catalysis plays a key role in converting natural gas into chemicals. It is increasingly being involved in the use of natural gas in the energy sector. Catalytic combustion, chemical recuperation, flue gas cleaning and fuel cells are examples from the power industry. The indirect conversion via syngas is the most feasible route for production of commodity chemicals such as ammonia and methanol. Chemical conversion of natural gas may become important for providing transportation fuels and for the transition to a hydrogen economy.

Key words: Syngas, ammonia, gas to liquids, fuel cells, chemical recuperation, CO₂ sequestration

1. INTRODUCTION

Catalysis plays a key role in converting natural gas into chemical products and it is increasingly being involved in the use of natural gas for the energy sector.

The remaining resources of natural gas amounts to ca. 6600 trillion ft³ (180 trillion Nm³) cft corresponding to around 70 years of production at the 2001 production level. The Middle East has the greatest share of the remaining resources (39%) followed by the former Soviet Union [1].

The gross production of natural gas was about 100 trillion cuft (ca. 3 trillion Nm³) in year 2000 with ca. 92 trillion cuft sold and the remaining part being reinjected or flared as shown in Table 1:

Table 1. Natural Gas Production 2000 (billion cuft) (EIA/DOE)

	Gross production	Flared	Marketed*
North America	33343	383	28437
Central & South America	5678	406	3927
Western Europe	11963	120	10374
Eastern Europe & former Soviet Union	26516	244	26239
Middle East	11258	534	8273
Africa	8990	1291	4879
Asia & Oceania	10340	272	9758
Total	103088	3250	91889

*) Reinjection not shown

North America (US) remains the largest producer followed by the former Soviet Union. About 3% of the natural gas production is flared. This corresponds to ca. 170 mio. t CO₂ per year or about 0.7% of total world CO₂ production from fossil fuels.

Africa is the largest contributor to flaring of natural gas.

The resources are not always located in areas with high population and present markets for natural gas as fuel. The price of natural gas reflects this. When natural gas can be made available at the fuel market, the price will be high. At present, a typical price in the US is 3 €/GJ (USD/MM BTU) or above. However, with big seasonal changes up to say 10 €/GJ. In Europe, the prices will be 4 USD/MM BTU or above, whereas in many remote areas the costs will be between 0.5-1 USD MMBTU. In areas, where flaring of natural gas is prohibited, the real price of natural gas may even be negative. It means that the use of natural gas as feed for chemicals can hardly be feasible in areas where there is a big market for natural gas as fuel.

The options for conversion of remote natural gas are listed in Fig. 1:

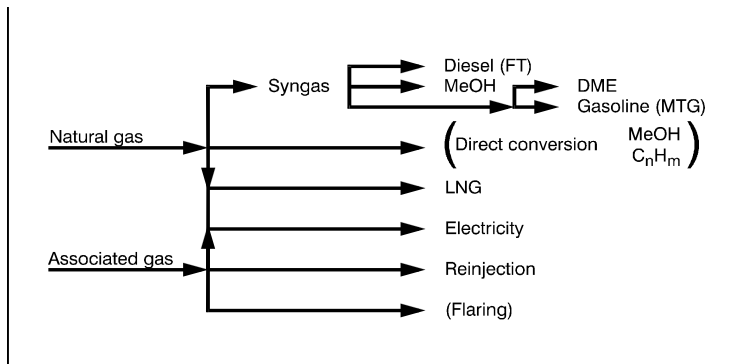


Figure 1. Options for Conversion of Remote Natural gas [2]

The conversion of natural gas into liquid products has been discussed for decades and recently as a solution for “validation of stranded natural gas”, but in most situations projects involving liquified natural gas, LNG, have proven to be more feasible [3]. The gas conversion has suffered from the small price differential between product and natural gas. The regulations on flaring of natural gas as well as lower investments in the chemical plants have changed this picture as described below.

2. POWER GENERATION AND CATALYSIS

2.1 General

The maximum useful work which can be obtained by combustion of natural gas is equal to the decrease of free energy in the reaction:



This amounts to 801 kJ/mole (1 bar, 25°C). The change in enthalpy is almost the same 802 kJ/mole, since the entropy change is very small. This means that almost as much energy can be obtained as heat as would have been obtained as work if the process had been carried out reversibly. The subsequent conversion of the thermal energy to mechanical energy is limited by the Carnot efficiency $((T_2 - T_1)/T_2)$. In practice, the efficiency of any steam engine or turbine is determined by a highest temperature in the system, T_2 , and the temperature of the cooling water, T_1 , in the condenser. In conventional power plants, only 25-50% of the heat taken from the steam can be recovered as electricity.

The combustion of natural gas with air is accompanied by the formation of nitrogen oxides. This becomes significant above 1450-1500°C. These temperatures are easily surpassed in normal diffusion flames. The problem is solved by the use of low NO_x burners and cleaning of the flue gas by selective catalytic reduction (SCR) with ammonia [4].

2.2 Gas Turbines

Advanced gas turbines have the potential for higher electric efficiencies as new materials allow high operating temperatures (1300°C). These temperatures are below the 1800-2000°C being required for complete thermal combustion of methane without unconverted carbon monoxide and hydrocarbons in the flue gas. Hence, the hot flue gas from the combustor is

diluted with air to meet the maximum 1300°C by the gas turbine. By *catalytic combustion*, it is possible to ignite the pre-mixed gas at 400°C and burn it at $1300\text{--}1500^{\circ}\text{C}$ with less than $1\text{--}2$ ppm NO_x -formation [5]. This is illustrated in Fig. 2. The entire feed of air and fuel is mixed and passed through the catalytic combustor which leaves the maximum temperature for a turbine ca. 1350°C .

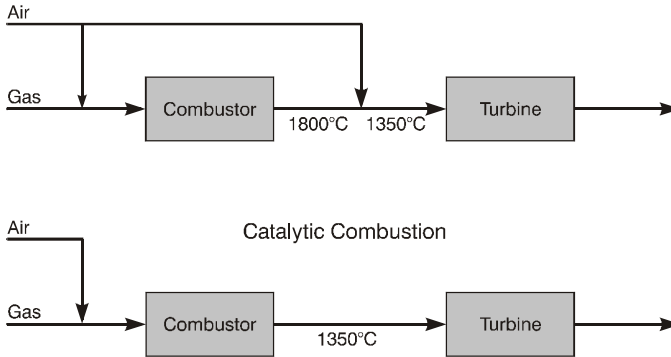


Figure 2.: Catalytic and Thermal Combustion [6]

Catalytic combustion is a challenge to catalyst development and reactor design. In a conventional, catalytic system, the reaction rate will be controlled by film diffusion and the temperature of the catalyst will increase quickly to the adiabatic exit temperature of the combustor (i.e. 1300°C). At this temperature, the catalyst will suffer severe deactivation. This problem has been solved by stage-wise combustion [5]. The success of catalytic combustion depends on the scale-up as well as the competition from non-catalytic means with low NO_x technology and the costs compared to downstream cleaning by selective catalytic reduction (SCR).

2.3 Chemical recuperation for gas turbines

The combustion temperature for gas turbines is normally controlled by operating with surplus air, but the dilution causes production of entropy and a corresponding loss of exergy or a decrease in the maximum efficiency which can be achieved. One way of solving this problem [6,7] is to use the exhaust heat from the gas turbine for converting the methane feed by the steam reforming reaction to a fuel gas with less heating value per volume and thereby decreasing the demand for dilution as illustrated in Fig. 3.

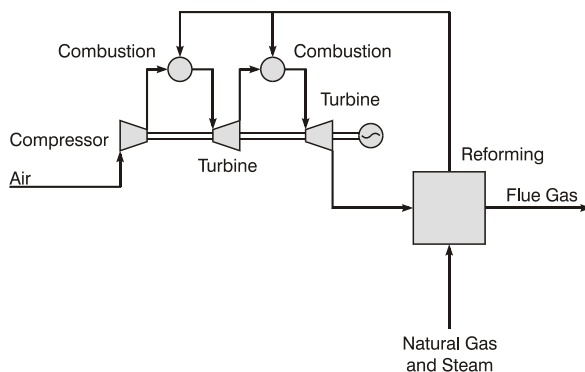


Figure 3. Chemical Recuperation for Gas Turbines [6]

Still, at a turbine inlet temperature, 1350°C , the benefits of chemical recuperation remains marginal, because only 18% of the natural gas is converted into synthesis gas due to thermodynamic constraints in a heat exchange reformer. At a future turbine inlet temperature at 1500°C , the higher exhaust temperature from the second turbine creates more useful heat for heat exchange reforming and it means that more than $1/3$ of the natural gas can be converted resulting in a similar gain in efficiency [6]. A similar increase in efficiency can be achieved by steam injection without reforming reaction, but the amount of steam has to be almost doubled up compared with the steam reforming case.

Chemical recuperation has been considered also for energy transportation systems. This was studied 25-30 years ago in a German ADAM/EVA scheme [8] in which the heat produced at the high temperature, gas cooled nuclear reactor was converted into chemical energy by the steam reforming reaction. The heat was transferred in a close loop of helium at 950°C and 40 bar which was efficient to drive the tubular reformer. The converted syngas was meant to be transported over long distances and converted into high pressure steam by high temperature methanation [9]. Similar schemes are being considered today for converting solar energy produced at remote locations into chemical energy by CO_2 -reforming of methane [10]. CO_2 is used instead of steam to avoid the problem of raising steam.

2.4 Fuel Cells

With fuel cells, it is possible to convert the free energy of methane (or hydrogen and other fuels) directly into electric energy as expressed by the Nernst equation ($E^{\circ} = nF\Delta G^{\circ}$). It means that the electric ideal efficiency of a fuel cell is expressed simply by $\Delta G^{\circ}/\Delta H^{\circ}$ for the overall combustion

reaction. Hence, for methane combustion, the ideal efficiency is close to 100% independent of temperature [11]. The ideal efficiency for hydrogen fuel is less than 100% and decreases strongly with temperature because of a negative entropy. This is illustrated in Fig. 4 showing the exergy changes going from methane to electricity directly or via hydrogen. The data reflects a system at 25°C. At higher temperatures, the difference between the ideal efficiency for the direct and indirect route increases. At 650°C, the ideal efficiency for direct methane conversion remains close to 100% whereas for hydrogen, it is about 80% [11].

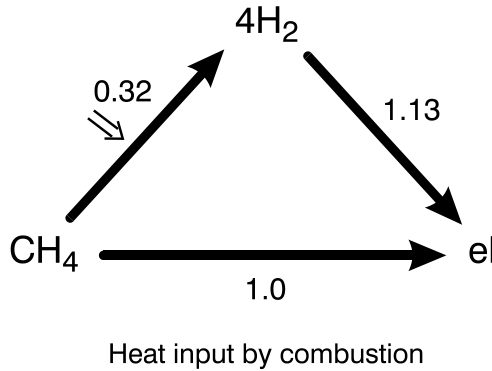


Figure 4. Conversion of Methane into Electric Power.

Ideal conditions, 25°C (relative exergy) in order to achieve the high efficiency from natural gas, it is essential that the conversion of methane to hydrogen is coupled with the electro-chemical reaction of hydrogen meaning that the two reactions are taking place at the same temperatures [11]. This is possible in high temperature fuel cells like the solid oxide fuel cell (SOFC) [12]. If the steam reforming of natural gas to hydrogen takes place in an external, fired reformer, there is a loss in efficiency because of the high temperature created in the flame which is not utilized fully for work because the waste heat can be recovered only with the Carnot cycle [6,11].

Large scale process schemes have been proposed in which high temperature fuel cells with internal reforming are integrated into advanced gas turbine cycles as illustrated in Fig. 5 [13].

The exhaust gas from an SOFC fuel cells provides a hydrogen containing mean fuel gas mixture for the combustion chamber of the gas turbine allowing a more efficient control of the maximum temperature than is achievable by adding the surplus air. In this way, the thermodynamic constraints described above for chemical recuperation are by-passed. Such schemes are claimed to have electric efficiencies close to 70%. [13]. The

fuel cell is able to achieve higher methane conversion than the scheme for chemical recuperation shown in Fig. 3.

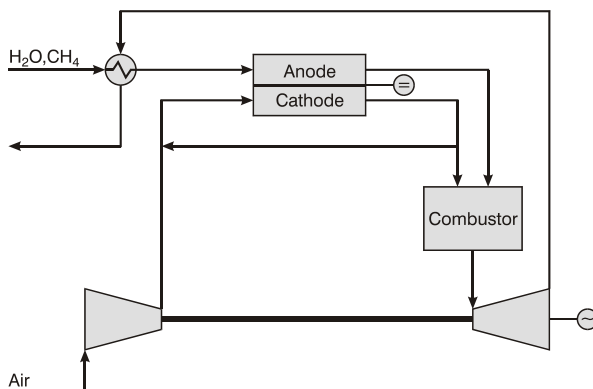


Figure 5. SOFC and Gas Turbine Cycle [2]

3. NATURAL GAS AS FEEDSTOCK

3.1 General

The most important parameter for large volume chemicals is production costs (variable and fixed costs). The *variable* costs are related to the feed costs, the use of energy, process selectivity and environmental costs. It is essential at an early stage to establish a primitive process scheme showing the overall material balance. By-products may easily have a negative value and high consumption of energy is often equivalent to high CO₂-production. Apart from the mass and thermodynamic balance is also important to establish the ΔP simply being the difference of the price of the product minus the price of the feedstock and energy consumed per unit product [14].

The *fixed* costs are related to plant scale and to the heat of reaction (heat loss) and the transfer of energy [15]. The economy of *scale* can be expressed by:

$$\text{Cost (1)} = \text{Cost (2)} \left(\frac{\text{capacity (1)}}{\text{capacity (2)}} \right)^n \quad (2)$$

n varies typically between 0.6-0.8.

The *management of heat* of reaction and potential energy loss makes the plant more complex. It can be shown that the plant costs for a variety of

processes correlates with the energy transfer (heat transfer, compression) within the process scheme [15].

It is evident that *catalyst life*, i.e. on-stream factor is crucial for large scale commodity plants in contrast to batch-wise manufacture of fine chemicals. For each case, there is a minimum *space time yield* (production rate) and corresponding stability that is commercially applicable [15]. Economic arguments will limit the minimum space time yield to ~ 0.1 ($t_{\text{product}}/(\text{m}^3_{\text{reactor}}/\text{h})$) corresponding to the stability that is commercially applicable for commodity manufacturing processes. On the other hand, the heat removal capacity of conventional space time yield reactors rarely permits a reactor productivity in excess of ~ 10 $t_{\text{product}}/(\text{m}^3_{\text{reactor}}, \text{h})$ [15].

The main commodity products based on natural gas are shown in Table 2. It is evident by comparing with figures in Table 1 that the chemical conversion of natural gas is marginal to the total natural gas production.

Table 2. Main Chemical Products based on Natural Gas

Product	Yearly product. (mio t/y)	Energy Consum. (GJ/t)	Thermal Efficiency (LHV)		CO ₂ (t/t)	Main Technology
			Practical (%)	Ideal (%)		
Ammonia	120	29	65	89.2	1.6 ^a	Syngas/synthesis
Ethylene	100	15 ^b	62	93 ^c	0.65	Steam cracking of C ₂ H ₆
Propylene	55	-	-	84.2	0.28	Steam cracking
Methanol	30	28	72	91.8	9.0	Syngas / synthesis
Hydrogen	20	12.6	84 ^d	78	a.1	Steam reforming
Synfuels	15 ^e	67	60			Syngas / synthesis

a) incl. CO₂ converted into urea

b) data kindly provided by F. Dautzenberg, ABB Lummus.

c) H₂ used for reaction heat. No credit for surplus H₂. Credit for by-product C₃H₆ < 1%

d) CH₄ used for reaction heat. No steam export

e) excl, 3 mio t/y under construction

Most of the large scale conversion of methane [16] into products is carried out via oxidation to provide a thermodynamic potential.



Direct conversion of methane into products remains a challenge [17] as it is difficult to eliminate complete oxidation. Therefore, the *indirect* conversion via syngas is the dominating route:



In most plants, the heat is utilized for running the plant. This requires that the heat is available at sufficiently high temperatures to raise high pressure steam. As an alternative, the heat may be exported but it is not always that there is a need for that. The overall thermal efficiencies are shown in Table 2. The practical efficiencies are ca. 80% of the ideal values expressed as [17]:

$$\eta_{\text{ideal}} = \frac{LHV_{\text{product}} / \text{mol}}{LHV_{\text{methane}} / \text{mol}} \cdot \frac{\text{mol}_{\text{product}}}{\text{mol}_{\text{methane}}} \tag{5}$$

For endothermic reactions (ethylene, hydrogen), the LHV of the fuel providing the reaction heat should be added to the nominator.

3.2 Ammonia

For *ammonia*, the natural gas consumption is decisive for the ammonia production costs as illustrated in Fig. 6. It is evident that ammonia production in a new plant is hardly feasible at a typical natural gas price above 2.5 Euro/GJ. The energy consumption of ammonia production has been decreased over the years [18] by introduction of high pressure steam reforming, integration of the steam turbine cycle and process and by the application of better catalysts.

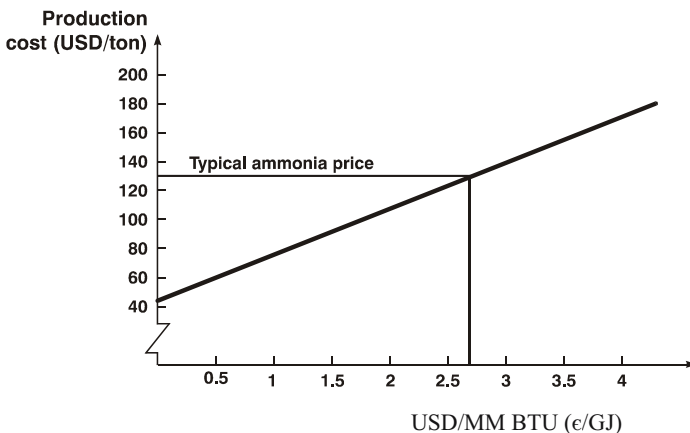


Figure 6. Ammonia Production Costs

3.3 Gas-to-Liquids (GTL)

It is a challenge to convert the natural gas into *liquid fuels* which can be moved readily around the world to markets where they are most needed. The manufacture of synfuels from natural gas is technically feasible as demonstrated by the MTG-plant in New Zealand [19], and the Fischer-Tropsch units in Malaysia [20] and Mossel Bay, South Africa. Further units are under design in Nigeria and Qatar. The GTL plants have suffered from production costs being too high and mainly related to the capital costs. The syngas unit including the manufacture of oxygen amounts to ca. 2/3 of the investments with the air separation unit responsible for ca. 50% [21]. Hence, a key parameter is tons of oxygen consumed per ton of fuel F-T product.

GTL plants may now appear feasible because of a number of factors: the oil price has increased and synfuels may have a premium value because they are sulphur-free, and because they have high cetane and octane numbers. It has been unacceptable to flare natural gas from oil fields and it has become possible to build larger plants taking advantage of the economy of scale. Finally, process development has resulted in more efficient processes for the F-T synthesis and the syngas technology.

3.4 Methanol and Derivatives

Large scale *methanol* plants have been discussed for decades considering methanol as an energy carrier [22]. So far, methanol has been used primarily for petrochemical purposes giving a higher ΔP . As an example, the MTG-plant in New Zealand was soon reduced to a methanol production plant. Methanol is an important intermediate in the petrochemical industry as illustrated in Fig. 7. It is converted directly into formaldehyde. It is used as a reactant with CO for *acetic acid* [23] and potentially for methyl formate and *dimethyl carbonate* [24], which might be used as a gasoline additive. Methanol is also an active alkylation agent in reactions with aromatics etc. and it is one of the reactants for *MTBE* [25], a product which however cannot be used anymore in some parts of the world (California and probably rest of US and some European countries).

Dimethylether (DME) can easily be made from methanol [26] and it may play a role in the energy sector as a replacement for LNG for gas turbines [27] or for LPG as domestic fuel. DME can also be used as a pollution-free diesel substitute in existing diesel engines [26,27]. This would however require a special infra-structure. DME can also be used as an intermediate for acetic acid [29]. If the manufacture of acetic acid is not based on important of cheap large scale produced methanol, an integrated scheme may be advantageous. Syngas is converted in a combined synthesis of

methanol, dimethylether [26] and unconverted syngas and dimethylether is reacted with CO in the carbonylation reactor into acetic acid [17, 29].

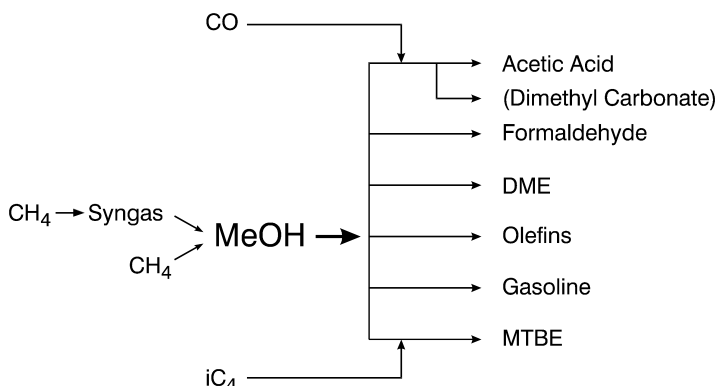


Figure 7. MeOH as Petrochemical Intermediate

Methanol and DME can be converted into *olefins* over zeolite catalysts (MTO-synthesis). Various process schemes [25, 30, 31] have been proposed which break the yield structure in the thermal steam cracking process allowing higher yields of propylene. It may be difficult to compete with the process economy of steam cracking of ethane or LPG, but there may be situations in connection with big natural gas fields where the availability of gas streams may favor conversion of natural gas with low contents of C₂₊ hydrocarbons. This production could also be made feasible by the co-production of synthetic fuels taking advantage of the economy of scale of the syngas unit.

3.5 Hydrogen

Natural gas will play an increasing role in providing the hydrogen in *refineries* for hydrotreating, hydrocracking and removal of aromatics and olefins to adjust to H/C ratio to close to 2 being optimum for transportation fuels [32]:



Hydrogen as “*energy vector*” has been discussed for decades [33]. Key applications for hydrogen are as carbon-free fuel in general and as fuel for hydrogen-driven fuel cells for automotive or stationary applications. Many technologies for production of hydrogen that do not involve with the CO₂ are being considered. In spite of efforts to produce hydrogen by schemes

involving solar energy, bio-fuels etc, natural gas remains the most feasible feedstock for hydrogen generation in the near term [34].

The steam reforming process for hydrogen (with the steam credit) has a high efficiency (87.7%) being 94% of the theoretical energy efficiency. Without steam production, the efficiency drops to 84.3%. In locations with high natural gas prices, the energy efficiency becomes critical [35]. For a natural gas price of 4 €/GJ (4 USD/MM BTU), the feedstock and utility costs makes about 2/3 of the total H₂ production costs. This, on the other hand, means that the potential for reduction in hydrogen production costs are limited, if the energy costs are high.

Significant efforts are being made to develop technologies for hydrogen production based on fossil fuels combined with *CO₂-sequestration*. The aim is to develop effective methods to capture significant amounts of CO₂ from power generation and store the CO₂ in geological formations [36]. Fig. 8 shows a scheme for large scale power production based on air-blown reforming of natural gas coupled to CO₂-sequestration [34].

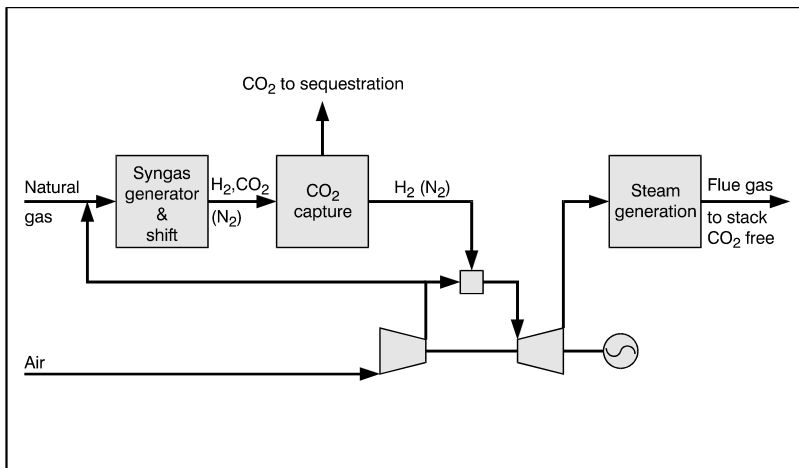


Figure 8. Hydrogen by Air-blown Reforming for CO₂-free Power Production [33]

Hydrogen is being considered for *fuel cells* in units from 1-500 kW, but the application has not grown as fast as predicted because of the high investment costs and competition from advanced gas turbines. Hydrogen and fuel cells have attracted great interest for mobile applications. The issue is then where to produce the hydrogen - in large centralised plants at the gas stations or in the cars [37].

4. TECHNOLOGY OPTIONS

4.1 Direct conversion of natural gas

It remains a challenge to find routes for direct conversion of methane into petrochemicals and synfuels. Attempts to convert methane by direct oxidation into methanol have not been encouraging [14, 17]. High selectivities of about 90% may be achieved, but at low conversions per pass of about 7.5% corresponding to a yield per pass less than 7%. As illustrated in Fig. 9, this means large recycle ratios, ca. 12, and a difficult separation due to low partial pressure of the product.

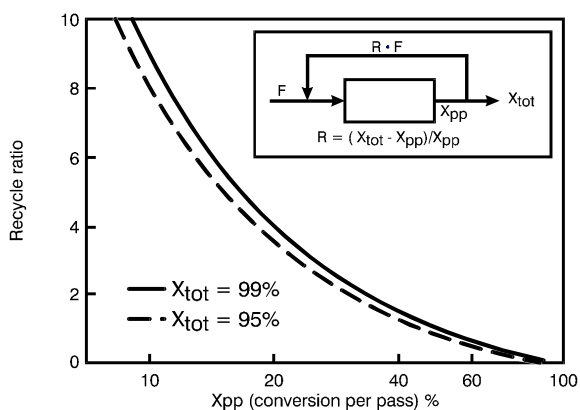


Figure 9. Recycle Ratio and Conversion [14]

In comparison, the commercial syngas based methanol synthesis has a conversion per pass of 50% and a total recycle ratio of 4, using the recycle to control the temperature in the reactor [14]. This does not harm the economy, because the selectivity is 99.9% meaning a yield per pass close to 50%.

Other attempts have aimed at creating a carbon-carbon bond from methane. Direct conversion of methane to higher hydrocarbons is not favored by thermodynamics. This constraint can be circumvented in a two-step process via carbides, but so far yields have been insignificant [38]. Other studies have explored the direct conversion of methane into benzene [39]. Selectivities of 70% were obtained close to equilibrium conversion at 600°C (12%). Most work in direct conversion has focused on the oxidative conversion of methane into ethylene [40]. It has proven to be more promising than high temperature pyrolysis of methane into primarily acetylene. However, the process suffers from ethane being a significant part

of the products (low ΔP) that above 20% of the converted methane is oxidized to carbon oxides. C_{2+} -yields at industrial conditions are less than 20% at a conversion of 24-35% per pass. As a result of the process scheme ends up being rather complex meaning that the oxidative coupling is not economically feasible with the present low selectivities to C_2 -hydrocarbons.

Catalytic partial oxidation at high temperature and ultra-short residence time over noble metals gauze has shown formation of olefins and oxygenates [41]. The feasibility of this route is still to be analyzed. The indirect route via methanol appears to be more a more promising route for olefins.

4.2 Syngas-based Routes

4.2.1 General

A syngas based route has often been characterised as being inefficient. In fact, syngas manufacture is very efficient [42]. The thermal efficiency of a tubular reformer approaches 95%, as most of the heat input to the process is recovered from the flue gas and the product stream. The main advantage of the indirect routes via syngas is the very high *carbon efficiency* [2, 3], but it involves a high exchange of energy and thereby high capital costs.

It may be argued that energy efficiency is of less importance when natural gas is cheap, but high energy efficiency means small feed pretreat units and reduced requirements for utilities and hence less investments. Moreover, high efficiency means less CO_2 -production.

The size of the synthesis gas plant is directly related to the carbon efficiency of the synthesis. Non-converted syngas and light synthesis products may be recycled to the syngas unit or used as fuel as illustrated in Fig. 10 [21, 43]. As an example, low syngas utilisation means larger syngas unit per ton of F-T product and hence a higher oxygen consumption per ton liquid product. Therefore, it is important that the syngas composition is tuned (or adjusted for maximum conversion per pass) in the F-T synthesis. CO_2 is not a reactant in the low temperature FT synthesis for GTL [43]. This means that CO_2 in the syngas represents a loss in carbon efficiency. In contrast, CO_2 and CO as well are both reactants in the synthesis of methanol, dimethylether and gasoline via the Mobil MTG [19] or TIGAS process [26]

Most large volume petrochemical plants are usually designed as stand-alone plants being autonomous in energy balance. This is achieved by high carbon yield and highly integrated steam and process streams. Methanol and synfuels might be produced cheaply in once-through synthesis units if the

non-converted syngas can be used for power production in gas turbine for instance in a scheme shown in Fig. 11. Such units (disregarding recycle streams and energy recovery) would of course be very cheap if the natural gas is available at a low price.

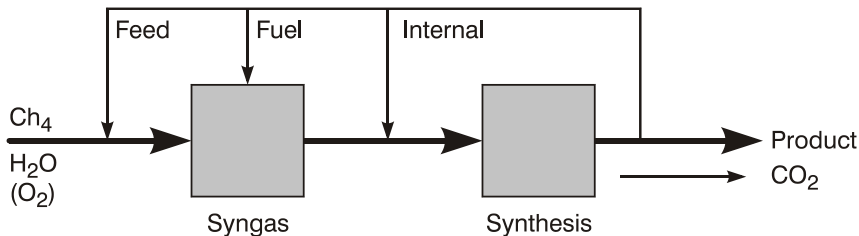


Figure 10. Indirect Conversion of Natural Gas. Recycle Streams

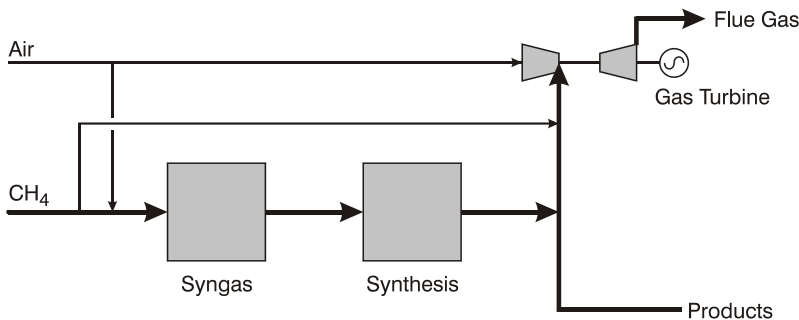


Figure 11. Once-through Synthesis coupled with Power Production

A typical ammonia plant (1500 MTPD) has steam turbines with a power output of 35 MW. It might be considered to apply the more efficient gas turbines [17] by integrating the ammonia plant with a power plant operating with steam turbines, but it is rare that there is a need for more electric power at locations where cheap natural gas is available.

4.2.2 Steam reforming

Syngas is made by the endothermic steam reforming or CO_2 -reforming or by oxidative reforming processes [2,42]. The choice of syngas technology is dictated by the needs for high conversion, the requirements of the syngas composition, and by the scale of operation.

As shown in Table 3, the *steam and CO_2 reforming* reactions are strongly endothermic and hence the manufacture of syngas requires a high temperature to achieve a high methane conversion [2]. The overall heat of

reaction becomes negative which implies that heat must be supplied to reaction. In industry, the reforming reactions are carried out in a heated furnace with the presence of a nickel catalyst. The catalyst is placed in a number of high alloy reforming tubes and the product gas leaves the reformer at 800-950°C depending on the application [2, 44]. The reformer furnace consists of a box-type radiant section including the burners and the convection sections to recover the waste heat of a flue gas leaving the radiant section as illustrated in Fig. 12.

Table 3. Synthesis Gas Reactions

Process	$-\Delta H_{298}^{\circ}$ kJ/mole
Steam Reforming:	
1. $\text{CH}_4 + \text{H}_2\text{O} \rightleftharpoons \text{CO} + 3\text{H}_2$	-206
2. $\text{C}_n\text{H}_m + n\text{H}_2\text{O} \rightleftharpoons n\text{CO} + (n+m/2)\text{H}_2$	-1175 ^{*)}
3. $\text{CO} + \text{H}_2\text{O} \rightleftharpoons \text{CO}_2 + \text{H}_2$	41
CO₂ Reforming:	
4. $\text{CH}_4 + \text{CO}_2 \rightleftharpoons 2\text{CO} + 2\text{H}_2$	-247
Autothermal Reforming (ATR):	
5. $\text{CH}_4 + 1/2\text{O}_2 \rightleftharpoons \text{CO} + 2\text{H}_2\text{O}$	520
6. $\text{CH}_4 + \text{H}_2\text{O} \rightleftharpoons \text{CO} + 3\text{H}_2$	-206
7. $\text{CO} + \text{H}_2\text{O} \rightleftharpoons \text{CO}_2 + \text{H}_2$	41
Catalytic Partial Oxidation (CPO):	
8. $\text{CH}_4 + 1/2\text{O}_2 \rightleftharpoons \text{CO} + 2\text{H}_2$	38

*) for $n\text{C}_7\text{H}_{16}$

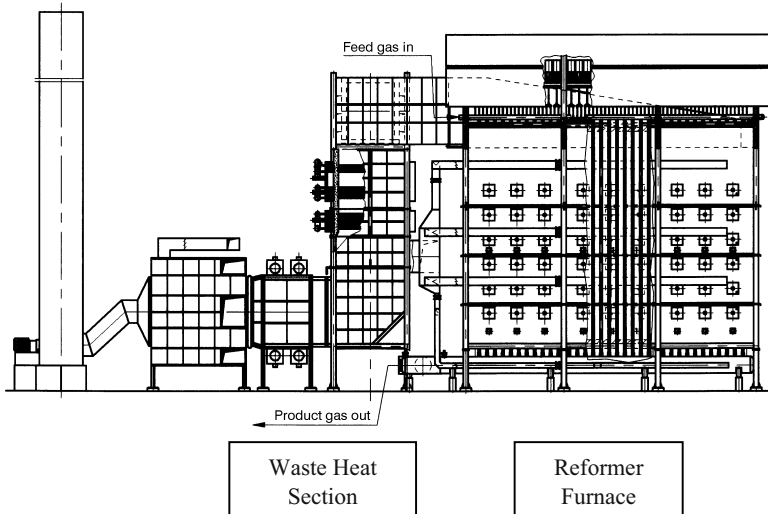


Figure 12. Reformer Furnace. Waste Heat Section
(only every second tube is shown. Number of tubes: 66)

Hydrogen production often results in a by-product of steam which in many cases should be minimized [34]. About 50% of the heat generated in the reformer is transferred through the tubes to the process. The remainder is recovered from the flue gas in the waste heat section [2]. It is possible to increase the amount transferred to the process gas to about 80% of the supplied heat when using a convective heat exchange reformer in which the flue gas as well as the hot product gas are cooled by heat exchange with the process gas flowing through the catalyst bed [42, 44]. This means less steam production, but the convective heat exchange reformer operate at lower heat fluxes than the reformers with radiant transfer. Hence tubular reformer remains the most economic solution for large scale plants.

The steam reforming may appear straight-forward from an overall consideration as the product composition is determined by simple thermodynamics, but in reality it is a complex coupling of catalysis, heat transfer and mechanical design. In recent years, there has been progress in steam reforming technology [42] resulting in less costly and more efficient plants, in part because of better materials for the reformer tubes, better control and understanding of carbon limits and better catalysts and process concepts with high feedstock flexibility. Progress has been accompanied by a better understanding of the reaction mechanism [2].

4.2.3 Partial oxidation

Partial oxidation represents an alternative to steam reforming. The heat for the methane conversion is created “in-situ” thus eliminating the big heat transfer area of the tubular reformer and its flue gas waste heat section.

The water formed during partial oxidation is recovered as condensate meaning utilizing the higher heating value of the combusted methane, whereas the water formed by combustion in the reformer leaves with flue gas in vapor phase, meaning utilizing only the lower heating value of the fuel. This leaves room for a slightly higher energy efficiency for the partial oxidation routes.

Partial oxidation can be carried out in three ways [16]: The *non-catalytic* partial oxidation (POX) requires high temperature to ensure complete conversion of methane and to reduce soot formation. The thermal processes typically result in a product gas with H₂/CO ratio in the range of 1.7-1.8.

The *autothermal reforming* process [42] is a hybrid of partial oxidation and steam reforming using a burner and a fixed catalyst bed for equilibration of the gas. This design allows the decrease in the maximum temperature and hence the oxygen consumption can be lowered. Soot formation can be eliminated by addition of an appropriate amount of steam to feedstock and by a specific burner design. The autothermal reformer is a simple piece of equipment with a specifically designed burner and a fixed catalyst bed in brick-lined reactor. Irrespective of whether the burner is thermal or catalytic or whether fixed or fluidized, catalyst bed is used, the product gas will be determined by the thermodynamic equilibrium at the exit temperature which in turn is determined by the adiabatic heat balance.

A flow scheme of an advanced unit for syngas for GTL [21] is shown in Fig. 13.

The natural gas is desulphurized and mixed with steam and passed through a prereformer converting all higher hydrocarbons. The core is the autothermal reformer where the prereformed gas is partially burned with oxygen in the mixer/burner and further reacted over the catalyst bed to equilibration of the reforming and shift reactions. The product gas from the ATR is normally cooled by production of steam, but in Fig. 13 is shown how the heat is utilized for steam reforming in a heat exchange reformer – a scheme resembling the chemical recuperation shown in Fig. 4. This allows further optimisation of the GTL-plant resulting in less oxygen consumption [21]. The choice of technology for off-shore GTL-plant raises special problems related to size, safety etc [45].

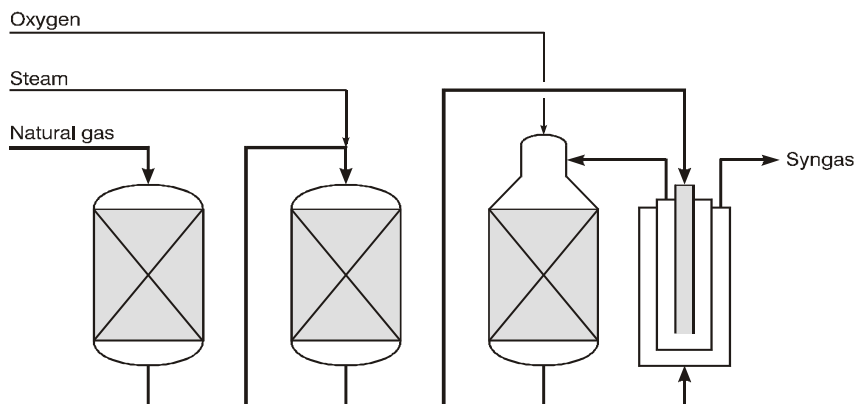


Figure 13. Syngas Plant for GTL with Chemical Recuperation

In *catalytic partial oxidation* (CPO), the reactants are premixed and all the chemical conversions take place in the catalytic reactor without the burner. The direct CPO reaction appears to be the ideal solution and provides a H_2/CO ratio of 2 and has a low heat of reaction (38 kJ/mole). However, in practice the reaction is accompanied by the reforming of water gas shift reactions, but high conversions of product gas will be close to thermodynamic equilibrium. If so, the same exit temperature is required in ATR and CPO to achieve similar syngas compositions for given feedgas streams. As the CPO requires a lower preheat temperature (ca. 250°C) than ATR (ca. 650°C). It means that CPO inherently has a higher oxygen consumption per ton of product than does ATR.

Up to 50% of the costs of the syngas based on ATR is related to the oxygen plant [40]. Consequently, *routes based on air* and eliminating cryogenic air separation have been suggested. The use of air in the process stream is possible only in once-through synthesis schemes, otherwise huge accumulation of nitrogen is unavoidable. Attempts to use air instead of oxygen result in large gas volumes and consequently in large compressors and feed effluent heat exchangers [46,47]. These are hardly feasible for large-scale stand-alone plants. Although steam reforming is the preferred choice for hydrogen, catalytic partial oxidation (CPO) may have special applications where it is acceptable that a hydrogen stream contains nitrogen (i.e. small fuel cells) [34].

Another attempt, *catalytic membrane reforming* (CMR) involves eliminating the oxygen plant and including a reactor concept with oxygen addition through a membrane. Reported oxygen diffusivities and laboratory results are encouraging [48], but the feasibility of this scheme is still to be demonstrated during the planned scale-up. A key parameter is the oxygen

price above which the CMR scheme will become feasible. This will depend on the scale of operation.

4.2.4 Economy of scale

The choice of syngas technology is dictated by the scale of operation [43,46]. The economy of scale for syngas production is different for the steam reforming and partial oxidation routes. The tubular reformer costs increase almost linearly with capacity because of the number of tubes, hair pins and pig tails being proportional with capacity, whereas the autothermal reforming technology is related to the economy of scale for the oxygen plant, where n is close to 0.7. For an intermediate capacity, a two-step reforming combining tubular reforming followed by autothermal reforming appears to be the optimum choice, whereas for the large scale GTL or methanol plants (10.000 t/d), the autothermal reforming is the most feasible as illustrated in Fig. 14. A similar trend is to be expected for CMR-plants. If the membrane costs become a dominating element of total plant costs, CMR will be most favourable for small scale operation.

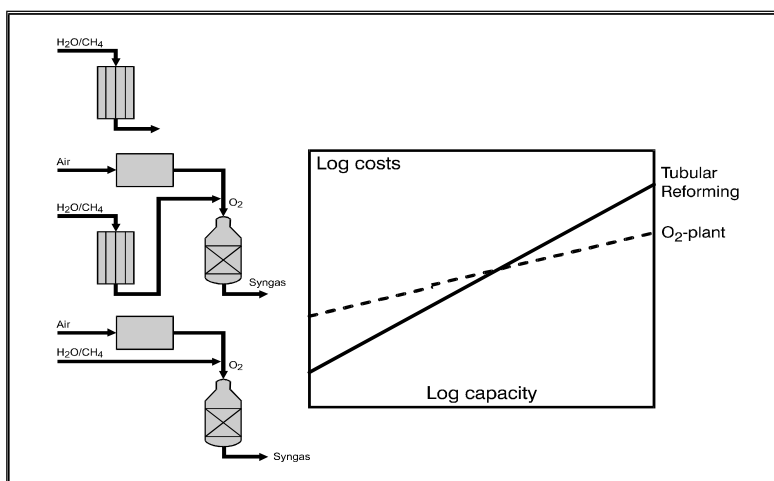


Figure 14. Impact of Scale of Operation [44]

5. CONCLUSIONS

Whether natural gas is used as fuel or feed for chemical production will more and more depend on the geographic location. Production of chemicals

and synthetic fuels will be feasible only where the natural gas price is low, meaning at locations where there is not a market for natural gas as fuel or for power generation. In both situations, high efficiency and carbon yield are important for the process economy. Catalysis will play an important role using natural gas as feed as well as fuel.

Natural gas may become important for the introduction of a hydrogen economy. One may ask whether it would not be cheaper to use natural gas conversion to make transport fuels via the GTL-technologies – awaiting a break-through in hydrogen technologies based on non-fossil fuels [49]. On the long-term, it might be better to use natural gas primarily for purposes where it offers special advantages, i.e. for chemicals, transportation fuels and direct use in fuel cells.

6. REFERENCES

- [1] Chew, K. (2003) in “Fundamentals of Gas to Liquids”, Petroleum Economist, p. 11.
- [2] Rostrup-Nielsen, J.R., Sehested, J., and Nørskov, J.K. (2002), *Adv.Catal.*, 47, 65.
- [3] Fleisch, T., Sills, R., Briscoe, M., and Freide, J.F. (2003) in “Fundamentals of Gas to Liquids”, Petroleum Economist, p. 39.
- [4] Topsøe, N.-Y (1997), *Cattech* 1, 125.
- [5] DallaBetta, R., and Rostrup-Nielsen, T., (1999), *Catal.Today* 47, 369.
- [6] Rostrup-Nielsen, J.R. (1997), *Stud.Surf.Sci.Catal.* 107, 473.
- [7] Mills, G.A. and Rostrup-Nielsen, J.R. (1994) *Catal.Today* 22, 335.
- [8] Fedders, H., Harth, R., Höhlein, B. (1975), *Nucl.Eng.Des.* 34, 119.
- [9] Harms, H., Höhlein, B., Jørn, E. and Skov, A. (1980), *Oil Gas J.* 78 (15) 120.
- [10] Diver, R.B., Fish, J.D., Levitan, R., Levy, M., Meirovitch, E., Rosin, H., Paripatyadar, S.A. and Richardson, J.T. (1992), *Sol.Energy*, 48, 21.
- [11] Rostrup-Nielsen, J.R. (2001), *Chem.Phys.Phys.Chem.*, 3, 283.
- [12] Christiansen, N., Kristensen, S., Holm-Larsen, H. (2002), 5th Eur. SOFC Forum Lucerne, July 2002, 1, 34.
- [13] Selimovic, A., Palson, J., and Sjunneson, L.(1998), in Abst. Fuel Cell Seminar 1998, Palm Springs, CA, p.88.
- [14] Rostrup-Nielsen, J.R. (2000) in ”Combinatorial Catalysis and High Throughput Catalyst Design and Testing” (E.G. Derouane et al, eds.), 337, Kluwer Academic Publishers, Dordrecht, NL, 2000.
- [15] Lange, J.P. (2001), *Cattech*, 5 (2) 85.
- [16] Rostrup-Nielsen, J.R. (1994), *Catal.Today*, 21 257.
- [17] Rostrup-Nielsen, J.R. (1998), Proc. 15th World Petr. Congr., John Wiley & Sons, New York p. 767.
- [18] Dybkjær, I. (1995) in “Ammonia” (A. Nielsen, ed), Springer Verlag, Berlin, p. 199.
- [19] Yurchak, S., (1988), *Stud.Surf.Sci.Catal*, 36, 251.
- [20] Couvaras, G. (2003) in “Fundamentals of Gas to Liquids”, Petroleum Economist, p. 4.
- [21] Dybkjær, I. (2003) in “Fundamentals of Gas to Liquids”, Petroleum Economist, p. 16.
- [22] Deam, R.J., Leather, J., and Hale, J.G. (1975), Proc. 9th World Petr.Congress, Tokyo 1975, 5, 397.

- [23] Yoneda, N., Kusano, S., Yasui, M., Pujado, P. and Wilcher, S. (2001), *Appl.Catal. A*, 221, 235.
- [24] Fang, D. and Cao F. (2000), *Chem.Eng.Jour.* 78, 237.
- [25] Sanfilippo, D. (this volume)
- [26] Bøgild Hansen, J. and Joensen, F. (1991), *Stud.Surf.Sci.Catal.* 61, 457.
- [27] Fleisch, T.H., Puri, R., Sills, R.A., Basu, A., Gradassi, M., and Jones, Jr, G.R. (2001), *Stud.Surf.Sci.Catal.* 136, 423.
- [28] Mikkelsen, S.E. and Sorenson, S.C., Int. Congr. & Exposition Detroit 1995, SAE Technical paper Series 950064, Warrendale, PA.
- [29] Hansen, J.B., Proc. 2nd Petroleum Symp., Saudia Arabia 1996, p. 1.
- [30] Andersen, J., Bakas, S., Foley, J., Gregoz, J., Vora, B., Kvisle, S., Reier Nilsen, H., Fuglerud, T., and Grønvold, Al. (2003), Paper at ERTC Petrochemical Conf, Paris, March.
- [31] Rothsemel, M., Wagner, J., Jensen, S.F. and Olsvik, O. (2003), paper at ERTC Petrochemical Conf., Paris, March.
- [32] deJong, K.P. (1996), *Catal.Today*, 29, 171.
- [33] "Hydrogen as an Energy Vector" (A.A. Strub and G. Imarisio, eds.), Reidel, Dordrecht 1980.
- [34] Rostrup-Nielsen, J.R. and Rostrup-Nielsen, T. (2002b), *Cattech*, 6, 150.
- [35] Middleton, P., Søgaard-Andersen, P., Rostrup-Nielsen, T. (2002) Abstr. 14th World Hydrogen Energy Conference, June, Montreal, Canada, p. 45.
- [36] Rostrup-Nielsen, J.R. and Sehested, J. (2003), ACS Preprints Petr.Chem.Div.
- [37] Ogdan M.M., Steinbugler, T.G. Kreutz (1999), *J. Power Sources*, 79, 143.
- [38] Koerts, T., Deelen, M.J.A.G and van Santen, R.A. (1992), *J.Catal.*, 138, 101.
- [39] Wang, D., Lunsford, J.H. and Rosynek, M.P. (1996), *Topics in Catalysis*, 3, 289.
- [40] Fox, III, J.M. (1993), *Catal.Rev.Sci.Eng.* 35, 169.
- [41] Goetsch, D.A., and Schmidt, L. (1996), *Science*, 271, 1560.
- [42] Aasberg-Petersen, K., Bak Hansen, J-H., Christensen, T.S., Dybkjær, I., Seier Christensen, P., Stub Nielsen, C., Winter Madsen, S.E.L., and Rostrup-Nielsen, J.R. (2001), *Appl.Catal. A: General*, 221, 379.
- [43] Rostrup-Nielsen, J.R., Dybkjær, I., Aasberg-Petersen, K. (2000), ACS Preprints Petr.Chem.Div. 45 (2) 186.
- [44] Dybkjær (1997) and Winter Madsen, S.E.L. (1997/98), *Int.J.Hydrocarb.Eng.* 3 (1) 56.
- [45] Trimm, D.L. (this volume)
- [46] Rostrup-Nielsen, J.R. (2000), *Catal.Today*, 63, 159.
- [47] Dybkjær, I., and Christiansen, T.S. (2001), *Stud.Surf.Sci.Catal.* 136, 441.
- [48] Shen, J., Venkataraman, V. (2003) in "Fundamentals of Gas to Liquids", Petroleum Economist, p. 24.
- [49] Rostrup-Nielsen, J.R. Proc. 16th ECOS Conference (Houbak, N., Elmegaard, B., Qvale, B., and Moran, M.J. eds.), Copenhagen 2003, p. 25.

Chapter 2

MOLECULAR CHEMISTRY OF ALKANE ACTIVATION

Aromatization of hydrocarbons on supported Mo₂C catalysts

Frigyes Solymosi

Institute of Solid State and Radiochemistry, University of Szeged and Reaction Kinetics Research Group of the Hungarian Academy of Sciences¹

P.O. Box 168, H-6701 Szeged, Hungary

¹This laboratory is a part of the Center for Catalysis, Surface and Material Science at the University of Szeged

Fax: +36-62-424-997; e-mail: fsolym@chem.u-szeged.hu

Abstract: The effects of Mo₂C/ZSM-5 found to be active in the aromatization of methane has been investigated on the reactions of various hydrocarbons. It was found that Mo₂C enhances the conversion of hydrocarbons and promotes the formation of aromatics, benzene and xylene. As in the case of aromatization of methane, Mo₂C deposited on silica also catalysed the reactions of the hydrocarbons, mainly the dehydrogenation processes. In addition, however, the aromatization reaction also occurred on Mo₂C/SiO₂ catalyst. The examination of the acidic properties of supported MoO₃ during calcination and carburization showed a significant decay in the number of Brönsted sites for ZSM-5 and the formation of stronger Lewis sites for silica samples. From the study of the reaction pathways of hydrocarbon species (CH₂, CH₃, C₂H₅, C₃H₅, C₄H₉ and C₆H₅) on Mo₂C/Mo (100) in UHV with different spectroscopic methods it appeared that the dominant processes are the dehydrogenation and hydrogenation of C_xH_y. In addition, their coupling was also experienced. This finding suggests that the Mo₂C is not only activate the methane and other hydrocarbon molecules, but it may also participate in the further reactions of the primary dissociation products.

Key words: Reaction of methane, reaction of ethane, reaction of propane, reaction of butane, formation of benzene, formation of aromatics, catalytic effect of ZSM-5, Mo₂C/ZSM-5 catalyst, Mo₂C/SiO₂ catalyst, acidic properties of supported Mo₂C, chemistry and reaction pathways of hydrocarbon fragments.

1. INTRODUCTION

This paper gives a survey of our studies on the most important features of the reactions of several hydrocarbons on supported Mo_2C catalysts. An account is also presented on the chemistry of hydrocarbon fragments, the primary dissociation products of the activation of hydrocarbons, on $\text{Mo}_2\text{C}/\text{Mo}$ (100) surface.

The upgrading of lower alkanes is an important subject of heterogeneous catalysis [1]. It is particularly true for the reaction of methane, which has been a great challenge for catalysis. The discovery of Wang *et al.* [2,3] that methane can be converted into benzene on $\text{MoO}_3/\text{ZSM-5}$ opened a new route for the utilization of methane. It turned out, however, that not the MoO_3 but Mo_2C is the key component for the activation and aromatization of methane, which is formed from MoO_3 during the induction period of the reaction [4-9]. In the subsequent works a great attention has been devoted to this catalytic system [10].

In our laboratory we continued our work in two directions: (i) elaborating the effect of Mo_2C on the aromatization of other hydrocarbons [11-14], and (ii) studying the chemistry of hydrocarbon species, C_xH_y , the primary products of the activation of the above compounds, on $\text{Mo}_2\text{C}/\text{Mo}$ (100) in UHV by several spectroscopic methods [15-19]. In addition, we paid a great attention to the effects of the preparation of Mo_2C . Other laboratories dealt with the interaction of MoO_3 and Mo_2C with ZSM-5, with their location in the zeolite, and with structural and other properties of Mo_2C [20-25].

2. EXPERIMENTAL

2.1 Materials

MoO_3 -containing catalysts were prepared by impregnating H-ZSM-5 or SiO_2 with a basic solution of ammonium heptamolybdate to yield different wt% of MoO_3 . The suspension was dried at 373 K and calcined at 863 K for 5 h. Supported Mo_2C catalysts were prepared by the carburization of calcined $\text{MoO}_3/\text{ZSM-5}$ or $\text{MoO}_3/\text{SiO}_2$ [26]. About 0.5 g of MoO_3 was heated in 1:4 methane- H_2 mixture flowing at 300 ml (STP)/min in quartz cell with two stopcocks. Preparation temperature was increased rapidly to 773 K and at 30 K/h between 773 and 1023 K, and maintained at 1023 K for 3 h. In another case, supported MoO_3 was heated under 10% v/v $\text{C}_2\text{H}_6/\text{H}_2$, from room temperature to 900 K at a heating rate of 0.8 K min^{-1} [27].

Unsupported Mo₂C has been prepared in the similar ways. After carburization, the samples were cooled down to room temperature under argon. Before exposure to the atmosphere, the carbides were passivated in flowing 1%O₂/Ar at 300 K, as suggested by Lee *et al.* [26]. In some cases, the samples were treated with H₂ at 873 K for 30 min to remove the excess carbon. The catalysts were characterized by XPS measurements. The binding energies for Mo(3d_{5/2}) and Mo(3d_{3/2}) were 227.8-228.2 and 230.7-231.1 eV, and for C(1s) 283.8 eV. These values are consistent with those attributed to Mo₂C [6, 7, 18].

The gases used were of commercial purity (Linde). NH₄-ZSM-5 was a commercial product (Zeolite Intern.), which was calcined to produce H-ZSM-5 in air at 863 K for 5 h. In most of the studies we used ZSM-5 with SiO₂/Al₂O₃ ratio of 55. The surface area of the sample was 425 m²/g. SiO₂ was Cab-O-Sil, surface area: 200 m²/g.

The hydrocarbon fragments, C_xH_y, have been prepared by the thermal and/or photo-dissociation of the corresponding iodo compounds. The completeness of the dissociation was established by XPS measurement.

2.2 Methods

Catalytic reaction was carried out at 1 atm of pressure in a fixed-bed, continuous flow reactor consisting of a quartz tube connected to a capillary tube [4-6]. The flow rate was 12 ml/min. The carrier gas was Ar. The hydrocarbon content was in most cases 12.5%.

The surface science studies were performed in an UHV chamber with a routine base pressure of 5x10⁻¹⁰ mbar produced by turbo molecular, ion-getter and titanium sublimation pumps. The chamber was equipped with facilities for AES, HREELS and TPD. XPS measurements were performed in a separate chamber with a Kratos XSAM 800 instrument using MgK α primary radiation (14 kV, 10 mA). To compensate for possible charging effects, binding energies (BE) were normalized to the Fermi-level for the Mo₂C. The pass energy was set at 40 eV, and an energy step width of 50 meV and dwell time of 300 ms were used. Typically 10 scans were accumulated for each spectrum. Fitting and deconvolution of the spectra were made using the VISION software (Kratos). The pretreatment of the samples and the reaction were performed in the preparation chambers attached to the UHV system.

3. RESULTS AND DISCUSSION

3.1 Reaction of methane

Following the initial works on the conversion of methane into benzene [2-4], an extended research has been devoted to this reaction, which was recently reviewed by Goodman *et al* [10]. Nevertheless, there are still several open questions which should be answered. One of them is the possible role of the Mo–O species in the activation of methane. As the Mo₂C/ZSM-5 samples were prepared by the carburization of supported MoO₃, one can assume that the presence of unreacted MoO₃ or Mo–O species may play an important role in the catalytic performance of Mo₂C/ZSM-5 samples. This idea was apparently supported by the observation that a partial oxidation of a less active Mo₂C mixed with ZSM-5 improved the yield of hydrocarbons and benzene produced [5].

In order to clarify the picture Mo₂C/ZSM-5 was prepared in situ by decarbonylation and carburization of Mo(CO)₆. This sample also proved to be an active and selective catalyst in the conversion of methane into benzene. In this case we cannot count on the presence of Mo oxides, although if the reactive OH groups of the support are not removed completely, 2σ-O⁻-Mo²⁺ species can be transitorily formed during the preparation in the reaction



as was postulated for alumina [28]. However, we did not find H₂O, CO, and CO₂ in the reaction products, which suggests that the Mo–O species was not present.

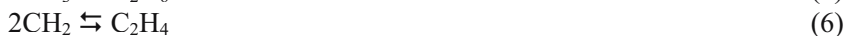
Accordingly, we may conclude that the presence of Mo–O species is not required for the activation of methane and for the further reaction steps. Mo₂C on the ZSM-5, produced by the transformation of highly dispersed MoO₃, is the active site for the cleavage of the C–H bond in the methane molecule. This explanation, however, is not sufficient as Pt metals on ZSM-5 even more active towards methane activation and decomposition without giving benzene or other aromatic compounds. Therefore we have to assume that Mo₂C is active for the first step of the methane decomposition,



but it is far less active for the decomposition of CH₃ and CH₂ species produced



compared to the Pt metals. As a result, these radicals have a certain lifetime to recombine into C_2H_6 and C_2H_4



either on the catalyst surface or in the gas phase. Further reactions, the oligomerization and aromatization of ethylene, occur on Brönsted sites of the ZSM-5 support [4-10, 20-25]. The finding, however, that Mo_2C on silica, which does not contain Brönsted sites, also catalyses the aromatization of methane is in an apparent disharmony with this picture. One can assume that new acidic sites are generated in the course of the conversion of MoO_3 into Mo_2C on silica or at the Mo/SiO_2 interface, which facilitates the aromatization of ethylene. We return to this problem later.

For the illustration of the effect of $\text{Mo}_2\text{C}/\text{ZSM-5}$ prepared from $\text{Mo}(\text{CO})_6$ some data are shown in Fig. 1.

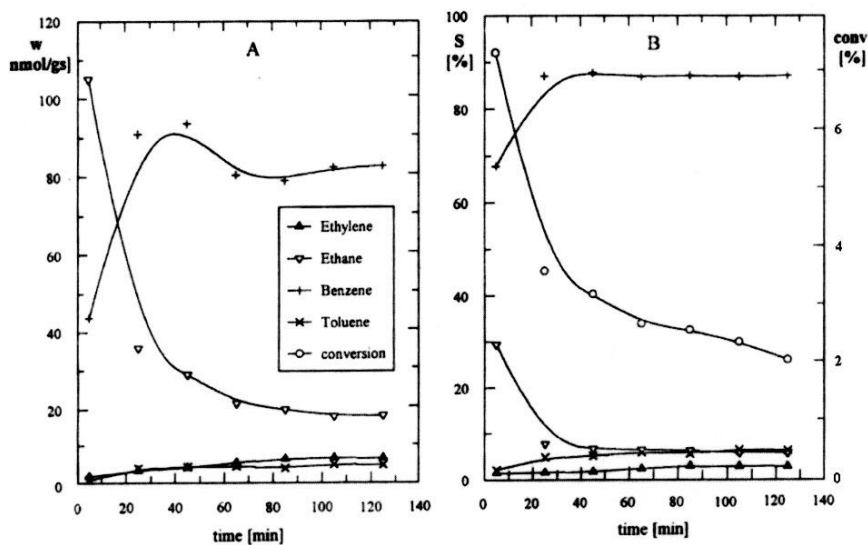


Figure 1. Conversion of methane, rate, and selectivity of the formation of various products on $\text{Mo}_2\text{C}/\text{ZSM-5}$ at 973 K. Mo_2C was prepared by decarbonylation and carburization of $\text{Mo}(\text{CO})_6$ deposited on ZSM-5 [6].

3.2 Reaction of ethane

The aromatization of ethane over promoted ZSM-5 has been the subject of extensive research [1, 29-36]. The effects of several additives (Ga, Zn, Pt etc.) have been examined, and active and selective catalysts have been prepared [29-36]. At high temperature, above 823 K, the aromatization of ethane proceeds on undoped ZSM-5 itself: the preparation, the composition of the ZSM-5 and the experimental conditions all influence the conversion and product distribution [29-36].

On ZSM-5 sample used by us the reaction of ethane was measurable at 873 K. The dehydrogenation reaction was the dominant pathway. The formation of benzene was limited, the selectivity was only 3-5%. At 973 K, this value increased to ~22%. These characteristics are consistent with the results of Schultz and Baerns [33] and differ from the behaviour reported recently by *Wong et al* [36]. They found aromatics (with 51.8% selectivity) and methane (with 48.2% selectivity) at ethane conversion of 5.9% at 923 K. No data for ethylene formation was given.

The reaction of ethane with unsupported MoO₃ was detected above 850 K when H₂O, CO₂, C₂H₄, CO, H₂ and CH₄ were produced. The conversion of ethane at 973 K approached the value of 10%.

The situation was different when MoO₃ was deposited on ZSM-5 and calcined at 973 K. This treatment resulted in high dispersion of MoO₃ and very likely in an interaction between MoO₃ and ZSM-5. As a result, the reduction of MoO₃ started at higher temperature. The conversion of ethane significantly increased and the product distribution also differed. This is illustrated in Fig. 2, which also shows the effects of other supports.

Both the yield and the selectivity of benzene formation markedly increased (Table 1).

Note that even the mechanical mixture of MoO₃ with ZSM-5 exhibited an improved performance as regards the conversion of ethane and the formation of benzene. Whereas at lower temperatures, below 873 K, the dehydrogenation of ethane



is the main reaction, above 873 K the formation of CH₄ and C₆H₆



or





came into prominence. In addition to step 7, the decomposition of ethylene



also contributes to the deposition of surface carbon.

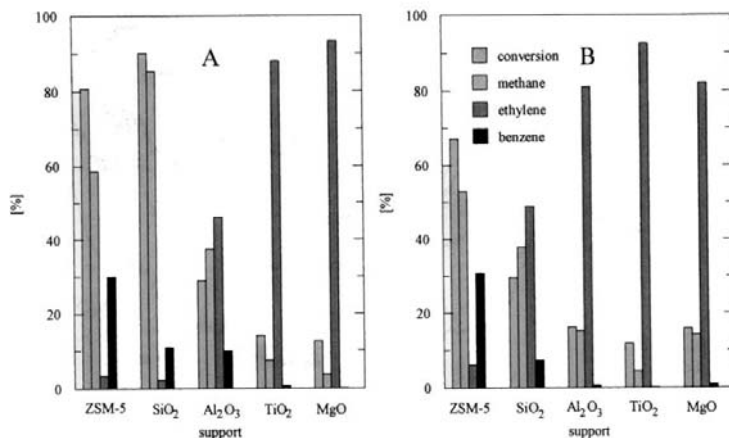


Figure 2. Effects of supports on the reaction of ethane on MoO₃ at 973 K. Reaction time: (A) 15 min; and (B) 60 min. [11].

Table 1. Some characteristic data for the ethane reaction on different catalysts.

Catalyst	Temperature (K)	Conversion (%)	Yield ^a (%)				
			CH ₄	C ₂ H ₄	C ₃ H ₈	C ₆ H ₆	C ₇ H ₈
H-ZSM-5	873	1.6	19.9	53.6	11.7	3.2	2.3
MoO ₃ /ZSM-5	873	14.5	21.7	24.8	7.8	22.2	12.9
Mo ₂ C/ZSM-5	873	36.1	38.6	11.5	5.5	25.2	10.2
H-ZSM-5	973	22.4	20.1	36.3	5.4	20.5	10.1
MoO ₃ /ZSM-5	973	54.1	37.5	14.5	3.1	26.6	7.8
Mo ₂ C/ZSM-5	973	67.2	48.5	5.7	1.1	28.3	8.2

^a The yield value shows the percentage of the converted ethane that transforms into the specified product.

Changes in the conversion and in the rates of product formation occurring in time on stream suggest an alteration of MoO₃ during the reaction. This may consist of (i) reduction of MoO₃, (ii) deposition of carbon and (iii) transformation of MoO₃ into Mo₂C, as experienced in the cases of the reaction of CH₄ on this catalyst [4-6, 37].

A partial reduction of MoO_3 is clearly indicated by the initial formation of H_2O and CO . The deposition of carbon was also observed which increased with the time on stream. XPS data also suggest the reduction of MoO_3 which, however, proceeds much slower than with CH_4 . The signal around 235.5-236.0 eV, indicative of the presence of Mo^{6+} , is still strong even after a reaction of 2 hr at 773 K (Fig.3).

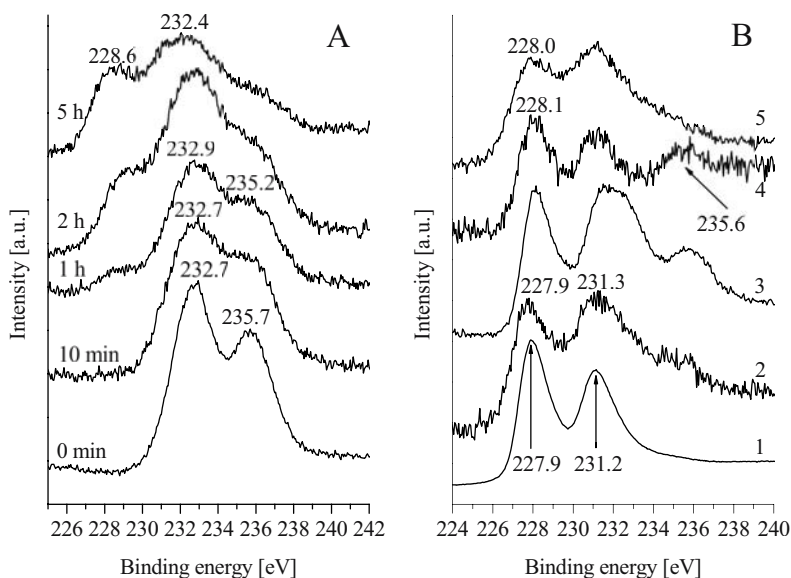


Figure 3. XPS spectra of Mo-containing catalysts. (A) Effects of reaction time with ethane at 773 K on the XPS of $\text{MoO}_3/\text{ZSM-5}$. (B) 1, Mo_2C ; 2, $\text{MoO}_3/\text{ZSM-5}$ treated with CH_4 at 973 K for 1 h; 3, $\text{MoO}_3/\text{ZSM-5}$ treated with C_2H_6 at 973 K for 10 min; 4, for 120 min; and 5, 2% $\text{Mo}_2\text{C}/\text{ZSM-5}$ prepared from MoO_3 [11].

The characteristic binding energies of $\text{Mo}(3d)$ in the Mo_2C are at ~ 231.1 and $227.8\text{-}228.3$ eV [6]. Deconvolution of the spectra suggests that - in contrast to the $\text{CH}_4 + \text{MoO}_3/\text{ZSM5}$ system - the complete transformation of MoO_3 into Mo_2C does not occur even at 973 K, but Mo_2C is produced in an increased amount with the increase of the temperature and the reaction time with C_2H_6 . Note that exact stoichiometry of carbide formed is not certain as the molybdenum carbide species having a different stoichiometry gives nearly the same XPS spectrum.

As regards the catalytic behavior of Mo_2C we can say the following. Unsupported Mo_2C catalysed the dehydrogenation of ethane at 973 K

without production of benzene. A significant improvement in the catalytic performance of Mo_2C occurred when it was prepared on ZSM-5. Apart from the very initial values, no changes in the conversion and selectivities to various products were experienced in time on stream. Qualitatively, we observed the formation of the same C - containing compounds as in the case of $\text{MoO}_3/\text{ZSM-5}$, which suggests the occurrence of similar reaction as was suggested for $\text{MoO}_3/\text{ZSM-5}$. An important difference is that the products of the reduction of MoO_3 (H_2O , CO_2 , CO) were missing. The advantageous properties of this catalyst were particularly exhibited above 873 K, when the steady state conversion reached a value of 65% with a 30% selectivity to benzene. These results suggest that the highly dispersed $\text{Mo}_2\text{C}/\text{ZSM-5}$ is a better catalyst for the transformation of ethane than the $\text{MoO}_3/\text{ZSM-5}$ and the enhanced production of benzene in time on stream is possibly due to the formation of Mo_2C . Another difference is that on $\text{Mo}_2\text{C}/\text{ZSM-5}$ less ethylene and more methane are formed at the same ethane conversion.

As in the aromatization of methane we may suppose that the role of the Mo_2C is mainly the activation of ethane and the promotion of the formation of ethylene. The further reactions, namely the oligomerization and the aromatization of ethylene proceed on the acidic sites on ZSM-5. In the light of these results it is interesting that a relatively large amount of ethylene is released from the ZSM-5-based catalysts, or in other words, a large fraction of ethylene produced escapes the aromatization. This suggests that the Mo_2C and/or the carbon formed in the reaction of ethane poisons the acidic sites of ZSM-5 and prevents the aromatization of ethylene.

As the aromatization of methane was investigated on the same $\text{Mo}_2\text{C}/\text{ZSM-5}$ catalyst, we may compare the results obtained in the two reactions. The remarkable difference is that the conversion of ethane is markedly higher than that of methane. As a result, the rates of the formation of all products were higher. Comparing the selectivities at nearly the same conversion, ~6-10%, (which was measured at 773 K for the reaction of ethane, and at 973 K for the reaction of methane), we obtain that the selectivity of benzene formation is much less (15%) for ethane reaction than in the case of methane aromatization (~85%). We attribute this to the more extended formation of excess carbon, which may block some of the acidic sites of ZSM-5.

3.3 Reactions of ethylene

Pure ZSM-5 effectively catalyses the aromatization of ethylene [1]. Deposition of Mo_2C on ZSM-5 affected the reaction pathways of ethylene observed on previous samples. At 773 K it somewhat decreased the conversion obtained for pure ZSM-5. Toluene formed with the highest

selectivity (~33%), followed by propane (~25%) and benzene (~15%). A complete conversion of ethylene into other products was experienced at 973 K. The selectivity to benzene production was practically the same as for Mo₂C-free ZSM-5. Toluene and propane formed with lower selectivities, while the methane production was significantly higher. Some data are displayed in Fig 4.

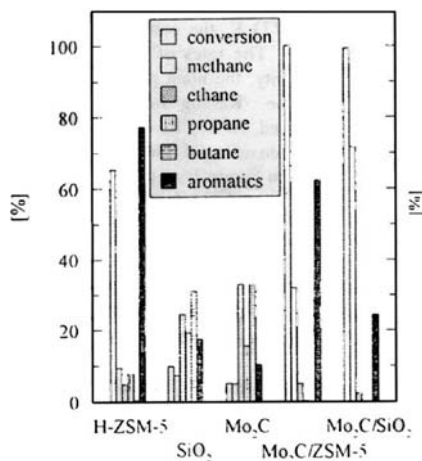


Figure 4. Conversion of ethylene and selectivities of the formation of various products on different catalysts at 973 K [13].

On the basis of these features we can conclude that Mo₂C deposited in highly dispersed state on ZSM-5 influences only slightly the aromatization of ethylene on the acidic sites of ZSM-5. The decrease in the selectivity of aromatics may be attributed to the reduction of the number of acidic sites, or to blocking some of the active area of the ZSM-5.

Different feature was found on silica support. Deposition of Mo₂C on silica exerted a dramatic influence on the reaction of ethylene. Whereas on pure silica we observed no reaction at 773 K, on Mo₂C/SiO₂ we detected all the products reported before. After an initial fast decay, the conversion of ethylene was about 10%. The main gaseous products were H₂, C₂H₆ (S ≈ 40%), propane (S ≈ 23%) and benzene (S ≈ 10%). Raising the temperature to 973 K caused the complete decomposition of ethylene. Besides H₂, CH₄, (S ≈ 70%) and C₆H₆ (S ≈ 20%) were identified. Changes of the conversion and selectivities in time of stream are presented in Fig. 4. The results suggest that Mo₂C in highly dispersed state can activate the ethylene molecule on the rather inactive silica support. The enhanced formation of benzene over Mo₂C/SiO₂ may be the result of the creation of acidic sites on the silica surface.

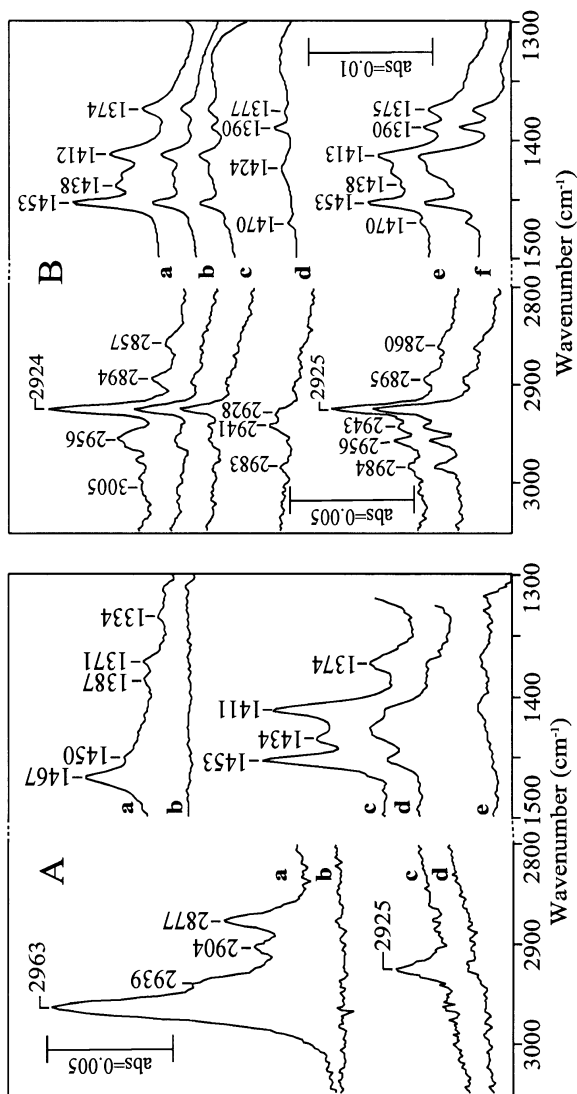


Figure 5. Infrared spectra of $\text{Mo}_2\text{C}/\text{SiO}_2$ following the adsorption of propane (A) and propylene (B). For (A): 1 Torr propane at (a) 173 K; (b) 273 K; (c) 10 Torr propane at 573 K; (d) evacuation of (c) at 300 K; (e) Propane flow at 373 K for 10 min and evacuation at 300 K. For (B): 1 Torr propylene at (a) 225 K; (b) 273 K; (c) 293 K; (d) after evacuation at 300 K; (e) 300 K; (f) 373 K. When the spectra were taken in the presence of gases, their spectra have been subtracted [14].

Table 2. Absorption bands (in cm^{-1}) observed following the adsorption of propane and propylene on $\text{Mo}_2\text{C}/\text{SiO}_2$.

assignment [24]	propane gas [24]	propane on $\text{Mo}_2\text{C}/\text{SiO}_2$ at 173K	assignment [25]	propylene		propane on $\text{Mo}_2\text{C}/\text{SiO}_2$ at 573 K
				gas [25]	propylene on $\text{Mo}_2\text{C}/\text{SiO}_2$ at 225 K	
$\nu_{\text{as}}(\text{CH}_3)$	2977	2963	$\nu_{\text{as}}(\text{CH}_2)$	3090	3080 (I/II)	
$\nu_{\text{as}}(\text{CH}_3)$	2973	2939	$\nu(\text{CH})$	3010	3005 (I/II)	
$\nu_{\text{as}}(\text{CH}_2)$	2968	2904	$\nu_{\text{s}}(\text{CH}_2)$	2990	2975 (I/II)	
$\nu_{\text{s}}(\text{CH}_3)$	2887	2877			2983 (III)	
$\delta_{\text{as}}(\text{CH}_3)$	1476	1467	$\nu_{\text{as}}(\text{CH}_3)$	2960	2956 (I/II)	
$\delta(\text{CH}_2)$	1462	1450			2941 (III)	
$\delta_{\text{s}}(\text{CH}_3)$	1392	1388	$\nu_{\text{s}}(\text{CH}_3)$	2930	2924 (II/I)	2925 (II/I)
$\delta_{\text{s}}(\text{CH}_3)$	1378	1371	$\nu_{\text{s}}(\text{CH}_3)$	2870	2894 (I/II)	
$\omega(\text{CH}_2)$	1338	1334	$\nu(\text{C}=\text{C})$	1650	2857 (I/II)	
					1637 (I)	1606 (I)
					1613 (I)	
					1470 (III)	
			$\delta_{\text{as}}(\text{CH}_3)$	1470	1453 (I/II)	1453 (I/II)
			$\delta_{\text{as}}(\text{CH}_3)$	1440	1438 (I/II)	1434 (I/II)
			$\delta(\text{CH}_2)$	1420	1412 (I/II)	1411 (I/II)
					1390 (III)	
			$\delta_{\text{s}}(\text{CH}_3)$	1380	1374 (I/II)	1374(I/II)

I: π -bonded propylene

II : di- σ bonded propylene

III: propylidyne

3.4 Adsorption and reaction of propane

In this case we studied thoroughly the interaction of propane with Mo₂C-containing catalysts by means of FTIR spectroscopy. Some characteristic spectra are displayed in Fig. 5A.

As shown in Table 2 the absorption bands observed following the adsorption of propane on Mo₂C/SiO₂ at 150-250 K correspond very well to the different vibrations of adsorbed propane. At higher temperature, however, new spectral features appeared at 2925, 1453, 1429, 1411 and 1374 cm⁻¹, which suggests that a fraction of propane interacted strongly with Mo₂C. As the possible process was the dehydrogenation of propane, the interaction of propylene with supported Mo₂C was also investigated. The characteristic absorption bands of π and di- σ -bonded propylene can be clearly established in the IR spectra (Fig. 5B). In addition, the appearance of bands at 2983, 2941, 1470 and 1390 cm⁻¹ suggests that adsorbed propylene is converted into propylidyne at 273 K. Taking into account the spectral features of adsorbed propylene and propylidyne on Mo₂C/SiO₂, the absorption bands at 2925, 1453, 1411, 1374 cm⁻¹ found following the adsorption of propane at 573 K can be attributed to adsorbed propylene. We cannot exclude that the vibration of propylidyne also contributes to these absorption bands. We assume that the two weak features remained on the spectrum (e) in Figure 5A are definitely due to the strongly adsorbed propylidyne. The characteristic absorption bands of propylidyne are as follows: 2960, 2920, 2870, 1450, 1410, 1365 cm⁻¹ [38-42]. These spectral features were also established following the adsorption of propane on Pt/SiO₂ by Sheppard *et al* [38-42]. Accordingly, the reactivity of highly dispersed Mo₂C towards propane and propylene is not much less than that of supported Pt catalyst.

The presence of strongly adsorbed species remained on supported Mo₂C after contact with propane is also suggested by TPD measurements. This species is converted into propylene and ethylene at higher temperature.

Pure Mo₂C exerted a much larger influence on the reaction of propane compared to methane and ethane. The initial conversion was 24% at 873 K yielding different hydrocarbons without benzene. A completely different picture was obtained on Mo₂C/ZSM-5 catalysts. The formation of aromatics came into prominence. The aromatization of propane proceeds readily on undoped ZSM-5 alone at and above 823 K: the preparation, the composition of the ZSM-5 and the experimental conditions all influence the conversion and product distribution [1]. On our ZSM-5 sample, the reaction of propane was measurable at 773 K. The main products were ethylene, methane and propylene. The selectivity of the aromatics (benzene and toluene) at 873 K

was around 16-18%, which increased to ~34% at 973 K. When Mo₂C was deposited over ZSM-5, the catalytic performance of ZSM-5 markedly changed. The conversion of propane slightly decayed, but the selectivity to benzene and toluene significantly increased. The effects of temperature on the product distribution of the reaction of propane on 2% Mo₂C/ZSM-5 are shown in Fig.6.

In the description of the aromatization of propane on ZSM-5 it is assumed that propane is activated through the abstraction of hydride ions by carbonium ion [1]. The dimethyl carbonium ions formed may give propylene or react with alkenes. Parallel with this reaction route the cracking of alkenes (ethylene and propylene) also proceeds to yield lower alkanes. The oligomerization of propylene on the acidic sites in the zeolite cavities leads to the formation of aromatics [1]. The favourable effect of Mo₂C can be explained by its high activity towards the dehydrogenation of propane. The results obtained for Mo₂C/SiO₂ clearly showed that Mo₂C is an effective catalyst to produce propylene from propane. For comparison of the performance of different catalysts some data are collected in Table 3.

Table 3. Characteristic data for the reactions of propane at 873 K for steady state.

	Mo ₂ C/SiO ₂	ZSM-5	Mo ₂ C/ZSM-5
Conversion of propane	24%	53%	46%
Selectivity for			
Propylene	48%	12%	8%
Ethylene	14%	32%	13%
Methane	13%	30%	26%
Ethane	5%	6%	5%
Benzene	12%	10%	33%
Toluene	5%	6%	13%

3.5 Reactions of propylene

As in the aromatization of lower alkanes the oligomerization of alkenes on the acidic sites of ZSM-5 play an important role, it seemed necessary to examine the influence of Mo₂C on the reaction of propylene on ZSM-5. Under the reaction conditions applied 80% of propylene reacted on pure ZSM-5 at 873 K producing all the products measured in the reaction of propane. The selectivity to benzene and toluene was 27 and 24%, respectively. Other main product was ethylene with 25% selectivity. The main effect of Mo₂C over ZSM-5 is that the formation of ethylene was reduced, and at the same time the selectivity to benzene and toluene was somewhat increased. The conversion of propylene remained at high level, above 80%. Note that on unsupported Mo₂C the cracking of propylene was the main reaction route, aromatics were only very minor products. Results obtained for ZSM-5 and Mo₂C/ZSM-5 at 873 K are listed in Table 4.

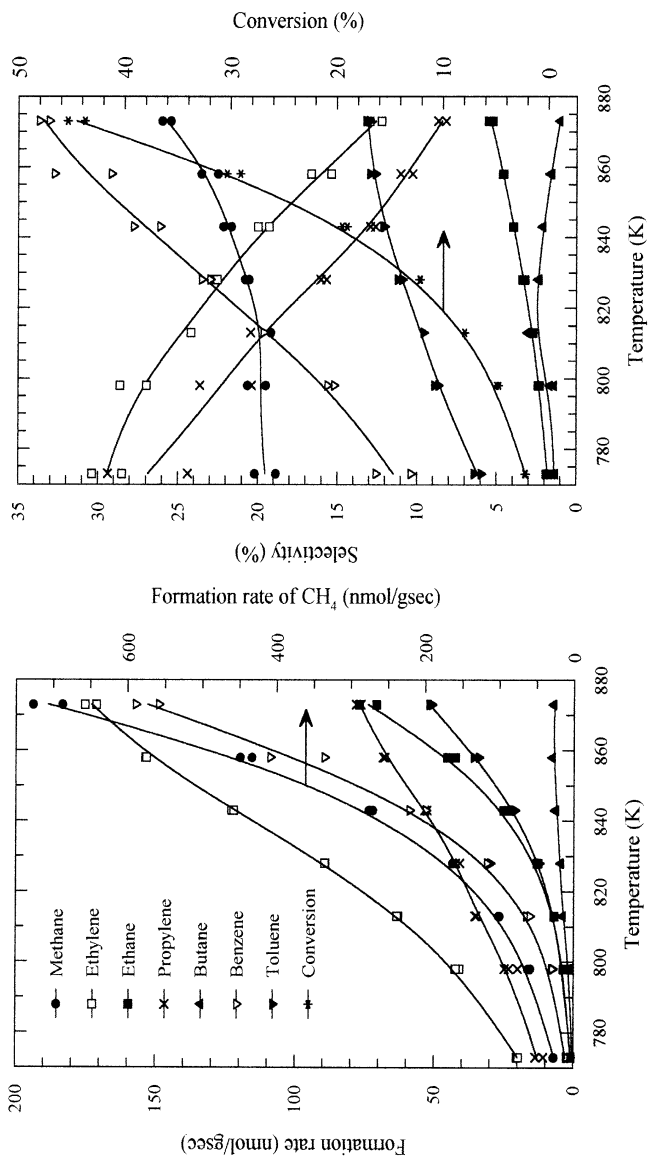


Figure 6. Conversion of propane, rates and selectivities of the formation of various products on Mo₂C/ZSM-5 at different temperatures. Data were obtained after 60 min of reaction. The same sample was used at every temperature. Measurements were started at the highest temperature [14].

Table 4. Characteristic data for the reaction of propylene on ZSM-5 and 2% Mo₂C/ZSM-5 at 873 K.

	ZSM-5	Mo ₂ C/ZSM-5
Conversion, %	10	82
Selectivity for		
methane	7.5	8.5
ethane	3.5	4.0
ethylene	25.5	10.5
propane	5.0	2.0
butane	7.0	3.0
pentane	0.3	0.0
benzene	27.0	39.0
toluene	24.0	34.0

3.6 Reaction of *n*-butane and iso-butane

The interaction of *n*-butane with MoO₃ on ZSM-5 and the aromatization of *n*-butane on Mo₂C/ZSM-5 has been recently studied by Derouane's school [44, 45]. We also gave a short account on this reaction on Mo₂C/ZSM-5 [46]. Both laboratories showed that while *n*-butane is mainly cracked on ZSM-5, the production of aromatics is markedly promoted when Mo₂C is deposited on ZSM-5. In our more detailed study we paid a great attention to the effects of the composition of ZSM-5.

Reaction was measurable above 700 K. In harmony with the literature data, the product distribution sensitively depended on the composition of ZSM-5.

As shown in Fig.7, the highest conversion was obtained for the sample with SiO₂/Al₂O₃ ratio = 30 and the lowest with SiO₂/Al₂O₃ ratio of 280. There was no or only a slight decay in the conversion and in the rate of formation of various products. Whereas the cracking of butane was the dominant reaction pathway, yielding propane, propene, ethylene, ethane and methane in decreasing amounts, the production of aromatics (benzene, toluene and xylenes) occurred on all samples. The selectivity of aromatics was the highest on ZSM-5 with high alumina content (SiO₂/Al₂O₃ ratio = 30).

As this ZSM-5 alone exhibited relatively high activity, a great improvement of its catalytic performance with Mo₂C addition was not expected. Nevertheless, depending on the preparation and pretreatment of Mo₂C/ZSM-5, the conversion of *n*-butane approached or even exceeded the value measured for pure ZSM-5. Better catalytic performance was obtained by the Mo₂C/ZSM-5 sample prepared by the carburization of MoO₃ with ethane. Elimination of excess carbon of Mo₂C with H₂ at 873 K before the catalytic reaction also caused an increase in the conversion of *n*-butane.

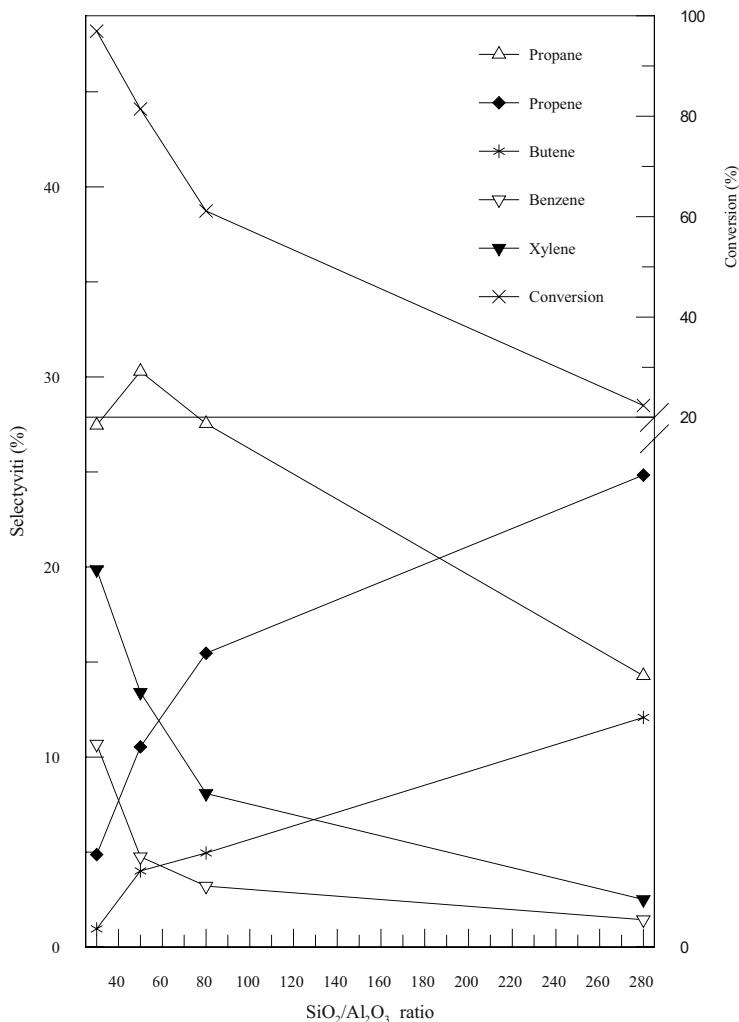


Figure 7. Effects of SiO₂/Al₂O₃ ratio on the reaction of *n*-butane at 773 K.

Figure 8A shows the effects of the amount of Mo₂C prepared on ZSM-5 on the reaction of *n*-butane. The addition of even 2% Mo₂C to ZSM-5 (SiO₂/Al₂O₃ ratio = 80) increased the selectivity to aromatics from 12% to 27% mainly at the expense of the formation of propane. On increasing the amount of Mo₂C we observed a decrease in the conversion and in the selectivities of aromatics, methane, ethane and propane, and a marked increase in that of butenes (Fig. 8A).

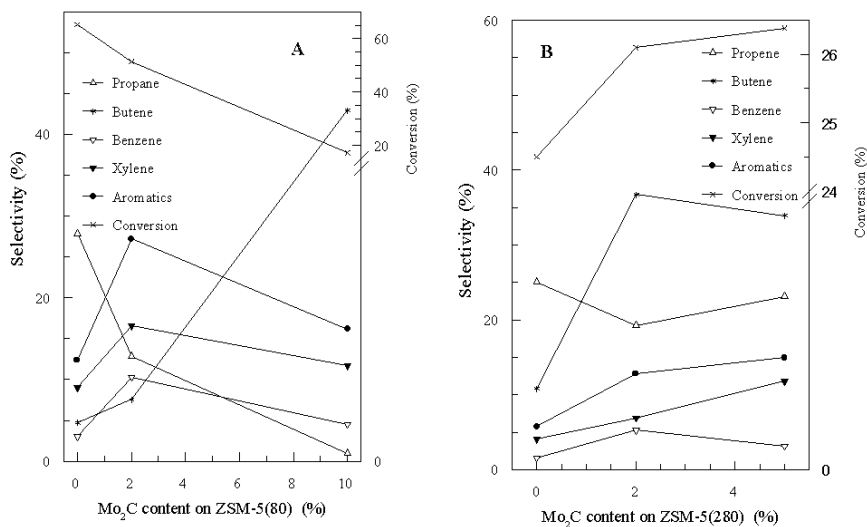


Figure 8. Effects of Mo₂C content of ZSM-5 (80) (A) and ZSM-5 (280) (B) on the reaction of *n*-butane at 773 K.

The results obtained for ZSM-5 (SiO₂/Al₂O₃ ratio = 280) are plotted in Fig.8B. While this zeolite exhibited very little aromatizing tendency, the presence of 2 and 5% Mo₂C promoted the formation of both benzene and xylene. The selectivity of aromatics attained a value of 16-17%. A significant increase was observed in the selectivity of butenes, whereas the formation of lower hydrocarbons has been reduced. Detailed analysis of butene showed that it consists of 1-butene, trans 2-butene, iso-butene and cis 2-butene. Their distribution is shown in Table 5. It appears that iso-butene is produced with higher selectivities.

Table 5. Distribution of different butanes formed in the reaction of *n*-butane at 823 K.

Catalyst	Conversion (%)	Selectivity (%)			
		Trans-2-Butene	1-Butene	Iso-Butene	Cis-2-Butene
H/ZSM-5 (80)	69,3	1,1	1,2	2,4	1,1
2%Mo ₂ C/ ZSM-5 (80)	51,4	0,01	2,2	3,6	1,7

The important role of Mo₂C in the conversion of *n*-butane into other compounds is clearly demonstrated by the results obtained when Mo₂C was

dispersed on almost inactive SiO_2 , as pure silica exhibited only slight catalytic activity. The decomposition of *n*-butane at 823 K was less than 1.5% which reached ~3-4% at 923 K, yielding the same cracking products observed for ZSM-5 without any sign of aromatics. On $\text{Mo}_2\text{C}/\text{SiO}_2$ not only the cracking and dehydrogenation of *n*-butane were catalyzed, but the aromatization reaction was also promoted. Some data for the illustration of the effects of $\text{Mo}_2\text{C}/\text{SiO}_2$ on the catalytic conversion on *n*-butane are presented in Table 6. We may assume that the deposition of Mo_2C created some active acidic sites on SiO_2 or at the $\text{Mo}_2\text{C}/\text{SiO}_2$ interface which facilitated the coupling of reactive hydrocarbon species formed.

ZSM-5 effectively catalysed the conversion of iso-butane, too. The composition of the zeolite played again an important role: the activity of the ZSM-5 decreased with the increase of the $\text{SiO}_2/\text{Al}_2\text{O}_3$ ratio. Qualitatively, the same compounds were produced as in the case of the reaction of *n*-butane. Aromatic compounds formed with higher selectivity on ZSM-5 ($\text{SiO}_2/\text{Al}_2\text{O}_3$ ratio = 30), whereas ZSM-5 at large $\text{SiO}_2/\text{Al}_2\text{O}_3$ ratios exhibited very little aromatization property. Deposition of Mo_2C on ZSM-5 varied only slightly the conversion of iso-butane and significantly promoted the reaction pathway for aromatics. The promoting effect of Mo_2C was well exhibited on ZSM-5 with $\text{SiO}_2/\text{Al}_2\text{O}_3$ ratio of 80 and 280. At 2% Mo_2C on ZSM-5 (80) the selectivities of xylene and benzene reached the values of 40 and 20%, respectively. As the conversion of iso-butane also increased, the yields of aromatics were considerably higher compared to pure ZSM-5. Higher loading of Mo_2C (10%) favored the formation of butenes and left practically unchanged the selectivities of aromatics. The conversion of iso-butane, however, fell to a low value. Whereas the aromatization of iso-butane occurred to a very limited extent on ZSM-5 ($\text{SiO}_2/\text{Al}_2\text{O}_3$ ratio = 280), aromatic compounds were formed with high selectivities and yields when 2% Mo_2C was deposited on this zeolite. This is illustrated in Fig. 9. Mo_2C was also advantageous for the production of different butenes. Highest selectivity was again calculated for iso-butene.

Table 6. Characteristic data for the reaction of n-butane on Mo₂C/SiO₂ at 823 K

Catalyst	Conversion(%)	Selectivity(%)							Yield of aromatics
		Methane	Ethane	Ethylene	Propane	Propene	Butene	Aromatics	
2%Mo ₂ C/SiO ₂ * (cabosil)	25,8	6,2	2,3	19,7	0,4	13,5	40	16,2	4,2
2%Mo ₂ C/SiO ₂ (cabosil)	15	1,8	0,5	7	0,2	10	0,267	8	1,2
2%Mo ₂ C/SiO ₂ (aerosil)	37	5,52	2,45	11,73	0,67	14,06	42,59	19,13	7
10%Mo ₂ C/SiO ₂ (cabosil)	33,24	2,78	1,28	9,14	0,28	8,78	61,2	12,58	4,18
10%Mo ₂ C/SiO ₂ (aerosil)	35,15	3,88	2,1	9,46	0,50	10,91	55,35	14,56	5,1

* data were taken at 873 K

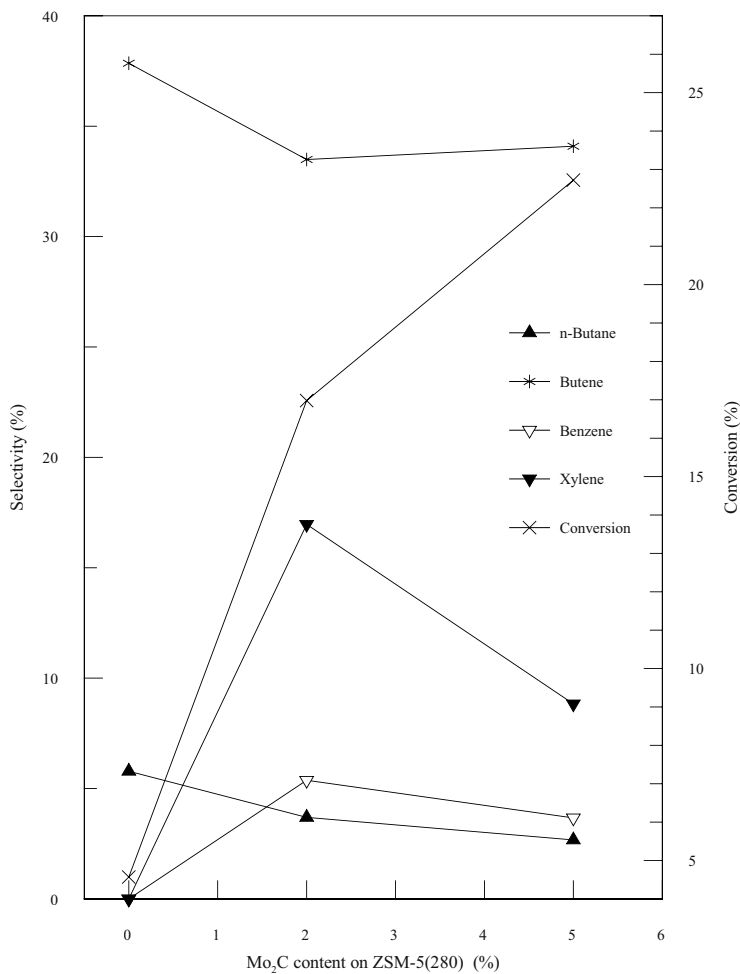


Figure 9. Effects of Mo₂C content of ZSM-5 (280) on the reaction of iso-butane at 773 K.

3.7 Reaction of butene-1 on supported Mo₂C

As the products of the dehydrogenation of butane is butene, some measurements have been carried out concerning its reaction on the previously studied catalysts. Since the reaction pathway is strongly influenced by the temperature, the reaction was studied near the temperature of former experiments, 723 K. At this temperature the conversion of 1-butene on pure ZSM-5 samples was very high, more than 90%. The main

products on ZSM-5 with $\text{SiO}_2/\text{Al}_2\text{O}_3 = 30$ was propane ($S = 33\text{-}35\%$) followed by xylene ($S = 26\%$), benzene ($\sim 10\%$). Depositing 2% Mo_2C on this zeolite resulted in an increase in the selectivities of aromatic compounds to 31-32% and 11-12%, respectively, and in a decrease of that of propane ($\sim 30\%$). At lower temperature, 623 K, the selectivities of all the these compounds were drastically reduced, whereas the formation of iso-butane, *n*-butane and pentane greatly increased. The selectivities of aromatics were lower (xylene (24%), benzene (4%)) on ZSM-5 of higher silica content ($\text{SiO}_2/\text{Al}_2\text{O}_3 = 80$), but both values were enhanced on the effect of 2% Mo_2C to 31-32% and 5-6%, respectively.

3.8 Determination of acidic centers

As regards the aromatization of methane on $\text{Mo}_2\text{C}/\text{ZSM-5}$ we assumed before that the primary role of the Mo_2C is the mild activation of methane and the coupling of C_xH_y fragments into ethylene. Further reactions, the oligomerization and aromatization of ethylene occur on the Brønsted sites of zeolite. In the case of higher hydrocarbons it is safe to conclude that Mo_2C promotes the dehydrogenation process, and the aromatization of alkene compounds proceeds on the same centers of ZSM-5. A surprising result obtained in an early study was that $\text{Mo}_2\text{C}/\text{SiO}_2$ also catalyzed the aromatization of methane [4], although its catalytic performance was far behind that of $\text{Mo}_2\text{C}/\text{ZSM-5}$. As was demonstrated above, $\text{Mo}_2\text{C}/\text{SiO}_2$ exerted a similar influence on the aromatization of ethane, propane and butane. As silica contains no Brønsted sites, the question arose as to how olefins are converted into benzene on $\text{Mo}_2\text{C}/\text{SiO}_2$.

One possibility was that the transformation of MoO_3 into Mo_2C creates new acidic sites, which are not present on pure silica. In order to check this assumption detailed infrared spectroscopic measurements were carried out to characterize the catalysts and to determine changes in the nature and the number of acidic centers in the course of calcinations and carburization of MoO_3 .

Spectra registered for $\text{MoO}_3/\text{SiO}_2$ are displayed in Figs. 10 and 11. We obtained the following results [46]:

- A decrease of all the OH stretching bands in the IR spectrum of $\text{MoO}_3/\text{ZSM-5}$ was observed during calcination. Both pyridine and CO adsorption measurements showed the decrease in the number of Brønsted acidic centers due to deposition of Mo on ZSM-5.
- Carburization did not lead to regeneration of Brønsted acidic OH groups.
- Mo deposited on SiO_2 reacts with the OH groups of the support during calcination and induces Lewis acidity.

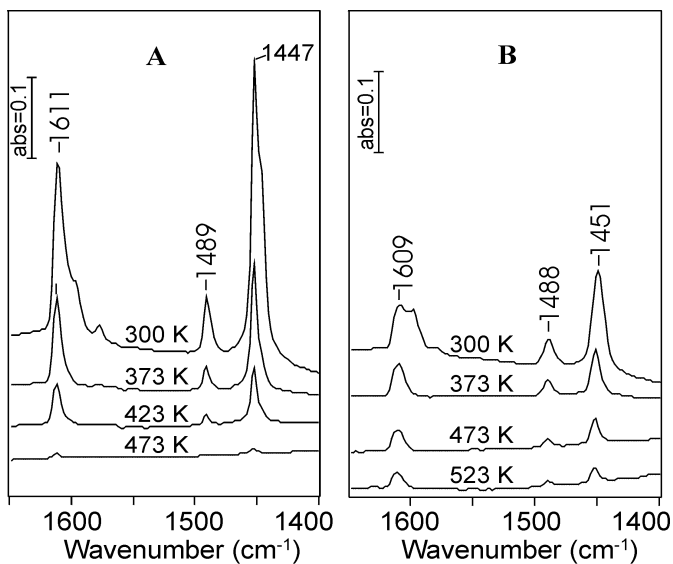


Figure 10. FTIR spectra of pyridine adsorbed on 2%MoO₃/SiO₂ (A) and carburised 2%MoO₃/SiO₂ (B) [46].

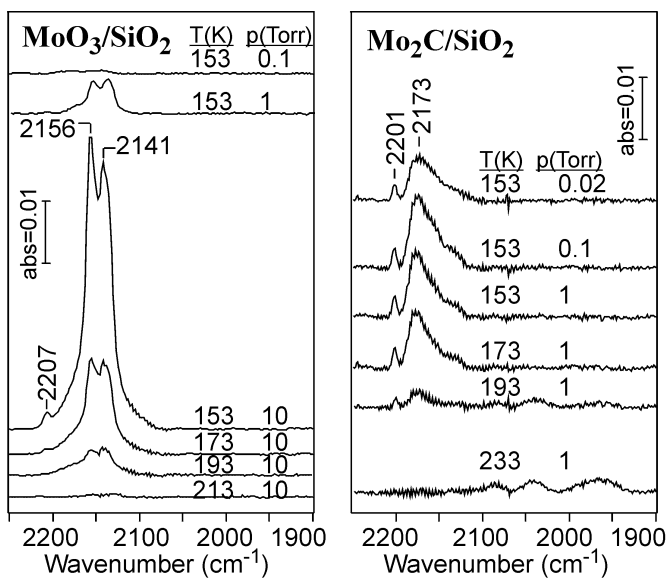


Figure 11. FTIR spectra of CO adsorbed on 2%MoO₃/SiO₂ (A) and carburised 2%MoO₃/SiO₂ (B) [46]. The spectrum recorded before CO adsorption and that of the gas phase were subtracted.

- Carburisation resulted in further OH consumption and the appearance of stronger Lewis acid sites. The generation of Brønsted sites was not observed either by pyridine or by CO adsorption.

In the light of these results we came to the conclusion that the oligomerization and aromatization of the C_xH_y formed can also occur on Lewis acidic sites very probably at Mo_2C - SiO_2 interface.

3.9 Main features of the chemistry of hydrocarbon fragments

As regards the chemistry of different hydrocarbon fragments we established the following features.

The main products of adsorbed CH_3 over $Mo_2C/Mo(100)$ is hydrogen, methane and surface carbon. The coupling of CH_3 into C_2H_6 was not observed, but the formation of ethylene was detected. CH_2 species undergoes self-hydrogenation to CH_4 at $T_p=300$ K, and dimerization into C_2H_4 at and above 222-280 K. The reaction of C_2H_5 yields C_2H_6 and C_2H_4 . Neither the cleavage of the C–C bond nor the coupling of C_2 compounds occurred to detectable extent under the experimental conditions. Allyl species, C_3H_5 , underwent hydrogenation to propane and propene, which desorbed with $T_p=280-300$ K, and 400-420 K. Analysis of HREEL spectra of the annealed adsorbed layer suggests the formation η^1 -allyl and η^3 -allyl groups at 100-200 K and the presence of di- σ bonded propene at 250-410 K. The latter species is converted into propylidyne, which decomposes at higher temperatures leaving carbon on the surface. At higher surface concentration, allyl species coupled into hexadiene ($T_p=172$ K) and hexane ($T_p=230$ and 325 K). The reaction of butyl, C_4H_9 , gave butane, butene and a small amount of octane. The chemistry of benzyl, C_6H_5 , has been also examined on this Mo_2C surface. A very limited part is coupled into biphenyl ($T_p=510$ K). Other part was hydrogenated to a benzene which desorbed with a $T_p=290-278$ K. The third part of $C_6H_{5(a)}$ decomposed to hydrogen and benzyne groups. This species could be also hydrogenated into benzene, but its most part decomposed at higher temperature, as shown by H_2 desorption peaks at 600 and 700 K. HREEL spectra suggested that the aromatic ring was preserved on the surface up to ~ 430 K. Elevating the adsorption temperature to 400 K enhanced the amount of strongly bonded C_6 species by a factor of ~ 3 as evidenced by the increased hydrogen desorption.

4. CONCLUSIONS

- Mo₂C deposited on ZSM-5 increased the conversion of the reactions of various hydrocarbons measured on pure ZSM-5 and promoted the formation of aromatics. This effect appeared mostly at low (~2%) Mo₂C content.
- The extent of the promoting effect of Mo₂C was the highest on ZSM-5 with high SiO₂/Al₂O₃ ratio.
- Qualitatively similar features were observed in the case of silica support, which alone exhibited no or only negligible catalytic activity.
- Both the deposition of MoO₃ on ZSM-5 and subsequent carburization of MoO₃ decreased the number of Brønsted acidic sites. On SiO₂ surface the carburization of MoO₃ led to stronger Lewis sites.
- Although the hydrocarbon fragments produced by the dissociation of iodo compounds decompose and dehydrogenate readily on Mo₂C/Mo(100) surface, their couplings were also observed.
- It is assumed that the Mo₂C is not only activate the methane and other hydrocarbon molecules, but it may also participate in the further reactions of the primary dissociation products.

5. REFERENCES

- [1] Y.Ono, Catal. Rev. -Sci. Eng., 34 (3) (1992) 179
- [2] L.Wang, L.Tao, M.Xie, G.Xu, J.Huang, Y.Xu, Catal. Lett. 21 (1993) 35
- [3] Y.Xu, L.Wang, M.Xie, X.Gou, Catal. Lett. 30 (1995) 135
- [4] F.Solymosi, A.Erdőhelyi, A.Szőke, Catal. Lett. 32 (1995) 43
- [5] F.Solymosi, A.Szőke, J.Cserényi, Catal. Lett. 39 (1996) 157
- [6] F.Solymosi, J.Cserényi, A.Szőke, T.Bánsági, A.Oszkó, J. Catal. 165 (1997) 150
- [7] D.W.Wang, J.H.Lunsford, M.P.Rosynek, Topics in Catal. 3(4) (1996) 299
- [8] J.H.Lunsford, M.P.Rosynek, D.W.Wang, Stud. Surf. Sci. Catal. 107 (1997) 257
- [9] D.W.Wang, J.H.Lunsford, M.P.Rosynek, J. Catal. 169 (1997) 347
- [10] T.V.Choudhary, E.Aksoylu, D.W.Goodman, Catal. Rev. 45 (2003) 151
- [11] F.Solymosi, A.Szőke, Appl. Catal. A166 (1998) 225
- [12] F.Solymosi, R.Németh, Catal. Letts., 62 (1999) 197
- [13] F.Solymosi, A.Szőke, Stud. Surf. Sci. Catal. 119 (1998) 355
- [14] F.Solymosi, R.Németh, L.Óvári, L.Egri, J. Catal. 195 (2000) 316.
- [15] F.Solymosi, L.Bugyi, A.Oszkó, Catal. Lett. 57 (1999) 103
- [16] F.Solymosi, L.Bugyi, A.Oszkó, I.Horváth, J. Catal. 185 (1999) 160
- [17] L. Bugyi, A. Oszkó, F. Solymosi, Surf. Sci. 516 (2002) 74
- [18] L. Bugyi, A. Oszkó, F. Solymosi, Surf. Sci. 519 (2002) 139
- [19] L. Bugyi, A. Oszkó, F. Solymosi, Surf. Sci. in press
- [20] R.W.Borrey III, E.C.Lu, K.Young-ho, E.Iglesia, Stud. Surf. Sci. Catal. 119 (1998) 403
- [21] J-Z.Zhang, M.A.Long, R.F.Howe, Catal. Today 44 (1998) 293
- [22] L.S. Liu, L.Wang, R.Ohnishi, M.J.Ichikawa, Catal. 181 (1999) 175

- [23] S.B.Derouane-Abd Hamid, J.R.Anderson, I.Schmidt, C.Bouchy, C.J.H.Jacobsen, E.G.Derouane, *Catal. Today* 63 (2000) 461
- [24] Y-Y.Shu, D.Ma, L-L.Su, L-Y.Xu, Y-D.Xu, X-H.Bao, *Stud. Surf. Sci. Catal.* 136 (2001) 27
- [25] R.Ohnishi, L.Xu, K.Issoh, M.Ichikawa, *Stud. Surf. Sci. Catal.* 136 (2001) 393
- [26] J.S.Lee, S.T.Oyama, M.Boudart, *J. Catal.* 106 (1987) 125
- [27] A.J.Brungs, A.P.E.York, J.B.Claridge, C.Márquez-Alvarez, M.L.H.Green, *Catal. Lett.* 70 (2000) 117
- [28] R.G.Bowman, R.L.Burwell, *J. Catal.* 63 (1980) 463
- [29] M.Guisnet, N.S.Gnep, F.Alario, *Appl.Catal.* 89 (1992) 1
- [30] K.H.Steinberg, U.Mroczek, F.Roessner, *Appl. Catal.* 66 (1990) 37
- [31] O.V.Bragin, E.S.Shapiro, A.V.Preobrazenskij, S.A.Isaev, T.V.Vasina, B.B.Dyusenbina, G.V.Antoshin, Kh.M.Minachev, *Appl. Catal.* 27 (1986) 219
- [32] Y.Ono, H.Nakatami, H.Kitagawa, E.Suzuki, *Stud. Surf. Sci. Catal.* 44 (1988) 279
- [33] P.Schulz, M.Baerns, *Appl. Catal.* 78 (1991) 15
- [34] O.V.Chetina, T.V.Vasina, V.V.Lunin, *Appl. Catal. A:General* 131 (1995) 7
- [35] O.P.Keipert, D.Wolf, P.Schulz, M.Baerns, *Appl. Catal. A:General* 131 (1996) 347
- [36] S.T.Wong, Y.Xu, L.Wang, S.Liu, G.Li, M.Xie, X.Guo, *Catal. Lett.* 38 (1996) 39
- [37] A.Szöke, F.Solymosi, *Appl. Catal. A:General* 142 (1996) 361
- [38] G.Shahid, N.Sheppard, *Spectrochim. Acta.* 46 (1990) 999
- [39] M.A.Chesters, C.De La Cruz, P.Gardner, E.M.McCash, P.Pudney, G.Shahid, N. Sheppard, *J. Chem. Soc. Faraday Trans.*, 86(15), 2757 (1990).
- [40] N.Sheppard, *Ann. Rev. Phys. Chem.* 39 (1988) 589 and references therein.
- [41] N.Sheppard, C.De La Cruz, *Adv. in Catal.* 41 (1996) 1
- [42] N.Sheppard, C.De La Cruz, *Adv. in Catal.* 42 (1998) 181
- [43] S.Yuan, S.B.Derouane-Abd Hamid, Y.Li, P.Ying, Q.Xin, E.G.Derouane, C.Li, *J. Mol. Catal. A: Chem.* (2002) 1
- [44] S.Yuan, S.B.Derouane-Abd Hamid, Y.Li, P.Ying, Q.Xin, E.G.Derouane, C.Li, *J. Mol. Catal. A: Chem.* 180 (2002) 245
- [45] F. Solymosi, R. Németh, A. Széchenyi, *Catal Lett.* 82 (2002) 213
- [46] F. Solymosi, L. Óvári, *J. Mol. Catal. A: Chem.* in press.

Chapter 3

ECONOMICS OF ALKANE CONVERSION

Economic guidelines and techno-economical evaluation of alkane conversion processes

Jean-Paul Lange

Shell Chemicals Int.

Abstract: The conversion of methane and C₂₋₄ alkanes to fuels and chemical intermediates represents a major challenge for the 21st century. Due to the chemical and thermodynamic stability of these feedstocks, their upgrading requires expensive manufacturing plants. This paper will review the basics of manufacturing economics and then discuss the economic peculiarities of methane and alkane conversion technologies. On the basis of manufacturing economics, the value of various feedstocks and the importance of energy management on plant costs will be discussed. The economic information disclosed in press releases will then be analysed, showing the clear trade-off between plant and feedstock costs in methane conversion processes, and briefly reviewing the major syngas and non-syngas routes. It will finally look at the C₂₋₄ alkanes as potential chemical feedstock. It will highlight a trade-off between plant and feedstock costs, address the consequences of selectivity and discuss the economic potential of alternative oxidants such as SO₃, N₂O and H₂O₂.

Key words: economics, investment, feedstock, energy management, methane, alkane, gas-to-liquid, methanol, Fischer-Tropsch, synthesis gas, oxidative coupling, partial oxidation

1. INTRODUCTION

Coal was the major source of energy during the 18th and 19th century. It was the source of aromatics and acetylene that formed the main feedstock of the emerging chemical industry. During the 20th century, crude oil replaced coal as an energy carrier and supplied the lower alkenes that formed the basis of the petrochemical industry. As the 20th century ends, the oil and

petrochemical industry recognises the increasing availability of cheap natural gas and C₂₋₄ alkanes and their potential as feedstock for fuels and chemicals. However, the Industry has also realised that the present alkane conversion technologies lead to the design of expensive conversion plants, which is dictated by the chemical inertness and thermodynamic stability of these alkanes. The present lecture will try to provide guidelines to help academia and industry in developing cheaper and more efficient alkane conversion technologies.

It will review the principles of manufacturing economics by defining the major contributions to production costs and trying to identify the parameters that influence them the most. It will then apply these concepts to methane and alkane conversion in attempt to distil their major chemical and technological features.

For didactic purpose, we will focus on the principles and concepts. We therefore will not attempt to present and evaluate all the most recent technological developments.

A valuable compilation of relevant literature is available in the proceedings of the “Natural Gas Conversion” Symposia published in ‘Studies in Surface Sciences and Catalysis’ as volumes 36 (1987), 61 (1990), 81 (1993), 107 (1995), 119 (1998) and 136 (2001).

2. BASICS OF MANUFACTURING ECONOMICS

The manufacturing cost of fuels and chemicals is typically composed of two major contributions:

- **variable costs**, which include feed, chemicals (e.g. catalysts and solvents) and utilities (e.g. water and energy). The variable costs depend on the actual consumption and price of the various streams needed for the manufacture. They could be minimised by improving the plant operation, improving the conversion technology or utilising cheaper feedstock.
- **fixed costs**, which include labour, maintenance and overhead as well as a provision for recovering the investment of the plant and the lost interests. The fixed costs depend largely on the size, complexity and reliability of the plant. Reduction of fixed costs will therefore rely heavily on technology improvement.

The sum of variable and fixed costs, excluding the provision for investment, defines the **cash cost**, i.e. the cost of operating an existing plant. The true profitability of existing and future plants is described by the

profited cost, i.e. the sum of cash cost and provision for investment. These terms will be used throughout this lecture.

The following paragraphs will look at the major cost contributions in an attempt to identify their importance and unravel the major factors that affect them. For further details, the reader is referred to a recent review [1] and relevant textbooks [2, 3].

2.1 Variable costs

2.1.1 Feed costs

The feedstock costs usually account for the largest portion - e.g. ~80% - of the profited cost. It depends on the consumption and price of the feedstock. The consumption rarely exceeds 110-120% of the stoichiometry in modern plants. As for the feedstock prices, they generally vary from [1].

- \$150-\$250 per ton for fuels such as gasoline, kerosene, diesel or naphtha, to
- \$300-\$600 per ton for base chemicals such as lower olefins and aromatics and
- \$500-\$1,500 per ton for chemical intermediates, e.g. lower alcohols, epoxides, (di)acids and anhydrides.

Interestingly, lower prices can be attributed to feedstocks and products that are not easily amenable to their market. For example, this is the case for methane and ethane that are produced at low cost in the Middle East and in remote areas. Typical prices could be \$0.5/GJ (or \$20/ton) for methane and \$0.75-1.25 /GJ (or \$40-60/ton) for ethane. When produced close to a market such as the USA or Western Europe, however, methane and ethane are traded at \$2.5-3.5 /GJ, i.e. much nearer to the price of crude oil.

More information on feedstock - and product - prices is available in journals and Web sites [4]. These sources show that the prices vary within a wide range, sometimes by a factor of two, as illustrated in Fig. 1.

Products that are first derivatives of the crude oil (e.g. naphtha and benzene) closely follow the crude prices. More distant derivatives (e.g. ethene and polyethene) are priced in a broader range that depends only weakly on the crude price. They are in fact priced according to the balance between supply and demand. Sedriks [5] has nicely illustrated this by showing how the added value varied with the utilisation of the global production capacity: the margins are low at moderate capacity utilisation, i.e. when the demand exceeds the, but increases steeply when the market

gets tight and the capacity utilisation approaches 100% (Fig. 2). The same holds true for the crude oil prices themselves, which are determined by the production quotas set by the OPEC countries [6].

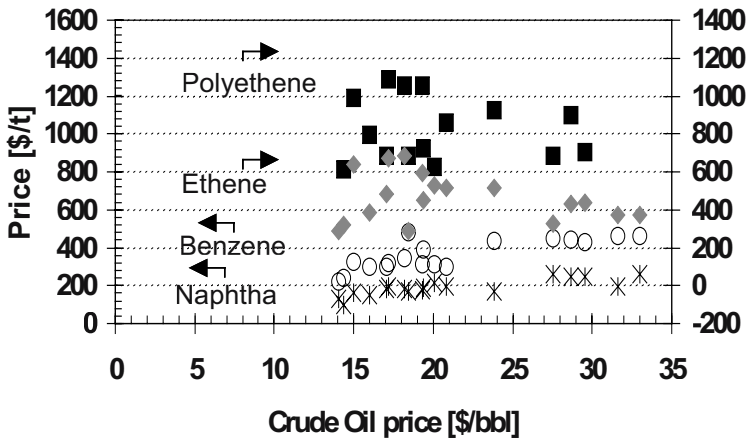


Figure 1. price of various feedstock and products (annual averaged price over 25 years).

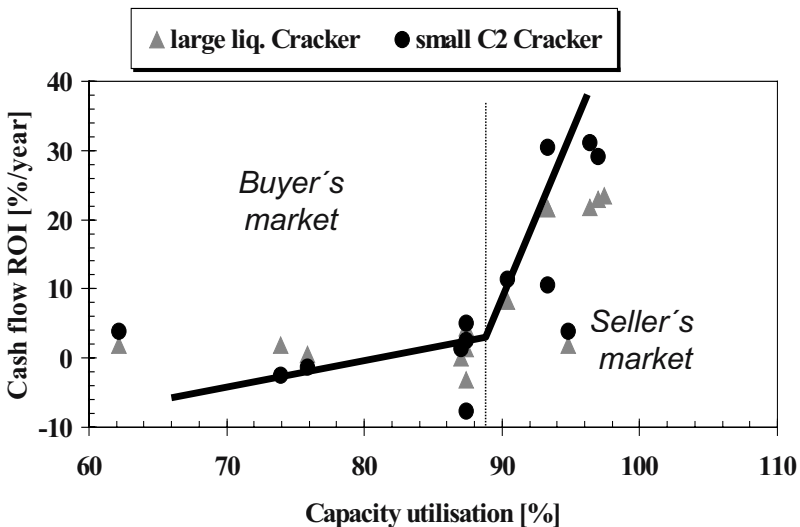


Figure 2. the margin (defined as cash flow ROI) increases with increasing tightening of the product supply [5].

How can one then identify the relevant price within such a large range? A producer that needs to purchase its feedstock on the external market could reasonably expect to have to pay the market price reported. A mid-range or average feedstock price could be fairly representative for him.

In contrast, a producer that is integrated with the feedstock production does not need to pay the market price but only the manufacturing cost. He will probably obtain his feedstock at the bottom of the price range, which represents the manufacturing cost of the high-cost producer [5]. He might even obtain it at a lower price if he is producing his feedstock in a world-scale, well-located and modern plant.

2.1.2 Other variable costs: catalyst and utility

Beyond the feedstock, the variable costs also account for the costs of utilities, mainly energy, as well as catalyst and chemicals. These contributions are usually much smaller [1].

The energy costs amount to between \$15-30 /ton for endothermic or thermoneutral reactions and are obviously much lower for exothermic reactions. They can occasionally become revenues in the case of net production of energy.

The catalyst costs typically fall between \$0.1 and \$10 per ton of product.

2.2 Fixed costs

The total fixed costs of a process can be related to the plant complexity and, thereby, to the total investment costs. This obviously holds for the provision for recovering the investment but also for the other fixed costs such as labour and maintenance. A simple and convenient practice is to assume that the annual fixed costs amount to ~35% of the total investment costs: 10% accounts for the operating fixed costs such as labour, maintenance and a 25% capital charge accounts for the provision for investment recovery. The capital charge is equivalent to the sum of the targeted Return On Investment (**ROI**) and the plant depreciation used in some studies.

The capital charge is calculated based on numerous factors such as expected plant life as well as interest and tax rates (Appendix B). The percentage is therefore not universal and may vary with cases and investors. For instance, capital charges of 10% are often encountered for natural gas conversion plants.

The concept of capital charge is valuable for comparing the economics of different process options. However, more comprehensive approaches are

needed to support real investments. These are beyond the scope of this paper but are available in dedicated textbooks [3].

2.2.1 Investment costs

An accurate determination of investment cost is labour intensive. Simpler methods are needed to help researchers in guesstimating investment costs or, at least, ranking process schemes according to relative investment costs at the early stage of their research. For this purpose, we have identified three critical parameters that determine the investment costs: the plant scale, the heat of reaction and the heat transfer duty. While these parameters will be briefly reviewed below, the reader is referred to the literature for a more detailed discussion and justification [1].

Plant scale:

For similar plants, the investment costs I_i are well known to increase with the capacity C_i raised to the power $n = 0.6-0.8$ according to eq. 1 [1, 2, 3]. Specific values for n are reported in the literature for various types of plants [3, 7]. Accordingly, any doubling of the capacity results in 50-75% increase in investment or a 12-25% decrease in investment per ton of product. This explains why fuel and chemical producers are relentlessly working at maximising plant size.

$$I_i/I_j = (C_i/C_j)^n \quad (1)$$

Heat of reaction:

Eq. 1 can only be applied to compare plants of identical design. It can, however, be adapted to compare plants of different designs. For this purpose, one needs to realise that, while converting a feed into a product, a manufacturing plant is also releasing heat, e.g. from the reaction or from burning fuel. The energy flux appears to be a better scaling-factor than the mass flux (i.e. the capacity) when comparing processes of various designs [1]. The investment of a large variety of fuel and chemical processes can indeed be scaled upon substituting the overall 'energy loss' E_i of a plant for its capacity C_i in eq. 1 (eq. 2).

$$I_i [\text{mill. \$ 1993}] = 3.0 (E_i [\text{Mw}])^{0.84} \quad (2)$$

The energy loss E_i is defined here as the difference between the low-heating value LHV[▲] of the stream entering the plant, i.e. feed and fuel, and the low-heating value of the product stream leaving the plant.

▲ LHV = heat of combustion to gaseous CO₂ and H₂O

This cost-scaling rule not only recognises the plant scale but also the chemistry involved. The heat of reaction can indeed be a major contribution to the energy loss. The investment is therefore expected to increase with the $|\Delta H_{\text{reaction}}|$. The absolute value $|\Delta H_{\text{reaction}}|$ needs to be used here to account for the energy lost by firing a fuel to drive endothermic reactions.

Eq. 2 is based on total installed cost. It includes the costs of the reaction and separation segments, i.e. the **ISBL** costs (inside battery limit), as well as that of the energy supply, tank park and other utilities, i.e. the **OSBL** costs (outside battery limit). The OSBL costs are specific to the process and location considered. It is however convenient to calculate them as a fixed fraction of the ISBL costs, e.g. 20-40%.

Heat transfer:

One can further refine the scaling rule to the ISBL costs only and even to specific reaction or separation segments. Such segments indeed consist of reactors, heat-exchangers, pumps and compressors that transfer energy from one stream to another. The global energy transfer duty D_i of a given segment appears to be a proper indicator for its installed costs (eq. 3) [1]. This cost-scaling rule allows one to push the analysis to the level of process segment in identifying major cost contributions within a complex plant. The data used for deriving eqs. 2 and 3 are displayed in Fig. 3.

$$I_i [\text{mill. \$ 1993}] = 2,9 (D_i [\text{Mw}])^{0.55} \quad (3)$$

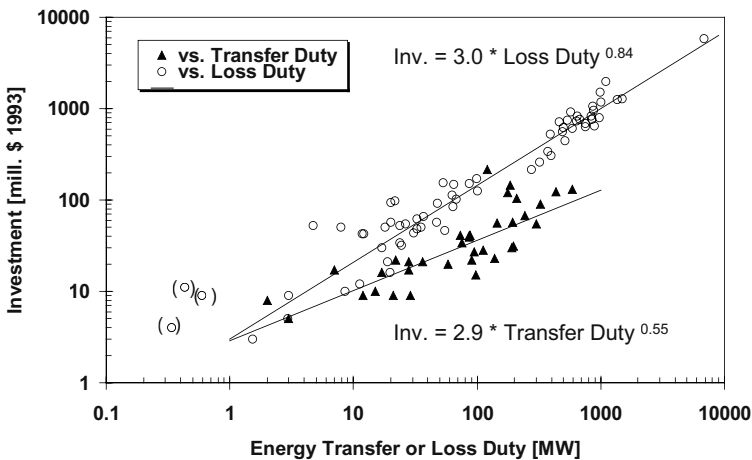


Figure 3. the plant investments increase with increasing energy loss for complete plants (open symbols) or with increasing energy transfer duty for plant segments (filled symbols) - adapted from [1].

Minimising the investment:

Based on this crude correlation between capital cost and heat transfer duty, effort in reducing investment can be best directed by a few simple guidelines:

- **maximise the selectivity** to avoid having to accommodate the enthalpy of side-reactions, i.e. to minimise the heat of reaction.
- **maximise the concentration of the desired product** in the reactor effluent to minimise the duty of the feed-effluent heat-exchanger. This implies maximising the yield per pass, which may conflict with the need for maximising selectivity stated above. It also implies avoiding feed dilution and avoiding the build-up of inert components in the recycle loop.
- **minimise gas recycling** to minimise the duty of the gas compressor, which is an energy-consuming and capital-intensive equipment. Liquid recycling is much less of a problem.
- **minimise the number and amount of components to be vaporised** to minimise the distillation duty. The recovery and purification of the product usually requires multiple distillation columns for separating the desired product from lighter and heavier component. The duty of the distillation column is mainly determined by the enthalpy needed to vaporise the lighter components. This enthalpy is added by boiling the bottom stream of the column and is withdrawn in condensing the top stream of the column. To a first approximation, the distillation duty can therefore be minimised by minimising the amount of component to vaporise, for example it is preferable to recycle a heavy stream than a lighter one.
- **minimise changes in pressure and temperature** between successive process steps. This often implies avoiding or minimising the need for separating product streams between process steps. Combining several process steps into a single reactor is ideal as long as it does not harm the overall selectivity.

Although crude, these guidelines should be valuable in most cases. It should be noted that none of them addresses the activity of the catalyst. Catalyst activity is indeed not critical above the minimal level of $\sim 0.5 \text{ T}/(\text{m}^3 \text{ h})$, except when a low activity results in excessive losses of an expensive homogeneous catalyst [1].

Costs inflation:

The reference data available in the literature do not all refer to the same construction year. Before being compared with one another, plant costs should therefore be corrected for cost inflation. Inflation indices are

available in the literature [2, 8]. These indices show a general cost inflation of 1-2% per year since 1955, with an exceptional inflation of 7-9% throughout the 70's.

Environmental costs

Besides the variable and fixed costs discussed above, we also have to consider the costs needed for minimising the environmental damages of manufacturing. These costs have to cover the cleaning of the air and water emissions as well as the responsible destruction or disposal of the wastes produced. Depending on the solution adapted these costs could be seen as variable or fixed costs. We will not elaborate on this matter here but refer to the literature [1], for the production of waste is usually moderate during the manufacture of fuels and petrochemicals [9, 10].

2.3 Dynamics of manufacturing costs

New technologies often take between 10 and 20 years to be developed and will hopefully operate economically for several decades thereafter. It is therefore important to consider the long-term dynamics of manufacturing cost in preliminary economic evaluations. One of the most striking trends observed for a wide variety of products is a steady decrease in manufacturing cost as the market matures (eq. 4). Accordingly, the cost decreases by about 50% for every 10-fold increase in demand. This is often called the "experience curve".

$$\text{Manufacturing cost} = A * (\text{world demand})^{-0.3} \quad (4)$$

The experience curve holds for fuel and petrochemicals as well [5]. It is due to the continuous development of new or improved technologies, to the construction of larger plants and/or the access to cheaper feedstocks that provide lower costs. These cheaper plants are preferentially implemented, squeezing the margin of the older plants and eventually pushing them out of production. As the new technology gets older, however, it encounters increasing difficulties in competing with the newer plants and sees its margin melting away.

To get commercialised, it is therefore not sufficient for a new technology to be economical under the present price and cost structure. It has to promise a long and profitable life. Economical parity is not good enough to justify the cost and risks of research, development and commercialisation. In short, the new technology needs to beat the best technology in place by e.g. 25%.

2.4 Summary

The manufacturing cost is often dominated by feedstock costs, hence the drive for using cheaper feedstocks such as lower alkanes and particularly remote natural gas. The complexity of the plant defines much of the remaining fixed costs and provision for investment recovery. These costs appear historically to mainly depend on the overall energy lost through the process and, at a more detailed level, on the overall energy transferred in the plant. Based on this, a few guidelines have been formulated for minimising the plant cost.

3. THE ECONOMICS OF NATURAL GAS CONVERSION PROCESSES

3.1 Business case

3.1.1 A new economic environment

The two oil crises of the 70's and the further discovery of abundant natural gas reserves have stimulated a large global R&D effort in converting natural gas to liquid fuels. Some research groups, like Shell Research, opted for routes based on synthesis gas [11, 13] while others focused their efforts on the direct functionalisation of methane [12, 13]. Economic evaluation studies of the 90's generally concluded that the syngas routes were more attractive, though none was economically attractive at the targeted oil prices of <20 \$/bbl [14, 15]. When commercialising its SMDS process (Shell Middle Distillate Synthesis) in Malaysia in 1993, Shell had to convert a significant fraction of the distillates to high value products (such as solvents, lubricating oil and waxes) to make it economically viable. Sasol remained also active in this area as well, whereas most oil companies shelved their technologies, waiting for better times.

Better times have apparently arrived, for several GTL (gas-to-liquid) plants are under construction or consideration now [16]. Two factors can explain this recent development. Firstly, the OPEC has announced its desire to target oil prices of \$22-28/bbl, which is considerably higher than the \$15-20/bbl found between 1985 and 2000. Secondly, the new plants will benefit from economies of scale by producing up to 75,000 barrel/day (i.e. 3.0 Mt/a), compared to the 12,000 barrel/day (or 0.5 Mt/a) of Shell's SMDS

plants. What is then the economics of emerging GTL plants? Let us have a look at press releases.

3.1.2 Reading the press releases

When announcing new GTL (gas-to-liquid) projects, the specialised press usually provides valuable economic information. A few simple calculations suffice to place the economics in perspective. We will review these calculations through two examples.

In 2003 Sasol and Qatar Petroleum announced the construction of a 34,000 bbl/day in Qatar that will cost \$675 mill. for engineering, procurement and construction (EPC) – a investment of \$19,800/daily barrel [17]. This project will be taken to illustrate the basis of GTL economics based on the following reasonable assumptions:

- The variable costs are based on a gas price of \$0.5/GJ and a thermal efficiency of 64% (i.e. 80% carbon efficiency)
- The fixed cost amount to 10% of the investment
- The target capital charge amounts to 10% of the investment, though 25% would offer more robust economics.

It should be noted that the true investment is significantly higher than the EPC costs, since they include all the cost made to get to the EPC contract such as detailed design.

Using the conversion factor reported in Appendix A, the various costs contributions would amount to

Variable cost:	
$0.5 [$/GJ_{NG}] * 5.1 [GJ_{distil.}/bbl] / 0.64 [GJ_{distil.}/GJ_{NG}]$	= \$ 4.0/bbl
Fixed cost:	
$0.1[1/a] * 19,800 [$/bpd] / 330 [day/a]$	= \$ 6.6 /bbl
Cash cost:	
	= \$ 10.6 /bbl
Plant cost:	
$0.1 [1/a] * 19,800 [$/bpd] / 330 [day/a]$	= <u>\$ 6.6 /bbl</u>
Profited cost (10% cap. charge):	
	= \$ 17.2 /bbl

These very simple calculations indicate that the announced GTL plant should be profitable at oil prices above \$17.2/bbl and be cash neutral at \$10.6/bbl. Based on the true investment rather than the EPC costs, the profited cost might increase from \$17.2 to \$19-20/bbl. Such economics are quite promising when considering that OPEC is setting its production quotes

for oil price at \$22-28/bbl. It should however be mentioned that the oil industry does not believe that such oil prices are sustainable. They use therefore lower prices of \$16-18/bbl as long-term screening value.

As a second example, one can consider the methanol-to-polymer plant announced by Eurochem Technologies for Nigeria [18]. The plant, which is estimated at \$2 bill. (probably EPC costs), should convert 6,16 Mm³/d of gas (at \$0.6/GJ) into 7.5 kt/d of methanol as an intermediate and 800 kta polyolefins (i.e. HDPE and PP). Using the conversion factors reported in Appendix A, the various costs contribution would amount to:

Variable cost:	
$0.6[\$/\text{GJ}] * 36,500[\text{GJ}/\text{Mm}^3] * (330 * 6,16 [\text{Mm}^3/\text{a}]) / 800[\text{kt}/\text{a}]$	= \$ 56 /t
Fixed cost:	
$0.1 [1/\text{a}] * 2 [\$/\text{bill.}] / 800 [\text{kta}]$	= \$ 250 /t
Cash cost:	
	= \$ 306 /t
Plant cost:	
$0.1 [1/\text{a}] * 2 [\$/\text{bill.}] / 800 [\text{kta}]$	= \$ 250 /t
Profited cost (10% cap. Charge):	
	= \$ 556 /t

Considering the market price of \$600-1000/ton for polyolefins (Fig. 1), this plants should be profitable as well. Upon using true investments instead of EPC costs, the profited cost might increase to \$600 /t, which looks still competitive. However, it will not offer leading cash costs, which are reported to be \$100-150/t [19]. It might therefore become a high-cost producer too early. It does not offer secured profits either when one uses a capital charge of 25%. This indeed results in a profited cost of \$931/t (based on EPC but possibly \$1,000-1,100/t based on true investments), i.e. in the upper half of the polyolefin price band.

3.2 Sizing the challenges

3.2.1 Plant costs

The press releases discussed above illustrate nicely the impact of selecting a cheap feedstock. The profited cost of gas conversion consists of \$4/bbl in variable costs and \$12/bbl in fixed cost (incl. plant cost), which is almost the opposite of an oil refinery. Oil refining typically requires

\$~20/bbl in variable costs and \$2-3/bbl in plant cost* [20]. In short, a NG conversion plant is, at least partially, trading higher capital cost for lower feedstock [21].

The major challenge is therefore to reduce the investments involved. The fact that the feedstock is cheap does not allow us to use it inefficiently, however, for an inefficient conversion would result in high energy-losses and, consequently, high plant cost. On the contrary, energy efficiency – i.e. feedstock efficiency – has been used as a first indicator of plant cost.

3.2.2 Chemistry

The major routes for upgrading methane are illustrated in Fig. 4. Traditionally, methane is converted to methanol or distillates (paraffinic liquids) via syngas (CO/H₂). Methanol can also be subsequently converted to aromatics or paraffinic distillates (via ethene/propene). Alternatively, methane can be converted to ethene, either by high-temperatures (Pyrolysis) or high-temperatures and O₂ (oxidative coupling). It can also be converted to methanol, either directly or via a methyl-ester such as methylchloride or methyl-bisulphate. Both routes require an oxidant.

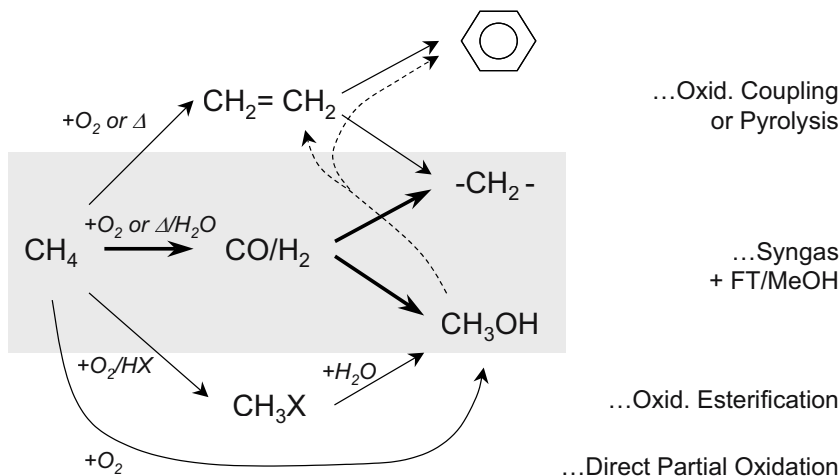


Figure 4. syngas and 'direct' routes for converting methane to fuels and chemicals.

The elegance of the conventional syngas route is to convert the unreactive CH₄ to a thermodynamically stable intermediate, i.e. syngas. The

* based on 10% capital charge and \$1-1.5 bill. Capex for 150,000 bpd capacity, i.e. \$7,000-10,000/daily barrel

subsequent CO hydrogenation reaction can be performed fairly selectively towards the desired product [11, 22].

In contrast, the 'direct' routes attempt to directly convert the inert methane to less stable and more reactive products. These products tend to subsequently decompose to thermodynamic sinks such as coke or CO₂. The catalytic sciences seem not to have been able to block this undesired decomposition, for the highest yield reported so far for the 'direct' routes decrease with decreasing stability of the desired product (Fig. 5), defined as the pseudo equilibrium constant K of eq. 5 [12, 22]. This apparent thermodynamic limitation on yields was later expressed in terms of C-H and C-C bond strength of reactant and products, as we will see in a later chapter on alkane conversion.

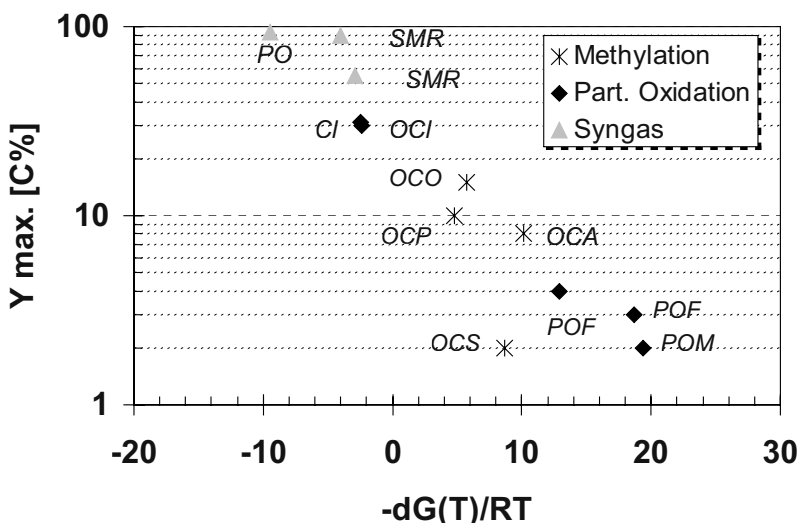


Figure 5. the yields of methane conversion reactions decrease with decreasing thermodynamic stability of the product, as defined by eq. 5 (PO – partial oxidation to syngas; SMR – steam reforming to syngas; (O)Cl – (oxy)chlorination; OC(O,P,S,A) – oxidative coupling to olefins, paraffins, acrylonitrile or styrene; PO(F,M) – partial oxidation to formaldehyde or methanol [22]).

Fig. 5 reveals that the so-called 'direct' routes are not more direct than the syngas routes since they also require several process steps - the exception being the direct oxidation of methane to methanol. Fig. 5 further

suggests that the 'direct' routes face a trade-off between high selectivity and high yield per pass: the high selectivity implies high energy transfer due to the low conversion whereas the high conversion results in high energy losses due to the low selectivity.

3.2.3 Overall economics

Prior to discussing the economics of the various routes, it is revealing to compare the estimation of various processes as reported in the literature (Table 1). These plants have been evaluated for a comparable scale of 10,000-15,000 bbl per day, with the exception of the two Fischer-Tropsch plants announced at 2-4 times larger scale. Table 1 confirms the crude trend of increase in plant cost with decreasing thermal efficiency – see, for example, the improvement in cost and thermal efficiency upon adding an alkylation unit to a MeOH/aromatisation plant. It also indicates higher costs and lower thermal efficiencies for plants that produce gasoline compared to paraffinic distillates. It finally shows the cost reduction achieved by scaling up the distillate plant of 15,000 by a factor of 2-4.

Table 1. Plant costs and thermal efficiency of various methane conversion plants.

Route	Capacity bbl/day (Mta)	Plant cost ^(a) \$/daily bbl (\$/annual t)	Thermal efficiency % LHV	Reference
PARAFFINIC DISTILLATE				
FT + cracking	13,500 (0.6)	55,600 (1260)	67	15
FT + cracking	34,000 (1.5)	19,800 (450)	67	17
GASOLINE				
FT + aromatisation	10,300 (0.4)	89,400 (2300)	41	15
MeOH + aromatisation	14,700 (0.6)	65,300 (1680)	43	23
MeOH + aromatisation + alkylation	14,900 (0.6)	55,800 (1440)	59	15
Ox. coupling + aromatisation	10,200 (0.4)	100,400 (2586)	41	15
Ox. coupling + aromatisation	15,700 (0.6)	69,200 (1782)	36	24

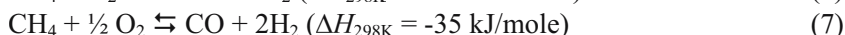
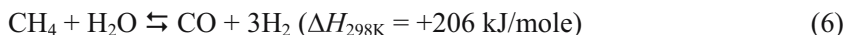
(a) EPC Plant costs re-calculated to 2003 using 1.5% inflation per year.

3.3 Economics of the Syngas-based conversion routes

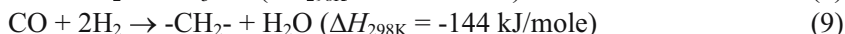
3.3.1 Basic reactions

Numerous publications discuss the economics of natural gas conversion processes. It is not the intention to review them here in any detail. In contrast, we will discuss the main process concepts and try to identify their economic impact based on the economic guidelines discussed above. We will focus on their potential capital cost based on their energy efficiency and/or energy transfer duty. Such an analysis has been already applied to review the major developments in methanol synthesis [21 43, 44] and for evaluating various “*direct*” conversion routes [43]. This approach could also be applied to distillate synthesis processes.

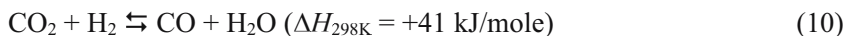
The syngas-based routes consist of two process steps, namely syngas manufacture and syngas conversion. The syngas manufacture proceeds via either the steam reforming reaction (eq. 6) or the partial oxidation reaction (eq. 7), which are thermodynamically favoured by high temperatures and low pressures (e.g. 900°C and < 20 bar for the former and 1,200°C and < 20 bar for the latter).



The syngas conversion proceeds either via the methanol synthesis reaction (eq. 8) or the Fischer-Tropsch synthesis (eq. 9), which operate best at moderate temperature and high pressure, e.g. around 260°C and 80 bar for the former and around 220°C and 20 bar for the latter.



The manufacture as well as the conversion of syngas can be accompanied by the water-gas shift equilibrium (eq. 10) that converts CO to CO₂ and vice versa.



Rather than discussing the fascinating chemistry of these reactions, we will review the energetic aspects that affect the capital cost of the plant.

3.3.2 Syngas manufacture

Energy loss:

The steam reforming reaction is highly endothermic. It is, therefore, carried out in a large furnace. About 50% of the firing energy liberated in the furnace is efficiently used for driving the reaction. The remaining energy is recovered in pre-heating the feed and producing steam to drive gas compressors. Hence, the overall energy losses of the steam reforming typically amount to twice the heat of reaction, i.e. to about 6.4 GJ/t (400 kJ/mole) of converted methane.

In contrast, the partial oxidation is largely exothermic; typically about twice the 0.56 GJ/t_{CH₄} (35 kJ/mole) reported in eq. 7 due to the small fraction (~5%) of the H₂ and CO that is burned to bring the reaction mixture to the 1,200°C required for a favourable equilibrium. This energy is partially recovered for raising steam to drive gas compressors. With ~1 GJ/t_{CH₄} liberated by the reaction, partial oxidation would be a cheap alternative to steam reforming if it did not require the use of pure O₂ that is generally produced by means of cryogenic distillation from air.

Fig. 6 indeed shows that the savings made by substituting the low-cost partial oxidation (or its parented autothermal reformer in Fig. 6) for the expensive steam reformer are offset by the cost of the air separation unit ASU.

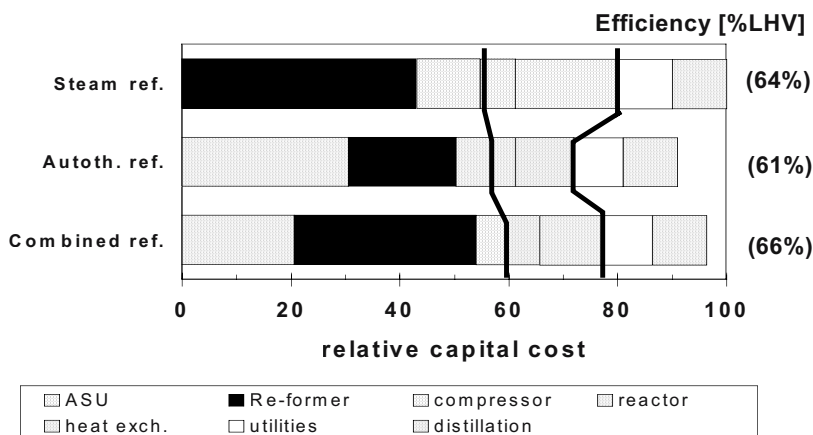


Figure 6. cost breakdown of methanol synthesis processes (adapted from [28]).

Pure O₂ is required because the syngas is usually not fully converted in a single pass in the second reaction step and the unconverted syngas is thus

recycled back to the reactor. An inert gas like N_2 that is present in the syngas would rapidly accumulate in the recycle loop and can then only be removed by purging a fraction of the recycle gas, losing valuable syngas in the process. This leads to undesirable losses of syngas and heating and cooling of inert gas in the recycle loop.

Syngas Stoichiometry:

Accumulation of inert gas will also result from using a syngas that has not the desired stoichiometry, since the reactant in excess will also build-up in the recycle loop; hence, the need for stoichiometric syngas. According to eq. 6 and 7, both syngas conversion processes require a H_2/CO ratio of 2:1. This is only partly true for the methanol synthesis, which utilises CO and CO_2 through their interconversion via the water-gas shift reaction (eq. 10). Its syngas stoichiometry is therefore defined by the stoichiometric number $SN = (H_2 - CO_2)/(CO + CO_2) = 2$, which boils down to $H_2/CO = 2$ at low CO_2 concentration.

Once again, the partial oxidation is advantaged over the steam reforming by providing a better syngas stoichiometry, as illustrated in Fig. 6. The partial oxidation of methane delivers a stoichiometric number of 1.7 and H_2/CO ratio of 1.7-2.5, depending on the amount of steam added to the feed[▲], whereas the steam reforming provides a stoichiometric number of 3 and a H_2/CO ratio of 3-8 [25, 26]. The build-up of excessive H_2 from steam reforming results in larger transfer duties and, therefore, higher costs in the syngas conversion segment. The purge of syngas from the recycle loop results in a larger syngas consumption and larger energy losses, i.e. in higher costs in the syngas manufacturing section.

Both arguments, i.e. the energy losses and the syngas stoichiometry, favour the partial oxidation. Combining these two processes appears to be even better, however [27, 28, 29]. For instance, the steam reforming can supplement the partial oxidation in H_2 and, thereby, increase in thermal efficiency from ~64% to 66-67% LHV [27, 28]. A more intimate integration can allow the exothermic partial oxidation to drive the endothermic steam reforming, thereby reducing the O_2 consumption of the one and the firing duty of the other. The heat integration further increases the thermal efficiency to 67-69% [27]. All these improvements have resulted in an “asymptotic” reduction of capital cost of large-scale methanol synthesis processes from 100% for steam reforming, to 80-90% for partial oxidation schemes and 75-80% for heat-integrated processes (Fig. 7) [30]. This cost ranking again follows the ranking in thermal efficiency.

[▲] Addition of steam to the feed results in an increase in H_2/CO due to the water-gas shift reaction (eq. 10)

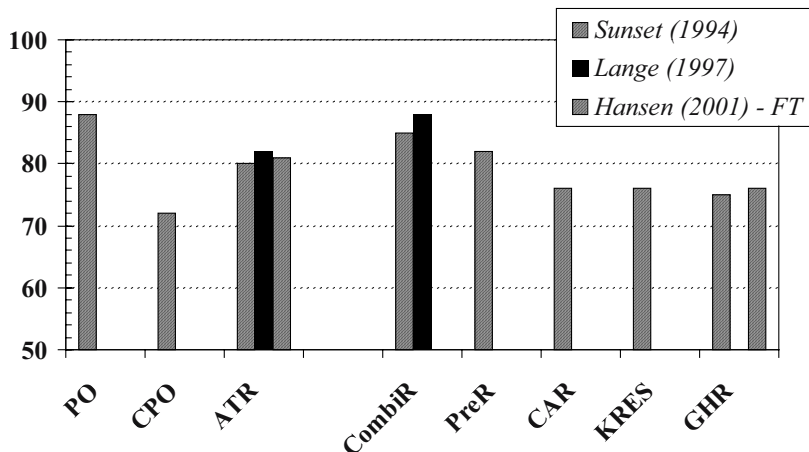


Figure 7. costs of methanol and Fischer-Tropsch plants based on various syngas manufacturing technologies, relative to the steam reforming set at 100% (partial oxidation (PO, CPO, ATR), combined reformer (CombiR, PreR) and heat-integrated reformers (CAR, KRES, GHR) based on [28, 30, 31]; see list of symbols).

Although omitted here, economy of scale is also an important factor. For instance, the cost of an air separation unit increases less steeply with scale than does the cost of a steam reformer. Hence, partial oxidation – incl. the parented autothermal reformer - becomes increasingly advantageous over steam reforming at very large scale. From being comparable in a 660 kta methanol plants, the autothermal reformer process shows a 25% cost advantage at 3-times the scale [32].

3.3.3 Syngas conversion

The conversion of syngas to methanol and distillates are highly exothermic with -91 and -144 kJ/mole CO, respectively. It requires large cooling duty, which contributes significantly to the cost of the process. Various reactor designs have been proposed to accommodate this reaction heat as effectively as possible. The distillate synthesis reactors are commonly cooled by means of cooling spirals in the reactor, being a fixed bed, a slurry phase or a fluidised bed reactor [33, 34, 35]. Since the methanol synthesis is less exothermic it can also be cooled by the injection of cold syngas [21].

Both syngas conversion processes are characterised by large heat transfer duties in the syngas recycle loop. They operated at low-to-moderate conversion per pass with a large recycle of the unconverted syngas. This syngas recycle requires large and expensive heat exchangers and gas

compressors. The gas recycle is particularly large for the methanol synthesis process, since the thermodynamic equilibrium prohibits high conversion of the syngas. Major efforts were devoted to reducing the size of recycle stream by improving the stoichiometry of the syngas, as discussed above. Various options have also been explored for shifting the equilibrium [21, 28]. Reactors were designed to offer low exit temperatures. Catalysts were improved to operate at lower reactor temperatures. Schemes were conceived to remove methanol from the reaction, for example by means of membranes, absorbents or condensation. While some options may offer small reductions in investment, none seems to offer dramatic savings.

Increasing the scale of the equipment can also reduce the investment per ton of product. Fluidised and slurry bed reactors have the potential of larger scale. They have therefore been seriously studied for both methanol and distillate synthesis [33, 34, 36].

3.3.4 Methanol Upgrading

Methanol is a valuable intermediate that can be converted to various products. Its main chemical derivatives are formaldehyde, methyl-tertiarybutyl ether and acetic acid [2]. The economics of these chemical derivatives is clearly outside the scope of the present paper. It is however very relevant to mention the conversion of methanol to lower olefins and gasoline, so called MTO [37, 38] and MTG [39] technologies, which are often proposed to be integrated with the syngas manufacture and syngas conversion plants. Both processes apply zeolite-type catalyst. The production of lower olefins is favoured by applying a very short residence time and a zeolite with small pores (3.4 Å) while aromatics are favoured at longer residence times and with larger pore zeolites (5.5 Å).

The upgrading of methanol to more valuable products has its costs, however. The reaction operates with 75-80% carbon efficiency, is highly exothermic and proceeds with high steam dilution. All these aspects result in high energy-losses and high energy-transfer duties. The rapid deactivation of the zeolite catalyst requires the use of multiple fixed beds or expensive fluidised beds to allow for frequent catalyst regeneration.

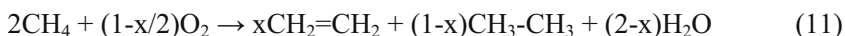
3.4 Economics of the '*direct*' conversion processes

Various '*direct*' and '*indirect*' process schemes for methanol and hydrocarbons have been evaluated in the past [13, 14, 15, 40, 41, 42, 43, 44]. Some were quantitative and based on complete flow sheeting. Others were rather comparative. We will highlight here the key features that affect the economics of the major processes illustrated in Fig. 4, namely the

oxidative coupling, the direct partial oxidation and the oxidative esterification. The reader will be referred to more extensive studies for further reading.

3.4.1 Oxidative coupling

The oxidative coupling of methane [12, 45, 46] consists of converting CH_4 to $^\circ\text{CH}_3$ radicals in the presence of O_2 and a basic oxide catalyst at $\sim 700^\circ\text{C}$. The $^\circ\text{CH}_3$ radicals couple to form ethane, which thermally dehydrogenates to ethene under reaction conditions. The overall reaction proceeds according to eq. 11. The C_2 hydrocarbons are more reactive than methane and are subsequently burned to CO , CO_2 and H_2O . This results in a decreasing selectivity at increasing conversion that follows the rule of thumb “conversion + selectivity = 100%”. A typical performance is 16 % yield at 20 % conversion and 80 % selectivity.



Ethene is produced at high dilution in unconverted methane. It is further contaminated with ethane. Its low boiling point makes the recovery by means of cryogenic distillation very expensive. All this results in a large heat-transfer duty.

The use of air directly as an oxidant is also prohibited, as the N_2 present in air further dilutes the ethylene. Alternatively, ARCO has proposed a “redox” operation, in which the catalyst is used as an oxygen carrier. The catalyst is initially oxidised by air in a first reactor vessel and then brought into contact with methane in a second reactor vessel for performing the coupling reaction. Whilst this scheme offers two advantages in that it avoids the need for an oxygen plant and avoids the dilution of ethene in N_2 it also requires a complex double-vessel reactor system.

Finally, the oxidative coupling does not produce an easily transportable liquid product. It therefore needs to be complemented by an ethene oligomerisation or aromatisation unit, which adds to the costs.

Several studies concluded that the catalyst selectivity needs to be improved beyond the rule “selectivity + conversion = 120-130 %” to be economically attractive [40, 43].

3.4.2 Direct partial oxidation

In the direct partial oxidation [46, 47, 48], methane is directly oxidised to methanol at 500°C at high pressure (eq. 12). Operation at low pressure favours consecutive oxidation to formaldehyde (eq. 13). Various catalysts have been proposed but the reaction has been shown to proceed reasonably

well in the absence of any catalyst. Being much more reactive than methane, methanol and formaldehyde tend to burn to CO₂ at increased conversion. Hence, the yield rarely exceeds 2 %.



Compared to the oxidative coupling, the direct partial oxidation route delivers a product that is in principle much easier to condense or wash out of the unconverted stream. However, its low concentration means the recovery is still quite expensive.

Here again, pure oxygen is more attractive as an oxidant than air. This is particularly the case for methanol synthesis, which proceeds at high pressure. Indeed compression of the air beyond 10-20 bars is usually more expensive than O₂ separation.

The production of methanol is more desirable than that of formaldehyde. It liberates less heat, consumes less oxygen and provides a product that is more easily recovered from a diluted stream. Nevertheless, a methanol yield of ~10% is often seen as pre-requisite for enabling the direct partial oxidation route to compete with the syngas-based processes [40, 43]. The partial oxidation is often combined with a condensation step to convert the methanol to a gasoline fraction. This obviously adds to the production cost.

3.4.3 Oxidative esterification

Two major oxidative esterification routes have been pursued, one to CH₃Cl and the other to CH₃OSO₃H.

Methylchloride route:

Oxidative chlorination (eq. 14) consists in converting methane to methyl chloride in the presence of O₂/HCl as oxidant mixture over an oxychlorination catalyst. The methyl chloride can undergo subsequent chlorination to less desirable methylene dichloride and higher chlorinated species. The electronegativity of the Cl atom seems to partially protect the methyl group from further oxidation. Hence yields up to 30% can be achieved, which is significantly higher than the ~2% reported for the direct partial oxidation reaction.



With a boiling point of -24°C, methyl chloride is not as easily recovered from the unconverted feed as methanol.

Obviously, the process cannot stop at the methyl chloride and a subsequent condensation to gasoline fraction is required. This condensation resembles the one applied to convert methanol to gasoline, with the difference that it co-produces HCl instead of water.

A very important issue here is the potential corrosion of equipment by wet HCl, which requires the use of expensive materials. Traces of Cl need also to be removed from the gasoline product to protect the consumers against excessive corrosion of their car.

Methylbisulfate route:

Alternatively, the methyl group can be protected from further oxidation by attaching a group that is even more electronegative than Cl, e.g. HSO₄⁻. Accordingly, methane can be oxidised to methylbisulfate with 80% yield per pass, using SO₃ as oxidant (eq. 15). In a second step, the methylbisulfate is then hydrolysed to methanol and, in a third step, the SO₂ re-oxidised to SO₃.



So far no alternatives to SO₃ have been found for this chemistry and this is the Achilles' heel of this route. Since SO₃ reacts with traces of water to give H₂SO₄, the reaction needs to proceed in very dry H₂SO₄. The water/H₂SO₄ stream that comes out of the hydrolysis reactor needs to be dried to a very high degree before being recycled to the methane oxidation step. The use of concentrated and corrosive H₂SO₄ also imposes severe limitations on construction material choices.

3.4.4 Non-oxidative routes

Several routes have been proposed to convert methane to olefins and/or aromatics without the use of oxidants. They include:

- the high-temperature, thermal pyrolysis of methane to ethene and ethyne [49],
- the high-temperature, methane aromatisation using Mo-ZSM-5 catalyst [50, 51],
- the low-temperature methane coupling via surface carbides [52, 53].

Our discussion will be again limited to a few critical aspects here. The first two reactions are endothermic, require high-temperatures and are prone to coke formation. Like steam reforming, they are likely to require costly and energy-consuming furnace reactors. Alternatively, the aromatisation reaction might also be operated in a swing mode, alternating between a

reductive phase, which produces the desired product and coke, and an oxidative phase, which burns off the coke and reheat the reactor. Whatever the design, these processes are likely to imply high energy-losses and high energy-transfer duties.

The surface carbide route requires a swing operation that alternates between methane dehydrogenation to surface carbide and carbide rehydrogenation to methane and higher hydrocarbons. The step proceeds with low efficiency and produces very little condensable C5+ hydrocarbons. The swing operation will require either large solid recycling or pressure or temperature swing of large gas streams. Both options are expected to be very expensive.

3.5 Summary

We have seen that the economics of methane conversion processes are dominated by the plant costs. Fuel production plants can be profitable under the present economics of \$22-28/bbl at a plant cost of about \$20,000/daily barrel produced. Obviously, chemical plants produce a higher valued product and can, therefore, support higher plant costs.

To a 1st approximation, plant costs are dictated by the energy loss and transfer duties of the processes. It is, therefore, of prime importance to design processes with high thermal efficiency.

Syngas processes operates indeed at high thermal efficiency by converting methane with high selectivity and conversion to syngas, the thermodynamically most stable product under the prevailing conditions, and subsequently converting it to the desired product with high selectivity using well-designed catalysts. High thermal efficiencies (nearing the 70% LHV) and low plant costs are achieved through optimisation of syngas stoichiometry and heat integration as well as the selection of technologies with good scale-up potential.

So far, the '*direct*' processes do not achieve the same thermal efficiency and low plant costs as the syngas technologies. Several reasons can be mentioned. Firstly, these technologies are not simpler or more direct than the syngas technologies and, therefore, do not offer the promised reduction in equipment costs. Secondly, the methane conversion step usually achieves high selectivity only at low-to-moderate conversion because of the high reactivity of the products when compared to methane. This implies high heat-transfer duties and difficult product recovery. The '*direct*' processes that achieve high selectivity at high conversion, i.e. the oxidative esterification routes, have their own problems such as the use corrosive co-reactants and/or the need for expensive dehydration of the acid.

4. THE ECONOMICS OF ALKANE CONVERSION PROCESSES

4.1 Business case

Ethane, propane and butanes are abundant and cheap feedstocks. They are produced in large amounts in refineries. Propane and butanes can be liquefied to LPG (Liquefied Petroleum Gas) at moderate pressure, which represents a fair but limited market. $C_{2,4}$ alkanes also form excellent feedstocks for olefins via thermal cracking or dehydrogenation.

Lower alkanes are increasingly found in remote areas together with crude oil or natural gas. Their production cost is then very low. Liquefaction is a feasible option for bringing the C_{3+} fraction to the market. However, the producing countries in the Middle and Far East seem increasingly interested in upgrading these cheap alkanes to sell the more expensive chemical derivatives. The Middle East has indeed grown into a major Chemical producer over the last 20 years. It produces now about 10% of the global ethylene capacity and has growth plans of ~42% per year for the coming decade [19, 54]. Efficient alkane conversion is therefore a very popular subject.

The major route for converting alkanes to chemical intermediates is so far the thermal (or steam) cracking to ethene and propene. Alternative upgrading routes consist in the (oxidative) dehydrogenation to the corresponding alkene or the selective oxidation to acetic acid or vinyl chloride (from ethane), to acrylic acid and acrylonitrile (from propane) and to maleic anhydride and methacrylic acid (from butanes). All these routes show several defining characteristic, which have been already encountered in the methane conversion routes.

4.2 Plant vs. Feedstock Costs

As a first characteristic, alkanes are thermodynamically very stable. Their conversion requires, therefore, large energy losses, necessitating the firing of a fuel to drive highly endothermic reactions or the adoption of an exothermic oxidative route. Thermal cracking and catalytic dehydrogenation routes typically require 2.5-4.5 GJ/ton of product (i.e. 80 to 140 kJ/mole), which often implies firing duty of 5-9 GJ/ton of product. Similarly, the exothermic reactions liberates between 2.8 GJ/ton (for propane oxydehydrogenation) to 13.4 GJ/ton (for butane oxidation to maleic anhydride). In fact, most alkane conversion processes imply higher energy losses than the competing routes based on more expensive but more reactive

feedstocks [1]. This is, for example, the case for the production of acetic via ethane oxidation or methanol carbonylation (with 10.7 vs. 2.3 GJ/ton) or for the production of acrylic acid from propane or propene oxidation (with 10.6 vs. 8.2 GJ/ton). Hence, the overall processes are expected to require high investments, which might largely offset the savings achieved by using a cheaper feedstock. This expectation is indeed confirmed by the economic analysis reported by Nexant/Chem systems for the following route (Fig. 8) [55]:

- Vinyl chloride from ethane or ethene,
- Acetic acid from ethane or methanol,
- Acrylic acid and acrylonitrile from propane or propene.

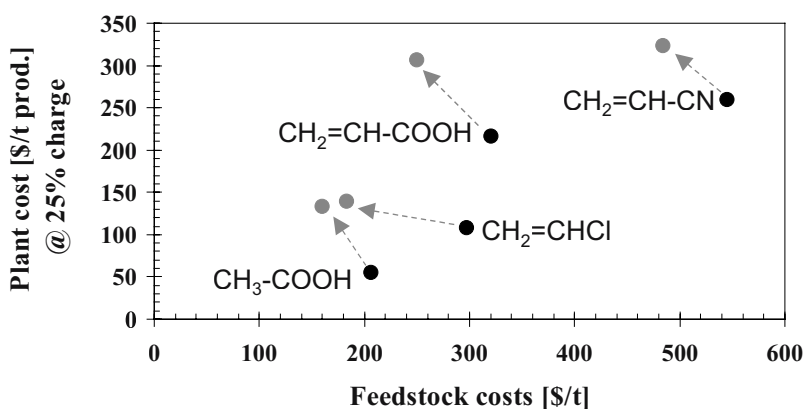


Figure 8. Trade-off between plant and feedstock costs upon shifting from alkenes or methanol (black symbols) to alkanes (grey symbols) as feedstock (plant costs from [55]).

This trade-off between plant and feedstock costs has not been encountered in past feedstock changes [1]. For instance, the switch from acetylene to alkenes offered savings in feedstock and plant costs.

4.3 Selectivity

As a second characteristic of alkanes, the product is usually more reactive than the feedstock. Hence the selectivity usually decreases with increasing conversion. Cassidy and Hodnett [56] illustrate this trade-off nicely by displaying the selectivity obtained at 30% conversion as function of the difference in bond strength between the weakest C-H or C-C bond in the product and the feed (Fig. 9). Only two alkane conversion routes proceed with > 80% selectivity (@ 39% conversion), i.e. the dehydrogenation of

ethane to ethene and the oxidation of butane to maleic anhydride. Alkane conversion reactions are therefore carried out at low-to-moderate conversion per pass. This results from a trade-off between minimising the feed-effluent heat exchange and product recovery duties, which decrease with increasing yield per pass, and minimising the energy and feed losses, which decrease with increasing selectivity. The energy losses are particularly sensitive to the selectivity of the oxidation reactions, for undesired alkane combustion results in the impressive release of 43 GJ/t of $-\text{CH}_2-$ burnt (i.e. 607 kJ/mole C). 10% of undesired combustion could easily double the overall heat release.

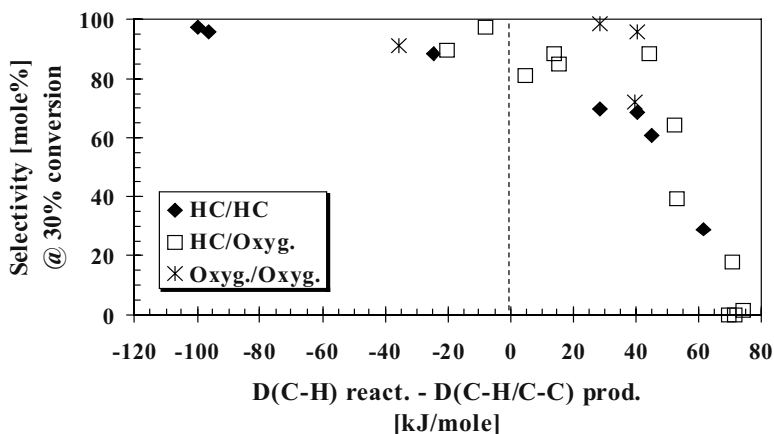


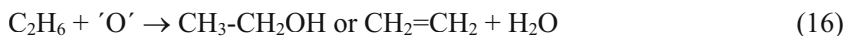
Figure 9. The selectivity of oxidation reactions decreases with increasing reactivity of product, expressed as the difference in the weakest C-C or C-H bond between product and feedstock [56].

4.4 Oxidant selection

Air is commonly accepted as being the cheapest oxidant that one can use in oxidation reactions. More expensive oxidants such as H_2O_2 , N_2O or even SO_3 have been reported to be more selective for given oxidation reactions. They might thereby offer savings in feedstock cost - via improvement in selectivity - and in investment - via lower energy losses or energy transfer duties.

In a first approach, we can evaluate the potential of alternative oxidants by ensuring that the margin that exists between the product and feedstock is sufficiently large to pay for the cost of the oxidant and still leave enough room for plant cost. For this purpose, we have calculated the margins

between various alkanol or alkene (+water) and the corresponding alkane, as illustrated by eq. 16, and compared them with the price of oxidant, after normalisation per oxygen 'O' consumed*.



Although this comparison depends significantly on the prices considered, clear conclusions can be drawn from the resulting Fig. 10.

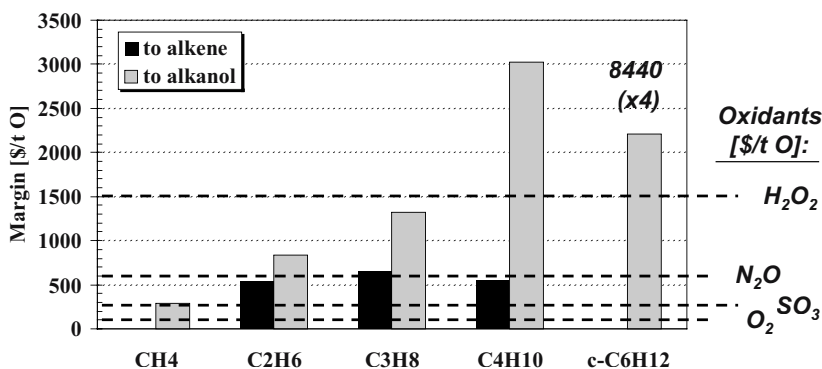
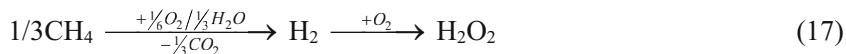


Figure 10. Margin of alkanes oxidation reactions and costs of oxidants.

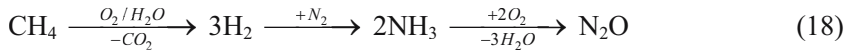
The margins between methanol or the C₂₋₄ alkenes and the corresponding alkanes are too small to allow for any expensive oxidant. Pure oxygen is the about as much as one can afford.

The margin between alcohols and the corresponding alkanes increase with increasing chain length to the point of – in theory – affording more expensive oxidants such as SO₃, N₂O or even H₂O₂. Notice that the margin for converting alkanes to aldehydes and ketones is about twice that of alcohol manufacture, when normalised per oxygen consumed.

This crude analysis needs, of course, to be refined to provide clear economic incentive. A dimension that was omitted here is the overall CO₂ emission needed to manufacture the oxidant. This emission is low in the case of pure O₂ and SO₃. It amounts, however, to 1/3 mole per mole H₂O₂ and 1 mole per mole N₂O (eq. 17 and 18).



* The costs of oxidants are crude estimates that include the capital needed for producing it from air (for pure O₂), NH₃ (for N₂O), SO₂ (for SO₃) or H₂ (for H₂O₂).



4.5 Summary

C₂₋₄ alkanes are promising feedstocks for the 21st century because they are abundant and cheap. However, their conversion to fuels and chemicals intermediates offers several challenges, which resemble those of methane conversion. The savings achieved by using a cheap feedstock are largely offset by more expensive plants that transfer large amounts of energy. The high plant costs are further exacerbated by the difficulty of achieving high selectivity at high conversion, which is due to the high reactivity of the desired product compared to the alkane feedstock.

Oxidants such as H₂O₂, SO₃ or N₂O have been proposed as selective alternatives to air or pure O₂. However, the number of alkane oxidation reactions that can afford such oxidants appears to be very limited.

5. APPENDIX A: SYMBOLS, DEFINITIONS AND CONVERSION FACTORS

Symbols and Definitions

ASU	air separation unit
ATR	autothermal reforming
Bbl	barrel (159 L)
CAR	combined autothermal reformer
CombiR	combined reforming
CPO	catalytic partial oxidation
GHR	gas-heated reformer
GTL	gas-to-liquid process
ISBL	inside battery limits; the process and purification segments
KRES	Kellogg heat reforming exchanger system
LHV	low-heating-value; the heat of combustion of a fuel to gaseous H ₂ O and CO ₂
MT(G,O)	methane-to-gasoline process, methane-to-olefin process
OCI	oxidative chlorination

OC(O,P,S,A)	oxidative coupling of methane to olefins paraffins, styrene or acrylonitrile
OSBL	outside battery limits; utilities and other facilities of plant, excl. ISBL
PO	non-catalytic partial oxidation
PO(M,F)	direct partial oxidation of methane to methanol or formaldehyde
PreR	combined reformer with pre-reformer
ROI	Return on investment; fraction of investments covered by the profits made annually
SMR	steam methane reforming
Cash cost:	cost to operate a plant, without considering prior investment
Fixed costs:	contribution of the cash cost that does not vary with plant loading, e.g. labour or maintenance
Profitable cost:	cost to operate a plant and reimbursed prior investment.
Variable cost:	contribution of the cash cost that varies with the plant loading, e.g. feed cost, energy or chemicals
Capital charge:	fraction of the investments that is plant to covered by annual profits

Conversion factors

Oil:	1 t = 42 GJ = 7.3 bbl
Paraffins:	1 t = 44 GJ = 7.5 bbl
Aromatics:	1 t = 40 GJ = 8.5 bbl
Gas:	1 t = 50 GJ = 1,370 m ³ = 1.23 toe = 48,928 ft ³
Coal:	1 t = 27-33 GJ = 0.63-0.77 toe
MeOH:	1 t = 20.0 GJ = 0.47 toe
Power:	1 MWh = 3.6 GJ = 0.083 toe
Prices:	1 \$cent/lb = 22 \$/t = 3 \$/bbl oil
Working year:	8000 hours or 330 days

6. APPENDIX B: DERIVING A CAPITAL CHARGE

The capital charge represents the minimum level of profit that is needed to recover the past investment and the lost interests, after taxes. Hence, the 25% capital charge does not imply that the total investment is written off in four years. It accounts for the expected life of the plant, the level of interest, the tax rate and additional factors. Let us illustrate this:

- In 1st approximation, the capital charge accounts for an even reimbursement of the capital over the production life. For a minimum production life of e.g. 10 years, the capital charge amounts to 10%.
- One can then include the lost interests. When the investment is reimbursed linearly over the 10 years together with 15% interest on the part that is still to be reimbursed, the total reimbursement amounts in fact 168% of the initial investment. The capital charge needs therefore to be increased from 10 to 16,8%.
- One can then include the tax rate. If the investment is reimbursed after having paid 35% tax on the profits, the capital charge (before tax) needs to be further increased by a factor $1/(1-35\%)$, from 16.8 to 25.6%. If, however, the 35% tax allows a 20% depreciation of the investment for the first five years, the capital charge increased from 16.8 to 20.4% only.

The same calculations can be made for an estimated production life of 20 years, resulting to a capital charge that increases from 5% (in 1st approximation), to 12% (including interests), to 19% (including tax) or 16% (including tax and depreciation).

Clearly, the interest and tax rates have a strong influence on the capital charge, much stronger than the expected production life.

7. REFERENCES

- [1] Lange, J.-P., *CatTech* 2001, 5, 82-95
- [2] Chauvel A. and Lefebvre G., in "Petrochemical processes: 1. Synthesis-gas derivatives and major hydrocarbons" Ed. Technip (1989)
- [3] Holland, F.A., Watson, F.A., Wilkinson, J.K., in "Perry's chemical engineers' handbook", 6th ed., p. 25-1 to 25-79 (eds. R.H. Perry, D.W. Green and J.O. Maloney), Mc-Graw-Hill (1984)
- [4] product prices are quoted in *European Chemicals News*, *Chemical week*, *Chemical market reporter* as well as on <http://www.chemexp.com>
- [5] Sedriks, W., *ChemTech* 1995, November, 56-60
- [6] Sedriks, W., *ChemTech* 1998, February, 47-53
- [7] Sommerfeld, J.T., *Hydrocarbon Proc.* 2001 (June), 103-108
- [8] Brown, T.R., *Hydrocarbon Process.* 2000, October, 93

- [9] Sheldon, R.A., *ChemTech* 1994 (March), 38-47
- [10] Lange, J.-P., *Green Chemistry* 2002, 4, 546-550
- [11] Lange, J.-P., *Chimie Nouvelle* 1995, 13, 1433-1436
- [12] Lange, J.-P., *Chimie Nouvelle* 1994, 12, 1403-1406
- [13] Fox III, J.M., *Catal. Rev.-Sci. Eng.* 1993, 35(2), 169-212
- [14] Fox III, J.M., Chen, T.-P. and Degen, B.D., *Chem. Eng. Progress* 1990, April, 42-50
- [15] Gradassi, M.J., Green, N.W., *Fuel Processing Technology* 1995, 42, 65-83
- [16] *Cat. Rev. Newsletter* 2002, December, 4-7
- [17] *Eur. Chem. News* 2003, February 10, 22
- [18] *Chem. Week* 2002, October 2, 14
- [19] Pickover, B., *Eur. Chem. News* 2000, September 25, 51
- [20] disclosed costs of plants under constructions are regularly reported in *European Chemicals News* and the *Oil and Gas Journal*
- [21] Lange, J.-P., *Catalysis Today* 2001, 64, 3-8
- [22] Lange, J.-P., de Jong, K.P., Anson, J., Tijm, P.J.A., *Stud. Surf. Sci. Catal.* 1997, 107, 81-86
- [23] Maiden, C.J., *Stud. Surf. Sci. Catal.* 1988, 36, 1-16
- [24] Raimbault, C., Cameroun, C.J., *Stud. Surf. Sci. Catal.* 1991, 61, 479-487
- [25] Rostrup-Nielsen, J., Dybkjaer, I.B., Christiansen, L.J., in "Chemical Reactor Technology for Environmentally Safe Reactors and Products" (de Lada et al., eds.), Kluwer, 1993, 249
- [26] Rostrup-Nielsen, J.R., in "Catalysis - Science and Technology" (J.R. Anderson and M. Boudart, eds), vol. 5, Springer (1984)
- [27] Solbakken, A., *Stud. Surf. Sci. Catal.* 1991, 61, 447-455
- [28] Lange, J.-P., *Ind. Eng. Chem. Res.* 1997, 36, 4282-4290
- [29] Schneider, R.V. III, LeBlanc, J.R., Jr., *Hydrocarbon Process.* 1992, 71(3), 51
- [30] Sundset, T., Sogge, J., Strøm, *Catal. Today* 1994, 21, 269-278
- [31] Hansen, R., Sogge, J., Wesenberg, M.H., Olsvik, O, *Stud. Surf. Sci. Catal.* 2001, 136, 405-410
- [32] Dybkjaer, I., Hansen, J.B., *Stud. Surf. Sci. Catal.* 1997, 107, 99-116
- [33] Sie, S.T., Senden, M.M.G., van Wechem, H.M.H., *Catal. Today* 1991, 8, 371-394
- [34] Jager, B., *Stud. Surf. Sci. Catal.* 1997, 107, 219-224
- [35] Eisenberg, B., Fiato, R.A., Maulding, C.H., Say, G.R., Soled, S.L., *Stud. Surf. Sci. Catal.* 1998, 119, 943-948
- [36] Saito, Y., Kuwa, M., Hashimoto, O., *AIChE Symp. Series* 1988, 84, 102-113
- [37] Vora, B.V., Marker, T.L., Barger, P.T., Nilsen, H.R., Kvisle, S., Fuglerud, T., *Stud. Surf. Sci. Catal.* 1997, 107, 87-98
- [38] Vora, B.V., Pujadó, P.R., Miller, L.W., Barger, P.T., Nilsen, H.R.; Kvisle, S., Fuglerud, T., *Stud. Surf. Sci. Catal.* 2001, 136, 537-542
- [39] Chang, C.D., *Catal. Rev. - Sci. Eng.* 1983, 25, 1-118
- [40] Parkyn, N.D., Warburton, C.I., Wilson, J.D., *Catal. Today* 1993, 18, 385-442
- [41] Sundset, T., Sogge, J., Porcelli, R., *Stud. Surf. Sci. Catal.* 1994, 81, 561-567
- [42] Lee, A.K.K., Aitani, A.M., *Fuel Sci. and Technol.* 1991, 9(2), 137-158
- [43] Kuo, J.C.W., in "Chemical reactor technology for environmentally safe reactors and products" (H.J. de Lasa et al., eds.) Kluwer, 1993, 183-226
- [44] Lange, J.-P., Tijm, P.J.A., *Chem. Eng. Sci.* 1996, 51(10), 2379-2387
- [45] Maitra, A.M., *Appl. Catal. A: General* 1993, 104, 11-59
- [46] Hutchings, G.J., Scurrell, M.S., Woodhouse, J.R., *Chem. Soc. Rev.* 1989, 18, 251-583
- [47] Pitchai, R., Klier, K., *Catal. Rev. - Sci. Eng.* 1986, 28, 13-88
- [48] Chun, J.-W., Anthony, R.G., *Ind. Eng. Chem. Res.* 1993, 32, 259-263

- [49] Weill, J., Chevron, F., Raimbault, C., Genier, R., Renesme, G., Capogna, L., Muller, Y.,
Rev. Inst. Fr. de Pétrole 1992, 47, 255-267
- [50] Wang, L., Tao, L., Huang, J., Xu, Y., Catal. Lett. 1993, 21, 35
- [51] Lunsford, J.H., Rosynek, M.P., Wang, D., Stud. Surf. Sci. Catal. 1997, 107, 257-261
- [52] Koerts, T., Delen, M.J.A.G., van Santen, R.A., J. Catal. 1992, 138, 101-114
- [53] Mielczarski, E., Monteverdi, S., Amariglio, A., Amariglio, H., Appl. Catal. A: General
1993, 104, 215-228
- [54] Tullo, A.H., Chem. Eng. News 2003, March 17, 25-26
- [55] Morgan, M., Eur. Chem. News 2002, Nov. 18, 26-28
- [56] Cassidy, F.E., Hodnett, B.K., CatTech 1998, 2, 173-180

Chapter 4

THEORETICAL BASIS OF THE ACTIVATION OF LIGHT ALKANES

M. Witko, R. Tokarz-Sobieraj, R. Gryboś

*Institute of Catalysis and Surface Chemistry, Polish Academy of Sciences,
ul. Niezapominajek 8, 30239 Kraków, Poland
ncwitko@cyf-kr.edu.pl*

1. INTRODUCTION

Activation of alkanes requires a presence of a catalyst, which by interacting with organic species modifies its electronic and geometric structures and facilitates rearrangement of the selected bonds. As a result, the reaction is directed along a certain, selected pathway that is usually not the most convenient from a thermodynamic point of view. A richness of the different catalytic reactions, which are possible among the particular reactants, follows from a fact that the formed product depends on properties of a particular catalyst.

Table 1 collects spectrum of various reactions, which may proceed between oxygen and propene molecules. We can deal with cyclization, oxidation (into ether, acrolein and acrylic acid, mixture of two aldehydes, or ketone), dehydrogenolysis, dimerization and total oxidation processes. So one can obtain different products depending on the catalyst that is applied, which proves that each of the catalysts directs the reaction into one, out of many possible, selected pathway.

At present, a main goal of catalytic science is to tailor the most active and selective catalyst for a particular reaction. In order to do it one should understand a mechanism of the reaction and the role of the catalyst. This cannot be obtained without a detailed knowledge of the physical and chemical properties of the catalyst surface together with a description of the

elementary steps of the reactions enriched by a full characterization of the transition complex, which is formed.

Table 1. Products of propene oxidation and the catalysts used.

$\text{CH}_2=\text{CH}-\text{CH}_3 + \text{O}_2$	
Product	catalyst
$\text{CH}_2\text{COHCH}_3$	Th_2O_3
$\text{CH}_2=\text{CH}-\text{CHO}$	$\text{Bi}_2(\text{MoO}_4)_3$
$\text{CH}_2=\text{CH}-\text{COOH}$	$\text{NiMoO}_4 + \text{MoO}_3$
$\text{HCHO} + \text{CH}_3\text{CHO}$	CoTiO_3
CH_3COCH_3	$\text{SnO}_2 + \text{MoO}_3$
$\text{CO}_2 + \text{H}_2\text{O}$	CuCo_2O_4
C_6H_6	BiPO_4
$\text{CH}_2=\text{CH}_2 + \text{CH}_2=\text{CH}-\text{C}_2\text{H}_5$	$\text{Mo}(\text{CO})_6$
$\text{CH}_2=\text{CH}-\text{CH}_2-\text{CH}_2-\text{CH}=\text{CH}_2$	Bi_2O_3

Two parallel and complementary approaches are requested: experimental and theoretical ones. Both provide needed information of the atomic and molecular levels and synergy between these paths leads to full understanding of the studied process giving the opportunity to tailor the catalyst for a particular reaction. During last decades the role of theoretical studies is constantly increasing due to very well developed theories as well as a fact that computers are widely available, relatively cheap and fast.

2. THEORETICAL MODELLING

Each model used in theoretical description of a chemical reaction is by its definition incomplete with respect to a real system. By constructing a model one should remember that it has to be done in such a way that it gives not only the interpretation of a phenomenon to which it has been elaborated but also enables one to predict different behavior/properties of the system. Theoretical model has to fulfill several criteria, and among them simplicity, self-consistency, stability and generality are the most important.

Usually two components of each model are discussed: geometrical and physical/chemical. Geometrical component describes a portion of a matter that is taken into consideration whereas physical/chemical component deals with mathematical methods and approximations that are used to describe physical/chemical interactions, which operate among the elements (mostly atoms) constituting the geometrical model.

In heterogeneous catalysis two models, which approximate the real systems from two opposite directions, are applied: cluster and slab/bulk models. *Cluster model* assumes a localized interaction near the adsorption sites and approximates a catalyst by a finite section that is cut out from the

surface or bulk. This section (a cluster) is assumed to interact with the incoming molecule forming a fictitious supermolecule (cluster + adsorbate) that can be treated by any method originating from a standard quantum chemistry. Clusters can be of different geometries and electronic states. **Slab/bulk model** bases on a periodic arrangement of all atoms and molecules at the surface so surface system is described by a two-dimensional slab (surface slab) of full translation periodicity and finite thickness. Such slabs are repeated in the direction perpendicular to the surface with vacuum separating adjacent slabs forming three-dimensional system. Here, standard solid-state physics methods are applied.

Both models have their advantages and limitations. The main drawback of the cluster model follows from a fact that long-range interactions are neglected; the unsaturated bonds appear and the results of calculations strongly depend on size/geometry of the cluster. Therefore, the application of cluster model requires systematic studies where clusters of different geometries are considered. In every case it is advisory to start from a small cluster and then enlarge it to the point in which results of the calculations start to be independent of the cluster size. The limitation of periodic approach appears when adsorbate molecule is involved because it forms two-dimensional periodic arrangement where artificially strong coupling between adsorbate molecule may appear. To solve this problem a balance between cell size and computation effort is needed and adsorption of a single molecule can be described in a limit of a very large supercell.

Electronic properties of both mentioned above models can be obtained by two approaches: *ab initio* and semiempirical calculations. In ***ab initio methods***, which can be based either on Hartree-Fock (HF) approximation [1] or on density functional theory (DFT) [2], no experimental neither fitting parameters appear. All needed integrals are calculated explicitly. Such a procedure allows to obtain highly accurate electronic states and potential energy surfaces with all characteristic points (minima and saddle points) and gives a quantitative account but only for relatively small model systems. ***Semiempirical methods***, which base on HF formalism, give quantitative trends in large model systems; usually one order of magnitude larger than those used in *ab initio* approaches. Here, only valence electrons are taken into account and most of the integrals are approximated by experimental data or fit into *ab initio* results.

All computational methods give detailed information on electronic and geometric parameters of the studied systems. The most commonly used parameters are: ***electronic charge distribution*** that can be obtained by many different population analyses and gives information on ionic contribution to the binding between atoms, ***bond orders*** that give indication concerning covalent contribution to the interatomic bonds and are often used to estimate the bond strength, ***total and partial, atom projected density of states (DOS)***,

PDOS) that provide a description of the discrete electron energy levels and contribution to them from the selected atoms, *energetics* of surface reactions i.e. energies of subsequent reaction steps with respect to different desorption limits and *bond angles* as well as *bond distances* that reflect changes in geometry as a consequence of bond making/breaking. Other parameters that can be extracted from calculations are: *charge density difference* that quantifies the charge rearrangement due to the bond formation giving therefore direct information about bond formation, *electrostatic potential* that characterizes local charging and bonding at the surface suggesting the place of attack of an adsorbate and many types of *reactivity indices*, which indicate the fragment (atom) of the molecule where the attack of nucleophilic or electrophilic reagent will happen.

3. SURFACE OF A CATALYST

The most important and first to be studied is the surface of a catalyst as it is responsible for interaction and binding with an adsorbate, for a resulting bond changes, for a reaction between reactants and finally, for a desorption process. One has to determine, which atoms at the surface act as active centers, and how the properties of the active center depend on its geometric and chemical environment.

As an example of a catalyst surface the (010)V₂O₅ surface is discussed. Vanadia based catalysts are used in many different processes that belong to various types of chemical reactions proceeding with or without insertion of oxygen into organic species. They catalyze mild (ammo)oxidation, oxidative dehydrogenation, dehydrocondensation, dehydrocyclization and many oxidation processes. Vanadia with a mixture of other oxides (MoO₃, TiO₂, Sb₂O₅ etc.) is used in such industrial processes as oxidation of propylene into acrolein and acrylic acid, benzene to maleic anhydride, anthracene to anthraquinone or propylene to acrylonitrile.

A wide application of V₂O₅ as a catalyst follows a fact that its crystallites may exhibit two structural types of surface: surface built of chemically saturated atoms and those built of unsaturated cations and anions. First type of surfaces expose either metal cations with empty d shells, which may function as lowest unoccupied orbitals (LUMOs) and behave like electron acceptor sites, or oxygen ions with free electron pairs that may act as highest occupied orbitals (HOMOs) and play role of electron donor sites. The second type of surfaces can accumulate excess charge, enabling significant variations of the potential along the surface. Both types of surfaces show different behavior in catalytic reactions by performing a complex multi-step operation on the reacting molecule through activation of some of the bonds

within reactant and hindering those interactions which could result in unwanted products.

Bulk vanadium pentoxide, V_2O_5 , is described by a layer-type crystal with orthorhombic structure [4] where layers extend parallel to the (010) net plane (nomenclature used in [3]), which forms the cleavage plane of the crystal. Depending on the choice of the orthorhombic crystal axes, the layer net plane orientation may be also denoted by (001), as, e.g. in ref. [4]. The crystallographic structure of a bulk can be described using a distorted octahedron [5] with V-O distances ranging from 1.58\AA for the vanadyl groups to 2.79\AA between the cleavage planes, see Fig.1. As a consequence, the layers (including (010) surface) are characterized by periodic arrangements of edge- and corner-sharing VO_5 pyramids sticking out at both sides.

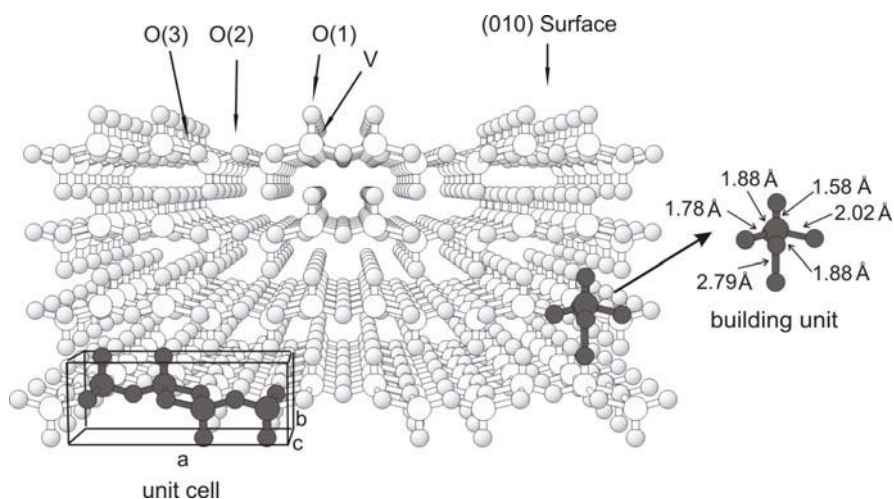


Figure 1. Crystal structure of orthorhombic V_2O_5 with netplane stacking along (010) direction. Vanadia centers are shown by large light balls and oxygen centers by small darker balls. Elementary unit cell, and building unit are indicated in the bulk. Additionally the bond lengths in the building unit are given.

The (010) plane contains three types of structurally different oxygen centers, the oxygen coordinated to one vanadium atom, O(1), the oxygen bridging two vanadium atoms, O(2), and the oxygen linking three vanadium atoms O(3). Singly coordinated, terminal oxygen atoms (each bonded to one vanadium through a short bond equal to 1.58\AA) are sticking out of the surface, whereas doubly and triply coordinated bridging oxygen atoms (with V-O bond distances ranging between 1.78 and 2.01\AA) are approximately at the surface.

The local environment of the different surface oxygen sites is modeled by series $V_6O_{20}H_{10}$, $V_{10}O_{31}H_{12}$, $V_{10}O_{34}H_{18}$ and $V_{20}O_{62}H_{24}$ clusters, which differ in sizes and geometries (see Fig.2). All clusters are cut out from the (010) surface or bulk, and their dangling bonds are saturated with hydrogen atoms (forming the typical OH groups) to account for long range interactions and to obtain electrostatic neutrality of the model.

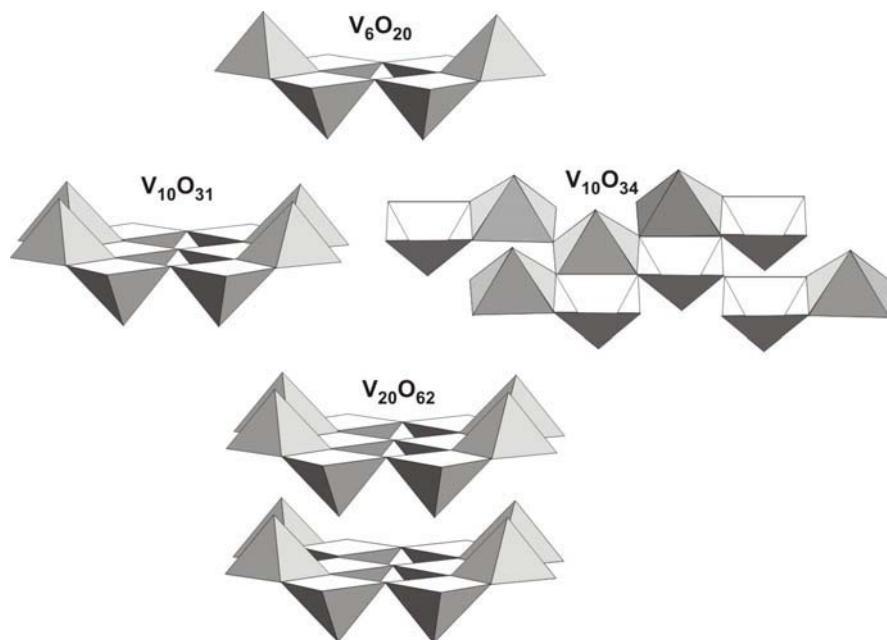


Figure 2. Surface sections used to model (010) V_2O_5 surface. In addition, the building units, corner-sharing VO_5 pyramids are shown.

The electronic structure of the above clusters is determined by ab initio DFT where the Kohn-Sham orbitals are represented by linear combination of atomic orbitals (LCAOs) using extended all-electron basis sets of contracted Gaussian, which are taken from DFT atom optimizations [6]. For the calculations the program package StoBe [7] is applied where electron exchange and correlation is approximated by the gradient corrected RPBE functional [8, 9]. Detailed analyses of the electronic structure are performed using Mulliken population [10] and Mayer bond order indices [11, 12]. Additional information is obtained from total and partial (atom projected) density of states, diagrams of molecular orbitals and energetics of the reactions.

3.1 Undefected (010)V₂O₅ surface

Table 2 lists results of Mulliken populations and Mayer bond orders analysis for the central V and O atoms of the present V₂O₅(010) surface clusters V₆O₂₀H₁₀, V₁₀O₃₁H₁₂, V₁₀O₃₄H₁₈ and V₂₀O₆₂H₂₄. The data are almost identical for the three largest clusters which indicates size and geometry convergence and shows that each of these clusters can be considered a realistic representation of the extended V₂O₅(010) surface. The charges obtained for the smallest V₆O₂₀ cluster are a bit smaller however the tendency in charging is kept.

Table 2. Atomic charges obtained from Mulliken population analysis for O(1-3) sites, Mayer bond order indices and bond lengths in [Å] describing the V-O bonds of the V₆O₂₀H₁₀, V₁₀O₃₁H₁₂, V₁₀O₃₄H₁₈, V₂₀O₆₂H₂₄ clusters. All values are associated with selected atoms and bonds closest to the cluster center.

Clusters	V ₆ O ₂₀ H ₁₀	V ₁₀ O ₃₁ H ₁₂	V ₁₀ O ₃₄ H ₁₈	V ₂₀ O ₆₂ H ₂₄
Atoms	Charges			
V	1.39	1.59	1.59	1.64, 1.76
O(1)	-0.34	-0.34	-0.34	-0.33
O(2)	-0.66	-0.69	-0.67	-0.71
O(3)	-0.87	-0.87	-0.86	-0.87
Bond distances [Å]	Bond orders			
V=O(1) 1.58	1.78	2.06	2.05	2.08
V-O(2)-V 1.78; 1.78	0.85; 0.85	0.83; 0.83	0.80; 0.89	0.82; 0.82
V-O(3)-V 1.88; 1.88	0.50; 0.50	0.49; 0.54	0.53; 0.63	0.45; 0.55
V 2.02	0.42	0.39	0.29	0.41

As expected from chemical reasoning, all vanadium atoms are positively charged (V^{1.59+}) and all oxygen atoms are negative in the clusters. The nucleophilic character of oxygen sites scales with their coordination number and they are described as follows O(1)^{0.34-}, O(2)^{0.69-}, O(3)^{0.87-}. Thus, the local charging is found to be much smaller than the formal valence (V⁵⁺, O²⁻), which indicates sizeable covalent contributions to the interatomic binding in V₂O₅.

While atom charges in the clusters can give information about ionic (electrostatic) binding between the V and O atoms, bond order results can serve as a rough estimate of covalent contributions to the total V-O binding. The data of Table 2 confirm general expectations based on simple coordination and valence concepts. The bond order of V-O(1) bond yields value close to 2, which suggests V=O double bond in agreement with the single coordination of this oxygen. Bond order referring to binding between doubly coordinated bridging oxygen and each of their two neighboring vanadiums results in values smaller than 1 (0.8 - 0.9), corresponding to two, almost single bonds per oxygen, which is again reasonable based on O(2)

coordination. Finally, V-O bond orders involving bridging O(3) atoms, coordinated to three vanadium each, give meaningful values of 0.4 to 0.6 per bond.

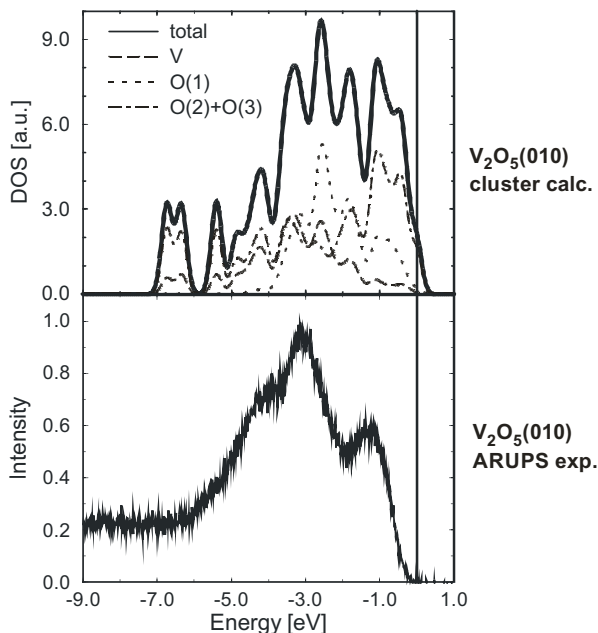


Figure 3. Total (DOS) and atom projected (PDOS) densities of states curves of the $V_{10}O_{31}H_{12}$ cluster and angle resolved He-II ultraviolet photoemission spectrum of a $V_2O_5(010)$ surface.

Alternatively, the electronic structure of the (010) V_2O_5 surface can also be described by energy level distributions of the occupied Kohn-Sham valence orbitals. The dense distribution of V and O derived cluster levels in $V_{10}O_{31}H_{12}$ cluster allow the definition and discussion of a cluster total density of states (DOS) as well as atom projected partial densities of states (PDOS). Fig. 3 shows calculated total and atom projected DOS for the $V_{10}O_{31}H_{12}$ cluster together with the experimental data, i.e. an ARUPS spectrum for V_2O_5 taken with HeII light in normal emission geometry [13].

To make a comparison possible, the theoretical data is shifted appropriately. As one can see the shape of the experimental intensity is well reproduced by the calculations what indicates that the origin of peaks observed in the photoemission spectrum may be identified by a comparison with the calculated PDOSs. This allows to assign the most prominent peak at about 5eV in the experimental spectrum into emission from terminal oxygen (O1) and to characterize the peak at a binding energy about 7eV as a mixture of vanadium with O(2) and O(3) induced intensity. The experiment

data concerning the surface imperfections that are taken from different $V_2O_5(010)$ surface samples [13] obtained by several cleavages shows that the spectra vary only in the region of 7eV whereas the dominant feature at about 5eV is less influenced. Therefore, the ARUPS data suggest that the concentration of surface imperfections involving vanadyl species changes only little between different cleavages. This can be understood as vanadyl oxygen being more strongly bonded to the surface than the bridging ones, and as a result, the more weakly bound bridging oxygen atoms contribute more to surface imperfections. This will be discussed later on. In addition, based upon the agreement between theoretical and experimental spectra, the $O2sp$ peaks can be suggested as monitors for reaction of different surface oxygen centers.

3.2 Modified (010) V_2O_5 surface

Surface of any catalyst may undergo several types of modifications. It can be changed on purpose for example by introducing promoters or using support. It can be also modified by local imperfection or by adsorption of atoms/molecules, which are present due to the reaction conditions.

3.2.1 Surface hydroxyl/water species.

In the oxidation of hydrocarbon surface OH or H_2O species may be formed due to the adsorption of hydrogen abstracted from the organic molecule in the first step of the reaction. They can be also present as the result of water traces that may adsorb at the local surface vacancies.

The easiest way to study surface OH/ H_2O species is to adsorb one/two hydrogen atom(s) at different surface oxygen atoms. The last processes (adsorption of one/two hydrogen atoms) was modeled by $V_{10}O_{31}H_{12}H=V_{10}O_{30}H_{12}OH$ and $V_{10}O_{31}H_{12}2H=V_{10}O_{30}H_{12}H_2O$ clusters. The OH/ H_2O species were optimized. The geometric and electronic parameters for $V_{10}O_{31}H_{12}$, $V_{10}O_{30}H_{12}OH$ and $V_{10}O_{30}H_{12}H_2O$ clusters are summarized in Table 3.

The results of Table 3 show that first hydrogen atom stabilizes at all oxygen sites with sizeable binding energies. So does the second hydrogen atom, however, the adsorption energies are smaller [14]. In all cases adsorption leads to the formation of very stable surface OH/ H_2O species.

The hydroxyl/water species involving terminal oxygen O(1) site are bent with respect to the surface normal and oxygen is shifted from its position towards adsorbed hydrogen atom(s). Both surface species formed at the bridging O(2) site, due to symmetry reason, point normal to the surface and again the involved oxygen is shifted out of the surface. Further, OH/ H_2O

formed with the participation of triply coordinated O(3) site are bent, pointing away from the adjacent vanadyl group. The geometries of all surface species are presented at Fig. 4. At all sites, the distances between oxygen and its nearest V neighbors at the V_2O_5 surface are enlarged by the adsorption, which indicates a weakening of V-O binding near the adsorption site. Such a weakening is seen also from the bond orders of the respective bonds. Results of the calculations indicate that adsorption of hydrogen, which is equivalent to the formation of surface OH/H₂O species, is a local process and results in the reduction of the nearest vanadium center.

Table 3. Atomic charges obtained from Mulliken population analysis and Mayer bond order indices for the selected atoms (V, O adsorption sites) from $V_{10}O_{31}H_{12}$ cluster with H, and 2H adsorbed at different oxygen sites O(1-3). For comparison, in the first position electronic parameters for each atom in the “clean” cluster are shown. In addition, H adsorption energies, $E_B(H^{1st})$, $E_B(H^{2nd})$, $E_B(2H)$, at the $V_{10}O_{31}H_{12}$ with OH and H₂O surfaces species are given.

	O(1)	O(2)	O(3)
Atoms	Charges (cluster / OH / H ₂ O)		
V	1.59 / 1.60 / 1.63	1.59 / 1.53 / 1.39	1.59 / 1.51 / 1.40
O	-0.34 / -0.67 / -0.91	-0.69 / -0.89 / -0.93	-0.87 / -0.99 / -0.93
bonds	bond orders		
O-V	2.04 / 1.15 / 0.37	0.83 / 0.45 / 0.19	0.54 / 0.24 / 0.16
	Energies [eV]		
$E_B(H^{1st})$	2.34	2.21	1.88
$E_B(H^{2nd})$	1.56	0.66	1.08
$E_B(2H)$	3.90	2.87	2.96

3.2.2 Surface oxygen vacancies.

Surfaces of all catalysts contain complex imperfections (various defects) that are generally very difficult to model. One of the easiest defects to mimic are local vacancies that may play a role of active centers, and in addition, may propagate into a long-range defects giving even rise to the formation of the shear planes.

Surface local vacancy may be modeled by discussing several possible scenarios of its formation see Fig. 5. First, surface oxygen may desorb leaving the vacancy behind. But local defect may form also due to the desorption of surface species such as for example OH and H₂O. Table 4 presents energies needed to create a vacancy at differently coordinated oxygen sites through a different scenarios i.e. via desorption of surface O, surface OH group and surface H₂O species. The energies are calculated according to the following formulae:

$$E_D(O) = E(V_{10}O_{30}H_{12}) + E(O) - E(V_{10}O_{31}H_{12})$$

$$E_D(\text{OH}) = E(\text{V}_{10}\text{O}_{30}\text{H}_{12}) + E(\text{OH}) - E(\text{V}_{10}\text{O}_{30}\text{H}_{12}\text{OH})$$

$$E_D(\text{H}_2\text{O}) = E(\text{V}_{10}\text{O}_{30}\text{H}_{12}) + E(\text{H}_2\text{O}) - E(\text{V}_{10}\text{O}_{30}\text{H}_{12}\text{H}_2\text{O})$$

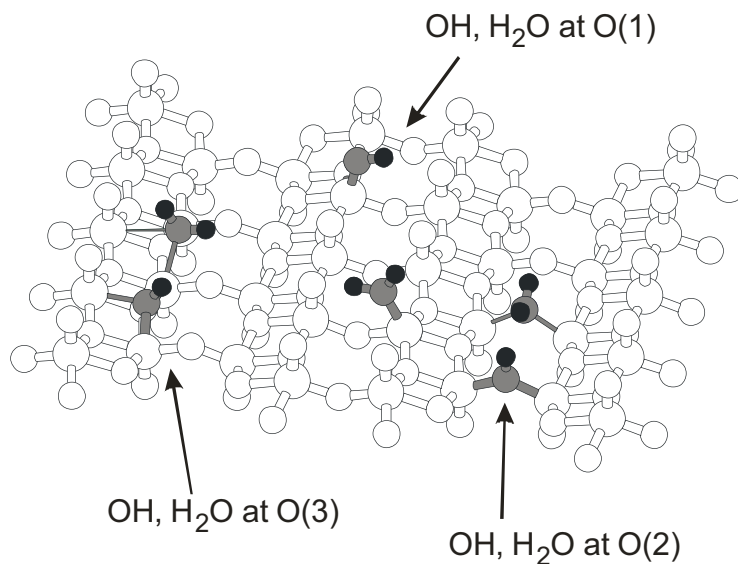


Figure 4. Calculated equilibrium geometries of hydrogen binding at different oxygen sites of the (010) V_2O_5 surface: surface OH groups, and surface H_2O groups obtained from optimizations of $\text{V}_{10}\text{O}_{31}\text{H}_{12}+\text{H}$ and $\text{V}_{10}\text{O}_{31}\text{H}_{12}+2\text{H}$, respectively. The surface species are shown by darker shaded balls while the surface lattice is sketched by light balls.

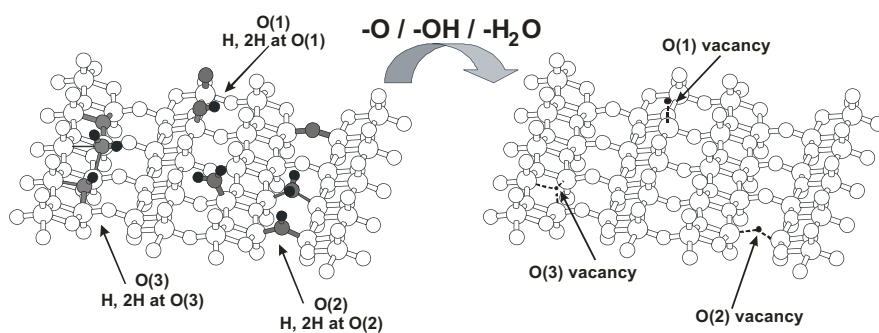


Figure 5. Scheme of different ways of vacancy formation (by removal of surface O sites, OH and H_2O species) and the sketch of different vacancies (black dots) at different surface sites at the $\text{V}_2\text{O}_5(010)$ surface.

Table 4. Desorption energies $E_D(O)$, $E_D(OH)$, and $E_D(H_2O)$ for different oxygen sites at the $V_2O_5(010)$ surface. All energies are given in [eV].

	O(1)	O(2)	O(3)
$E_D(O)$	7.16	7.95	7.01
$E_D(OH)$	4.67	5.33	4.06
$E_D(H_2O)$	1.17	0.92	0.08

Results of Table 4 show that surface oxygen atoms are strongly bonded to the surface, the energies required to create vacancies are of the order of 6-7 eV. Hydrogen assists the formation of vacancies. The energy needed to desorb surface hydroxyl is smaller by 2-2.5 eV, whereas to desorb surface water species the required energies are of the order of 1 eV. Thus removal of oxygen from the $V_2O_5(010)$ surface is energetically unfavorable, however the pre-adsorbed hydrogen can facilitate this process substantially.

Formation of oxygen vacancies is found [15] to result in chemical reduction of neighboring vanadium centers. Further, local relaxation affects inter-layer binding at the surface and may lead major reconstruction of the surface.

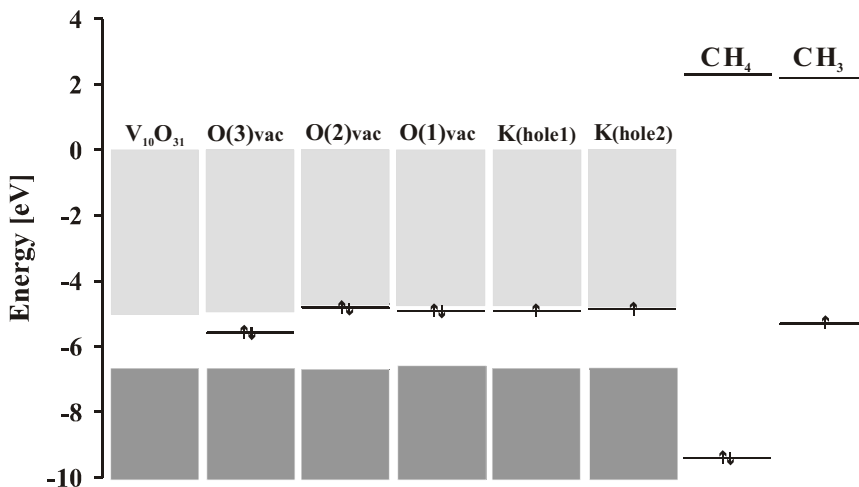


Figure 6. Molecular energy diagram for the interaction of methane and CH_3 radical with $V_{10}O_{31}H_{12}$ cluster modeling ideal $V_2O_5(010)$ surface (column denoted as $V_{10}O_{31}$), with $V_{10}O_{30}H_{12}$ cluster modeling the formation of O(3), O(2), and O(1) vacancies (columns denoted as O(3)vac, O(2)vac, and O(1)vac, respectively), as well as with K/ $V_{10}O_{31}H_{12}$ cluster modeling the adsorption of potassium at the $V_2O_5(010)$ surface (columns denoted as K(hole1) and K(hole2)). Dark shaded columns refer to dense occupied energy levels (conduction bands) whereas light shaded columns to empty levels (conduction bands) of the appropriate clusters. Local states occurring for modified surface are shown.

Surface vacancy may change the electronic structure of the surface and lead to the new active site. Fig. 6 shows molecular diagram for undefected and defected (by existing local oxygen vacancies) $V_2O_5(010)$ surface. As one can see, formation of surface vacancies at O(2) or O(1) site creates a local, doubly occupied state that lies very near to the conduction band, whereas O(3) vacancies results in the local state in the middle between the valence and conduction bands.

3.2.3 Alkali metal dopants.

From many experiments it is known that the addition of dopants to the active phase modify its performance in the catalyzed reaction. In particular, alkali metals increase the selectivity and decrease activity of V_2O_5/TiO_2 systems in oxidative dehydrogenation of propane; potassium having the strongest effect. The dopant influence on the electronic and, what follows, catalytic properties of the (010) V_2O_5 surface was studied by adsorbing potassium atom at the $V_{10}O_{31}H_{12}$ cluster in different positions/sites.

Results of performed calculations suggest two places for K adsorption: the hole between four vanadyl O(1) oxygen sites – referred to as hole 1 and the hole between the two bridging O(2) and two O(3) oxygen sites – denoted as hole 2 (see Fig. 7).

Potassium interacts with the surface with relatively large energies: ~ 3.5 and 2.8eV/mol for hole 1 and hole 2, respectively. Upon adsorption it transfers an electron to the surface and becomes stabilized as a cation. A new, singly occupied local state of V3d character is formed close to the conduction band (see Fig. 6, columns denoted as K(hole1) and K(hole2)) and leads to the modification of surface reactivity. Adsorption of potassium activates the surface oxygen by weakening V-O bonds, however, due to short range of this effect the activated oxygen sites are at the same time sterically blocked by the adsorbed potassium. The same effect is observed for other alkali dopants [16].

3.2.4 Vacancy re-oxidation

Surface oxygen vacancies may be filled by the adsorption of oxygen molecule from gas phase. Molecular O_2 can adsorb at different vacancies (of O(1), O(2), O(3) type) and with different geometric orientation (perpendicular or parallel to the surface). The re-oxidation process was modeled by $V_{10}O_{30}H_{12}O_2$ cluster. Fig.8 shows adsorbates geometries obtained from calculations whereas Table 5 lists the energies associated with O_2 adsorption at different oxygen sites at $V_2O_5(010)$ surface.

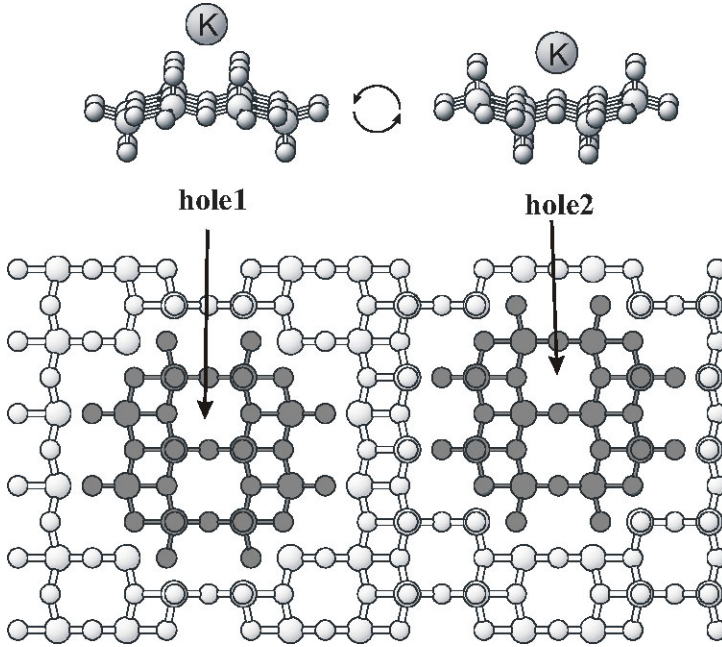


Figure 7. Two preferred sites for potassium (K) adsorption (hole 1 and hole 2) at $V_{10}O_{31}H_{12}$ cluster (used to represent the (010) V_2O_5) are indicated.

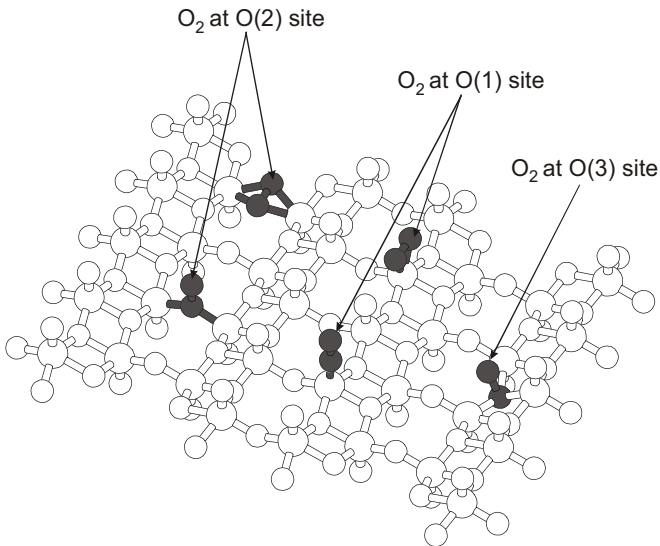


Figure 8. Sketch of computed equilibrium geometries of an adsorbed O_2 molecule at different vacancy sites of the V_2O_5 (010) surface.

The adsorption energy of molecular oxygen, $E_B(O_2)$, is defined as the difference between the energy of the adsorbate system (a defected cluster with and O_2 molecule adsorbed at a vacancy) and the sum of the energies of the defected cluster and a free O_2 molecule, i.e.

$$E_B(O_2) = E(V_{10}O_{30}H_{12}O_2) - [E(V_{10}O_{30}H_{12}) + E(O_2)]$$

where a negative value of the binding energy indicate that adsorption is an exothermic, favorable process.

Re-oxidation of the O(1) and O(2) vacancies by gaseous oxygen yield parallel adsorption of oxygen molecule more favorable than the perpendicular one. At the O(3) vacancy the adsorbate is pulled towards to bulk leading to orientation intermediate between parallel and perpendicular, the O_2 molecule is incorporated into the surface. The ordering of preferred adsorption sites follows the energies of vacancy formation; molecular oxygen is most stable at the O(2) vacancy, less stable at O(1) and is the least stable at O(3), see Table 5. The total charge of the O_2 molecule at the oxygen vacancy is very close to that of the lattice O atom occupying the corresponding site at the undefected surface [17]. Further, upon adsorption oxygen molecule becomes activated. Its O-O bond elongates and the corresponding bond order decreases indicating single O-O bond.

In order to restore the initial state (an undefected surface, an undefected cluster) one oxygen from the adsorbed O_2 molecule must be removed. In analogy to the adsorption energy of molecular oxygen, $E_B(O)$, can be defined as

$$E_B(O) = E(V_{10}O_{31}H_{12}O_2) - [E(V_{10}O_{30}H_{12}) + E(O)]$$

The results of calculations show that for V_2O_5 system, the removal of O atom from the O_2 molecule adsorbed at O(3) vacancy is a spontaneous process (positive value of $E_B(O)$, see Table 5). In contrast, bond splitting of the O_2 adsorbate at other vacancies required energy up to 1.5eV.

Table 5. Energies of vacancy formation E_D , molecular oxygen adsorption at a vacancy $E_B(O_2)$, and atomic oxygen adsorption at the surface $E_B(O)$ for surface sites O(1), O(2), O(3) at the $V_2O_5(010)$ surfaces using $V_{10}O_{31}H_{12}$ cluster. All energies are given in eV.

	O(1) parallel /perpendicular	O(2) parallel/perpendicular	O(3) "parallel"
E_D	7.16	7.95	7.01
$E_B(O_2)$	-2.53 / -2.16	-3.27 / -2.76	-1.03
$E_B(O)$	-1.50 / -1.13	-1.38 / -0.87	0.05

Adsorption of gaseous oxygen at a surface oxygen vacancy can be described as replacing lattice O atom with an O₂ molecule. Adsorbed molecular O₂ can replace the surface O occupying a specific lattice site with almost no change in electron distribution of the crystallographic neighborhood. Thus, the vanadium oxide surface is able to incorporate large amounts of (weakly bound) oxygen atoms. The charge characteristic for the lattice oxygen is redistributed between the two oxygen atoms of the O₂ adsorbate providing less nucleophilic surface oxygen (defined by Mulliken charges) as compared to the clean, undefected surface.

3.3 Interaction of CH₄ with (010)V₂O₅ surface

Oxidation processes may be discussed as reactions that consist of the abstraction of hydrogen atom(s) and addition of one or several oxygen atoms to reactant, resulting in products which differ in the C/H and C/O ratios. Depending on whether oxygen or organic molecule is activated the reactions can be classified as electrophilic or nucleophilic oxidation processes [18, 19]. They require the participation of different types of oxygen: in electrophilic oxidation O₂^{*}, O₂⁻, and O⁻ species are involved whereas in nucleophilic oxidation the lattice oxide O²⁻ ions perform the nucleophilic attack on the activated organic molecule [20]. The first class of processes lead in the conditions of heterogeneous catalysis to total oxidation (combustion), the second class can be carried out with high chemo-, regio- and stereo selectivity [21]. Oxidation of organic molecules proceeds usually by the Mars-van-Krevelen mechanism in which the molecule is oxidized by the catalyst that is then reoxidized by gas-phase oxygen. Thus, the catalyst must be characterized by a facile change of oxidation state of its cations. Transition metal oxides belong to systems that may change in a wide spectrum the electronic state of metals. Therefore, they are the components of all active and selective catalysts. The oxidation cycle involves thus two adsorbed redox couples:



of which the first injects electrons into the oxide catalyst whereas the second one extracts them from the oxide.

From results of spectacular surface science techniques and theoretical computational methods it is known that the activation of the molecule takes place at surface active sites composed of a transition metal ion and oxide

ions. The injection of electrons from an adsorbed redox couple into a transition metal oxide of semiconducting properties can take place spontaneously only if the redox potential of this couple is situated above the Fermi level and above the bottom of the conductivity band. On contrary, the extraction of the electrons from the solid may occur only when the redox potential is located below the Fermi level and below the top of the valence band.

The mechanism of electron transfer between organic molecules and solid catalysts will be examined on an example of $\text{CH}_4/\text{V}_2\text{O}_5(010)$ interaction.

At Fig. 6 in addition to the valence and conduction bands of ideal cluster ($\text{V}_{10}\text{O}_{31}\text{H}_{12}$), clusters ($\text{V}_{10}\text{O}_{30}\text{H}_{12}$) with different oxygen vacancies as well as cluster doped with potassium ($\text{V}_{10}\text{O}_{31}\text{H}_{12}\text{K}$) the HOMO and LUMO of CH_4 and CH_3 species are plotted. Since HOMO of methane is located in the energy range of valence band of the solid, no interaction can be expected. Its LUMO partner lies very high, which means that transfer of electrons from the solid would require very high energy. It is evident that the energies of interacting systems have to be matched either by activation of the reacting molecule or by modification of the electronic structure of the solid surface.

To discuss the interaction of methane with V_2O_5 , the surface was modeled by $\text{V}_6\text{O}_{20}\text{H}_{10}$ cluster. Repulsive potential was found for methane molecule approaching the surface irrespectively of its orientation (see Fig. 9). Therefore, a priori activation of CH_4 was assumed and the adsorption of isolated fragments (CH_3 and H) was studied.

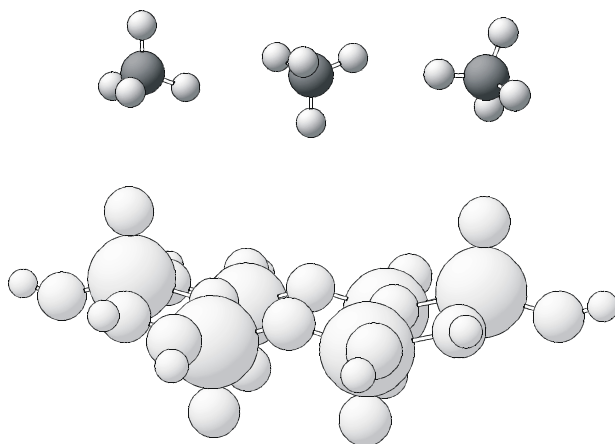


Figure 9. Different orientations of methane molecule above the V_2O_5 surface.

The results of calculations involving interactions of CH_3 and H fragments with $\text{V}_6\text{O}_{20}\text{H}_{10}$ cluster are presented in Tables 6 and 7. They indicate that CH_3 fragment is preferentially adsorbed at the doubly

coordinated oxygen site O(2) ($E_b = 1.31\text{eV}$) forming O(2)-C bond ($R_{O(2)-C} = 1.46\text{\AA}$) whereas H radical becomes stabilized at terminal oxygen ($E_b=2.26\text{eV}$) leading to the typical O(1)-H bond ($R_{O(1)-H} = 0.99\text{\AA}$) (see Fig.10).

Table 6. Bonding energy of H and CH₃ species on different oxygen centers at (010) V₂O₅ surface. Most favourable adsorption site is indicated by boldface font.

$E_b[\text{eV}]$	O(1)	O(2)	O(3)
CH ₃	1.28	1.31	0.74
H	2.26	2.15	1.80

Table 7. Selected electronic parameters (or changes in parameter values upon adsorption) of H and CH₃ species adsorbed on different oxygen centers at (010) V₂O₅ surface. Parameters include: R – bond lengths, P – Mayer bond orders, Q – Mulliken atomic charges.

	O(1)	O(2)	O(3)
CH ₃ species			
R(O-C) [Å]	1.42	1.46	1.34
P(O-C)	0.96	0.87	0.82
$\Delta R(\text{O-V})$ [Å]	+0.12	+0.11	+0.18
$\Delta P(\text{O-V})$	-1.06	-0.73	-0.56
Q(CH ₃)	+0.29	+0.32	+0.37
H-species			
R(O-H) [Å]	0.99	0.99	0.98
P(O-H)	0.66	0.67	0.67
$\Delta R(\text{O-V})$ [Å]	+0.17	+0.14	+0.09
$\Delta P(\text{O-V})$	-0.91	-0.72	-0.63
Q(H)	+0.51	+0.52	+0.53

However, moving the fragments further apart lowers the total energy of the system (see ref. [22]) and indicates possible H and CH₃ surface diffusion. Both fragments transfer electrons to the surface cluster, which results in the weakening of V-O surface bonds. A general conclusion can be thus formulated that the cleavage of the C-H bond in case of primary carbon proceeds with transfer of two electrons to the empty vanadium surface levels and formation of adsorbed alkoxy and surface hydroxyl species.

Generation of local energy levels in the band gap of the V₂O₅ through formation of surface oxygen vacancies (local level doubly occupied) or doping with potassium (local level singly occupied) has a strong influence on the type of species that are formed as the result of the cleavage of C-H bond and hence the CH₃/surface interaction can be different. This was checked by simple calculations where V₂O₉H₈ cluster was taken as model for V₂O₅(010) surface and its interaction with CH₃ species was examined [22]. It was found that when the CH₃ radical approaches doubly coordinated oxygen in such a small non defected cluster the alkoxy group is also formed. However, when methyl radical interacts with the V₂O₈H₈ cluster,

which models O(2) vacancy, no alkoxy group is formed and the surface becomes blocked by strongly bound (chemisorbed) CH_3 species, strongly bound to neighboring metals. The electron transfer, which is different in both cases (to the surface for $\text{V}_2\text{O}_9\text{H}_8$ cluster, and from the surface for cluster with vacancy, $\text{V}_2\text{O}_8\text{H}_8$), can be explained by using molecular orbital diagram (see Fig.6). Local states generated via formation of oxygen vacancy or via adsorption of potassium lie below/above the SOMO of CH_3 , mediate the electron transfer and decide on its direction.

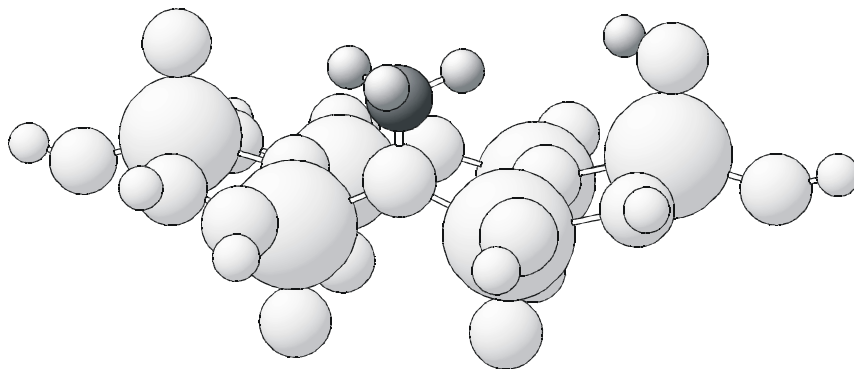


Figure 10. Energetically favoured adsorption sites of CH_3 and H radicals. Both species are shown on one picture for simplicity, in reality both fragments would diffund away to minimize unfavourable interaction energy.

In the next step, the activation of second C-H bond from CH_3 species stabilized either on O(2) or on molecular oxygen adsorbed at O(2) type vacancy was studied by discussing the reaction path, in which C-H bond was elongated and the hydrogen was moving to the nearest O(1) oxygen. It was found that activation of second CH bond from CH_3 radical adsorbed on O(2) proceeds with the energy barrier following from the necessity of C-H bond breaking. Reaction leads to the formation of adsorbed formaldehyde and OH species (see Fig. 11).

The situation is different when methyl radical is stabilized at molecular oxygen. Here, a small elongation of C-H bond results immediately not only in the formation of CH_2O species but also in the V-O bond breaking that leads to the desorption of formaldehyde. As products free formaldehyde and adsorbed hydroxyl are formed (see Fig. 12).

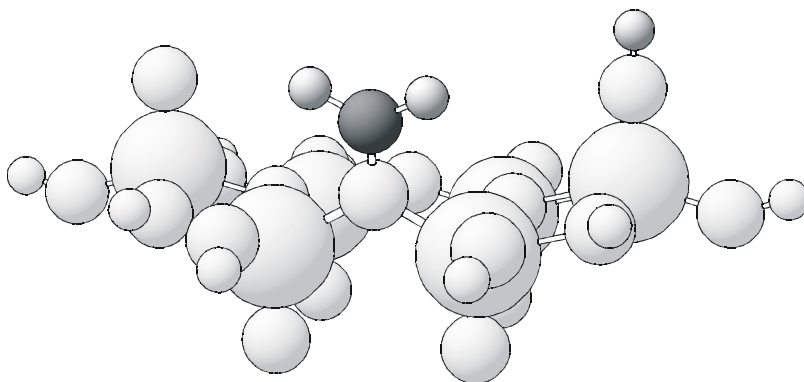


Figure 11. Formaldehyde formed from methoxy species adsorbed on O(2) oxygen center by forcing one hydrogen atom to move over O(1) oxygen center. The CH_2O molecule remains at the surface – compare with Fig. 12.

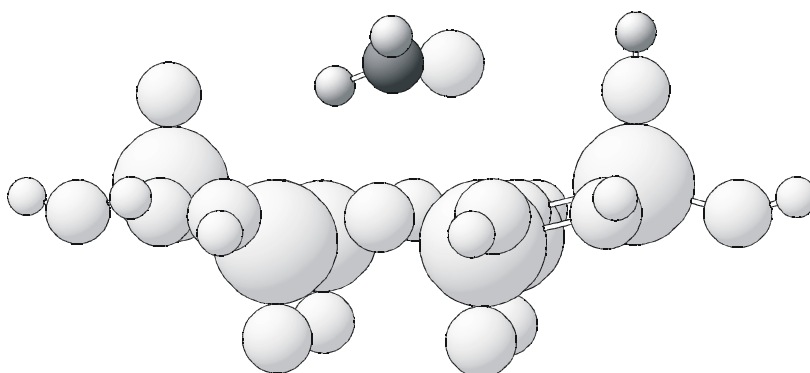


Figure 12. Formaldehyde formed from methoxy species adsorbed on an oxygen molecule in the place of O(2) vacancy. Even moderate C-H bond elongation leads to spontaneous CH_2O desorption.

4. CONCLUSIONS

The above discussion reports an importance and impact of quantum chemical approach on the field of catalysis. By applying theoretical methods to study microscopic properties of vanadium pentoxide surface and bulk it is shown that theory is able to answer several problems concerning surface/bulk binding, role of surface defects, impurities and dopands, as well as adsorption and surface reactions. It is evident that nowadays the

synergy between experimental techniques and theoretical, computational methods enables a better understanding of a mechanism of a catalytic reaction. Such knowledge gives an opportunity to tailor a catalyst with the required properties.

5. ACKNOWLEDGEMENT

This work was partly financed by Polish Research Committee (KBN) through grant (number 4 T09A 048 22).

6. REFERENCES

- [1] A. Szabo, N. S. Ostlund, *Modern Quantum Chemistry: Introduction to Advanced Electronic Structure Theory*, Macmillan, New York 1982.
- [2] J. K. Labanowski, J. W. Andzelm (Eds.), *Density Functional Methods in Chemistry*, Springer, Heidelberg 1991.
- [3] R. Ramirez, B. Casal, L. Utrera and E. Ruiz-Hitzky, *J. Phys. Chem.*, 94 (1990) 8960.
- [4] R.G.Wyckoff, *Crystal Structures*, 2nd ed., Vol.2, Interscience, New York, 1964.
- [5] H. G. Bachmann, F. R. Ahmed, W. H. Barnes, *Z. Kristallogr. Kristallgeom. Kristallphys. Kristallechem.* 115 (1981) 110.
- [6] N. Godbout, D.R. Salahub, J. Andzelm and E. Wimmer, *Can. J. Phys.*, 70 (1992) 560.
- [7] The program package StoBe is a modified version of the DFT-LCGTO program package DeMon, originally developed by A. St.-Amant and D. Salahub (University of Montreal), with extensions by L. G. M. Pettersson and K. Hermann.
- [8] J. P. Perdew, K. Burke, M. Ernzerhof, *Phys. Rev. Lett.* 77 (1996) 3865.
- [9] B. Hammer, L. B. Hansen, J. K. Norskov, *Phys. Rev. B* 59 (1999) 7413.
- [10] R.S. Mulliken, *J. Chem. Phys.* 23 (1955) 1833, 1841, 2388, 2343.
- [11] I. Mayer, *Chem. Phys. Lett.* 97 (1983) 270.
- [12] I. Mayer, *J. Mol. Struct. (Theochem)* 149 (1987) 81.
- [13] K. Hermann, M. Witko, R. Druzinic, A. Chakrabarti, B. Tepper, M. Elsner, A. Gorschluter, H. Kuhlenbeck, H-J. Freund, *J. Electron. Spectrosc. Relat. Phenom.* 98/99 (1999) 10583.
- [14] K. Hermann, M. Witko, R. Druzinic, *Faraday Discuss.* 114 (1999) 53.
- [15] K. Hermann, M. Witko, R. Druzinic, R. Tokarz, *Appl. Phys. A* 72 (2001) 429.
- [16] R. Gryboś, M. Witko, B. Grzybowska-Świerkosz, in-preparation.
- [17] R. Tokarz-Sobieraj, R. Gryboś, M. Witko, K. Hermann, *Collect. Czech. Chem. Commun.* 69 (2004) 121.
- [18] J. Haber, in "Solid State Chemistry in Catalysis", (Grasselli R.K., Brazdil J.F., eds) ACS Symposium Series 279, American Chemical Society, Washington, p.3, 1985.
- [19] J. Haber, *Proc.8th Intern.Congr.Catalysis*, Berlin 1984, Verlag Chemie-Dechema, vol.1 Plenary Lectures, p.85, 1984.
- [20] J. Haber, Turek W., *J.Catal.* 190 (2000) 320.
- [21] J. Haber, in "Heterogeneous Hydrocarbon Oxidation" (Warren B.K., Oyama S.Ted,eds) ACS Symposium Series 638, American Chemical Society, Washington, p.20, 1996.
- [22] J. Haber, M. Witko, *J. Catal.* 216 (2003) 416.

Chapter 5

SURFACE ORGANOMETALLIC CHEMISTRY OF TANTALUM: APPLICATION TO THE METATHESIS OF ALKANES CATALYZED BY A TANTALUM HYDRIDE SUPPORTED ON SILICA

J. Thivolle-Cazat, C. Coperet, S. Soignier, M. Taoufik, J.M. Basset

Laboratoire de Chimie Organométallique de Surface

UMR-9986 CNRS – ESCPE Lyon, 43 Bd du 11 Novembre 1918

F-69626 Villeurbanne Cedex (France)

1. INTRODUCTION

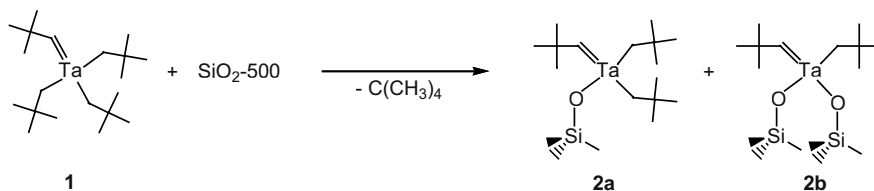
Heterogeneous catalysts are widely used in industry because they can usually be conveniently separated from the reaction medium. From a fundamental point of view, it is always difficult to define and control the real coordination sphere and then to determine the various elementary steps of a catalytic reaction. On the contrary, homogeneous catalysis has been developed on the rules of Molecular Organometallic Chemistry, which affords a better understanding of what are the active species and the elementary steps of a process. Surface Organometallic Chemistry (SOMC) is aimed at the preparation of highly reactive well-defined supported organometallic species which would obey the concepts and the rules of Molecular Organometallic Chemistry. The formation of such supported organometallic species usually involves the reaction of molecular complexes with functional groups of a surface. Surface Organometallic Chemistry found application in the field of the activation and valorisation of alkanes which has been the subject of numerous studies during the last two decades [1,2]. The transformation of alkanes may involve the activation of C-H or C-C bonds or both [3-5]. Among the various modes of C-H bond activation of alkanes, the use of highly electrophilic organometallic complexes of early

transition metal, lanthanides or actinides usually with a d^0 configuration, is believed to involve a σ -bond metathesis mechanism [6-12]. In the field of surface organometallic chemistry, we have initially synthesized a silica supported zirconium hydride, $(\equiv\text{SiO})_3\text{Zr-H}$ [13] with a d^0 configuration which proved able to activate stoichiometrically the C-H bond of methane and alkanes from 25°C to form the corresponding zirconium-alkyls [14,15]. The same surface complex [16,17] as well as its titanium [18] or hafnium [19] analogues were also found able to catalyze at low temperature, the hydrogenolysis of several alkanes such as propane, butane, isobutane or neopentane; the zirconium complex could also cleave under hydrogen the C-C bonds of polyethylene [20]. In the same way, a silica supported tantalum hydride, $(\equiv\text{SiO})_2\text{Ta-H}$ [21] was prepared which not only can cleave but also reform the C-C bonds of alkanes in a new catalytic reaction we have called the alkane metathesis; various organometallic species of tantalum supported on silica will be presented thereafter as well as their properties regarding the activation of alkanes.

2. PREPARATION AND CHARACTERIZATION OF TANTALUM ORGANOMETALLIC COMPLEXES SUPPORTED ON SILICA.

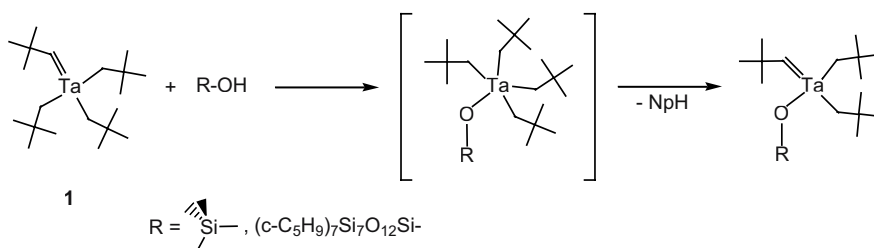
2.1 Preparation and characterization of surface alkyl-alkylidene tantalum complexes.

The tris(neopentyl)neopentylidene tantalum complex $\text{Ta}(-\text{CH}_2-\text{C}(\text{CH}_3)_3)_3(=\text{CH}-\text{C}(\text{CH}_3)_3)$ **1** [22] reacts with the surface hydroxyl groups of silica affording the irreversible grafting of the metal on the surface and leading to the formation of alkyl-alkylidene complexes. The mono-siloxy complex $(\equiv\text{SiO})\text{Ta}(-\text{CH}_2-\text{C}(\text{CH}_3)_3)_2(=\text{CH}-\text{C}(\text{CH}_3)_3)$ **2a** and the di-siloxy complex $(\equiv\text{SiO})_2\text{Ta}(-\text{CH}_2-\text{C}(\text{CH}_3)_3)(=\text{CH}-\text{C}(\text{CH}_3)_3)$ **2b** were formed selectively when silica was previously treated under vacuum at 700°C or 300°C respectively [23], whilst a 65/35 mixture of **2a** and **2b** was obtained after a treatment at 500°C [24]. The reaction is accompanied by the liberation of the corresponding amount of neopentane in the gas phase (scheme 1).



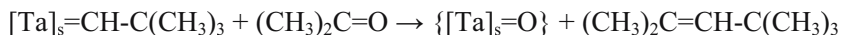
Scheme 1

Contrarily to the reaction of complex **1** with the tris(*tert*-butyl)silanol which led to ((*t*-Bu)₃SiO)Ta(-CH₂-C(CH₃)₃)₂(=CH-C(CH₃)₃) by the direct protonolysis of a Ta-C bond [25], the formation of species **2a** and **2b** turns out to involve first the addition of the OH bond onto the neopentylidene ligand affording the tetrakis(neopentyl) intermediate (≡SiO)Ta(-CH₂-C(CH₃)₃)₄ **2**. The evolution to **2a** goes through the liberation of one equivalent of neopentane via an α -hydrogen abstraction (scheme 2); indeed when the OH groups of silica were fully exchanged with deuterium, the neopentane evolved was only 38% monodeuterated which corresponds to the statistics of α -hydrogen elimination in intermediate **2** [24]. Moreover, the ¹³C NMR spectrum of **2** when enriched with ¹³C on the CH₂ carbon could also be obtained showing a typical evanescent peak at 110 ppm before the evolution to **2a** [26]; finally, the grafting reaction of **1** with silica could be modelled by the use of the silsesquioxane (c-C₅H₉)₇Si₇O₁₂SiOH affording the formation of the corresponding tetrakis(neopentyl) intermediate [26].



Scheme 2

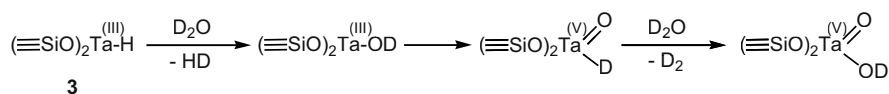
Complexes **2a** and **2b** were further characterized by elemental analysis and reaction with heavy water leading to the liberation of the complementary amount of mono- and bisdeuterated neopentane. The pseudo-Wittig reaction with acetone indicated on average, the presence of one carbene function per grafted complex [23, 24]:



All these data combined with infrared and MAS NMR characterizations supported the formation of surface species **2a** and **2b**.

2.2 Preparation and characterization of a surface hydrido-tantalum complex.

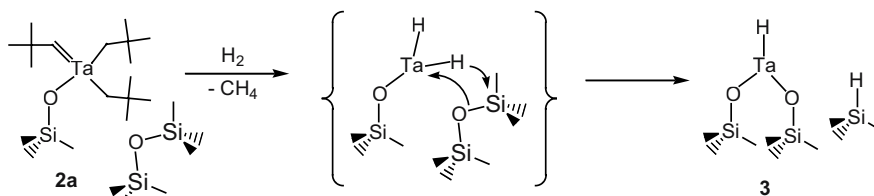
When the mixture of complexes **2a** and **2b** was heated under hydrogen at 150°C overnight there was formation of a new surface species: the tantalum hydride $(\equiv\text{SiO})_2\text{Ta}-\text{H}$ **3** [21]. This transformation was first evidenced by the infrared spectroscopy which showed the disappearance of $\nu(\text{C}-\text{H})$ and $\delta(\text{C}-\text{H})$ bands and the appearance of a new band centered at 1830 cm^{-1} for the tantalum hydride as well as smaller ones in the 2200-2300 cm^{-1} region assigned to surface silicon hydrides. An EXAFS study of the tantalum hydride gave a first coordination sphere of two oxygens at 0.189 nm for tantalum and a contribution of about 70% for a third oxygen at 0.263 nm. The infrared band at 1830 cm^{-1} was the unique one which could exchange reversibly with deuterium at room temperature. Titration of the tantalum hydride by reaction with methyl iodide or di(*tert*-butyl)ketone showed the presence of one hydride per tantalum. Interestingly, the reaction of the tantalum hydride with D_2O led to the liberation of 2 equiv. of an equimolecular mixture of HD and D_2 ; this result was still consistent with the presence of one hydride on the tantalum center but enlightened the occurrence of an oxidative process of the hydrido-tantalum(III) to a tantalum(V) species (scheme 3).



Scheme 3

After C-H bond activation of cycloalkanes (*vide infra*), the reaction with oxygen took only 1 equiv. per metal leading to an oxo-alkoxy complex which confirms that tantalum has the oxidation state +3 in complex **3** [21]. These results indicate that tantalum was reduced from oxidation state 5 to 3 during the transformation of complexes **2a** and **2b** to **3**. Furthermore, titration of the Si-H groups by KOH indicated the formation of only 0.63 Si-H per grafted tantalum. This value quite close to the amount of species **2a** enlightens the understanding of the process affording the transformation of two species **2a** and **2b** into a unique one **3**; indeed, a second Ta-O bond is

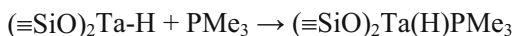
formed when **2a** is transformed into **3**; this can be explained by a surface reaction during which the tantalum environment is modified: a surface siloxane formed during the thermal treatment of silica would open to afford the formation of a Ta-O bond whereas the remaining silicon atom would receive an hydride from the metal center (scheme 4).



Scheme 4

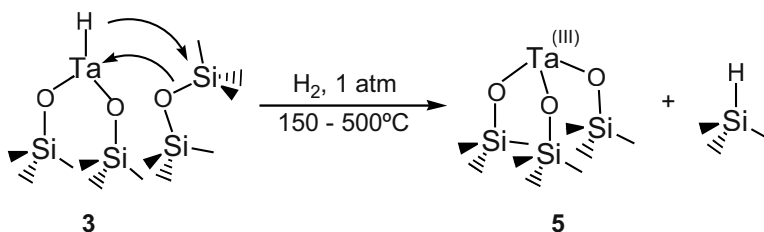
2.3 Further transformation of the tantalum hydride.

The silica-supported tantalum hydride $(\equiv SiO)_2Ta-H$ **3** reacts with an excess of PMe_3 to form a new surface species $(\equiv SiO)_2Ta(H)PMe_3$ **4** where only 1 equiv. of phosphine is coordinated to the metal [27]. The coordination of PMe_3 brings a shift of the $\nu(Ta-H)$ band from 1830 cm^{-1} to a larger band centered at 1690 cm^{-1} which still exchanges reversibly with D_2 . EXAFS experiments on this new species are consistent with a first coordination sphere of two oxygen atoms at 0.195 nm and one phosphorus at 0.26 nm . This complex was further characterized by elemental analysis and NMR; the ^{31}P CP MAS NMR spectrum confirms the coordination of PMe_3 with a unique signal at -8 ppm different from the simply physisorbed phosphine (-57 ppm) whereas the ^{13}C CP MAS NMR spectrum indicates, with a unique peak at 12 ppm , the absence C-H bond activation on the methyl groups.



The thermal stability under hydrogen of $(\equiv SiO)_2Ta-H$ **3** was also investigated. Monitoring of the reaction by infrared spectroscopy showed the progressive decrease of the $\nu(Ta-H)$ band for the benefit of the growth of $\nu(Si-H)$ bands at 2215 , 2270 and 2300 cm^{-1} ; at $500^\circ C$ all the $\nu(Ta-H)$ band had disappeared. Under such a treatment, the tantalum hydride **3** was transformed into a new surface compound, the trisiloxy-tantalum $(\equiv SiO)_3Ta$

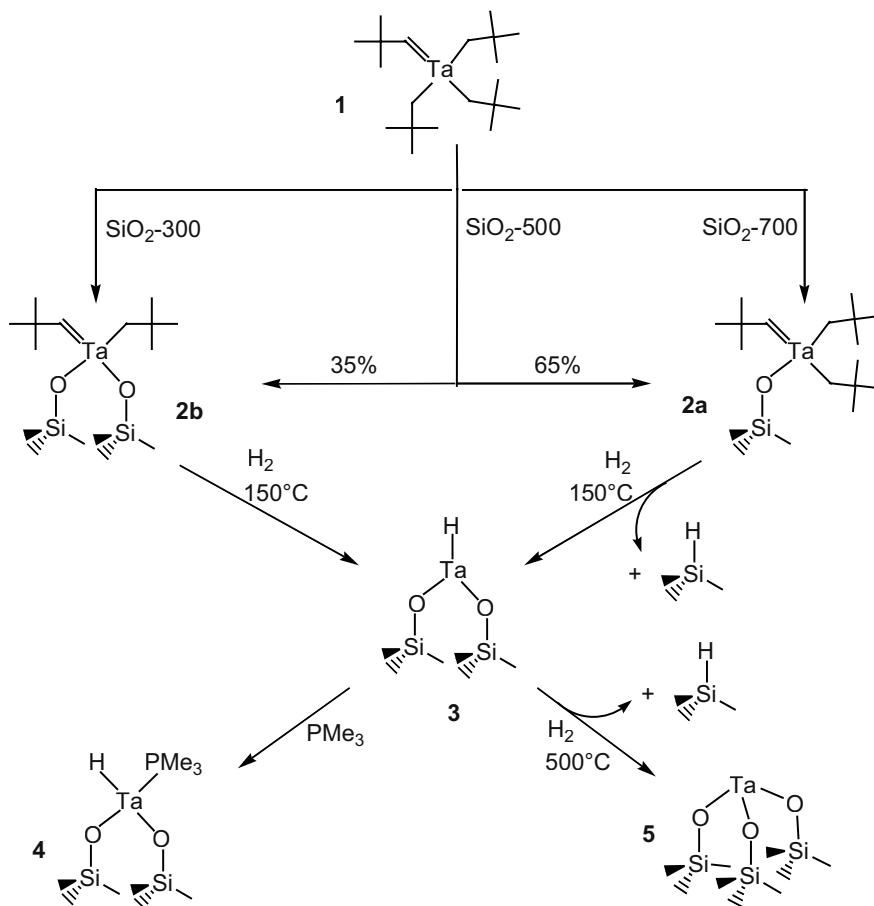
5 [28]. This new complex was characterized by its reactivity with protic reagents like water or alcohol affording the liberation of 1 equiv. of hydrogen and the formation of tantalum(V) species $(\equiv\text{SiO})_3\text{Ta}^{(\text{V})}(\text{OR})_2$ with $\text{R} = \text{H}$ or Et ; it could fix exactly 0.5 equiv. of O_2 to form $(\equiv\text{SiO})_3\text{Ta}^{(\text{V})}(=\text{O})$ or coordinate 1 equiv. of PMe_3 or pyridine. EXAFS analysis of complex **5** was also consistent with the presence of three oxygens at 0.19 nm around the metal. The formation of such a tripodal structure from the hydride **3** accompanied by the growth of Si-H groups can still be understood in the way of a rearrangement of the silica surface around the tantalum atom. Similarly to the formation of **3** this process should involve the cleavage of a siloxane bridge in the vicinity of the tantalum hydride resulting in a concerted transfer of the hydride from tantalum to a silicon atom and of a siloxy group to tantalum (scheme 5).



Scheme 5

So, the grafting of the tantalum complex **1** on silica and its further transformation leads to a series of surface species whose probable structures are summarized in scheme 6.

The following parts will be devoted to the presentation of some properties of these various species.



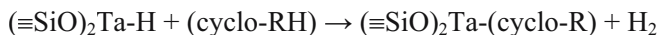
Scheme 6

3. STOICHIOMETRIC C-H BOND ACTIVATION OF ALKANES.

3.1 Activation of cyclic alkanes.

The $(\equiv\text{SiO})_2\text{Ta-H}$ complex **3** is a d^2 species with 8 valence electrons (or 12 if we consider the π -donation of oxygens) which shows a very high

degree of coordinative and electronic unsaturation. Thus, it shows specific properties in the activation of alkanes. First of all, it can activate from room temperature the C-H bonds of cycloalkanes (cyclopentane to cyclooctane) to stoichiometrically form the corresponding tantalum-cycloalkyl species along with the evolution of one equivalent of hydrogen [21,23].



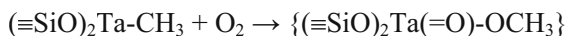
This reaction can be monitored by infrared spectroscopy which shows the progressive decrease of the $\nu(\text{TaH})$ band and the concomitant appearance of $\nu(\text{CH})$ bands. The initial activity at 25°C increases from cyclopentane to cyclooctane and for each cycloalkane a plateau is reached after a few hours; the conversion becomes complete after further heating at 100°C. So, the comparative evolution versus time of the $\nu(\text{TaH})$ bands for the various cycloalkanes indicates that the reactivity increases with their molecular weights; this result can be related to the absorption isotherms of the cycloalkanes at 25°C on silica(500) which show that the amount of the physisorbed cycloalkane, that is their surface concentration, also increases with the molecular weight [29]; a similar behavior was reported in the case of light alkanes [30]. Then, the difference in the initial rate between the various cycloalkanes could be ascribed to the variation in their surface concentrations whereas the limitation of the conversion of each cycloalkane to a different plateau suggests a variation in the reactivity of the tantalum hydride according to its surface environment.

3.2 Activation of methane.

The $(\equiv\text{SiO})_2\text{Ta-H}$ complex also activates the C-H bonds of methane but this later requires heating at 150°C and the infrared spectroscopy indicates an incomplete conversion of the tantalum hydride even after 10h; the $\nu(\text{CH})$ bands of the corresponding surface tantalum-methyl cannot be detected because of the proximity of the surface. The ^{13}C NMR spectrum of the resulting surface complex shows mainly a large peak centered at 55 ppm.



The formation of a tantalum-methyl species was confirmed by the release of methane after hydrolysis or the liberation of methyl acetate after oxidation with O_2 then extraction with acetic acid [31].



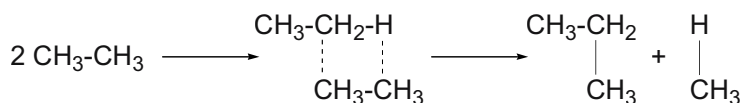
The low reactivity of methane towards the tantalum can again be ascribed to its lowest surface concentration [30] and also to its higher C-H bond energy (105 Kcal/mol [32]) amongst all the alkanes. The incomplete conversion of the tantalum hydride supports the presence of surface species with low reactivity.

4. METATHESIS REACTION OF ACYCLIC ALKANES.

4.1 General reaction

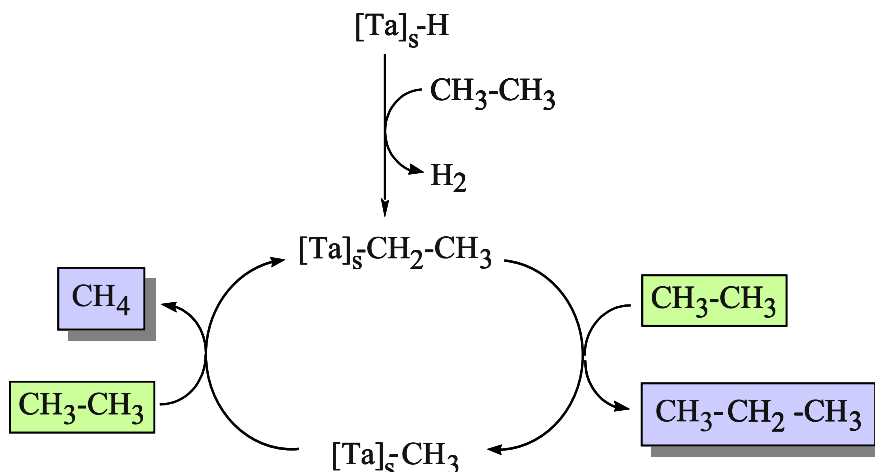
The surface tantalum hydride catalyses at moderate temperature (25-200°C) a novel reaction: the metathesis of acyclic alkanes which has been thus called by analogy with the olefin metathesis [33]. By this reaction, carbon-carbon and carbon-hydrogen bonds seem to be reversibly broken and formed allowing the transformation of C_n alkanes into higher and lower homologues.

A typical example is the metathesis of ethane. When ethane is contacted pure with the tantalum hydride (ethane/Ta molar ratio of 800) at 150°C there is progressive formation of methane and propane in quite similar amounts and traces of butane and isobutane (n/iso = 4) [33]. The main process results in fact in the transfer of a methyl group from one molecule of ethane to the second one; this involves the concomitant cleavage and formation of C-H and C-C bonds (scheme 7).



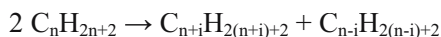
Scheme 7

This reaction reasonably begins by a C-H bond activation step of the ethane molecule by the tantalum hydride, in a quite similar way to the cyclic alkanes, leading to the formation of a surface tantalum-ethyl species (scheme 8); the interaction of this species according to a process not yet clarified, with a new molecule of ethane would lead to the liberation of propane and the formation of a tantalum-methyl intermediate; in this latter, the methyl ligand would be displaced by an other incoming ethane affording methane and the regeneration of the tantalum-ethyl species.



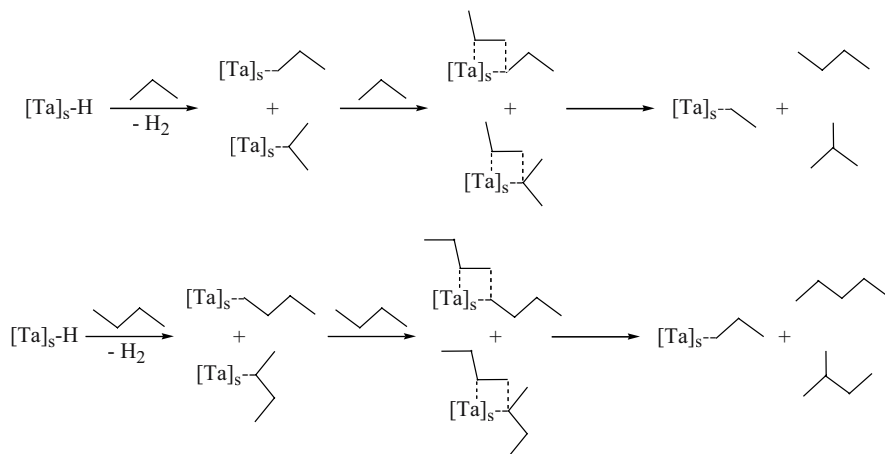
Scheme 8

A distribution of higher and lower homologues is also obtained from propane, butane, pentane as well as from branched alkanes like isobutane or isopentane according to the general equation:



where $i = 1, 2, \dots, n-1$, but with $i = 1$ generally favoured.

It turns out that the reaction is not fully selective even if the C_{n+1} and C_{n-1} alkanes are always the major products. For example the metathesis of butane, in a batch reactor, led to methane (2%), ethane (12,5%), propane (36%), n-pentane (26,5%), n-hexane (10%) and heptanes (4,5%). The other products (8,5%) were mainly isoalkanes. In the case of isobutane, propane and the higher isoalkanes were the major products, n-butane being formed only in very small amount (less than 0,6%), showing that isomerization was negligible. The formation of isoalkanes during the metathesis of n-alkanes can be explained easily by the C-H bond activation step; indeed, it can take place both on primary or secondary carbon atoms, leading to the formation of n-alkyl and sec-alkyl tantalum surface species; these species can further interact with the starting alkane in the gas phase, affording the corresponding linear and iso C_{n+1} alkanes with a selectivity directly governed by their distribution (scheme 9).



Scheme 9

The alkane metathesis reaction turns out to be an equilibrated reaction as indicated by the thermodynamic calculations. For the first terms of light alkanes, the Gibbs energy values ranges between -2 to $0,5$ Kcal/mol, according to temperatures usual for catalytic reactions [34]; this leads to equilibrium conversions ranging between 50 to 90% at 300K and gathering at higher temperatures (Figure 1). As a consequence, it seems that any C-H and C-C bonds of alkane can be involved in such a reaction; in particular, according to the reverse of scheme 7, methane could loose a C-H bond to engage into a C-C bond formation with any alkane.

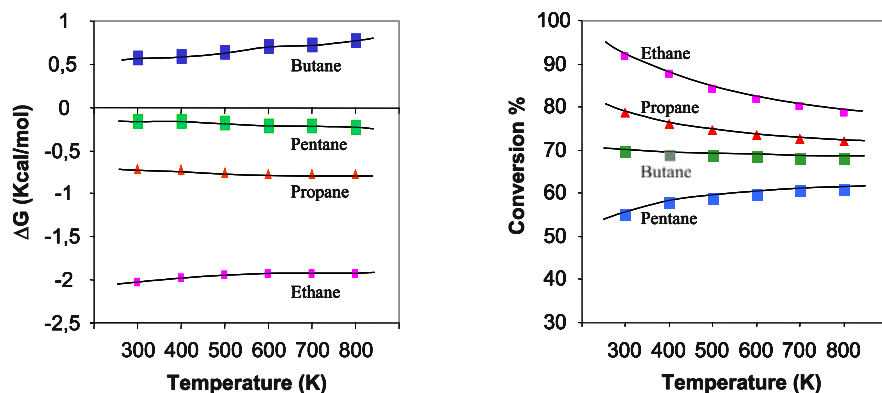
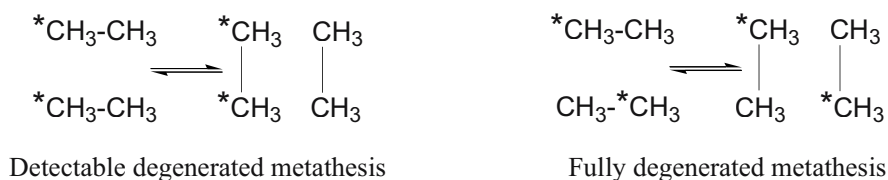


Figure 1. Thermodynamic data concerning the metathesis reaction of various alkanes: $2 C_n = C_{n-1} + C_{n+1}$; a) Gibbs Energy ΔG° ; b) Conversion at equilibrium.

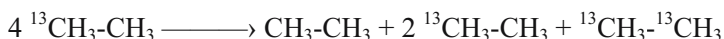
4.2 Metathesis of ^{13}C monolabelled ethane.

When ^{13}C monolabeled ethane was used, the formation of the usual metathesis products, e.g. methane, propane and butanes was still observed (productive metathesis); however, the production of non- and dilabeled ethane was also evidenced indicating the occurrence of a degenerated metathesis process leading to the scrambling of carbon atoms [35]. This detectable degenerated metathesis is necessarily accompanied by an undetectable process (fully degenerated metathesis) where two ^{13}C monolabeled ethane molecules exchange their methyl groups with each other to form two different ^{13}C monolabeled ethane molecules (scheme 10):



Scheme 10

The total scrambling process of ^{13}C methyl groups proves to be at least 5 times faster than the productive metathesis and can be written as follows:



Otherwise, all the propane isotopomers: non-, mono-, di-, and trilabeled propane are formed and their distribution proves to be rather stable all along the reaction time (figure 2); the experimental values (15-39-34-11 or 1.2-3.12-2.72-0.88) are quite close to the statistical distribution (12.5-37.5-37.5-12.5 or 1-3-3-1).

This result brings some interesting information on how the reaction proceeds; if we assume that propane arises from an interaction between an ethane molecule from the gas phase with a tantalum-ethyl species, the consideration of all the possible configurations of such an interaction leads to the conclusion summarized in table 1; if we consider too, the two extreme possibilities, that is ethane in the gas phase and the tantalum-ethyl species can be totally scrambled (distribution 1-2-1) or not (distribution 0-1-0), it turns out that one possibility to reach the statistical distribution in the propane isotopomers is given by the involvement of a totally scrambled tantalum-ethyl species (1-2-1) whatever the isotopomeric distribution of ethane in the gas phase. According to this observation and the results in

figure 2, it indicates that the scrambled ethyl fragment cannot dissociate from the metal before its transformation into propane.

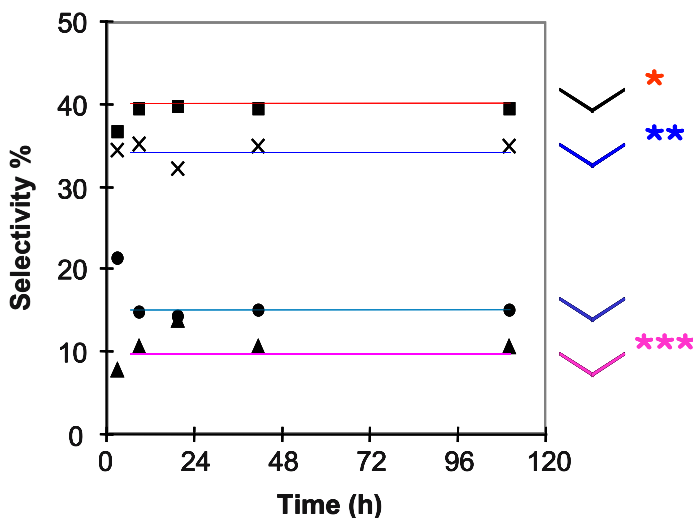


Figure 2. Distribution of propane isotopomers during the metathesis reaction of ^{13}C mono-labeled ethane at 150°C .

Table 1: Theoretical determination of the isotopomeric propane distribution according to those of ethane in the gas phase and of the tantalum-ethyl species (a: experimental values).

[Ta]-C ₂	ethane	propane	methane
0-1-0	0-1-0	0-1-1-0	1-1
0-1-0	1-2-1	0-1-1-0	1-1
1-2-1	0-1-0	1-3-3-1	1-1
1-2-1	1-2-1	1-3-3-1	1-1
		1.2-3.12-2.72-0.88 ^a	

4.3 Stoichiometric Cross-Metathesis of Alkanes.

So far the alkane metathesis reaction was initiated with the supported tantalum hydride **3** as a catalyst precursor whereas surface tantalum-alkyl species are assumed to be involved as intermediates. Then, new experiments were checked using the mixture of alkyl-alkylidene tantalum complexes **2a** and **2b** as catalyst precursors for the metathesis of alkanes from C₂ to C₄. In this case, it turns out that the reaction also proceeds with activities and selectivities quite comparable with those obtained from the tantalum

hydride. More interestingly, the reaction starts with the liberation of neopentane but also some amount of 2,2'-dimethylbutane, 2,2'-dimethylpentane or 2,2'-dimethylhexane depending on whether the initial alkane is ethane, propane or butane (figure 3) [36].

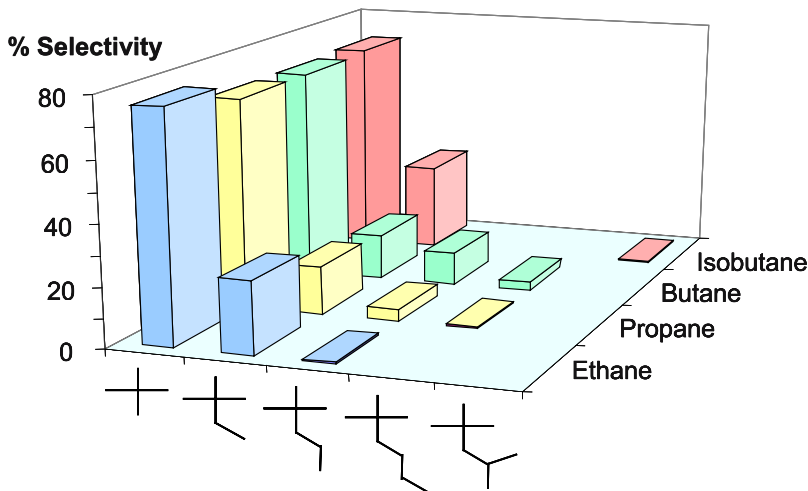
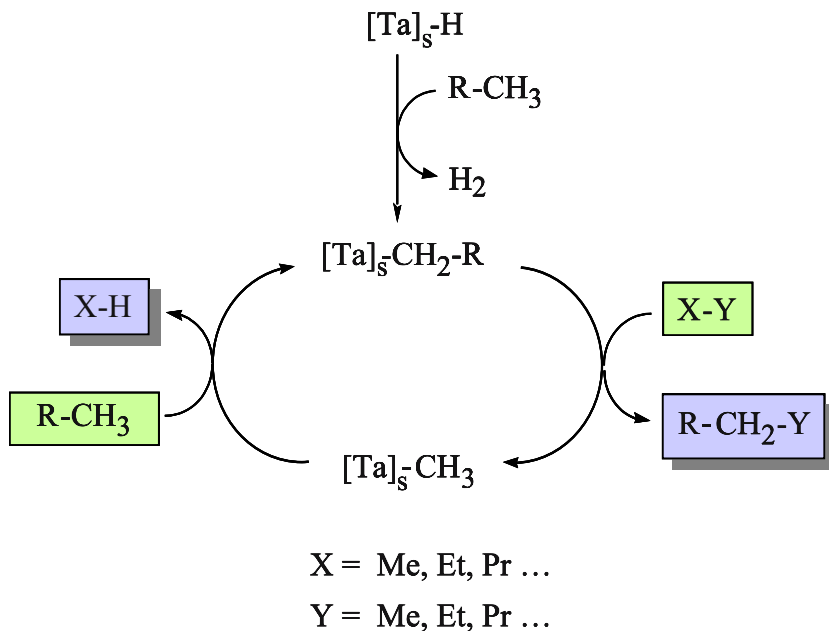


Figure 3: Distribution of cross-metathesis products released during the initiation period of the metathesis of various alkanes catalyzed by complexes 2a and 2b.

Reasonably, neopentane results from a displacement of the initial neopentyl or neopentylidene ligands by the incoming alkane molecule whereas the other products involve the addition of methyl, ethyl or propyl groups respectively, on the same ligands. The liberation of such products illustrates the occurrence of a stoichiometric cross metathesis process. These results also show that the alkane metathesis reaction can be initiated with surface tantalum(V) complexes and that higher alkyl groups like ethyl or propyl can be transferred even if it is in a moderate way compared to methyl. The order of ability to transfer decreases with the increasing size of the groups: hydrogen > methyl > ethyl > propyl.

The occurrence of this stoichiometric cross metathesis reaction opens the route to the investigation of catalytic cross-metathesis processes between two different alkanes where an alkane X-Y could transfer its Y alkyl fragment to a second R-CH₃ alkane and liberate the corresponding X-H hydrocarbon (scheme 11).



Scheme 11

5. CONCLUSION.

In the course of this short review, we have described the formation of various silica-supported tantalum complexes and presented some interesting catalytic properties of these surface species particularly, the tantalum hydride. This hydride was formed after reaction of the tris(neopentyl)neopentylidene tantalum complex **1** with the hydroxyl groups present on silica, then treatment of the obtained alkyl-alkylidene surface species **2a** and **2b** under hydrogen at 150°C. The tantalum hydride ($\equiv SiO$)₂Ta-H **3** can evolve further at 500°C under hydrogen into the tri(siloxy) species ($\equiv SiO$)₃Ta **5**. All these surface species were fully characterized by numerous physico-chemical methods.

The highly unsaturated tantalum hydride shows interesting properties in the stoichiometric C-H bond activation of cycloalkanes and methane but above all, it revealed itself as a catalyst precursor for the new reaction of alkane metathesis which leads to the transformation of an alkane into its

higher and lower homologues. The alkyl-alkylidene surface complexes **2a** and **2b** also proved to be catalytic precursors for the alkane metathesis affording the initial stoichiometric liberation of cross-metathesis products which opens the route to the investigation of catalytic cross-metathesis processes.

6. REFERENCES

- [1] Hill C.L., *Activation and Functionalisation of Alkanes*, Wiley, New-York, 1989.
- [2] Bhasin M.M., Slocum D.W., Eds., *Methane and Alkane Conversion Chemistry*, Plenum Press, New York, 1995.
- [3] Gozin M., Weisman A., Ben-David Y., Milstein D., *Nature* 364 (1993) 699.
- [4] Rybtchinsky B., Vigalok A., Ben-David Y., Milstein D., *J. Am. Chem. Soc.* 118 (1996) 12406.
- [5] Van Der Boom M.E., Ben-David Y., Milstein, D., *J. Chem. Soc. Chem. Commun.* (1998) 917 and references cited therein.
- [6] Watson P.L., Parshall G.W., *Acc. Chem. Res.* 18 (1985) 51.
- [7] Rothwell I.P., *Acc. Chem. Res.* 21 (1988) 153.
- [8] Fendrick C.M., Marks T.J., *J. Am. Chem. Soc.* 108 (1986) 425.
- [9] Thomson M.E., Baxter S.M., Bulls A.R., Burger B.J., Nolan M.C., Santarsiero B.D., Schaefer W.P., Bercaw J.E., *J. Am. Chem. Soc.* 109 (1987) 203.
- [10] Mimoun H., *New J. Chem.* 11 (1987) 513.
- [11] Rabaa H., Saillard J.Y., Hoffmann R., *J. Am. Chem. Soc.* 108 (1986) 4327.
- [12] Watson P.L., *J. Am. Chem. Soc.* 105 (1983) 6491.
- [13] Corker J., Lefebvre F., Lecuyer C., Dufaud V., Quignard F., Choplin A., Evans J., Basset J.M., *Science* 271 (1996) 966.
- [14] Quignard F., Choplin A., Basset J.M., *J. Chem. Soc. Chem. Commun.* (1991) 1589.
- [15] Quignard F., Lecuyer C., Choplin A., Olivier D., Basset J.M., *J. Mol. Catal.* 74 (1992) 353.
- [16] Lecuyer C., Quignard F., Choplin A., Olivier D., Basset J.M., *Angew. Chem. Int. Ed. Engl.* 30 (1991) 1660.
- [17] Quignard F., Lecuyer C., Choplin A., Basset J.M., *J. Chem. Soc. Dalton Trans.* 1994 (1994) 1153.
- [18] Rosier C., Niccolai G.P., Basset J.M., *J. Am. Chem. Soc.* 119 (1997) 12408.
- [19] d'Ornelas L., Reyes S., Quignard F., Choplin A., Basset J.M., *Chem. Lett.* (1993) 1931.
- [20] Dufaud V., Basset J.M., *Angew. Chem. Int. Ed. Engl.* 37 (1998) 806.
- [21] Vidal V., Théolier A., Thivolle-Cazat J., Basset J.M., Corker J., *J. Am. Chem. Soc.* 118 (1996) 4595.
- [22] Shrock R.R., Fellmann J.D., *J. Am. Chem. Soc.* 100 (1978) 3359-3370.
- [23] Lefort L., Chabanas M., Maury O., Meunier D., Copéret C., Thivolle-Cazat J., Basset J.M., *J. Organomet. Chem.* 593-594 (2000) 96-100. Dufaud V., Niccolai G.P., Thivolle-Cazat J., Basset J.M., *J. Am. Chem. Soc.* 117 (1995) 4288-4294.
- [25] Lapointe R.E., Wolczanski, P.T., Van Duyne G.D., *Organometallics*, 4 (1985) 1810-18. Chabanas M., Quadrelli E.A., Fenet B., Copéret C., Thivolle-Cazat J., Basset J.M., Lesage A., Emsley L., *Angew. Chem. Int. Ed.* 40 (2001) 4493-6.

- [27] Taoufik M., De Mallmann A., Prouzet E., Saggio G., Thivolle-Cazat J., Basset J.M., *Organometallics* 20 (2001) 5518-21. Saggio G., De Mallmann A., Maunders B., Taoufik M., Thivolle-Cazat J., Basset J.M., *Organometallics* 21 (2002) 5167-71. Maury O., Saggio G., Théolier A., Taoufik M., Vidal V., Thivolle-Cazat J., Basset J.M., *C.R. Acad. Sci. Paris* 3 (2000) 583-7.
- [30] a) Olivier M.G., Jadot R., *J. Chem. Eng. Data* 42 (1997) 230-33; b) *ibid.* 43 (1998) 568-72; c) Paniego A.R., Guil J.M., *An. Real Soc. Esp. Fisic. Quim.* 69 (1973) 1247-53; d) Paniego A.R., Guil J.M., *J. Coll. Interf. Sci.* 57 (1976) 166-74.
- [31] Vidal V., Théolier A., Thivolle-Cazat J., Basset J.M., *J. Chem. Soc. Chem. Commun.* (1995) 991.
- [32] Weast R.C., Ed., *Handbook of Chemistry and physics* 67th Ed. CRC Press, Inc., Boca Raton, Florida, p.F-178.
- [33] Vidal V., Théolier A., Thivolle-Cazat J., Basset J.M., *Science* 276 (1997) 99.
- [34] Stull D.R., Westrum Jr. E.F., Sinke G.C., *The Chemical Thermodynamics of Organic Compounds*, R.E. Krieger publishing company; Malabar, Florida, 1987.
- [35] Maury O., Lefort L., Vidal V., Thivolle-Cazat J., Basset J.M., *Angew. Chem. Int. Ed.* 38 (1999) 1952.
- [36] Coperet C., Maury O., Thivolle-Cazat J., Basset J.M., *Angew.*

Chapter 6

THE CHALLENGES IN CONVERTING REMOTE NATURAL GAS TO VALUABLE PRODUCTS

David Trimm

CSIRO Petroleum

Kinnoull Grove, Syndal Vic. 3149 Australia

1. INTRODUCTION

The realization that supplies of crude oil are finite and that the known remaining large reserves are mainly located in politically sensitive locations has focused attention on the development and production of alternative fuel sources. These include biofuels, natural gas, and gas derived sources such as liquid natural gas (LNG), liquid petroleum gas (LPG) and the conversion of natural gas to liquid fuels (GTL). The use of LPG and LNG as fuels is well developed, but the large and growing demand for transport fuels emphasises the need for alternative liquid fuels. Although processes to achieve the conversion of natural gas to liquids are well known [1, 2], having been developed early in the 20th century, the capital intensive processes have been regarded as economically unattractive. A potential decrease in the availability of crude oil and a consequent possible increase in price has led to re-assessment of this evaluation and several commercial scale gas to liquids (GTL) plants are now under serious commercial consideration.

Although there are abundant reserves of natural gas in the world, major gas fields supplying large population centres and major markets are being depleted. There are concerns, for example, about gas reserves in America and Europe, where industrial applications, power generation and residential heating annually consume large and increasing quantities of gas. Gas transported by pipeline from Siberia or Alaska provides a finite reserve but access to more remote fields will need to be considered if long term demand

forecasts are to be accommodated. Key factors in this consideration are the economics and practicality of transporting these supplies to market via overland pipeline. Currently the high costs of pipeline construction generally tend to limit economic transport via pipeline to distances up to 5,000 km, at which point alternative means of transport such as LNG or liquid fuels obtained from gas, become more commercially attractive.

The option of transporting gas to market as a liquid raises the prospect of being able to monetise the worlds major gas reserves through linking them to major population centers or regional markets. This has led to active consideration of the exploitation of the large gas reserves in Qatar, Nigeria, Argentina, Trinidad, Sakhalin Island and other more remote locations such as North West Australia.

A further challenge for the development of a world wide gas based fuels industry is that, in many locations there are abundant undeveloped gas reserves located offshore at distances or water depths that make transport to shore by pipeline uneconomic. In Australia, for example, *ca.* 80% of the total 115 TCF gas reserves so far discovered are considered to be stranded or non commercial. The challenge then is to exploit these reserves by offshore processing, either as LNG or GTL products or by some alternative process. Such exploitation must produce products which can compete in the market place with those supplied from more accessible gas fields or, alternatively, to be in position to be brought on stream at a time when more accessible reserves are exhausted.

The market for LNG is very competitive and is dominated by major players. As a result, conversion of gas to liquid fuels to meet the growing demand for transport fuel is a particularly attractive option. The magnitude of this interest is demonstrated by the fact that more than 15 GTL project developments are currently under commercial consideration world wide. The number of plants that will eventually be built will depend on market demand, gas prices, government incentives and fiscal support, as well as on technical advances that reduce the cost of conversion and improve the return on the significant level of funds invested.

The most commonly considered scenario for these GTL processes is well established. Natural gas is converted to syngas (a mixture of carbon monoxide and hydrogen) which is then converted to synfuel via the Fischer-Tropsch process. It is also possible to generate syngas from coal or biomass, but the cost is generally greater and carbon dioxide (an unwanted greenhouse gas) generation is higher. The capital cost of a GTL plant has been estimated to be of the order of US\$ 750M for a 30,000 BPD plant (US\$ 25,000/BPD) [3], and the process technology is closely patent protected [1, 2]. As a result, commercial exploitation so far has been limited to only a few major players, who direct their attention to large gas reserves

where favourable gas prices and financial or tax advantages exist. Even then, the size of the investment is such that only a limited number of plants will be built at any given time.

The problems associated with the exploitation of remote natural gas are even greater, particularly in the context of developing offshore gas reserves. The location, the weather to be expected and the necessity to erect plant on a platform or a vessel introduces new challenges and a new set of boundary conditions. These are the subject of the present text, with some suggestions as to possible lines of research and development.

2. APPROACHES TO THE PROBLEM

A major objective for any GTL process is to reduce capital cost. This is intensified for remote gas, where the size of a vessel or platform will limit the size of the process plant. Thus, for example, the North Rankin platform (one of the largest gas producing platforms in the world) which is located offshore in north West Australia has an area of 60 x 38 m (and a weight of 54,000 tons) while a deck space of *ca.* 25,000 m² has been suggested for a suitable floating production and processing vessel [4]. In contrast a compact land based unit should cover *ca.* 20,000 m² and *ca.* 60,000 m² for storage. Based on a typical GTL plant configuration a process facility located offshore would currently be limited to a capacity of the order of 5-15,000 BPD. The economics of scale may well be limited. The options then become either to reduce the size or the number of units on the vessel, to change the process or to produce an intermediate easily transportable liquid which can be upgraded at an on-shore facility.

This immediately suggests that size and the number of units associated with a remote GTL plant should be minimized. It also suggests that it may be necessary to think outside the boundaries of conventional GTL processes. As a result, attention is focused here both on conventional syngas/Fischer-Tropsch processing and on possible alternatives.

3. CONVENTIONAL GTL PROCESSES

3.1 Syngas production

The production of syngas involves the conversion of natural gas to syngas which, in turn, is converted to syngas. *ca.* 65% of the overall cost is associated with the production of syngas.

Several routes to syngas are possible and different processes give different ratios of carbon monoxide to hydrogen.



Selectivity to C_5+ products in the subsequent Fischer-Tropsch process increases with decreasing $\text{H}_2:\text{CO}$ ratios [5] and a ratio of *ca.* 2 is preferred. The most common means of achieving this ratio is via partial oxidation (POX) or autothermal reforming (ATR [6]) possibly combined with gas heated reforming (GHR [6]). Autothermal reforming involves combustion of part of the fuel inside the reactor in order to produce the heat needed for endothermic reforming (reactions 1 and 2).

Both ATR and POX involve the reaction of gas with oxygen and, under conventional conditions, this is supplied by air separation [3, 6]. Systems have been designed using air [7], but the residual nitrogen has to pass through the Fischer-Tropsch reactor and reduces partial pressure and efficiency. As a result, air separation prior to syngas manufacture is favoured.

Conventional air separation plants can be mounted on a vessel [4] and operate even when rocking in a swell-albeit with reduced efficiency. However, considerable effort has been focused on the development of an ion transport membrane for oxygen production that may reduce significantly the cost of syngas [8]. These inorganic membranes show much promise, with estimates of saving on installed capital ranging from 20 to 50%, but have yet to be commercialized.

Although oxygen based syngas production is efficient, avoidance of an air separation process has the potential to save space on a platform or offshore facility. This re-directs attention towards steam and dry reforming, which are carried out with external firing in a furnace box [6]. Steam reforming produces a hydrogen rich syngas (reaction 1), but combination

with dry reforming (reaction 2), for example leads to the desired CO: H₂ ratio. Such a system has been considered for commercial application [9, 10], with a pre-reformer used to reduce the size of the tubular reformer by some 13% [10]. Systems involving dry reforming may be particularly advantageous when the gas reserve contains carbon dioxide.

The high temperatures of operation of reforming processes introduce problems of coking, which can be minimized by control of the steam:carbon ratio [6]. Supply of water to an offshore rig is expensive but the excess heat from the furnace block could be used to raise steam and distill fresh water from sea water.

One of the problems with reforming is the size of the furnace. Tubular reformers may contain up to 1,100 tubes, some 7-12 m in length, with the unit weighing some 12,000 tons. They are usually constructed on site which adds to the difficulties. One alternative is the gas heated reformer (GHR), which involves a combination of two reactors [6]. *Ca.* 75% of the natural gas is reformed in the first reactor at about 1,000 K and 40 atms pressure. The second reactor is an autothermal system (ATR) where residual methane is oxidized to produce more syngas and a hot gas stream which is used to heat the first reactor.

The size of the system is significantly reduced, but the GHR introduces some new problems. The obvious one is the need for an oxygen separation plant for the ATR reactor with all the associated space requirements. The second arises from metal dusting – a corrosion process that occurs on alloy surfaces exposed to carbon monoxide at temperatures between *ca.* 750 and 1050 K [11]. Metal dusting leads to tube failure, and there is considerable work in progress to research cause and prevention – mainly by choice of suitable alloys [12]. Some companies have announced that the problem is solved while others continue to do research even at a pilot plant scale.

Another option to reduce the size of plant required for reforming, currently under consideration, is the integrated compact reformer built into a synfuel pilot plant at Nikiski, Alaska [13]. The reformer tubes are heated by enhanced convection rather than by radiation and this leads to major space saving. A compact reformer for a 17,000 bpd synfuel plant is stated to weigh about 4,000 tons and can be manufactured off site and delivered as a 7,500 ton module [13].

The process is based on steam reforming, associated with a membrane separator for hydrogen. However there seems to be no reason not to combine steam reforming (SR) with dry reforming (DR) to produce syngas of the desired composition.

Pilot plant testing has been carried out at Warrensville, USA and a small unit has just come on stream in Alaska. It will be very interesting to follow the test results in the context of possible offshore applications.

The processes discussed above produce syngas by reacting natural gas with water or carbon dioxide, but it is also possible to react natural gas with oxygen to produce syngas (reaction 3). Although the theoretical yields give a ratio of CO:H₂ of 1:2, other, more exothermic reactions can occur which may affect the selectivity.



Non catalytic partial oxidation is used in industry and has the advantage of lower capital cost and simplicity of operation [6]. The reaction is carried out at temperatures of the order of 1,300-1,400 K, which is high enough to favour non-catalytic reforming. As a result, the exit gases are close to thermodynamic equilibrium and some carbon is produced by thermal cracking. The CO:H₂ ratio produced is somewhat higher than desired, and an alternative source of hydrogen may be needed.

The homogeneous reaction can be operated at high pressures and the reactor assembly is cheap. On the other hand, an oxygen plant is necessary, which increases cost and space requirements.

Catalytic partial oxidation reactions (CPOX) has also attracted much attention in recent years [6]. The selectivity of the reaction is excellent, the process is carried out at high temperatures using millisecond residence times [6]. This results in small monolithic catalyst beds, which would appear to be ideal for remote location operations. Unfortunately, industrial application has not been developed since methane/oxygen mixtures need to be fed to the reactor under flammable or near explosive conditions. In addition, the space requirements of the oxygen plant and of the heat exchanger (required to drop the exit gas temperature from *ca.* 1,100 K) are considerable.

Pene *et al* [6] report an economic summary of the relative costs of producing syngas via different processes. This showed that gas heated reforming was significantly cheaper than steam reforming, a conclusion also reached by Hansen *et al* [5]. Dybkjaer and Christensen [14] favour ATR, but their calculations are more relevant to larger scale plants.

Thus the production of syngas from natural gas in the context of remote gas fields introduces interesting optimization problems. From a size viewpoint, the integrated compact reformer appears to offer many advantages – but the design has not been extensively tested at a pilot plant scale. In addition, the process is based on steam reforming, which will give a

high $H_2:CO_2$ ratio. This could be adjusted through the use of a hydrogen separation membrane and using the hydrogen for electricity generation, or by combining steam reforming with dry reforming – a concept not yet examined in this system.

Alternatively, non catalytic partial oxidation, GHR or ATR offer many advantages, but suffer from cost and size demands. Cryogenic oxygen separation is expensive, particularly for a small syngas plant as would be the case offshore. Oxygen transport membranes are predicted to be able to reduce by better than 35% the cost of syngas [8], but have yet to be developed commercially. Commercial flux targets are only met by operation above 1,200 K with conventional membranes, but research has improved performance at lower temperatures [8]. As a result, membrane separation remains a promising but as yet unproven means of separating oxygen from air.

Of the oxygen based processes, non catalytic partial oxidation does produce syngas containing less hydrogen than desired. On shore, this is corrected by a small steam reformer, but the dictates of space limit this combination offshore. As a result, GHR or ATR appear to offer the most promising source of syngas, provided an oxygen supply is available.

3.2 Syngas conversion

Classic Fischer Tropsch processing to convert syngas to synfuel is well established, and significant advances have been made in catalyst technology [1, 2, 15] and reactor design. Cobalt based catalysts have been found to be effective, but iron based catalysts are also in use, being particularly suitable for the processing of syngas derived from coal.

In the context of the exploitation of remote gas, the need is to produce material that can easily be transported. Much conventional Fischer-Tropsch processing produces waxes, which are hydrocracked to produce diesel [16] and other material. The inclusion of a hydrocracking unit on board a vessel has been suggested [4], but the alternative would be to transport wax to an on-shore site for processing. This may mean the application of heat in order to maintain wax in the liquid state.

The Fischer Tropsch process leads to the formation, over an appropriate catalyst, of products essentially made up of more than 90% *n*-paraffins together with olefins and alcohols. The molecular weight distribution follows the Anderson-Flory-Schultz model [17], and a wide range of products is produced under conventional conditions. Cobalt-based catalysts produce *ca.* 5-20% naphtha, 40-60% $C_{10} - C_{22}$ and 60 – 40% heavier

products [16]. Iron-based catalysts favour somewhat lighter product ranges. Adjusting the reaction conditions to favour more liquid products does not necessarily help, since the as produced material does not have good cold flow properties and the amount of unwanted gaseous products increases.

All in all, the inclusion of a mild hydrocracking unit on board the vessel or platform seems desirable provided sufficient space is available. It simplifies transport requirements and produces fuel that can be taken to a distribution centre direct.

Choice of a reactor introduces some complexity [18] Lowe *et al* [4] favour a fixed bed system, in order to minimize the effects of list and wave motion. However, modern technology favours the use of slurry bed systems [19] where vessel movement should not be a disadvantage with careful design. Such reactors also have the advantage of a lower profile, which can have real advantages with respect to insurance requirements for tall structures on board vessels.

Overall, the best alternative would seem to be a slurry reactor with an associated mild hydrocracking system.

Although some of the designs and assumptions may not be totally appropriate, the assembly of a combined syngas/synfuel process on a vessel has been considered by Lowe *et al* [4]. They show that it is possible to assemble an oxygen blown plant on a vessel some 300 m long and 53 m wide, with a total deck space of 22,100 m². The size of the superstructure dictates hull size, and the resultant storage space for liquid fuels is high (*ca.* 1,240,000 bbls).

The high point loading of some of the reactors does mean that a purpose built vessel will be required, and this will add to the cost. Catalyst replacement and handling will also be difficult. However, both oxygen blown [4] and air blown [20] plants have been seriously considered for offshore exploration.

The disadvantage with conventional processing lies in the continuing generation of greenhouse gases, although partial oxidation tends to give a CO:H₂ ratio of the desired value without too much CO₂ generation. One can optimize most systems to minimize emissions, but disposal of carbon dioxide by, for example, sequestration will be difficult or impossible from an offshore operation. Thus the sustainability of such operations will always be questionable to an extent that depends on the actual processes in use.

4. ALTERNATIVE TECHNOLOGY

The problems of sustainability with conventional processing are concerned with carbon dioxide generation, and alternative routes to synfuel which minimize such emissions are desirable. One such route is based on methane pyrolysis to acetylene, followed by acetylene processing to produce a more gasoline like product.

The basis of the process has been discussed elsewhere [21]. Methane is flash pyrolysed to acetylene, which is then oligomerised over a zeolite catalyst to produce hydrocarbons as shown in Table 1 [22]. The product is seen to be consistent with gasoline, and the average molecular weight is 98.4 [22]. The small amounts of light hydrocarbons produced can be recycled through the pyrolysis stage [23], while the heavier hydrocarbons could be separated for middle distillate or combusted to provide some of the heat needed for pyrolysis.

Not surprisingly, the process is more complex than the description above. Pyrolysis of methane may be achieved using a plasma furnace, an electric arc or a thermal reactor. Hall *et al* [21] gain part of the necessary heat by combusting excess hydrogen produced in the reaction, but the necessary temperature (*ca.* 1,600K [23]) may require combustion of some of the natural gas.

Table 1. Typical product distribution from pyrolysis/oligomerisation: adapted from ref. 22.

Component	Mol %	Component	Mol %
Ethane	0.180	Ethylcyclopentane	0.488
Propane	3.143	Trimethylpentanes	0.701
Isobutane	4.511	Toluene	6.164
n-Butane	6.440	Methylheptanes	2.130
2,2 Dimethylpropane	0.016	Dimethylcyclohexanes	0.465
Isopentane	9.703	Methylethylcyclopentanes	1.384
n-Pentane	5.817	Ethylbenzene	2.708
Dimethylbutanes	0.683	Xylenes	9.597
Methylpentanes	8.199	n-Octane	0.276
n-Hexane	2.577	Nonane Paraffins	1.394
Methylcyclopentane	1.655	Nonane Naphthenes	1.012
Benzene	0.755	Nonane Aromatics	3.143
Cyclohexane	2.844	Decane Paraffins	6.871
Dimethylpentanes	2.539	Decane Naphthenes	0.593
Methylhexanes	1.674	Undecanes	2.685
Dimethylcyclopentanes	1.230	Dodecanes	1.232
n-Heptane	0.771	Tridecanes	1.130
Methylcyclohexane	1.161	Tetradecanes +	2.317

The process demands millisecond residence times in order to minimize coke production, and rapid quenching is essential to obtain larger yields of acetylene. This is usually done using a water quench, which requires provision and removal of water to the gas stream and an extra heat exchanger to cool the gas to the oligomerisation catalyst temperature.

Liquid products are separated from the exit stream of this reactor, while gaseous products are compressed to remove useful fuel and then taken to a separation unit. Hydrogen and methane are returned to the pyrolysis unit.

Catalytic processes require removal of sulphur from the feedstock to minimize catalyst deactivation. While removal of sulphur is not a requirement for pyrolysis processes, it is desired, mainly because sweeter fuels are more profitable and removal of sulphur from the feedstock is probably easier.

As compared to the syngas/synfuel route, the process has the advantage of relative simplicity and of a more desirable product. This has been suggested to lead to a reduction in CAPEX to *ca.* \$17,000/bbl/day, but the process is still only at the pilot plant stage and such estimates may be optimistic.

However, the process footprint can be expected to be smaller, and catalyst management is limited only to the second reactor. Both of these attributes make application to remote location gas seem attractive but, again, it is essential to review carefully the results of pilot plant testing as they become available.

5. SUMMARY

The realization that supplies of crude oil based liquid fuels are finite has focused attention on alternative fuels and, in particular, fuels based on natural gas. Various possibilities exist, but the future demand for environmentally sensitive transport fuels favours GTL processes. Existing processes based on large, easily accessible gas fields currently provide only marginal returns but the economics are expected to improve with the next generation of larger scale plants. Large gas reserves located in remote locations pose additional economic and technical problems.

As a result, the upgrading of remote location gas, with or without sustainability, is at an interesting stage with an unknown future. Conventional Fischer-Tropsch processing would be much improved with the successful development of the ion transport membrane for oxygen separation, and the further development of the integrated compact reformer. The alternative pyrolysis/oligomerisation route to synfuel appears to offer

much promise, but pilot plant testing is still underway. In all cases, CAPEX and OPEX will have to be examined carefully, particularly in the context of the relatively small GTL plants that can be accommodated on a platform or vessel.

It is only when these initial problems have been solved that the questions of sustainability may be addressed. The pyrolysis/oligomerisation route does seem to have advantages, but much development work is required before the first plant is constructed.

There seems to be no show-stopper on the construction and operation of a remote location GTL plant except the demands of economics. One doubts that serious attention will be directed to remote gas while large reserves remain that are easily accessible. This has the advantage of allowing time for process development, provided the long term necessity of upgrading stranded gas is recognized as a future necessity.

6. REFERENCES

- [1] Schultz, H.(1999) *Appl. Catal. A. General* 186,3
- [2] Van der Laan, G.P. & Beenackers, (1999) *Catal. Revs. Sci. Eng.* 41, 255
- [3] Gradassi, M.J.: (2001) *Studies in Surface Science & Catalysis* (ed. Spivey, J.J., Iglesia, E. & Fleisch, T.H.) p429 Elsevier Science BV
- [4] Lowe, C., Gerdes, K., Stupin, W., Hook, B. & Marriott, P.: *Ibid* p57
- [5] Hansen, R., Sogge, J., Wesenberg, M.H. and Olsvik,: O. *Ibid* p405
- [6] Pena, M.A., Gomez, J.P. & Fierro, J.L.G: (1996) *Appl. Catal. A General* 144, 7
- [7] Schubert, P.F., Bayens, C.A., Weick, L. & Haid, M.O. (2001) *Studies in Surface Science & Catalysis* (ed. Spivey, J.J., Iglesia, E. & Fleisch, T.H.) p459 Elsevier Science BV
- [8] Mazanec, T.J., Prasad, R., Odegard, R., Steyn, C. & Robinson, E.T.: *Ibid* p147
- [9] Wakatsuki, T., Morita, Y., Okado, H., Inaba, K., Hirayama, H., Shimura, M. Kawazuishi, K., Iwamoto, O., & Suzuki, T., *Ibid* p117
- [10] Holm-Larsen, H., *Ibid* p441
- [11] Grabke, H.J., Krajak, R. & Müller-Lorenz, E.M. (1993) *Werkst. Korros.* 44,89
- [12] Grabke, H.J., Müller-Lorenz, E.M., Klöwer, J. & Agarwal, D.C. (1998) *Materials Performance* 37,58
- [13] Font Freide, J., Gamlin., T. & Ashley, M.: (Feb 2003) *Hydrocarbon Processing* p52
- [14] Dybkjaer, I. & Christensen, T.S. (2001): *Studies in Surface Science & Catalysis* (ed. Spivey, J.J., Iglesia, E. & Fleisch, T.H.) p435 Elsevier BV
- [15] Bromfield, T.C. & Vosloo, A.C. (2003) *Macromolecular Symposia* vol 193 p 2934
- [16] Colemma, V., Peratello, S., Pavoni, S., Clerici, G. & Parego, C. (2001) *Studies in Surface Science & Catalysis* (ed. Spivey, J.J., Iglesia, E. & Fleisch, T.H.) p 307 Elsevier BV
- [17] Andersen, R.B. (1984) *The Fischer Tropsch Synthesis*. Academic. N.Y.
- [18] Davis, B.H.: (2002) *Catalysis Today* 71,249

- [19] Krishna, R., Van Baten, J.M., Urseanu, M.I. & Ellenberger J., (2001) Chem. Eng. Sci. 56, 537
- [20] Hutton, J. (2003) Fundamentals of Gas to Liquids p38 The Petroleum Economist London ECI
- [21] Trimm, D.L., Alternative Routes to Synfuel from Natural Gas: this volume page XXX
- [22] Hall, K.R., Akgerman, A., Anthony, R.G., Eubank, P.T., Bullin, J.A., Cantrell, J.G., Weber Jr., B.R. & Betsill, J.: (2002) APPEA Journal p59
- [23] Holmen, A., Olsvik, O. & Rokstad O. A. (1995) Fuel Processing Technology, 42, 249.

Chapter 7

ALTERNATIVE ROUTES TO SYNFUEL FROM NATURAL GAS

David Trimm

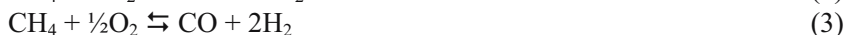
CSIRO Petroleum

Kinnoull Grove, Syndal Vic. 3149 Australia

1. INTRODUCTION

The realization that world reserves of crude oil are limited has focused attention on the conversion of coal and gas to synthetic liquid fuels (synfuel). Suitable processes have been developed for the conversion, but a combination of economic and environmental constraints has limited their wide applicability. As a result, the more efficient production of higher value products from natural gas and coal remains a major objective.

The conversion of natural gas to methanol or to synfuel is the most widely practiced route to add value. Methane is first converted to syngas, which is then processed to give hydrocarbons and alcohols (1-5):



The production of methanol (reaction (4)) is an important industrial reaction. The production of synfuel via the Fischer-Tropsch process (reaction (5)) is economically less attractive and is practiced in only a few locations. However, the expected future shortage of crude oil has led to

serious consideration of wider scale applications and to detailed studies of the associated environmental problems [1].

The obvious attractions of the direct processing of natural gas to obtain more valuable products has led to the study of oxidation (oxidative coupling, (OCM [2], NO catalysed oxidation [3] and direct oxidation to formaldehyde [4]), of reactions of natural gas with halides or sulphates [5] and of pyrolysis based reactions – which are the subject of the present text. Of these, only pyrolysis has been exploited industrially and, even then, only on a limited scale [6].

The thermal processing of natural gas is best explained in terms of the thermodynamics of simple hydrocarbons (Figure 1) [7]. Natural gas consists mainly of methane, which is seen to be more stable than carbon and hydrogen below 803 K. The production of other hydrocarbons is not favoured until *ca.* 1,300 K where the production of benzene is favoured. The production of acetylene is favoured at temperature above *ca.* 1,400K. Thus the most promising conversion routes for natural gas would appear to involve carbon formation, benzene formation or acetylene formation.

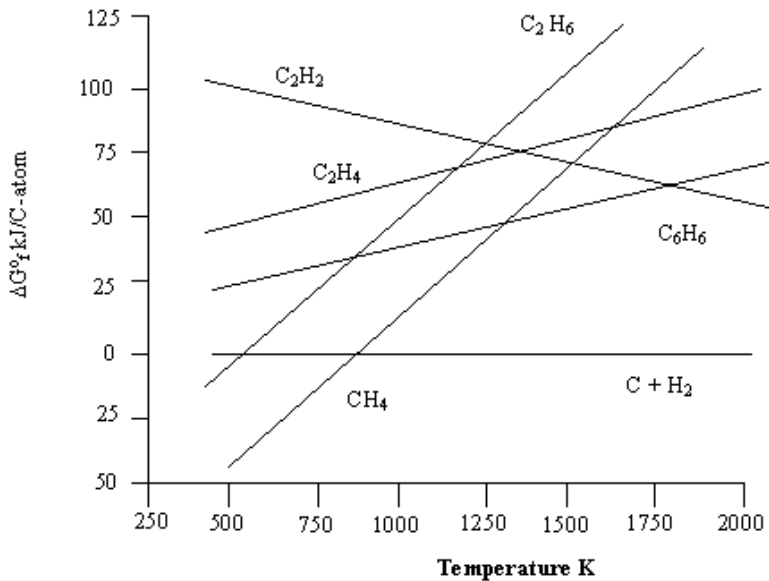


Figure 1. Methane Pyrolysis: Standard free energy of formation (ΔG_f^0) of products as a function of temperature (K).

Thermodynamic calculations have been extended by Gueret [8] to predict the yield of products at various temperatures (Figure 2). Although the formation of carbon is not shown, it is clear that different products may be produced at different temperatures and that the production of hydrogen and acetylene is favoured at temperature in excess of 1,400 K. As would be expected from figure 1, benzene and ethylene are also produced, but not in particularly large amounts.

Exploration of the opportunities predicted by the thermodynamics can conveniently be considered as three routes; via carbon, via conversion to aromatics and via high temperature pyrolysis. Of these, only the latter has been developed industrially.

It is also obvious that most of the products of pyrolysis are not necessarily economically attractive. Thus any consideration of upgrading natural gas by this route must include subsequent processing of pyrolysis products. Luckily, most of these are valuable intermediates which can be converted to more useful end products. This processing is also considered in this article.

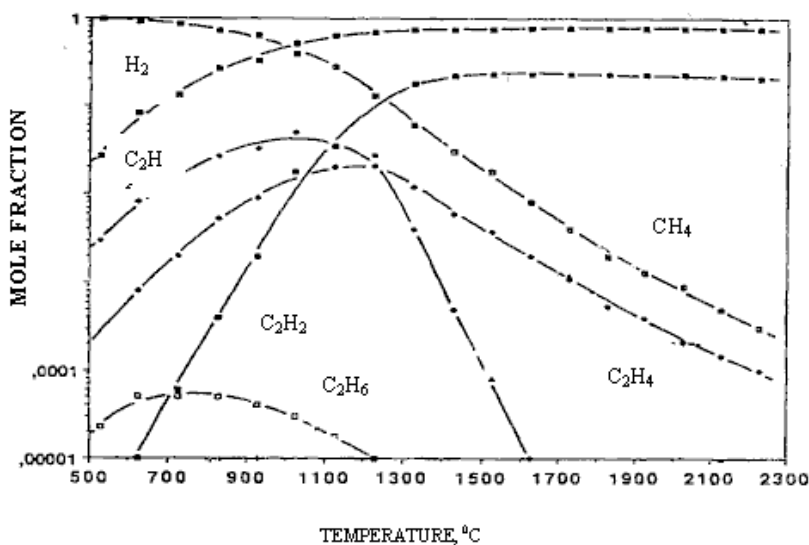


Figure 2 Mole fractions of products in gas-phase equilibrium calculated from thermodynamic data. Total pressure = 1 bar, H:C = 4: adapted from Gueret [8].

2. NATURAL GAS CONVERSION VIA CARBON

The possibility of obtaining higher value hydrocarbons from natural gas via carbon was first recognized by two groups in 1991 [9, 10]. The basis of the conversion essentially rests on the fact that reactive forms of carbon can be obtained by decomposition of hydrocarbons at relatively low temperature (Figure 1).

Van Santen and co-workers [9] developed a two stage process, where methane was decomposed on silica supported Ru, Rh and Co at 700 K, followed by hydrogenation of surface carbonaceous species at *ca.* 373 K. The products of reaction obeyed the Flory – Schulz – Anderson distribution pattern, with a maximum yield of 13% C₂₊ hydrocarbons over Ru/SiO₂.

Amariglio *et al* [10] studied the same reaction but under isothermal conditions. The two stage process, operated at 523 K, gave 19% conversion of methane to C₂₊ hydrocarbons.

Ru was again found to be the most active catalyst, with optimal C₂₊ yields of *ca.* 37% being obtained on hydrogenation at 433 K. The thermodynamic limitations could be adjusted by removal of hydrogen in the carbon deposition stage, followed by supplying hydrogen during the hydrogenation stage, but the increase in yield was too small for industrial exploitation.

There are striking differences between the product spectra from the two processes and this has led to some controversy over the reaction mechanism [6]. The evidence appears to favor formation of a C-C bond during methane decomposition rather than during hydrogenation [6].

Although the reaction is of considerable academic interest, particularly with respect to the formation and reactivity of various carbonaceous species [11], the process suffers from deactivation on repeated cycle operations [12]. The catalysts could be rejuvenated by oxidation of carbonaceous deposits but avoidance of carbon deposition is highly desirable.

Some progress in this direction has been made by the use of bimetallic catalysts. Guczi *et al* [13] found that Co-Pt/NaY zeolite supported catalysts gave complete conversion of methane with *ca.* 84% C₂₊ selectivity. Garnier *et al* [14] used a Pd-Ag membrane to enhance removal of hydrogen and to allow lower temperature decomposition of methane. No deactivation was observed, but testing was limited to six cycles.

The most probable reaction pathway involves the formation of active C α [11]. Inactive C γ may be formed over some catalysts and conversion of C α to C γ can be expected over all catalysts in the fullness of time. As a result, an inactive C γ layer can be expected to accumulate on the surface and slowly to deactivate the catalyst – inferring that all catalysts will, eventually,

became encapsulated and inactive for methane decomposition. This, coupled with the necessity to operate through two cycles, will almost certainly preclude industrial application.

It is interesting to note that the products of reaction follow the Flory-Schulz-Anderson distribution and, as such, will mainly produce useful hydrocarbons. Provided these can be separated and captured, there should be few expectations of producing unwanted greenhouse gases.

3. CONVERSION TO AROMATICS

A second approach to the direct upgrading of methane was pioneered by Wang *et al* [15] in 1993, who discovered that zeolitic materials promoted the conversion of methane to benzene. MoZSM-5 catalysts were found to offer the best activity (*ca.* 7%) with high selectivity to benzene. Subsequent studies [16] showed that various factors affected catalyst performance.

Methane conversion was found to vary with the nature of the transition metal ion on the zeolite [17]



but 2-3% metal loading was critical. Larger loadings led to pore blockage, an effect which appears to be dependent, at least in part, on carbon formation [18]. However, the deposition of carbon was found to be critical, in that clusters of molybdenum carbides were formed within well defined zeolitic channels containing Brønsted acid sites [18]. This combination was found to promote the formation of aromatics – both benzene and naphthalene.

The addition of a second metal ion has also been found to increase activity and selectivity, with Fe-, Co- [19] and Cu-Mo/ZSM-5 [20] improving activity and selectivity.

The zeolite structure and acidity were found to play an important role in determining catalyst activity and selectivity [21]. Zeolites containing two dimensional pore diameters of the order of the dynamic diameter of benzene (*ca.* 0.6 nm) offered best performance. In practice, HZSM-5 supports have been widely used but MCM-22 also yields *ca.* 80% selectivity to light aromatics [22].

Work by Howe *et al* [23] and Lunsford *et al* [18] has clarified some aspects of the process. An induction period observed with fresh catalysts is associated with the production of coke modified MoC_x clusters. At steady

state, *ca.* 8-10% methane could be converted to give *ca.* 70% selectivity to benzene. Naphthalene could be produced (*ca.* 20% selectivity) but the production dropped away, presumably as a result of steric hindrance caused by the formation of carbonaceous species in the pores.

Some interesting results have been obtained by removing and co-feeding components that could well be present in natural gas. Liu *et al* [24] investigated the effect of the continuous removal of hydrogen during the reaction. Methane conversion at 900 K was increased slightly (*ca.* 7%) but C_{12+} selectivity improved and deactivation increased. The co-feeding of small amounts of carbon dioxide gave much improved C_{2+} - C_{12+} selectivities and minimised deactivation.

Choudhary *et al* [23] achieved high conversions over a galloaluminatite substituted HZSM-5 by co-feeding methane with higher hydrocarbons, apparently as a result of enhanced hydrogen transfer. Despite this, conversions and selectivities appear to be too low to encourage industrial exploitation, but again the reaction produces a minimum of greenhouse gases.

4. HIGH TEMPERATURE PYROLYSIS

As would be anticipated from the thermodynamics, methane can be directly converted to C_2 hydrocarbons by thermal coupling. More than 90% selectivity may be obtained, with high yields of acetylene (>85%) being obtained under optimal conditions (high temperatures and short residence times). Despite the fact that the reaction is highly endothermic and that coke is liable to be formed, the reaction has been exploited industrially over several years.

The thermal dissociation of methane starts to become significant at *ca.* 750 K and is complete by 1,200 K. At these temperatures, carbon and hydrogen should be formed (figure 1), but the rate of formation of unsaturated compounds (acetylene and ethylene) is much faster than complete decomposition [32]. Optimal yields of acetylene can be expected at around 2,000-3,000 K.

The overall reaction can be described as a free radical process involving stepwise dehydrogenation of methane (Figure 3).

The Huels process has been using an electric arc to produce acetylene since the 1940's [33]. A wide range of feed stocks (from low boiling components of fuels to methane and natural gas) was passed through an electric arc at millisecond residence times to give up to *ca.* 50% yield of acetylene [33]. A modified process from Dupont magnetically rotated the

arc to give *ca.* 65-75% yield of acetylene [32]. In both cases, rapid quenching of the exit gases is an essential.

Plasma jets in which natural gas is injected into a stream of hot gas have also been investigated using *ca.* 10 kW units [34]. Acetylene yields of 75-85% have been reported [34, 35] but no full scale plant has been developed.

BASF has taken a different path to acetylene, using the so-called Sachsse process [36]. Natural gas and methane are preheated before entering a specially designed burner that gives a stream of gas containing *ca.* 8% acetylene. This gas is stripped of carbon dioxide, compressed and adsorbed into a suitable solvent. Subsequent separation gives 99.8% pure acetylene.

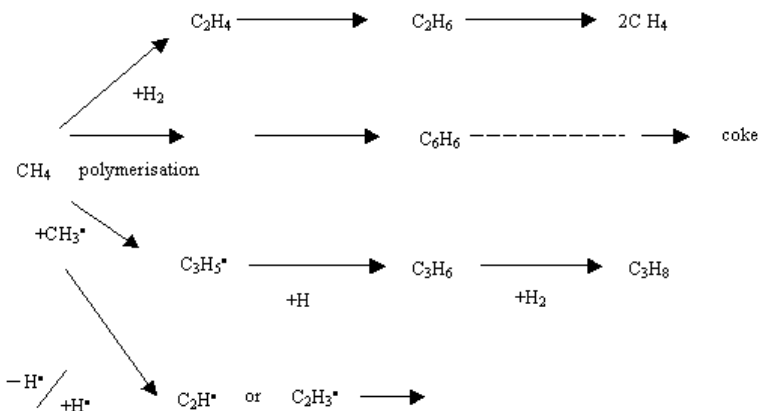


Figure 3. Possible reactions of acetylene. All are probably free radical reactions and further reactions of products with or separate from acetylene are possible.

The process has the advantage of producing valuable by products and the disadvantage of producing carbon dioxide – a greenhouse gas. Nevertheless, there is considerable industrial operating experience with the process [36], with plants built in Germany, Italy and the U.S.

Hall *et al* [37] have focused attention on an electrically heated furnace, although there are indications that hydrogen combustion may be used to increase operating temperature. A pilot plant, operated in conjunction with acetylene to gasoline, has been described [37].

It is clear that methane and natural gas pyrolysis offers a route to acetylene that is of some commercial interest and that has the advantage of minimising greenhouse gas emissions.

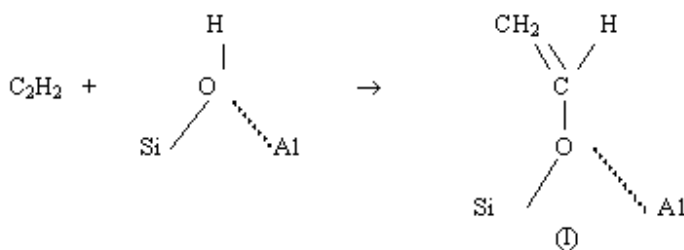
5. ACETYLENIC FEEDSTOCKS TO SYNFUELS

The use of acetylene as a chemical intermediate to a range of useful products has been well described [38]. Until the advent of cheap olefins, acetylene based chemistry was considered to be of great potential. Most acetylene processing was based on polymerisation or hydrogenation [38] but Reppe and Wolfe [39], as early as 1934, reported a reaction with methanol to produce dimethoxyethane, an excellent cetane enhancer for diesel.

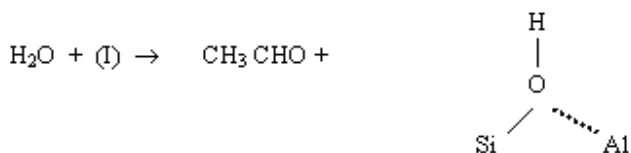
A major breakthrough occurred with the recognition that acetylene could be converted to liquid hydrocarbon fuels by reaction over zeolitic catalysts [40, 41]. Thus, Tsai and Anderson [41] reported that ZSM-5 catalysts converted up to 40% of acetylene to (predominantly) C₁₀ and C₁₁ aromatics. Operated at > 530 K, it was suggested that Brønsted acid sites in the zeolite pores catalysed first the polymerisation via vinyl cations followed by cyclisation to produce aromatics.

Deactivation of the catalyst was reported but He *et al* [42] have shown that metal modified zeolites can be used with minimal coking. The main modifying metal was nickel and steam was added to enhance gasification. Up to 93% conversion to 11% olefins, 67% paraffins and 21.5% aromatics could be achieved by operating a 13% Ni/ZSM-5 catalyst at 823 K, with a steam:acetylene ratio of 0.63.

In contrast to Pereira *et al* [43] and Anderson [41], who favour acid catalysed polymerisation/cyclisation, He *et al* [42] argue the importance of a vinyl alkoxy intermediate in the presence of steam.



which, in turn, reacts with steam to form acetaldehyde



Aldehydes were observed among the products of reaction, but there was no conclusive evidence that the aldehyde route was a major pathway to liquid fuels. Indeed, it is possible to suggest that the main role of steam and nickel is to catalyse the gasification of coke laid down during the polymerisation/cyclisation reactions [44].

6. NATURAL GAS TO HYDROCARBON LIQUIDS

The potential importance of these reactions to the sustainable upgrading of natural gas is illustrated by the work of Hall *et al* [37]. They have described a process based on pyrolysis and acid catalysed reactions to produce a range of hydrocarbons compatible mainly with gasoline. The liquid contains *ca.* 20 mol% aromatics and the remainder is mostly iso & cycloalkanes. A pilot plant has been constructed and ongoing tests leading to commercialisation are proceeding.

The advantages of the process revolve around minimising greenhouse gas emissions and producing mainly gasoline compatible liquids. The capital cost is estimated at US\$25,000 p.a. BPD (barrel per day) to give a product cost (based on US\$0.5 MSCFD natural gas) of US\$ 12-15 per barrel.

Certainly, these figures are optimistic. Certainly, pyrolysis/polymerisation is a process that shows much promise for the sustainable upgrading of natural gas. Certainly, further study and development is needed and warranted.

7. REFERENCES

- [1] Guczi, L. & Kiriese, I: (1999) *Appl.Catal. A* 186, 375
- [2] Keller, G. E, & Bhasin, M. M: *J.Catal.* (1982) 73, 9
- [3] Yan, Z., Xiao, C-X & Kou, Y: (2003) *Catal.Lett.* 85, 129
- [4] Keene, D., Cullis, C.F. & Trimm, D.L: (1970) *J.Catal.* 19, 378

- [5] Anderson, J.R: (1989) *Appl.Catal.* 47, 177
- [6] Choudhary, T.V., Aksoylu, E. & Goodman, D.W: (2003) *Catal Revs Sci. Eng.* 45, 151
- [7] Holmen, A., Olsvik, O. & Rokstad, O.A: (1995) *Fuel Processing Technology* : 42, 249
- [8] Gueret, C: PhD Thesis: (1993): Institut National Polytechnique de Lorraine : Quoted in reference 7
- [9] Koerts, T. & Van Santen, R.A: (1991) *J. Chem.Soc-Chem.Comm.*1281
- [10] Belqued, M., Pareja, P., Ameriglio, A. & Aurariglio, H: (1991) *Nature* 352, P789
- [11] McCarty, J. G. & Wise, H: (1979) *J.Catal.* 57, 406
- [12] Koranne, M.M., Goodman, D. W, & Zajac, G.W: (1995) *Catal. Lett.* 30, 219
- [13] Guzzi, L., Sarma, K.V. & Borko, L: (1997) *J. Catal* 167, 495
- [14] Garnier, O., Shu, J., Grandjean, B. P.A (1997): *Ind.Eng.Chem.Res* 36, 553
- [15] Wang, L. S., Tao, L. X., Xie, M.S., Xu, G.F., Huang, J.S. & Xu, Y.D: (1993) *Catal.Lett* 21, 35
- [16] Xu, Y.D., Liu, S.T., Wang, L.S., Xie, M.S. & Guox, X. (1995) *Catal.Lett.* 30, 135
- [17] Weckhuysen, B. M., Wang, D. J., Rosynele, M.P. & Lumsford. J.H: (1998) *J.Catal* 175, 338
- [18] Wang, D.J., Lumsford, J.H. & Rosynek, M.P: (1997) *Catal* 169,347
- [19] Liu, S.T., Dong, Q., Ohnishi, R., Ichikawa, M: (1997) *Chem Comm* 1455
- [20] Li, S., Zhang, C.L., Kan, Q.B, Wang, D.Y., Wu, T.H., Lin, L. W:(1999) *Appl. Catal.A. General* 187, 199
- [21] Zhang, C.L., Li, S.A., Yuan, Y., Zhang, W.X., Wu, T.H. & Lin, L.W: (1998) *Catal.Lett.* 56, 207
- [22] Shu, Y.Y., Ma, D., Su, L-L., Xu, L-Y., Xu, Y-D. & Bao, X-H.(2001) *Studies in Surface Science & Catalysis* (ed. Spivey, J.J., Iglesia, E. & Fleisch, T.H.) 27 (Elsevier Science BV)
- [23] Zhang, J.Z., Long, M.A. & Howe, R.F: (1998) *Catal.Today* 44, 293
- [24] Liu, Z., Liu., L. & Iglesia, E: (2002) *Catal. Lett.*82, 175
- [25] Choudhary,V.R., Kinage, A. K. & Choudhary, T.V: (1997) *Science*, 275, 1286
- [26] Olsvik, O. & Billaud, F. (1994) *Thermochim Acta* 232 155 - 169
- [27] Palmer, H.B.,Lahaye, J. & Hou, K.C: (1968) *J Phys. Chem* 72, 348
- [28] Schneider, I.A., Z. (1963) *Phys. Chem.* 223, 234
- [29] Rokstad, O.A., Olsvik, O. & Holman. A: (1991) *Natural Gas Conversion* p533: Elsevier (Amsterdam)
- [30] Billaud, F.G., Baronnet, F., Gueret, C.P: (1993) *Ind Eng Chem Res* 32, 1549
- [31] Holmen, A., Rokstad, O.A. & Solbakken, A: (1976) *Ind. Eng. Chem Process Design Dev.* 15,439
- [32] Anderson, R.P., Fincke, J. R. & Taylor, C.E: (2002) *Fuel* 81,909
- [33] Gladisch, H: (1962) *Hydrocarbon Process Petrol Refiner* 41,159
- [34] Anderson, J. E. & Case, L. K : (1962) *Ind. Chem Proc. Des. Dev.* 1, 161
- [35] Ibberson, V.I. & Sen, M: (1976) *Trans. Inst. Chem Eng.* 54, 265
- [36] Forbath, T.P. & Gaffney, B. J: (1954) *Petroleum Refiner* 33, 160
- [37] Hall, K.R., Akgerman, A., Anthony, R.G., Eubank, P.T., Bullin, J. A., Cantrell, J. G., Weber Jr., B.R. & Betsill, J: (2002) *APPEA Journal* 55
- [38] Nieuwland, J.A. & Vogt, R.R: (1945) *The Chemistry of Acetylene ACS Monograph* 99 Amer. Chem. Soc.
- [39] Reppe, W. & Wolfe, W: (1934) *USP* 2, 066, 076
- [40] White, N., Kagi, D.A., Creer, J.G. & Tsai, P: (1991) *Australian Patent* 608, 502
- [41] Tsai, P. & Anderson, J.R: (1983) *J Catal* 80, 207

- [42] HeY, Jang B., W-L, & Timmons, R.B: (1993) ACS Symposium Series No 517 p 355
Amer. Chem. Soc. Washington
- [43] Pereira, C., Kokotailo, G.T. & Gorte, R. J : (1991) J Phys. Chem 95, 705
- [44] Trimm, D. L. & Bernardo, C.A. Carbon (1979) 17

Chapter 8

NEW TECHNOLOGIES FOR LIGHT ALKANE UPGRADING

Membrane and redox reactors

Jorge Gascon, Carlos Tellez, Javier Herguido, Miguel Menendez

Department of Chemical Engineering, University of Zaragoza, Spain

Abstract: An overview of recently developed technologies for alkane activation is presented, the main emphasis being in two kinds of reactor: membrane reactors and redox. The first type provides a wide range of possibilities, with the membrane acting as a reactant distribution only, or separating a reactant or a product, simultaneously with the reaction. The redox reactor includes several possibilities for carrying out a reaction in a reactor with reducing and oxidizing zones, allowing the decoupling of two steps of a catalytic reaction or the carrying out of two reactions simultaneously. The advantages and limitations of each type of reactor are discussed, as well as the challenges that their development poses to researchers.

Key words: alkane activation, oxidative dehydrogenation, maleic anhydride, Fischer-Tropsch, membrane reactor, redox reactor

1. INTRODUCTION

Alkane activation is currently performed in several ways. Methane is transformed into synthesis gas, this being the intermediate step in several processes. Various technologies are available for the dehydrogenation of alkanes. The formation of oxygenated products is performed large scale in the synthesis of maleic anhydride. Many new technologies have been proposed over the last few years, mainly during the last decade, with the aim of improving the economical performance of such transformations. This presentation will focus on two kinds of chemical reactor that have been the subject of intense research in many laboratories and industrial companies, the University of Zaragoza among them.

The first kind of reactor described here is the membrane reactor. A large variety of catalytic reactors can be included in this category, and very often the processes for which they have been developed include the use of alkanes as reactants. Given the high temperatures usually required for these processes, the application of polymeric membranes is limited, since in general they can not operate at temperatures over 200°C, and inorganic membranes are the usual choice. The use of inorganic membranes in catalytic reactors opens up many ways of improving the effectiveness of the process: by increasing the conversion or the selectivity to a given product, allowing milder operating conditions, or simply allowing operating conditions that would not be possible in a conventional reactor.

The second kind of reactor includes several alternatives for feeding an alkane and a stream containing oxygen to separate points of a reactor, with solid circulation between those points. This may be employed in catalytic oxidations, e.g. butane to maleic anhydride, but also in processes where the catalyst is deactivated by coke. In the first case, the catalyst acts as a carrier of oxygen, the oxidation of the hydrocarbon being carried out with the oxygen from the crystal lattice whilst the catalyst is reduced. The catalyst is reoxidized with a stream containing oxygen in a separate zone of the reactor. In the second case, the catalyst is deactivated by coke during the hydrocarbon reaction, and the coke is burnt with oxygen.

2. MEMBRANE REACTORS

A large number of catalytic reactors have been described in the literature where the use of a membrane as part of the reactor improves the reaction performance. Several extensive reviews [1-4] have been published recently, and the developments in membrane reactor technology may be followed in the proceedings of the last International Conferences on Catalysis in Membrane Reactors [5, 6]. The present work focuses on those reactors applicable to alkane activation. Although several classifications are possible, here reactors are categorized in four main groups according to the role of the membrane.

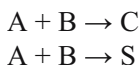
- a) The membrane is ideally inert and not selective, i.e. has not separation selectivity, and only acts as a gas distributor. This is the situation where the only aim is to distribute a reactant uniformly throughout the reactor.

- b) The membrane can separate one of the reactants from a feed, avoiding its separation before the reactor. The most interesting case is the separation of oxygen by a selective membrane.
- c) The membrane can selectively separate a product from the reaction mixture. There are several possible advantages in such case, depending on the reaction, e.g. the removal of a reaction product in an equilibrium limited reaction can provide a reactant conversion higher than that achievable in a conventional reactor.
- d) The membrane has catalytic activity. This is the situation where there are less results available, although some applications have been described.

The above list is not comprehensive, since the ingenuity of researchers always offers new methods to take advantage of the properties of membranes in the development of improved reactors. However, the main possibilities described in the literature can be grouped in any of the above classes.

2.1 MEMBRANES AS GAS DISTRIBUTORS

A first possibility is to use the membrane as a gas distributor to a catalyst bed located inside (or outside) the membrane. This kind of membrane reactor, sometimes called the Membrane Enclosed Packed Bed Reactor, has as its principal advantage the lower concentration (or partial pressure) of one of the reactants in the entire reactor. When several reactions occur simultaneously, and the effect of the partial pressure of one reactant is different for each of them, it is well known [7] that the way the reactants are fed will affect the selectivity. The following example shows in a simple way the basis of this reactor. Consider a set of series-parallel reactions as:



C being a suitable product and S an undesired subproduct. This scheme can represent many catalytic oxidations, where carbon oxides are formed simultaneously with the desired product. If the reaction order with respect to B is higher for the production of S, a lower partial pressure of B will improve the selectivity. In many catalytic oxidations of hydrocarbons a simple kinetic analysis shows that a decrease in the partial pressure of oxygen will increase the selectivity towards the desired product-

The first application of a membrane reactor for improving the selectivity by distributing oxygen was described for the oxidative coupling of methane [8, 9]. Given the large reserves of natural gas, the search for an alternative method to obtain liquids from methane is of strategic interest. Methane coupling has been the subject of intense research since Keller and Bhasin [10] showed that many catalysts can produce ethane and ethylene from methane. Many compounds have been tested for this reaction, although the per pass yield considered as desirable to be economical (around 35%) has not been achieved. Several reviews [11, 12] show the large variety of catalyst tested in the literature. It has been proved that the membrane reactor provides increased selectivity for a given degree of methane conversion, and therefore the per pass yield achievable is larger than in a conventional reactor with cofeeding of reactants. An additional advantage of the distributed feed of oxygen lies in the increased safety [13], since the formation of hot spots is largely reduced and also the formation of explosive mixtures is avoided since the oxygen concentration is kept low throughout the reactor.

Another kind of reaction where the distribution of oxygen can provide increased selectivity is the oxidative dehydrogenation of alkanes. Membrane enclosed packed bed reactors have been employed for oxidative dehydrogenation of ethane, propane and butane. The oxidative dehydrogenation of alkanes is an alternative method for the production of a olefin from a paraffin, with several advantages:

- The conversion is not limited by the thermodynamic equilibrium
- The reaction is endothermic, and therefore the need for an external heat supply is avoided.
- Operation temperatures are lower, allowing the use of cheaper materials.
- Catalyst deactivation by coke is avoided, since any carbon that may be formed will immediately be burnt.

The main problem of these reactions is the formation of carbon oxides, which reduces the selectivity to the desired products. Significant improvements in the selectivity to olefins have been achieved using membrane reactors for oxidative dehydrogenation of ethane [14], propane [15, 16] and butane [17]. High yields have been also obtained in the oxidative dehydrogenation of methanol to formaldehyde [18] and the partial oxidation of propane to acrolein [47].

As an example, the results obtained in the oxidative dehydrogenation of ethane are shown in Figure 1. It may be seen that the selectivity to ethylene is quite high (around 85%), and that the conversion achieved is higher than the thermodynamic equilibrium for conventional dehydrogenation. In this

case, the equilibrium conversion for ethane dehydrogenation at 660°C is around 30%, whereas in the membrane reactor conversions up to 45% are achieved.

The advantage in safety provided by the membrane reactors is shown in Figure 2. It may be seen that whereas in the conventional reactor the feed is inside the flammable limit, and the reacting mixture remains inside this limit in a large section of the reactor, the concentration of oxygen is kept low in the membrane reactor, always outside of such limit.

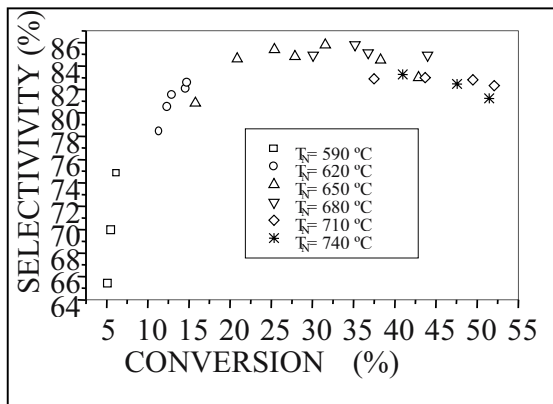


Figure 1. Selectivity vs. conversion for oxidative dehydrogenation of ethane in a membrane reactor

Another selective oxidation where the membrane reactor has been applied successfully is the synthesis of maleic anhydride by oxidation of butane [19]. This reaction is unique among catalytic oxidations, since it is the only industrial process where oxygen is inserted in an alkane by reaction with molecular oxygen. Two different configurations (see Figure 3) were tested: the IMR (conventional Inert Membrane Reactor), in which the catalyst bed is located inside the membrane, and the OFIMR (Outwards Flow Inert Membrane Reactor) [20]. The second configuration allows a larger amount of catalyst for a given membrane area, but it also provides better selectivity for a given spatial time. Some results in these reactors are shown in Figure 4. It may also be seen that the presence of significant amounts of CO₂ in the feed changes the selectivity to maleic anhydride. Since CO₂ is a subproduct of the reaction it is easy to recover and recycle it, providing the atmosphere needed to increase the selectivity. Another point to emphasize is that the membrane reactor allows the use of a higher butane concentration than conventional cofeed reactors, where the maximum

butane concentration in the feed is 1.5%, because otherwise the feed would be in the explosive region.

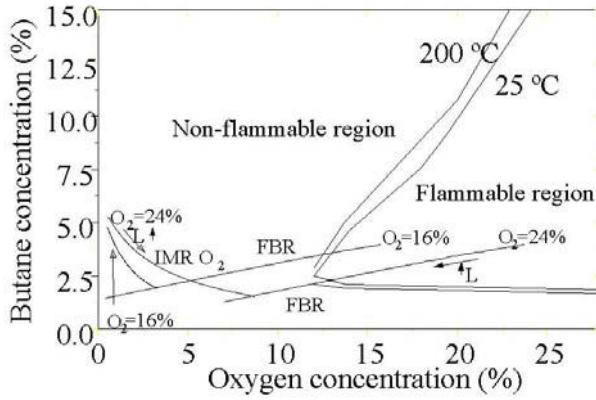


Figure 2. Variation of the concentration of reactants during the oxidative dehydrogenation of butane in a fixed bed reactor with cofeeding and in a membrane reactor

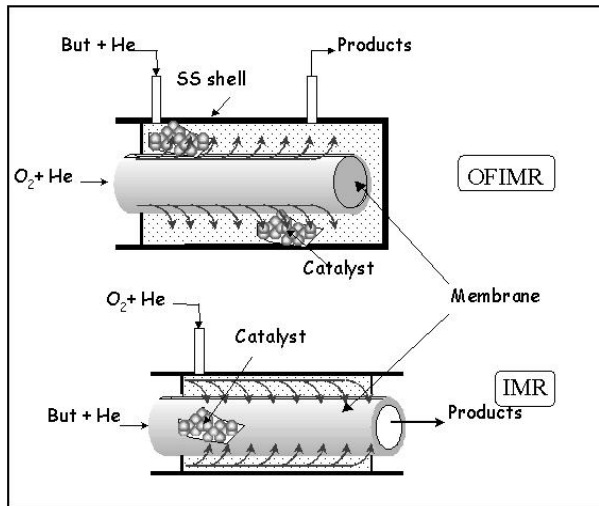


Figure 3. Two configurations of membrane reactor employed in the oxidation of butane to maleic anhydride

The use of the membrane reactor thus allows a drastic change in the whole process design. Since we can employ larger butane concentrations the unreacted butane can be more easily recovered and recycled, and the recycling of CO₂ helps to improve the selectivity [21].

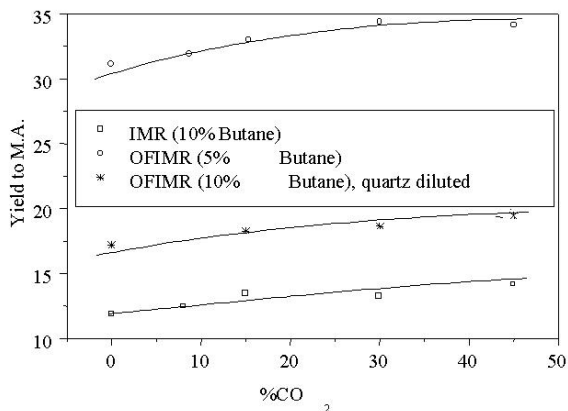
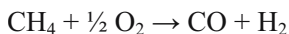


Figure 4. Effect of carbon dioxide and reactor configuration in the oxidation of butane to maleic anhydride

2.2 FEED PURIFICATION

The separation of oxygen is an expensive part of many oxidation processes. If oxygen is not separated from air before the reaction, the products will be highly diluted with nitrogen. A highly promising approach is to employ a membrane to separate the oxygen, such a membrane being an integral part of the reactor. The discovery of inorganic membranes selective to oxygen at high temperatures enabled their use to supply oxygen to the reaction [22-25]. An additional advantage of this integration of reaction and separation lies in the improved driving force for oxygen transfer through the membrane, since the oxygen partial pressure at the side where the hydrocarbon is fed can be kept very low, as it is being consumed. The application of such a membrane reactor to the activation of methane by partial oxidation to synthesis gas:



has been the subject of intense research.

The use of dense membranes, selective to oxygen, avoids the need to separate oxygen from air in a different unit, and thus the operation costs are reduced by roughly 30%. A pilot plant with a production of 0.1 ton/day has already been built, and a contract recently assigned by the US-DOE to Eltron Research Ind. and ITN Energy Systems, will allow a scale up to 25 ton/day [26]. The most recent advances include the use of mixed phase materials, which exhibit improved mechanical properties [27].

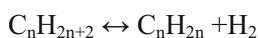
2.3 REMOVAL OF A PRODUCT

The integration of a selective membrane in a catalytic reactor allows the removal of a reaction product out of the bed. This requires a membrane selective to this product under the operating conditions of the catalyst. Two main categories of membranes can be considered:

- a) those selective to hydrogen
- b) those selective to water

2.3.1 HYDROGEN REMOVAL

The first opportunity is offered by membranes selective to hydrogen. These have been widely employed for dehydrogenation reactions, where the removal of the product displaces the reaction equilibrium, in accordance to the Le Chatelier's principle. Such reactions correspond to the general equation:



and the conversion achievable in conventional reactors is limited by the thermodynamic equilibrium.

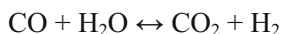
Dense palladium membranes, which can be fully selective, are the most commonly used [3]. The economy of such reactors is drastically affected by the thickness of the Pd membrane. A thinner membrane implies a lower cost per unit of membrane area, since Pd is the most expensive component, and also a smaller area of membrane, since the permeation ($\text{mol}/\text{m}^2 \cdot \text{s} \cdot \text{Pa}^{1/2}$) increases. Initially thin palladium films were employed, but recent works usually support the Pd film over a porous substrate, providing mechanical strength. This allows the use of very thin Pd membranes (of only a few micrometers in thickness) with sufficiently high enough hydrogen flux. Among the large number of techniques that have been described (e.g.

thermal deposition, sputter coating, chemical vapor deposition or electrochemical plating), electroless plating is the most promising, since the cost is relatively low, and the equipment needed is quite simple [28].

A disadvantage of this kind of membrane reactor in dehydrogenation reactions is the increased coke formation when a large percentage of the hydrogen has been removed. Finding catalysts with lower coking thus poses a challenge to catalyst developers.

The use of porous membranes has also been suggested, but their achievable selectivity is given by the Knudsen diffusivity ratio, i.e. the square root of the ratio of molecular weights. Therefore, except for very large molecules the H₂/hydrocarbon selectivity is only moderate. The increases in conversion reported in the literature using porous membranes are usually similar to those achievable by merely mixing the hydrocarbon and the purge gas stream. Microporous membranes, in particular zeolite membranes, have also been proposed for this kind of reactor, since a molecular sieving mechanism may be expected, and the theoretical selectivity could be very large. However the values to date of H₂/hydrocarbon selectivity at high temperatures are not significantly larger than the Knudsen diffusivity ratio.

The same principle may be applied to the water gas shift reaction, which is also limited by equilibrium, and where the removal of hydrogen can provide increased conversion.



A membrane reactor employing this process has been proposed as a method to avoid CO₂ emissions during the burning of hydrocarbons. The hydrogen can be used as a clean fuel, and the recovered CO₂ could be stored, e.g. underground. This is one of the techniques being evaluated by the CCP (Carbon dioxide Capture Project) consortium to reduce the CO₂ emissions, following to the Kyoto agreements [29]. Many of the leading oil companies in the world are participating in this consortium. An economical evaluation [30] showed that the CO₂ recovery cost may be acceptable if the thickness of the Pd membrane is lower than 10 micrometers and permeabilities around 100-200 Nm³/h m² bar^{1/2} are obtained. Even lower permeabilities may be acceptable if the membrane cost is kept low enough.

Membrane reactors with hydrogen removal have been also applied for steam reforming of methane, which is a similar case to the above described.

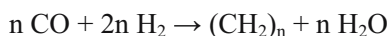
2.3.2 REMOVAL OF WATER

Whereas the use of a membrane to remove hydrogen was first described many years ago, its use to remove water from a reaction is quite recent. Two inorganic membranes have been reported to have the required selectivity:

- a) microporous silica membranes, which are amorphous and show high selectivity to water.
- b) zeolite membranes, new materials which have been developed with a large variety of compositions. Zeolite A membranes are already commercial and are employed industrially for the removal of water from solvents by pervaporation. However, they suffer from a lack of stability under acid or basic conditions. Other zeolitic materials (e.g. MFI or mordenite) seem more promising for such conditions.

The use of inorganic membranes for the removal of water or other condensable products has been proposed for the following processes:

- Fischer-Tropsch. This process can be represented schematically as:



Since for each CO molecule that reacts to form the hydrocarbon a molecule of water is formed, and given the high pressure of the operation, the partial pressure of water may be of the order of ten bars. It is known that the presence of water decreases the reaction rate, and for some catalysts causes deactivation. It has been found that zeolite membranes can remove water from the reaction environment. Table 1 shows some results of separation in conditions that simulate those existing in a Fischer-Tropsch reactor [31,32]. It may be seen that the presence of water, due to its strong adsorption, blocks the permeation of smaller molecules. Water fluxes close to 10 kg/h.m² have been obtained, and suitable selectivity is achieved even at temperatures up to 360°C.

Table 1. Separation of hydrogen under conditions simulating a Fischer-Tropsch reactor

Memb	Temp (°C)	P _{H₂O} (bar)	Water Flux (kg/h.m ²)	Sel. H ₂ O/ /C ₈	Sel. H ₂ O/ /H ₂	Sel. H ₂ O/ /C ₈	Sel. H ₂ O/ /CO ₂
MOR	150	3.8	6.4	80	76	72.1	58.3
Alumina	196	3.3	5.9	63	66	44.5	10.7
	355	7.9	12.8	9.7	4.5	5.4	10
ZSM5/	244	7.9	9.5	25.4	48.4	41.5	13.8
SS	359	4.4	11.7	23.5	18.3	25.5	36.6

- Methanol synthesis. The mechanism of selective separation is similar to that described for Fischer-Tropsch. Since zeolite membranes can separate vapors from permanent gases, their use in methanol synthesis could be advantageous to obtain higher conversions or to perform the operation at lower pressure. This concept was proven using polymeric membranes [33], but the use of inorganic membranes could be useful for operation at higher temperatures [34], decreasing the need for high pressure during the operation, or allowing higher conversion per pass. This concept has been experimentally proven using zeolite A membranes [48].
- Esterifications. Again the target is to remove the water formed in the reaction. A discussion on the design of pervaporation membranes reactor was presented by Lim et al. [49].

2.4 CATALYTIC MEMBRANES

It has been suggested [35] that providing catalytic activity to a membrane can help to improve the selectivity, by feeding each reactant to a different side. Figure 5 shows an explanation of this idea: The membrane has an active zone and an inert zone. Due to the diffusion, the partial pressure of one reactant can be kept low in the reaction zone, and by operating with a slightly higher pressure at one side, the products can be transported to the side where the partial pressure of this reactant is almost null. This has been checked experimentally for the oxidative dehydrogenation of butane [35]. Figure 6 shows a catalytic membrane where the active zone, where Vanadium has been deposited, is in black color (the color has been obtained by reduction of the vanadium oxide). This is achieved by controlled impregnation techniques, similar to those employed for obtaining the egg-shell catalysts. The selectivity obtained by feeding each reactant to a different side of the membrane was higher than flowing both reactants through the membrane, which constitutes the experimental proof of the concept.

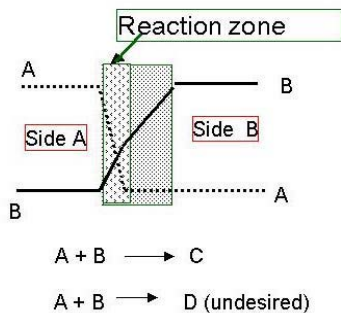


Figure 5. Scheme of the concentration of reactants in a catalytic membrane

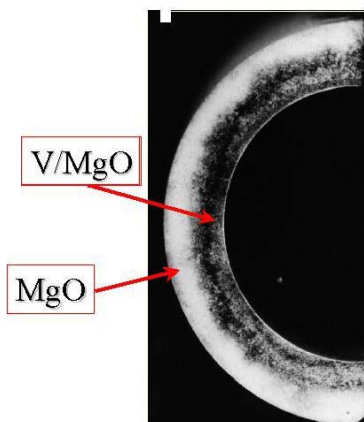


Figure 6. Picture of a catalytic membrane (V/MgO) showing the active layer

2.5 SOME COMMENTS ON MEMBRANE REACTORS

The applications described above do not constitute an exhaustive list of applications of membrane reactors, although the main advances related with alkane upgrading have been included. The ingenuity of researchers has proposed a large variety of reactions where the use of membrane reactors could provide some kind of advantage.

A serious problem with membrane reactors is the cost of the membrane. Typical prices for inorganic membranes (including the module) are around \$5000/m², and it has been calculated that a cost reduction to \$1000/m² is needed to achieve an economic operation in most applications [50]. This has to be achieved by means of improved production technologies and new designs.

In most laboratory experiments the catalyst bed is enclosed in the membrane. This is a suitable configuration for an easy operation in the laboratory and elegant results for an academic presentation, but the separation of the catalyst bed and the membrane provides greater flexibility in the design, since the permeation area and the catalyst weight can be tailored independently.

Ceramic supports are employed in many laboratory scale experiments, for palladium, silica or zeolite membranes. The use of stainless steel porous supports may be an alternative, avoiding the problems of brittleness and allowing an easier sealing of the membrane in the reactor.

3. REDOX REACTORS

Those systems where a reduction and an oxidation are carried out in separate points of a reactor are grouped in this category. This includes those systems in which a catalyst is oxidized at one point of the reactor and is reduced at another point by reaction with a hydrocarbon, which is oxidized. The best known example is the oxidation of butane to maleic anhydride, as is performed by DuPont in a plant recently built in Asturias (Spain). This technology employs a circulating fluidized bed reactor (CFBR) as shown in Figure 7 [37-39]. The butane is fed to a riser reactor, where it is converted to maleic anhydride, whilst the VPO catalyst is partially reduced. The catalyst is reoxidized with air in a fluidized bed reactor. A similar system was employed in a pilot plant built by ARCO for the oxidative coupling of methane [40]. Vrieland and Murchison [41] also proposed this kind of reactor for the oxidative dehydrogenation of butane to give butadiene, which can be transformed to styrene by a Diels-Alder reaction.

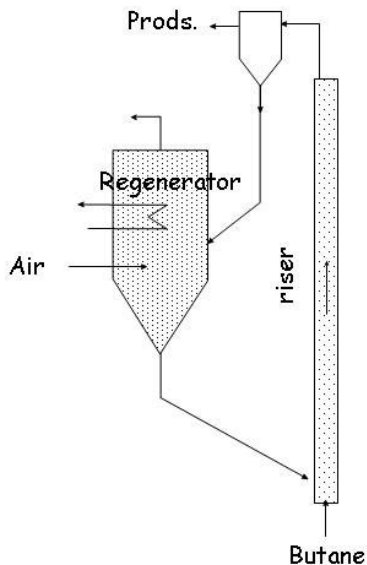


Figure 7. Scheme of the Circulating Fluid Bed reactor employed for the oxidation of butane to maleic anhydride

Two types of redox reactor, alternative to the CFBR have been studied at the University of Zaragoza

- a) The Two Zone Fluidized Bed (TZFBR)
- b) The Internally Circulating Fluidized Bed Reactor (ICFBR)

The aim in both cases is to provide separated oxidation and reduction zones, but avoiding the problems associated with the flow of solids through standpipes, as in the CFBR.

3.1 THE TWO ZONE FLUIDIZED BED REACTOR

In the TZFBR (Figure 8) the oxygen, together with an inert gas, is fed into the lower part of the fluidized bed while the hydrocarbon is fed at an intermediate point. The catalyst is oxidized in the lower part of the reactor, and under suitable operating conditions the gas stream reaches the hydrocarbon entry point with a low or even negligible oxygen concentration. The oxygen is transported to the upper part of the reactor in the crystal

lattice of the catalyst, by means of the solid mixing characteristic of fluidized beds: bubbles that rise in the reactor carry a wake of solid, whereas there is a return of solid in the emulsion phase. In the upper zone the hydrocarbon reacts with the oxygen from the catalyst lattice, which is reduced. In this way the hydrocarbon oxidation is carried out in the absence of gas phase oxygen, reducing the extent of undesired reactions.

This mode of operation was first applied to the oxidative coupling of methane [42]. It was found that the separation of the oxidation and the reduction zones was possible, although no improvements in the yield to the desired products was observed. The results for the oxidative dehydrogenation of butane [43] were much more interesting: for a given set of operating conditions the selectivity to olefins was higher in the TZFBR than in a conventional reactor with cofeeding of the reactants. The most remarkable result was that the yield to butadiene increased by almost 200% (i.e. it was up to three times higher). Several catalysts were tested, including V/MgO, V/Al₂O₃ and Mo/MgO [44]. The best results were obtained with V/MgO. Mo/MgO also gave good results but it became deactivated after several hours on stream.

This reactor has also been tested for the oxidation of butane to maleic anhydride [45]. It produced yields similar to those reported in the literature for CFBR or pulse reactors, and clearly higher than those achievable with conventional fixed bed reactors with cofeeding of the reactants when the percentage of butane in the feed is higher than 1.5%. A comparison of the results obtained in the TZFBR and a fluidized bed reactor with the same catalyst, operating in conventional mode, i.e. with cofeeding of reactants, is shown in Figure 9. It is clear that the yield to maleic anhydride achievable with the TZFBR is higher than in the conventional contact mode. It is worth pointing out that the feed introduced in the conventional fluidized bed reactor was inside the explosion limits and thus these experiments should be repeated only under carefully controlled safety conditions.

The TZFBR can also be employed in conventional dehydrogenation processes. In this case the catalyst is deactivated by coke formation in the upper part of the bed and the coke is burnt in the oxidizing zone. The operation of this reactor has been tested for butane dehydrogenation [46], and some results for propane dehydrogenation are presented below.

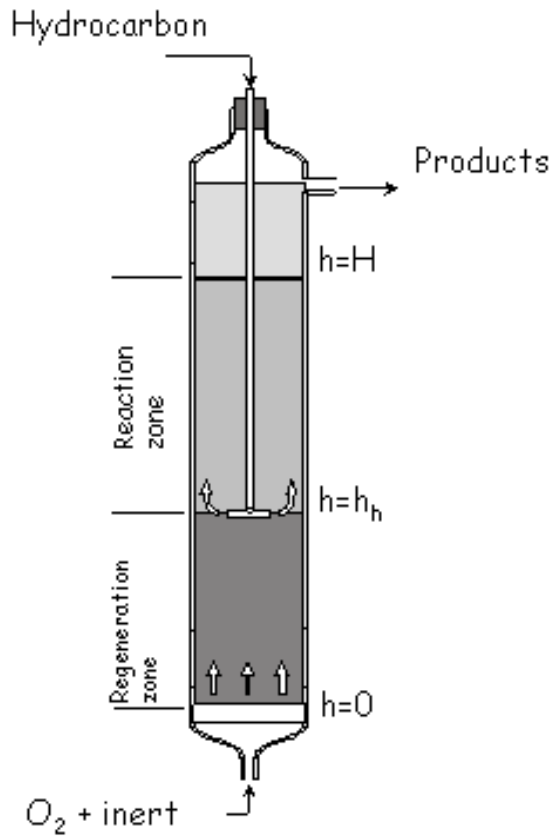


Figure 8. Scheme of the Two-zone fluidized bed reactor

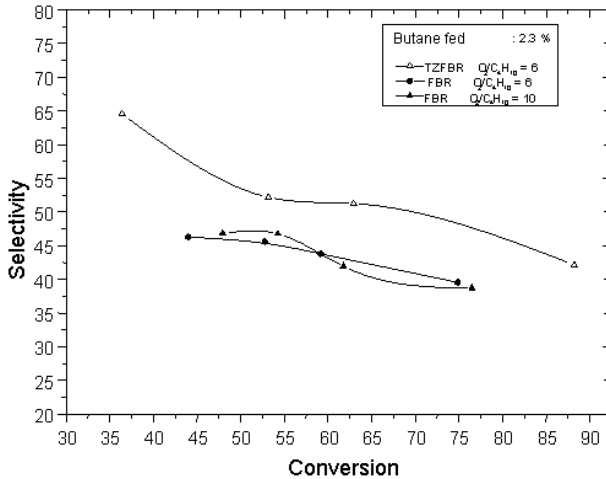


Figure 9. Comparison of the results obtained in a fluidized bed with cofeeding (FBR) and in a TZFBR, for the oxidation of butane to maleic anhydride

3.2 THE INTERNALLY CIRCULATING FLUIDIZED BED REACTOR

The CFBR is only one among many combinations of reactor that can provide a solid circulation between two zones. Another possibility is to employ two fluidized beds connected by the upper and lower zones. This has been done at our laboratory by inserting a vertical plate in a 6 cm i.d. stainless steel reactor, as shown in Figure 10.

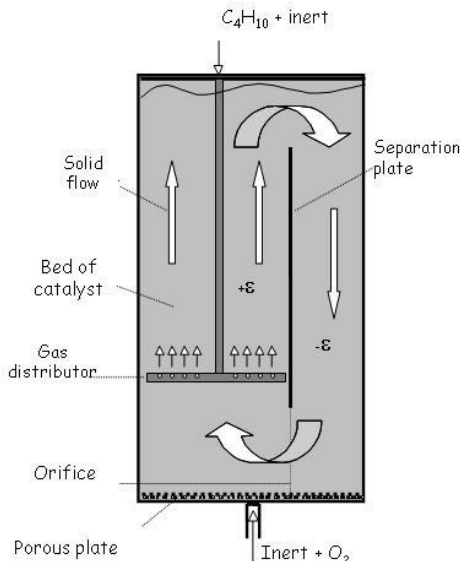


Figure 10. Scheme of the Internally Circulating Fluidized Bed Reactor

In the zone where the hydrocarbon is introduced the catalyst bed has a lower porosity, since the gas flow is larger. Therefore the pressure drop of the gas is smaller in that zone and a pressure gradient appears in the lower part of the reactor, in the orifice connecting both beds. This generates a solid circulation between both beds, which is roughly one order of magnitude larger than the solid flow carried in the wake of the bubbles. This reactor provides several advantages compared with the TZFBR:

- a) a larger solid circulation, and thus the possibility of transferring a larger amount of oxygen between zones;
- b) better control of the solid circulation rate. In the TZFBR the solid flow is given only by the bubbles, whereas in the ICFBR there are several variables: aeration rate, size of the orifice connecting the two zones, and the gas flow rate of the hydrocarbon-inert mixture;
- c) better separation between the oxidizing and reducing zones. In the TZFBR there is an exchange between the solid rising in the bubbles and that descending in the emulsion. In the ICFBR the solid in the emulsion is also rising, since the total solid circulation is larger than that produced by the bubbles.

A comparison between the results obtained with the TZFBR and the ICFBR for the oxidative dehydrogenation of butane is shown in Figure 11 (with the optimum conditions for each reactor). It may be seen that the ICFBR provides similar or higher selectivity than the TZFBR, despite the fact that smaller spatial times are employed.

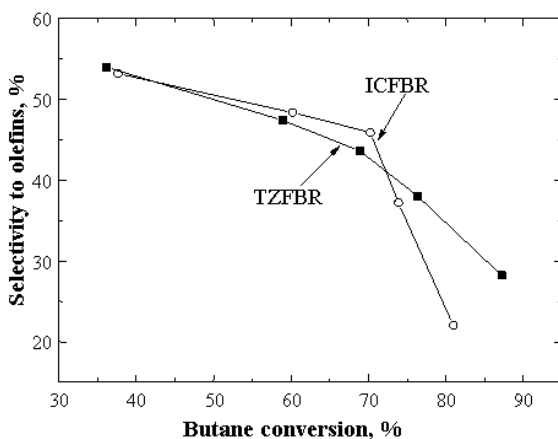


Figure 11. Results obtained in the TZFBR and the ICFBR for the oxidative dehydrogenation of butane

Results for propane dehydrogenation with the TZFBR and the ICFBR, using a commercial $\text{Cr}_2\text{O}_3/\text{Al}_2\text{O}_3$ catalyst, are shown in Figure 12. It is remarkable that stable operation was achieved even with small amounts of oxygen. The selectivity to carbon oxides was very small (1-2% in most cases) and the largest part of the subproducts are methane and ethylene. This is a considerable advantage with respect to oxidative dehydrogenation processes, where the subproducts are mainly carbon oxides. The achievable selectivity to propene is similar to the values reported for industrial operation (85-90%), but this is obtained with the advantage of operating under steady state conditions.

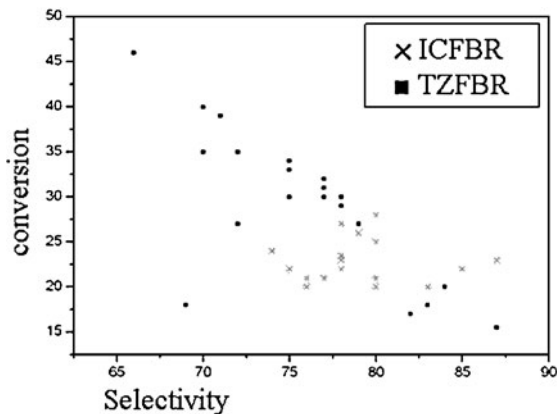


Figure 12. Dehydrogenation of propane in TZBFR and ICFBR with simultaneous regeneration of the catalyst

4. CONCLUSIONS

Several processes involved in the upgrading of alkanes may be improved by the use of advanced reactors. Membrane reactors can provide advantages in dehydrogenation of alkanes, selective oxidations, water gas shift or steam reforming, as well as in the transformation of synthesis gas to liquid hydrocarbons by Fischer-Tropsch or to methanol.

Reactors with separated oxidizing and reducing zones are promising for some catalytic oxidations and for simultaneous reaction and regeneration in processes where the catalyst is deactivated by coke formation.

5. ACKNOWLEDGEMENTS

Research on redox reactors at the University of Zaragoza is currently supported by DGI (Spain), project PPQ2001- 2519.

6. REFERENCES

- [1] Sanchez, J.G., Tsotsis, T.T. "Catalytic membranes and membrane reactors", Wiley, 2003.
- [2] Coronas, J., Santamaría, J., "Catalytic reactors based on porous ceramic membranes", *Catal. Today*, 51, 377-389 (1999)
- [3] Dixon, A.G., "Innovations in catalytic inorganic membrane reactors", *Catalysis*, 14, 40-92 (1999)
- [4] Saracco, G., Neomagus, H.W.J.P., Versteeg, G.F., van Swaaij, W.P.M., "High-temperature membrane reactors: potential and problems", *Chem. Eng. Sci.*, 54, 1997-2017 (1999)
- [5] Hojlund-Nielsen, P.E., and Clausen, B.S. (eds), *Catal. Today*, 56 (1-3), (2000)
- [6] Santamaría, J., Menéndez, M.(eds), *Catal. Today*, 67 (1-3), (2001); W. Yang, T.T. Tsotsis (eds.) *Catal. Today* 82 (1-4) (2003)
- [7] Levenspiel, O., "Chemical Reaction Engineering" (2nd ed), Wiley, 1972
- [8] Coronas, J., Menéndez, M., Santamaría, J. "Methane oxidative coupling using porous ceramic membrane reactors-II. Reaction studies", *Chem. Eng. Sci.*, 49, 2015-2025 (1994)
- [9] Tnkovich, A.L.Y., Jimenez, D., Zilka, J.L., Roberts, G.L., Cox, J.L. "Inorganic membrane reactors for the oxidative coupling of methane", *Chem. Eng. Sci.*, 51, 2051-3056 (1996)
- [10] Keller, G.E., Bhasin, M.M., "Synthesis of ethylene via oxidative coupling methane. I. determination of active catalysts", *J. Catal.*, 73, 9-19 (1982)
- [11] Wolf, E.E. (ed), "Methane conversion by oxidative processes", Van Nostrand Reinhold, 1992.
- [12] Amenomiya, Y., Birss, V.I., Goledzinowski, M. , Galuszka J., Sanger, A.R., "Conversion of methane by oxidative coupling". *Catal. Rev.- Sci. Eng.* 32, 163 (1990).
- [13] Coronas, J., Menéndez, M., Santamaría, J., I. "The porous-wall ceramic membrane reactor: an inherently safer device for gas-phase oxidation of hydrocarbons", *J. Loss Prev. Process Industries*, 8, 97-101 (1995).
- [14] Coronas, J., Menéndez, M., Santamaría, J., Use of ceramic membrane reactor for the oxidative dehydrogenation of ethane to ethylene and higher hydrocarbons", *Ind. Eng. Chem. Res.*, 34, 4229 (1995)
- [15] Pantazidis, A., Dalmon, J.A., Mirodatos, C. "Oxidative dehydrogenation of propane on catalytic membranes reactors", *Catal. today* 25, 403-308 (1995)
- [16] Ramos, R., Menéndez, M., Santamaría, J. "Oxidative dehydrogenation of propane in an inert membrane reactor", *Catal. Today*, 56, 239-245 (2000)
- [17] Tellez, C., Menéndez, M., Santamaría, J., "Oxidative dehydrogenation of butane using membrane reactors", *AIChE J.*, 43, 777-784 (1997)
- [18] Diakov, V., Varma, A., "Methanol oxidative dehydrogenation in a packed-bed membrane reactor: yield optimization experiments and model", *Chem. Eng. Sci.*, 58, 801-807 (2003)
- [19] Mallada, R., Menéndez, M., Santamaría, J. " Use of membrane reactors for the oxidation of butane to maleic anhydride under high butane concentration", *Catal. Today*, 56, 191-197 (2000)
- [20] Mallada, R., Pedernera, M., Menéndez, M., Santamaría, J. "Synthesis of Maleic anhydride in an Inert Membrane reactor. Effect of Reactor configuration", *Ind. Eng. Chem. Res.*, 39, 620-625 (2000)

- [21] Perregaard, J., Santamaría, J., Menéndez, M., Mallada, R., Patience, G., Ross, J.R.H., Xue, E., Volta, J.C., Julbe, A., Farrusseng, D. "Process for catalytic selective oxidation of a hydrocarbon substrate", European Patent EP 1081124, assigned to Dupont Iberica, Haldor Topsoe and the University of Zaragoza (2001)
- [22] Ten Elshof, J.E., Martin, J.P., Cook, C.F., Kinble, J.B., "Activation of methane using solid oxide membranes", *Catal. Today*, 25, 397 (1995)
- [23] Shao, Z., Dong, H., Xiong, G., Cong, Y., Yang, W., "Performance of a mixed-conducting ceramic membrane reactor with high oxygen permeability for methane conversion", *J. Membr. Sci.*, 183, 397 (2001)
- [24] Tsai, G., Dixon, A.G., Moser, W.R., "Dense Perovskite membrane reactors for partial oxidation of methane to syngas", *AIChEJ.*, 43, 2741 (1997)
- [25] Lu, Y., Dixon, A.G., Moser, W.R., Ma, Y.H., Balachandran, U., "Oxygen permeable dense membrane reactor for the oxidative coupling of methane", *J. Membr. Sci.*, 170, 27 (2000)
- [26] Bose, A.C., Richards, R.E., Sammels, A.F., Schwartz, M., "Beyond state-of-the art separation processes using ion-transport membranes", *Desalination* 122, 91-92 (2002)
- [27] Van Calcar, P., Mackay, R., Sammels, A.F., "Mixed ionic and electronic conducting ceramic membranes for hydrocarbon processing", US patent 6471921, Assigned to Eltron Research, Ind., (2002)
- [28] Yeung, K.L., Christiansen, S.C., Varma, A. "Palladium composite membranes by electroless plating technique. Relationships between plating kinetics, film microstructure and membrane performance", *J. Membr. Sci.*, 159, 107-122 (1999)
- [29] www.CO2captureproject.org
- [30] Middleton, P., Solgaard-Andersen, H., Rostrup-Nielsen, T., "Hydrogen production with CO2 capture using membrane reactors", World Hydrogen Energy Conference, Montreal, (2002)
- [31] Espinoza, R.L., Du Toit, E., Santamaría, J., Menéndez, M., Coronas, J., Irusta, S., "Use of membranes in Fischer-Tropsch reactors." *Stud. Surf. Sci. Catal.*, 130, 389-394 (2000)
- [32] Espinoza, R.L., Santamaría, J., Menéndez, M., Coronas, J., Irusta, S., "Production of hydrocarbons", PCT patent WO 99/64380 (1999)
- [33] Struis, R.P.W.J., Stucki, S., Wiedorn, M., "A membrane reactor for methanol synthesis", *J. Membr. Sci.*, 13, 93-100 (1996)
- [34] Menéndez, M., Piera, E., Coronas, J., Santamaría, J., "Zeolite membrane reactor for obtaining methanol and other alcohols from synthesis gas", Spanish Patent nº 2164544 (2002)
- [35] Harold, M.P., Zaspalis, V.T., Keizer, K., Burgraaf, A.J., "Intermediate product yield enhancement with a catalytic inorganic membrane-I: analytical model for the case of isothermal and differential operation", *Chem. Eng. Sci.*, 48, 2705-2725 (1993)
- [36] Alfonso, M.J., Menéndez, M., Santamaría, J., "Oxidative dehydrogenation of butane on V/MgO catalytic membranes", *Chem. Eng. J.*, 90, 131-138 (2002)
- [37] Contractor, R.M. "Dupont's CFB technology for maleic anhydride" *Chem. Eng. Sci.* 54, 5627-5632, (1999).
- [38] Contractor R.M., Bergna H.E., Horowitz H.S., Blackstone C.M., Malone B., Torardi C.C., Griffiths B., Chowdhary U., Sleight A.W. "Butane Oxidation to Maleic Anhydride over Vanadium Phosphate Catalysts" *Catal. Today*, 1, 49-58 (1987).
- [39] Contractor R.M., Garnett D.I., Horowitz H.S., Bergna H.E., Patience G.S., Schwartz J.T., Sisler G.M. "A New Commercial Scale Process for n-Butane Oxidation to Maleic Anhydride using a Circulating Fluidized Bed Reactor" *Stud. Surf. Sci. Catal.*, 82, 243-251 (1993).

- [40] Jones, C.A., Leonard, J.J., Sofranko, J.A., "Fuels for the future: remote gas conversion" *Energy and Fuels*, 1,12-16 (1987)
- [41] Vrieland G. E., Murchison C. B. "Anaerobic oxidation of butane to butadiene over magnesium molybdate catalyst. I. Magnesia supported catalysts". *Appl. Catal. A*, 134, 101-121 (1996).
- [42] Ramos R., Herguido J., Menéndez M., Santamaría J. "Oxidation of Hydrocarbons in an in Situ Redox Fluidized Bed Reactor" *J. Catal.*, 163, 218-221 (1996).
- [43] Soler, J., López-Nieto, J.M., Herguido, J., Menéndez, M., Santamaría, J., "Oxidative dehydrogenation of n-butane in a two-zone fluidized bed reactor", *Ind. Eng. Chem. Res.*, 38, 90-97 (1999)
- [44] Lopez Nieto, J.M, Soler, J., Concepción, P., Herguido, J., Menéndez, M., Santamaría, J., "Oxidative dehydrogenation of alkanes over V-based catalysts: Influence of redox properties on catalytic performance", *J. Catal*, 185, 324-332 (1999)
- [45] Rubio, O., Mallada, R., Herguido, J., Menéndez, M. "Experimental study on the oxidation of butane to maleic anhydride in a two-zone fluidized bed reactor", *Ind. Eng. Chem. Res.*, 41, 5181-5186 (2002)
- [46] Callejas, C., Soler, J., Herguido, J., Menéndez, M., Santamaría, J., "Catalytic dehydrogenation of n-butane in a fluidized bed reactor with separate coking and regeneration zones.", *Stud. Surf. Sci. Catal.*, 130, 2717-2722 (2000)
- [47] Kolsch, P., Smejkal, Q., Noak, M., Schafer, R., Caro, J., "Partial oxidation of propane to acrolein in a membrane reactor. Experimental data and computer simulation", *Catal. Comm.*, 3 (2002) 465-470.
- [48] Gallucci, F., Paturzo, L., Basile, A., "An experimental study of CO₂ hydrogenation into methanol involving a zeolite membrane reactor", *Chem. Eng. Proc.*, (2004) in press.
- [49] Lim, S.Y., Park, B., Hung, F., Sakimi, M., Tsotsis, T., "Design issues of pervaporation membrane reactors for esterification", *Chem. Eng. Sci.*, 57 (2002) 4933.
- [50] Tennison, S., Current hurdles in the commercial development of inorganic membrane reactors, *Membrane Technol*, 128 (2000) 4.

Chapter 9

FUNDAMENTALS OF THE FISCHER-TROPSCH SYNTHESIS

A.L. Lapidus

The N.D.Zelinsky Institute of Organic Chemistry, Russian Academy of Sciences, Moscow, Russia

Hydrocarbon synthesis from CO and H₂ is among of rear heterogeneous catalytic polymerization reactions. In the simplest case the reaction could be expressed by the following equilibrium $\text{CO} + 2\text{H}_2 \rightarrow [-\text{CH}_2-] + \text{H}_2\text{O}$. But really the synthesis includes a numerous of consecutive and parallel reactions.

It should be noted that the maximal yield of products formed at stoichiometric CO/H₂ ratio is 208.5 g produced from 1 m³ of synthesis gas converted to normal conditions.

Hydrocarbon synthesis from CO and H₂ was named after Germany chemists Franz Fischer and Heinrich Tropsch elaborated first commercial catalysts and technology of their application.

Some thermodynamics and kinetics regularities of the Fischer-Tropsch synthesis are known. For example, Formation probability decreases in the row: methane>other alkanes>alkenes. Increase in total pressure leads to higher molecular weight products.

- Olefins/paraffins ratio increases with temperature.
- Olefins with a short chain increase at $T > 300^\circ\text{C}$.
- Reaction rate is proportional to hydrogen partial pressure in degree of 2 and inversely proportional to CO partial pressure.

Hydrocarbon synthesis from CO and H₂ is strongly exothermic reaction. The reaction enthalpy is -165 KJ. Thermal effect of the reaction is 600 Kcal/m³ of synthesis gas or 41 Kcal/mol. And heat removal is the main technological problem. VIII Group transition metals catalyze hydrocarbon synthesis from CO and H₂. Ni, Co, Fe, and Ru are among them. The catalysts operate at different conditions. For example, nickel is the most

active at atmospheric pressure and temperature of 150-250°C. Cobalt operates at the same temperatures and at both atmospheric and moderate pressures. Stronger conditions are applied for iron. It can operate at moderate pressure only. Ruthenium is active at low temperature (about 100°C), but needs pressure higher than 1000 bar.

The catalysts differ also in products. Methane is formed on Ni. Cobalt is highly selective to liquid and solid paraffins, that is paraffins containing more than five carbon atoms. Mixture of olefins, paraffins and aromatics is formed on iron. Ruthenium is the most active in polymerization producing polymethylene, but conditions of the reaction are very strong in terms of pressure.

From these four of catalysts cobalt and iron are applied in practice. For example, Shell uses cobalt catalysts in Malaysia, and iron catalysts operate on Fischer-Tropsch plants in South Africa.

Co and Fe catalysts produced from CO and H₂ different hydrocarbon products. For example, in fixed bed cobalt is highly selective to straight paraffins (90% and more). In similar conditions iron produces more olefins and oxygenates (about 30% total). Olefins are main products over iron catalysts in fluidized-bed (up to 70% and more). In this case liquid products also contain oxygenates and aromatics.

Cobalt and iron catalyst are often compared in terms of cost. Iron is well known to be much cheaper than cobalt 1-5 and 20-40\$/pound, respectively). But if the most productive fixed-bed reactor with Co catalysts and the most prevalent fluidized-bed reactor with iron catalyst compared, the share of Fe catalyst in the product cost is more than doubled because iron catalyst life is much shorter in comparison with cobalt one.

The good Fischer-Tropsch catalyst satisfies certain requirements.

- The catalyst has to be mechanically strong and resistant to overheating.
- For high productivity gas hour space velocity has to be more than 1000/h.
- For economic reasons selectivity to liquid hydrocarbons has to be higher than 95% and selectivity to methane lower than 5%.

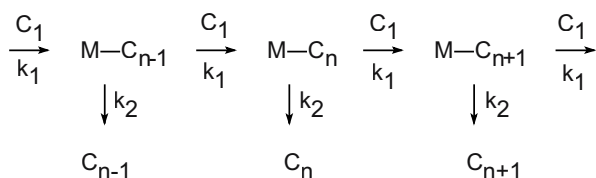
Mechanism of the reaction and principles of catalyst operation have to be clarified to elaborate the catalyst satisfying these requirements. As a heterogeneous reaction the Fischer-Tropsch synthesis proceeds through a certain stages such as

- Adsorption of reactants.
- Formation of intermediates.
- Polymerization and other transformations of intermediates.
- Desorption of products.

Polymerization is the most important stage in terms of the Fischer-Tropsch mechanism. In common case chain growth can be presented as $C_n + C_1 = C_{n+1}$, where C_1 is an elementary link of a growing chain and n is a number of C atoms in the chain. Three main mechanisms of the Fischer-Tropsch synthesis are dependent on C_1 nature:

- C_1 does not contain oxygen. (The mechanism is named "dissociative theory"). According to the mechanism, dissociative adsorption of CO is rate-determining stage. Carbon produced undergoes the partial hydrogenation to initiate appearance of CH_x species that are readily polymerized.
- C_1 contains oxygen and hydrogen. (The mechanism is named "polymerization-condensation mechanism".) In this case the propagation of hydrocarbon chain occurs *via* polycondensation of the intermediates that is polymerization accompanied with water elimination.
- C_1 is CO. (The mechanism of chain propagation *via* CO insertion.) It assumes that CO molecule incorporates into $M-C$ bond and forms new bonds with the surface metal atom and the terminal carbon atom by which the hydrocarbon chain is attached to catalyst surface.

Since hydrocarbon synthesis from CO and H_2 is the polymerization reaction, in steady-state molecular weight distribution of the FT products follows a formal kinetics of polymerization. It can be described by the following way:



This scheme is based on several assumptions:

- Every insertion of C_1 specie can be followed either by one link chain growth or by termination;
- Rate constants of propagation and termination (k_1 and k_2 , respectively) are independent on chain length.

According to the scheme, molecular weight distribution of FT products is unambiguously defined by the ratio of propagation and termination rates, that is by a value of $\alpha = k_1/(k_1+k_2)$.

Based on this model, Schulz derived the equation describing the molecular weight distribution of the products formed by the radical polymerization:

$$W_n = n \alpha^n \ln^2 \alpha,$$

whereas Flory suggested the equation related to the distribution of products yielded by the polycondensation of the bifunctional molecules:

$$W_n = n \alpha^{n-1} (1-\alpha)^2$$

Later Friedel and Anderson showed that both equations are valid for the distribution of the FT products.

Hydrocarbon distribution at a certain alpha could be calculated from Schulz or Flory equations substituting the alpha value and 1, 2, 3, 4 etc. for n (see Fig.1).

Schulz-Flory equations impose some limitations on Fischer-Tropsch the products distribution:

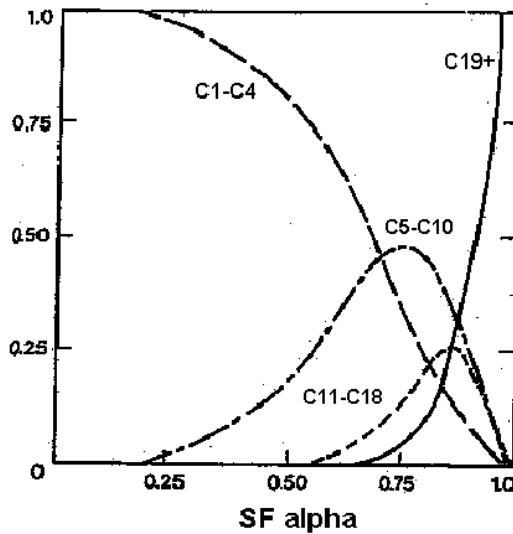


Figure 1.

- Share of gasoline (C₅-C₁₀) in products could not be more than 48 wt.%.
- Share of diesel (C₁₁-C₁₈) in products could not be more than 30 wt.% Methane could be produced with selectivity of 100% .Wax could

formed with selectivity of 100%. It should be noted that molecular weight distribution of Fischer-Tropsch products is a straight line if presented in semi-logarithmic coordinates (Fig.2). And Schulz-Flory alpha characterizing the distribution could be calculated from tangent of angle slope.

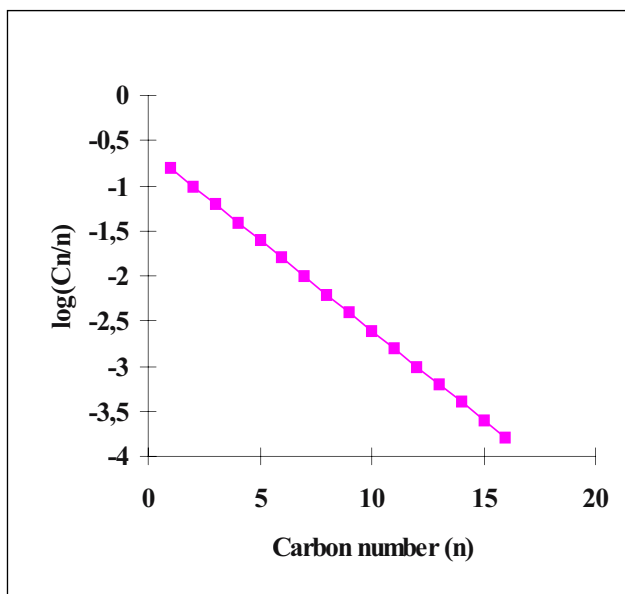


Figure 2.

But normally some deviations from the theoretical distribution could be founded when a composition of real Fischer-Tropsch products is examined. In particular, amount of methane formed in real conditions is always higher than calculated theoretically. The matter is that methane is formed in the Fischer-Tropsch synthesis as a product of two different reactions. In the first place, methane is a first member of polymerization row. And its yield could be calculated according to the Schulz-Flory equations.

Excess methane appears in products due to direct hydrogenation of carbon monoxide. Thus, normally total methane (from polymerization and from hydrogenation) is fixed in Fischer-Tropsch products.

Our investigations of many years give grounds to expect that two noted reactions of methane formation proceed on different sites of catalytic surface. Polymerization site is located on the cobalt—oxide interface. CO is adsorbed on it in molecular form. A low-temperature peak with maximum at temperature lower than 200°C characterizes the site in CO TPD spectrum.

CO hydrogenation site is defined as a small cobalt crystallite. CO is adsorbed on it in dissociative form. In CO TPD spectrum the site is characterized by peak with maximum over temperature interval of 250-350°C.

Obviously, to be effective in the Fischer-Tropsch synthesis a catalyst has to contain mainly polymerization sites. Hydrogenation sites have to be minimized, as less as possible.

Chemical modification is the famous way to increase the number of polymerization sites on Fischer-Tropsch catalyst and, respectively, to reduce CO methanation. Support modification with such oxides as, for instance, ZrO_2 is effectively used in case of cobalt Fischer-Tropsch catalysts. What is its action on Co/SiO_2 catalyst?

Silica gel suited to be a support for cobalt Fischer-Tropsch catalyst has to demonstrate some function of acidity due to the presence of small amount of alumina. Normally, NH_3 TPD spectrum of silica gel contains two main peaks with T_{max} of about 100 and 190°C (Fig.3).

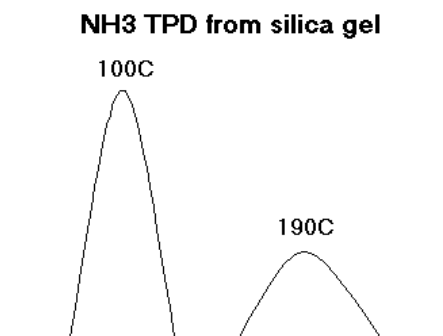


Figure 3.

After silica gel modifying with ZrO_2 total acidity of the support grows up (intensity of NH_3 TPD spectrum of silica gel modified is higher). Moreover, an additional peak appears in low-temperature range due to formation of additional weak acid sites (Fig.4).

$Co-ZrO_2$ catalyst is very effective in the Fischer-Tropsch synthesis. The catalyst operates at low temperature of 160°C. At atmospheric pressure it produces liquid hydrocarbons with the yield of 160 g/m³ (that is about 80% from theory) and selectivity of about 90%. Selectivity of the catalyst to methane is very low and accounts for 3% only. SF alpha of the catalyst is very high for atmospheric pressure (0.9). And the catalyst produces wax at very mild conditions.

Thus, chemical modification is very effective way to reduce methane formation on Co Fischer-Tropsch catalyst. But another way exists also.

It follows from the two-site model of cobalt Fischer-Tropsch catalyst two cobalt sites are different in terms of energy. Polymerization sites are weaker. They are characterized by reversible CO adsorption in molecular form. Hydrogenation sites are much stronger. And CO is adsorbed on them in dissociative form.

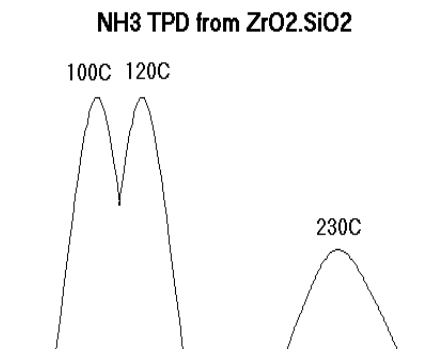


Figure 4.

In such situation, an idea arises to block selectively stronger methane formation sites by catalytic poisons, for example, ammonia.

In fact ammonia could be adsorbed on both Co sites when passed through the cobalt Fischer-Tropsch catalyst. But it is adsorbed reversibly on weaker polymerization sites. And they lost it when ammonia passage is stopped. Contrary, stronger sites continue to keep in place molecules of ammonia. Thus, CO hydrogenation sites remain to be selectively blocked by ammonia whereas polymerization sites could take part in the Fischer-Tropsch synthesis.

How does this show itself in the catalytic experiment?

Practically no change in C₅₊ yield is observed when 1-4% of ammonia is added to synthesis gas (SG). The index remains the same after ammonia removal from the reaction zone (Fig.5).

C₅₊ selectivity grows when ammonia is introduced into synthesis gas (Fig.5) And it remains high after ammonia removal. Both CH₄ yield and selectivity fall down drastically when ammonia is added to synthesis gas (Fig.6). And they both remain low after ammonia removal.

It should be noted that effect of ammonia on liquid product composition has been founded besides methane suppression (Fig.7). This effect is twofold.

First, ammonia treatment leads to higher n/iso ratio in liquid hydrocarbons formed. Second, Schulz-Flory alpha grows after the treatment.

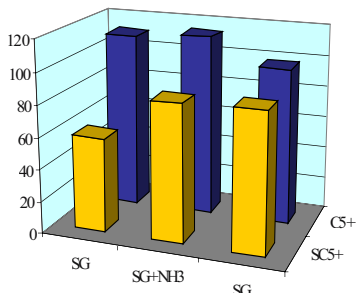


Figure.5. Influence of NH3 on C5+ yield and selectivity

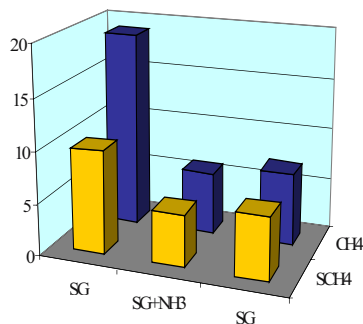


Figure.6. Influence of NH3 on CH4 yield and selectivity

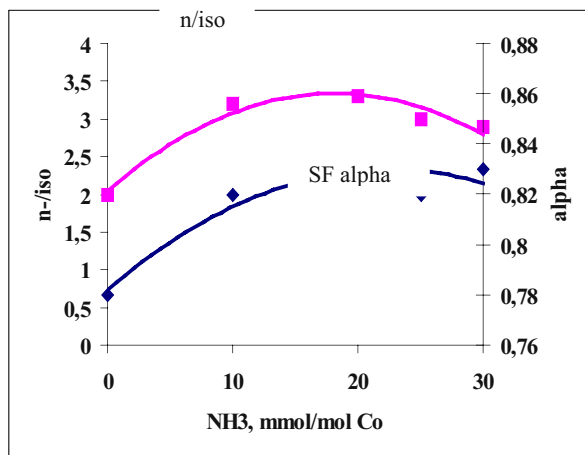


Figure 7.

No surprise that n/iso ratio in liquid products grows up. There are some acid sites on the surface of cobalt Fischer-Tropsch catalysts apart from Co-containing centers. These acid sites take part in secondary isomerization of

hydrocarbons or, more exactly, in isomerization of intermediates. Usually they are relatively strong and could be irreversibly blocked by ammonia. Naturally, this leads to lower amount of iso-paraffins.

Ammonia influence on Schulz-Flory alpha that is on molecular weight product distribution requires more detailed examination. Polymerization site of cobalt Fischer-Tropsch catalyst is bifunctional. It located on cobalt—oxide interface and contains metallic cobalt taking part in red-ox process and an oxide part responsible for polymerization. Oxide part of such site shows property of Lewis acid. That is why a part of cobalt electron density near the interface is shifted from cobalt to oxide.

Formation of Fischer-Tropsch products on such site could proceed by the following way. CO is adsorbed on cobalt—oxide interface. And hydrogen is adsorbed on metal cobalt. CO and hydrogen being activated interact with each other forming an oxide-containing radical. And then two radicals react on Lewis acid site forming C₂ and taking water away. And with time the chain is terminated by reaction with hydrogen.

We suggest that ammonia could be adsorbed on the acid part of the polymerizing site. And a part of its electron density is transferred to the oxide. Thus, ammonia modifies polymerizing site making its acid part weaker and more favorable to polymerization. (Effective size of Lewis site is about 10 Å. Due to smaller size of ammonia molecule polymerizing site still remains accessible for further CO and hydrogen adsorption and interaction.)

Thus, it could be suggested that a combination of chemical modification and selective poisoning is a way to produce "pure" Fischer-Tropsch catalysts. For example, Co supported on zirconia-silica mixed oxide and treated with ammonia produces liquid hydrocarbons with selectivity of about 90% and Schulz-Flory alpha of 0.87. CH₄ selectivity was closed to theoretical one.

It should be noted that natural gas, coal, or any other combustible organic materials could be used as a feed for synthesis gas production. And any Fischer-Tropsch technological scheme based on natural gas or coal as a raw material, includes some indispensable stages. They are synthesis gas production, synthesis gas purification (mainly from sulfur), hydrocarbon synthesis from CO and H₂ (strictly the Fischer-Tropsch synthesis), and product upgrading.

The Fischer-Tropsch synthesis was lucky in commercialization. Its technology was elaborated in 1920th in Germany and commercialized in 1930th. Nine Fischer-Tropsch plants operated in the country during World War II. But all of the nine were stopped after the war on economic reasons.

Only two plants were in operation in 1950th. They were a small unit in Russia, one of the nine Germany plants, with cobalt fixed-bed. It is stopped now. Another, larger scale "Sasol" plant in South Africa operates till now using iron fixed bed.

Arabian-Israel crisis in 1973 led to oil cost jump and faced the world to the Fischer-Tropsch synthesis. The crisis stimulate investigations in the field of synthetic hydrocarbons production. As a result in 1980th-1990th several plants and large-scale pilot-plants have been build.

First of all, two "Sasol" plants with total capacity of about 4 mil.ton/year have to be mentioned. They are in operation since 1980 and 1983 and manufacture liquid hydrocarbons in iron fluidized-bed using coal as the row material. Later, in 1990th "Mossgas" plant has been coming into service using the same "Sasol" technology but natural gas as a feed.

In 1990 "Exxon" pilot-plant was constructed in USA. The unit contains slurry-reactor with cobalt catalyst. Since 1993 "Sasol" has a similar unit in South Africa but operating with iron catalyst.

Since 1993 "Shell" exploits in Malaysia "Shell Middle Distillate" process, two-stage Fischer-Tropsch technology. The process includes production of high molecular weight hydrocarbons from CO and H₂ followed by wax hydro-cracking or hydro-isomerization to produce middle distillates (diesel oil, jet kerosene). Initial capacity of the unit was about 500 kton/year but two years ago it was doubled.

In the middle of 1980th "Mobil" plant in New Zealand has been coming into service. It used an unusual technology differed from the Fischer-Tropsch one. The technological scheme contained stages of synthesis gas production, synthesis gas purification, methanol synthesis from CO and H₂, methanol dehydration, and liquid hydrocarbon production from the mixture of methanol and dimethyl ether over ZSM-5 zeolite. High octane number gasoline was the product in this case. Octane number was about 96 but it was result of high amount of aromatics in the hydrocarbon mixture. Moreover, lifetime of zeolite catalyst was too short because of coking, and inter-regeneration period was about 14 fays only. That is why afterwards the stage of liquid hydrocarbon production was stopped. Now the plant produces methanol only.

"Sintroleum" company (USA) plans to build in Australia a plant for lubricants production from CO and H₂ using Co catalysts. One of the technology features is hydrocarbon synthesis from nitrogen-diluted synthesis gas. The synthesis gas is formed during methane partial oxidation with air but not with oxygen as usual.

Now Fischer-Tropsch synthesis looks very attractive to transport carbon-containing feed from distant regions to developed countries. And the leading

companies such as "Shell", "Sasol" etc. plan to build new plants in different countries (for example, in Indonesia, Nigeria, Qatar).

Chapter 10

REACTOR TECHNOLOGY FOR SYNGAS AND HYDROGEN

Applications, Innovation, Performance and Reactor Engineering

E H Stitt

Johnson Matthey Catalysts

Abstract Changes and developments in the markets for synthesis gas and hydrogen, driven largely by environmental and remote gas monetization, are leading to innovation in the reaction engineering of syngas generation. The opportunities vary in scale from the order of liter volumes of catalyst (fuel cell hydrogen preparation) up to 100 te catalyst (gas-to-liquids). A variety of process options are available, based on steam reforming, partial oxidation and combinations thereof, with varying degrees of integration. Autothermal and Gas-Heated reforming designs are compared. The performance of a reforming process is critically dependent on design, operation and maintenance and aspects of this are reviewed.

Key words: Synthesis gas, Hydrogen, Steam Reforming, Reaction engineering

1. INTRODUCTION

The generation of, what is today recognizable as synthesis gas dates from the first quarter of the last century, with the deployment of the classical Haber Bosch process in 1917, based on the reaction of steam with coke. In 1931 Standard Oil built a plant to generate hydrogen from refinery off-gases at Baton Rouge; the reforming reaction took place over a catalyst in vertical tubes in parallel rows in a radiant, fired furnace. Work in ICI in the 1950s led to a more stable catalyst, operated at economic steam ratios without excessive carbon formation and resistant to poisons. In 1959 ICI started up the first large-scale pressure steam reformer using naphtha as a feed. This plant and technology became the forerunner to over 400 plants subsequently licensed around the world in areas where natural gas was not readily

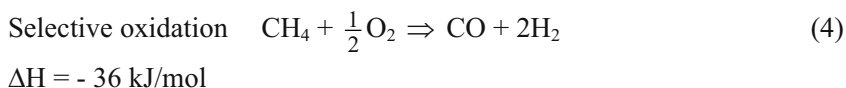
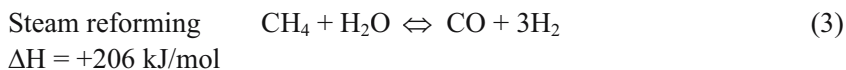
available. From 1959 to present, development of the catalyst has allowed plants to be run at higher pressure and temperature, using feedstocks with different hydrogen:carbon ratios and the processing of unsaturated and aromatic containing feeds.

In the last 25 years the increased availability of natural gas has resulted in its use as the main feedstock for steam reforming with development of the catalyst for longer life, higher activity, reduced carbon formation and with improved physical attributes.

The last 5 years have however seen a shift in emphasis. While the use of reformed gas has historically been dominated by hydrogen manufacture for commercial use, and for ammonia and methanol synthesis this may not remain the case. Two "new" applications of syngas are becoming of increasing importance: the manufacture of liquid fuels from remote, marginal or stranded natural gas - so called "gas-to-liquids" or GTL - where Fischer Tropsch chemistry is currently the favored route, and generation of hydrogen from natural gas or liquid fuels to power mobile and stationary fuel cells.

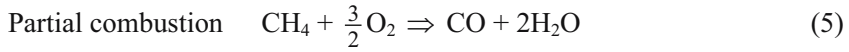
2. ROUTES TO SYNGAS AND HYDROGEN

There are, in essence, two means to generate syngas from a hydrocarbon fuel. These are (exemplified for methane):

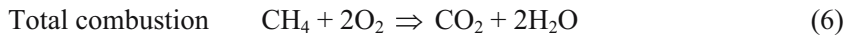


All syngas manufacturing routes are based on one or both of these, idealized, catalytic reactions. Note importantly that the reforming reaction is equilibrium limited and high conversion is thus favored by high temperature. It is important also to note the opposing thermochemistry of these reactions - with the steam reforming reaction being highly endothermic whereas the partial oxidation reaction is slightly exothermic. In steam reforming, an excess of steam is used to suppress carbon formation but also beneficially serves to reduce the adiabatic temperature fall.

The reality for the oxidation reaction is of course that it has a propensity, especially if uncatalyzed and not oxygen limited, to give the fully oxidized products, thus increasing the exotherm. This can be summarized by the following reactions



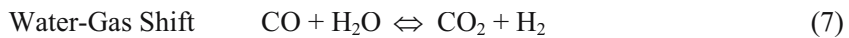
$$\Delta H = -519 \text{ kJ/mol}$$



$$\Delta H = -802 \text{ kJ/mol}$$

Given this, it is easy to theoretically envisage systems where the heat of reforming is balanced by combustion or oxidation. The significant differences between alternate processes relate to the nature of the oxidation and combustion, the extent to which they are decoupled (spatially, temporally) and the relative reliance on each reaction.

In both reforming and oxidation reactors the water gas shift reaction will occur:



$$\Delta H = -41 \text{ kJ/mol}$$

At the temperatures prevailing in either type of reactor this reaction is fast and non-catalytic and will probably be near equilibrium. The reaction, as shown, is slightly exothermic and therefore high temperatures encountered in oxidation or reforming will push conversion in favor of CO. CO_2 incidentally produces syngas via the catalyzed reaction

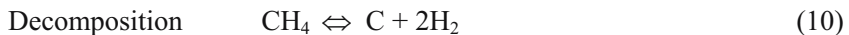


$$\Delta H = +247 \text{ kJ/mol}$$

The other important side reactions are those leading to the formation of carbon. In reforming these are as follows



$$\Delta H = -172 \text{ kJ/mol}$$



$$\Delta H = +75 \text{ kJ/mol}$$



$$\Delta H = -131 \text{ kJ/mol}$$

In oxidation conditions, carbon forms due to soot formation mechanisms and oxidative dehydrogenation of the hydrocarbon. In either case the formation of carbon species is suppressed by use of steam. The control of

carbon formation is important in all forms of syngas generation for reasons not only of catalyst longevity but also materials of construction.

3. CONVENTIONAL STEAM REFORMING

The overall flowsheet for steam reforming is dependent on the required end product. Figure 1 shows a generalized flowsheet, which is in fact the flowsheet for the generation of ammonia synthesis gas.

In ammonia manufacture the purpose of the secondary reformer is to add heat but also a convenient means to introduce the nitrogen. Clearly in the case of methanol only the primary reformer is required although an oxygen fired secondary reformer can be employed. For FT, primary reforming alone gives too high a $H_2:CO$ ratio and an oxygen fired secondary reformer is required, or an alternative reactor. For hydrogen generation the secondary reformer would normally be omitted. The key and common feature of all the flowsheets is the large, fired box reformer, where the firing may be from the roof or the walls. The steam plus hydrocarbon is passed over the nickel catalyst in tubes, typically 100-150 mm diameter. Extreme conditions are required to provide the reaction heat and high temperature and pressure are required to achieve good equilibrium methane conversion.

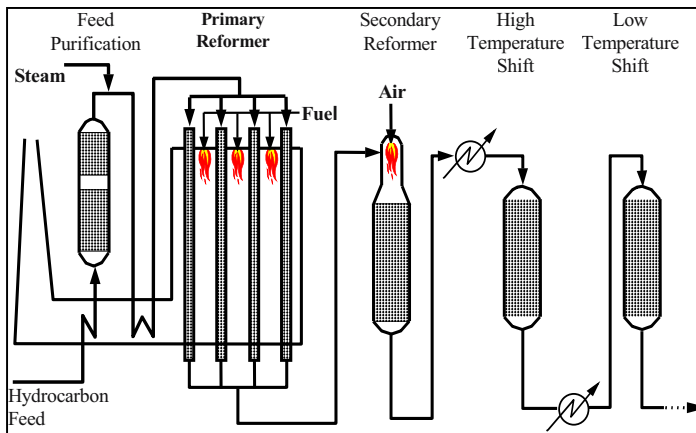


Figure 1. Generalized Steam Reforming Plant

While this is the most commonly used approach for all the applications mentioned, it has a number of disadvantages including large size, high cost, slow response, higher $H_2:CO$ ratio than required for methanol and FT. It is

certainly unsuitable for a floating or mobile facility due to weight and size, sensitivity to motion and safety hazard potential

Cost analysis of a methanol plant [1] indicates that the syngas generation section comprises 50% of the total capital cost, rising to 70% if the syngas compression is included. In order to achieve significant cost reductions and location flexibility a significant shift in the underpinning reactor technology and its cost base is required.

4. APPLICATIONS AND MARKETS

As a preamble to considering the alternate syngas technologies it is worth reviewing the demands of both the conventional and the perceived "new" applications. These will be considered in approximately the reverse order of scale.

4.1 Gas-to-Liquids

There are a number of potential scales and environs. The monetization of remote and marginal gas through chemical conversion to is generally associated with Fischer Tropsch (FT) synthesis. In general, for FT, a syngas with a $H_2 - CO$ ratio of approximately 2 is required. There are a limited number of FT plants operating, of which two are gas fed (PetroSA in South Africa and Shell in Malaysia). The opportunity falls into two categories:

- Remote Gas: Alaska, Middle East, Africa, Caribbean, North Sea, China etc. An opportunity for GTL to generate a transportable clean fuel. Projected plant sizes are several times larger in syngas capacity than any existing operating single train reformer.
- Marginal Gas. Gas associated with oil fields is predominantly flared as a waste product at present. Environmental pressure will push for this gas to be used beneficially. The gas rate here is lower than for remote gas and some applications are offshore.

There is a clear future driver to extract value from remote and marginal gas where an economic case can be made and where environmental factors dictate. This will probably become a reality over the next 3-10 years, providing the economics of GTL can be made competitive with liquefied natural gas (LNG).

4.2 Refinery Hydrogen

The major use of hydrogen is in refineries. The hydrogen required mostly comes from two sources, catalytic reformers and 'on-purpose' hydrogen plants. Over 85% of 'on purpose' hydrogen production is by steam reforming. Environmental regulations for cleaner fuels, related mainly to sulfur or aromatics content, lead to increased hydrogen demand via hydrodesulfurization and hydrogenation respectively.

Choices for meeting the increased hydrogen demand include new capacity, revamping existing capacity and purification and recovery of hydrogen from other refinery streams. There is much debate in the industry at present as to how the regulations can be achieved in each particular refinery. It is evident however that over the next 5 years significant additional hydrogen production will be required.

4.3 Methanol

This is a traditional user of syngas technology, with the vast majority of the world's methanol plants being based on fired steam reformers. The future of methanol is currently a little uncertain.

The trend now appears set against the use of MTBE as a gasoline additive. A number of States in the USA have already put plans in place to phase out its use over the next 3-5 years. It is however not clear that the rest of the world will follow this trend. MTBE through the 1990s accounted for 25-30% of methanol usage and the possible loss of a portion of that market is having a significant effect on the future expectations of the methanol producers; an industry that historically swings between glut and high margins may be on a downwards path, unless alternative uses for methanol can be found.

Methanol is a very effective means of fixing hydrogen into the liquid state and has potential use as a liquid hydrogen source for automobile fuel cells, either through reforming to hydrogen or in "direct methanol" fuel cells. The main alternative is a gasoline fraction. If it is methanol, then this will provide an enormous boost to that industry and in due course encourage increased production. As a measure of the possible tonnages involved, the American Methanol Institute estimates [2] that 10 million Fuel Cell Vehicles will consume 13-14 million tons of methanol per annum, to be compared with the current global methanol market of 30 million tons.

Recent presentations from BP [3, 4] propose the concept of a "gas refinery" in which methanol is a key intermediate from which chemical and fuel products can be made. Methanol utilization chemistries are several and

include di-methyl ether and methanol-to-gasoline (MTG) process [5] and methanol-to-olefines (MTO) as examples. These are potentially important future markets for large scale methanol manufacture.

4.4 Ammonia

One of the earliest users of reforming technology, ammonia production is used to fix nitrogen into a form from which it can be effectively used as a fertilizer. The main use of ammonia is still into the fertilizer industry and thus its production is inextricably linked to the trends in that market. Minority uses, amounting to approximately 20% of ammonia use, are for explosives and nylon. The use of inorganic fertilizers in Europe and North America has been in decline for 10 years or more. This is a low growth market, with mature technology. The trend is to move production to locations with the cheapest gas supply such as Australia, Caribbean and Middle East - while ammonia plants in Europe and North America are frequently in cost cutting mode to compensate for the natural gas price differential.

4.5 Reducing Gas Manufacture

The use of a synthesis gas mixture of carbon monoxide and hydrogen is now well established as a method for the direct reduction of oxides in metals manufacture. Unlike the cases above, the syngas is not required at pressure and so the technology has developed towards a much lower pressure reforming. The essential reformer design is unchanged, comprising vertical tubes in a fired box, but due to the lower pressure the tubes are larger diameter and the reforming pellets considerably larger than is the norm in the higher pressure operation. This market sector appears to command lower margins than the traditional syngas markets of hydrogen, methanol and ammonia.

4.6 Fuel Cells

The fuel cell is, simplistically, a device for turning hydrogen into water but generating electricity as part of the reaction energy. There is a wide range of applications here, dictated not only by the application and size but also the nature of the fuel cell. Large units (several MW) are likely to be based on solid oxide or molten carbonate fuel cells. In both of these the

operating temperature is such that internal reforming of a hydrocarbon fuel is realistic, especially for the former.

The focus for present purposes is on smaller units: say < 100 kW up to 1 MW . These are most likely to be based at or near ambient operating conditions in the fuel cell. Both the currently commercially available phosphoric acid fuel cell (PAFC) and its probable replacement, the polymer electrolyte membrane (a.k.a. proton exchange membrane) fuel cell (PEMFC), operate at relatively low temperatures: approximately 200 and 60-80°C respectively. As such, generation of the hydrogen must be decoupled. It may further be noted that for the PEM there is sensitivity to CO and hydrogen purification is required. There are two distinct applications in terms of scale and priorities

4.6.1 Mobile Power (Cars, Buses, Lorries),

The hydrogen will be generated from a liquid fuel (methanol, gasoline ...). The power rating is likely to be in the order of 20-100 kW and the design emphasis is on compactness, flexibility, automated operation, reliability and rapid start-up. While for methanol fuel decomposition may seem logical, the development emphasis does appear to be on reforming or partial oxidation [6].

4.6.2 Stationary Power Units

The power rating will be in the order of 100 - 500 kW and the hydrogen will be generated from natural gas or a liquid fuel (kerosene, gasoline, diesel). Units rated at up to 250 kW, based on PAFC, have been commercially available for a number of years from IFC (International Fuel Cells) with their own partial oxidation based hydrogen generation system.

4.7 Distributed Syngas and Hydrogen Manufacture

There is a large number of applications and manufacturing processes that require hydrogen or syngas in much smaller quantities than refineries and methanol plants. Traditionally these have taken hydrogen “over the fence” if pipeline hydrogen is available, such as on the US Gulf coast or in large petrochemical complexes. Alternatively the hydrogen has been sourced as a trailed import.

As an application example, consider a typical edible oil hydrogenation unit that has a hydrogen demand of approximately 0.25 – 0.5 te/day. This is only in the order of 1% of the capacity of a typical (refinery) hydrogen plant

but is of a similar order of magnitude to that required for stationary fuel cells (100 – 500 kW capacity). The development of smaller scale reforming technologies, particularly for offshore and fuel cell applications is promising to deliver a low cost compact hydrogen plant that may be competitive with trailered hydrogen.

5. SCALES OF OPERATION

The preceding section has given a brief summary of current and possible future major users of syngas and hydrogen. There are of course others, such as the manufacture of carbon dioxide. What is clear from the previous section is that the operations cover a wide range of scale, Figure 2. These data indicate a potential for a variation in reformer size over some four orders of magnitude.

6. OUTLINE OF ALTERNATIVE TECHNOLOGIES

From the above it is evident that future demands on syngas and hydrogen generation will straddle the existing scale of operation. Despite this, similar approaches appear valid across the scale ranges. There are thus a number of distinct, almost generic approaches vying with the conventional fired reformer, and all at varying stages of development.

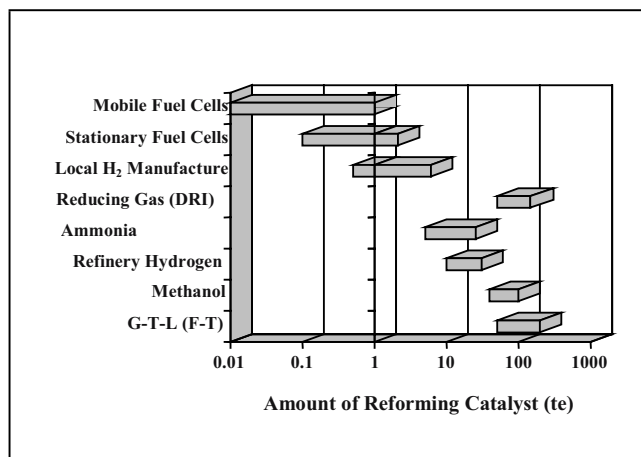


Figure 2. Scales of Operation for Reforming

6.1 Autothermal Reforming

The gas or vapor is burned in air (or oxygen) and the resulting gas passed over a nickel reforming catalyst (Figure 3). This has been proposed for both Fischer Tropsch and fuel cell systems, and indeed methanol in the past. It has the ostensible advantage of simplicity. This is not however strictly true. The process gas exits the reformer still at elevated temperature ($> 800^{\circ}\text{C}$) and thus significant heat exchange and recovery duty are required. Large-scale adiabatic autothermal reformers have already been built in the industry, whether as secondary reformers on ammonia plants or as pre-reformers for the processing of heavier feedstocks. The existing leading catalyst and technology suppliers in syngas therefore have considerable experience here.

6.1.1 Use of Air or Enriched Air

In a variation within the theme, the use of air, or enriched air, rather than oxygen has been proposed for both methanol plants [7] and for FT [8, 9]. Operation is at higher total pressure to maintain reactant partial pressures. The use of air has the ostensible benefit of removing the requirement for an oxygen plant, reducing cost, but with the knock on effect that the synthesis reactor now includes significant volumes of nitrogen inert thus increasing costs. The penalty would appear to be the higher in methanol where there is a significant recycle in the synthesis "loop". It is not clear that the overall cost considerations favor the use of air for either methanol or FT.

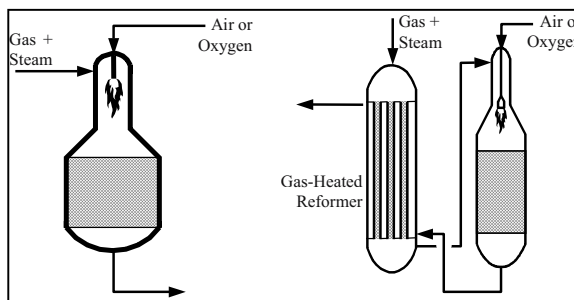


Figure 3. Autothermal and Gas-Heated Reforming Concepts

6.1.2 Coupled Reactions

In a further development from the concept of autothermal reforming, a number of workers [10 – 12] have suggested direct heat exchange coupling of oxidation and reforming. The reactions, both catalyzed, occur on opposite sides of a rigid, impermeable barrier through which the heat will transfer. It is not clear how operable these systems will be in terms of local and overall dynamics, steady state multiplicity and working lifetime.

6.2 Partial Oxidation (Thermal)

Syngas may be generated by simply burning the methane (or vaporized liquid fuel), in the absence of a catalyst, under oxygen starved conditions. This does lead to carbon formation, but also very low CO₂ content of the product and low methane slip. It leads also to a naturally low H₂ : CO ratio: 1.6 or thereabouts. In practice this requires a dedicated hydrogen plant operated alongside to achieve required H₂: CO ratios.

This technology is believed to be used in the Shell GTL plant at Bintulu, Malaysia, plus a conventional fired steam reformer, fed with FT tail gas, to generate a higher H₂ content syngas to adjust the overall H₂ : CO ratio upwards.

6.2.1 Fluidized Bed Partial Oxidation

A similar process to that above has been explored, but using a fluidized bed, with both catalytic and non-catalytic fluidized particles. The non-catalytic process has been observed by some to generate excessive soot/carbon. The catalytic approach may be more interesting and has been developed further by BP [13]. Subsequently Shell [14] has developed the non-catalytic route. None of these developments appears to be commercial, nor are they believed to be still under development

6.3 Catalytic Partial Oxidation.

It has been shown that by running at very high space velocity and temperature over a platinum group metal gauze catalyst or supported on a honeycomb monolith, it is possible to obtain partial oxidation of the methane to CO and hydrogen. Thermodynamically, the formation of CO and H₂ is favored at high temperatures. Feed ratios and/or the shift reaction can be used to obtain the correct H₂ : CO ratio for downstream processing or

synthesis. Considerable work has been done in this area; most notably by Schmidt [15]. A commercial development project is believed to be ongoing for this technology

Extensive work on metal oxides for catalyzed partial oxidation, with structured or packed bed catalyst is reported in the literature [16]. There is currently no known drive for commercialization.

6.4 Fluidized Bed Reforming

Exxon has developed a dual-functional fluidized bed process [17] where the feed gas is subject to both oxidation and reforming actions. The oxygen is introduced into the middle of the methane/steam fluidized bed. The heat released by the oxidation drives the reforming reactions. The fluidized bed ensures good heat transfer. Operating temperatures lower than those typical of the partial oxidation are claimed, leading to improved oxygen efficiency and improved thermal efficiency. This technology has been demonstrated at pilot scale over a three year period.

6.5 Gas Heated Reforming

This is a two step process (Figure 3). The net heat generation is by a "secondary" autothermal reformer, but the exit gas is fed back into a primary, heat exchange reformer (or Gas Heated Reformer - GHR) where the incoming process gas plus steam is reformed over a conventional nickel catalyst prior to feeding to the secondary, autothermal reformer. The primary reformer is thus essentially replaced by a heat exchange reactor based on multiple tubes. Originally developed by ICI in the late 1980s [18], this technology has been successfully applied at the manufacturing scale for ammonia, and more recently over an extended period at the pilot scale for methanol with an oxygen fired secondary reformer [19].

6.6 Separative Reforming

There is significant effort to try and exploit the separative capability of membranes and adsorption in conjunction with the reforming reaction.

6.6.1 Membrane Reforming I - Hydrogen Removal.

A palladium membrane is used to remove hydrogen from the reformat in situ and thus remove the equilibrium barrier[20]. This has only been achieved to any extent at the laboratory scale. Major problems remain with

obtaining a Pd membrane of sufficient integrity but with sufficient flux. This barrier to success will probably lead to this technique remaining a laboratory and theoretical curiosity for many years.

6.6.2 Membrane Reforming II - Oxygen Separation.

A mixed oxide (e.g. perovskite) membrane is used to separate oxygen from air and in so doing feed oxygen into the flowing gas stream [21]. The transport mechanism is in fact an electrical counter transport and requires temperatures in the order of 700-800°C to achieve practical transport rates; which is of course in the same temperature range as required for reforming. The oxygen permeate promotes a partial oxidation reaction, essentially at the membrane surface. It has in fact been found necessary to use a catalyst in situ to promote the oxidation [22]. In reality a reduction catalyst may also be required at the "air face" of the membrane. The eluent from this reactor is then passed over a reforming catalyst to maximize methane conversion. This technology is currently the subject of two major consortia funded projects [23]; one led by Air Products the other by Praxair and BP.

6.6.3 Adsorptive Reforming

Work in Russia in the 1970s (although not published in the west until the 80s-90s) considered the use of a solid adsorbent to remove CO₂ from a reforming or shift reactor, as a means of pushing the reforming and/or shift reactions towards full conversion. In principle this will allow a simplified, even single step, process for the generation of high purity hydrogen at high methane conversion. This original work [24, 25] used dolomite as the adsorbent with a thermal swing regeneration. This idea has been revisited by Harrison et al [26]. Air Products (with DOE support) is also exploring this approach [27] but with a hydrotalcite adsorbent that can operate at lower temperatures than the dolomite and be regenerated through pressure swing. The two approaches differ also in the process concept. The former explores a fluidized / raining bed approach, similar to the original Russian work, while Air Products proposed adiabatic fixed cycling beds (similar to PSA).

6.7 "Dry" Reforming.

The principle here is that CO₂ is ostensibly able to fulfill a similar role to steam in respect of both reforming and carbon inhibition. The dry reforming reaction is given in Equation (8). This gives a lower H₂/CO ratio than the

use of steam, and thus a syngas more suited to FT is available, and is also of interest as an increased efficiency route to the manufacture of CO. This is not yet practiced commercially and there are development uncertainties in the catalysis. The recycle of CO₂, or its specific use in conjunction with steam is however known.

6.8 Reforming for Fuel Cell Hydrogen

There is considerable effort, both actual and reported in this area. Companies and academics are making a significant input not previously active in the syngas or reforming area. Unsurprisingly however, the solutions being proposed generally comprise a mix of POx, ATR and compact reforming, with of course shift and CO removal steps downstream to give a hydrogen rich stream that can be fed to the PEM fuel cell. It is clear that the drivers for automobile and stationary applications are not the same, other than capital cost minimization. The stationary systems appear to favor reforming. In the context of fuel cells there is a need to move the balance of oxidation vs. reforming towards reforming in order to obtain maximum hydrogen yield and hence also fuel efficiency. However for automobiles simplicity, robustness and size are the dominating drivers. With this exception, the general thrusts are similar to those for GTL despite the difference in scale, noting however that while for GTL the question is how far a technology will scale up, for fuel cells, and especially automobile applications, the problems are scaling down (or miniaturization).

7. GAS HEATED REFORMING TECHNOLOGY

The first gas heated reforming process, a syngas generation technology that combines autothermal reforming and a heat recovery based primary reformer, was developed by ICI in the late 1980s. The first commercial examples were ammonia plants, successfully commissioned in the late 1980s. These plants have thus now been operating successfully for more than 10 years. This "LCA" (Leading Concept Ammonia) technology was later modified, in a joint venture with BHP Petroleum, to feature an oxygen (rather than air) fired secondary reformer for the LCM (Leading Concept Methanol) process [28], which was demonstrated at pilot scale over a three year period from 1994. This required the development of the autothermal secondary reformer for oxygen fired operation.

7.1 Gas Heated Reformer Development

The original GHR designs featured a bayonet tube construction. This was used to avoid problems of tube and tube-sheet stresses arising due to differential thermal expansion of the tubes and the shell. This however led to high costs and poor scalability. In the late 1990s development work was focused on the development of a “hot end” tube-sheet seal that would allow tube movement during start-up and shut down, thus allowing a more conventional design featuring two tube-sheets [29] - the Advanced Gas Heated Reformer (AGHR). This allows simplification of the mechanical design of the upper tube sheets. The benefit is that the AGHR is cheaper to manufacture and can be scaled up to a methanol plant size equivalent to 6,000 mtpd in a single reformer shell [30].

7.2 BHP Petroleum Methanol Research Plant

In order to verify and develop the LCM process for offshore operation BHPP first built the Methanol Research Plant (MRP) as an onshore plant near Melbourne, Australia. The MRP was successfully commissioned in October 1994 with a BHPP operating team supported by a team from Johnson Matthey. The plant was running at 100% of flowsheet after 2 weeks and towards the end of 1994 a high trial rate of 200 mtpd was achieved without any impact on product methanol quality.

The GHR has performed well from start-up, in fact slightly better in terms of catalyst activity and heat transfer performance than design, and with no evidence of metallurgical attack. Similarly, the secondary reformer performed excellently. Inspection of the burner at planned shutdowns has indicated no observable wear and deterioration of the hot face of the refractory has also been found to be minimal. The high quality of mixing in the header space of the secondary is evidenced by the fact that the exit gas is found to be virtually at the steam methane equilibrium.

After the development of the AGHR, it was possible to directly replace the GHR on the MRP in a shutdown in 1998 as part of the ongoing R&D program. The cost savings of the AGHR in fabrication were proven to be as predicted and upon commissioning the operational efficiency validated the success of the seal design (no methane leakage from tube to shellside). The plant was tripped and restarted a number of times in the first few month's operation to ensure that the sliding seal did not bind or seize. The vessel has been opened and the seals inspected. They showed no signs of wear or deterioration.

7.3 Gas Heated Reforming for GTL

While the development by Johnson Matthey and BHPP discussed hitherto has focused on methanol, the syngas section of the plant will remain substantially the same for a Fischer Tropsch (FT) unit. The optimal syngas for FT synthesis is usually at 20 - 30 bara with a $H_2:CO$ ratio exit the syngas generation plant section of 1.9-2.1. FT is also favored by low concentrations of all of CO_2 , CH_4 and N_2 . Many similarities exist between the synthesis gas requirements of FT and methanol processes, but key differences include lower optimal steam content and $H_2:CO$ ratios. Conventional steam reforming generate a $H_2:CO$ ratio higher than required for FT stoichiometry, and also allows a relatively high methane slip and CO_2 production and is thus not really ideal on its own. Clearly, all of the oxygen-based processes are applicable, namely POx, ATR and GHR processes.

7.4 Gas Heated Reforming for FT Syngas

Based on published studies [31, 32] and internal work it is possible to build a comparison of the main features of the autothermal and gas heated reforming alternative routes to FT syngas, Table 1, based on process simulations [33]. These data show that the GHR based process gives not only the highest carbon efficiency but also the lowest oxygen requirement and lowest CO_2 emission.

Table 1. Comparison of Routes to FT Syngas

Reformer		ATR	GHR	
Steam Ratio		0.6	1.0	0.6
Carbon Efficiency	%	75.2	80.7	82.8
Total Energy	GJ/bbl	9.6	9.0	8.7
Oxygen	kg/bbl	210	162	160
CO_2 Emissions	kg/bbl	120	87	75
Water Produced	kg/bbl	181	153	152
HP Steam	kg/bbl	868	273	225
Power Required	kWhr/bbl	162	130	128
Air Cooling	kWhr/bbl	937	698	650

There are of course a number of features in common. Both require oxygen that is reacted with the process gas, in the presence of steam, prior to passing over a catalyst. The inherent feature of the GHR technology is that the combustion takes place at a lower temperature, explained simply by the fact that, for the same exit temperature (equilibrium conversion) less endothermic reforming takes place downstream of the combustion in the GHR flowsheet than in an autothermal reformer alone. That is, the

combustion heat is more effectively recovered through the convective heat transfer that occurs in the GHR and this results in a higher carbon efficiency and lower oxygen requirement. This difference is at the root of the process differences Table 1. In summary:

- The GHR flowsheet produces around 7 – 10 % more FT liquid product from the same gas feed rate.
- The GHR flowsheet requires only approximately 75 % of the air separation duty of ATR. The ATR requires more power in the process, but as a penalty also generates more steam and therefore has a tendency to export more power.
- The emission of CO₂ from an AGHR plant is 38 – 60 % lower than for the ATR.

All of these factors affect the unit capital cost. While the GHR + Secondary is more expensive than a single (but larger) autothermal reformer for the same FT product duty, the above analysis indicates that other sections of the plant are considerably smaller. Overall the LCL process has a lower capital cost than the ATR based process in addition to the ongoing operational benefits from the AGHR based flowsheet.

One operational advantage of the GHR lies in a higher carbon efficiency and lower CO₂ emission. While this may not appear important in the overall context of gas at a marginal value this will probably not remain so. Resulting from the various international protocol agreements, taxes on CO₂ emissions may become reality.

7.5 GHR Development for FT Syngas

The key to improving the economics of gas heated reforming based syngas generation for GTL lies primarily in reducing the operating steam - carbon ratio (S/C). The main calculations in this paper are based on an S/C of 2.0 and 0.6. The former is within the known operating window for the existing metallurgy and catalyst and is thus proven.

This can be reduced to 1.5, offering significant benefits, as can be inferred from the data above. The existing metallurgy is believed to be satisfactory, although this does need running on a plant to be demonstrated. A steam ratio of 0.6 would give further significant benefits in cost. This is an achievable target for the catalyst (activity at lower temperatures) and thus the process is feasible at this reduced steam-carbon ratio. The main development requirement here is however on the shellside, where a metallurgy development and materials testing program is ongoing. The viability of materials developed for this application is now the subject of an

evaluation on a pilot scale AGHR “Materials Demonstration Unit” operating in New Zealand in collaboration with Methanex.

As an alternate approach to syngas generation using the GHR, the concept of a Flue Gas Heated Reformer has been developed [34]. This is intended to give options for replacing the oxygen fired secondary, and thus because air is used in the burner for the flue gas, avoids the cost of the oxygen plant without incurring the penalty of high nitrogen concentrations in the synthesis loop.

8. ENGINEERING OF SYNGAS PROCESSES

This section will address some practical issues of reforming, focusing primarily on steam, autothermal and heat exchange reformers. Issues addressed will include:

- Firing and burner design
- Flow distribution
- Catalyst loading
- Catalyst shape and heat transfer

8.1 Reformer Firing and Burner Design

Steam reforming is a strongly endothermic reaction (Eqn 1), and equilibrium limited. High heat input is required to maintain temperature and reaction rate, while high temperature is needed to achieve high conversion. But high temperatures increase carbon formation and wear on tubes. Hot tubes rapidly deteriorate. It is thus essential to obtain correct design of the burners in order to achieve good operation of the reformer.

There are essentially three general burner design approaches: top fired, side fired and terrace wall fired: Figure 4. Top fired reformers usually have the higher radiant efficiency, typically 50-55% compared to 40-45% for side fired reformers. Side fired furnaces tend to can achieve higher exit temperatures with little no detrimental effect on tube life.

With tubes numbering in the hundreds, and a similar order of magnitude of burner heads obtaining uniform conditions across the reformer is no simple matter. This entails obtaining not only similar flow of process gas through each tube but also good mixing of the air-fuel mixture in the headers and a similar flow of the fuel/air mixture to each burner. A key aspect for the tubes is the catalyst packing and resulting pressure drop - and this is addressed in a later section.

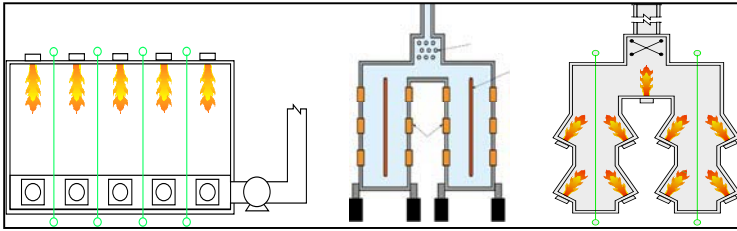


Figure 4. Top, Side and Terraced Wall Firing for Steam Reformers

For the burners, detailed design of headers, distribution manifolds and burners is required in order to ensure uniformity and to avoid flame impingement on the tubes (which will lead to rapid failure). CFD may be successfully used to predict the gas mixing and flow within the manifolds and the combustion behavior from the burner.

Figure 5 shows the output from a furnace-side CFD simulation for a top fired furnace [35]. The benefit of this type of calculation is the direct prediction of tube heat fluxes, enabling the assessment of the impact of burner or firing changes. Flow distribution in the headers feeding the tubes is equally important and poor design of these can impact significantly on performance, even with properly and uniformly packed tubes. CFD can equally be applied in this application.

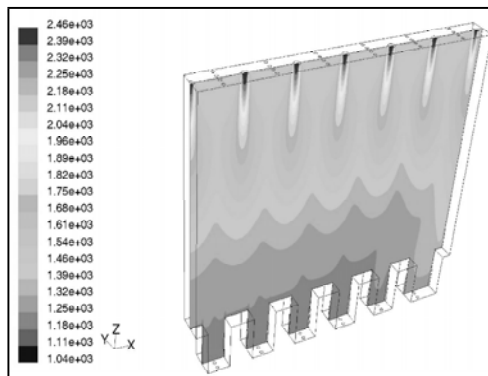


Figure 5. CFD Results for Design of Furnace Side Burners and Headers

The performance of autothermal and secondary reformers is critically dependent on the mixing of the oxygen and hydrocarbon in the headspace above the bed, and in achieving a uniform temperature over the cross section as the gas enters the bed. The effects of poor mixing on the performance of

an air fired autothermal secondary reformer are shown in Table 2 [36], and can readily be seen in terms of methane slip even though a higher average exit temperature is obtained. These effects are considerably worse for an oxygen-fired reactor.

Table 2. Effect of Poor mixing on Secondary (Autothermal) Reformer Performance

	Good Mixing	Poor mixing		
		Half @ +20% air	Half @ -20% air	Combined average
Reformer Exit Temperature	957	902	1034	971
Methane exit concentration (mol% dry)	0.62	1.89	0.13	0.97
Approach to Reforming Eqm. (°C)	10	10	10	53
Approach to Shift Eqm. (°C)	0	0	0	6

Considerable effort is therefore required to assure good mixing and uniformity of temperature at the bed entry. Again, CFD is an invaluable tool for this when coupled with the gas phase oxidation kinetics, allowing mapping of flows, concentrations and temperatures in the header space, Figure 6, and the optimization of the design of the burner [37].

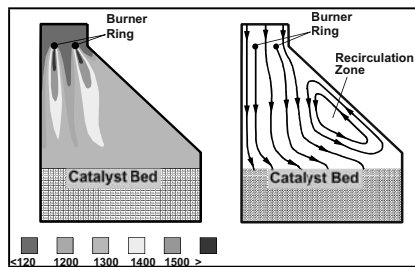


Figure 6. CFD Results for Flow and Temperature in an Autothermal Reformer

8.2 Catalyst loading

There are essentially two types of catalyst loading problem in reforming. One is the large fixed bed, typified by the adiabatic Autothermal reformer. The other is where the catalyst is contained within tubes, such as the fired reformer of the gas heated reformer. Either may involve specialized catalyst handling techniques. Different methods are used, but the goal is always the same: to achieve as near as possible a uniform distribution of catalyst.

8.2.1 The Importance of Even Catalyst Loading

Uneven catalyst loading, characterized by a distribution on bed porosity leads to uneven flow, with higher flow rates through the areas of low voidage. The effects of this are dependent on the type of reactor. In all cases however this leads to radial temperature gradients and non-uniform conversion. This is never as good as uniform flow. There are specific effects in tubular, fired reformers that will be addressed later.

In general the packing of a catalyst is dependent on the way in which the particles fall and settle. If particles are allowed to collide with other particles before they settle into position, this tends to lead to bridging, and thus high voidage. Likewise, particles that roll rather than fall into position tend to align differently, and thus present different porosity and pressure drop characteristics. Loading techniques are thus aimed at providing a uniform discharge and settling pattern to all particles to obtain as near as possible a uniform porosity

8.2.2 Adiabatic Fixed Beds (Autothermal Reformers)

The catalyst bed is supported on either a support plate or on inert ceramic balls, or in some cases a combination thereof. The catalyst will normally be loaded from a "big bag" - containing in the order of 1 m^3 of catalyst. In large vessels, it is important to move the "sock" through which the catalyst is charged from the bag around the area of the vessel to prevent systematic variation in the way the catalyst particles arrive and settle, and thus in voidage. In order to prevent breakage it is normal to limit the free fall of the particles to 1m.

8.2.3 Flow in Packed Tubes and Packed Beds

The fluid flow patterns in a packed bed are a direct result of the porosity structure of that bed. Areas of large voidage, or large inter-pellet dimensions will have larger flows than tightly packed regions. Magnetic resonance imaging (MRI) of liquid flows in packed tubes gives significant insight into the distribution of not only voidage but also the resulting fluid flow.

The MRI can be used to map the bed matrix, and propagator measurements (similar in output to a tracer) can be used to map the velocity vectors of the fluid flow. Flow simulations can be carried out based on the digital mapping of the bed, based on a uniform voxel size. Lattice Boltzmann (LB) simulations are particularly suited to this. Figure 7 shows the MRI image and a LB simulation [38] for flow through a random packed

bed of cylindrical extrudates, whose length/diameter ratio is larger than typical for reforming catalysts. Statistical analysis of these data shows that approximately 40% of the total flow through the image slice is passing through only 10% of the pores. Note also that the visualization and simulation point to regions of reverse flow. This is a very important observation. At larger inter-pellet dimensions this proportion is probably higher. This highlights that large voids carry a disproportionate amount of the flow. It is therefore important to avoid these in packing the bed if bypassing is to be avoided.

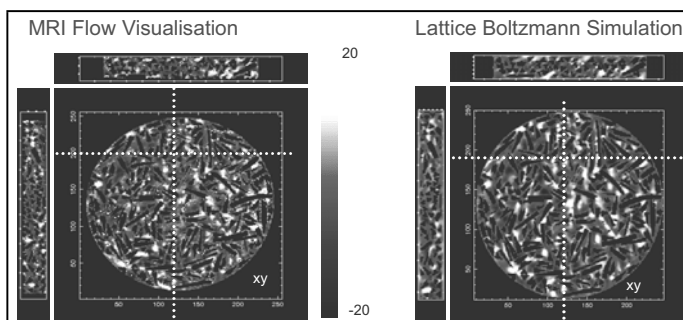


Figure 7. MRI Flow Visualization and Lattice Boltzmann Simulation for Flow in a Random Packed Bed (Black is the solid cylindrical packing)

8.2.4 Effects of Uneven loading in Tubular Reactors

Loading ideally aims to achieve uniform catalyst packing in every tube to obtain the same gas flow in every tube resulting in the same pressure drop across every tube, and thus the same tube wall temperature (TWT) profile down every tube

Voids and bridging within catalyst are observed as “hot spots” and “hot bands” multiple occurrences referred to as “giraffe necking” and “tiger tails”. Their occurrence is influenced by catalyst shape and size and care with loading. Increases tube wall temperature 30°C (86°F) are typical for small voids, and large voids are worse.

In a fired reformer the endotherm of reaction is essential to maintain a low tube wall temperature. If this heat sink is absent or reduced then the tube wall temperature will increase. Anything that leads to reduced volumetric activity will cause this, such as large voids due to poor catalyst loading, low flow due to a relatively high packing density (also a loading fault or a result of breakage) or deactivated catalyst.

The effect of flow variation between tubes is demonstrated in Table 3. Uneven gas flow is observed as variance in pressure drop and affects peak tube wall temperature. A $\pm 10\%$ PD spread results in a $\pm 20^\circ\text{C}$ TWT spread. A $\pm 3\%$ PD spread, which is achievable by good loading practice, limits TWT variability of only 6°C . The effective life of a reforming tube is a direct function of the tube temperature during operation. A 20°C increase in TWT can half the life expectancy from, for example, 10 yrs to 5 yrs. A reformer re-tube is a significant expense and lengthens the period of any turnaround.

Table 3. Effect of Uneven Catalyst loading on Reformer Performance

	Units	Flows well balanced	Flow poorly balanced	Mixed Gas Exit
Process gas temperature	$^\circ\text{C}$	870	834-992	872
Approach to equilibrium	$^\circ\text{C}$	2	1 - 3	9
Methane slip	Mol % (dry)	3.6	1.6 - 6.5	3.9
Max. TWT	$^\circ\text{C}$	891	860-930	

Uniform catalyst loading influences not only tube life, as noted above, but also steam reformer performance. Note from Table #2 that the methane slip (viz. unconverted methane exit the reformer) from the reformer is higher for the unevenly packed version. Two wrongs do not make a right! An increased methane slip results in increased methane build up in the downstream synthesis sections. Good practice in catalyst loading rewards itself not only in extended tube life but also in improved reformer and thus overall plant performance

From the above it is clear that catalyst loading into reformer tubes is to be undertaken with great care and planning. The key to this is consistency of technique and rigorous checking of pressure drop of each tube before, during and after filling of the tube. If the PD is away from the norm by greater than 5% then adjustment is required, normally by vibrating the tube to achieve some catalyst settling. Tubes with too high a pressure drop should be discharged and reloaded. As noted above, a $\pm 3\%$ variation is achievable. Uniformity of pressure drop is the critical measurement, more important than absolute pressure drop or even mass or volume flow. Note however that insufficient packed height of catalyst, after settling leads to a catalyst free volume at the top of the tube that will lead to excessive TWT and tube failure.

8.2.5 Loading Techniques for Tubular Reformers

There are a number of techniques used to charge reformer tubes, of which three are common:

- Water fill method: all the tubes are filled with water and the catalyst poured in slowly using funnel. The displaced water overflows. Once filled with catalyst residual water drained out. The catalyst and header refractory are wet and careful drying is required. Not commonly used - mostly small upflow reformers
- Sock loading. This is a well-established "classical" method, and probably the most common. catalyst supplied in plastic "socks" with a calculated weight per sock that is intended to give whole number of socks per tube. The sock is connected to a rope at the top, and the bottom of the sock folded over. The sock is lowered into tube to near the existing level, and the rope "jerked" to release the flap, allowing the catalyst to fall from the sock. It is recommended to vibrate the tube after each sock. This settles the catalyst and minimizes voids. Vibration methods include electric or pneumatic vibrators (noisy) or a soft-faced shot-filled hammer (blows must be consistent). The key is that the method must be consistent for every tube and to avoid over-vibration
- Trickle (or Dense Loading) methods. These have been used increasingly since mid-1990s and are gaining widespread acceptance. This technique uses a device to break catalyst fall in tubes, such as a knotted line, or discs or brushes fitted onto a rope. The rope is raised as the tube fills. The underlying principle is that each catalyst particle is allowed to settle without collision with another moving particle. The effectively minimizes bridging and the occurrence of large voids.

8.3 Catalyst Design & Heat Transfer in Reformer Tubes

Good heat transfer is essential in all tubular reformers. This is equally true of fired reformers and heat exchange reformers, although for different reasons. The need for good heat transfer in fired reformers will be apparent from the above discussion of loading. Poor heat transfer from the tube to the gas will result in an increased tube wall temperature. In heat exchange reformers the rate of heat transfer can limit the rate of reaction, as the catalyst temperature cannot be maintained at the correct temperature. Both effects apply to both reformer types to a greater or lesser extent.

There are three distinct transfer restrictions to heat transfer in tubular reformers (Figure 8):

- Heat transfer on the furnace or shell side: heat transfer to the tube. In a fired reformer this is a mixture of radiative and convective mechanisms. In a heat exchange reformer it is solely convective
- Heat transfer through the reformer tube. This is effectively the tube wall conductivity
- Heat transfer into the catalyst bed. Convective transfer through the gas film adjacent to the wall into process gas

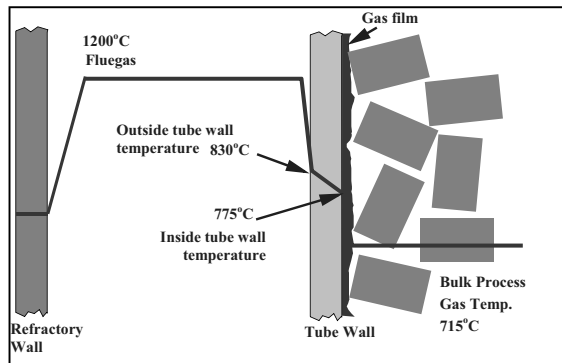


Figure 8. Heat Transfer in Steam Reforming

The heat transfer in a reformer tube is essentially from the tube wall to the catalyst surface, with the flowing gas as a heat transfer medium. Solid phase conduction between pellets is not significant. The nature of steam reforming catalysts is that activity is substantially a direct function of the geometric surface area. This would normally lead to the use of small catalyst particles. In the case of reforming however, this would lead to high pressure drop, which is unacceptable. It is equally important however that high tube to particle diameter ratios lead to low effective radial mixing, and thus poor heat transfer from the wall to the centre of the tube.

There are therefore requirements in reforming that might normally be considered mutually incompatible:

- Low pressure drop and thus high voidage and large particles
- High surface area for high activity which normally requires small particles
- Good radial mixing for heat transfer that requires a large particle
- High strength to avoid breakage during handling and charging

- (Note that no catalyst is strong enough to resist the stresses of tube contraction during cooling but that the fracture patterns are important to preventing pressure drop build up)

The general outcome of this is that simple spherical or cylindrical pellets are not used. The reforming industry uniformly uses pellets of a length to diameter ratio in the range 0.8 - 1.2 with internal holes. At their simplest these may be Raschig rings, but 4 to 10 axial holes are now commonly used. Tube to particle diameter ratios also vary but at the top, entry region where good heat transfer is essential, they will normally be 5-10. Smaller catalyst particles tend to be used in the lower portion of the tube where the reaction becomes activity rather than heat transfer limited and where high tube temperatures are less likely. This is especially true of top fired reformers.

At the tube to particle diameters typical in reforming, radial heat transfer is in fact good, and only small temperature gradients exist across the bulk of the tube. The rate limiting step is the transfer from the wall to the gas and significant temperature differences exist across the boundary layer. The heat transfer within the packed tube is substantially convective, with little contribution from radiation. Accordingly the heat transfer has been traditionally modeled using two heat transfer coefficients:

h_K - representing the heat transfer coefficient for radial convection in the bulk of the tube

h_W - the so-called wall coefficient representing transfer from the tube to the gas.

The impact of the tube-side heat transfer coefficients on the tube wall temperature is shown in Figure 9: a two-fold improvement in the coefficients facilitates approximately a 40°C lowering of the TWT.

This is an entirely empirical approach, but one that has been successfully used by reforming technology licensors and contractors over many years. This success is however based on extensive experimental work to validate and fit the correlations. The correlations are not however strictly predictive. This technique also averages the heat transfer and thus spatial resolution of tube wall temperatures is not possible. Maximum tube wall temperatures are therefore predicted based on experientially empirical models.

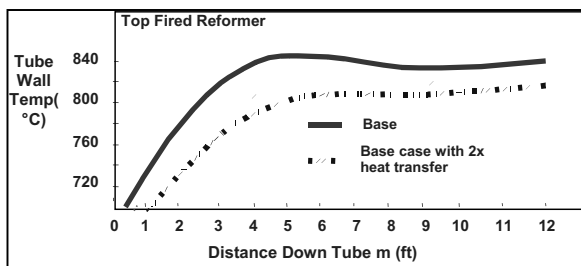


Figure 9. Impact of Tube-Side Heat Transfer coefficients

Table 4. Benefits of Modern Catalyst Pellet Design on Reformer Performance

	17mm Raschig Rings	17mm Raschig Rings	LxD 19x14mm 4-Hole
Plant rate (relative)	100	112	112
Maximum TWT (°C)	921	940	921
CH ₄ slip (mol% dry)	4.4	4.8	4.3
Approach to Eqm. (°C)	3	6	2
Pressure Drop (kg/cm ²)	2.3	3.1	2.8

The overall effect of catalyst pellet geometry on not only heat transfer but also the performance of the reformer is shown in the simulation results presented in Table 3, where the performance of the traditional Raschig ring (now infrequently used) and a modern 4-hole geometry. The benefits in terms of tube wall temperature, methane conversion and pressure drop are self-evident.

While it is possible to predict flow patterns and velocities in a given porosity network of considerable complexity using lattice Boltzmann approaches, this technique does not allow the interrogation of heat transfer and is limited to Re values below those in typical reforming applications.

A randomly packed tube, see Figure 10 for example, is geometrically extremely complex and thus hard to represent. The randomness of the packing makes it hard to construct mappings with periodicity - an absolute necessity for CFD calculations that can be completed using existing codes and hardware. Until recently therefore the computational evaluation of catalyst tube heat transfer performance based on phenomenological approaches has not been feasible.

Recent developments in structuring geometrical segments have allowed the CFD calculation to be reduced to a manageable size. Critical to this has been the demonstration of the validity of "wall segment models, where only an angular segment is considered, Figure 11, with periodicity at all internal

boundaries [39]. These studies, based on simple geometric shapes, have demonstrated that the actual wall coefficient is a complex function of the overall flow structure and not a simple correlation dependent on the velocity vectors adjacent to the wall. This work has been extended to evaluate the overall effect of the reaction, on the temperature profiles and heat transfer [40].



Figure 10. Tube Packed with Reforming Catalyst

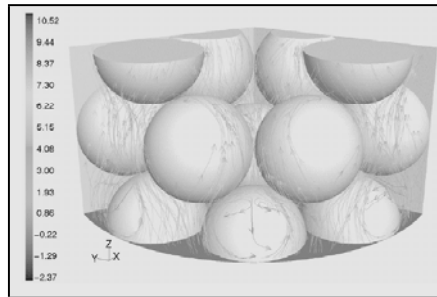


Figure 11. Velocity Vectors for a Wall Segment model of a Tube with Spheres (N=4)

9. SUMMARY

9.1 Markets and Technologies

While syngas and hydrogen markets and technology are often considered mature, this is not entirely true and there are significant changes occurring.

Many of these are actually driven by changing energy needs and environmental drivers. Most significant amongst these are:

- The potential growth in the need to monetize stranded and process marginal gas through gas-to-liquids (viz. Fischer Tropsch or methanol-to-gasoline) technology,
- The changing specification of gasoline and diesel with not only increasing hydrogen processing requirement but also the apparent phasing out of MTBE (with impact into methanol markets)
- The potential growth of fuel cell powered vehicles and the need for hydrogen rich fuels (methanol or gasoline) to be processed on-board to generate hydrogen. Clearly if methanol is to be the fuel of choice then this will impact in a major style on the methanol industry
- The potential growth of fuel cell distributed electricity generation with the associated need to process locally the gas (or liquid fuel) to generate hydrogen.
- The development of cost effective small scale hydrogen generation technology from the fuel cell applications may lead to growth in distributed manufacture of hydrogen and syngas for chemicals applications beyond ammonia and methanol.

As a direct result of the perceived future changes and challenges in syngas and hydrogen markets, there is significant effort world-wide aimed at developing technology for syngas generation, with the primary alternative goals of gas-to-liquids and fuel cell hydrogen. The leading technologies are based on steam reforming and/or partial oxidation, with partial oxidation, autothermal reforming and compact (two step) reforming being the leading contenders for all applications.

9.2 Gas Heated Reforming

The development and performance of the Johnson Matthey two step, compact reforming process based on a primary gas heated reformer and a secondary autothermal reformer has been considered in detail. With regards to this "GHR" based technology the following have been established.

- The GHR is a proven reforming technology, with over 10 years operating experience at commercial scale.

- The gas heated reformer provides a compact reformer design, with excellent heat transfer design, suited to small and very large scale reforming applications.
- The GHR produces the optimal gas composition for Methanol and Fischer Tropsch
- In GTL duties, the GHR based process has a lower oxygen requirement than POx or autothermal reforming.
- The GHR process also leads to lower CO₂ emissions and a lower power export
- The GHR process has a small footprint, low weight and has a competitive capital cost
- Continuing development of the GHR is aimed at achieving further reductions in operating and capital costs:
- Development work will focus on operability at lower steam to carbon ratios. This requires development of metallurgy and catalysts plus continued flowsheet optimization.

9.3 Engineering of Syngas Processes

This section has addressed on a few of the engineering issues of reforming. It can be seen that it is an extremely complex reactor - even the ostensibly simple autothermal version. Important features are the design and operation of the firing/burner, catalyst loading, materials of construction (including tube metal and tube fabrication), heat transfer design and catalyst shape, catalyst loading, and many more. The successful operation of a syngas generation based process is critically dependent on the design and operation of the reforming section.

10. ACKNOWLEDGEMENTS

The author is indebted to many colleagues in Johnson Matthey Catalysts for collaborations, recent papers and presentation materials that form the basis for parts of this chapter. Particular thanks are expressed to Jim Abbott, Mike Davies, Peter Farnell and Barry Fisher.

11. REFERENCES

- [1] Abbott PEJ, Conduit MR & Mansfield K (1989) Methanol - A New Process for the 1990s, *Proc. World Methanol Conf.*, Crocco & Associates Inc., Houston TX, Paper 14-1

- [2] Anon (1998) Looking Beyond the Internal Combustion Engine : the Promise of Methanol Fuel Cell Vehicles, *American Methanol Institute Report*, May 1998
- [3] Atkins M (2003) The transition from oil to natural gas as a fuel and feedstock, NATO-Advanced Study Institute, Sustainable Strategies for the Upgrading of Natural Gas: Fundamentals, Challenges, and Opportunities, Vilamoura, Portugal, 6 – 18 July, 2003
- [4] Fleisch, T (2003) Strategies, technologies and opportunities for oxygenates derived from light alkanes, NATO-Advanced Study Institute, Sustainable Strategies for the Upgrading of Natural Gas: Fundamentals, Challenges, and Opportunities, Vilamoura, Portugal, 6 – 18 July, 2003
- [5] Kvisle S et al. (2000) Methanol to Olefins Future Challenges, *The Catalyst Group, CAP2000 Meeting*, Lisbon, 13-14 Feb. 2000.
- [6] Prigent M (1997) On Board Hydrogen Generation for Fuel Cell Powered Electric Cars: *Revue IFP*, 52 (3), 349 - 360.
- [7] Van Dijk CP & Fraley LD (1993) Process for Producing and Utilizing Oxygen Enriched Gas *US Patent 5,245,110*, 14 Sept 1993.
- [8] Agee KL (1989) Process and apparatus for the production of heavier hydrocarbons from gaseous light hydrocarbons *US Patent 4,833,170*, 23 May 1989.
- [9] Agee KL (1990) Apparatus for the production of heavier hydrocarbons from gaseous light hydrocarbons, *US Patent 4,973,453*, 27 Nov 1990.
- [10] Charlesworth RJ, Gough A & Ramshaw C (1995) : Combustion and Steam Reforming of Methane on Thin Layer Catalysts for Use in Catalytic Plate Reactors: *Proc 1st Int Conf.Sci.Eng.& Technol.of Intensive Processing*, p85, Nottingham.
- [11] Piga A & Varykios XE, (2000) An advanced reactor configuration for partial oxidation of methane to synthesis gas, *Catalysis Today*, 60, 63-71.
- [12] Frauhammer J, Eigenberger G, Von Hippel L & Armtz (1999): A New Reactor Concept for Endothermic High Temperature Reactions: *Chem. Eng. Sci*, 54, 3661-3670.
- [13] Brophy JH & Telford CD (1988) Process for Producing Synthesis Gas by Partial Combustion of Hydrocarbons, *US Patent 4,758,375*, 19 July 1988
- [14] Sie ST (1993) Partial oxidation of a hydrocarbon-containing fuel using entrained catalyst, *GB Patent 2,249,555*, 16 Feb. 1993.
- [15] Hickman DA & Schmidt LD (1993) Production of Syngas by Direct Catalytic Oxidation of Methane, *Science*, 259, 343.
- [16] Pena MA, Gomez JP & Fierro JLG (1996) New Catalytic Routes for Syngas and Hydrogen Production: *Applied. Catalysis A*, 144, 7-57.
- [17] Eisenberg B et al. (1994) Advanced Gas Conversion Technology for Remote Natural Gas Utilisation, *73rd Gas Processors Association*, New Orleans.
- [18] Armitage PM, Elkins KJ, Kitchen D & Pinto A (1992) Leading Concept Ammonia Process: First Two Years; *AIChE Ammonia Plant Safety Meeting*, 32.
- [19] Farnell PW (1995) Commissioning and Operation of ICI Katalco's Leading Concept Methanol Process, *AIChE Ammonia Plant Safety Meeting*.
- [20] Sogge J & Strom T (1997) Membrane Reactors - A New Technology for Production of Synthesis Gas by Steam Reforming: *Studies Surf. Sci. Cat.*, 107, 561-566.
- [21] Balachandran U et al (1997) Ceramic Membrane Reactor for Converting Methane to Syngas: *Catalysis Today*, 36 (3), 265-272
- [22] Sammells AF (1999) Catalytic Membrane Reactor Improvements for Syngas and Gas to Liquids: *The Catalyst Group, CAP Annual Meeting*, Clearwater Beach
- [23] a) Anon (1997) *Oil & Gas Jnl*, 95(31) p35 28 July 1997, & b) Anon (1997) *Oil & Gas Jnl*, 95(37) p37 8 Sept 1997

- [24] Brun-Tsekhovoi, AR Kurdumov SS, Sidorov NV & Katsobashvili YaR (1988) The Process of Catalytic Steam Reforming of Hydrocarbons in the Presence of a Carbon Dioxide Acceptor, *Proc. 7th World Hydrogen Energy Conference*, 2, 885
- [25] Kurdumov SS, Brun-Tsekhovoi AR & Rozental AL (1996) Steam conversion of Methane in the Presence of a Carbon Dioxide Acceptor : *Petroleum Chemistry*, 36(2), 139-143
- [26] Balasubramanian B, Lopez-Ortiz, Kaytakoglu S & Harrison DP (1999) Hydrogen from Methane in a Single Step Process, *Chem. Eng. Sci.* 54, 3543-3552
- [27] Anand M et al, Hufton J, Mayorga S, Nataraj S, Sircar S & Gaffney T (1996): Sorption Enhanced Reaction Process (SERP) for Production of Hydrogen, *Proc US DOE Hydrogen Program Review*, 1, 537-552
- [28] Farnell PW (1995) Commissioning and Operation of ICI Katalco's Leading Concept Methanol Process, *AIChE Ammonia Plant Safety Meeting*
- [29] Farnell PW (1999) Syntex's Advanced Gas Heated Reformer: *AIChE Ammonia Plant Safety Meeting*, Seattle, (27-30 Sept 1999)
- [30] Fitzpatrick TJ (2002) Large Scale Methanol Production using AGHR-based Syngas Generation, *World Methanol Conference*, Rome, 9-11 December, 2002
- [31] Tindall R (1998) Natural Gas Reforming Technologies: *Intertech Conf. Gas to Liquids Processing*, San Antonio, 18-20 Mar 1998
- [32] Karp AD & Dickenson RL (1998) Syngas Production for Gas-to-Liquids Applications: Technologies, Issues and Outlook: *2nd Annual Conf. Monetizing Stranded Gas Reserves*, San Francisco, 14-16 Dec.1998
- [33] Abbott PEJ & Crewdson BJ (2003) Syngas Production for GTL Using Gas Heated Reforming – A Highly Efficient, Environmentally Friendly Process, *CatCon 2003*, Houston, TX, 5 – 6 May, 2003
- [34] Kirpatrick R & Fitzpatrick TJ (1999) A Methanol Technology for the 21st Century, *World Methanol Conference*, San Diego, 29 Nov – 1 Dec (1999)
- [35] Cotton WC, Davies M & Fisher B (2003) Modeling Tools and Applications for Methanol Plants, *IMTOF*, London, July 2003
- [36] Lywood WJ (1996) Process Design, Rating and Performance. *Twigg MV (Ed) Catalyst Handbook (2nd Ed.)*, Manson Publishing
- [37] Farnell PW & Hughes RJ (1994) Secondary Reforming: Theory and Application, *AIChE Ammonia Plant Safety Conf.*
- [38] Mantle MD, Sederman AJ & Gladden LF (2001) Single- and two-phase flow in fixed-bed reactors: MRI flow visualization and lattice-Boltzmann simulations, *Chem. Eng. Sci.* 56, 523-529
- [39] Nijemeisland MJ & Dixon AG (2003) Simulation and Analysis of Gas Flow and Heat Transfer in a Wall-segment Model of an N=4 Fixed Bed of Spheres, *A.I.Ch.E. Journal*, submitted for publication
- [40] Dixon AG, Nijemeisland MJ & Stitt EH (2003) CFD Simulation of Reaction and Heat Transfer Near the Wall of a Fixed Bed, *Int. J. Chem. Reactor Eng.*, Vol. 1, paper A22 <http://www.bepress.com/ijcre/vol1/A22>.

Chapter 11

ENGINEERING ALKANES TO OLEFINS AND HIGHER VALUE CHEMICALS

The technological world of olefins, building blocks of the current Industrial Chemistry

Domenico Sanfilippo, Ivano Miracca, Marco Di Girolamo
Snamprogetti SpA Viale DeGasperi, 16 . 20097 S.Donato Milanese – Italy
domenico.sanfilippo@snamprogetti.eni.it

Abstract: Olefins are the building blocks of choice for manufacturing a huge amount of commodities and specialties. A network of technologies connects the fossil raw materials (crude oil, Natural Gas, condensates etc.) with the olefins and the final products. The basic concepts of these technologies are reported, together with the expected trends in their evolution.

Key words: alkanes, olefins, ethylene, propylene, butenes, isobutylene, butadiene, natural gas, steam cracking, FCC, DCC, dehydrogenation, MTO, metathesis, etherification, isooctane, MTBE

1. INTRODUCTION

The vigorous development of the human society in the second half of the past century has been sustained by the parallel development of the modern Industrial Chemistry and has been based on the exploitation of oil and gas hydrocarbons as well as energetic source, as well as raw materials. The geo-biological processes that generated the natural fossil resources have formed mainly saturated or aromatic hydrocarbons. As a consequence, available primary feedstock for chemical industry (Natural Gas and petroleum from the fractionation of crude oil), are mainly of saturated, paraffinic and naphthenic hydrocarbons. The generally feeble reactivity of these compounds (*paraffin* etymology is from the Latin words *parum* + *affinis* = *with little affinity*), makes difficult to get the target finished products.

The manufacture of some of the most important chemicals, such as polymers, synthetic fibers, elastomers, detergents and fuel components, has been based on the use of molecules offering a definite attack point for further selective reactions, like unsaturated aliphatic or aromatic hydrocarbons. Therefore light olefins are favored feedstock fundamental and building blocks for the petrochemical downstream and the refining industry. Ethylene and propylene derivatives form the core of the commodities chemical industry and C₄–C₅ olefins are transformed into valuable components for fuels. Unfortunately light olefins production requires sophisticated technologies highly demanding in terms of energy and investment.

This chapter highlights the basis for the conceptual design of some technologies and shows the strict integration of the engineering aspects and the chemistry of the involved reactions. Need for integration of diversities is not a new concept. Menenius Agrippa (494 B.C.) persuaded the Roman plebs on strike on Sacred Mount to come back to their duties telling them:

"No organ of the human body can claim the right to consider itself more important than the other ones and refuse to cooperate with them, otherwise the entire body will die". Obvious, tough, doable.

2. USES AND SOURCES OF OLEFINS

Olefins are the starting material for manufacturing an impressive number of commodities and specialties of our daily use. Main use of olefins is the production of polymers (table 1) that are the most popular materials of our "plastic world".

Table 1. Main derivatives of light olefins (share %) [1]

Ethylene derivatives		Propylene derivatives		butadiene derivatives	
LDPE	17.2	Polypropylene	59.8	Polybutadiene	26.2
LLDPE	14.3	Acrylonitrile	9.1	SB Latices	12.5
HDPE	25.1	Cumene	5.6	SB Rubber	33.9
Ethylene oxide	12.8	Isopropyl alcohol	2.4	ABS	12
Ethylene dichloride	13.9	Oxo alcohols	7.7	MBS	1.4
Ethylbenzene	7.1	Propylene oxide	7.3	NB Copolymers	3.5
Acetaldehyde	0.9	Oligomers	1.7	Chloroprene	2
Ethanol	0.9	Acrylic acid	3.6	Adiponitrile	5
Vinyl Acetate	1.4	EPDM	0.6	Miscellaneous	2.4
Linear olefins	3.5	Miscellaneous	2.2		
EPDM	0.6				
Miscellaneous	2.2				

As concerns the C_4 olefins, main use of isobutylene is its etherification to MTBE to be blended in gasoline, with minor destination to butyl rubber, polybutenes, and methylmetacrylate. Butene-1 is almost completely absorbed by the LLDPE and HDPE production.

Figure 1 shows the commercial and pricing routes utilized for manufacturing light olefins and the main relevant derivatives. Major traditional source of light olefins is *Steam Cracking* and, particularly for the C_3^+ ones, *Fluid Catalytic Cracking*.

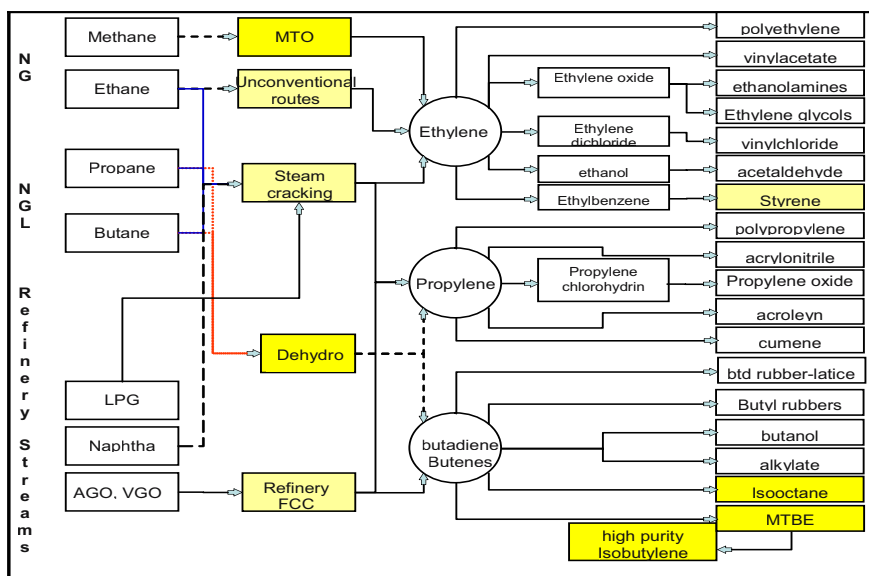


Figure 1. Olefins at crossroad between fossil sources and end uses.

Feeds heavier than ethane to the Steam Cracking co-produce a variety of intermediates mandating a complex downstream integration of chemical productions that has represented in last decades the base of petrochemistry or “Petroleum-to-chemicals”. The combination of the relevant facilities has determined the creation of mega-petrochemical complexes.

Methane has been used in the past as raw material for the production of petrochemicals, according to the so called “acetylene chemistry”. Acetylene (via methane partial oxidation in oxygen-deficient flame at 1,200-1,500°C) has been the starting point for the development of the petrochemical industry in countries like Italy, Germany and South Africa. These old processes have been almost completely abandoned since they were not competitive with the growing ethylene (from crackers) chemistry.

But, today, the interest for the use of Natural Gas ("clean", hydrogen-rich, abundant) is again very high. This aspect has stimulated the development of technologies aimed at transforming natural gas components, methane as well as C_2-C_4 , to higher valued chemicals or liquid fuels, easily transportable to end-user markets. The development of chemical conversion technologies of the NG components makes closer the growth of an economy of "Gas-to-Chemicals" and "Gas-to-fuels".

3. ETHYLENE/PROPYLENE VIA STEAM CRACKING

Until the Second World War ethylene was industrially produced mainly via the liquefaction and fractionation of coke oven gas. Union Carbide studied pyrolysis of ethane and propane at pilot scale in 1920s. Small industrial units were built also utilizing heavier petroleum fractions (NGL/LPG, naphtha, gas oil). In Europe first cracker (6,000 t/y of ethylene from gas oil) was commissioned in 1942. Technological development and economy of scale have allowed plant production capacity progressively to grow from 10,000 t/y of the 1950s, to typically 300,000 t/y of 1980s, and to the 1.4 million t/y of the largest gas-based unit today under construction [2].

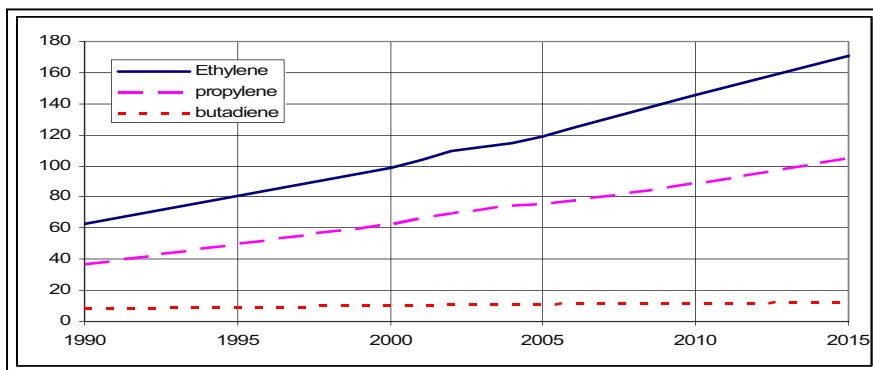


Figure 2. World Olefins capacity, MM t/y [1].

The world capacity of olefins has been growing significantly in the last decades and it is expected to continue the trend of growth (Figure 2).

The worldwide feedstock slate for ethylene production is about 43% based on Natural Gas (Ethane, propane, butanes, NGL) and 57% petroleum-based [3] with huge geographic differences. Europe and Asia historically have developed a liquid feed petrochemistry. North America, where an ethane distribution infrastructure has been developed, and gas rich Middle East

largely utilize lighter feeds (Table 2). Steam cracking produces, together with ethylene, and according to the feed, propylene, a C₄ cut rich in butylenes/butadiene and a C₅⁺ cut with a high content of aromatics (BTX). Table 3 reports typical distributions of products for the most used feeds. Ethylene remains in any case the main product, but heavier the feeds, higher the amount of different products formed.

Table 2. Distribution (%) of Feedstocks for Ethylene production (2002) [4].

Feed	Western Europe (22% of World production)	North America (25% of World production)
Ethane/light gases	10.3	50.8
LPG	8.6	23.4
Naphthas	67.2	12.5
Middle distillates	5.7	3.5
Heavy condensates	8.2	9.8

Table 3. Influence of feedstock on Steam cracker yields (%wt) [5].

Products	Ethane	Propane	Butanes	Naphtha	Atm. Gasoil	Vac. Gasoil
H ₂ (95% vol)	8.8	2.3	1.6	1.5	0.9	0.8
Methane	6.3	27.5	22	17.2	11.2	8.8
Ethylene	77.8	42	40	33.6	26	20.5
Propylene	2.8	16.8	17.3	15.6	16.1	14
Butadiene	1.9	3	3.5	4.5	4.5	5.3
Other C ₄	0.7	1.3	6.8	4.2	4.8	6.3
C ₅ -200 gasoline	1.7	6.6	7.1	18.7	18.4	19.3
Fuel oil	-	0.5	1.7	4.7	18.1	25

Yields with recycle of primary ethane and propane. Modern very high severity unit can increase C₂ yields up to 83-84% [2] at expenses of propylene and heavier products.

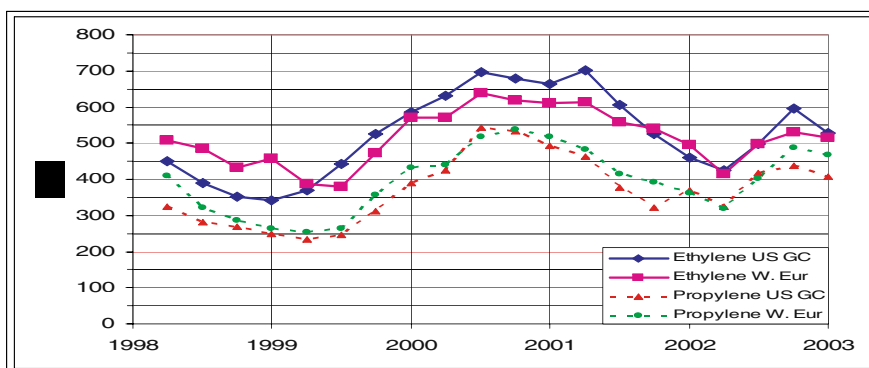


Figure 3. Historical trend of contract prices for olefins [1].

Steam cracker remains also the main source of propylene (65.7%). Balance comes from refinery (31.7%) and dehydrogenation (2.6%) [1].

Figure 3 shows the evolution of the quarterly average contract prices for ethylene and propylene recorded in the last five years in the North American and European markets. The trend includes a typical petrochemical cycle with peaks (2001) and troughs (1999 and 2002).

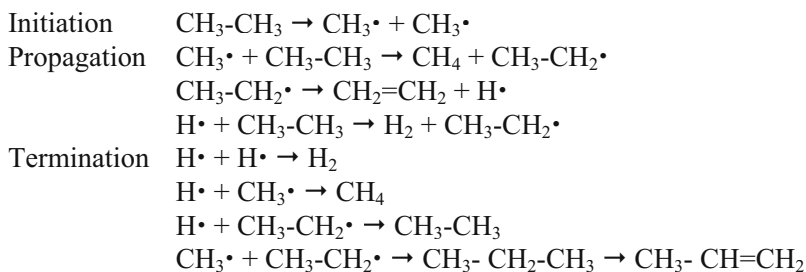
3.1 Cracking reactions features

Steam cracking utilizes the thermal pyrolysis of saturated hydrocarbons in the presence of steam. The characteristics of involved reactions (cracking, dehydrogenation, dehydrocyclization, dealkylation, etc.) condition the design of the industrial processes.

The unsaturated products are *thermodynamically* stable in relation to the saturated parents at relatively high temperatures. For ethylene formation temperatures above 750-800 °C are required.

From the *kinetic* viewpoint, pyrolysis proceeds by a free radical and chain mechanism [5]. Initiation is through the homolytic cleavage of a C-C bond with the formation of radicals. Reaction chain propagates via extraction of hydrogen and formation of a new radical.

Considering the simplest case of ethane:



More generally, with longer chain paraffins, primary radical formed are stabilized by the cleavage of the C-C bond at the β position (β -scission). As concerns the C-H bonds of a tertiary carbon is broken more easily than on a secondary, or a primary one.

In the case of C_3^+ saturated aliphatic hydrocarbon their so-called *primary cracking* produces a paraffin and an olefin. Secondary cracking reactions of remaining fragments yield several light products according with the selected operating conditions. Consecutive dehydrogenation of olefins generates acetylenic or diolefinic impurities, undesirable since they are precursors of heavy products via the Diels-Alder or cycloaddition reaction. Condensation

reactions produce a number of aromatic hydrocarbons eventually followed by polyaromatic paste or solid materials (tars and coke).

With an increasing temperature gradient, cracking reactions start first (above 700 °C), followed by dehydrogenation (above 800-850 °C), and by the formation of polyaromatic hydrocarbons and coke (high rate above 900 to 1,000 °C). Of course, higher molecular weight compounds in each hydrocarbons family show higher reactivity. Light olefins are therefore favored by short residence times and lower temperatures.

Kinetics of the steam cracking reactions have been widely investigated [6, 7]. Kinetic models describing in detail the thousands of elementary reactions occurring during pyrolysis have been developed and are very helpful either for accurate predictive reactor coil and firebox design either for the optimization of industrial units operation.

Reaction engineering must consider the involved reaction enthalpies. Global reaction is highly endothermic. Typically to crack a paraffin to an olefin and a lighter paraffin requires around 20 kcal/mole. About 30 kcal/mol are needed to dehydrogenate a paraffin to the corresponding olefin.

Thermodynamics and kinetics of pyrolysis therefore force precise constraints in the design of industrial units:

- Supply substantial amount of heat at very high temperature
- Operate at the lowest hydrocarbon partial pressure in the reactor
- Use very short residence times, to limit the consecutive reactions
- Quick quench the reactor effluents to avoid composition change

These requirements can be fulfilled in several ways, in particular as concerns the principle of supplying heat to the reagents. Some alternatives will be discussed later. In industrial operation the still unbeaten technique consists in feeding hydrocarbons and steam into empty tubes or coils placed in a fired furnace. Products are quenched and separated.

3.2 Engineering aspects of steam cracking

Once the feed composition has been fixed, the main operating variables at the designer disposal are the coil *temperature profile*, the *residence time* and the *partial pressure* of the hydrocarbons. The optimization of their combination determines the profitability of the process.

Temperature profile is determined by the design of the furnace and by the choice of the coil outlet temperature, which is considered a significant

indicator of the operation mode of the furnace. These temperatures range from 750 to 950 °C according to the type of feedstock treated. Heavier hydrocarbons, having greater intrinsic reactivity, require lower temperatures. Residence time is longer for heavy than for light feedstock, ranging typically between 0.1 - 0.6 s. Short residence times increase the yield of olefins and reduce aromatics and heavy byproducts. Several technical and economic limits (higher heat fluxes, materials metallurgy, furnace costs etc.) determine the minimum values. In any case the concept has reached the extreme in the millisecond technology (< 0.1 s), developed initially by Kellogg. Millisecond design has minor advantages on light feed.

Thermodynamics (increase of moles number) and kinetics (presence of condensation reactions) make preferable a low hydrocarbon partial pressure. Indeed exit pressures are kept close to the atmosphere, requiring more recompression energy in the cold section. A further decrease in the partial pressure of the hydrocarbons is obtained by dilution with steam. Steam plays additional beneficial role by helping with its heat capacity the heat balance of the furnace and by reducing coke deposits. On the other hand, its presence increases the flow rate and requires a separation from the hydrocarbon effluents through large condensation surfaces (steel = investment) and higher utility consumption. The amount of steam employed is typically 0.25-0.40 t/t of feed for ethane, and increases with the molecular weight of the feed.

For the global optimization of operating parameters and furnace design the concept of severity (or conversion) is used. Its definition varies with the different licensors, particularly for liquid feeds. Industrial operations are "at low, medium, high and very high severity". From a general viewpoint, at low and medium severities, the primary cracking and dehydrogenation reaction prevail and lighter products (methane, ethylene, propylene and C₄ cut) increase. Very high severities are indicated for liquid feed in order to convert also heavier less valuable products, but at the same time propylene yields decline. As a consequence, the ratio of propylene to ethylene decreases with severity, which increases the formation of ethylene. Typical single pass (alkanes and other products are recycled to the furnace) performances are:

Table 4. Typical single pass conversions and selectivities for different feed.

	Ethane	Propane	<i>n</i> -Butane	Naphtha
Conversion %	70	95	98	92
C ₂ ⁻ selectivity	80	43.3	40.4	30
C ₃ ⁻ selectivity	1.4	12.1	14.4	17.3

A steam cracking unit consists of two main sections: a *hot section* that includes furnaces and cracked gas quench and conditioning, and the *cold section*, for products separation and purification. A rough share of TIC (Total Investment Cost) indicates that furnaces contribute for about 35%, compressors and turbines for 30% and the balance is given by columns, drums, pumps etc [2].

Figure 4 shows a very simplified flowsheet of a steam cracker. It includes several furnaces in parallel, quench boilers, and very complex fractionation scheme.

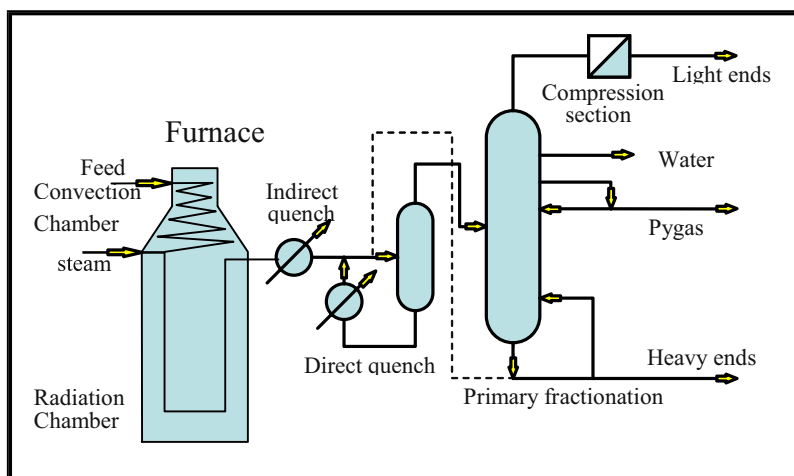


Figure 4. Conceptual scheme of a hot section of a steam cracker.

The hydrocarbon feedstock is preheated in the convection chamber of the furnace, and after addition of steam, enters the coils in the radiant chamber where reactions take place. Some fouling on the walls of the coils forces for periodic decoking, via controlled combustion. Run lengths range between 10-15 days up to 30-60 or, in special conditions, up to 100 days. Typical furnace characteristics are reported in table 5.

Within the reported ranges, parameters have also allowed or typical combination, like in table 6 [5].

Cracked gas after quenching is compressed, caustic-washed, dehydrated with molecular sieves and finally sent to a separation and purification train that includes hydrogenation of impurities, demethanization, deethanization, depropanization and gasoline hydrotreating.

Table 5. Furnaces typical characteristics.

Max. Ethylene capacity, tons per year	Current ca. 100,000; Studies 200,000
Number of coils	< 180
Inside coil diameter, mm	30 – 200
Coil length, m	< 80
Process gas outlet temperature, °C	750 – 950
Max. coil skin temperature, °C	1,040 - 1,150
Max. Heat flux, kJ/m ² ext. area	Approx. 400,000
Residence time, seconds	0.06 - 0.6
Outlet Pressure, kPa	150 - 275
Clean coil pressure drop, kPa	10 - 200

Table 6. Steam cracking, tube performances [5].

Max. skin temp. °C	Tube length m	Pres. drop kPa	Average heat flux kJ/h m ²	Min. res. time s
925	55	115	190,000	0.46
980	40	90	250,000	0,35
1,040	35	70	315,000	0.27

3.3 Commercial technologies

Several factors determine the cracking profitability (feed value, optimum yields, maximum recovery of energy, maintenance requirements, etc.). Of great importance are all the technologies used in the cold section and in the one for purification from byproducts (e.g. acetylenes and diolefins hydrogenation) for reaching the severe polymerization grade specs.

A limited number of licensors-contractors possess the expertise and know how of the ethylene unit design. Typically licensors offer both hot and cold sections. Some characteristics, as claimed by licensors, are [8]:

ABB Lummus Global, with the Short Residence Time design of furnaces (SRT VI), claim energy consumption of 3,300 kcal/kg ethylene for ethane as feed, or 5,000 for naphtha, reduced to 4,000 with turbine integration.

KBR (Kellogg Brown & Root), in agreement with ExxonMobil, license the SCORE technology (Selective Cracking Optimum REcovery). Very short residence times (0.1 s) are used to maximize ethylene yields (84% for ethane feed, 38% for naphtha, 32% for gas oil). Flow-schemes for the cold section (demethanizer-, deethanizer- or depropanizer-first) are optimized case by case. Capacities up to 1.3 MM t/y ethylene have been designed.

S&W (Stone & Webster, now part of the Shaw Group) offer USC (Ultra Selective Cracking) and ARS (Advanced Recovery System). Ethylene yields of 57% (ethane high conversion) to 28% (heavy gas oils), with energy requirement correspondently of 3,000-6,000 kcal/kg are reported.

Linde AG, with the PyroCrack furnaces, claim ethylene yields of 83, 45, 35, 25% respectively for ethane, LPG, naphtha, and gas oils feed.

Correspondently energy consumption are 3800 - 4,600 - 5,400 and 6,000 kcal/kg. Reported Gulf Coast investment (ISBL) are 500 US\$/t ethylene installed capacity for Gas crackers and 750 for naphtha feed. It means about 500 MM US\$ for 1,000,000 t/y ethylene from ethane plant.

TPL/Technip-Coflexip. Special design furnaces for gas, (GK coil res. time 0.15-0.25 s) and for liquid (SMK coil res. time 0.35-0.4 s) are available. Ethylene yields are 83% from ethane (conversion 65-75%), 35% from naphtha, 25% from gas oils. Correspondent energy consumption is 3,000 kcal/kg for gas- 4,700 naphtha and 5,500 for gas oil. Overall thermal efficiency is 93-95%. A very sophisticated proprietary kinetic model (SPYRO) is used for optimizing the cracker design.

In order to provide flexibility to the ethylene to propylene ratio, some technologies for cracking C₄-C₅ cuts to propylene are under study [9]. PROPYLUR by Lurgi/Linde operates in fixed-bed over shape selective zeolitic ZSM-5 type (Si:Al 10-200:1): oligomerization, disproportionation, cracking and hydrogen transfer reaction happen.

Mobil/Kvaerner have proposed MOI, Mobil Olefin Interconversion: steam cracker by-products, including pygas, are converted to ethylene and propylene in a circulating fluidized bed reactor with continuous regeneration with a ZSM-5 based catalyst. Similarly KBR/Arco propose SUPERFLEX to offer flexibility in C₂/C₃ ratio [10].

4. ETHYLENE/PROPYLENE FROM REFINERY

Ethylene (*ca.* 14%wt) and propylene (*ca.* 16%wt) are contained in **FCC** (Fluid Catalytic Cracking) offgas. FCC is the heart of the so called "conversion refineries" (450 FCC in the 722 worldwide refineries [11]), therefore, influences operations for a majority of the units in the refinery and it contributes directly to the gasoline pool. FCC transforms heavier molecules of different feeds (atmospheric or vacuum gas oil) to products in the range of valuable fuels (gasoline, diesel). A number of catalytic reactions take place: the basic mechanism involves the formation of carbenium ions that can lead to isomerization, β -scission, de/trans-alkylation, and hydrogen transfer. In the recent years the catalyst formulation (ZSM-5 based additives) and FCC units run (overcracking with conversion >75%wt) have been adapted to meet gasoline stringent reformulation tasks, reducing high olefins and increasing the branched high octane products. Undesired heavier olefins are converted primarily to

propylene and isobutylene. As a result, FCC tends to increase its role of olefins provider.

In this direction a new technology has been developed: **DCC** (Deep Catalytic Cracking), a modified version of FCC, operating at more severe conditions, to increase the production of light olefins from liquid heavy feedstock. The process, originally developed by the Chinese RIPP, is commercialized by S&W and, depending upon the circumstances, can show good economics. Two commercial units are in operation [12].

Ethylene and propylene contained in refinery streams together with lots of impurities can be recovered via a number of ways, including use of offgas as feed to a conventional steam cracker, or through the use of expanders and cryogenic separation. Refinery, through the insertion of a P-P (propane-propylene) splitter, supplies over 30% of market propylene. New technologies are under evaluation based on:

- Physical absorption on hydrocarbon solvent OGR (OffGas Recovery) by KTI/AET [13] or
- Chemical complexing, on Cu(I) compounds [14] or on CF_3COOAg [15] or on AgNO_3 promoted liquid membranes (BP-S&W) [3, 16] or on Fe-promoted AgNO_3 (Snamprogetti) [17].

5. ETHYLENE BY NON-CONVENTIONAL PROCESSES

Steam cracking is the technology of choice for producing ethylene, but the ingenuity of chemical engineers has proposed several alternative concepts. Even if it is unlikely a next-coming revolution in ethylene field, some of them merit to be mentioned since in some conditions they could deserve some industrial interest. Several attempts have been made for applying *catalysts* to the thermal cracking reactions [3]: $\text{KVO}_3/\text{In}_2\text{O}_3$ (VNIIOS process), Ca-Fe aluminates (Toyo), various zeolites (Asahi), Pd-based membranes (MITI), all of them do not show breakthrough advantages.

Another approach has been to look for a different way of supplying heat.

Ethylene by *circulating fluidized bed cracking*: heat supply can be done via accumulation of heat on a circulating solid carrier raised to a high temperature in a separate vessel and brought into contact with the feed (heavy cuts or crude oil) in the reactor. Endothermic cracking absorbs heat and generates coke on the solid that must be removed. The solid initial state is restored by coke combustion. According to this concept the Lurgi Sand Cracker [3] was used in commercial units in the 1960s and is no longer in operation. Also BASF has developed the same concept, using coke fine

particles as heat carrier. BASF has operated commercial units in the 1960-1970s.

A different concept of heat supply has been applied in the ACR (Advanced Cracking Reactor) Process developed by Union Carbide (merged recently into Dow Chemical): oil is injected in the hot gas coming from the combustion in a burner of a fuel with pure O_2 in the presence of steam. The advantages are the high flexibility and good yields [3]. Drawbacks are represented by the costs of O_2 and by the complex downstream separation.

A different approach proposed to overcome the ethane thermodynamic conversion limit at low temperature has been to remove H_2 either via selective permeation through membranes either via catalytic combustion (ODH Oxidative Dehydrogenation). Standard catalytic oxidation route has not yet given appealing results.

Recently the unconventional SCT-CPO of ethane (Short Contact Time Catalytic Partial Oxidation) deserves some attention at R&D level.

Ethane, premixed with oxygen, flows through a thin layer of catalyst (typically Pt-based) with a contact time of milliseconds ($SV > 100,000 \text{ h}^{-1}$). Due to the heat transfer limitations the surface catalyst temperature reaches values ($>900\text{-}1,000 \text{ }^\circ\text{C}$) higher than the gas phase, enhancing the reaction rate. The SCT oxidation occurs in a thin solid-gas inter-phase layer where extremely localized and high temperatures are realized. The contact time of the molecules in this layer corresponds to few microseconds. The short permanence in the reaction environment freezes the chemical processes into their initial stages and stops the dehydrogenation to the olefin products. Moreover the high surface temperature hastens the reactions. Recycle of hydrogen, the co-feed of other fuels and/or steam is used to improve the yields. Reported yields are slightly lower than the ones of ethane-fed crackers, but the expected investment is lower. Extensive scientific activities were performed by L.D. Schmidt [18]; the route is also studied at industrial level [19].

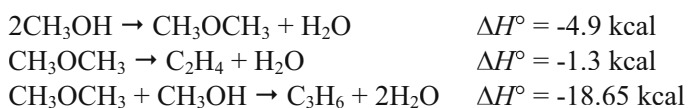
5.1 Olefins from methane via methanol

Since the oil price crises a number of methane-based ethylene routes, like OCM (Oxidative Coupling of Methane), Chlorinating Flame (Benson Process), dehydro-polymerization, have been explored, and up to now for different reasons have failed. Only the methanol to olefins (mainly ethylene and propylene) has overcome the exploratory phase. Two technologies of this type have been recently developed:

- MTO (Methanol-To-Olefins) by Hydro/UOP and
- MTP (Methanol-To-Propylene) by Lurgi/Statoil.

The ancestor of these technologies is the MTG (Methanol-To-Gasoline), developed by Mobil and implemented in a commercial unit in New Zealand in 1985. MTG utilized the ZSM-5 zeolites capable of partially converting methanol to Di-Methyl-Ether (DME) that further reacts to olefins, paraffins and aromatics in the gasoline range. The New Zealand unit currently produce mainly methanol.

Both MTO and MTP technologies use modified zeolites and tailored operating conditions to maximize the yield to light olefins. Oxygen leaves the system in the form of co-produced water (> 50%wt). Once methanol is produced from Natural Gas, main reactions involved are:



MTO [20] uses a SAPO-34 zeolite that with a pore size of 3.8 Angstroms controls the size of olefins that may emerge from the pores. Ethylene and propylene yields are about 80%, and the molar ratio between the two main products may be varied between 0.75 and 1.5 by adjusting the operating severity, with higher temperatures increasing the percentage of ethylene. Butylenes account for about 10%.

The process uses a fluidized bed reactor/regenerator system with continuous circulation of solid between reactor and regenerator, where coke is burnt with air and heat is removed from the system. The reactor operates at temperatures between 350°C and 550°C and slightly over-atmospheric pressure. The product gas is compressed and unconverted DME is recycled to the reactor. After the recovery of DME the effluent is further processed in a series of distillation columns, also including selective hydrogenation of acetylenic compounds, to recover polymer-grade ethylene and propylene.

A demonstration plant has been operated at Hydro's research facilities in Norway since 1995, at capacities of up to 1 ton per day of methanol.

MTP [21], currently under development by Lurgi/Statoil, is based on the same theoretical background than MTO, but claims the use of a proprietary zeolite catalyst, tailored to maximize the selectivity to propylene. The yield to propylene is also enhanced by partly recycling both higher and lower boiling by-products to the reactor. The produced propylene/ethylene mole ratio is in the range of 6-7. MTP works in two steps: methanol is fed to a first fixed bed adiabatic reactor where it is converted to DME at about

300°C. A subsequent reactor at 420-490°C and 1.3-1.6 bars converts DME to olefins. For lower capacity units a multitubular reactor cooled by evaporating water may be employed. For the large capacities associated to “mega-scale” methanol units, a single train may be maintained only using a series of adiabatic reactors with intermediate cooling. Periodically, the catalyst in each reactor (one at a time) is regenerated with air. MTP is also at the demonstration unit stage since 2002.

It is interesting to compare the different ways in which the developers of MTO and MTP face the features of the reaction:

- Exothermicity of reactions. Since ethylene and propylene formation reactions are very differently exothermic, variations of their ratio, force the reactors to be largely flexible in the heat removal design.
- Equilibrium shifted toward the products.
- Periodical regeneration of the catalyst due to Coke deposition.

The circulating fluidized catalyst of MTO with its high degree of gas and solid mixing avoids hot spots, keeping uniform the temperature. The high heat exchange coefficient, typical of fluid bed systems, allows efficient heat removal through submerged heat exchange surfaces. Regeneration of the catalyst is continuous. Moreover continuous replacement of fines with fresh catalyst keeps constant the bed activity and steady operating conditions are maintained throughout the life of the plant.

MTP relies on multiple fixed bed reactors in series. This choice allows complete conversion of DME, due to the plug-flow of the gas phase. Water must however be recycled to the reactors to keep under control the adiabatic temperature increase, divided in steps via intermediate quench with cold DME. In any case coke/tar build up on the catalyst requires a regeneration. A decay of performances between start- and end-of-run conditions has to be considered.

The methanol to olefins route appears economically attracting when low cost (remunerated price 80-100 US\$/t) methanol is available. This situation could be realistic for stranded gas (priced at 0.5 – 1 US\$/MMBTU) with "Mega-scale" methanol units ($\geq 5,000$ MTPD). This route could become a different way of GTL (gas-to-liquids) for converting "remote" gas to a transportable liquid (methanol) as feedstock for derivatives in end user areas.

5.2 The revival of metathesis

The word "metathesis" stems from old Grecian and means transposition or interchange. In effects this process involves the reaction between two olefins where their double bonds are broken and each moiety of the first olefin is reconnected with a moiety of the second one, forming different olefins. The following simple scheme (four centre of quasi-cyclobutane) is very useful for predicting primary products of metathesis:

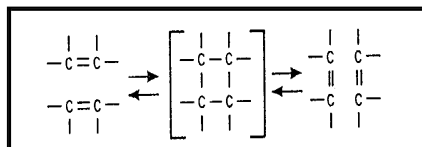


Figure 5. "Cyclobutane" model for prediction of metathesis products

Metathesis takes place by double bonds cleavage while the C-C bonds adjacent to the double bonds are unchanged. The mechanism involves carbene complexes as key intermediates with formation of transition metal-carbon bond with cyclobutane structure [22]. Olefins metathesis is an equilibrium limited reaction essentially thermo-neutral because the total number and type of C-C bonds remain unchanged.

The history of industrial application of metathesis is very interesting and represents a curious and instructive case of chemistry following market requests. This reaction was discovered, in the 1960s, independently in several industrial laboratories, mostly devoted to research in transition metal application in the polymerization field. The first industrial application of metathesis (32,000 t/y in 1966) was the Phillips "Triolefins Process" used to convert propylene into polymerization grade ethylene and high purity linear butenes:



Due to the increase in the demand of propylene this plant was shut down in 1973. At the moment, the market situation is completely inverted with a high propylene demand not covered by Steam Crackers, currently addressed to maximize ethylene. As seen before, the ratio of propylene to ethylene of crackers could be increased, operating at lower severities, but it would sacrifice ethylene yield and produce undesired heavies.

In this scenario, a possible alternative to reverse the "direction" of the old metathesis to get propylene from ethylene and 2-butenes:



The growing interest for propylene production with metathesis reaction is confirmed from the following industrial activities:

- Lyondell, using Phillips technology, has commercially proven propylene production using ethylene from an ethane cracker and 2-butenes from ethylene dimerization [23]. Potential capacity is 400,000 t/y propylene.
- ABB Lummus has purchased and improved the Phillips process (now OCT "Olefins Conversion Technology"). Three plants under design or construction [24].
- IFP is promoting its metathesis process Meta-4 jointly developed with Chinese Petroleum Corporation (CPC) of Taiwan [24].

Metathesis is another good example of how, for the same reaction, different "chemical" choices determine different solutions in the reaction engineering.

ABB process employs as catalyst WO_3 on SiO_2 together with a skeletal isomerization catalyst (MgO on Al_2O_3): catalyst operates at 300 - 375°C and simultaneously converts 1-butene to 2-butenes. Propylene selectivity of 98% is claimed. The catalyst beds are periodically regenerated by controlled coke deposit combustion.

IFP process employs a rhenium based catalyst which is active at very low temperatures (30 - 80°C); under these conditions equilibrium conversion is favored and it is possible to achieve longer catalyst length due to less catalyst fouling. Optimal reactor/regenerator system is determined by the plant size. For large units continuous catalytic reforming technology is the more cost-effective design; in this configuration the reagents enter the bottom of reactor in countercurrent with the fresh catalyst which enters (from the regenerator) the top of reactor; a small amount of less active catalyst is removed from the bottom and sent to regenerator. For smaller units fixed beds with cyclic regeneration are the best solution.

6. DEHYDROGENATION OF ALKANES

Dehydrogenation is the most direct and selective way to get a defined olefin and introduces a preferential point of attack for subsequent reactions.

Reaction characteristics pose inherent difficulties and some constraints [25] in developing commercial processes.

- *Conversion is limited by thermodynamics. High temperature needed*

Equilibrium conversion increases with temperature. In order to achieve reasonable economic conversion high temperatures, exceeding 500°C, are a prerequisite (table 7). Lighter paraffins are more difficult to dehydrogenate.

Table 7. Equilibrium conversion (%) for light paraffins dehydrogenation.

Paraffin/T°C	400°C	450°C	500°C	550°C	600°C	650°C
Ethane	1	2	5	10	17	29
Propane	3	6	11	20	32	51
Isobutane	5	11	18	30	47	71

These temperatures are critical for the paraffins and olefins stability: several side reactions take place. Oligomerization to heavier compounds, cracking to lighter hydrocarbons, skeletal isomerization, aromatization, alkylation of the formed aromatic rings, eventually leading to coke formation, lower the yields (figure 6).

The use of a suitable catalyst is necessary in order to get high reaction rates and, above all, high selectivity toward the desired olefin at convenient conversion per pass, taking into consideration that most side-reactions are accelerated by the same catalyst components. At temperature higher than 700°C about, thermal reaction become very fast and compete with the catalytic ones. The presence of several consecutive reactions is responsible of the typical trade-off between conversion and selectivity to the desired olefin: increasing conversion, selectivity drops off.

Many different catalysts have been studied since many years for the dehydrogenation of paraffins [26], but in practice only promoted chromia/alumina and platinum/alumina are industrially applied. Commercial Cr- and Pt-based are duly optimized, to achieve a suitable couple of activity/selectivity values. Pt is less active in the heavier products formation respect to Cr, but induces some skeletal isomerization of C₄ (a slight complication of C₄ process schemes) that Cr does not [27]. Recent promising results have been obtained on ethane dehydrogenation on mordenite modified with Zn, or Ru, or Pt, or Ga [28].

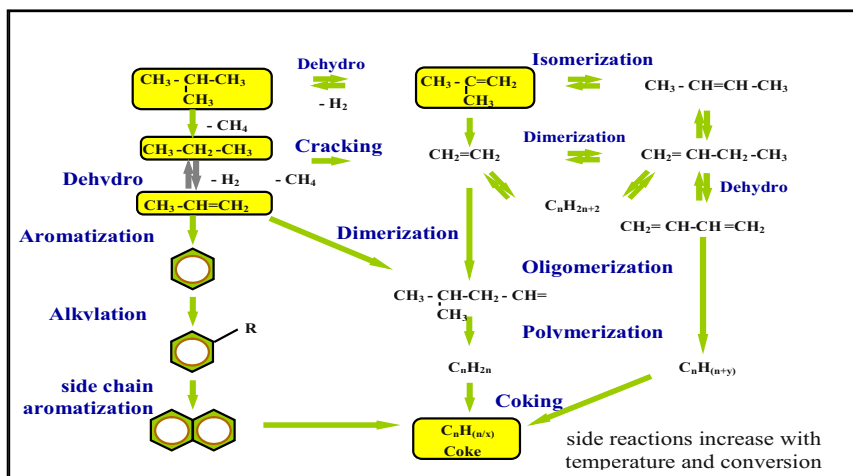


Figure 6. Dehydrogenation reactions network.

The chain of condensation reactions brings fatally heavy by-products and coke that accumulate on the catalyst during the reaction period. A periodical regeneration, normally with air, of all catalysts is mandatory. Any catalyst will follow a cycle of a hydrocarbon atmosphere, and a period in the presence of oxygen (and/or some steam). It is required to preserve their morphology, structure, chemical stability in severe hydrothermal conditions. The length of the time on hydrocarbon stream depends on the active phase: typical values are “minutes” for Cr catalysts and “hours” for the Pt ones.

- *Dehydrogenation is strongly endothermic:*

About 30 kcal/mole of extracted hydrogen are requested, resulting in a higher heat demand on weight basis for producing lighter olefins. High endothermicity means high adiabatic temperature decrease of the gas phase, e.g. 200°C to convert 25% propane or 35% isobutane. Since no catalyst is able to operate in a so wide range of temperature, it is clear that a single step adiabatic converter cannot be used and heat has to be supplied in the course of the reaction. The way in which the heat is supplied to the gas characterizes the industrial processes.

- *Reactions increase the number of moles:*

Equilibrium conversion increases lowering the pressures. Some technologies operate at paraffin partial pressure lower than one atmosphere (vacuum, H₂ or steam dilution) to get a higher driving force.

6.1 Conceptual design for reactor configurations.

Several different conceptual reactor types and configurations can satisfy the basic dehydrogenation system operating requirements. The heat supply philosophy determines the other choices: catalytic system, regeneration mode, cycle length. Licensors claim significant advantages to their particular choices outlining low investment requirements, low utilities, and large capacity capability.

- *Adiabatic fixed bed reactors* commercialized by ABB Lummus (Catofin technology - figure 7a [27]). Heat is stored on the catalyst during the regeneration step and released by the catalyst during the reaction period. Reactors operate batchwise cyclically, quickly alternating reaction, purging and regeneration periods. Continuous operation is achieved using more reactors in parallel. The quick switching between oxidizing and reducing atmosphere and the short time on hydrocarbon stream is compatible with a Cr catalyst. The reactor temperature profile is complex, due to the alternating reaction taking place, but in principle, during the reaction period it is expected to be decreasing with the time on stream and from the reactor inlet to the outlet. Commercial plants for C₄ and C₃ dehydrogenation are in operation.

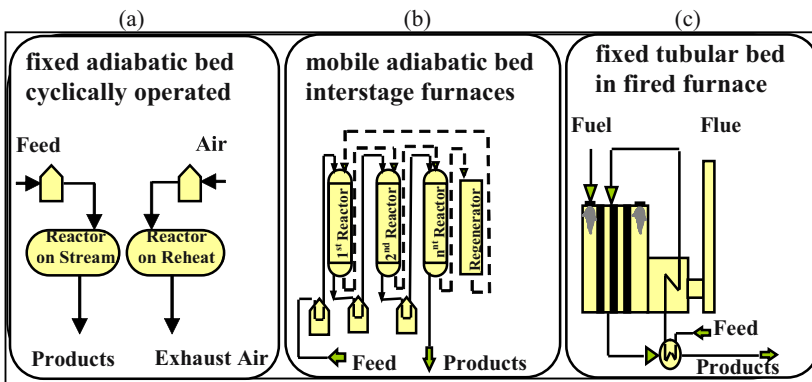


Figure 7. Dehydrogenation reactor conceptual design.

- *Adiabatic moving bed reactors in series* commercialized by UOP (Oleflex technology - figure 7b [29]). Reaction heat is supplied to the gas by interstage heating in furnaces between several reactors in series. For the regeneration the catalyst slowly downflows and it is collected at the

end of the last reactor, conveyed to the regenerator and then back to the first reactor. The slow movement of a mobile bed forces a relatively long period on hydrocarbon stream, and suggests the use of a Pt catalyst. Reactor temperature profile is a typical sequence of re-heating steps. The technology is commercially applied for C₄ and C₃ dehydrogenation.

- *Tubular fixed bed in furnace* fireboxes (figure 7c): heat is supplied similarly to a steam-reforming process by burning fuel in a furnace. For regeneration more reactors in parallel are used, some of these being alternatively in regeneration. In principle it is possible to use both Pt or Cr catalyst. Depending on this choice and on its resistance to coke build-up at the actual operating conditions, the number of tubes necessary to be alternatively in regeneration varies. In principle the reactor could be isothermal, but the actual temperature profile will be determined by the balance of heat exchange of the packed tubes according to the internal heat absorption rate and the furnace temperature profile. Two technologies follow this concept. STAR (Steam Active Reforming), developed by Phillips, and now licensed by Krupp-Uhde [30] is applied commercially for C₄ (Pt catalyst). Recently Linde-BASF-Statoil have developed a new technology based on Cr catalyst [31].
- *Fluidized bed reactor* applied in the FBD technology, by Snamprogetti–Yarsintez based on circulating solid and described below. Over 30 industrial units of isobutane, *n*-butane and isopentane fluidized bed dehydrogenation units have been built since 1960s. The largest unit is a single line 475,000 t/y isobutylene (FBD-4) plant in Saudi Arabia [32].

6.2 Dehydrogenation in a fluidized bed

A fluidized bed is a bed of solid particles kept suspended by an upward gas flow. At very low gas velocity the bed behaves like a fixed bed; increasing the gas velocity, for a given density and particle size of the solid, fluidization begins and above a certain value the solid particles are blown away [33]. Some principles and images are shown in figure 8 and 9.

A fluid bed behaves like a liquid and the solid can be transferred in pipes; the high efficiency of mixing of solid particles enhances heat and mass transfer; pressure drop across the bed is low (equal to the catalyst weight divided by the cross sectional area).

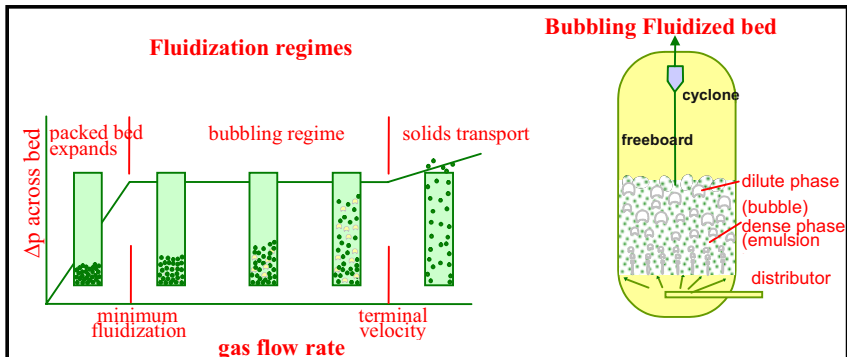


Figure 8. Fluidized beds main concepts.

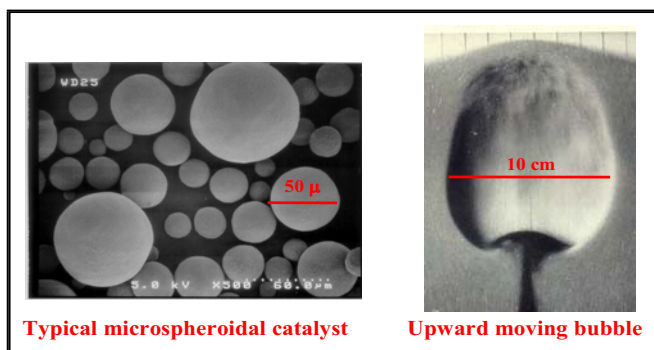


Figure 9. Particle size-distribution and bubble shape

Fluidization regimes applied in the industrial practice range from a very smooth bubbling stationary bed of solid, up to a highly turbulent co-current flow of gas and solid. Fluidized beds are currently applied to a huge variety of chemical reactions, including dehydrogenation.

The core concept of the FBD process is the design of the reactor-regenerator system (figure 10). The reaction is carried out in a bubbling fluidized bed operating at 500 - 700°C and slightly above atmospheric pressure. Catalyst circulates like a liquid between reactor and regenerator.

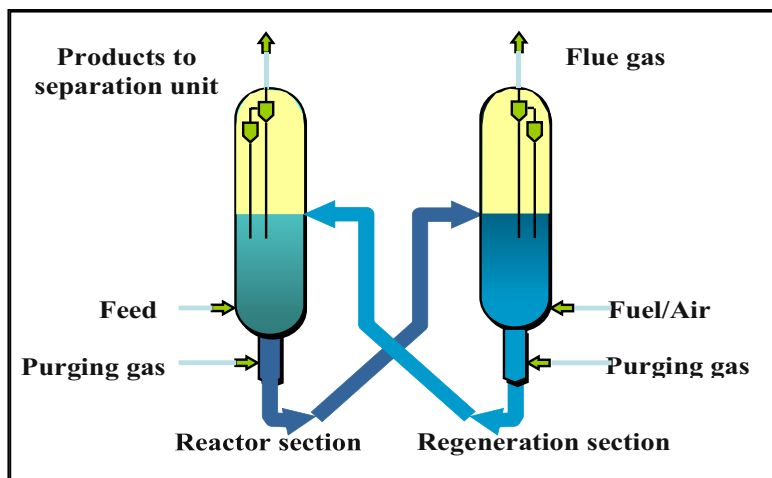


Figure 10. FBD Reactor - regenerator cycle.

Reaction heat is supplied by the heat capacity of the “hot” ($>650^{\circ}\text{C}$) solid catalyst (hotter than reaction temperature) continuously arriving to the reactor top from the regenerator bottom. Catalyst vice-versa goes back “cold” ($<560^{\circ}\text{C}$) from the bottom of the reactor to the top of the regenerator through a transfer line system. A countercurrent flow of gas and solid both in the reactor and in the regenerator is obtained. Pneumatic transfer of the catalyst between the two vessels is obtained reducing the density of the rising side of the transfer lines by a suitable lift gas injection. Commercial technologies applying this principle reach catalyst circulation of thousands of ton per hour.

The FBD processes use a chromia/alumina catalyst with promoters. The microspheroidal catalyst with average diameter less than 10^{-4} m and density less than $2,000\text{ kg/m}^3$ is typical of "A" group according to Geldart [33], and it is very similar to a FCC catalyst. Molar selectivity to olefin of 90 - 95% is obtained at conversion level optimized for each paraffin and local economic parameters.

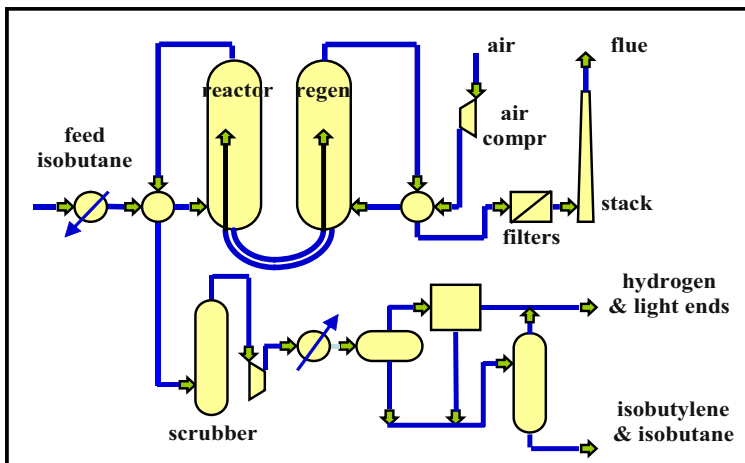


Figure 11. FBD-4 Process scheme.

In the regenerator, the catalyst restores its initial state by burning the small quantity of coke formed on it during the reaction; catalytic active sites are also restructured. Main task of the regenerator is to generate all the heat required by the system: reaction heat, enthalpy of reactants, heat losses. In order to heat up the catalyst and satisfy the overall thermal balance the small quantity of coke formed by the selective catalyst is not enough. Additionally some fuel is burned directly on the catalyst in the regenerator, acting as a catalytic combustor. Heat requirements (and not deactivation) dictate the catalyst circulation rate. Catalyst flowrate is easily calculated since it is directly proportional to the total heat to be supplied, inversely proportional to the solid heat capacity and to the ΔT of the catalyst leaving from and returning to the regenerator.

A typical fluidized bed shows a top-to-bottom mixing which makes the bed nearly instantaneously homogeneous, approaching an ideal CSTR (Continuous Stirred Tank Reactor). To achieve optimal yields and reactor volumes, it is desirable a sharp distribution of residence time of solid particles, as well of gas molecules. To approach that it is necessary to minimize the axial backmixing of both phases. A practiced way is to stage the bed through the insertion of baffles [34] that reduces gas backmixing. Staging makes a fluidized bed similar to a tray distillation column dividing the bed in a series of well-mixed CSTR. Baffles are usually (e.g. FCC or fluid-coke strippers) chevron, inclined slabs; other shapes like perforated trays are also used. A simplified flowscheme for isobutane dehydrogenation is reported in figure 11.

7. TECHNOLOGIES FOR C₄s EXPLOITATION

MTBE (Methyl-tert-butyl-ether) with its over 20 million t/y of capacity is the largest utilization of C₄. It appeared in the gasoline pool in 1973 with the first commercial plant (100,000 t/y by Snamprogetti/Anic in Italy). The MTBE superior blending properties as gasoline component (octane booster, substitute for lead, low volatile, full fungible with gasoline, combustion improver for abating tailpipe emissions) made it the fastest growing chemical in 1980s. The Clean Air Act Amendments of 1990s, mandating the 2% oxygen in Reformulated Gasoline, sealed the success of MTBE, the oxygenate of choice. As the acceptance of MTBE increased all available sources of isobutylene (steam crackers C₄s, FCC C₄s, dehydration of tert-butanol) were “dried up” and new routes were developed particularly the Isobutane from field butane Dehydrogenation.

Any great success provokes reactions. In the late 1990s it was widely emphasized in the US that MTBE finds a way into drinking water supplies, making the water taste and smell badly. MTBE arrived to water from leaking underground storage tanks, gasoline pipelines, spills, use of motorboats on lakes for water supplies, i.e. from infrastructure defects. Its detectable presence should warn that other really harmful components of gasoline were there. A “war” against MTBE inflamed involving many parties: oil companies, MTBE producers, farmers, ethanol producers, car producers, public authorities, politicians, greens, each one having different viewpoint and interests. On this emotional wave crest, California decided to ban the use of MTBE (delayed at January 1st, 2004). The outlook for MTBE in the US is still uncertain and difficult to predict, although a strong reduction of its use is likely. In Europe, where gasoline distribution infrastructures were safer, and in Asia MTBE use is not under discussion. In any case, guilty or messenger, villain or victim, MTBE has lost its golden age, but still maintain a worldwide prominent role in gasoline formulation.

7.1 MTBE TECHNOLOGY

MTBE is produced by the liquid-phase addition of methanol (MeOH) to isobutene with acid ion-exchange resins as catalyst. Since the reaction is exothermic and limited by the chemical equilibrium, the reactor outlet temperature is maintained as low (40 and 80°C) as allowed by the catalyst activity in order to maximize the isobutene conversion.



Several companies have developed MTBE processes which differ principally for the particular kind of reactors employed while separation section is generally very similar. A typical MTBE process scheme is reported in figure 12 [35].

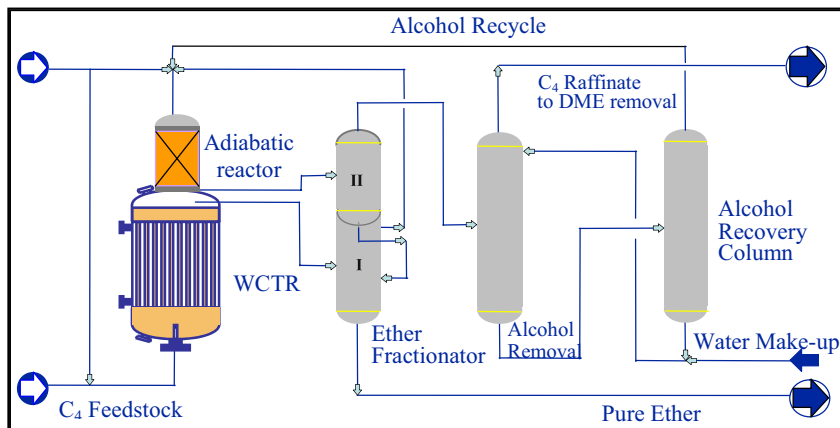


Figure 12. Snamprogetti High Conversion MTBE process scheme.

All licensors claim advantages for their technology.

Snamprogetti. The key feature of this process is the water-cooled multitubular reactor (WCTR) as first reactor. This reactor allows a temperature profile that represents the optimal trade-off between kinetics and thermodynamics, i.e. high temperature at reactor inlet, to allow high reaction rates, and low temperature in the outlet zone, to maximize the conversion. The height of temperature peak is controlled in order to be sufficiently high to allow high reaction rate but low enough to avoid negative effect on the catalyst life.

Catalytic Distillation Technologies (CDTech). CDTech process is based on a two step reactor design consisting in a boiling point fixed bed reactor (BPR) followed by a catalytic distillation (CD Tower). BPR is designed so that the liquid is allowed to reach its boiling point by absorbing the heat of reaction, after which a limited amount of vaporization takes place thereby maintaining precise temperature control. Catalytic distillation combines reaction and fractionating in single unit operation. Recently CD Tech and Snamprogetti agreed to combine and market their expertise in C₄ fraction upgrading. The combined technology, based on a vast experience in etherification field, can offer a variety of solutions (BPR, WCTR and CDtower) in order to optimize revamping or grass root construction with reduction of capital cost [36].

IFP. A typical feature of IFP technology is an expanded bed reactor as first reactor. This reactor prevents local overheating or bed channeling by keeping the catalysts moving to maintain an uniform reaction environment. The finish conversion step of isobutene can be achieved with a fixed bed or with a distillative column (CATACOL) [37].

UOP. UOP Ethermax process combines the UOP/Huels fixed bed etherification process with catalytic distillation from Koch (KATAMAX packing). A possible option of this technology is the removal of residual oxygenates from spent C₄ hydrocarbons with MRU (Methanol Recovery Unit) and ORU (Oxygenates Removal Unit) [38].

Fortum. The most distinctive property of Fortum process is the total absence of conventional alcohol recovery section. In this process the synthesis is made with some adiabatic reactors while methanol is recovered as side stream with one or two distillation column [39].

7.2 ISOCTANE TECHNOLOGY

Gasoline standards throughout the world are continuing to move toward cleaner burning gasoline (reduction of aromatics, benzene, sulfur, RVP and distillation characteristics maintaining or increasing octane). Apart from MTBE, alkylate and isooctane could fulfill the above requirements. Conventional alkylation units use as catalyst liquid acids that raise significant environmental concerns. In this scenario, Iso-Octane, from selective dimerization of isobutene by revamping existing MTBE units, can meet economic and quality requirements.

Isooctane technology definitely permits to make a non-oxygen-containing alkylate-like product by using existing MTBE (or ETBE) units. Isooctane (2,2,4-trimethyl-pentane) is the reference compound for the measurement of octane and, by definition, has a clear RON and clear MON of 100. Iso-OctAne refers to a product very rich in isooctane, produced by selective isobutylene dimerization, with acid catalyst, followed by olefin saturation. The olefinic product from the dimerization, prior to being saturated, is rich in isooctene (2,2,4-trimethyl-pentenenes or DIB) and is referred to as Iso-OctEne product.

Although this dimerization technology has been used since during World War II, it has not found further applications because of its high exothermicity which makes temperature control very difficult, favoring the excessive formation of heavier oligomers. Snamprogetti since 1994 studied how to make more flexible its MTBE technology by co-producing simultaneously a high quality alkylate [40]. The key of the success has been

the use of an oxygenate (selectivator) which influences the dimerization reaction rate. Due to its polarity the oxygenate compound (alcohol or ether) is preferentially adsorbed on the active sites of the catalyst. The presence of oxygenates reduces the strength of acid sites and, as a result, the rate of oligomerization reaction is much reduced and the selectivity increased.

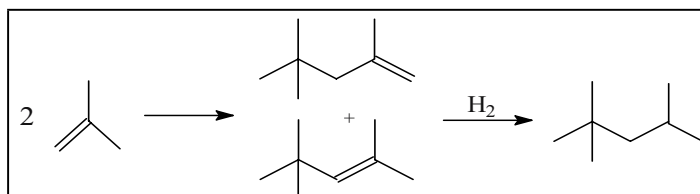


Figure 13. Dimerization of isobutylene to isooctenes.

When methanol in substoichiometric molar ratio oxygenate/isobutene is the selectivator, a simultaneous isobutene etherification and dimerization occurs and the final product will be a mixture of MTBE and dimers/trimers. Product composition depends on the alcohol/isobutene molar ratio in the feed (figure 14). Alternatively, when TBA or the same MTBE are used as oxygen bearing selectivator pure dimerization is achieved.

In the presence of linear olefins, reaction mechanism is more complex because linear butenes react with isobutene to form codimers with dimethyl-hexane structure having much poorer octane properties.

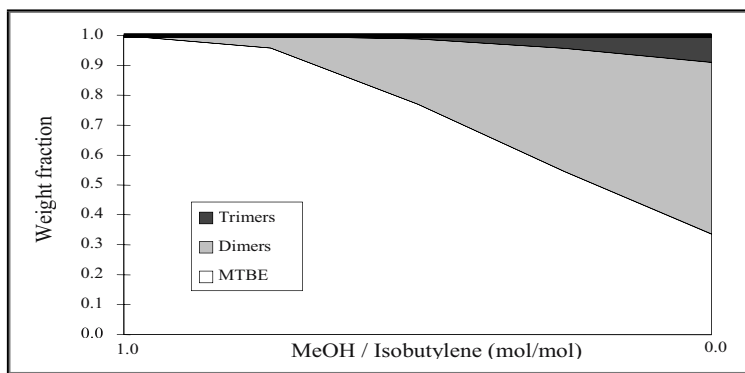


Figure 14. Isobutylene Etherification /dimerization; typical product composition.

On the contrary trimers have not a marked influence of Iso-Octane properties. Operating under optimal conditions, trimers content is limited at about 5-15 wt %, while tetramers are present at the level of only a few

thousand ppm. Iso-OctAne and Iso-OctEne properties are better than those of the normal alkylate produced by commercial technologies with higher RON and MON and lower RVP (Table 8).

Table 8. Comparison of properties for fuel use of some high performance component

	Iso-OctAne product	Iso-OctEne product	Normal Alkylate	MTBE	Iso-OctAne - MTBE 1/1 vol.
Clear RON	100.2		90		
Clear MON	100.3		94		
Blending RON *	101 - 103	114 - 118	97 - 99	116	108 - 110
Blending MON *	96 - 98	95 - 97	90 - 92	100	98 - 99
RVP (psi)	1.7	1.5	4.5	8	5.4
Sp. Gravity	0.72	0.733	0.697	0.745	0.725

* Base Gasoline RON = 95; MON = 85. RVP = Reid Vapor Pressure

Commercially available dimerization technologies are oriented to US MTBE revamping market. MTBE plants revamping to produce Iso-OctAne can be made easily because dimerization occurs utilizing the same catalyst, reactors, operative parameters (temperature and pressure) and isobutene conversion; in this case C₄ purification section is not necessary.

Snamprogetti/CDTech is the only technology that can offer also a solution with MTBE as selector (more efficient for C₄ feedstock with high isobutene concentration) or with MeOH to produce a mixture of high quality alkylate and ether if there is some market request.

Hydrogenation is carried out in a typical trickle-bed reactor on noble or non-noble metals according to the level of contaminants.

UOP InAlk and IFP Selectopol are alternative technologies to convert isobutene. These processes could be a solution for new plants but are not indicated for MTBE revamping due their different process design, catalyst (inorganic solid acid) and operating conditions.

7.3 High Purity Isobutylene

Very purity isobutylene (>99.99%) is obtained via the combination of MTBE synthesis and cracking. This is an effective and cleaner way of separating isobutylene from 1-butene since a direct fractionation is impossible being the difference of boiling points of only 0.6°C.

The scheme of the High Purity Isobutylene process [41] is very simple since it constituted by a MTBE synthesis section in which only isobutylene reacts. MTBE is easily separated from unreacted butenes and sent to a cracking section that requires only methanol washing steps and separation columns to recover isobutylene. Unconverted MTBE (conversion per pass

80-85%) is recycled back to the cracking reactor. The tubular MTBE cracking reactor operates in gas phase and utilizes a proprietary catalyst (a particularly prepared silica/alumina). Its key feature is the fine tuning of acidity to prevent the formation of by-products such as dimers/oligomers (catalyst fouling) and DME-water (detrimental for polymerization grade). The tetrahedral coordination of aluminum atoms of the active centers is the key factor for catalyst performances. Four plants (up to 62,000 MTPY) are in operation.

8. REFERENCES

- [1] Parpinelli Tecnon: World Petrochemical Industry 2002. Olefins
- [2] E. Dupont, A. Laghate, S. Barendregt, ERTC Petrochemical 2003 Paris.
- [3] SRI Menlo Park, Ca. Private Report 29F Ethylene by Non-conventional Processes
- [4] ATEC Parpinelli, May 13, 2003
- [5] Chauvel, G. Lefebvre Petrochemical Processes Vol 1 - Editions Technip Paris (1989)
- [6] Dente, M., Ranzi, E., Goossens, A. G., *Comp. Chem. Eng.*, 3 (1979), 61
- [7] T. Detemmerman G.F. Froment, *Rev. Inst. Fr. Petr.*, 53, 2, 181-, 1998
- [8] *Hydroc. Proc.* March 2003
- [9] USP 5,981,819 (1999) to Metallgesellschaft AG. *ptqcatalysis* 8, (2), 57, 2003; *Chem. Eng.* July 1998, 25;
- [10] <http://www.mwkl.co.uk/pdf/Superflex.pdf>; R. Ware, World Petrochem. Conf., CMAI, Houston, Apr. 1, 1998
- [11] *O&GJ* Dec. 23 2002, 96
- [12] *Hydrocarbon Asia*, January/February 43 2002,
- [13] *ECN* April, 4 1993, 31
- [14] USP 4,434,317 (1983) to Exxon; USP 5,639,935 to BP (1998), 6,395,952 (2002) to S&W
- [15] Alter, 4,328,382 (1982) to Erdolchemie
- [16] D. Tsou, *Ind. Eng. Chem Res.* 33, 3209, (1994); USP 5,135,547 to Standard Oil (1992)
- [17] C.Pirovano, D. Sanfilippo, F. Saviano, L. Piovesan USP 6,414,210 to Snamprogetti (2000)
- [18] A.S. Bodke, D.A. Olshcki L.D. Schmidt E. Ranzi, *Science* 1999, 285, 712.; A. Beretta, E. Ranzi, P. Forzatti, *Cat. Today* 2001, 64, 103-111
- [19] USP 4,940,826 (1990), WO200037399 to BP. WO200014035 to Dow
- [20] J. Andersen, ERTC Petrochem. Conf. 2003, Paris; E. Arnold, J. Andersen, 17th Ann. World Methanol Conf., San Diego, 1999.
- [21] M. Rothemael, J. Wagner, S. Staale Forre, O. Olsvik, ERTC Petrochem. Conf. 2003, Paris
- [22] R.L. Banks "Catalysis" vol IV, 100, Chem. Society London, 1984 - R. Streck, *J. Mol. Cat.*, 46 (1988) 305 - P.H. Wagner, *Chem Ind.*, 4 May 1988, 331
- [23] Anon, *Petrochemical News*, 18 nov (1985), 4.
- [24] *Hydroc. Proc.* March 2003, 126 - J.A. Chodroge, J.Cosyns, USP 6358482, 2002
- [25] F. Buonomo, D. Sanfilippo, F. Trifirò, in G. Ertl, H. Knotzinger, J. Weitkamp eds. *Handbook of Heterogeneous Catalysis*, 5, chap. 4.3.1, 2140-51, VCH (1997)
- [26] P.H. Emmett *Catalysis*, 3 chap. 10, Reinhold Pub.Corp. (1955)

- [27] F. Trifirò, F. Cavani, Catalytica Studies Div., Study # 4192 OD, (1993) - http://www.sud-chemieinc.com/houdry_isobutane.shtml
- [28] WO 96/34843 to Dow (1996)
- [29] <http://www.uop.com/gasprocessing/TechSheets/Oleflex.pdf>. P. Pujado, B. Vora: Hydroc. Proc. 1990, 65,
- [30] S. Wenzel et al.; ERTC Petroch.. Paris 03.03.03; Achema, Frankfurt May, 19-21 2003
- [31] /H. Zimmermann, F. Verluis: USP 5,378,350 (1995) to Linde - <http://www.linde-anlagenbau.de/en/p0001/p0002/p0007/p0007.jsp>
- [32] D. Sanfilippo, Chemtech 35-9, Aug. 1993; CatTech, 7, Sept. 2000, 56; I. Miracca, L. Piovesan, Cat. Today, 52, 259-269 (1999)
- [33] D. Kunii, O. Levenspiel, Fluidization engineering, Butterworth-Heinemann Series in Chem. Eng. (1991); D. Geldart, Gas fluidization technology, Wiley, New York (1986)
- [34] Overcashier, Todd, Olney, AIChE J. 5, (1), 54-60 (1959); G. Papa, F.A. Zenz, Chem. Eng. Progress, 32-6, April 1995
- [35] Miracca, L. Tagliabue, R. Trotta, Chem. Eng. Sci., 32 (1993), 178
- [36] Hydrocarbon Processing., November 2002, 106
- [37] Hydrocarbon Processing., November 1994, 109
- [38] R.A. Becker et al, NPRA 1994, San Antonio
- [39] Hydrocarbon Processing, March 1995, 112
- [40] M. Di Girolamo et al. Cat. Today, 52 (1999), 307 - M. Di Girolamo, Ind Eng Chem, 1997, 36, 4452 - M. Marchionna, M. Di Girolamo, R. Patrini, Cat. Today, 65 (2001), 397
- [41] O. Forlani et al., 12th North Am. Meet. Cat. Soc., Lexington Ky (USA), May 5-9, 1991

Chapter 12

MEMBRANE REACTORS FOR THE FISCHER-TROPSCH SYNTHESIS

Alexander A. Khassin

Boriskov Institute of Catalysis, 5 Prospect Lavrentieva, Novosibirsk 630090 Russia

Abstract: The analysis of the specific features of the Fischer-Tropsch synthesis helps formulating the most important requirements to the FTS reactor. Membrane reactor designs can be useful for the FTS process application. Semi-permeable hydrogen-selective distributors allow to control the $H_2:CO$ ratio along the catalyst bed and thus enhance the selectivity of the process. Membranes of extractor type can help to improve the FTS performance by selective removing water from the reaction volume. On the other hand, plug-through contactor membrane reactor design (PCM) seems to meet all the other requirements, ensuring the high concentration of the catalyst, isothermicity, high gas-liquid interface area, small effective diffusion length and reasonable hydraulic resistance. Varying the membrane composition and conditions of its preparation leads to the changes in porous structure parameters of the PCM membrane. This allows to weaken the diffusion constraints in a predictable way and, therefore, to control the productivity and selectivity of the Fischer-Tropsch process.

Key words: Fischer-Tropsch, membrane, extractor, contactor, ceramic-metal composite, monolith

1. INTRODUCTION

1.1 Advantages of the use of membranes in catalysis

During the last two decades, numerous publications were devoted to the application of membranes in catalysis. In some catalytic processes, the use of membranes have already provided technological breakthrough and are

expected to improve the other. These are subjects of several review papers [1, 2] but out of scope of the present report. Table 1 presents a short list of the supposed roles of membranes in catalysis. Better understanding of potential benefits of membrane reactors for the Fischer-Tropsch synthesis (FTS) needs formulation of basic requirement to this process and analysis of difficulties of the process implementation.

Table 1. The possible roles of membranes in catalysis and some recent examples of their application.

A. Reagent supply (distributors)	
1. A reagent is supplied continuously along the entire reactor length, so that its concentration along the catalyst bed is never high. Therefore, the successive reactions are not favored	Selective oxidation reactions, chemical valve membranes [3]
2. A reagent can be separated from the diluted mixture feed (e.g. oxygen from air)	Partial oxidation of methane, Extraction of H ₂ from syngas [4]
B. Removal of a product (extractors)	
1. Extracting one of products from the reaction volume may increase this product yield in the equilibrium-restricted processes due to:	dehydrogenation (H ₂ removal) WGSR (water removal) [5]
a) increasing the conversion;	pervaporation-aided
b) suppressing overreaction.	esterification processes [6, 7]
2. Extracting one of products can suppress the undesirable secondary interactions of the product with another reaction mixture component or with the catalyst	isobutene oligomerization to isooctene [8]
C. Increasing the gas-liquid interface (contactors)	
Application of permeable porous membranes with the active component supported on the membrane surface can help to increase the rate of multiphase processes	hydration of propene [9] aqueous nitrate reduction [10] multiphase hydrogenation [11]

1.2 Specific features of the FTS process and principal requirements to the process design

1.2.1 Temperature sensitivity of the process selectivity

Fischer-Tropsch synthesis is a highly exothermal process ($\Delta H_{500\text{K}}$ is *ca.* -160 kJ/mol). The process selectivity depends strongly on the reaction temperature and it decreases as the temperature increases [see e.g. 12-16]. According to [16], the temperature dependence of the Anderson-Schulz-

Flory (ASF) parameter α for cobalt-containing catalysts at 1 bar follows the equation:

$$\alpha = \left(1 + \gamma_0 \exp\left(-\frac{\Delta E + \xi/d}{RT}\right) \right)^{-1} \quad (1)$$

where γ_0 is the parameter depending on the reaction conditions, ξ depends on the nature of active metal, d is the mean size of the active metal crystallites. Parameter α decreases monotonously with temperature (Fig. 1). Elevation of temperature results not only in acceleration of the reaction but also in undesirable shifting of the process selectivity towards methane and light hydrocarbons. The conflict between the process acceleration and detriment of the selectivity puts forward the *requirement of strict temperature control and isothermicity of the process.*

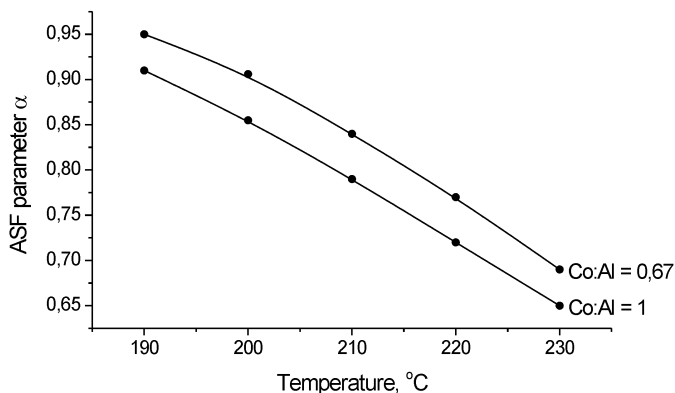


Figure 1. ASF parameter α as a function of the reaction temperature according to [15], Co/CoAl₂O₄ catalysts, H₂:CO = 2, P = 0,1 MPa

1.2.2 Slow reaction kinetic rate

FTS is a rather slow process. In 1975, Vannice [17] reported the reaction rate as low as $2 \cdot 10^{-2}$ CO molecules per 1 surface cobalt atom per second (i.e. 1.4 g of hydrocarbons per 1 g of cobalt loading per hour) at 275°C, 0.1 MPa over 2% Co/Al₂O₃ with cobalt dispersion of 8%. The effective activation

energy of the process is *ca.* 113 kJ/mol that indicates a strong dependence of the reaction rate on temperature. Taking into account the above mentioned sensitivity of the process selectivity to temperature, the reaction rate at the optimal temperature range 210-230°C is even ten times lower and no more than 0.15 mg_{HC} g_{Co}⁻¹ hr⁻¹. The later experimental reaction rates over cobalt-containing Fischer-Tropsch catalysts at the typical FT conditions (H₂:CO ratio *ca.* 2; P = 1-3 MPa, T = 220-250°C) were consistent with the data obtained by Vannice, they were no more than 0.6 g of hydrocarbons per 1 g of catalyst per hour. For example, the 39 wt% Co/SiO₂ catalyst was reported to produce 385 mg_{HC} g_{cat}⁻¹ hr⁻¹ at 220°C; 2 MPa; H₂:CO = 2; 23.4% CO conversion [18].

In view of the fact that the catalytic activity is low, it seems strongly undesirable to allow additionally any kinds of mass transfer hindrances. This calls two specific demands to the CO hydrogenation reactors, which are discussed below. Anyway, *any kind of the catalyst dilution should be avoided.*

1.2.3 Hindered mass-transfer at the gas-liquid interface

Fischer-Tropsch synthesis is a three-phase process, since the liquid hydrocarbons are accumulated in the reaction volume (in particular, inside the pores of a catalyst grain). Therefore, the gas phase reactants must first dissolve in the liquid phase before the catalytic interaction occurs, and the formed light hydrocarbons must evaporate. The rate of these interphase mass-transfer processes affects strongly the productivity of the process [19]. *The presence of a large gas-liquid interface area and the intensification of the convective mass-transfer inside the liquid phase* (including that inside the catalyst grain pores) are crucial requirements for the process.

1.2.4 Intraparticle diffusion constrains and their impact on the process productivity and selectivity

Another consequence of catalyst grain flooding is significant deceleration of the molecular diffusion of both the reactants and products inside the catalyst grain. The reactant molecular diffusivities in liquid hydrocarbons can be estimated from the well-known Wilke-Chang correlation [20]:

$$D = 7.4 \cdot 10^{-8} (M_L)^{1/2} T / \mu_L (V_{bG})^{0.6} \quad (2)$$

Here M_L and μ_L are the molar weight and dynamic viscosity of the liquid phase, respectively; V_{bG} , cm³/mole is the reactant molar volume at the

boiling point. At 200°C, $n\text{-C}_{14}\text{H}_{30}$ as the liquid phase, these estimated coefficients are $1.6 \cdot 10^{-4} \text{ cm}^2/\text{s}$ for CO and $2.2 \cdot 10^{-4} \text{ cm}^2/\text{s}$ for H_2 . These values are much lower than those for gas phase. Simple estimation leads to the conclusion that the particle radius should be less than 100 μm to have no effect on the catalyst activity. A more accurate analysis of the role of intraparticle diffusion constraints reported in [21, 22] led to similar values of the maximal effective diffusion length, which ensures no effect of the intraparticle diffusion on the reaction rate.

Notice that the intraparticle diffusion limitations not only hinder the activity of the process, but also affect the process selectivity. The nature of this influence is thoroughly analyzed in articles [23, 24] and review [25]. The diffusion impact upon selectivity was estimated by the value of complex $\chi = R^2 \theta \varepsilon / r$, which is a part of the Thiele modulus. Here R is the effective grain radius (m), θ is the concentration of active sites (m^{-2}), ε is the grain porosity, r is the effective pore radius (m). Figure 2 shows the trend of the impact of χ complex on the C_{5+} selectivity. At low values of $\chi < 2 \cdot 10^{18} \text{ m}^{-1}$, the diffusion constraints have positive effect on the C_{5+} selectivity, since the mass-transfer constraints hinder the release of olefins from the pore structure thus increasing the probability of their re-adsorption and continuation of the hydrocarbon chain growth (see dash line). At higher χ values, the pore volume becomes depleted with CO, since diffusion coefficient is significantly lower for carbon monoxide than for hydrogen. This results in higher probability of chain termination and in diminishing C_{5+} selectivity (dash-and-dotted line in Figure 2). Maximum of the C_{5+} selectivity is therefore achieved at the effective diffusion length of 0.02-0.04 mm. It is noteworthy that if olefins are considered as target products, the effective diffusion length should be even less than 20 μm .

1.2.5 Inhibiting the reaction rate in the presence of water vapor

Water is one of the main FT products. As reported earlier by Espinoza and co-authors, introduction of water vapor into the reaction mixture deactivates iron-based catalysts [26] and cobalt-containing catalysts [27] due to oxidation of a part of Co metal. These data are in agreement with the observations made with $\text{Co}/\text{Al}_2\text{O}_3$ catalysts [28-30]. Moreover, some data [28, 31] argue for partial (10-30%) irreversibility of the oxidation. Davis and co-workers reported that the water addition decreased the activity of Co/TiO_2 as well as Ru-promoted Co/TiO_2 catalysts [32]. Kogelbauer et al. [33] also studied the effect of treatment of Co/SiO_2 with water on the formation of Co silicates (including the treatment under near-FTS conditions) and reported the formation of both “hard-reducible” and

“unreducible” Co species during the water treatment. In light of Ref. [34], this may be an evidence of formation of the Co-stevensite phase, $\text{Co}_3[\text{Si}_4\text{O}_{10}](\text{OH})_4 \cdot n\text{H}_2\text{O}$, during the treatment.

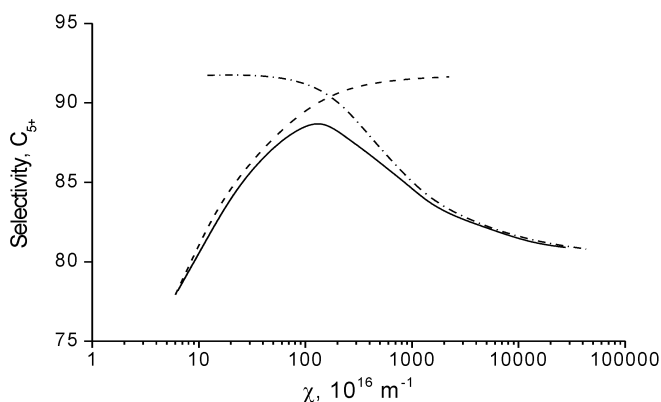


Figure 2. The role of diffusion constrains on the Fischer-Tropsch selectivity towards liquid hydrocarbons, C_{5+} (from Ref. [25]).

On the other hand, Iglesia and co-authors [25] reported the favorable effect of water on the activity and C_{5+} selectivity of Co/ SiO_2 catalysts, and supposed this to be due to higher CO diffusion rates through the intraparticle water-enriched liquid phase stabilized by capillary condensation at high partial pressure of H_2O . However, later these researchers showed that this phenomenon is not responsible for the observed enhancement of the catalyst performance in the presence of water vapors [35]. They also found no effect of water on the magnitude of the kinetic isotope effects ($r_{\text{H}}/r_{\text{D}}$) for CO conversion or C_{5+} formation nor that on the density of available Co atoms and the structure of adsorbed CO. At the same time, they reported cobalt oxidation at $\text{H}_2\text{O}/\text{H}_2$ ratios higher than 0.8 at 200°C . Thus, the nature of the observed positive effect of water is still unclear.

Again, Claeys and van Steen have reported recently [36] that the addition of water during FTS over a supported ruthenium catalyst leads to a significant increase in the rates of products formation and significant changes in the selectivity to the products, in particular in a lower selectivity to methane and improved chain growth.

Some literature data argue in favor of the idea of increasing the water partial pressure, whereas quite a few studies evidence that high water concentration should be avoided, if possible, in the FTS because of probable

oxidation of active metal. Therefore, it is quite reasonable to include the necessity of low water concentration to the list of important features of the Fischer-Tropsch reactor.

1.2.6 General requirements to the Fischer-Tropsch reactors

Now we can summarize the requirements to the FTS reactor as follows:

- Isothermal catalyst bed
- High concentration of the catalytically active substance in the reactor volume
- High gas-liquid interface surface area
- Small effective size of catalyst grains (i.e. small effective diffusion length)
- Low pressure drop
- Low water concentration (e.g. low backmixing in the reactor volume)

These requirements are common for any Fischer-Tropsch process with no concern about the raw material source or product market.

The traditionally used slurry bed reactor designs satisfy the demands 1) and 3)-5), however the catalyst concentration in the reactor volume is rather low due to the conflict between the loading of a particular matter in the slurry and the effective dynamic viscosity of the latter, which promotes coalescence of gas bubbles and a decrease in gas hold-up in the slurry. The experimental studies [37] demonstrate that increasing the loading of particulate matter in slurry to above 38 vol% leads to a dramatic decrease in the gas-liquid interface area down to naught. It is reported [38] that the interphase mass-transfer in the bubble slurry reactors diminishes strongly when the catalyst loading is above 20-25 vol%. Hence, the optimal catalyst loading in the slurry bed reactor is approx. 250-300 kg/m³ of the reactor volume or even less. As a result, the space-time yield of hydrocarbons is low and the dimensions of industrial apparatuses are huge: the SASOL Slurry Phase Distillate (SPD) reactor with productivity of 2,500 barrels (ca. 290 tons) per day is 22 m in height and 5 m in diameter [39], while the proposed Conoco reactor with productivity 10 thousand barrels (1,160 tons) per day is 7.6 m in diameter and 30.5 m in height [40].

In another traditional reactor design – circulating fluidized bed (CFB) reactors [41] – the catalyst concentration in the reactor volume is of the same value. However, the construction of the reactor is much more complicated and the prevalent part of the catalyst is stored in the loading hopper. The fixed catalyst bed is more dense, but the conflict between the

reasonable hydraulic resistance (large catalyst grains needed) and low diffusion constrains (small catalyst grains needed) result in even worse process performance. This contraposition can be resolved using the “egg-shell” catalysts [25, 42, 43] with, however, a low concentration of the active component in respect to the entire particle volume.

2. USE OF SEMI-PERMEABLE MEMBRANES IN FTS

2.1 Hydrogen- and CO- selective semi-permeable membranes for the reagents supply

The semi-permeable membranes selective to hydrogen or carbon monoxide have been extensively studied in respect to synthesis gas production and upgrading. These studies include separation of the synthesis gas flow into the flow of hydrogen-enriched and hydrogen-depleted gas flows (see e.g. patents owned by Texaco Dev. Corp. [4]). Originally, these inventions aimed mainly at the production of hydrogen from syngas. These methods also may improve the overall gas-to-liquid process through efficient diminishing of the $H_2:CO$ ratio to values close to the Fischer-Tropsch stoichiometry, but they still leave the FTS in its traditional conditions with $H_2:CO$ ratio of above 2. More significant decrease in the inlet $H_2:CO$ ratio is desirable, since it will definitely improve the selectivity of the process since the rate of the elementary step of chain termination is more sensitive to the $H_2:CO$ ratio than the step of chain propagation. However, the exhaust of hydrogen into the reaction mixture at a high CO conversion makes this way unreasonable for improving the selectivity over cobalt-containing catalysts. Application of hydrogen-selective distributors is one of the possible solutions for the problem.

Despite the idea of distributing one of the reactants along the catalyst bed has been many times shown effective for numerous processes (e.g. partial oxidation), the first experimental works on the separate reactants supply via membrane for the FTS have only recently appear. Vanhove and co-authors applied a γ -alumina/ α -alumina membrane with pores of *ca.* 5 nm in size for distributing H_2 flow along the fixed bed reactor [44]. As a result, a significant increase in the selectivity to middle distillates and waxes (C_{10+}) has been observed with the reactants fed separately at the ratio $H_2:CO \approx 3:1$ compared to that in the traditional Fischer-Tropsch process with $H_2:CO$ flow premixed at the 2:1 ratio. At the same inlet ratio $H_2:CO = 2$, the selectivity to C_{10+} fraction reaches 42% (with the use of membrane) compared to 36%

(with mixed reactants). On the other hand, the enhanced selectivity is achieved at the expense of catalyst activity, which is reported 50% lower than that for the pre-mixed feed. Therefore, the compromise between selectivity improvement and activity loss needs careful examination.

The application of the hydrogen-selective distributors opens even more prospects for regulation of the process selectivity in the case of membranes which exhibit specific catalytic activity in hydrocarbons conversion. In [45], the same team of authors report that introduction of ZSM-5 zeolite into the membrane composition gave rise to the production of intermediate weight hydrocarbons C_6 - C_{10} at the expense of C_{11+} fraction. At the same time, the gain in the process efficiency reaches the level observed with the traditional reactor design. The authors attribute these effects to the secondary reactions (like hydrogenolysis, cracking etc.) of heavy hydrocarbons over acid sites of the zeolite component of the membrane.

Even though the reported data are as yet incomplete and quite a few questions need clarification, the feasibility and effectiveness of separate feeding the syngas components is obvious.

Notice that the separate feed technique also is a new tool for investigation of the Fischer-Tropsch mechanism and kinetics. It has allowed, for example, the kinetic parameters for the elementary steps of chain propagation and chain termination, including the kinetic orders with respect to H_2 and CO to be estimated [44].

2.2 Water-selective semi-permeable membranes for water removal

Among the above formulated important demands for the FTS is the one of minimization of water concentration in the catalyst bed. The most natural way to do that is to mount a hydrophilic semi-permeable membrane in the reactor. The attempt of the use of membranes for *in-situ* removal of the Fischer-Tropsch water has been successful [46, 47]. Zeolites (ZSM-5, mordenite) on stainless steel have been shown effective for selective separation of water from the simulated FTS reactor for both gas phase and gas-liquid two-phase system in the retentate side of membrane. Hence, water-selective membranes can be used for both fluidized and slurry bed Fischer-Tropsch reactors at 1.7 – 2.2 MPa and temperatures from 150°C to 350°C. The highest separation factors and separation selectivity are observed at 240°C. Notice that water removal also is believed to improve the overall efficiency of the Fischer-Tropsch synthesis due to decreasing carbon monoxide consumption by water-gas-shift reaction [47]. Unfortunately, we

failed to find any further publications dealing with experimental data on the effect of water removal on the productivity and selectivity of the Fischer-Tropsch process.

3. THE USE OF NON-SELECTIVE POROUS MEMBRANES IN FTS

3.1 Concept of the plug-through contactor membranes using the permeable composite monolith (PCM)

The origin of the PCM concept lies in high loading of the active component in the catalyst grain combined with the low void volume in the reactor volume. This demand being formulated above in Section 1.2 comes into an obvious conflict within the traditionally proposed slurry reactor designs, since an increase in the particulate matter (catalyst) loading into a slurry leads to high values of viscosity and provides a dramatic decrease in the gas-liquid interface area [37, 38].

A high catalyst concentration and an intense mass-transfer can be achieved together by directing the gas flow through the porous catalytically active membrane. The benefit of enhancing the gas-liquid interface area with the use of porous membranes is demonstrated for reduction of nitrates from their aqueous solution [10] and for hydrogenation of liquid hydrocarbons [11]. In both processes, one of the reactants is supplied to the reaction zone inside the catalytic membrane via liquid phase, while another (hydrogen) is supplied by gas and the permeation of the gas flow through the membrane is not required. Despite that, it looks tempting to apply the similar approach to the three-phase process that needs gas permeation through the membrane.

Figure 3 shows a schematic of the Fischer-Tropsch process using such a permeable membrane with gas flow permeating via a set of the partially wetted transport pores. In this case, the high area of the gas-liquid interface can be created if the concentration of such pores is high enough and their effective diameter is quite small. Assuming that the mass-transfer coefficient on the gas-liquid boundary, k_L , is about 10^{-4} m/s (estimated by the Moo-Young equation [48]), the reaction rate not higher than 6 moles(CO)/(m³ s) (i.e. 300 kg/(m³ hr) of hydrocarbons produced) and the solubility of CO in hydrocarbons about 52 moles(CO)/(m³ MPa) (measured for octacosane at 250°C [49]), one can estimate that the specific area of the gas-liquid interface should be above 20 cm²/cm³ to relieve the mass-transfer

restrictions at the interface for the typical Fischer-Tropsch conditions (2 MPa, 33% of CO).

The effective diffusion length for the porous membrane under discussion can be considered as the mean distance between the neighboring transport pores. It is concluded [25] that for a typical Fischer-Tropsch catalyst, internal diffusion constrains do not worsen the process selectivity at the catalyst grain size less than 30 μm . With assumption of the close packing of pores, this corresponds to the concentration of the transport pores $n_p > 10^9 \text{ m}^{-2}$.

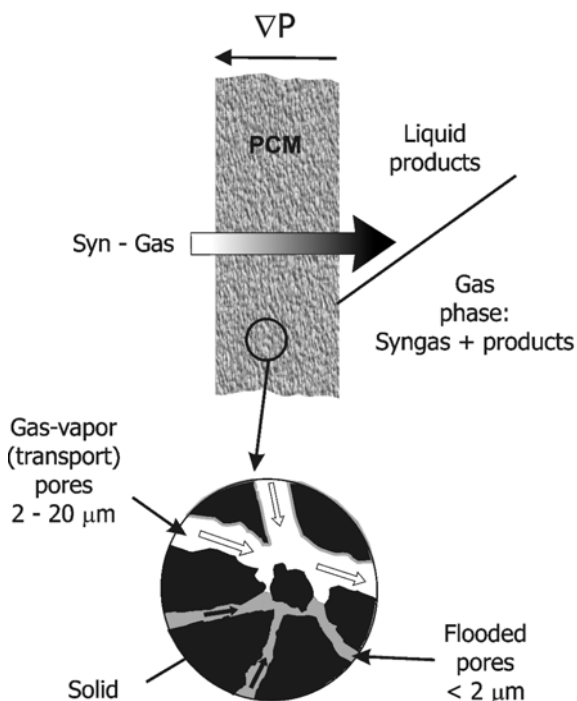


Figure 3. The principal scheme of the Fischer-Tropsch synthesis using the permeable catalytic membrane.

At the same time, the effective radius of the transport pores should be large enough to provide low pressure drop. Let us estimate the minimal permeability (the Darcy's coefficient) of a PCM grain by assuming that the gas feeding rate in the industrial Fischer-Tropsch synthesis can hardly be

higher than $1 \text{ m}^3/(\text{m}^3 \text{ s})$ and the minimal reasonable catalyst bed length is about 0.1 m. Then, the reasonable pressure drop, $\Delta P < 0.5 \text{ MPa}$, can be achieved if the permeability of the catalyst bed is above $2 \cdot 10^{-14} \text{ m}^2$ (20 mDarcy).

Therefore, the challenge is to prepare a catalytic membrane, which satisfies all the above criteria. The membrane should contain a catalytically active substance at a high concentration of (at least $0,7 \text{ g/cm}^3$) and possess a high heat conductivity to maintain the isothermal regime of the catalyst operation.

Lapidus and co-authors were first in 1994 who tried to prepare FTS catalytic membranes by impregnating carbon membranes with cobalt salt solutions [50]. This approach allowed active and stable under the FTS conditions membranes to be prepared, the optimal cobalt loading being about 2-4% wt. These Co/C membranes exhibited a very high selectivity towards methane and CO_2 . The authors supposed that the Co/C membranes may be prospective for methanation of CO and did not continue the research on the catalytic membranes for the FTS.

Another approach for preparation of the catalytic membranes by combining modern techniques for the preparation of composite materials has been tried recently in the Boreskov Institute of Catalysis [51]. This catalytic membrane are called “permeable composite monolith” (PCM) catalyst.

3.2 Preparation of PCM. The possibility to control the porous structure parameters at the preparation stage

3.2.1 Preparation procedure

The PCM is a three-component mixture of a catalytically active substance, pore-producing agent and reinforcing agent with a high heat conductivity, which is sintered and reduced in flowing hydrogen after mixing [52]. In general, any metal is an appropriate reinforcing agent provided that it is stable in the reaction mixture. Obviously, copper can be used for the purpose, since it is rather inert with respect to CO, hydrogen and water vapors and also it has a reasonable Tammann temperature (of about 410°C). Cobalt-containing catalyst should be stable to the thermal treatments up to Tammann temperature of the reinforcing metal. For example, the Co-Al-containing catalysts [53] can be used. Properties of PCM particles can be considerably varied by varying the component proportions, the nature of pore-producing agent and the preparation conditions. Two geometries of membranes were studied – flat plates with

thickness of *ca.* 6 mm and 14 mm in diameter (further denoted as “Plate”) and hollow cylinders with height of *ca.* 8 mm, diameter of *ca.* 17 mm and diameter of coaxial hole of *ca.* 7 mm (further denoted as “Cylinder”). In the latter case, the gas flow was directed radially from inside outwards or *vice versa*.

3.2.2 Characterization of PCM samples

Experimental dependencies of the gas flow through the dry PCM grain on the pressure drop follow the Darcy’s law for ideal gas:

$$Q_{vol} = K \cdot \frac{S}{l \cdot \eta} \cdot \Delta P \quad (3)$$

Here Q_{vol} is the gas flow rate (m^3/s), K is the PCM permeability (m^2), η is the dynamic viscosity of gas ($1.23 \cdot 10^{-5}$ Pa s), l is the grain height (m), ΔP is the pressure drop (Pa), S is the PCM grain cross-section area (m^2).

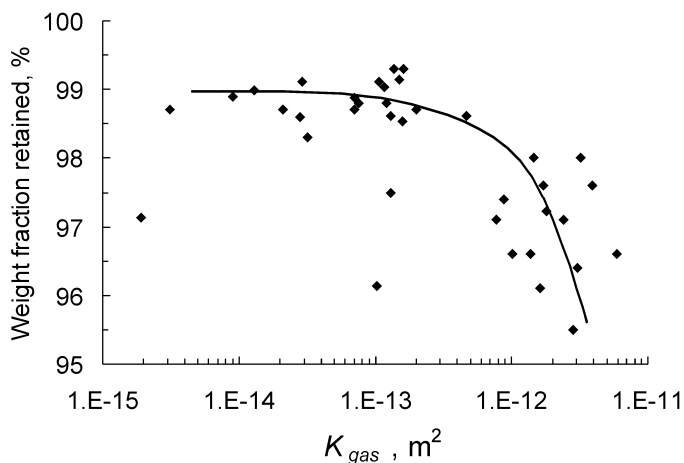


Figure 4. The correlation of the permeability, K_{gas} , and the mechanical strength for PCM samples in a wide range of the PCM composition and preparation conditions. The mechanical strength is expressed as the weight fraction of sample retained after the intense shaking (see the text).

Permeability of the prepared PCM samples can be varied over wide range by varying the composition and preparation conditions. However, a

lower mechanical strength is characteristic of high-permeable samples. Fig. 4 shows correlation between these two parameters. It is clear (see the plot) that the optimal permeability, K_{gas} , ranges between 10^{-14} and $5 \cdot 10^{-13} \text{ m}^2$ (10-500 mDarcy). Table 2 summarizes the experimental data on the unreduced catalyst loading, m , permeability, K_{gas} , and thermal conductivity, λ , of some PCM samples.

Table 2. The experimental data on the PCM samples under study.

Sample	Plate A	Plate B	Plate C	Plate D	Cylinder A	Cylinder B
$m, \text{g/cm}^3$	0.92	0.99	0.9	1.0	0.99	0.9
K_{gas}, mDarcy	120	106	71	75	-	-
$\lambda, \text{W/(m s)}$	4	4	3.5	> 5	-	-

Fig. 5 illustrates the effect of the pressure drop on the volume gas flow rate in the case, when the membrane is immersed into the bath of liquid n -tetradecane (i.e. at the “flooded” mode of operation, with liquid phase contacting the outlet boundary of membrane). Evidently, the observed pressure drop is a superposition of the capillary pressure and the pore resistance to the viscous gas flow:

$$\Delta P = \frac{l \cdot \eta}{K S} \cdot Q_{vol} + P_{cap} \quad (4)$$

Therefore, it is not proportional to the gas flow.

At a low gas flow rate, only the widest transport pores are open for the gas flow, i.e. the ones which satisfy the necessary condition $P_{cap} < \Delta P$. The observed hysteresis loop indicates the complicated geometry of the pores: the critical value of the pressure drop needed to open a transport pore corresponds to the most narrow spot in the pore, while on decreasing the gas flow rate the same pore can be only closed at a somewhat lower pressure drop equal to the capillary pressure at the pore neck. The experimental dependence $Q_{vol}(\Delta P)$ allows estimating the density of the transport pore distribution by diameter $n(D)$. The estimated pore density distribution, $\partial n/\partial D$, is exemplified in Fig. 6 (curve 4).

Curves 1, 2 and 3 in Fig. 6 correspond to the calculated transport pore size distribution of the gas flow the at the value of $\Delta P = 15 \text{ kPa}$.

The measured PCM permeability K_{g-l} , estimated effective (weighted average) transport pores size, $R_{tp\ cap}$, their concentration, n_{tp} , volume fraction, ε_{tr} , specific surface area, a_{tp} , as well as the transport pore size measured by optical microscopy, $R_{tp\ opt}$, are summarized in Table 3.

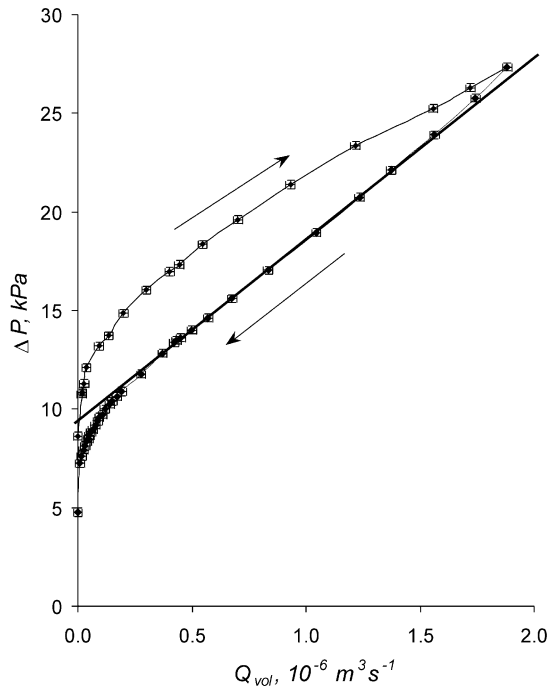


Figure 5. Experimental dependence of the pressure drop on the volume gas flow “flooded” operation mode. Sample Plate-A.

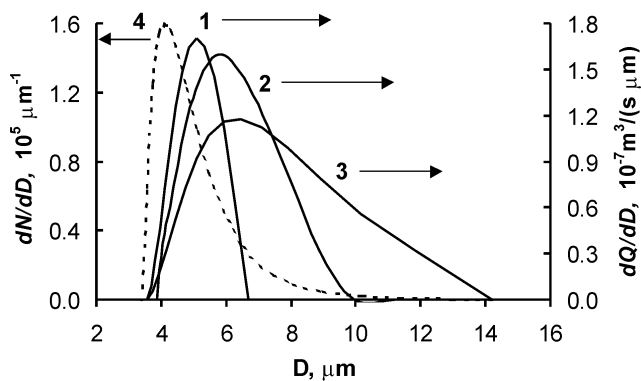


Figure 6. The estimated density functions of the gas flow distribution with respect to pore diameter (right axis): 1 – Plate-B; 2 – Plate-C; 3 – Plate-D; and pore diameter distribution (left axis) 4 – Plate-D.

The permeability, K_{g-l} , corresponds to the slope of the $Q_{vol}(\Delta P)$ plot at $\Delta P > 15$ kPa (see Fig. 5). The concentration of the pores is calculated as the total amount of the pores related to the area of the PCM grain cross-section, S .

The data of Tables 2 and 3 indicate that the PCM membranes satisfy all the requirements postulated in the Section 1 of this article. Thus, it is quite natural to expect their high performance in the FTS. Moreover, it is quite clear, that the pore structure of the PCM membrane can be controlled at the preparation stage in a rather wide range of parameters. The performance of the PCM membrane reactor in the FTS is discussed below.

Table 3. The estimated transport pore structure parameters.

Sample	Plate A	Plate B	Plate C	Plate D	Cylinder A	Cylinder B
K_{g-l} , mDarcy	66	30	60	53	63	140
$R_{tp, bp}$, μm	3.6	2.5	3.6	3.9	4.2	5.5
$R_{tp, opt}$, μm	-	2.5	-	5.0	-	-
n_{tp} , 10^9 m^{-2}	1.0	2.7	1.2	2.0	0.77	0.55
ε_{tp} , %	3.6	4.5	3.6	4.2	3.2	3.5
a_{tp} , cm^2/cm^3	210	370	230	320	174	140
L_{tp} , μm	38	23	35	27	38	46

3.3 Fischer-Tropsch synthesis in a PCM membrane reactor. Effect of the pore structure of the PCM on its catalytic performance

3.3.1 Dry mode of operation

Figure 7 shows comparative dependencies of conversion on the contact time for the same catalytically active substance in the slurry bed reactor (grain diameter less than $140 \mu\text{m}$) and in the PCM membrane reactor at 0.1 MPa, 483 K, $\text{H}_2:\text{CO} = 2$. Here, the contact time is the ratio of the gas flow rate to the volume of initial catalyst powder with the bulk density of *ca.* $1 \text{ g}/\text{cm}^3$. The fed syngas flow is saturated with n-tetradecane vapor at the reaction temperature ($P_{\text{sat}} = 33 \text{ kPa}$) to make the comparison possible. Since the experiment was performed at low pressure, the conversion of CO was moderate and no liquid phase was added to the reactor volume before starting the test, the pore volume can be considered as almost dry. At this “dry” mode of the operation (dataset 1), the activity of the PCM samples is close to that observed in a slurry reactor over the catalyst powder, i.e. under the conditions, when neither internal nor external mass-transfer restrictions can be considered as significant. This allows to make the important

conclusion that almost all the active component particles are accessible to the gas (the isolated catalyst particles aren't present in the membrane). At that this is the evidence that preparation procedure didn't deactivate catalytically active substance.

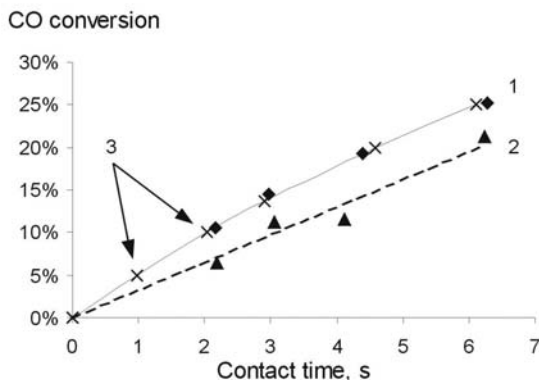


Figure 7. Experimental CO conversion versus contact time for the same Co-Al catalyst in PCM Plate B: 1 – dry mode; 2 – flooded mode in comparison to that in stirred slurry bed (dataset 3).

3.3.2 Flooded mode of operation, the effect of the pore structure and membrane geometry on the magnitude of the mass-transfer constrains

It is seen in Fig. 7 that the effectiveness factor decreases when the liquid phase is added to the system (dataset 2). Table 4 presents some experimental data on the activity and selectivity of three plate samples, pore structures of which are depicted in Fig. 6. These data evidence that the activity of flooded membranes is considerably lower at a wide pore size distribution. Again, lower Anderson-Schulz-Flory selectivity parameters, α , for saturated fraction of hydrocarbons are characteristic of these samples. This is the expected result at a non-homogeneous pore structure because the hydraulic resistance of the membrane is mainly determined in this case by the resistance of widest pores; as a result, the permeability is much higher and the pressure drop lower. When so, a significant part of narrow transport pores are flooded because the pressure drop on the membrane is lower than the capillary pressure in these channels. For these reasons, the catalyst is less effectively utilized while the diffusion constrains are more severe. The diffusion constrains reveal themselves also as decreasing α and C_3 \neq ratio

(please note, that the residence time of olefins is much higher in the slurry bed reactor than in PCM plates due to a larger slurry bed volume and, hence, the C_3 =/- ratio for slurry bed is not to be compared here).

The data on cylinder-shaped membranes look strange: The tests reveal striking difference between two series with the same membrane but counterflow gas. Even if so, the nature of some trends is well understood. For example, irrespective of the gas flow direction, the performance of Cylinder B is worse comparing to Cylinder A. Apparently, this is due to a smaller proportion of transport pores in Cylinder B: the estimated distance between two neighboring transport pores is about 46 μm for this membrane, and significant diffusion limitations are expected for this sample. On the other hand, parameters of the pore structure of Cylinder A are close to those of Plate C and this agrees with the similarity in their performance.

Table 4. Comparative performance of “flooded” PCM membranes at 0.1 MPa, 483 K, H_2 :CO = 2, ca. 10% CO conversion and the slurry bed at 21% CO conversion [51, 54].

<i>Plate membranes</i>				
Sample	Slurry bed	Plate B	Plate C	Plate D
$W, \text{mg}_{\text{HC}} \text{g}_{\text{cat}}^{-1} \text{hr}^{-1}$	18.8	16.5	12.3	10.5
$S_{\text{CH}_4}, \text{wt}\%$	13.4	11.9	9.1	8.0
ASF α , saturated	0.84	0.80	0.80	0.72
ASF α , olefins	0.81	0.60	0.66	0.74
C_3 =/- ratio	2.0	3.3	3.3	1.9
<i>Cylinder membranes</i>				
Sample	Cylinder A	Cylinder A	Cylinder B	Cylinder B
Direction of flow	inwards	outwards	inwards	outwards
$W, \text{mg}_{\text{HC}} \text{g}_{\text{cat}}^{-1} \text{hr}^{-1}$	10.2	14.4	8.0	8.4
$S_{\text{CH}_4}, \text{wt}\%$	17	13	21	19
ASF α , saturated	0.84	0.66	0.82	0.71
ASF α , olefins	0.74	0.46	0.67	0.48
C_3 =/- ratio	3.7	1.5	3.2	0.41

The effect of the gas flow direction on the membrane performance is not so plain. One can hardly imagine any kinetic process, whatever complicated is it, being sensitive to the direction of the gas flow. Discussion of this phenomenon will be easier using the effect of gas direction on olefins selectivity as an example.

3.3.3 The impact of gas membrane geometry on propylene-to-propane ratio

Dependence of the propene-to-propane ratio on CO conversion is plotted for Cylinder A in Fig. 8. This monotonous dependence agrees well with a simple model including three elementary steps: (1) formation of olefin; (2)

phase transition of olefin from liquid to gas phase (and its removal from the catalyst bed); (3) hydrogenation of olefin over the catalyst giving paraffin. If the primary products are olefins and paraffins in the ratio (paraffins:olefins) = Ratio⁰, phase transitions are close to equilibrium and hydrogenation of olefins is the first order reaction with respect to olefins, then the correlation between (paraffins:olefins) ratios can be written as follows:

$$\text{Ratio} = \text{Ratio}^0 (1 + k RT/(V_g \phi_{\text{liq}})), \quad (5)$$

where k , $\text{s}^{-1} \text{g}_{\text{cat}}^{-1}$ is the constant of first order effective reaction of olefins hydrogenation, V_g , $\text{m}^3 \text{g}_{\text{cat}}^{-1}$ is the specific gas flow rate, ϕ_{liq} is the olefin fugacity coefficient. It is important to note here, that the effective kinetic constant is sensitive to the magnitude of the intraparticle diffusion constrains. The more severe limitations, the higher is effective reaction rate constant. Fig. 9 illustrates that all of four datasets for cylindrical membranes fit well the above simplified model.

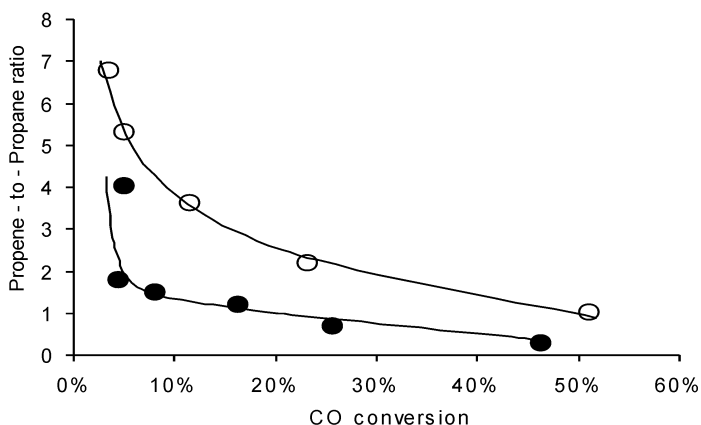


Figure 8. Experimental data on the propene-to propane ratio versus CO conversion. Black points are for outward gas directed from inside, white points for gas directed from outside.

As for any intermediate product of two consequent reactions, propylene concentration along the catalyst bed first increases, reaches maximum and then decreases. At the same time, the linear gas velocity increases as the gas flow nears the cylinder center, or *vice versa* decreases when it moves away from the center. Thus, the behavior of the linear gas velocity along the

catalyst bed is sensitive to gas flow direction. Similarly, the profile of the pressure gradient is sensitive to the gas flow direction, since it is proportional to the linear gas velocity. The fraction of dry transport pores increases with the pressure gradient, and, thus, diffusion constrains weaken. Therefore diffusion constrains weaken along the catalyst bed, if gas is directed from outside of the membrane cylinder inwards. Limitations become more severe if the gas permeates from inside of the membrane outwards.

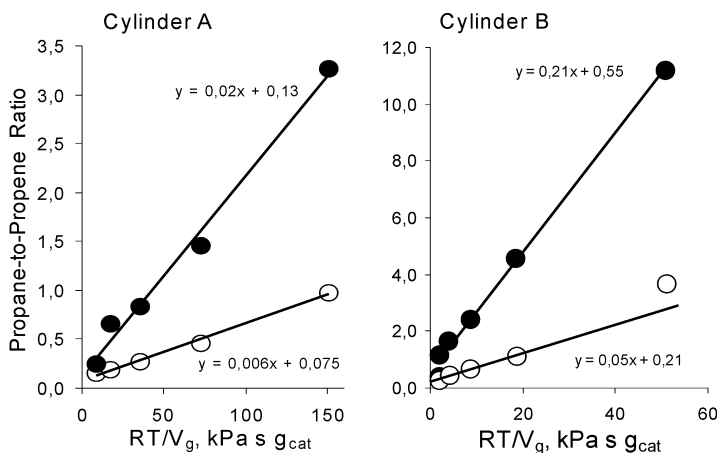


Figure 9. The linear anamorphism of the impact of the gas flow rate to the process selectivity to olefins for cylindrical membranes A (left plot) and B (right plot). Gas flows from inside (black points) and from outside (white points).

Hence, the maximal concentration of propylene is achieved in membrane fragment with the highest diffusion constrains and, therefore, the effective rate of propylene hydrogenation is the highest when reactants permeate through the cylindrical membrane from its inner void volume outwards, and *vice versa*. The observed phenomenon of the FTS sensitivity to the membrane geometry may be accounted for by sensitivity of the liquid phase distribution in the membrane pore structure to the gas flow direction. It is not easy to analyze the effect of membrane geometry on the process productivity and selectivity to methane and heavy hydrocarbons. Supposedly, the impact of membrane geometry is accounted for by a change in the profile of the diffusion constrains magnitude due to variations in the wetting profile along the membrane.

To conclude the discussion on properties of non-selective porous catalytic membranes, it is necessary to emphasize that PCM membrane

reactors satisfy all the requirements for the Fischer-Tropsch synthesis reactors formulated above. The highest efficiency of PCM usage is no more than 70%, but the catalyst loading is many times higher in PCM than in traditional reactors (approaching to 1 g/cm^3). Therefore, the unit volume productivity (space-time yield) of this reactors is significantly higher in comparison to bubble slurry bed of fluidized bed reactors. The results of the first catalytic tests at 2.0 MPa demonstrate that the space-time yield as high as $200 \text{ kg}_{\text{HC}}/\text{m}^3$ is allowed with PCM [55].

4. CONCLUSIONS

The research activities in application of membrane technologies for catalysis became very intense in the last decade but only few publications dealt with membranes in the Fischer-Tropsch synthesis. Meanwhile the results of these studies inspire that membranes could be helpful in improving the productivity of the process.

Hydrogen-selective semi-permeable distributors can give a chance to improve significantly the yield of middle distillates and heavy paraffins due to constantly low $\text{H}_2:\text{CO}$ ratio along the catalyst bed [44, 45].

Water-selective semi-permeable extractors can be efficiently used for highly selective in-situ removal of water from the Fischer-Tropsch reactor volume for both fluidized bed and slurry bed reactors to enhance productivity of the Fischer-Tropsch process and prevent deactivation of the catalyst due to active metal oxidation [46, 47].

On the other hand, the use of plug-through catalytic contactors gives rise to new design of the Fischer-Tropsch reactor to provide high space-time yield and no separation problems. [51, 52, 54, 55].

Obviously, the list of advantages provided by the use of membranes in the Fischer-Tropsch synthesis is not complete as yet. Therefore, application of membranes for the process should not be overlooked in future research and industrial development.

5. ACKNOWLEDGEMENTS

Author is very grateful to Profs. V.N. Parmon, T.M. Yurieva and V.A. Kirillov for fruitful discussions, Dr. I.Sh. Itenberg, Mr. A.G. Sipatrov, Mrs. G.K.Chermashentseva, and Mrs. I.A. Mikhailova for their collaboration in

the experimental and theoretical work. Communications with Prof. D. Vanhove and Mr. L. Guillou are highly appreciated.

6. REFERENCES

- [1] J.-A. Dalmon, in: G. Ertl, H. Knoezinger, J. Weitkamp (Eds.) *Handbook of Heterogeneous Catalysis*, VCH, 1997, Chapter 9.3, p.1387.
- [2] A.G. Dixon, *Catalysis* 14 (1999) 40.
- [3] A. Julbe, D. Farrusseng, D.Cot, C. Guizard, *Catal. Today*, 67 (2001) 139.
- [4] P.S. Wallace, K. Johnson, PCT Int. Appl. WO 0037356 (filed 29.06.2000) to Texaco Dev. Corp.
- [5] S. Umemiya, N. Sato, H. Ando, E. Kikuchi, *Ind. Eng. Chem. Res.*, 30 (1991) 585.
- [6] F. Lipnizki, R.W. Field, P.K. Ten, *J. Membr. Sci.* 153 (1999) 183.
- [7] K. Tanaka, R. Yoshikawa. C. Ying, H. Kita, K. Okamoto, *Catal. Today*, 67 (2001) 121 and references therein.
- [8] E. Piera, C. Tellez, J. Coronas, M. Menendez, J. Santamaria, *Catal. Today*, 67 (2001) 127.
- [9] A.A. Lapkin, S.R. Tennison, W.J. Thomas. 5th European Congress on Catalysis EUROPACAT-V (Limerick, 2-7 September 2001). Presentation 9-O-10.
- [10] K. Daub, V.K. Wunder, R. Dittmeyer, *Catal. Today*, 67 (2001) 257.
- [11] N.A. Kuzin, A.V. Kulikov, A.B. Shigarov, V.A. Kirillov, *Catal. Today* 79-80 (2003) 105
- [12] M.E. Dry, in: "Catalysis – Science and Technology" (J.R. Anderson and M. Boudart eds.) New York: Springer Verlag, 1981. Vol. 1, p. 139.
- [13] T.J. Donnelly, C.N. Satterfield, *Appl. Catal. A.: Gen.*, 52 (1989) 93.
- [14] R.A. Dictor, A.T. Bell, *J. Catal.* 97 (1986) 121.
- [15] A.A.Khassin, T.M.Yurieva, V.N.Parmon. *Doklady Phys.Chem.*, 367(1-3) (1999) 213.
- [16] A.A.Khassin, V.N.Parmon, *Doklady Phys.Chem.*, 368(4-6) (1999) 283.
- [17] M.A.Vannice, *J. Catal.*, 37 (1975) 449.
- [18] B. Ernst, S. Libs, P. Chaumette, A. Kiennemann, *Appl.Cat. A: Gen.*, 186 (1999) 145-168
- [19] V.A. Kirillov, V.M. Khanayev, V.D. Mescheryakov, S.I. Fadeev, R.G. Lukyanova, *Stud. Surf. Sci. and Catal.* 119 (1998) 149.
- [20] Perry's Chemical Engineers' Handbook 6th ed. (R.H. Perry, D.W. Green and J.O. Maloney eds.) New York: McGraw-Hill Book Company. 1984. Sec.3.
- [21] W.H. Zimmerman, J.A. Rossin, D.B. Bukur, *Ind. Eng. Chem.* 28 (1989) 406.
- [22] M.F.M. Post, A.C. van't Hoog, J.K. Minderhoud, S.T. Sie, *AIChE J.* 35 (1989) 1107.
- [23] E. Iglesia, S.L. Soled, R.A. Fiato, *J. Catal.* 137 (1992) 212.
- [24] E. Iglesia, S.L. Soled, J.E. Baumgartner, S.C. Reyes, *J. Catal.* 128 (1995) 108.
- [25] E. Iglesia, *Appl. Catal. A.: Gen.* 161 (1997) 59.
- [26] D.J. Duvenhage, R.L. Espinoza, N.J. Coville, *Stud. Surf. Sci. Catal.* 88 (1994) 351.
- [27] R.L. Espinoza, A.P. Steinberg, B. Jager, A.C. Vosloo, *Appl. Catal., A:Gen.* 186 (1999) 13.
- [28] A.M. Hilmen, D. Schanke, K.F. Hassen, A. Holmen, *Appl. Catal. A:Gen.* 186 (1999) 169.
- [29] P.J. van Berge, J. van de Loosdrecht, S. Barradas, A.M. van der Kraan, *Catal. Today.* 58 (2000) 321.
- [30] J. Li, G. Jacobs, X. Zhan, Y. Zhang, T. Das, B.H. Davis, *Appl. Catal. A.:Gen.*, 228 (2002) 203.

- [31] A.M. Hilmen, O.A. Lindvag, E. Bergene, D. Schanke, S. Eri, A. Holmen, Proc. of the 6th Natural Gas Conversion Symposium, Girdwood, Alaska, 17-22 June 2001, CD edition. Elsevier, 2001. Article 48.
- [32] J. Li, G. Jacobs, T. Das, B.H. Davis, Appl. Catal. A: Gen., 233 (2002) 255.
- [33] A. Kogelbauer, J.C. Weber, J.G. Goodwin Jr., Catal Lett 34 (1995) 259.
- [34] A.A. Khassin, T.M. Yurieva, G.N. Kustova, L.M. Plyasova, T.A. Kriger, I.Sh.Itenberg, M.P.Demeshkina, T.Larina, V.F.Anufrienko, V.N.Parmon. Mater. Res. Innov., 4(4) (2001) 251.
- [35] S. Krishnamoorthy, M. Tu, M.P. Ojeda, D. Pinna, E. Iglesia, J. Catal., 211 (2002) 422.
- [36] M. Claeys; E. van Steen, Catal. Today, 71(3-4) (2002) 419.
- [37] R. Krishna, J.W.A. de Swart, J. Ellenberger, G.B. Martina, C. Maretto, AIChE J. 43 (1997) 311.
- [38] A.A.C.M. Beenackers, W.P.M. van Swaaij, Chem. Eng. Sci. 48 (1993) 3109.
- [39] B. Jager, Proc. 1997 AIChE National Spring Meeting, Houston TX, 10-13 March 1997, Paper 27c.
- [40] J. Shen, E. Schmetz, 5th European Congress on Catalysis EUROPACAT-V, Limerick, 2-7 September 2001, Presentation 11-O-02.
- [41] B. Jager, M.E. Dry, T. Shingles, A.P. Steynberg. Catal. Lett. 7 (1990) 293.
- [42] E. Peluso, C. Galarraga, H. de Lasa, Chem. Eng. Sci. 56 (2001) 1239.
- [43] C. Galarraga, E. Peluso, H. de Lasa, Chem. Eng. 82 (2001) 13.
- [44] D. Vanhove, S. Leonard, Recent Progres en Genie des Procedes, 89 (2003) 297.
- [45] S. Leonard, S. Miachon, D. Vanhove, Recent Progres en Genie des Procedes, 89 (2003) 226.
- [46] R.L. Espinoza, E. Du Toit, J.M. Santamaria, M.A. Menendez, J. Coronas, S. Irusta, Stud. Surf. Sci. Catal. 130A (2000) 389.
- [47] R.L. Espinoza, J.M. Santamaria, M.A. Menendez, J. Coronas, S. Irusta, PCT Int. Appl. WO 9964380 A1, filed 16.12.1999 to Sasol Technology Ltd.
- [48] P.A.Ramachandran and R.V.Chaudhari, Three-phase catalytic reactors, Gordon and Breach Science Publishers, New York, 1983.
- [49] C.N. Satterfield, H.G. Stenger, Ind. Eng. Chem. Process Des. Dev., 24, 407 (1985)
- [50] A.L. Lapidus, A.Yu. Krylova, A.N. Strupov, V.M. Linkov, R.D. Sanderson, Kh.T.T. (Chemistry of Solid Fuels) Nos. 4-5, 1994, 69-72 (in Russian).
- [51] A.G. Sipatrov, A.A. Khassin, T.M. Yurieva, V.A. Kirillov, G.K. Chermashentseva, V.N. Parmon, Chem. Sustainable Dev., 11(1) (2003) 285.
- [52] A.A. Khassin, T.M. Yurieva, A.G. Sipatrov, I.Sh. Itenberg, V.N. Parmon, G.K. Chermashentseva. Patent Application RU 2003103899, filed 10.02.2003 to Boreskov Institute of Catalysis.
- [53] A.A.Khassin, T.M.Yurieva, G.N.Kustova, I.Sh.Itenberg, M.P. Demeshkina, T.A. Kriger, L.M.Plyasova, G.K. Chermashentseva, V.N.Parmon. J. Mol. Catal. A: Chem., 168 (2001) 193.
- [54] A.A. Khassin, A.G. Sipatrov, G.K. Chermashetseva, T.M. Yurieva, V.N. Parmon Abstracts of the Russian-American Seminar AUAC-2003, Moscow, Russia, May 28-30, 2003, p. 64. (OP-14)
- [55] A.A. Khassin, T.M. Yurieva, A.G. Sipatrov, V.A. Kirillov, G.K. Chermashentseva, V.N. Parmon. Catal. Today, 79-80, (2003) 465.

Chapter 13

SOURCES OF METHANE FOR SUSTAINABLE DEVELOPMENT

Prospects and Challenges

V.N. Parmon

Borshov Institute of Catalysis, Novosibirsk 630090, Russia
fax: +7 (383 2) 34-32-96, e-mail: Parmon@catalysis.nsk.su

Abstract: Under consideration are most valuable or remarkable sources of methane which can be used for both chemical industry and energy production in future.

Key words: Methane, methane hydrates, oil associated gas

1. INTRODUCTION

Methane, CH₄, is the lightest, omnipresent and most abundant organic compound both on our planet and in Universe. For chemists it is known also as the most stable and inert organic compound. This creates a lot of difficulties in the methane conversion into more valuable substances which restrict sufficiently its use in chemical industry. As the result, the most large scale use of methane is now, indeed, energetics. The main role of raw material for chemical and petrochemical industries is now played by fossil oil. However, the resources of fossil oil are known to be much smaller than that of methane and natural gas as a whole (see, e.g., [1,2]). Moreover, due to huge current consumption of motor fuels and many organic materials by our civilization, the sources of cheap oil are steadily exhausting. For this reason the oil-based chemical industry will unavoidably be shifted by a methane-based chemical industry possibly in the already neighboring future [3]. The arrival to the new resource-based steady state of the civilization is usually estimated as 20–40 years. How long will continue this new steady state? Indeed, the answer depends on both the existing available recourses of

methane as well as on its prospective consumption by our rapidly growing civilization.

In this paper we consider the most remarkable sources of methane to form a definite view on its availability in the future.

The known sources of methane can be classified as natural or technogeneous. The main sources of natural fossil methane are evidently natural gas, oil accompanying (or oil associated) gases, coal gas, and gas hydrates. These sources are evidently exhaustible and unrenovable, if only do not consider possibility of the practically inexhaustible supply of methane at the Earth' gasification (see below). Renewable sources of methane are natural and on-purpose produced biogas as well as methane available as either a product of gasification of some substrates or an industrial byproduct.

2. NATURAL SOURCES OF METHANE

2.1 Natural Gas

Natural gas (NG) is now the most exploited methane-containing fossil. Typically, fossil natural gas has a complicated composition, but however methane is everywhere its main component. Typically, in addition to methane, NG contains also heavier alkanes like C_2H_6 , C_3H_8 , etc., as well as CO_2 , H_2S and He. Geologists distinguish dry, fatty, and sour NG. Dry natural gas is comprised mostly of pure methane. Fatty natural gas contains a large admixture of heavier hydrocarbons. Sour natural gas contains large amount of hydrogen sulfide (up to vol. 40 %) and/or carbon dioxide. The most valuable component of NG is helium. Typically, its content is very low but, however, in some cases it reaches ca. 1 vol. %. In such cases its cost can exceed the cost of hydrocarbon components of NG.

The known deposits of NG are enormous. Only the NG deposits of the "proof" quality (it means the possibility to exploit industrially such deposits) contain ca. $(100-120) \times 10^3$ bln. m^3 of methane which is equal to ca. 100 bln. metric tons. Since the annual world consumption of NG can be estimated now ca. 3000 bln. m^3 , it means that the "proof" quality deposits of NG are able to satisfy the current needs of the civilization for 30-40 years ahead. The deposits of NG are distributed around the world nonuniformly. The location of main deposits is shown in Fig. 1. Note, that ca. 32 % of NG locates in Russia (mainly in North Siberia), ca. 15 % in Iran. Large deposits locate also in Qatar, Alaska, Malaysia, Australia, Algeria, Venezuela, etc.

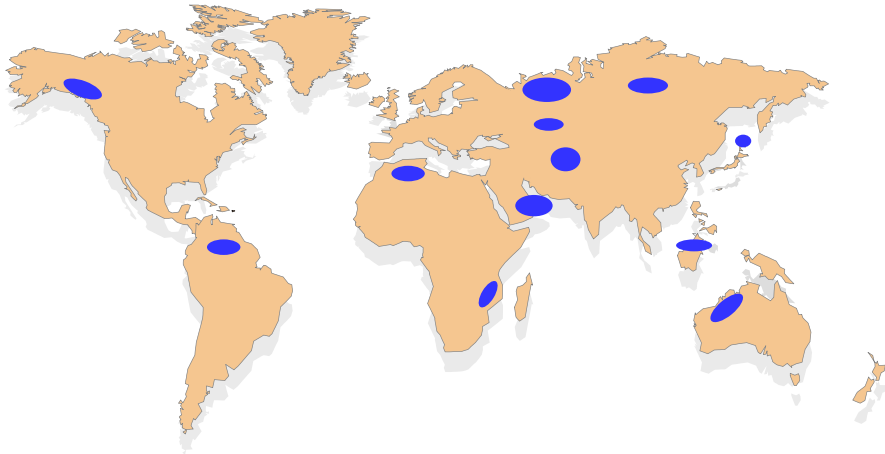


Figure 1. The location of the main Natural Gas deposits

The existence of large natural gas deposits is not the only necessary condition for their successful exploitation, since there is a lot of problems in utilizing the gas evolved by the wells. Typically, the main problem of the natural gas utilization is the location of its deposits. Indeed, the wells are sometimes located very far away from the largest NG consumers. For example, the length of pipeline from the largest Russian NG deposit at Yamal peninsula to Moscow area is ca. 5000 km. For this reason, in the Russian case, the major problem is, indeed, transportation of NG. Transportation in Russia occurs via pipelines typically at the NG pressure 45–80 bar. To drive the compressors which are pumping the transported gas, in the case of the Yamal NG deposit, one has to incinerate nearly half of its amount. Also, the easy condensing C_3 and C_4 components of NG are hardly transported at the severe Siberian climate. For this reason, a deep drying and the separation of nearly all NG components (except ethane) from methane are needed at the NG transportation in Russia. Sometimes this separation is done with the use of cryogenic technologies which have very high cost. Another problem is useful utilization of all components NG. For example, the current world market of He is much less than the helium content in a large East Siberian deposit “Kovytko”, which creates evident economical obstacles for large scale exploitation of that promising NG deposit. The same is sometimes the case with H_2S and CO_2 containing NG due to the absence of possibility of a large scale utilization of these compounds.

In case the NG deposit locate not so far away from see coast, the cheapest way is sometimes the transportation cryogenically liquefied NG by special boats.

2.2 Oil associated gases

The second large resource of fossil methane, which is now widely exploited, are oil-associated gases which are extracted from the wells simultaneously with crude oil. Typically, such gases contain methane and a large amount of heavier alkanes and thus can be attributed to a kind of the fatty NG. However, the oil-associated gases are usefully exploited till now in only a moderate scale (see Fig. 2). The reason for this is also typically a remote location of oil wells and a necessity to construct extremely expensive additional systems for transporting the gas in addition to liquid components of oil.

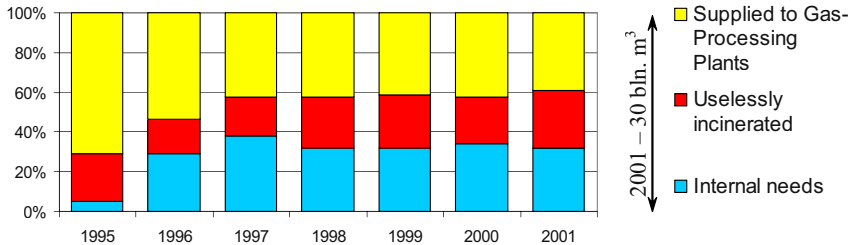


Figure 2. The annual data on the utilization of oil associated gases in Russia (according to [4]). The last bar corresponds to ca. 30 bln. m^3 (30 mln. tons) of the gas

2.3 Coal gas

Coal gas originates from degassing the coal deposits and coal mines. The main organic component of coal gas also is methane. The resources of methane in coal gases are also enormous and comparable with those of ordinary NG. According to some estimations, the content of methane in coal deposits can reach 10 wt. % of the coal itself. Note that the “proof” coal deposits are estimated as ca. 14.000 bln. metric tons.

Another source of coal methane is vent gases of coal mines. Such methane is emitted permanently from the mines but its utilization without specially designed catalytic technologies appears practically impossible since the methane content in vent gases does not exceed 2–3 vol. %.

The coal gas can be on-purpose produced by drilling special wells and extracted as nearly pure methane. Its main disadvantage is that it is produced as low-pressure gas that restricts sufficiently its application and transportation.

2.4 Methane hydrates

The methane hydrates are grey-colored solids with the composition $\text{CH}_4 \cdot x\text{H}_2\text{O}$, where $x \geq 6$. The natural hydrates were not discovered by the Russian geologists until 1950's (see, e.g., [5]). The deposits of such solids are estimated as $10 \div 10^5$ times larger than that of "usual natural gas". The global resources of methane in gas hydrates are most often estimated as $2 \cdot 10^{16} \text{ Nm}^3$ [18]. The location of methane hydrates is either bottom of arctic and deep seas or permafrost (see Fig. 3).

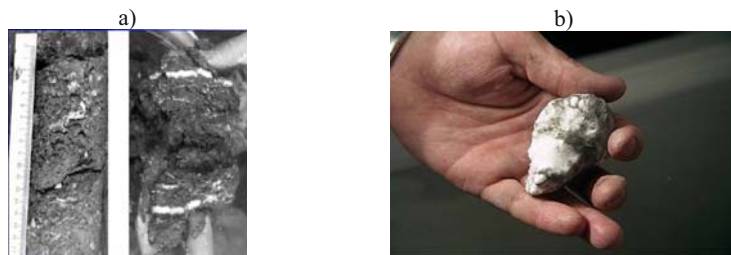


Figure 3. View of the gas hydrates excavated from the Siberian permafrost and a crystalline sample of methane hydrate (b)

Gas hydrates are typical examples of compounds of the clathrate family. Their structure can be expressed as "zeolites" with the framework created from the water molecules, while the "zeolite" cavities are filled with the included "guest" compounds (see Fig. 4 and [7]). Note, that common water ice can also be considered as a gas hydrate where the included molecule is the water one.

According to the specificity of the water-formed-zeolite structure, the extreme composition of gas hydrates with the largest content of hydrocarbons is $\text{M} \cdot 6\text{H}_2\text{O}$, where the guest compound M could be CH_4 , C_2H_6 , etc.

Till now there are only preliminary estimations of the gas hydrates' resources. These estimations vary very much (see, e.g., Table 1). However, all estimations assume that such resources are huge, with the content of methane definitely no less than in resources of ordinary NG.

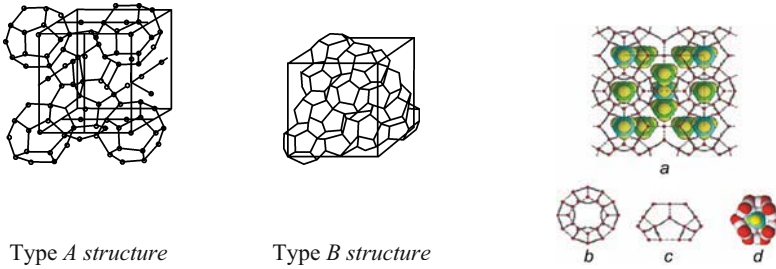


Figure 4. Typical structures of gas hydrates. Shown are two main crystalline structures of the framework of hydrates (*A* and *B*) as well as a molecular model of a hydrate with the methane molecules inside

Table 1. The year-to-year changes in the global evaluations of methane content in marine methane hydrates located at the bottom of the Ocean

№	Methane volume, Nm ³	Methane amount, metric tons	Year of evaluation	Authors of the evaluations
1	$(0.5 - 2.5) \times 10^{16}$	$(0.5 - 3) \times 10^{13}$	1977	Trofimuk et al.
2	7.6×10^{18}	8×10^{15}	1981	Dobrynin et al.
3	1.1×10^{15}	1×10^{12}	1981	Mclver
4	$(1 - 4) \times 10^{16}$	$(1 - 4) \times 10^{13}$	1988, 1990	Kvenvolden, Claypool, Makogon, Mac Donald
5	$(0.26 - 1.4) \times 10^{17}$	$(0.3 - 1) \times 10^{14}$	1994	Gornitz, Fung
6	$(2.3 - 9.1) \times 10^{16}$	$(2 - 9) \times 10^{13}$	1995	Harvey, Hung
7	1×10^{15}	10^{12}	1995	Ginsburg, Soloviev
8	7×10^{15}	7×10^{12}	1996	Holbrook et al.
9	$(0.2 - 2) \times 10^{16}$	$(0.2 - 2) \times 10^{13}$	1997	Makogon, Dickents et al.
10	2×10^{14}	2×10^{11}	1999	Soloviev, Ginsburg

For comparison: the known deposits of ordinary natural gas of the “proof” quality are known to contain ca. 10^{11} tons of methane.

Of extreme importance is that the methane hydrates were recently found on the bottom of many seas nearly the hydrocarbon resources-poor-countries like Japan and India (see [8] Fig. 5). This recent discovery has initiated an actual explosion of the interest to such potentially large resources of fossil hydrocarbons.

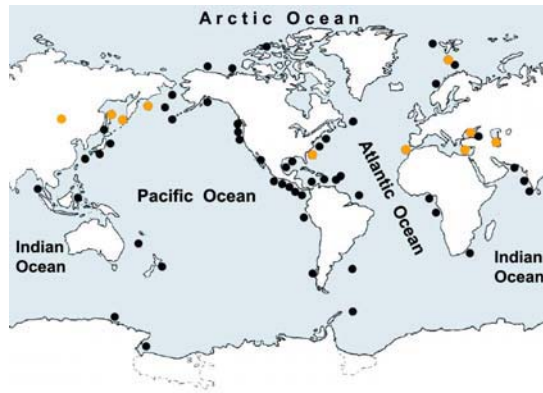


Figure 5 Location of the known deposits of gas hydrates at the sea bottom (black points)

The solid methane hydrates are known not only as potentially important resources of hydrocarbons. Vice versa, now these are known mostly as solids which can be formed inside tubes at drosseling the natural gas or simply at the emission of humid natural gas to atmosphere at low temperature seasons in, e.g., Siberia (see Fig. 6). For this reason, at the Siberian climate, the natural gas before its transporting, should be deeply dried (up to the dew point ca. $-50\text{ }^{\circ}\text{C}$).



Figure 6. A rock around a natural gas well formed by solid methane hydrates created at an emission of humid nature gas to atmosphere at $-60\text{ }^{\circ}\text{C}$ in Yakutia (Siberia)

The main physical-chemical peculiarity of gas hydrates is their PT-phase diagram (see Fig. 7). According to this diagram, these solid compounds are

stable if the temperature and pressure of ambient lie in the certain range of parameters which form an “island” (see Fig. 7 and Table 2). It means that the methane hydrates which locate at the sea bottom (at depth over 200 m) or deep in permafrost are thermodynamically stable. Thus, the main problem of extraction of methane from the gas hydrates is the necessity to increase the temperature or depressurize the hydrates just inside the gas hydrates deposits [10]. To now there is no evident technical solution to resolve this problem.

Table 2. The experimental data on the lower hydrocarbon hydrates dissociation pressure at 273 K

Guest hydrocarbon which forms the hydrate	Boiling temperature of the guest hydrocarbon, K (at 1 bar)	Hydrate dissociation pressure, bar
CH ₄	112	26.3
C ₂ H ₄	171	5.6
C ₂ H ₆	180	5.3
C ₂ H ₂	189	5.8
C ₃ H ₈	228	1.7

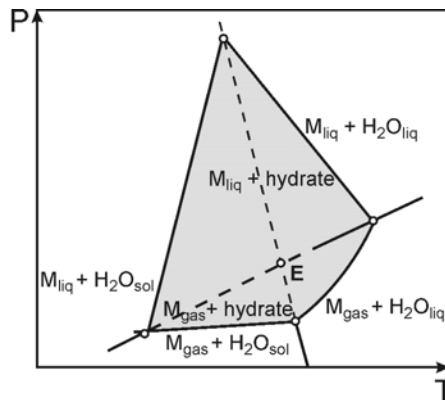


Figure 7. A typical PT-phase diagram for gas hydrates $[M \cdot nH_2O]$ for various guest substances M (according to [5, 6]). The area of the solid hydrate stability is marked. The “island” of the solid hydrate stability locates around the cross point E of the curve of coexistence of solid and liquid water and that of liquid and gas guest substance M

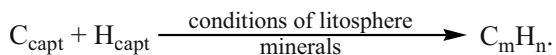
2.5 Methane as a product of the Earth degassing

A very peculiar but practically inexhaustible source of methane is a permanent degassing of our planet [11]. It is known that the annual CH₄ emission to the Earth atmosphere through volcanos, etc., at the current time

can be estimated as ca. 200 mln. tons [12]. One can assume that the origin of such methane is a steady release of carbon and hydrogen which were captured by the bulk of our planet at early stages of the planet Earth formation [13, 14]. One can expect that the captured amount of carbon corresponds to the average atomic fraction of carbon in Universe. If so, one can estimate the overall content of carbon in Earth as ca. 0.3 at % of Earth, which equals 10^{19} tons.

The idea of a continuous degassing of Earth is based on a hypothesis of the existence of inorganic and hydrocarbonic (cool, amagmatic) branches of geofluids in the Earth depth. This idea has found an experimental and theoretical support from both geology and geochemistry [15]. According to some estimates, even at minimal scales of hydrocarbon degassing, for the period of 500 mln. yeas, the supply of hydrocarbons to the Earth surface exceeded $2,5 \cdot 10^{16}$ tons [16].

The above statement is of a principal importance and relates with an old but still unresolved problem which concerns the origin the oil and natural gas deposits. Indeed, the most part of hydrocarbons in known and exploited deposits has unambiguously a biogenic origin. However, one cannot exclude that partly it has an abiogenic origin, too, and could be formed as a result of some chemical transformations of carbon and hydrogen in the Earth mantle, etc. [13, 14, 17]. Indeed, direct experiments show that in the presence of many common minerals of the Earth crust and at the common conditions of the upper levels of the crust there is possibility of “geocatalytic” hydrocarbon formation:



The natural minerals serve here the role of conventional heterogeneous catalysts (see, e.g., [15, 18]).

If this is really the case, one can expect that in future some new deposits of fossil hydrocarbons of “inorganic” origin (in addition to those of “biologic” origin) can be found [12, 16]. The location of these deposits can be different from what is considered now as common for geologists, but the overall content of hydrocarbons there can be enormous. In the latter case, our Civilization will have no problems of resources of fossil hydrocarbons for very long future.

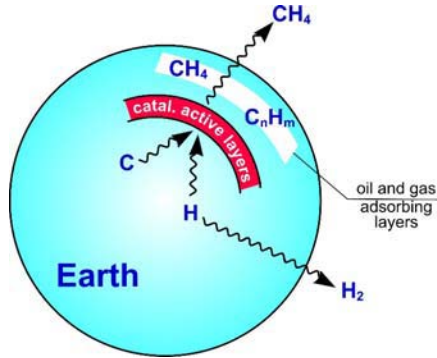


Figure 8. A scheme of the expected abiogenic hydrocarbon formation inside the Earth crust followed the methane emission as a sort of the Earth degassing

2.6 Methane in natural biogas

This resource is evidently renewable, since the origin of this methane is anaerobic fermentation of various biomass, i.e. organic substances produced as a result of natural photosynthesis. The fermentation can be represented by a generalized formula $C_nH_mO_1 \rightarrow xCH_4 + yCO_2$.

The main experimentally detected sources of so produced natural methane are forests, savanna, boreal swamps, rice plantations, uncontrolled fermentation in large municipal stockpiles.

The annual emission of CH_4 from such sources to atmosphere is estimated as ca. 40 mln. tons, while the total content of CH_4 in the Earth atmosphere is estimated as ca. 5 bln. tons [12, 19].

It is clear that it is not possible to utilize methane from the above sources due to its extremely diluted composition and, thus, due to its very low calorific value.

3. TECHNOGENEOUS SOURCES OF METHANE

3.1 On-purpose produced biogas

The origin of such biogas is on-purpose anaerobic fermentation of agricultural and communal wastes, typically municipal solid wastes, MSW. On-purpose produced biogas is a product of not very complicated biotechnological anaerobic fermentation of various organic substances

inside special batch reactors, so called “methane tanks”. In some countries this biotechnology received a wide application. For example, in China, under operation there are now more than 50 mln. units of not very large methane tanks at local agricultural enterprises. Usually, the on-purpose produced biogas contains up to 75 vol. % of CH_4 . The rest is mostly CO_2 .

The estimated resource potential of such renewable source of methane is huge and correlates with the general scale of agriculture and crops harvesting. Only for urban areas, in cities, the estimated flux of MSW is ca. 400 kg of MSW per year per capita, which allows to obtain ca. 30000 m^3 CH_4 per year. Unfortunately, biogas is now mostly used as only a fuel gas of a moderate calorific value.

3.2 Methane as an industrial byproduct

In addition to natural biological and biotechnological sources of methane, there is a lot of technogeneous sources, where methane is produced as a byproduct. The most important sources of this kind are pyrolysis processes, first of all numerous pyrolytic processes of oil refinery, production of coke from coal as well as on-purpose pyrolysis of biomass [3].

Typically, pyrolytic gases at oil and coal pyrolysis contain mostly light hydrocarbons, hydrogen and carbon oxides. Such pyrolytic gases can serve as very important raws for petrochemistry [20].

Also, in some cases of practical importance is on-purpose gasification of coal and biomass. For example, the largest Fischer–Tropsch industry erected in South Africa by SASOL is based namely on the large-scale gasification of coal. The scale of pyrolytic gases production at SASOL reaches several million tons of the pyrolysis gases per year.

The gas generated at the on-purpose gasification of coal contains mostly methane, hydrogen, and carbon oxides, while pyrolytic gases after the biomass gasification contain also a lot of oxygenates.

4. CONCLUSION

Our Civilization has in its responsibility large resources of methane which can serve as reliable background of chemical industry, in addition to methane from common natural gas.

The most expectable and considerable new sources of methane in the neighboring future seem to be oil-associated gases, coal assisted methane, methane hydrates, and bio-gas.

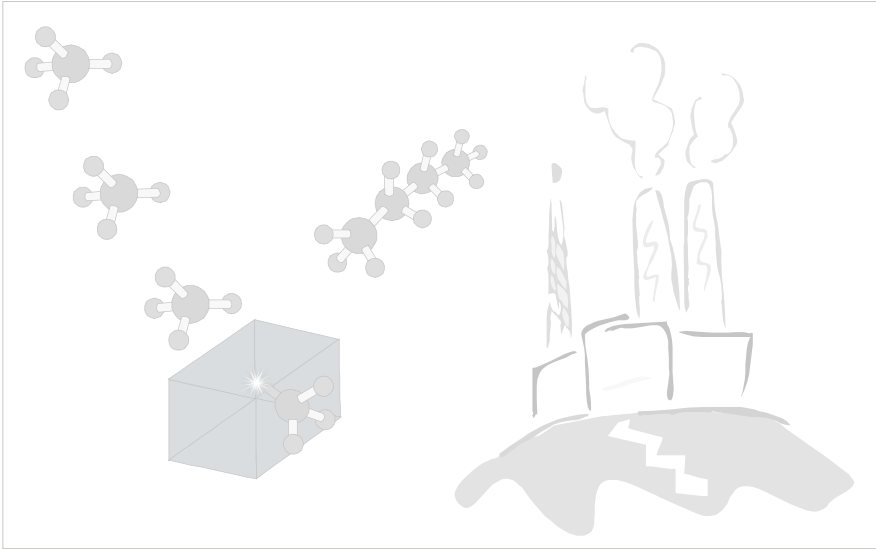
5. ACKNOWLEDGEMENTS

The author is cordially indebted to Prof. F.A. Kuznetsov for presenting the photos and tables on the gas hydrates problem.

6. REFERENCES

- [1] B.J. Skinner. *Earth Resources*. Third edition. Prentice–Hall: New Jersey, 1986.
- [2] A.A. Opalovskij. *Planned Earth by the Chemist' Vision*. Nauka: Moscow, 1990 (in Russian).
- [3] *Chemistry for the Energy Future*. V.N. Parmon, H. Tributsch, A.V. Bridgwater, and D.O. Hall etc. Blackwell: Oxford, 1999.
- [4] V. Kryukov, A. Sevast'yanova, A. Tokarev, V. Shmat. *Peculiarities of the regulation of the market of light hydrocarbon rays*. Edition of the Institute of Economics: Novosibirsk, 2002.
- [5] S.Sh. Byk, Yu.F. Makogon, V.I. Fomina. *Gas Hydrates*. Khimiya: Moscow, 1980 (in Russian).
- [6] *Degassing of Earth: Geodynamics, Geofluids, Oil and Gas*. A.N. Dmitrievskij, B.M. Valyaev, GEOS: Moscow, 2002, p. 320 (in Russian).
- [7] T. Uchida, S. Takeya, et al. *J. Phys. Chem. B*, 106, 12426 (2002).
- [8] J.P. Henriot, et al. *Nature*, 391, 648 (1998).
- [9] N.M. Bazhin, V.A. Ivanchenko, V.N. Parmon. *Thermodynamics for Chemists (textbook)*. Moscow: Khimiya, 2000.
- [10] W. Sung, H. Lee, C. Lee. *Energy Sources*, 24, 499 (2002).
- [11] N.P. Kropotkin. *Zhurn. Vsesoyuznogo Khimich. Obshchestva im. D.I. Mendeleeva*, № 5, 482, 540 (1986) (in Russian).
- [12] N.M. Bazhin. *Chemistry for Sustainable Development*, 1, 381 (1993).
- [13] A.A. Marakushev. *Origin of Earth and the Nature of its Endogenic Activity*. Nauka: Moscow, 1999.
- [14] V.N. Snytnikov et al. *Adv. Space Res.*, 30, 1461 (2002).
- [15] *Degassing of Earth: Geodynamics, Geofluids, Oil and Gas*. A.N. Dmitrievskij, B.M. Valyaev, GEOS: Moscow, 2002 (in Russian).
- [16] *ibid*, p. 379.
- [17] B. Sherwood Lollar, T.D. Westgate, J.A. Ward, G.F. Slater, G. Lacrampe-Couloume. *Nature*, 416, 522 (2002).
- [18] K.G. Ione, V.N. Parmon. *Doklady*,
- [19] J.E. Andrews, P. Brimblecombe, T.D. Jickels, P.S. Liss. *An Introduction to Environmental Chemistry*, Blackwell: Oxford, 1996.
- [20] D.L. Burdick, W.L. Leffler. *Petrochemicals in Nontechnical Language*. Penn Well Books: Tulsa, Oklahoma, 1990.

SECTION 2



COMMUNICATIONS

Chapter 14

CO₂ SEPARATION BY MEMBRANES IN NATURAL GAS PROCESSING

G. Clarizia, E. Drioli

Institute on Membrane Technology, ITM-CNR, via P. Bucci Cubo 17/C, 87036 Arcavacata di Rende (CS), Italy

Abstract: Aim of this work is the demonstration of how a proper distribution of the separation load in a multistage membrane system can make more efficient the operation. A single stage and a two membrane stages in cascade have been considered to process ternary mixtures representing natural gas and landfill gas streams. The quality of the separation has been evaluated in terms of purity of the more permeable component and membrane area per feed flow-rate, in correspondence of fixed global recoveries. The influence of different design variables such as feed pressure and pressure ratio, feed concentration, membrane selectivity on the separation extent has been investigated assuming co-current and complete mixing flow modes in the membrane units.

Key words: membrane gas separation, natural gas upgrading

1. INTRODUCTION

Carbon dioxide separation from industrial streams, where it is involved as pollutant, is an urgent need in order to reduce its impact on the environment. Natural and landfill gases represent some of the main sources of CO₂ and their treatment is important in CO₂ recovery strategy, also for its direct re-use (e.g. CO₂ enhanced oil recovery). Membrane technology is an innovative and efficient method to perform the upgrading of these gas streams, as reported in recent literature studies [1-5].

In this framework, our attention is mainly focused on how a proper distribution of the separation load on each membrane stage can make more efficient the operation.

2. MATERIALS AND METHODS

A single stage and a two membrane stages in cascade (with the permeate from the first compressed at the same pressure before to be fed to the second membrane stage) have been considered in this study. The stage cut for each stage (θ_i) is defined as ratio between permeate and feed flow-rates; in the case of two membrane units the stage cut for the whole system, θ , is the product of the single stage cuts: $\theta = \theta_1 \times \theta_2$. Thus, for instance $\theta=0.1$ can be realized with a single stage ($\theta_1=\theta$), but also combining two membrane stages operating at $\theta_1=0.5$ and $\theta_2=0.2$ or $\theta_1=0.2$ and $\theta_2=0.5$ respectively. These arrangements produce significantly different results.

The reference mixture consists of three species with different permeation rates through the membrane. CO_2 represents the fastest component, methane the slowest while impurities, that include different species depending on the specific source (e.g. light hydrocarbons, sulphur compounds, moisture), are characterised by an intermediate permeation rate.

Two different compositions (mol.%), that represent low (natural gas) and medium (landfill gas) CO_2 concentration respectively, have been investigated assuming in the membrane module two alternative flow modalities, complete mixing (CM) and co-current (CC), at both feed and permeate sides. Feed₁ contains 14% CO_2 , 8% impurities, 78% CH_4 , while Feed₂ is constituted by 42% CO_2 , 5.4% impurities, 52.6% CH_4 . In these mixtures the impurities/methane ratio was kept constant. All permeate streams leave the membrane units at atmospheric pressure. Three feed pressure values (10, 20 and 50 atm) and global stage cuts ($\theta=0.1, 0.4$ and 0.8) have been analysed. The main data used in the simulations are summarised in table 1.

The set of ordinary differential equations that describes the mass transport into the membrane unit for CC mode has been solved by a fourth order Runge-Kutta method, whereas the set of non linear algebraic equations for CM simulations has been solved using a Newton-Raphson algorithm [6].

Membrane system performances have been evaluated in terms of purity of the more permeable component in the permeate stream and specific membrane area per feed flow-rate (S_m), at fixed θ values. The influence of different design variables such as feed pressure and pressure ratio, feed concentration, membrane selectivity has been investigated.

Table 14. Gas permeation rate and feed composition considered as reference in the simulations.

	CO ₂	impurities	CH ₄
Permeance, GPU	120	30	6
Feed ₁ mol%	14	8	78
Feed ₂ mol%	42	5.4	52.6

1 GPU = 10⁻⁶ cm³(STP) cm⁻² cmHg⁻¹ s⁻¹

3. RESULTS AND DISCUSSION

In Figure 1 is shown the effect of the feed pressure on CO₂ purity in CC modality for a low θ value (10%). The same trend is observed for all the investigated pressures with a maximum in the curves at around $\theta_1=0.2$. An increase of the feed pressure (and pressure ratio) determines higher CO₂ purities in correspondence of equal θ_1 .

Under the same operating conditions, lower normalised membrane surface areas (S_m , m²/Nm³ feed) are required working at higher feed pressures, while a continuous increase of their values is observed at increasing of θ_1 (see Figure 2).

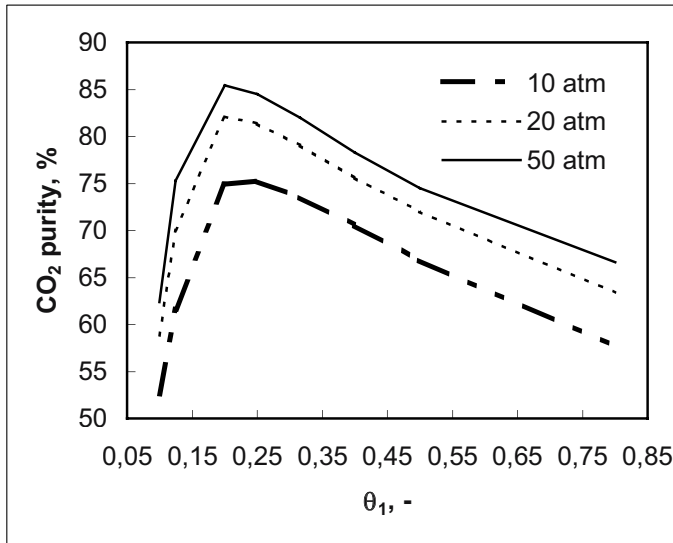


Figure 1. CO₂ purity (%) vs. θ_1 (-) as function of the feed pressure.

A similar behaviour is confirmed when medium (0.4) and high (0.8) global recovery values are analysed. In this case the maximum of the CO₂ purity curve is shifted toward an equally shared separation load between the

membrane stages, while the specific membrane requirements always increase with θ_1 . The same trend has been observed in CM calculations with the difference of lower purity levels and higher S_m values, as consequence of a worse use of the driving force with respect to CC mode. The results of some CM and CC simulations at $\theta=0.1$ and feed pressure of 10 atm are compared in table 2.

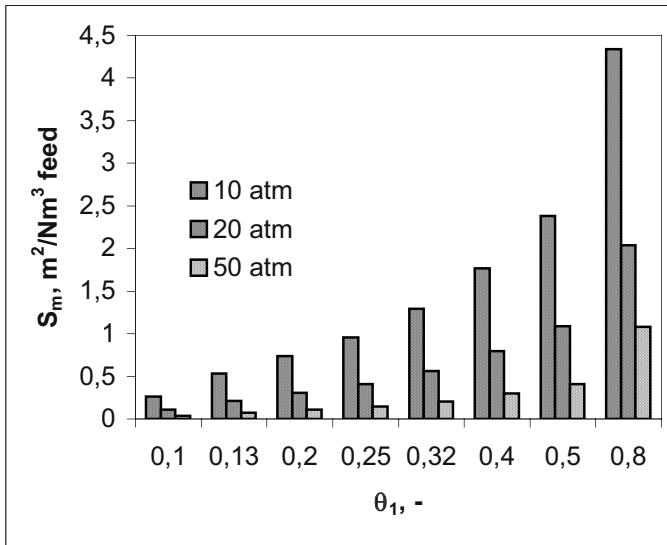


Figure 2. Influence of feed pressure on S_m (m^2/Nm^3 feed) at different stage cut combinations.

Table 2. Comparison of the membrane unit performances in CC and CM modes at $\theta=0.1$.

Flow mode	θ_1	CO ₂ purity, %	S_m , m^2/Nm^3 feed
CC	0.1	52.6	0.264
CC	0.2	74.9	0.741
CC	0.5	66.8	2.38
CM	0.1	49	0.29
CM	0.2	63	0.87
CM	0.5	60	2.5

An increase of CO₂ feed concentration (Feed₂) causes an improving in CO₂ purity level combined to a lower membrane area need due to the higher partial pressure of the more permeable species (CO₂) in the feed stream.

In addition to changes of the operating variables, the effect of the membrane selectivity, strongly linked to modifications in transport properties of the membrane material, on the separation performances has been also analysed. The permeance of CO₂ has been kept constant, while the

selectivity changes have been obtained considering a lower permeation rate for impurities and methane.

CO₂ purities for different membrane selectivities are shown in Figure 3 ($\theta=0.1$), at optimal θ_1 values in CC flow mode. The general trend already discussed (highest CO₂ purity at θ_1 around 0.2 and membrane area increasing with θ_1) is still confirmed independently on the membrane selectivity, that influences their absolute values.

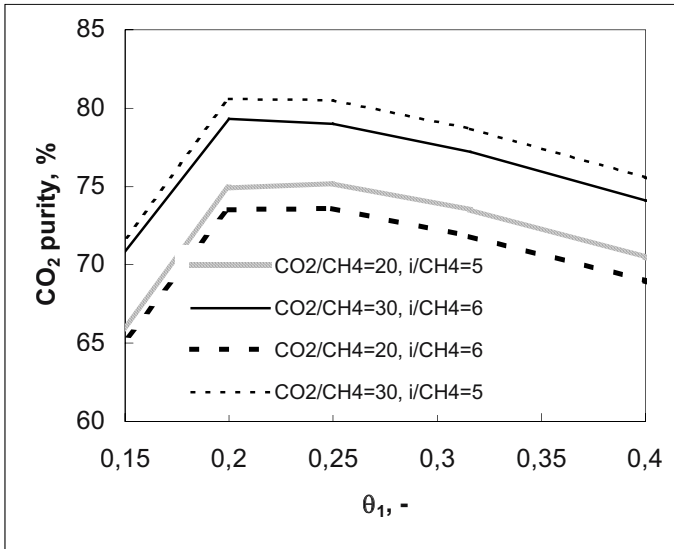


Figure 3. Membrane selectivity effect on CO₂ purity at low recovery value ($\square=0.1$).

Again at increasing global stage cut values (θ equal to 0.4 and 0.8), in particular for landfill gas concentration (Feed₂), the differences among single stage and two membrane stages in cascade are more reduced in terms of CO₂ purity, but they remain significant regarding to membrane area requirements. Moreover the best distribution of the separation load in the cascade arrangement requires to operate with $\theta_1=\theta_2$.

4. CONCLUSIONS

On the basis of the simulations performed on single and two membrane units in cascade operating in CC and CM flow modes and using two representative natural gas streams, some general considerations can be done.

At low recovery values, the purity of the most permeable component in the ternary mixture (CO₂) increases for low θ_1 values, it reaches a maximum

(θ_1 around 0.2) then it starts to decrease at higher θ_1 . For what concerns the membrane area requirement, it always increases with θ_1 . When higher θ values are analysed, the optimal performances for two membrane stages system are achieved when $\theta_1=\theta_2$ condition is realised. This trend is further confirmed when the CO_2 concentration in the feed stream increases (e.g. Feed₂).

It is possible to conclude that a single membrane stage is characterised by the lowest membrane area requirement but also the lowest CO_2 purity in the permeate stream. This result is valid for all different operating conditions investigated in this study, but it becomes less important with reference to the CO_2 purity when the total stage cut increases. In this case a single membrane stage, offering similar purity levels at the lowest membrane area, represents the best configuration.

5. REFERENCES

- [1] R. Baker, *Ind. & Eng. Chem. Res.*, 41, 2002, 1393.
- [2] A. Tabe-Mohammadi, *Sep. Sci. & Technol.*, 34(1), 1999, 2095.
- [3] B.D. Bhide, A. Voskericyan, S.A. Stern, *J. Membrane Sci.*, 140, 1998, 27.
- [4] P.J. Cook, M.S. Losin, *Hydrocarbon Proc.*, April 1995.
- [5] R. Rautenbach, K. Welsch, *J. Membrane Sci.*, 87, 1994, 107.
- [6] S.-T. Hwang, K. Kammermeyer, *Membranes in Separations*, J. Wiley & Sons, NY, 1975.

Chapter 15

STRUCTURAL AND TEXTURAL PROPERTIES OF MCM-41 MESOPOROUS MOLECULAR SIEVES CONTAINING NB, V, MO – ALTERNATIVE CATALYSTS FOR HYDROCARBONS OXIDATION

I. Nowak^a, B. Kilos^a, M. Ziolk^a, J.C. Volta^b

^a *A. Mickiewicz University, Faculty of Chemistry, Grunwaldzka 6, 60-780 Poznań, Poland; e-mail: ziolk@amu.edu.pl*

^b *Institut de Recherchers sur la Catalyse, CNRS, 2 Av. A. Einstein, 69626 Villeurbanne, Cedex, France*

1. INTRODUCTION

In 1992 the synthesis of a new family of mesoporous molecular sieves designated as M41S was reported [1]. MCM-41, one member of this family, exhibits uniform cylindrical pores in hexagonal arrangement and is produced using rod-like micelles of cationic surfactant molecules as a template. Mesoporous molecular sieves of MCM-41 type opened an opportunity for the design of catalytically active sites inside the uniform channels with controllable nano-order pore diameter. However, a pure silicate MCM-41 showed limited catalytic applications [2] and therefore, incorporation of metal centers in the silicate framework is necessary for their use in the catalysis. Isomorphous substitution of silicon with a transition metal is an excellent strategy in creating catalytically active sites for reactive molecules in the design of new heterogeneous catalysts. It is possible to obtain highly dispersed and isolated active sites in the silicate framework. Coordination and stabilization of the transition metal ion by the ordered matrix can significantly affect its catalytic behavior and lead to catalysts with new and often improved properties.

Special attention, in this work, has been devoted to develop new systems containing Nb, V, Mo mesoporous molecular sieves of MCM-41 type addressed to the partial oxidation of hydrocarbons.

2. EXPERIMENTAL

2.1 Catalyst Preparation

V, Nb and Mo were incorporated to MCM-41 material during the hydrothermal synthesis (373 K, 48 h). A sodium silicate and a salt of TME, i.e. niobium oxalate, vanadyl sulphate and ammonium molybdate were used as Si and Nb, V, and Mo sources, respectively, and cetyltrimethylammonium chloride was applied as a surfactant. The composition of the reactant mixture depended on the assumed R=Si/T ratio (where T = Nb, V, Mo). In the case of bi- and tri-functional systems a following sequence of admission of metal sources was used: niobium oxalate, vanadyl sulphate and ammonium molybdate. The general formula of obtained materials will be denoted as TMCM-41-R and their compositions are given in Table 1.

2.2 Characterization Techniques

The metal contents (Nb, V, Mo) in the calcined samples were determined by inductively coupled plasma emission spectroscopy (ICP) (Perkin Elmer M 1100).

X-ray diffraction (XRD) patterns were recorded between 1 and 40° (2 θ) on a Philips PW 1710 diffractometer (Cu K α radiation) with a step size 0.02°.

The N₂ adsorption/desorption data were measured by Micromeritics ASAP 2010 at 77 K. Prior to the adsorption measurements, the samples were degassed in vacuum at 573 K for 2h. Surface area was calculated by the BET method. The total pore volume (V_t) was estimated from the adsorbed amount of N₂ at $p/p_0 = 0.99$. The pore size distributions (PSD), the pore size (PD) and the mesopore volume (V_p) were determined from the adsorption isotherms using a corrected algorithm based on the Barret-Joyner-Halenda (BJH) procedure [3]. Moreover, the pore diameter (w) was achieved from the pore volume (V_p) and the lattice spacing (d) (obtained from X-ray diffraction data) in the following way: $w = cd_{100}[\rho V_p/(1+\rho V_p)]^{1/2}$, where $c = (8/(3^{1/2}\pi))^{1/2}$; ρ is the density of pore walls and is equal to 2.2 g cm⁻³. Additionally, the pore wall thickness, (w_t), was calculated under assumption of the hexagonal pore geometry and is equal to

the unit cell parameter, a ($a=2(3^{-1/2})d$), minus the distance between the midpoints of the sides of the hexagonal cross section (equal to $w/1.050$) [3]. The external surface area (S_{ext}) and the volume of mesopores were assessed using the α_s plot method [4] in the range of α_s from 1.8 to 2.2.

3. RESULTS AND DISCUSSION

The possibility of isomorphous substitution of silicon into MCM-41 materials with transition metals strongly depends on the metal nature. If two or three various metals are added during the MCM-41 synthesis, a competition will occur in their location in different positions.

The facility for transition metals inclusion into the mesoporous structure of MCM-41 type during the synthesis is not determined by the cation size and oxidation-state of metal cation in a simple way [5]. Table 1 clearly shows that the amount of metals in the final material differs from that in the gel and this behavior strongly depends on the metal nature. Using the same amount of metals in Nb, V, and Mo sources (together with sodium silicate) for preparing one transition metal containing MCM-41, the following order of metal content in the final material was observed: $\text{Nb} > \text{V} \gg \text{Mo}$ [5]. If two (Nb, V) or three (Nb, V, Mo) metals are introduced together during the synthesis, the V content is enhanced in comparison to one metal containing samples. Nb seems to be responsible for this feature. If V is introduced together with Nb, more vanadium is incorporated into the final mesoporous material than if only V together with Si sources is used. The introduction of Mo into the framework together with Si is extremely difficult (Si/Mo ratios > 3000). The use of a higher amount of Mo source leads to a higher content of Mo, but no more than ~ 0.01 part of Mo used in the reagent mixture is located in the final material.

It is worthy of notice that in the case of a low Si/Nb ratio (NbMCM-41-32 or 64) the real Si/Nb ratio in the final material is lower. It can suggest that not all of Nb is in the Si-O-Nb framework but part of Nb is localized in the extra framework position as Nb_2O_5 or $\text{Na}_2\text{Nb}_4\text{O}_{11}$ [6]. In the consequence, a chemical analysis gives rise to a lower Si/Nb ratio than assumed indicating that part of Si from the reactant mixture was not placed in the final material. A similar feature was observed for Co-MCM-41 [7]. If Si/Nb=128 is used in the gel the obtained material has the identical Si/Nb ratio.

The calcined TMCM-41 materials gave well-defined hexagonal XRD patterns with a main peak at $2\theta \sim 2^\circ$ and up to three signals in the region $3-8^\circ$. The introduction of metals slightly decreases the unit cell parameter and this decrease depends on the amount of metal introduced.

Table 1. The chemical composition of the samples (obtained from ICP analysis).

Catalyst*	Assumed atomic ratios	Atomic ratios					
		Si/Nb	Si/V	Si/Mo	V/Nb	Mo/Nb	Mo/V
NbMCM-41-32	Si/Nb=32	26	-	-	-	-	-
NbMCM-41-64	Si/Nb=64	45	-	-	-	-	-
NbMCM-41-128	Si/Nb=128	129	-	-	-	-	-
VMCM-41-32	Si/V=32	-	259	-	-	-	-
VMCM-41-128	Si/V=128	-	1950	-	-	-	-
MoMCM-41-32	Si/Mo=32	-	-	3274	-	-	-
MoMCM-41-128	Si/Mo=128	-	-	9440	-	-	-
NbVMCM-41-51	Si/Nb=256; Si/V=64	216	272	-	0.8	-	-
NbVMCM-41-64	Si/Nb=128; Si/V=128	129	879	-	0.08	-	-
NbVMoMCM-41-9.8 Mo/V=2/1	Si/Nb=128; Si/V=32 ; Si/Mo=16; V/Nb=4/1	134	133	1712	2	0.08	0.08
NbVMoMCM-41- 19.7 Mo/V=2/1	Si/Nb=256; Si/V=64 ; Si/Mo=32; V/Nb=4/ 1	230	255	<4043	0.9	<0.06	<0.06

* The last number in the catalyst symbol denotes Si/T assumed ratio; T= \sum of transition metal atoms

Table 2 summarizes the results of N₂ ads. and XRD measurements for all the materials studied. The N₂ isotherms are of type IV in the IUPAC classification (typical of MCM-41 materials). The steps of capillary condensation in primary mesopores are clearly pronounced and steep. The examples are given in Fig. 1. By contrast, the isotherms of the samples prepared with high concentrations of TME featured prominent hysteresis loops at p/p₀=0.9-1 indicating a considerable macroporosity. It is well known that this outcome is produced by such macropores that are connected through windows of smaller size (so-called bottleneck pores). Moreover, it seems that the incorporation of V or Mo besides Al leads to a larger hysteresis loops than that of pure silica and/or vanadium or molybdenum containing MCM-41. For NbMCM-41-32 and NbVMoMCM-9.8 an additional uncommon type-H4 hysteresis was observed in p/p₀=0.5-1.0 (Fig. 1). Mou et al. [8] on the basis of the analysis of TEM micrographs assigned this hysteresis loop at p/p₀=0.5-1.0 to extensive structural defect holes amid the nanochannels.

Table 2. Structural/textural properties of the TME-containing MCM-41 and pure siliceous sample on the basis of XRD and nitrogen adsorption data.

Catalyst	a_0 , nm ^a	S_{BET} (m ² g ⁻¹) ^b	S_{ext} (m ² g ⁻¹) ^b	V_t (cm ³ g ⁻¹) ^b	V_p (cm ³ g ⁻¹) ^b	PD (nm) ^b	W (nm) ^c	WT (nm) ^c
MCM-41	4.57	1090	70	1.01	0.99	4.02	3.89	0.87
NbMCM-41-32	4.29	960	130	0.93	0.87	3.66	3.46	0.99
NbMCM-41-64	4.34	1040	280	1.15	0.88	3.64*	3.47	1.02
NbMCM-41-128	4.33	930	110	0.79	0.80	3.65	3.45	1.04
NbVMCM-41-51	4.50	970	90	0.90	0.84	3.62	3.67	1.00
NbVMCM-41-64	4.44	1050	230	1.38	0.89	3.96*	3.63	0.98
VMCM-41-32	4.38	1070	100	1.03	0.99	3.94	3.71	0.85
VMCM-41-128	4.47	1090	80	1.02	1.01	3.98	3.81	0.84
VAIMCM-41-32	-	960	200	1.04	0.98	3.98	-	-
MoMCM-41-32	4.55	1040	130	1.04	1.02	3.94	3.72	0.94
MoMCM-41-128	4.39	1100	80	1.02	1.02	4.10	3.75	0.82
MoAIMCM-41-32	-	1040	270	1.27	0.89	3.96*	-	-
NbVMoMCM-41-9.8	4.36	1020	130	1.02	0.88	3.95*	3.71	0.94
NbVMoMCM-41-19.7	4.46	1020	70	1.36	0.93	3.97	3.73	0.90

^a – from XRD; ^b – from nitrogen adsorption data; ^c – from XRD and nitrogen adsorption data. * - secondary meso- or macropores were observed

As can be seen in Fig. 2, ads. capacities as well as width and positions of the pore size distribution peaks do not depend on the Si/T ratio. All of the materials have high SA and pore volumes. The mesopores diameter depends slightly on the nature of TME used for the synthesis and varies between 3.6 and 4.0 nm. A decrease in the Si/T molar ratio is leading to increase in the pore size that is also accompanied with a narrowing of pore size distribution. An opposite behavior was observed for the pore wall thickness, which is highest in case of higher amounts of transition elements introduced. All these features are especially visible when V or Mo are used as a sources of TME, whereas almost no influence was registered in case of Nb use only. The comparison of S_{ext} with the presence of secondary meso- and/or macroporosity evidenced in PSD confirms the presence of the additional porosity of the metallosilicates.

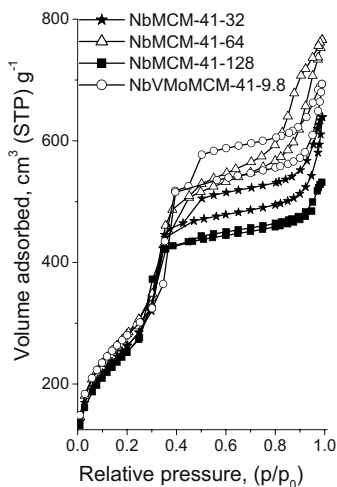


Figure 1. N₂ ads./des. isotherms of various TME-containing MCM-41.

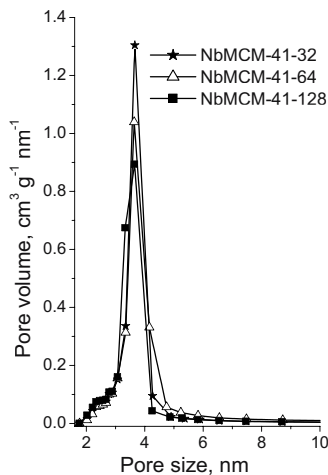


Figure 2. PSD of Nb-containing samples.

4. SUMMARY

Vanadium and molybdenum are difficult to incorporate into the MCM-41 skeleton. The presence of niobium tends to improve it. Well-ordered structures, typical for mesoporous solids with very uniform pore size distribution, were obtained for samples with high Si/T atomic ratio, whereas an additional porosity was registered for materials with high TME content.

5. REFERENCES

- [1] C. T. Kresge, M. E. Leonowicz, W. J. Roth, J. C. Vartuli, J. S. Beck, *Nature* 359 (1992) 710.
- [2] E. P. Reddy, L. Devydov, P. G. Smirniotis, *J. Phys. Chem. B*, 106 (2002) 3394.
- [3] M. Kruk, M. Jaroniec, A. Sayari, *J. Phys. Chem.*, 101 (1997) 583; *Langmuir* 13 (1997) 6267.
- [4] M. Jaroniec, M. Kruk, J. P. Olivier, *Langmuir* 15 (1999) 5410.
- [5] M. Ziolek, I. Nowak, B. Kilos, I. Sobczak, P. Decyk, M. Trejda and J. C. Volta, *J. Phys. Chem. Solids*, submitted.

- [6] B. Kilos, J. C. Volta, I. Nowak, P. Decyk, M. Ziolek, *Stud. Surf. Sci. Catal.*, submitted.
- [7] W. A. Carvalho, P. B. Varaldo, M. Wallau, U. Schuchardt, *Zeolites* 18 (1997) 408.
- [8] H.-P. Lin, S-T. Wong, Ch.-Y. Mou, Ch.-Y. Tang, *J. Phys. Chem. B* 104 (2000) 8967.

Chapter 16

ACIDIC AND CATALYTIC PROPERTIES OF DEALUMINATED BEA ZEOLITES

J. P. Marques ^{1,2}, I. Gener ², P. Ayrault ², J. C. Bordado ¹, J. M. Lopes ¹,
F. Ramôa Ribeiro ¹, M. Guisnet ²

¹ Centro de Engenharia Biológica e Química, Instituto Superior Técnico, Av. Rovisco Pais,
1049-001 Lisboa, Portugal

² Laboratoire de Catalyse en Chimie Organique, 40 avenue du Recteur Pineau, 86022
Poitiers, France

1. INTRODUCTION

BEA zeolite, firstly synthesized in 1967 [1], is a wide pore material. It has been shown to be a good catalyst for many industrial reactions such as aromatic alkylation [2,3], aromatic acylation [4], aromatic nitration [5] or aliphatic alkylation [6]. Because of its framework complexity, its structure remained unknown up to 1988 [7,8]. BEA zeolite exhibits a three-dimensional channel system with 12-membered ring apertures of 5.5 – 7.6 Å. This structure results from the coexistence of two distinct polymorphs. By this coexistence, unsatisfied linkages are present in the region connecting the polymorphous where defects and nests are concentrated. Consequently, zeolite BEA shows more pronounced variations in the nature and the reactivity of acid sites than those observed in more perfect lattices. Acidity of BEA is, therefore, a new target of investigation on the zeolite research.

2. RESULTS AND DISCUSSION

A series of dealuminated samples were prepared by dealumination through three different methods (steaming, treatments with hydrochloric acid and ammonium hexafluorosilicate (HFS) solutions) of a parent sample,

and the structural and acidic characteristics are investigated in order to identify the parameters that decide their catalytic behaviour. The samples were characterized by XRD, nitrogen adsorption and pyridine adsorption-desorption followed by IR spectroscopy. Whereas the three dealumination treatments have practically no effect on crystallinity and nitrogen adsorption properties, they cause large changes in the ranges of the O-H bond stretching modes (3300-3800 cm^{-1}) and of the most intense IR absorptions of pyridine (1400-1700 cm^{-1}). Treatments with HCl and HFS cause the most significant changes (Fig. 1): immediate disappearance of the 3662 and 3782 cm^{-1} bands corresponding to extraframework Al species (EFAL) and to tricoordinated Al species partially connected to the framework, respectively, most likely due to EFAL extraction but also via modification in the structure of the described species; appearance of additional bands at 1603 and 1446 cm^{-1} ascribed to a new type of pyridine species coordinated to Lewis sites (PyL₂). The detection of a set of bands near 1603 and 1446 cm^{-1} is usually assigned to the presence of labile hydrogen-bonded or sodium-bonded pyridine species. PyL₂ species are however much more resistant than the last ones on pyridine evacuation by increasing the temperature. An arrangement according pyridine molecules coordinated to Lewis sites and interacting through hydrogen bond with protonic sites was envisaged to explain PyL₂ formation.

Significant progress has been made in understanding the factors affecting zeolite acidity. The effect of higher framework Si/Al ratio on acidic and catalytic properties of dealuminated zeolites has been found to be influenced by the presence and structure of amorphous extraframework phases usually formed during dealumination. As exposed, HCl and HFS treatments cause the most significant changes in the structure of the resulting zeolites. Similar behaviour was verified in the catalytic performance of the dealuminated zeolites in methylcyclohexane transformation. In fact, the catalytic behaviour of the HCl and HFS treated samples shows important differences in products selectivity which, however, is apparently not sensitive to the extent of dealumination

The major rate of methane and toluene formation through protolytic cracking in the parent zeolite, comparatively to the HCl and HFS treated samples, is a fingerprint of the presence of very strong protonic sites. A positive effect of the EFAL species present on the parent zeolite, due to an inductive effect of the Lewis sites of EFAL species on the protonic sites, is expected. Nevertheless, it was verified that the number of EFAL species is not the only parameter that determines the presence of enhanced acidic sites. EFAL structure and/or location should also play an important role. Different dealumination methods induce different EFAL structure and location.

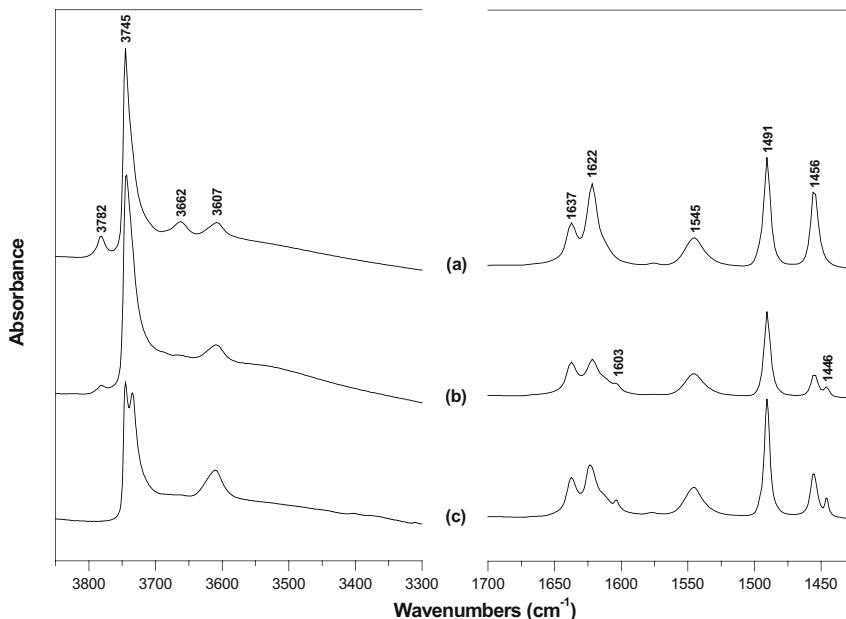


Figure 1. FTIR spectra of the parent sample (a) and HCl (b) and HFS (c) typical treated samples in the ranges 3900-3300 cm^{-1} and 1700-1400 cm^{-1} after pyridine adsorption and evacuation at 150°C.

3. REFERENCES

- [1] R.L. Wadlinger, G.T. Kerr, E.J. Rosinski, U.S. Patent 3 308 069, 1967.
- [2] G. Bellusi, G. Pazzuconi, C. Perego, G. Girotti, G. Terzoni, *J. Catal.* 157 (1995) 227.
- [3] T. F. Degnan, Jr., C. M. Smith, C. R. Venkat, *Appl. Catal. A.*, 221 (2001) 283.
- [4] A.J. Hoefnagel, H. van Bekkum, *Appl. Catal. A*, 97 (1993) 87.
- [5] M.S. Rigutto, H.J.A. de Vries, S.R. Magill, A.J. Hoefnagel, H. van Bekkum, *Stud. Surf. Sci. Catal.*, 78 (1993) 661.
- [6] K.P. de Jong, C.M.A.M. Mesters, D.G.R. Peferoen, P.T.M. van Brugge, C. de Groot, *Chem. Eng. Sci.*, 51 (1996) 2053.
- [7] J.M. Newsam, M.M.J. Treacy, W.T. Koetsier, C.B. de Gruyter, *Proc. R. Soc. London*, A420 (1988) 375.
- [8] J. B. Higgins, R. B. LaPierre, J. L. Schlenker, A. C. Rohrman, J. D. Wood, G. T. Kerr, W. J. Rohrbaugh, *Zeolites* 8 (1988) 446.

Chapter 17

INFLUENCE OF THE H-FERRIERITE SAMPLE ON THE SELECTIVITY OF SKELETAL N-BUTENE ISOMERIZATION

B. De Menorval, N. S. Gnep, M. Guisnet

Laboratoire de Catalyse en Chimie Organique, UMR 6503, CNRS-Université de Poitiers, 40 avenue du Recteur Pineau, 86022 Poitiers Cedex, France. Michel.guisnet@univ-poitiers.fr

Abstract: Very large differences can be observed in n-butene transformation at 623K over two H-ferrierite samples with Si/Al ratios of 10.2 (HFER10) and 18.8 (HFER19). At short TOS, the selectivity to isobutene is higher on HFER19 than on HFER10; with both zeolites, this selectivity increases with TOS, which can be related to an effect of coke deposit. The selectivity increase is more significant with HFER10 which becomes the most selective sample at long TOS. With HFER19, the yield in all the products decreases, the decrease being less significant for isobutene. In contrast, with HFER10, after a significant initial decrease, the isobutene yield increases with TOS becoming higher than on the fresh sample. Proposals are made to explain this large difference in the behaviour of the HFER samples.

1. INTRODUCTION

The skeletal isomerization of n-butene was extensively investigated in the last ten years [1-5]. This isomerization can be catalysed over a large variety of acid solids : doped aluminas, 10-membered ring zeolites such as ferrierite etc [6]. We show here that very large differences in catalytic behaviour can be observed between two HFER samples.

2. EXPERIMENTAL SECTION

Two samples of ferrierite in the ammonium form were purchased from Zeolyst International, London. Their total Si/Al ratios were 10.2 (HFER10) and 18.8 (HFER19). Prior to use, they were calcined in situ under dry air flow at 723K for 10h. The transformation of 1-butene was carried out in a flow reactor at 623K under atmospheric pressure; the reactant and nitrogen pressure were equal to 0.1 and 0.9 bar respectively and the weight hourly space velocity to 12.9 h⁻¹. Reaction products were analysed on-line by gas chromatography using a 50m Chrompack PLOT Al₂O₃/Na₂SO₄ capillary column and a 10-loop Valco valve.

3. RESULTS AND DISCUSSION

The micropore volumes of the two zeolite samples (determined by N₂ adsorption at 77 K) were practically similar, whereas the mesopore volume (interparticular) of HFER19 and the area of its external surface were twice greater than those of HFER10. Furthermore, as could be expected from its lower Si/Al ratio, the concentration of protonic sites n_B (able to retain NH₃ adsorbed as NH₄⁺ at 323K) of this zeolite was higher than that of HFER19.

The main products of n-butene transformation were isobutene (iC₄⁻), propene (C₃⁻) and pentenes (C₅⁻); n-butane (nC₄), ethylene (C₂⁻) and C₆-C₈ olefins (C₆⁻-C₈⁻) were also observed but in lower amounts. With both zeolites, there is an initial deactivation followed by a quasi plateau in activity. This deactivation can be related to a rapid initial formation of coke (Fig 1).

The product distribution depends on the zeolite and on the time on stream (TOS):

- With HFER10, at short TOS, butene isomerization is accompanied by a significant production of propene and pentenes, of n-butane and of C₆⁻-C₈⁻. At long TOS, isomerization into isobutene becomes very selective (S=90% at 1290 min). Whereas the effect of TOS on the yields in all the products, excepted isobutene, is similar to the one observed for n-butene conversion, the change of the yield in isobutene is very particular (Fig 2): fast initial decrease followed by an increase, the yield obtained at 1290 min being higher than the initial one. Other curious observations are that at this long TOS, the total pore volume accessible to nitrogen at 77K is less than 12% of the one of the fresh zeolite and the concentration of acidic OH groups equal to 6% of that of the fresh zeolite.

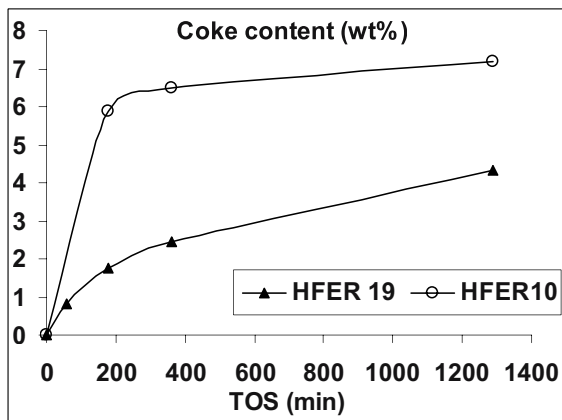


Figure 1. Coke formation as a function of time-on-stream (TOS).

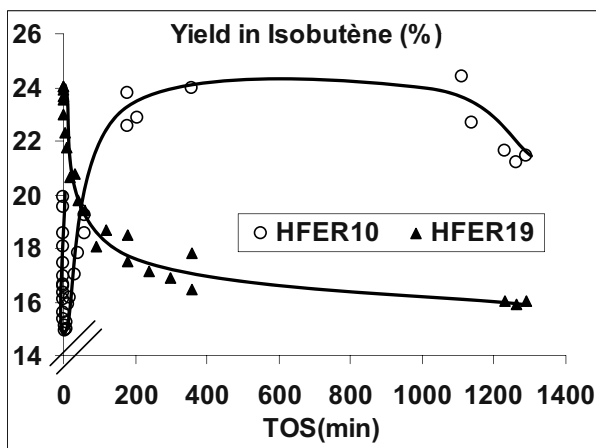
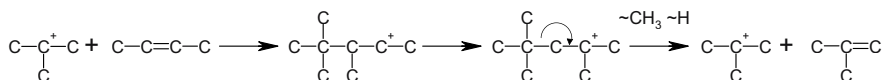


Figure 2. Yield in Isobutene as a function of TOS on HFER10 and HFER19

- With HFER19, the selectivity to isobutene also increases with TOS. However at short TOS the selectivity to isobutene is much higher than on HFER10 : 72% at 1 min instead of 38%. In contrast, at long TOS the selectivity to isobutene is lower on HFER19 than on HFER10 : 79% at 1290 min instead of 88% (Fig. 1.). This lower positive effect of TOS on isobutene selectivity can be related to the slower coke formation with consequently a smaller decrease in the adsorption capacity (-33% instead of -90%) and in the acidic OH groups (-60% instead of -94%).

The difference in behaviour between the two zeolites can be explained by considering that :

- n-butene can undergo three main different processes, the significance of which depends largely on the zeolite :
- Dimerization - Isomerization - Cracking process leading to isobutene and to a large amount of propene + pentenes.
- a similar process involving as first step the alkylation by n-butene of isobutene molecules which desorb slowly from the zeolite micropores. This process leads selectively to isobutene through the following easy steps. (autocatalytic mechanism)



- the formation of heavy secondary products which remain trapped within the zeolite micropores causing a deactivation of the inner sites [6].
- there are limitations in the desorption of isobutene from HFER zeolites and especially from the larger crystallites of HFER 10.

4. REFERENCES

- [1] H. H. Mooiweer, K. P de Jong, B. Kraushaar-Czarnetzki, W. H. J. Stork, and B. C. H. Krutzen, in J. Weitkamp, H. G. Karge, H. Pfeifer, and H. Holderich, (Eds.) "Zeolites and Related Microporous Materials : State of the Art 1994", Stud. Surf. Sci. Catal., Elsevier, Amsterdam 1994 Vol 84, p 2327.
- [2] M. Guisnet, P. Andy, N. S. Gnep, Ch. Travers, E. Benazzi, J. Chem. Soc. Chem. Commun. (1995) 1685.
- [3] J. Houzvicka, V. Ponec, Catal. Rev.-Sci. Eng. 39(4) (1997) 319.
- [4] P. Mériaudeau and C. Naccache. Adv. Catal, 44 (2000) p 505.
- [5] P. Andy, N. S. Gnep, E. Benazzi, Ch. Travers, M. Guisnet DGMK-Tagungsbericht, 9705 (1997) 43.
- [6] M. Guisnet, P. Andy, Y. Boucheffa, N. S. Gnep, Ch. Travers, E. Benazzi, Catal. Lett. 50 (1998) 159.

Chapter 18

STUDY ON THE LATTICE DEFECTS IN THE MIXED OXIDES OF NEODYMIUM AND ALKALINE EARTH ELEMENTS AND THEIR ROLE ON THE OXIDATIVE COUPLING OF METHANE

D. Filkova¹, R. Edreva-Kardjieva¹, N. Dragan², D. Crisan², L. Petrov¹

¹ Institute of Catalysis, Bulgarian Academy of Sciences, Acad. G. Bonchev Str., Bl. 11, 1113 Sofia, Bulgaria, e-mail dfilkova@ic.bas.bg

² I. Gh. Murgulescu Institute of Physical Chemistry, Romanian Academy, Sp. Independentei 202, 77208 Bucharest, Romania

1. INTRODUCTION

Along with realising the shortage of natural energy feedstock nowadays, their most effective and wise utilisation gains growing importance. For more than two decades now a great interest is manifested in the utilization of the huge natural gas resources. Different ways of methane activation are studied, as it is the main component of the natural gas. One of the most challenging tasks is the direct catalytic conversion of methane into higher hydrocarbons. It appears to be rather hard to realize with satisfactory yield mainly because of the high symmetry and very low reactivity of the methane molecule which is normally less reactive than the desired products.

A huge number of articles dealing with the catalytic oxidative coupling of methane (OCM) report data concerning almost all of the elements of the Periodic Table. It seems that a significant progress can be made only by designing complex catalytic compositions to improve the methane conversion and the selectivity towards the desired products.

According to Efstatiou et al. [1], the introduction of altrivalent cations into the oxide lattice gives an opportunity to control the activity towards

partial oxidation of methane by changing the host oxide electron structure, its oxidation/reduction potential, its acidity/basicity characteristics, and also oxygen ion mobility. These parameters are expected to influence methyl radical generation and bond strength between the surface and methyl radicals. So, one of the possibilities for improved catalyst performance is to apply complex compositions. In this connection a series of samples of mixed neodymium oxide with alkaline earth oxides (AEO) is studied to elucidate the complex relationships between the composition, catalyst structure and defects, and the catalytic performance.

2. EXPERIMENTAL

The catalyst samples (5 mol.% AEO) were coprecipitated from a solution of neodymium nitrate and nitrate of alkaline earth element (AEE) with 1M oxalic acid solution, dried and calcinated at 850°C for 24 h [2]. In order to compare the catalytic properties of pure and doped oxides, Nd_2O_3 and CaO were prepared by the same procedure.

Specific surface areas of fresh samples were measured by BET method.

The surface composition was studied by XPS. Leybold Heraeus LHS-10 spectrometer was applied with AlK_α radiation. Wagner's sensitivity factors were used for evaluation of the amount of respective elements.

XRD powder analysis was made using conventional Philips diffractometer with Ni filter and CuK_α radiation.

For the XRD data processing X RAY 3.0 program was applied [3]. The evaluation of the lattice constants is based on the minimisation of random errors by linear multiple regression [4-5]. The program determines the lattice constants, the average crystallite size and lattice strain, and gives a qualitative evaluation of their anisotropy.

Catalytic activity tests were performed using a fixed bed flow system with on-line gas chromatographic analysis. The total gas flow rate was 5.35 ml/sec with feed gas mixture of 60% methane, 6% oxygen, and 34% nitrogen and with 0.2 g catalyst sample in the reactor. The temperature range of 650–850°C was studied at atmospheric pressure.

3. RESULTS AND DISCUSSION

Due to the high temperature of calcination, the specific surface areas of the studied catalysts are rather low and do not differ much: Nd_2O_3 – 0.8, $\text{MgO-Nd}_2\text{O}_3$ – 1.5, $\text{CaO-Nd}_2\text{O}_3$ – 1.2, $\text{SrO-Nd}_2\text{O}_3$ – 1.3, $\text{BaO-Nd}_2\text{O}_3$ – 1.1 m^2/g .

XRD analysis was applied in attempt to follow the solid solution formation. According to the ionic radii fit (Table 1) calcium should incorporate into the Nd_2O_3 lattice most easily, as Ca^{2+} and Nd^{3+} possess very close cation radii. Sr^{2+} radius is bigger by 12% compared to Nd^{3+} and Mg^{2+} and Ba^{2+} are symmetrically situated by about 30% difference between each of their radii and Nd^{3+} radius. The XRD patterns show only lines characteristic of A-type Nd_2O_3 hexagonal structure. No other phases are detected.

Table 1. Cation radii in Å of Nd^{3+} and added AEE, calculated for coordination number 6 by Shannon and Prewitt [6] and Ahrens [7], average fit = 100 (average $R_{\text{AEE}^{2+}}$ /average $R_{\text{Nd}^{3+}}$)

	Nd^{3+}	Mg^{2+}	Ca^{2+}	Sr^{2+}	Ba^{2+}
Shannon	0.995	0.72	1.000	1.16	1.36
Ahrens	1.040	0.66	0.990	1.12	1.34
Average Fit (%)		67.8	97.7	112	133

The unit cell volumes are calculated for pure and doped Nd_2O_3 according to the formula $V = a^2 \cdot c \cdot \sin 120^\circ$: 76.21 Å³ for pure Nd_2O_3 , 76.42 Å³ for $\text{MgO-Nd}_2\text{O}_3$, 76.39 Å³ for $\text{CaO-Nd}_2\text{O}_3$, 76.38 Å³ for $\text{SrO-Nd}_2\text{O}_3$, and 76.20 Å³ for $\text{BaO-Nd}_2\text{O}_3$. Doping with Mg, Ca, and Sr increases the lattice parameters and unit cell volume, while the values calculated for the pure and Ba doped Nd_2O_3 are essentially the same. This may mean that the barium ion is constrained to some extent from incorporation into the neodymium oxide lattice because of its bigger radius. However, when comparing the lattice strain of the doped samples (Fig. 1) the barium containing oxide shows the highest value. Obviously, Ba^{2+} disturbs the host lattice, probably occupying interstitial positions.

As no crystal phases of AEE are detected by XRD, it is checked if the dopant elements are concentrated on the sample surface as amorphous substances applying XPS (Table 2). 1s orbital binding energy is calculated for oxygen, 4d - for Nd, 2p - for Ca, 3d - for Sr, and 3d_{5/2} - for Ba. No signal is observed for Mg, probably because of its low atomic weight and the weight concentration lying at the border of detectability. The data show an enrichment of the surface by Ca and Ba and almost random distribution of Sr. The bigger lattice strain established for the Ca and Ba doped samples (Fig. 1) may be the reason for such behaviour, since the lattice strain is easier compensated in the surface layers of the solid.

The dopant incorporation into neodymium oxide lattice was studied earlier by measuring electrical conductivity of the samples [2]. It was found to consists of two components: p-type conductivity and ionic conductivity (σ_i), and increases in the order: $\text{MgO-Nd}_2\text{O}_3 < \text{Nd}_2\text{O}_3 < \text{BaO-Nd}_2\text{O}_3 < \text{SrO-Nd}_2\text{O}_3 < \text{CaO-Nd}_2\text{O}_3$. The estimation of the ionic component shows that doping by Ca, Sr, and Ba increases the ion mobility while the presence of

Mg strongly decreases it and increases the enthalpy of activation of the conductivity. In the rare earth oxides σ_i has been attributed to O^{2-} migration what depends on oxygen vacancy concentration only according to the literature [8, 9].

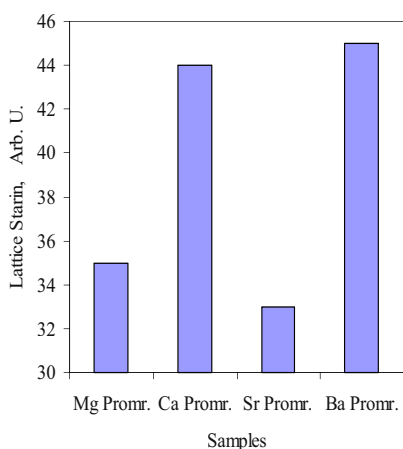


Figure 1. Lattice strain (arbitrary units) in the crystals of promoted Nd_2O_3 .

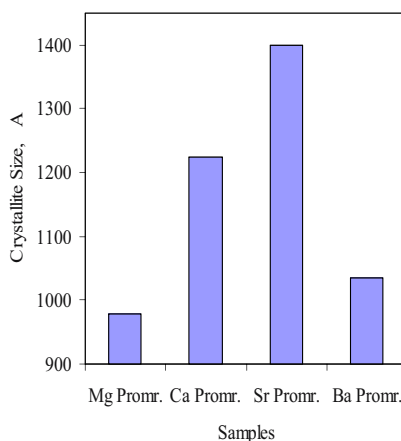


Figure 2. Average crystallite size (Å) calculated about promoted samples of Nd_2O_3 .

Table 2. XPS data about the dopant concentration on the surface of neodymium oxide promoted with 2.56 at. % of AEE.

Promoter	AEE (at. %)	Nd (at. %)
Mg	—	100
Ca	5.8	94.2
Sr	3.0	97.0
Ba	5.2	94.8

It is hard to explain how the magnesium doping would have decreased the number of oxygen vacancies in neodymium oxide lattice but it is very probable that because of the big difference between the cation radii of Mg^{2+} and Nd^{3+} a lattice distortion and clustering take place. Such phenomenon is reported by Kelly et al. [10] in a study on nickel ferrocyanide electrodes modified with alkaline elements. The electrodes are used as active cation-exchange matrices. The authors observed that in a system with mixed alkali cations a lattice site occupied by caesium ion causes neighbouring sites to prefer caesium thus forming micro-domains of the nickel ferrocyanide dominated by cesium and other areas dominated by sodium. For cation combinations that yield a variation in the nickel ferrocyanide lattice

parameter of less than 0.009 Å, i.e. sodium and potassium, a homogeneous nickel ferrocyanide phase is obtained. This way the lattice strain caused by the big difference between the cation radii is diminished but the clustering reduces the effective number of available current carriers below the expected level thus decreasing strongly the conductivity.

The introduction of AEE cations into Nd_2O_3 as expected, creates additional oxygen anion vacancies for attaining electroneutrality of the lattice, thus modifying the catalyst structure and performance. According to the electrical conductivity measurements the oxygen anion vacancy concentration increases in the order: $\text{Nd}_2\text{O}_3 < \text{BaO-Nd}_2\text{O}_3 < \text{SrO-Nd}_2\text{O}_3 < \text{CaO-Nd}_2\text{O}_3$.

The average crystallite size of the four promoted samples is given in Fig. 2. The poorest crystallinity is manifested by the magnesium-containing sample and strontium seems to stabilise the crystal lattice, causing higher crystallite size and lower lattice strain. This is an unexpected result since Ca^{2+} radius fits best the neodymium oxide lattice but the calcium promoted sample shows higher lattice strain and poorer crystallinity. The high concentration of oxygen vacancies leading to electrostatic repulsion between them may be a reason for such behaviour.

Considering the catalyst performance, the methane conversion does not differ much on pure and promoted neodymium oxide, being lower on CaO. Promoting with AEE increases the C_{2+} selectivity (summary selectivity towards ethane, ethylene, propane, and propylene, the latter two in small quantities up to 6 vol. %) (Fig. 3). Obviously, many factors influence the catalyst performance in the reaction of OCM. It is believed that the proper catalysts are basic substances, although there is not always direct correlation between the basicity and the catalyst performance [11–13]. Lattice defects, oxidation-reduction potential, oxygen mobility play important role, too [14, 15].

According to the catalyst selectivity data (Fig. 3), strontium promotion is the most effective and magnesium promoted catalyst shows the poorest selectivity at higher temperatures, in spite of the highest oxygen vacancy concentration under calcium promotion and the presence of strong basic centres under barium promotion. It seems that the high basicity and good incorporation of strontium into neodymium oxide lattice, the increased number of oxygen vacancies and high O^{2-} mobility are very important for attaining high selectivity of the process. The new data reveals that strontium promoter also stabilises the crystal lattice and spreads randomly in the bulk oxide.

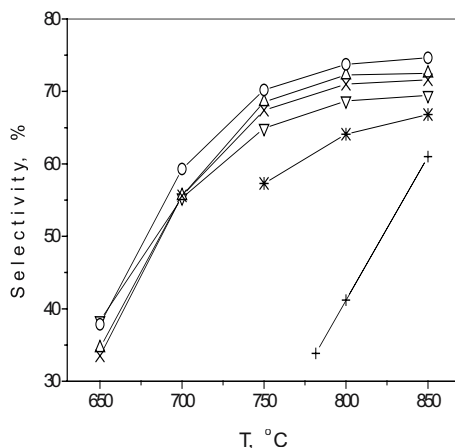


Figure 3. C_{2+} selectivity vs. the temperature. Reaction conditions: $F_{\text{tot}} = 5.35$ ml/s, $\text{CH}_4 : \text{O}_2 : \text{N}_2 = 60 : 6 : 34$, 0.2 g catalyst, symbols: + - CaO, * - Nd_2O_3 , ∇ - $\text{MgO-Nd}_2\text{O}_3$, Δ - $\text{CaO-Nd}_2\text{O}_3$, O - $\text{SrO-Nd}_2\text{O}_3$, X - $\text{BaO-Nd}_2\text{O}_3$.

4. CONCLUSIONS

Doping of neodymium oxide with AEO improves its selectivity in the reaction of oxidative coupling of methane, strontium promoted sample manifesting the best selectivity towards higher hydrocarbons.

It is strontium that stabilizes the host oxide lattice upon doping despite the best cation radii fit between Ca^{2+} and Nd^{3+} . Strontium promoter is randomly distributed in the catalyst bulk while calcium and barium enrich the catalyst surface about twice, probably because of the higher lattice strain under doping with Ca and Ba, what is easier to compensate in the surface layers of the solid.

The mobility of O^{2-} ions is restricted under magnesium doping. It is supposed to appear as a result of lattice distortion and clustering, corresponding to the poorest C_{2+} selectivity on this sample.

5. REFERENCES

- [1] Efstatiou A. M., D. Boudouvas, N. Vamvouka, X. E. Verykios, *Appl. Catal. A: General*, 92 (1992) 1
- [2] Filkova D., D. Wolf, G. Gayko, M. Baerns, L. Petrov, *Appl. Catal. A: General*, 159 (1997) 33

- [3] D. Filkova, R. Kardjieva, N. Dragan, D. Crisan, and L. Petrov, *Bulg. Chem. Commun.* 34 (2002) 469
- [4] Langford J. I., *J. Appl. Cryst.*, 11 (1978) 10
- [5] Langford J. I., R. Delhez, Th. H. Keijser, and E. J. Mittemeijer, *Aust. J. Phys.*, 41 (1988) 173
- [6] Shannon R. D. C. T. Prewitt, *Acta Cryst.*, B25 (1969) 925
- [7] Ahrens L. H., *Geochim. Cosmochim. Acta*, 2 (1952) 155
- [8] Szabo Z. G. and D. Kallo Eds., *Contact Catalysis*, Akademiai Kiado, Budapest (1976) p. 115.
- [9] Etsell T. H. and S. N. Flengas, *Chem. Rev.*, 70 (1970) 339
- [10] Kelly M. T., G. A. Arbuckle-Keil, L. A. Johnson, E. Y. Su, L. J. Amos, J. K. M. Chun, A. B. Bocarsly, *J. Electroanal. Chem.*, 500 (2001) 311
- [11] Dissanayake D., J. Lunsford, M. Rosinek, *J. Catal.* 143, 286 (1993).
- [12] Choudhary V., V. H. Rane, R. V. Garde, *J. Catal.* 145 (1994) 300
- [13] Ruckenstein E., A. Z. Khan, *Catal. Lett.* 18 (1993) 27
- [14] Borhert H., Z. L. Zhang, M. Baerns, Proc. Symp. Natural Gas Upgrading, ACS, San Francisco Nat. Meeting, Apr. 5-10, 1992, p.111.
- [15] Driscoll D. J., W. Martir, J.-X. Wang, J. H. Lunsford, *J. Am. Chem. Soc.* 107 (1985) 58

Chapter 19

MOLECULAR MECHANISM OF THE METHANE DISSOCIATION ON THE VANADIUM OXIDES CLUSTERS. DFT CALCULATIONS

Witold Piskorz¹, Ewa Broclawik²

¹*Faculty of Chemistry, Jagiellonian University, Cracow, Poland*

²*Institute of Catalysis, Polish Academy of Sciences, Cracow, Poland*

1. INTRODUCTION

The aim of this work was to elucidate the mechanism of the CH₄ molecule activation with the proximity of the V₂O₅ surface. The project is a continuation of the former calculations concerning small molecules of vanadium oxides VO_n (n=0...4) and concerns the mechanism change when moving from vanadium atom and small vanadium oxide molecules with gradually increasing number of oxygen ligands to the bi- and trimetallic clusters.

2. METODOLOGY

As a model the V₂O₉H₈ and V₃O₁₁H₉ clusters have been chosen with the geometry optimised starting with the cluster cut off the V₂O₅ lattice. The terminal bonds have been saturated with hydrogen atoms.

The software user for all the computations was Dmol-960 (Accelrys) with VWN correlation-exchange potential and DNP (double numerical augmented with polarization functions) basis set. For some species the computations have been verified with Gaussian-98 (B3LYP hybrid correlation-exchange potential, LanL2DZ basis set).

3. RESULTS AND CONCLUSIONS

The main conclusion of the project can be summarized as follows:

- Small complexes
 - $n(\text{O})=0,1$: oxidative addition of the C-H bond to the vanadium atom dominates.
 - $n(\text{O})=2,3$: oxidative addition becomes less stable and disappears for VO_3^- (not enough empty vanadium coordination places). With the presence of oxygen ligands the possibility of hydrogen capture into OH group appears, with methyl fragment bonded to the metal (most stable) and suggests the $\sigma(\text{CH})$ -bond metathesis. The structure with methyl group bonded to the oxygen and the hydrogen remaining in the metal coordination sphere shows negligible stability.
- Bi- and trivanadium clusters $\text{V}_2\text{O}_9\text{H}_8$ and $\text{V}_3\text{O}_{11}\text{H}_9$ (total charges of the assemblage 0 and -1. The calculations comprised determining the stable structures (minima on the potential energy surface) for all considered fragments (CH_4 , CH_3 and H) interacting with model clusters. In addition, the transition state structures were estimated for the process of C-H bond scission.
 - Single cluster model: weak physisorbed complex of CH_4 interacting with vanadium site occurred; for dissociated fragments both species (H^\cdot and CH_3^\cdot radicals or H^+ and CH_3^- ions) tried to locate concurrently on O(bridge) of the cluster. The localisation of the CH_3 on the V site lead to very high energy. The energy barrier for C-bond cleavage depended on the reduction advancement: it was estimated to be about 55 kcal/mol for the $\text{V}_2\text{O}_8\text{H}_6^0$ cluster and decreased to about 40 kcal/mol for $\text{V}_2\text{O}_8\text{H}_6^{-2}$.
 - Double cluster model:
 - $\text{V}_2\text{O}_9\text{H}_8$: The dissociation energy is as low as 34 kcal/mol (table below the text) in the case of homolytic dissociation with the overall charge equal to 0 ($\text{V}_2\text{O}_9\text{H}_8^0$). The homolytic dissociation is favored in the circumstances used in our calculations (vacuum). In the computational scheme used, the homolytic dissociation in vacuum costs 389 kcal/mol, and in heterolytic one costs 413 kcal/mol.
 - $\text{V}_3\text{O}_{11}\text{H}_9$: No stable intermediate complex and no product with the methyl group directly bound to the vanadium atom was found. The stability of the products with the hydrogen and the methyl bound to triply coordinated oxygens in the two clusters amounted to 98 kcal/mol (exothermic).

The analysis of the charge redistribution along the preliminary stages of the scission shows that the efficient C-H cleavage requires injection of

electrons into the methane which is in line with postulated activation via populating the antibonding σCH^* orbital. When the fragments reach their position on the bridging oxygens, they both become definitely positive ($Q(\text{CH}_3, \text{ads}) = +0.32$ a.u., $Q(\text{H}, \text{ads}) = +0.43$ a.u. according to Mulliken population analysis). Thus the hypothesis may be supported that the mechanism of the C-H bond scission on transition metal oxides is different from those previously postulated. Both fragments of the cleaved C-H bond become attached to the surface oxide ions. The proton forms an OH group, the hydrocarbon fragment forms an alkoxy group. Simultaneously, the two electrons of the cleaved bond are injected into the conductivity band of the V_2O_5 crystal.

As it was found in the forthcoming work, the V_6 -cluster is not large enough to study the regions of the transition state of the discussed reaction.

Table 1. The summary of the results for the CH_4 dissociation (energy in kcal/mol) on two separated $\text{V}_2\text{O}_9\text{H}_8$ and $\text{V}_2\text{O}_8\text{H}_6$ clusters in the different computational modes.

$\text{V}_2\text{O}_9\text{H}_8$		
Total charge	Dissociation mode	Dissociation energy
-1	heterolytic	136
-1	homolytic	255
0	heterolytic	127
0	homolytic	259

$\text{V}_2\text{O}_8\text{H}_6$		
Total charge	Dissociation mode	Dissociation energy
-1	heterolytic	208
-1	homolytic	92
0	heterolytic	152
0	homolytic	34

Chapter 20

ACIDITY, ACTIVITY AND MICRO-KINETICS STUDIES IN AN H-ZSM5

P. Borges¹, R. Ramos Pinto¹, M.A.N.D.A. Lemos¹, J. Védrine², E.G. Derouane³, F. Lemos¹, F. Ramôa Ribeiro¹

¹ Grupo de Zeólitos, Centro de Engenharia Biológica e Química, Departamento de Engenharia Química, Instituto Superior Técnico, 1049-001 Lisboa, Portugal.

² Laboratoire de Physico-Chimie des Surfaces, Ecole Nationale Supérieure de Chimie de Paris, 11, rue Pierre & Marie Curie - 75005 Paris, France.

³ Faculdade de Ciências e Tecnologia - Química, Universidade do Algarve, Campus de Gambelas, 8000-117 Faro, Portugal.

Abstract: An H-ZSM5 zeolite has been characterized by TPD of ammonia and its performance was tested with several olefins (ethylene and propylene) and n-hexane. The catalytic tests were performed at a wide range of temperatures (300 – 450°C) and molar fractions of reagent in the feed. The results from the TPD have been deconvoluted in order to obtain a distribution of the strength of the acidity of the active sites. A micro-kinetic model and a simplified kinetic equation have been developed and fitted to results for the conversion of n-hexane and the olefins, respectively.

Key words: H-ZSM5, TPD, Acidity, Activity, Micro-kinetic, Kinetics

1. INTRODUCTION

Acid catalysis is extremely important in the chemical industry and it is involved in the production of various chemical products and, in particular, in catalytic cracking, the industrial chemical process that has the largest catalyst consumption.

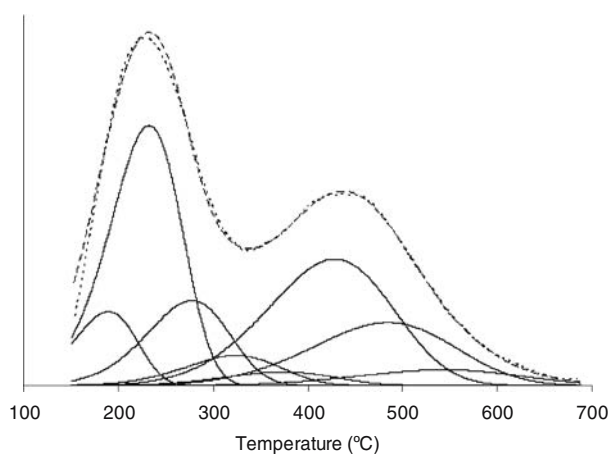
The demand for more efficient catalysts is making the understanding of the fundamental aspects of these transformations even more important; it is also creating the necessary drive force to the development of practical

models that enable the rapid analysis of new catalytic materials and that will allow the prediction of the catalytic behaviour of these materials based on very simple characterization tests. This need for faster analysis of results is being pressed by the more extensive use, by the industry research and development, of combinatorial catalysis techniques, which tend to produce an enormous amount of new materials, which have to be screened without resorting to extensive catalytic testing. Thus, the development of models that can relate the catalytic properties of a given solid with other type of information, which is easier to obtain from characterization techniques, is of enormous importance.

For the studies performed in this work, it was used a H-ZSM5 zeolite from Zeolyst with a Si/Al of 15.

2. TPD OF AMMONIA

The acidity of the H-ZSM5 catalyst was characterized by TPD of ammonia. This was intended to determine the acid strength distribution of the active sites of the catalyst. The acquired TPD curve was then deconvoluted by a method developed by C. Costa et al [1]. The obtained experimental curve, as well as the fitted curve and the partial deconvolution curves showing the distribution of acidity are shown in figure 1.



Experimental Curve -----, fitted curve ——— and deconvolution curves ———

Figure 1. TPD of ammonia of the H-ZSM-5 catalyst.

The object of this work is to, later on, develop a correlation between the distribution of acidity of different zeolites and their catalytic activity and by this way to be able to quickly predict the behaviour of new catalysts by simply determining its acid strength instead of having to perform several catalytic tests with different reactants, which is a more slow process.

3. CONVERSION OF OLEFINS

The acid-catalysed transformation of light olefins over ZSM5 was studied at various temperatures and partial pressures. It was observed that some of these olefins presented a decrease in reaction rate as the temperature increased. Despite the fact that this reaction proceeds by a rather complex mechanism, this well-known but rarely observed effect of apparent negative activation energy has been interpreted by the relevance of the adsorption energy in the complete catalytic cycle.

A simplified kinetic equation is proposed to describe the rate of reaction:

$$(-r_0) = \frac{k' \cdot p_{O \text{ initial}}^2 \cdot (1-x)}{1 + K \cdot p_{O \text{ initial}}} \quad (1)$$

where $p_{O \text{ initial}}$ is the fed partial pressure of olefin, x is the conversion, k' is the modified kinetic constant and the K is the adsorption constant. The dependence of these two last parameters with temperature can be expressed by equation 2.

$$k' = k'_0 \cdot e^{-\frac{E_A + \Delta H_{\text{ads}}}{R \cdot T}} = k'_0 \cdot e^{-\frac{E_{A \text{ app}}}{R \cdot T}} \quad \text{and} \quad K = K_0 \cdot e^{-\frac{\Delta H_{\text{ads}}}{R \cdot T}} \quad (2)$$

where k'_0 and K_0 are temperature independent constants, E_A and $E_{A \text{ app}}$ are, respectively, the true and apparent energies of activation for the oligomerization reaction, ΔH_{ads} is the enthalpy of adsorption of the olefin and is always a negative quantity, T is the absolute temperature and R is gas constant.

If, the absolute value of the enthalpy of adsorption is larger that the real activation energy, the apparent activation energy will come out with a negative value. If, at the same time, the denominator of the fraction on equation 1 is not much higher than one, that is, if the factor $K p_{O \text{ initial}}$ is sufficiently small, the kinetic constant decreases with the temperature.

3.1 Results and Conclusions

The experimental and fitted values of catalytic activity (estimated by equation 3), using the proposed model, are shown in figure 2, as a function of temperature.

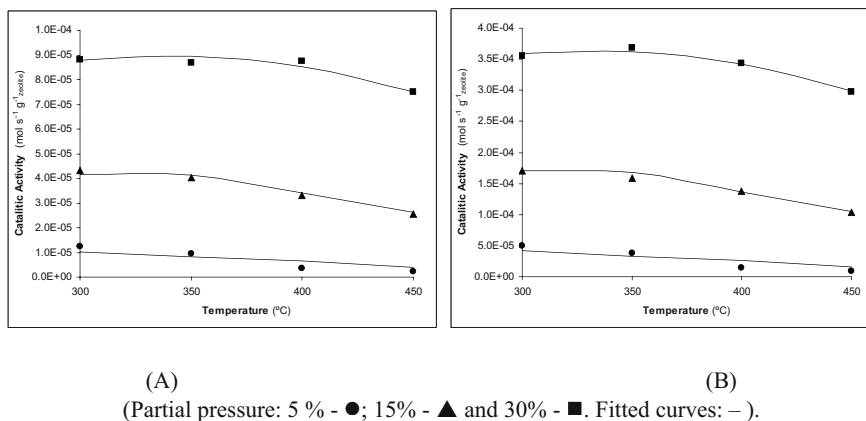


Figure 2. Evolution of the catalytic activity as a function of the temperature for ethylene (A) and propylene (B), at different partial pressures of reactant.

$$A_{C \text{ experimental}} = \frac{F_{O} \cdot x_{\text{final}}}{W_{\text{zeolite}}} \quad \text{and} \quad A_{C \text{ fit}} = \frac{x_{\text{final}}}{\int_0^{x_{\text{final}}} \frac{dx}{(-r_O(x))}} \quad (3)$$

where F_{O} initial is the molar flow of reactant at the inlet of the reactor and x_{final} is the conversion at the outlet of the reactor.

The experimental results show, clearly, a tendency for the decreasing of the catalytic activity above 350 °C. Although the kinetic rate of the oligomerization step increases with temperature, the raise of temperature also induces a reduction of the amount of reactant adsorbed on the surface of the catalyst, in view of the fact that the adsorption phenomena are always exothermic processes. This effect of depletion of the reactant leads, eventually, to be the limiting step of the global reactional rate, overlapping the increase of the kinetic constant of the oligomerization steps and conducting to the observed phenomenon.

The proposed equation, which results from a quite simple model attending the involved reactions, describes pretty well the evolution of the

reactional kinetics in the region of temperature where this is controlled by the adsorption equilibrium.

4. MICRO-KINETIC MODEL

The kinetic of the catalytic cracking has been extensively studied at the macro-kinetic level, which is sufficient for the dimensioning of equipment, but clearly insufficient when the aim is to obtain a more detailed description of the process, namely, to predict the behaviour of a certain catalyst when in contact with different charges.

The micro-kinetic model developed in this work considers paraffins and olefins separately, but lumped by their carbon number. This type of models involve a huge number of reactions and kinetic parameters, in order to reduce the number of kinetic constants, was performed a parameterization taking advantage of the relations between the reactions of similar species.

The developed micro-kinetic model is a continuation of the work done by C. Pinheiro *et al* [2] and H. Carabineiro *et al* [3].

4.1 Results and Conclusions

The catalytic tests, performed with n-hexane at a temperature of 450°C and a molar fraction of n-hexane in the feed of 0,48, were used to fit the developed micro-kinetic model and determine the kinetic constants. The micro-kinetic model only distinguishes paraffins from olefins, so the aromatics were included in the olefins with the same number of carbons.

As can be seen in figure 3, the molar distribution of the products predicted by the micro-kinetic model is reasonably similar to the experimental results.

Due to the great number of products, it becomes difficult to evaluate the micro-kinetic model only by the comparison of the products' molar distribution. In order make this task easier, several indexes were determined (conversion, activity, olefins/paraffins ratio and the medium molecular weight).

The data in table 1 corroborates the good behaviour of the developed micro-kinetic model in the simulation of the cracking of n-hexane in the conditions referred previously. Although, the model still presents an over-estimation of methane, ethylene and heavy olefins, which will have to be solved in future models, it can be considered to present a good agreement with the experimental data for the cracking of n-hexane.

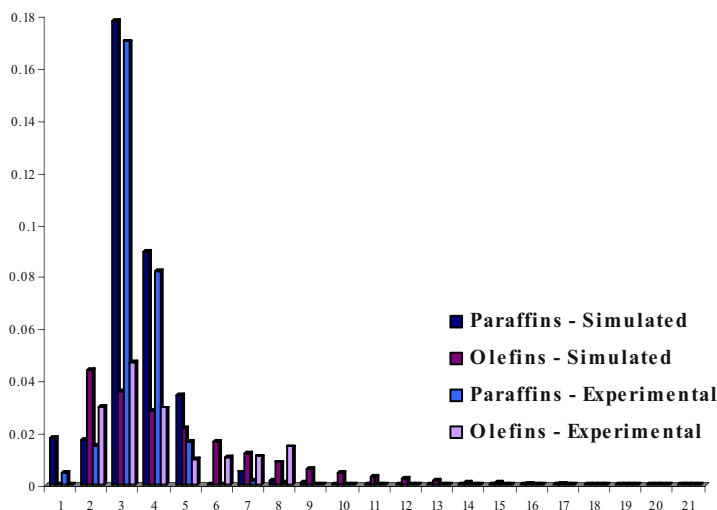


Figure 3. Molar distribution of the products of the cracking of n-hexane predicted by the micro-kinetic model developed in this work and the respective experimental results.

Table 1. Indexes which were determined in order to facilitate the evaluation of the micro-kinetic model

Indexes	Experimental	Simulated
Conversion (%)	32	37
Activity ($\text{mol s}^{-1} \text{kg}^{-1}$)	0,127	0,147
Olefins / Paraffins	0,52	0,56
Medium molecular weight (g mol^{-1})	71	78

5. REFERENCES

- [1] C. Costa, J.M. Lopes, F. Lemos, F. Ramôa Ribeiro, J. Mol. Catal. A: Chem, 144 (1999) 221.
- [2] C. Pinheiro, F. Lemos, F. Ribeiro, Chem. Eng. Sci., 1999, 54, 1735.
- [3] H. Carabineiro, C. Pinheiro, F. Lemos, F. Ribeiro, Chem. Eng. Sci., 59(6) (2004) 1221.

Chapter 21

MICROKINETIC MODEL FOR PROPANE ACTIVATION OVER H-ZSM5

X. Wang^{1,2}, H. Carabineiro², M.A.N.D.A. Lemos², F. Lemos², F. Ramôa Ribeiro²

¹*Dalian University of Technology, Institute of Industrial Catalysis,
116012 Dalian, China*

²*Instituto Superior Técnico, Centro de Engenharia Biológica e Química, Av. Rovisco Pais,
1049-001 Lisboa*

1. INTRODUCTION

Upgrade of light saturated hydrocarbons has received great deal of attention, strongly enhanced by the widespread use of natural gas. Due to their chemical inertness, light alkanes are hardly reactive and therefore their use is most often confined to combustion chambers. Alternative pathways towards valuable products are highly desired [1] and require the use of catalysts able to promote those hard transformations in an economical feasible way. Efficient routes for catalyst design and development for activation of light alkanes require a better understanding of the surface phenomena taking place at the catalyst surface. The microkinetic approach should be able to provide guidance in the search and tuning of materials having specific catalytic properties, by studying the correlations between surface phenomena in terms of elementary reaction steps and physico-chemical properties of the catalyst. Microkinetics differs from classical macrokinetics in that it provides detailed knowledge on the surface phenomena involving reactants, products and intermediates while the later is limited to a global rate expression which, although useful in reactor design, does not reflect the underlying chemistry of the surface processes. Knowledge on these surface processes supported by characterisation techniques will provide a better understanding on the origin of the catalytic

behaviour and thus assist in the design of improved catalysts (catalytic reaction synthesis [2]). Since no assumptions on rate limiting steps are involved, detailed microkinetic models are also valid over a wide range of reaction conditions and thus find interesting applications for predictive control purposes.

A microkinetic model for activation of propane over a H-ZSM5 catalyst is presented which successfully predicts products' yields with temperature ranging from 350 to 500 °C and propane partial feed pressures from 3 to 9 kPa.

2. EXPERIMENTAL

Catalytic tests were carried in a once-through flow reactor (10 mm ID). Propane (99.90% purity) was dried over a zeolite X bed. 100 mg of a H-ZSM5 catalyst (Si/Al = 30) were pretreated *in situ* in a purified nitrogen flow at 773 K for 4 hours prior to reaction. Reaction was carried at 623, 673, 723 and 773 K under atmospheric pressure. Contact time was kept constant (WHSV = 3.74 h⁻¹) and propane partial pressure was adjusted by dilution in nitrogen flow to obtain 3.0, 5.1, 7.1 and 9.1 kPa. The reactor outlet was directed through a heated line to a sampling valve connected to a gas chromatograph equipped with a 50 m KCl/Al₂O₃ PLOT-type column and a flame ionization detector. Preliminary tests revealed negligible thermal reactions products as well as no irreversible deactivation under reaction conditions. Conversions were kept low (under ca. 12%) in order to ensure differential mode operation.

3. MICROKINETIC MODEL

The microkinetic model consists of a sequence of elementary reaction steps (table 1) involving gas phase molecules as well as adsorbed carbocations. Free Brönsted acid sites are represented by "H⁺". Inclusion of alkyl transfer reactions is justified in order to account for the observed second partial order behaviour on reactant's concentration for methane. All reactions were considered to be irreversible due to the low conversions and strong dilution in nitrogen. Mass balances are established assuming steady-state behaviour for gas-phase (eq. 1) and adsorbed (eq. 2) species, respectively:

$$0 = F_{i,0} - F_i + \sum_j r_j(\bar{y}, T)W \quad (1)$$

$$0 = \sum_j r_j(\bar{y}, T) W \quad (2)$$

The resulting non-linear system is solved by proper numerical methods (IMSL routines for FORTRAN) for each set of temperature and reactant's feed pressure. Kinetic constants are assumed to follow the Arrhenius law. In order to reduce the number of adjustable parameters Evans-Polanyi relations were used (eq. 3).

$$E_a = E_0 + \alpha \Delta H_r \quad (3)$$

For each family of similar reactions as shown in table 1 (protolytic cracking excluded) we took $\alpha = 0.5$ and varied E_0 . Reaction enthalpies were calculated from standard enthalpies of formation without further correction. Standard enthalpies of formation of free carbocations are not experimentally available and therefore were calculated from proton affinities of the corresponding olefins and from the proton's enthalpy of formation. Kinetic parameters were obtained by fitting the model against a wide set of experimental data using a micro-genetic algorithm (by D. Carroll) with binary encoding and further refined using Nelder-Mead.

Table 1. Proposed microkinetic mechanism.

protolytic cracking	$C_3 + H^+ \rightarrow C_3^+ + H_2$ $C_3 + H^+ \rightarrow C_2^+ + C_1$	chain-growth	$C_2^= + C_3^+ \rightarrow C_5^+$ $C_2^= + C_5^+ \rightarrow C_7^+$ $C_3^= + C_2^+ \rightarrow C_5^+$ $C_3^= + C_4^+ \rightarrow C_7^+$
hydride transfer	$C_3 + C_2^+ \rightarrow C_3^+ + C_2$ $C_3 + C_4^+ \rightarrow C_3^+ + C_4$ $C_3 + C_5^+ \rightarrow C_3^+ + C_5$	desorption	$C_2^+ \rightarrow C_2^= + H^+$ $C_3^+ \rightarrow C_3^= + H^+$ $C_4^+ \rightarrow C_4^= + H^+$ $C_5^+ \rightarrow C_5^= + H^+$ $C_6^+ \rightarrow C_6^= + H^+$ $C_7^+ \rightarrow C_7^= + H^+$
alkyl transfer	$C_3 + C_3^+ \rightarrow C_1 + C_5^+$ $C_3 + C_3^+ \rightarrow C_2 + C_4^+$ $C_3 + C_3^+ \rightarrow C_2^+ + C_4$ $C_3 + C_2^+ \rightarrow C_1 + C_4^+$		

4. RESULTS

Calculated and experimental molar yields against conversion are plotted in figure 1. Propylene dominates the products distribution at low temperatures while at higher temperatures methane and ethylene prevail. The later are produced in equimolar amounts as revealed by initial selectivities obtained by extrapolating molar yields at zero conversion.

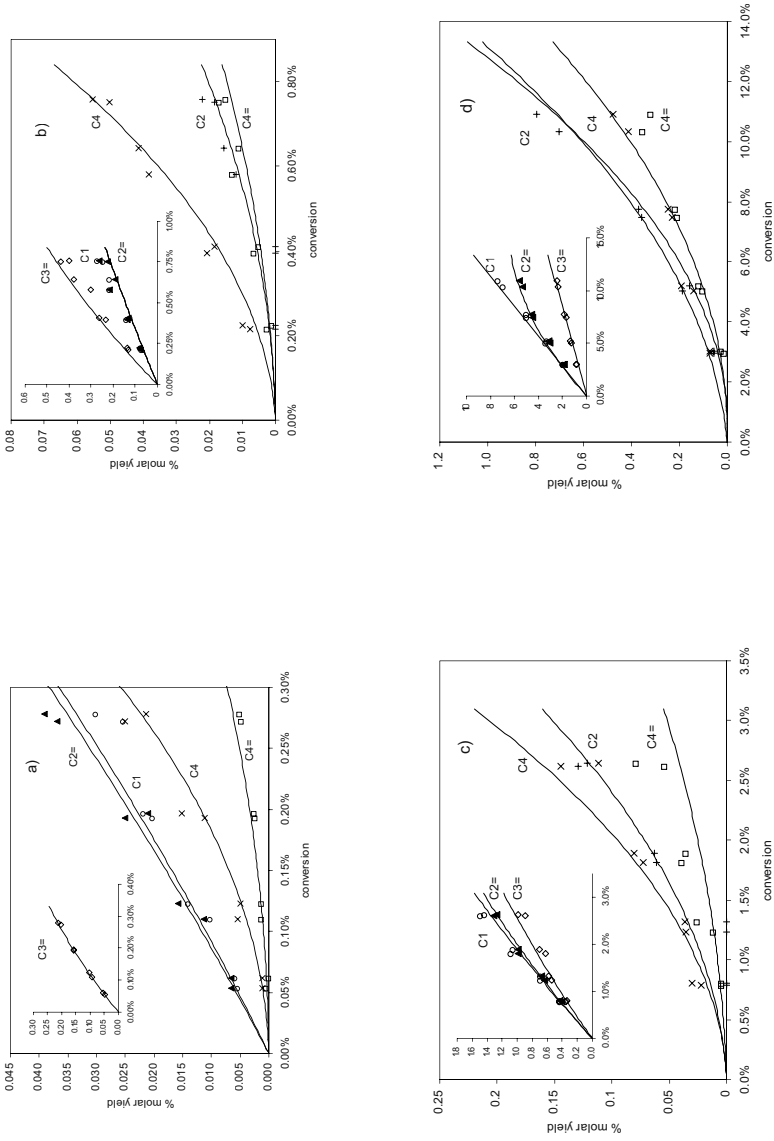


Figure 1. Experimental (dots) and calculated (—) molar product yields against conversion for propane cracking over H-ZSM5 at a) 350°C; b) 400°C; c) 450°C; d) 500°C. (WHSV = 3.74 h⁻¹, propane partial feed pressure 3.0, 5.1, 7.1, 9.1 kPa).

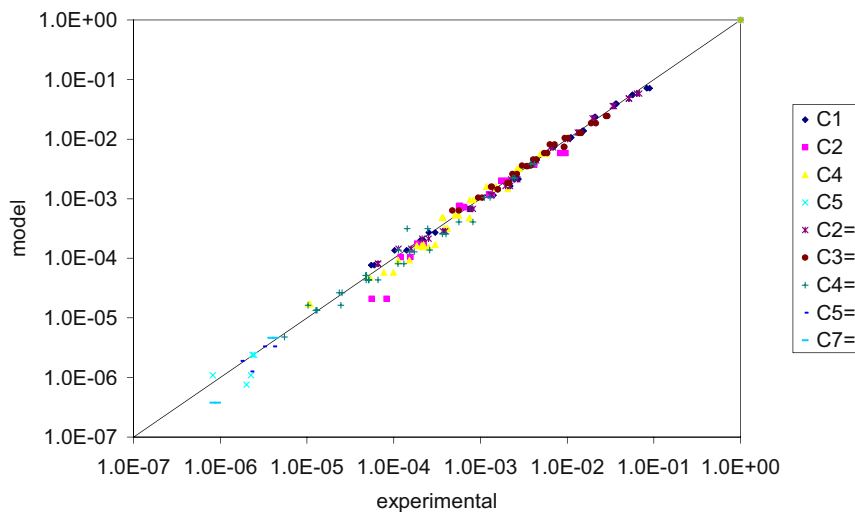


Figure 2. Parity plot between model response and experimental data.

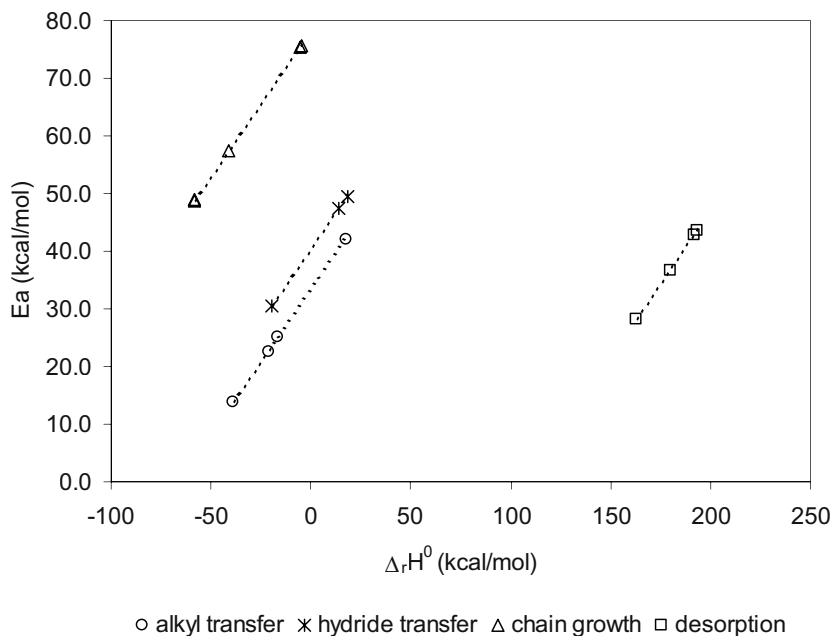


Figure 3. Evans-Polanyi relations obtained from model fitting against experimental data.

5. CONCLUSIONS

The proposed microkinetic model is able to describe propane activation over H-ZSM5 in the reactant's partial pressure and temperature range considered. Evans-Polanyi relations are effective in reducing the number of adjustable parameters. According to the microkinetic model, the activation energy for C-C bond breaking (155 kJ/mol) is substantially higher than the energy required to break a C-H bond in propane (63 kJ/mol).

6. ACKNOWLEDGEMENTS

We would like to thank the financial support from “Fundação para a Ciência e Tecnologia” through the scholarship SFRH/BD/6855/2001 attributed.

7. REFERENCES

- [1] E.G. Derouane, J. Haber, F. Lemos, F. Ramôa Ribeiro, M. Guisnet (Eds.), “Catalytic Activation and Functionalisation of Light Alkanes”, NATO ASI Series 3, Vol 44, Kluwer Academic Publishers, Dordrecht, 1998.
- [2] Dumesic, J. A., Rudd, D. F., et al, *The Microkinetics of Heterogeneous Catalysis*, American Chemical Society, Washington, DC 1993 (ISBN 0-8412-2214-2)

Chapter 22

¹³C MAS NMR MECHANISTIC STUDY OF THE INITIAL STAGES OF PROPANE ACTIVATION OVER Zn/H-MFI CATALYST

Yu.G. Kolyagin¹, J. Quartararo², E.G. Derouane³, F. Fajula⁴, I.I. Ivanova¹

¹Chemistry Dept., Moscow State University, Moscow, Russia

²Department of Chemistry, University of Liverpool, Liverpool L69 7ZD

³Universidade do Algarve, Algarve, Portugal

⁴UMR 5618 ENSCM/CNRS, Montpellier, France

Abstract: ¹³C MAS NMR was performed *in situ* to investigate the early stages of propane activation over Zn-modified H-MFI catalyst. Propane 2-¹³C and propane 1-¹³C were used as labelled reactants. The reactivity of propane 2-¹³C over the parent H-MFI was studied for comparison. While on H-MFI, the initial step of propane transformation involved ¹³C label scrambling, on Zn/H-MFI, formation of propene oligomers, methane and ethane was observed. The results confirmed the monofunctional carbonium ion type mechanism of propane activation suggested previously for H-MFI catalysts and pointed to bifunctional mechanism over Zn/H-MFI, involving propane dehydrogenation on Zn sites, propene oligomerization on acidic sites and propane hydrogenolysis on Zn sites.

Key words: Propane activation, ¹³C MAS NMR, zeolite ZSM-5, reaction mechanism.

1. INTRODUCTION

The mechanism of propane activation over MFI catalysts has been thoroughly studied by *in situ* MAS NMR during the last years [1-3]. The attention was focused mainly on acidic [1,2] and Ga-containing zeolites [3]. For Zn/MFI catalysts, the main reaction pathways were also established. However, no direct information on the mechanism of various steps, especially of the initial stages of propane activation, is available as yet.

This study aims to clarify the mechanism of propane activation over Zn/H-MFI using *in situ* ^{13}C MAS NMR technique.

2. EXPERIMENTAL

MFI zeolite with Si/Al = 35 was prepared as described elsewhere [4]. Acidic catalyst (H-MFI) was obtained by ion exchange of starting zeolite with 0.1 M NH_4NO_3 and subsequent calcination at 823 K for 6 h. Zn-containing catalyst (Zn/H-MFI) with Zn content of 8 % was prepared via impregnation with aqueous solutions of $\text{Zn}(\text{NO}_3)_2$ and subsequent drying at 393 K for 15 h and calcination at 823 K for 2 h.

^{13}C MAS NMR measurements were carried out on ADX-200 and ADVANCE-400 Bruker spectrometers operating at 50.3 and 100.6 MHz, respectively. Controlled-atmosphere experiments were performed in sealed pyrex NMR cells containing catalysts and adsorbates and fitting precisely into 7 mm Bruker zirconia rotors. Propane $1\text{-}^{13}\text{C}$ (99,9% enriched) and propane $2\text{-}^{13}\text{C}$ (99,9% enriched) purchased from ICON Services Inc were used as labelled reactants. In a typical NMR experiment, the sealed NMR cell was rapidly heated to the selected temperature and maintained at this temperature for a given period of time. The NMR spectrum was recorded after quenching of the sample cell down to 293 K. A more detailed description of *in situ* MAS NMR experiments is given elsewhere [1].

3. RESULTS AND DISCUSSION

Figure 1 shows ^{13}C MAS NMR spectra obtained at the early stages of propane $2\text{-}^{13}\text{C}$ reaction over H-MFI catalyst. The initial spectrum observed immediately after adsorption of propane- $2\text{-}^{13}\text{C}$ contains the only resonance at about 17 ppm, corresponding to the initially labelled methylene group of propane. After heating the sample up to at 598K, a signal at ca. 15.8 ppm corresponding to propane methyl group appears. No other significant signals were observed in the spectrum at this reaction step. Hence, the only rearrangement taking place at the beginning of the reaction is ^{13}C scrambling in propane molecule. Further heating of the sample at 623 and 648 K leads to the formation of i-butane ($\delta = 23.6$ ppm), ethane ($\delta = 5.9$ ppm) and methane ($\delta = -8.0$ ppm).

The results obtained over H-MFI catalyst are in line with our earlier observations [1] and are consistent with carbonium ion mechanism proposed previously (Fig. 2). According to this mechanism, propane activation over

H-MFI catalysts occurs via its protonation leading to carbonium ion type transition states, which further evolve via different reaction pathways involving ^{13}C scrambling in propane, cracking, dehydrogenation or disproportionation towards butane and ethane.

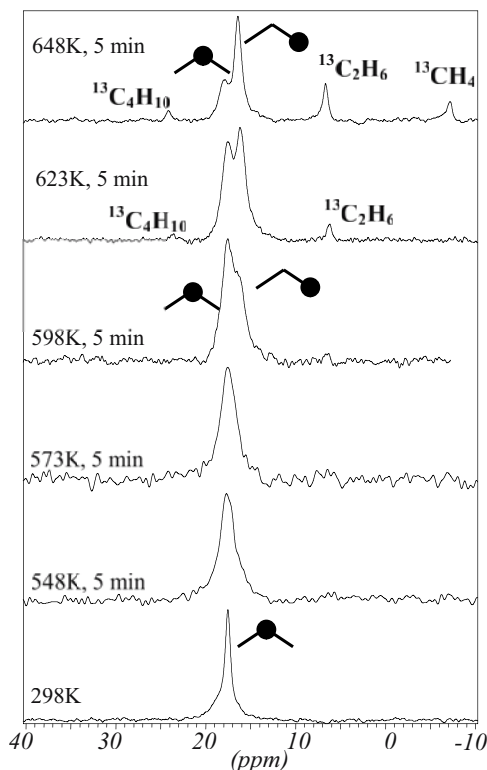


Figure 1. ^{13}C MAS NMR spectra observed in course of propane 2- ^{13}C reaction over H-MFI catalyst.

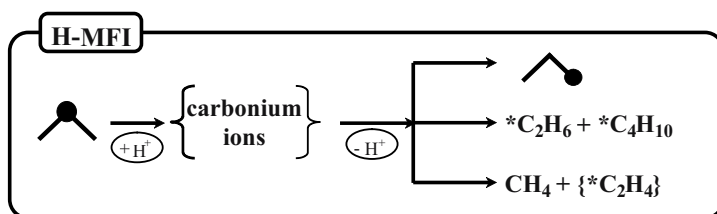


Figure 2. Initial products and intermediates observed at the initial steps of propane reaction over H-MFI catalyst

Modifying of H-MFI zeolite with Zn leads to significant changes in propane 2-¹³C reactivity (Fig. 3a):

- The reaction starts at much lower temperature (523 K instead of 598 K);
- No ¹³C scrambling is observed at the initial stages of propane conversion;
- The resonance line at ca. 19 ppm, which was not observed previously, appears at the onset of the reaction;
- No butanes and methane are observed at the beginning of the reaction, ethane, evidenced by the line at ca. 6.5 ppm, is the only labelled primary product.

The experiments carried with propane 1-¹³C are complementary to those observed with propane 2-¹³C (Fig. 3b):

- The reaction starts at 523 K;
- No ¹³C scrambling is observed;
- A broad resonance line at ca. 20 ppm appears at the onset of the reaction;
- Labelled ethane ($\delta = 6.5$ ppm) and methane ($\delta = -7$ ppm) are observed in equal amounts at the beginning of the reaction.

Formation of equal amounts of initially labelled methane and ethane from propane 1-¹³C and only labelled ethane from propane-2-¹³C points to the high probability of propane hydrogenolysis at the initial steps of the reaction. Such reaction pathway can occur on Zn-species, however, the source of dihydrogen required for this reaction pathway is not clear.

To understand the nature of the signals at ca. 19 and 20 ppm, ¹³C CP MAS NMR spectra were recorded at the onset of propane 1-¹³C and propane 2-¹³C conversion over Zn/HMFI (Fig. 4). The intensities of the lines at 19 and 20 ppm increased significantly with cross polarization, suggesting that these signals correspond to very rigid species attached to zeolite surface. In addition, another line at ca. 12 ppm became visible in the case of propane 1-¹³C conversion. The chemical shifts of the lines corresponding to the rigid species observed at the onset of propane 1-¹³C and propane 2-¹³C reactions suggest that they could be attributed to propene oligomers labelled either at methyl ($\delta = 20$ and 12 ppm) or at methylene ($\delta = 19$ ppm) groups, respectively. Observation of propene oligomers points to propane dehydrogenation occurring at the initial steps of the reaction, this step also accounts for the source of dihydrogen required for hydrogenolysis.

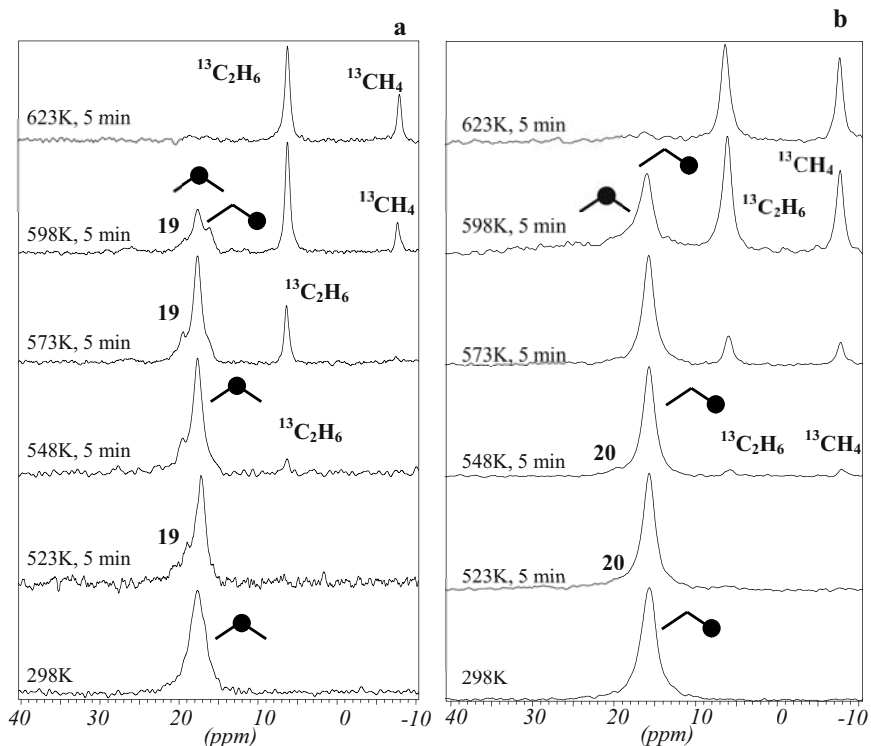


Figure 3. ^{13}C MAS NMR spectra observed in course of propane 2- ^{13}C (a) and propane 1- ^{13}C (b) reactions over Zn/H-MFI catalyst.

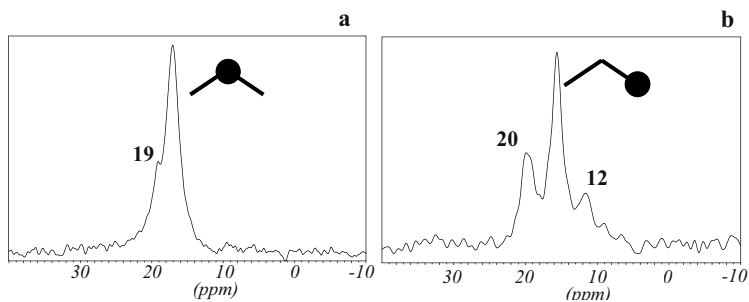


Figure 4. ^{13}C CP MAS NMR spectra observed after reactions of propane 2- ^{13}C (a) and propane 1- ^{13}C (b) over Zn/H-MFI at 523 K for 5 min.

The scheme presented in Fig. 5 rationalizes further all the above observations. Propane first undergoes dehydrogenation over Zn sites

towards propene and dihydrogen. Propene is further oligomerizes on acidic sites, while dihydrogen takes part in hydrogenolysis of another propane molecule over Zn sites. Formation of propene oligomers accounts for further aromatisation and explains higher aromatization activity of Zn-containing zeolites with respect to pure acidic.

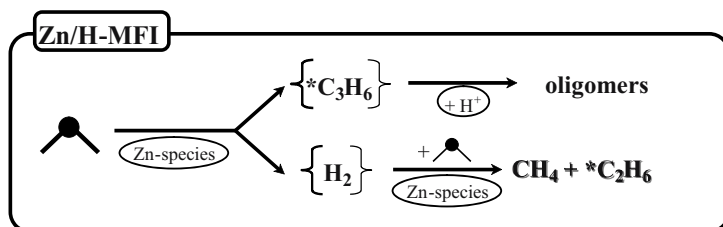


Figure 5. Initial products and intermediates observed at the initial steps of propane reaction over Zn/H-MFI catalyst.

4. CONCLUSIONS

It is proposed that propane activation over Zn-ZSM-5 catalysts occurs via a bifunctional mechanism involving propane dehydrogenation on Zn sites, oligomerization of propene on acidic sites and hydrogenolysis of propane on Zn sites.

5. ACKNOWLEDGEMENTS

The authors thank NATO Science for Peace Programme for the research grant. I.I. Ivanova is grateful to RFBR and Science support foundation for the financial support. Yu. G. Kolyagin thanks Haldor Topsoe A/S for a PhD fellowship.

6. REFERENCES

- [1] I.I. Ivanova, E.B. Pomakhina, A.I. Rebrov and E.G. Derouane, Topics in Catalysis 6 (1998) 49.
- [2] A.G. Stepanov, Russian Chemical Reviews, 068 (1999), 007, 563-580.
- [3] E.G. Derouane, S.B. Abdul Hamid, I.I. Ivanova, N. Blom and P.E. Højlund-Nielsen, J. Mol. Catal. 86 (1994) 371.
- [4] B. Czerwinska, J. Berak, J. Pieniasek, J. Mejsner, Polish Patent PRL 1215.146, 1981.

Chapter 23

DEHYDROGENATION OF PROPANE OVER CHROMIUM-BASED CATALYSTS

P. Michorczyk, J. Ogonowski, D. Ralowicz

*Institute of Organic Chemistry and Technology, Cracow University of Technology,
Warszawska 24, 31-155 Kraków, Poland*

1. INTRODUCTION

Catalytic dehydrogenation of light hydrocarbons has a considerable industrial impact, because it represents a method to obtain unsaturated hydrocarbons from feedstocks of the corresponding paraffins. Nowadays, the dehydrogenation of propane has become very important. Propene is used in chemical industry for the synthesis of cumene, acrylonitrile and high purity polypropylene. However, this reaction is limited by chemical equilibrium, and according to Le Chatelier's principle, higher conversion will require either lower pressures or higher temperatures. Furthermore, the high temperature favors thermal cracking reaction to coke and light hydrocarbons.

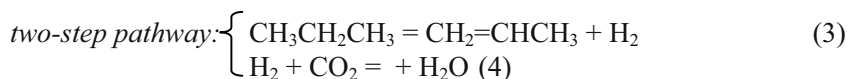
An attractive alternative is a catalytic oxidative dehydrogenation of propane (Eq. 1) since it does not present either thermodynamic limitations of the thermal dehydrogenation or typical catalysts deactivation.



Recently, a great variety of catalysts have been proposed for this reaction [1-3]. However, total oxidation reaction proceeds in parallel to the dehydrogenation reaction. Consequently, selectivity for the desired product decreases to a great extent.

In order to enhance the propene selectivity, it is interesting to study the same reaction by replacing oxygen by mild oxidant (CO_2 , N_2O) [4, 5].

The role of carbon dioxide in dehydrogenation is still not clear. There are two possible routes for propene formation in the presence of carbon dioxide (Eq. 2-4).



In the present work, we have studied the dehydrogenation of propane to propene over $\text{CrO}_x/\text{SiO}_2$ in the presence and absence of carbon dioxide. We also discuss the influence of promoter on catalytic activity and stability.

2. EXPERIMENTAL

The starting $\text{CrO}_x/\text{SiO}_2$ catalyst was prepared by equilibrium adsorption method. For the adsorption method, the support was contacted with a large amount of chromium (III) nitrate (POCH, Poland) solution at room temperature for seven days. The pH of the solution was kept at 4.5. After that the catalyst was dried at 397 K for 2 h and calcined at 923 K for 3 h in air. The potassium promoted $\text{CrO}_x/\text{SiO}_2$ catalysts were obtained by incipient wetness method. The $\text{CrO}_x/\text{SiO}_2$ catalyst was impregnated successively with aqueous solutions of KNO_3 (POCH, Poland), to yield the K/Cr atomic ratios of 0.2 or 1.0. After the impregnation, the catalysts were dried at 397 K for 2 h and calcined at 923 K for 3 h in air.

The dehydrogenation of propane to propene in the presence and absence of CO_2 was carried out at atmospheric pressure in a flow-type stainless steel reactor packed with 0.5 g of the catalyst. The feed was a mixture of 25:5 (ml/ml) of $\text{CO}_2/\text{C}_3\text{H}_8$. The total flow rate was 30 ml/min. The catalysts were first degassed in a helium stream at 873 K and then the reaction was started at this temperature. The reactants and products were analysed on-line using two gas chromatographs. One of them was equipped with a glass column packed with 3m x 3mm Porapak Q and a flame ionization detector. It was used to analyse the hydrocarbons (C_1 - C_3). The second chromatograph was equipped with a stainless steel column packed with 3x3mm Carboxen 1000 and, a thermal conductivity detector (for CO , H_2 and CO_2 analyses).

3. RESULTS AND DISCUSSION

3.1 Thermodynamic considerations

As shown in Table 1, the equilibrium conversion of propane can be improved by: (i) diluting the reactants with an inert gas, (ii) coupling the dehydrogenation reaction with the reverse water-gas shift and (iii) oxidative dehydrogenation of propane with oxygen.

Table 1. Percentage conversions at equilibrium for dehydrogenation and oxydehydrogenation of propane at atmospheric pressure and 873 K.

Process	Molar ratio CO ₂ (inert)/C ₃ H ₈	Equilibrium conversion of propane (%)
Dehydrogenation of propane	-	50
Dehydrogenation in atmosphere of inert gas	1:1	59
Oxidative dehydrogenation by O ₂	stoichiometric	100
Dehydrogenation in the presence of CO ₂ ^a	1:1	70

^a Calculation for two step pathway.

The introduction of inert gas at the molar ratio of (inert gas)/propane = 1/1 increases the equilibrium conversion of propane from 50 % to 59 % at 873 K. The propane conversion can be also improved by coupling the reaction with the water-gas shift (Eq.4). Carbon dioxide consumes hydrogen produced in the reaction 2. As the result, the dehydrogenation equilibrium is shifted towards products.

In the oxidative dehydrogenation of propane by O₂ (Eq.1) the shift towards products is complete (Tab.1).

3.2 Catalytic performance

The results obtained for the dehydrogenation of propane in the presence of CO₂ or Ar over the CrO_x/SiO₂ catalyst are shown in Table 2.

Table 2. Catalytic activity of CrO_x/SiO₂ catalysts^a

Catalyst	S _{BET} (m ² g ⁻¹)	Feed gas	Conv. (%)		Selectivity (%)		
			C ₃ H ₈	C ₃ H ₆	C ₂ H ₆	C ₂ H ₄	CH ₄
CrO _x (1wt%)/SiO ₂	333	C ₃ H ₈ /Ar	18.8	91.1	0.0	4.3	4.5
		C ₃ H ₈ /CO ₂	36.5	90.9	1.9	2.7	4.6

^a Reaction conditions: 873 K, 0.5 mg of catalysts, total flow rate 30 ml/min, CO₂:C₃H₈ = 5:1, reaction time 10 min..

As seen from Table 2, after 10 min of reaction propane conversion reached 36.5 %, while in the presence of argon under the same conditions only 18.8 % conversion of propane was achieved. The selectivities of propene in both processes were similar.

The catalytic stability of the unpromoted and potassium promoted catalysts is shown in Figure 1. All the catalysts exhibit deactivations with similar variation patterns.

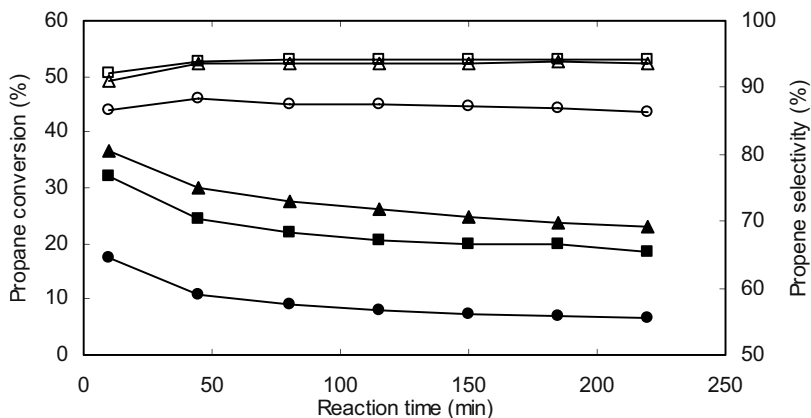


Figure 1. Propane conversion and propene selectivity on potassium promoted and unpromoted catalysts as a function of reaction time. Opened symbols: propene selectivity, solid symbols: propane conversion, (Δ) unpromoted $\text{CrO}_x/\text{SiO}_2$, potassium promoted $\text{CrO}_x/\text{SiO}_2$ catalyst (□) at K/Cr ratio = 0.2 and (○) at K/Cr ratio = 1. Reaction conditions are in the text.

The propane conversion and propene selectivity decrease with increasing K/Cr atomic ratio. Over the $\text{CrO}_x/\text{SiO}_2$ catalyst with K/Cr ratio of 0.2, the propane conversion and propene selectivity were 32.3 % and 90.9 %, while only 17.6 % and 86.6 % respectively in the case of $\text{CrO}_x/\text{SiO}_2$ with K/Cr ratio = 1. These results suggest that the excess of potassium blocks active sites for dehydrogenation of propane. However, the rate of coke deposition on potassium-promoted $\text{CrO}_x/\text{SiO}_2$ catalyst was much less than that on the unpromoted $\text{CrO}_x/\text{SiO}_2$ catalyst. After 4 h reaction time the mass of coke on the unpromoted catalyst was 1.08 wt % while only 0.23 wt % in the case of potassium promoted catalyst with the ratio Cr/K=1.

4. CONCLUSIONS

The obtained results lead to the following conclusions:

- Thermodynamic considerations show that the equilibrium conversion of propane to propene in the presence of CO₂ is higher than in the presence of an inert gas.
- Carbon dioxide exerts promoting effect on dehydrogenation of propane over CrO_x/SiO₂. The yield of propene in the presence of CO₂ is practically twice that in its absence.
- Proper modification of the acidity properties of the CrO_x/SiO₂ catalyst can suppress the formation of coke. However, the introduction of potassium to the CrO_x/SiO₂ catalyst leads to loss of the catalytic activity.

5. ACKNOWLEDGEMENTS

This research was partly supported by the State Committee for Scientific Research, KBN, under Project No. PB-1089/TO9/2003/24.

6. REFERENCES

- [1] Abello, M., Gomez, M., Cadús, L. (1996) *Ind. Eng. Chem. Res.*, 35, 2137.
- [2] Grzybowska, B., Słoczyński, J., Grabowski, R., Wcisło, K., Kozłowska, A., Stoch, J., Zieliński, J. (1998) *J. Catal.*, 178, 687.
- [3] Bettahar, M., Costentin, G., Savary, L., Lavalley, J. (1996) *Appl. Catal. A: General* 145, 1.
- [4] Vereshchagin, S., Kirik, N., Shishkina, N., Morozov, S., Vyalkov, A., *Stud. Surf. Sci. Catal.*, 130, 881.
- [5] Michorczyk, P., Ogonowski, J. (2003) *React. Kinet. Catal. Lett.*, 78, 41.

Chapter 24

CATALYTIC OXIDATION OF METHANOL TO FORMALDEHYDE

A. H. Yılmaz, F. S. Atalay, S. Atalay

Ege University, Faculty of Engineering, Chemical Engineering Department, Bornova-Izmir-Turkey

Abstract: Methanol is a clean burning fuel, containing no sulphur or nitrogenous materials. It produces power with very low emissions compared to those of a natural gas-fired, combined-cycle unit. Methanol can also be used as a feedstock for more sophisticated processes in the petrochemical industry. In this study, catalytic oxidation of methanol to formaldehyde was investigated. For this purpose, laboratory type, fixed bed catalytic reactor was used. For this gas-phase reaction iron-molybdate catalysts supported by silica or alumina were used. On silica and alumina supports, different Mo/Fe ratios were investigated for three different residence times (W/FA0) and six different temperatures were tried. The analysis of liquid product was performed by using gas chromatograph. From the results of GC analysis and CO₂ analyzer, conversion of methanol to formaldehyde, total conversion and selectivity to formaldehyde were obtained. After the determination of optimum operating conditions for this reaction, kinetic study was performed.

1. INTRODUCTION

A raw material for the methanol synthesis is natural gas. The technology for making methanol from natural gas is already in place and requires only efficiency improvements and scale-up to make methanol an economically viable alternative transportation fuel. Methanol is an inherently safe fuel and can be handled conventionally at the user's site without the substantial capital investment in special purpose tankers or unloading facilities required by other fuel systems. Methanol is an important industrial material and it is used in the manufacture of formaldehyde.

Formaldehyde, $\text{H}_2\text{C}=\text{O}$, is the first of the series of aliphatic aldehydes. It was discovered by Butlerov in 1859 and has been manufactured since the beginning of this century. Annual worldwide production capacity now exceeds 12.10^6 metric ton (calculated as 37 % solution). Because of its relatively low cost, high purity, and variety of chemical reactions, formaldehyde has become one of the world's most important industrial and research chemicals.

Formaldehyde's importance is proved by the fact that it is commonly used by industry to manufacture building materials and numerous household products. Because of its water resistance, formaldehyde is used in the manufacture of grocery bags, paper cups and plates, waxed paper, facial tissues, napkins, paper towels, and sanitary napkins. Formaldehyde is also used in cosmetics and fabric softeners besides in agriculture for seed treatment.

2. MATERIALS AND METHODS

Formaldehyde is produced industrially from methanol by three processes. First one is partial oxidation and dehydrogenation with air in the presence of silver crystals, steam and excess methanol at $680\text{-}720^\circ\text{C}$ (BASF Process, methanol conversion is about 97-98 %). Second one is dehydrogenation with air in the presence of crystalline silver, or silver gauze, steam and excess methanol at $600\text{-}650^\circ\text{C}$ (primary conversion of methanol is 77-87 %). The conversion is completed by distilling the product and recycling the unreacted product. Last process is the oxidation only with excess air in the presence of a modified iron-molybdenum-vanadium oxide catalyst at $250\text{-}400^\circ\text{C}$ (methanol conversion is 97-98 %). By-products are carbon monoxide and dimethyl ether, in addition to small amounts of carbon dioxide and formic acid.

In this study, the production of formaldehyde via catalytic oxidation of methanol was investigated by using fixed bed catalytic reactor. The experimental set-up used for the experiments was shown in Figure 1.

The aim of the study is to determination of the optimum conditions by changing catalyst type, support type, residence time and temperature. For this gas-phase reaction iron-molybdate catalysts ($\text{Mo}/\text{Fe}=1.5; 3; 5$), on two different supports, silica and alumina, were used. Experiments were performed at three different methanol flowrates. 5 g catalyst amount was kept constant and by changing methanol flowrates, three different residence times (W/F_{A0}) of 50.63, 33.75 and 20.25 g catalyst.h/mol methanol were tried. For all experiments temperature was changed between the range of

250-375°C. After determining the optimum conditions for this reaction, kinetic study searching by the effects of external and internal mass transfer resistances and the elaboration of suitable reaction mechanisms and kinetic constants were obtained.

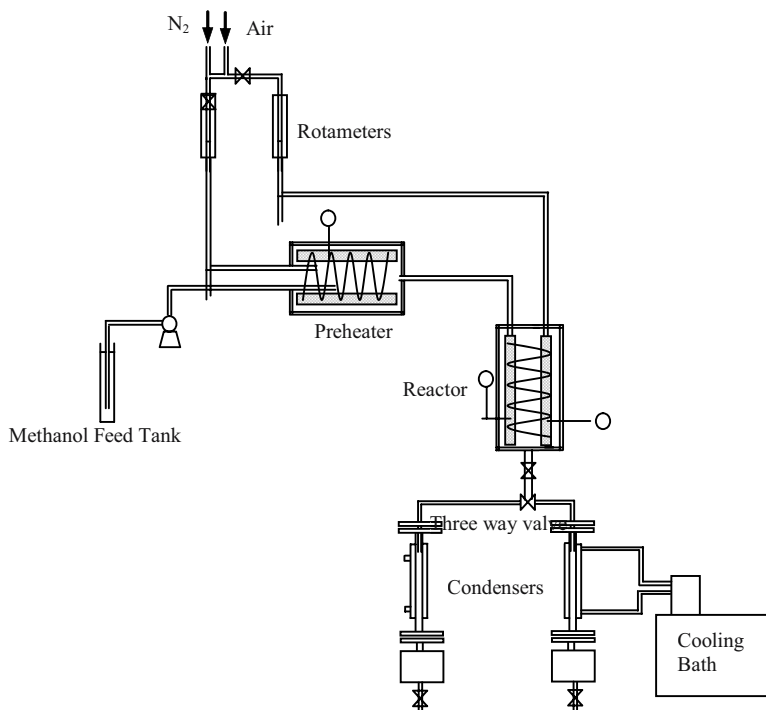


Figure 1. Experimental Set-up

3. RESULTS

In methanol oxidation, selectivity to formaldehyde and total conversion depend on the reaction temperature, residence time, Mo/Fe ratio of the catalyst and the type of the support. To study the effect of each parameter, the specified parameter is changed, as the others are being kept constant.

After calculations, it was found that, for all catalyst and support types, as temperature was increased, total conversion increased whereas selectivity to formaldehyde decreased. As Mo/Fe ratio was increased, it was seen that both total conversion and selectivity increased. At constant temperature,

total conversion and selectivity increased by increased residence times. Finally, silica support gave better results for conversion and selectivity than that of alumina support for all experiments.

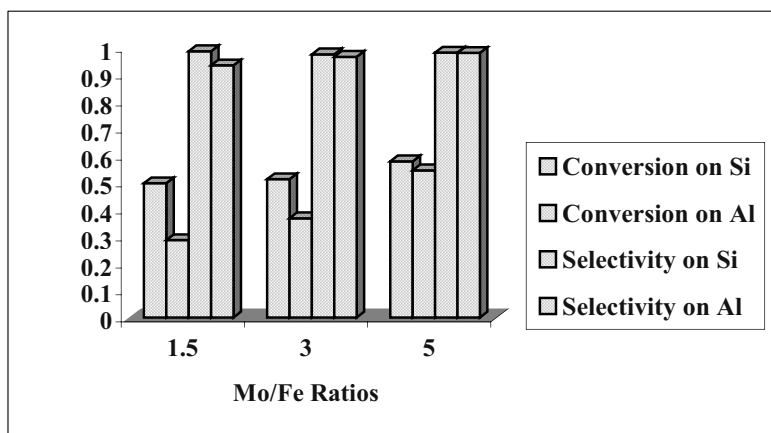


Figure 2. Change in total conversion and selectivity with respect to Mo/Fe ratios, for both silica and alumina supports at 275°C and $W/F_{A0}=20.25$ g/(mol/h). Kinetic study was started by searching for the effect of external diffusion and it was seen that the mass transfer from gas phase to the catalyst surface was taken as negligible when the air flowrate exceeded 0.03 mole/min. Then, internal diffusion effect was studied. For the kinetic study, six reaction mechanisms were searched for and it was obtained that this reaction was controlled by surface reaction.

4. REFERENCES

- [1] Cairati, L., di Fiore, L., Catalyst for the Oxidation of Methanol to Formaldehyde and a Method of Preparing the Catalyst", (1980), US Patent (4,181,629)
- [2] Carley, A.F., Davies, P.R., Mariotti, G.G., Read, S., Surface Science, 364 (1996), L525-L529
- [3] Fukui, K., Motoda, K., Iwasawa, Y., J. of Physical Chemistry B., 102 (1998), p. 8825-8833
- [4] Lafyatis, D.S., Creten, G., Froment, G.F., Applied Catalysis A: General, 120 (1994), 85-103
- [5] Burcham, L.J., Wachs, I.E., Catalysis Today 49 (1999), 467-484
- [6] Quina, M.M.J., Ferreira, R.M.Q., Chemical Eng. Science, 55 (2000), 3885-3897
- [7] Santacesaria, E., Morbidelli, M., Chemical Engineering Science, 36(5), p. 909-918, 1981
- [8] Soares. A.V.P., Portela. M.F., Kiennemann. Hilaire. L., Millet. J.M.M., Applied Catalysis A: General. 206 (2001). 221-229

- [9] Ullman's Encyclopedia of Industrial Chemistry, "Formaldehyde", Edited by W. Gerhartz, Vol. A-11, 1988
- [10] Valente, N.G., Cadús, L.E., Gorrioz, O.F., Arrúa, L.A., Rivarola, J.B.; Applied Catalysis A: General, 153(1997), p. 119-132
- [11] Wang, C.T., Willwy, R.J., Journal of Non-Crystalline Solids, 225(1998), 173-177
- [12] Yao, S., Yang, F.O., Shimamura, S., Sakurai, H., Tabat, K., Suzuki, E., Applied Catalysis A: General, 198 (2000), 43-50
- [13] <http://www.scidiv.bcc.ctc.edu/wv/Physical.html>
- [14] <http://www-personal.engin.umich.edu/~zjohn/Formaldehyde.html>.
- [15] <http://www.ag.ohio-state.edu/~ohioline/cd-fact/0198.html>.
- [16] <http://www.ethanol-gec.org/clean/cf05.htm>
- [17] <http://www.sciencedaily.com/releases/2003/03/030324064035.htm>
- [18] <http://www.epa.gov/otaq/07-meoh.htm>

Chapter 25

CONVERSION OF GAS CONDENSATE OVER METAL-CONTAINING MFI CATALYSTS

A.G. Popov¹, A.V. Smirnov¹, J. Krysiak², M. Derewinski², O.V. Barsukov³, E.G. Derouane⁴, F. Lemos⁵, F. Fajula⁶, I.I. Ivanova¹

¹*Chemistry Dept., Moscow State University, Moscow, Russia*

²*Institute of Catalysis and Surface Chemistry, Krakow, Poland*

³*Electrogorsk Refinery Institute, Electrogorsk, Moscow Reg., Russia*

⁴*Universidade do Algarve, Algarve, Portugal*

⁵*Centro de Engenharia Biologica e Quimica, Instituto Superior Tecnico, Lisbon, Portugal*

⁶*UMR 5618 ENSCM/CNRS, Montpellier, France*

Abstract: The conversion of gas condensate has been studied over monofunctional acidic MFI zeolites and bifunctional Zn-, Co-, Ni- and Mo-containing MFI catalysts. The active sites were characterized by IR spectroscopy of adsorbed pyridine. The correlation obtained between the catalytic activity of various MFI catalysts and the strength of their Lewis and Brønsted sites suggested that the strong Lewis sites and medium Brønsted are responsible for gas-condensate conversion into gasoline and propane-butane fraction.

Key words: Gas-condensate conversion, gasoline, MFI zeolites, IR spectroscopy,

1. INTRODUCTION

Gas-condensates consist of mixtures of C₃-C₁₂ hydrocarbons, including mainly alkanes and naphthenes, which are obtained in significant amounts as by-products in natural gas production fields. The most perspective route for gas condensate upgrading is based on the one step transformation of gas condensate into high-octane gasoline and propane-butane fraction on zeolite catalysts [1]. The main drawback of this process is rather low yields of gasoline and rapid catalyst deactivation [2]. Modification of zeolite catalysts with metal oxides results in bifunctional catalysts with improved properties:

higher gasoline yields and longer catalyst life times [3]. Further progress in this field will require the determination of the nature and strength of the active sites responsible for various reaction routes and the establishment of the optimal balance between hydro-dehydrogenation function provided by metal oxides and the acidic function provided by zeolite.

In this paper, we aimed to determine the relationship between the catalytic activity of the MFI type zeolite catalysts in gas condensate conversion and the nature and strength of their active sites characterized by IR spectroscopy of adsorbed pyridine.

2. EXPERIMENTAL

MFI type zeolites with Si/Al ratio of 20, 35 and 100 were synthesized following the procedure described in [4]. Monofunctional acidic catalysts were obtained by ion exchange of starting zeolites with 0.1 M NH_4NO_3 and subsequent calcination at 500°C for 6 h. Bifunctional catalysts were prepared via impregnation with aqueous solutions of $\text{Zn}(\text{NO}_3)_2$, $\text{Ni}(\text{NO}_3)_2$, $\text{Co}(\text{NO}_3)_2$ and $(\text{NH}_4)_6\text{Mo}_7\text{O}_{24}$ and subsequent drying at 120°C for 15 h and calcination at 500°C for 2 h. Two commercial hydrotreatment catalysts $\text{NiMo}/\text{Al}_2\text{O}_3$ and $\text{NiMo}/\text{MFI}/\text{Al}_2\text{O}_3$ (NiMo/MFI with 30% of Al_2O_3 matrix) were also studied for comparison. The main characteristics are given in Table 1.

Table 1. Characteristics of the catalysts

Sample	Si/Al	Metal content, wt%	Amount of sites*, $\mu\text{mol/g}$	Lewis/Bronsted sites* ratio
H-MFI-20	20	-	577	0.09
H-MFI-35	35	-	267	0.11
H-MFI-100	100	-	142	0.08
Mo/MFI-35	35	7	269	0.27
Co/MFI-35	35	6	348	4.12
Ni/MFI-35	35	8	317	2.08
Zn/MFI-20	20	8	464	13.06
Zn/MFI-35	35	8	448	6.47
Zn/MFI-100	100	8	224	5.59
$\text{NiMo}/\text{Al}_2\text{O}_3$	-	2; 10	112	2.11
$\text{NiMo}/\text{MFI}/\text{Al}_2\text{O}_3$	35**	4; 13	262	2.91

* Determined from IR spectra of adsorbed pyridine after evacuation at 150°C

** Si/Al ratio of zeolite

The catalysts active sites were characterized by IR spectroscopy of adsorbed pyridine (Py). The IR spectra were recorded on Nicolet 800 spectrometer after adsorption of Py and its evacuation at different

temperatures 150°C, 250°C and 350°C. The concentrations of the Brönsted (B) and Lewis (L) sites were determined on the basis of the absorbencies of the PyB band at 1545 cm⁻¹ and PyL band at 1455 cm⁻¹, respectively, according to the method described by C.A. Emeis [5]. The L and B sites desorbing Py in the temperature regions of 150 -250°C, 250 – 350°C and >350°C were defined as weak (w), medium (m) and strong (s), respectively.

Conversion of gas-condensate was studied in a continuous-flow catalytic unit at 10 atm, 400°C and WHSV of 4.3 h⁻¹. Methane was used as a carrier gas; CH₄/feed molar ratio was of 7. The reaction products were separated into liquid and gas fractions, which were analyzed on GC using 40 m SE-30 capillary columns.

3. RESULTS AND DISCUSSIONS

A series of catalysts prepared contained three monofunctional acidic catalysts with different Si/Al ratio (20, 35 and 100), four bifunctional catalysts with the same Si/Al ratio and different nature of metal oxide introduced (Co, Ni, Zn and Mo) and three Zn-containing catalysts with different Si/Al ratio (Table 1).

Table 2. Contents of weak, medium and strong Lewis and Brönsted sites (μmol/g) determined by IR spectroscopy of adsorbed Py.

	Lewis			Brönsted		
	w	m	s	w	m	s
H-MFI-20	14	0	40	104	85	341
H-MFI-35	8	0	20	8	35	197
H-MFI-100	0	0	14	0	38	97
Mo/MFI-35	45	7	6	126	56	29
Co/MFI-35	34	97	149	23	26	19
Ni/MFI-35	71	44	99	13	48	42
Zn/MFI-20	85	115	231	28	5	0
Zn/MFI-35	97	105	186	31	20	9
Zn/MFI-100	47	40	103	17	17	0
NiMo/Al ₂ O ₃	62	11	3	36	0	0
NiMo/MFI/Al ₂ O ₃	104	38	53	12	27	28

The contents of weak, medium and strong Lewis and Brönsted sites, determined as described in the experimental part are presented in Table 2. As it was expected, monofunctional acidic catalysts are characterized by high contribution of strong Brönsted sites and low content of Lewis sites. Impregnation of H-MFI-35 zeolite with metal (Co, Zn or Ni) nitrates results in drastic decrease of the number of Brönsted sites (Table 2). Simultaneously, the number and strength of Lewis sites increases. These

results can be accounted for by partial ion-exchange of zeolite protons with corresponding cations or deposition of highly dispersed metal oxide particles inside the zeolite pores. Modifying of H-MFI-35 with ammonium molybdate results only in minor decrease of the number of Brönsted sites and slight increase of weak Lewis sites content. $\text{Mo}_7\text{O}_{24}^{6-}$ polyanions cannot undergo ion-exchange, in addition, they are too bulky to enter zeolite channels and therefore molybdenum oxide is most probably agglomerated at the outer surface of zeolite crystals leading only to minor increase of Lewis acidity. Commercial $\text{NiMo}/\text{Al}_2\text{O}_3$ and $\text{NiMo}/\text{MFI}/\text{Al}_2\text{O}_3$ are characterized by comparatively low contents of both Brönsted and Lewis sites. The results of IR spectroscopic studies suggest that in the series of catalysts prepared, Brönsted sites are associated with bridging hydroxyl groups of zeolites, while Lewis sites are mostly due to the cations in the ion-exchange positions of the zeolite or highly dispersed metal oxides species.

The results of gas-condensate conversion over various catalysts are shown in Table 3. The hydrocarbons contained in starting gas-condensate feed and in the products of gas-condensate conversion are divided into four main groups: 1) propane-butane fraction ($\text{C}_3 - \text{C}_4$); 2) C_5+ n-paraffins; 3) C_5+ iso- and cycloparaffins and 4) aromatics. The research octane number (RON) of C_5+ fraction presented in Table 3 is calculated on the basis of product composition as described in [6].

Table 3. Conversion of gas-condensate over various catalysts

Sample	Composition of product, wt%				RON of C_5+ fraction
	$\text{C}_3\text{-C}_4$ gaseous fraction	C_5+ liquid fraction			
		Aromatics	n-Paraffins	Iso- and cycloparaffins	
Gas-condensate	6.8	9.7	33.1	50.4	63.6
H-MFI-20	52.8	26.0	1.3	20.0	91.0
H-MFI-35	45.0	23.5	3.9	27.6	89.6
H-MFI-100	38.2	20.0	7.2	34.6	84.1
Mo/MFI-35	39.4	20.4	7.9	32.3	84.9
Co/MFI-35	38.4	20.3	8.3	33.0	84.0
Ni/MFI-35	39.6	24.5	6.2	29.7	86.3
Zn/MFI-20	30.9	28.2	11.0	30.0	83.5
Zn/MFI-35	29.8	24.0	13.1	33.1	80.6
Zn/MFI-100	25.4	23.0	14.1	37.5	79.5
$\text{NiMo}/\text{Al}_2\text{O}_3$	7.2	9.8	32.6	50.4	65.3
$\text{NiMo}/\text{MFI}/\text{Al}_2\text{O}_3$	24.9	15.5	15.6	44.0	74.7

The catalytic conversion of gas-condensate over the catalysts studied results in transformation of n-, iso- and cycloparaffins into propane-butane fraction and aromatics, leading to the increase of RON of C_5+ liquid

fraction. Monofunctional acidic catalysts show the highest conversion of *n*-paraffins and therefore the highest octane number of C5+ liquid fraction. However, the yield of C5+ fraction over these catalysts is rather low. Modifying of zeolites with metal oxides allows for the increase of the yield of liquid fraction up to 75%, the RON being slightly lower. The best results with respect to the yield and RON of gasoline fraction are obtained over Zn/MFI-35 and Ni/MFI-35 catalysts. NiMo/Al₂O₃ is inactive in gas-condensate conversion, while NiMo/MFI/Al₂O₃ shows intermediate activity between NiMo/Al₂O₃ and zeolite catalyst without matrix.

The relationship between the catalysts activity and the nature and strength of their active sites was examined using the method of regional analysis [7]. According to this method, the catalysts active sites could be divided into *i* regions, within which their activity is considered to be constant and the overall activity over these catalysts can be described by the following equation:

$$A_j = \sum_i a_i * n_{ij} \quad (1)$$

where A_j - overall activity over catalyst *j*, n_{ij} - concentration of acid sites from region *i* on catalyst *j* and a_i - regional activity of the active site from region *i*. Calculation of regional activities a_i , from the series of the equations (1) obtained for a series of catalysts allows to determine the contribution of each type of active sites to the overall conversion.

In our case, active sites were divided into 6 regions as shown in Table 2. The catalytic activity was rationalized in terms of changes of the concentrations of various fractions in the products of gas-condensate conversion and in terms of calculated RON values of C₅+ fraction (Table 3). Since the initial contents of the fractions considered and the initial RON in gas condensate feed were not equal to zero, the model (1) was adjusted in the following way:

$$P_j = P_o + \sum_i p_i * n_{ij} \quad (2)$$

where P_j - content of various fractions or RON value over catalyst *j*, P_o - content of various fractions or RON value in initial gas-condensate at *t*=0 and p_i - regional deviation of the content of various fractions or regional deviation of RON value caused by an active site from region *i*. The regional deviations of the process parameters were calculated using the method of

least-squares on the basis of the results presented in Tables 2 and 3. H-MFI-20 catalyst was not taken into account during calculations, since the concentration n-paraffines over this catalyst approaches zero and the deviation of this parameter could not be estimated properly.

The calculated values of the regional deviations of the main process parameters and correlative coefficients of the model are given in Table 4. The values of the correlative coefficients obtained suggest that the model (2) satisfactory describes the experimental data.

The results of the regional analysis show that strong Lewis sites and medium Brönsted sites play the most important role in gas condensate conversion: medium Brönsted sites are the most effective in deep conversion of paraffins and formation of light alkanes, while strong Lewis sites are responsible for aromatics formation. The later produce lower amounts of light alkanes and therefore favor the higher yields of liquid gasoline fractions. The further catalyst improvement will therefore require the increase of the fraction of strong Lewis sites in the total amount of active sites.

Table 5. Regional deviations (p_i) of the main parameters of the gas-condensate conversion over the active sites of different nature and strength

	$P_{L(w)}$ $\times 10^4$, g/ μ mol	$P_{L(m)}$ $\times 10^4$, g/ μ mol	$P_{L(s)}$ $\times 10^4$, g/ μ mol	$P_{B(w)}$ $\times 10^4$, g/ μ mol	$P_{B(m)}$ $\times 10^4$, g/ μ mol	$P_{B(s)}$ $\times 10^4$, g/ μ mol	R
Aromatics	0.1	-21.4	18.0	3.4	10.5	3.2	0.99
n-paraffins	1.2	5.3	-11.3	-1.1	-39.4	-7.0	0.92
Iso- and cyclo- paraffines	3.9	12.2	-15.2	-5.8	-19.6	-6.4	0.99
C3-C4 fraction	-5.3	3.8	8.5	3.4	48.5	10.3	0.97
RON of C5+ fraction	-226	-901	1270	424	2711	721	0.95

4. CONCLUSIONS

The correlation obtained between MFI catalysts performance in gas-condensate conversion and the strength of their Lewis and Brönsted sites suggest that the strong Lewis sites and medium Brönsted are the most effective in this process and that the further improvement of catalyst performance can be achieved by the increase of the fraction of strong Lewis sites in the total amount of sites of the catalyst.

5. ACKNOWLEDGMENTS

The authors are grateful to NATO Science for Peace Programme for the research grant. I.Ivanova thanks RFBR and Science support foundation for the financial support.

6. REFERENCES

- [1] V.G.Stepanov, K.G.Ione, *Kchimia i Technologia Topliv i Masel*, 1, 2000, p.8-12 (Rus).
- [2] Y. Nagamori, M. Kawase, *Microporous and Mesoporous Materials*, 21, 1998, p.439-445.
- [3] J. Kanai, N. Kawata, *Applied Catalysis*, 55, 1989, p.115.
- [4] B. Czerwinska, J. Berak, J. Pieniazek, J. Mejsner, *Polish Patent PRL 1215.146*, 1981.
- [5] C.A.Emeis, *J. Catal.*, 141, 1993, p. 347-354.
- [6] S.V.Cherepitsa, S.M.Bichkov, S.V.Gatsiha, *Kchimia i Technologia Topliv i Masel*, 4, 2001, p.44-48 (Rus).
- [7] Y.Yoneda, *J.Catal.*, 9,1967, p.51-56.

Chapter 26

COKE FORMATION ON ALUMINA AND ALUMINA SUPPORTED PLATINUM CATALYSTS

Zenon Sarbak

Laboratory of Adsorption and Catalysis, Faculty of Chemistry, Adam Mickiewicz University, Poznań, Poland.

1. INTRODUCTION

Natural gas has become a most important chemical raw material for various syntheses. Raw natural gas contains valuable hydrocarbons mainly methane as well as undesirable water, hydrogen sulphide which should be removed before use. Many chemical syntheses based on the use of natural gas requires the presence of catalysts usually deposited on supports, very often a support is alumina and an active phase is platinum.

In the conditions of the catalytic process the hydrocarbons being the components of natural gas undergo many side reactions e.g. dehydrogenation and polymerisation. These processes lead to the catalyst deactivation as a result of the so-called coke deposition that is covering of the catalysts' surface with coke known also as carbonaceous deposit. Formation of carbonaceous deposits during conversion of hydrocarbons is related at the first stage with dehydrogenation of alkane and then with the polymerisation processes, which can be illustrated as [1]: alkane→ alkene→ oligomers→ naphthenes→ aromatic compounds→ carbonaceous deposit. The nature of the carbonaceous deposits can be studied by many methods [2], in this study the infrared spectroscopy (IR) has been used [3, 4].

2. EXPERIMENTAL

The material studied was alumina (Degussa C) with the surface area $100\text{m}^2/\text{g}$. Four series of measurements were performed. In the first ethylene was adsorbed on Al_2O_3 placed in the infrared cell [5, 6]. Prior to coke deposition, the samples were activated at 350°C for 1 hr at 10^{-3} Torr and then cooled down to R.T. After this procedure, the samples were exposed to ethylene at a pressure of 760 Torr for 6 hrs at temperatures 100, 250, 350 and 400°C . In the second series a similar procedure was applied for Al_2O_3 samples earlier subjected to hydrochloric acid or ammonium chloride activation. The samples were also exposed to ethylene at temperature 350°C . In the third series ethylene was replaced by buten-1 and 2-metylopropene which were deposited on Al_2O_3 . In the fourth series of measurements butene-1 was deposited on Al_2O_3 samples containing 0.3, 3.0 and 9.0 wt.%Pt.

In all series prior to IR measurement the cell was evacuated at 100°C and 10^{-3} Torr for 10 min. and then the spectra were taken on an Analect FX-6160 FT-IR spectrometer at a resolution of 2 cm^{-1} . The spectra were obtained as a result of 200 scans at R.T. The samples was pressed into self-supported discs of area about 2 cm^2 and the absorbance scales were normalised to 50 mg.

3. RESULTS AND DISCUSSION

FT-IR spectra of ethylene as a carbonaceous precursor deposited on alumina are shown in Fig.1a-e. The spectrum taken at 250°C (Fig.1c) shows that the main species formed are carboxylate groups responsible for two characteristic IR bands at 1575 and 1462 cm^{-1} . According to Lundlum and Eischens [3] the formation of carboxylate from the hydrocarbons indicates that the oxygen is provided exclusively by alumina. At 100°C we also observed band at 1633 cm^{-1} , which can be assigned to C=O stretching. Such species was proposed by Ermini at al. [7]. At higher temperatures new IR bands appear, which means that the coke composition is more complex. The main IR bands at about 1592 , 1390 and 1378cm^{-1} (Fig.1d) and 1593 , 1385 and 1378cm^{-1} (Fig 1e) can be assigned to the aromatic C=C stretching and C-H bending vibrations and according to Fetting et al.[8] and Karge [9] can be ascribed to alkyl naphthalenes.

In order to enhance acidic character of Al_2O_3 , Cl⁻ ions is often introduced on its surface. As a results of Cl⁻ ions introduction on Al_2O_3 , with te use of NH_4Cl and HCl solutions at 350°C a carbonaceous deposit formed from

ethylene was characterized by the IR bands similar to those obtained for the two types of deposits (Fig. 2a,b). The spectra of this sample indicate the presence of two types of deposits: the carboxylate type one and the one similar to alkyl naphthalenes. A comparison of the intensities of the bands assigned to these two types of deposits indicates that the content of the aromatic deposit in the samples (Fig. 2a,b) is lower than in the samples not exposed to Cl⁻ ions (Fig. 1d). The results also indicate that the presence of Cl⁻ ions irrespective of the source of their origin significantly affects the type of the carbonaceous deposit formed.

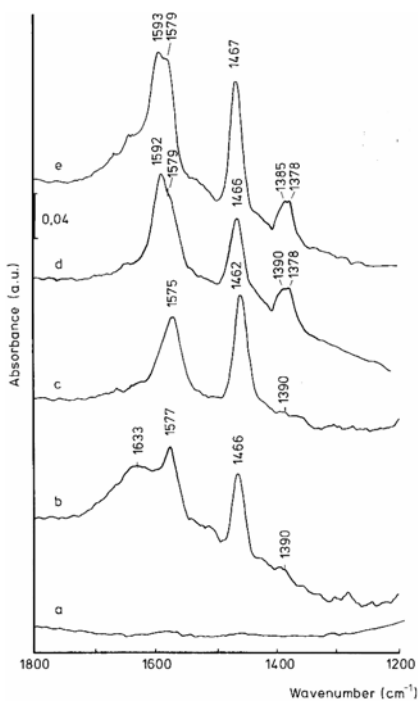


Figure 1. FT-IR spectra of carbonaceous deposit from ethylene on Al₂O₃ at: (a) R.T., (b) 100°C, (c) 250°C, (d) 350°C and (e) 400°C.

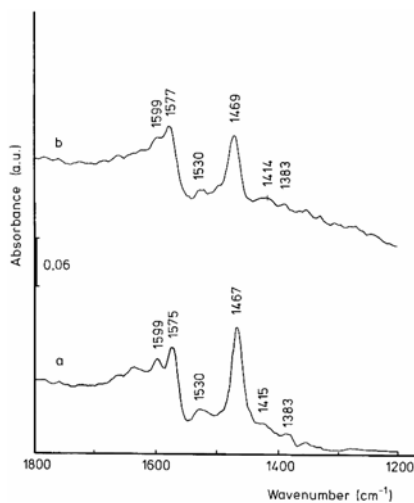


Figure 2. FT-IR spectra of carbonaceous deposit on Al₂O₃ containing Cl⁻: from (a) HCl and (b) NH₄Cl.

In the third series the source of the carbonaceous deposit were butene-1 and 2-methylpropene. The FT-IR spectrum of the sample with butene-1 used as a coke precursor (Fig.3b) shows two high intensity bands at 1572 and 1465 cm⁻¹ and a few low intensity bands at 1390, 1359 cm⁻¹. The character of the spectra indicates that the carbonaceous deposit formed is mainly of carboxylate character with a small content of aromatic deposit. The spectra of the samples with 2-methylpropene used as a coke precursor (Fig.3a)

reveal new intense IR bands at 1590cm^{-1} and 1376cm^{-1} assigned to conventional (aromatic) coke [7, 8].

In the fourth series of samples a source of the carbonaceous deposit was butene-1 chemisorbed at 350°C on $\text{Pt}/\text{Al}_2\text{O}_3$ catalysts containing Pt in a concentration of 0.3-9.0 wt.%.

The IR bands in the spectra of $\text{Pt}/\text{Al}_2\text{O}_3$ catalysts are characteristic of the coke obtained from butene-1 at 350°C . In general the spectra (Fig.4) of the catalysts studied are very complex. However, for the 0.3 wt.-%/ Al_2O_3 sample (Fig.4a) the bands at 1574 and 1469cm^{-1} are the most intense, while the other are comparably low intense. The spectra of the two catalysts containing 3.0 and 9.0 wt.% Pt show the bands at 1571 , 1470cm^{-1} (Fig.4b) and 1570 , 1463cm^{-1} (Fig. 4c) and low intensity bands at around 1540 , 1414 and 1383cm^{-1} . A comparison of the bands' intensity indicates that the carbonaceous deposit on the catalysts with 3 and 9 wt.% Pt contains the carboxyl and aromatic groups, and the deposit on the catalyst with 0.3 wt. %Pt contains mainly the carboxyl species. All examined catalysts show also strong bands at $1686 - 1688\text{cm}^{-1}$, which could be associated with $\text{C}=\text{O}$ stretching vibrations as was illustrated on scheme 2.

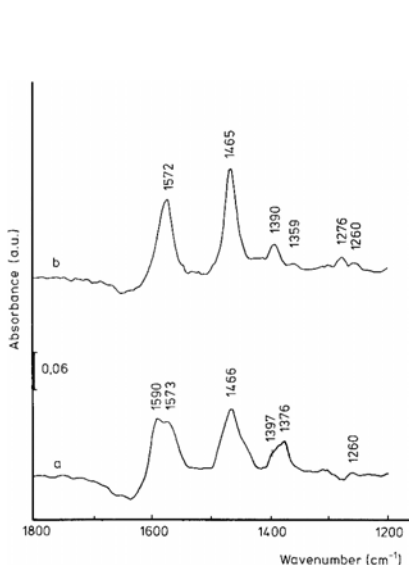


Figure.3. FT-IR spectra of carbonaceous deposit from: (a) 2-methylpropene and (b) butene-1 on Al_2O_3 at 350°C .

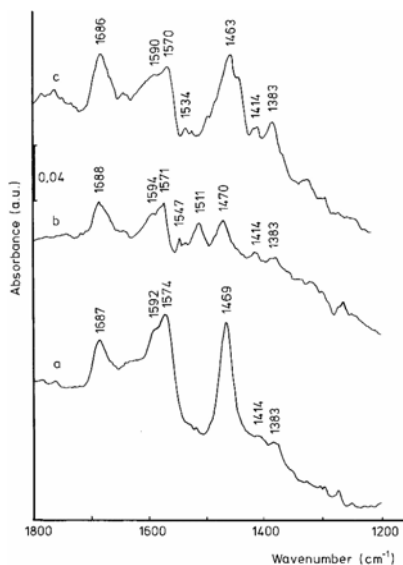
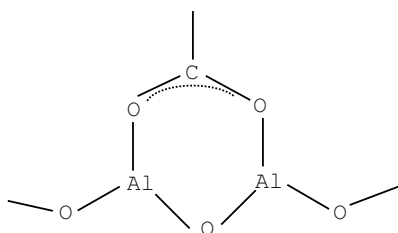


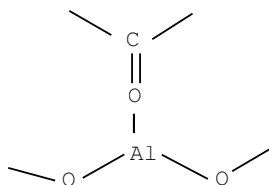
Figure 4. FT-IR spectra of carbonaceous deposit from butene-1 on: (a) 0.3 wt.-%Pt/ Al_2O_3 , (b) 3.0 wt.-%Pt/ Al_2O_3 , (c) 9.0 wt.-%Pt/ Al_2O_3 .

4. CONCLUSIONS

As follows from the FT-IR study the carbonaceous deposit obtained from decomposition of the chemisorbed ethylene and butene-1 used as precursors on Al_2O_3 is of typical carboxylic character (scheme 1). At 100°C deposit contain species with $\text{C}=\text{O}$ groups (scheme 2). In elevated temperatures also a deposit of aromatic character is formed.



scheme 1



scheme 2

The presence of Cl^- ions introduced from HCl and NH_4Cl inhibit the formation of the aromatic deposit.

For the samples with 2-methylpropene deposited on Al_2O_3 the coke obtained has both carboxylic and aromatic character.

The carbonaceous deposit formed on samples with butene-1 introduced on platinum catalysts has a more complex nature. With increasing concentration of platinum the carboxylic character of the deposit decreases, which indicates that it is related to the presence of Al_2O_3 . Moreover, $\text{C}=\text{O}$ species was also detected for examined catalysts (scheme 2).

5. REFERENCES

- [1] E. G. Derouane, B. Imelik, G. Gondurier, Y. Ben Taarit, J.C.Vedrine, *Stud. Surf. Sci. Catal.* 20, 221 (1985).
- [2] J. Góralski, J. Grams, I. Ludomirska, T. Paryjczak, I. Rzeźnicka, *Wiadomości Chemiczne* 54, 591 (2000).
- [3] K. H. Ludlum, R.P.Eischens, *Petroleum Division Preprint, ACS Meeting, New York, 1976*, p.375.
- [4] J. Datka, Z. Sarbak, R.P. Eischens, *J. Catal.*, 145, 544 (1994).
- [5] Z. Sarbak, *React. Kinet. Catal. Lett.*, 69, 177 (2000).
- [6] Z. Sarbak, *Polish J. Chem.*, 74, 439 (2000).
- [7] V. Ermini, E. Finocchio, S. Sechi, G. Busca, S. Rossini, *Appl. Catal. A*, 190, 157 (2000).

- [8] F. Fetting, E. Gallei, P. Kredel, *Ger. Chem. Eng.*, 7, 32 (1984).
- [9] H. G. Karge, *Introduction to Zeolite Science and Technology* (Eds. H. Van Bekkum, E. Flanigen, J. C. Jansen), Elsevier, Amsterdam, 1991, p. 531.

Chapter 27

ACTIVATION STUDIES OF THE Cs-DOPED Cu/ZnO CATALYST FOR THE HIGHER ALCOHOL SYNTHESIS

L. Nowicki, T. Olewski, T. Bedyk, S. Ledakowicz*

*Faculty of Process & Environmental Engineering, Technical University of Lodz, Wolczanska 213, PL-93 005 Lodz, Poland, *e-mail: stanleda@p.lodz.pl*

Abstract: In the present study the effect of different pre-treatment procedures on the modified methanol synthesis catalyst, Cs-doped Cu/ZnO catalyst, was studied in a fixed bed micro-reactor. The catalyst was provided by Institute of Chemical Engineering PAN, Gliwice, Poland. Prior to synthesis in the micro-reactor the process of the catalyst reduction was investigated in the thermo-balance TGA/SDTA851 LF, Mettler-Toledo, coupled with the mass spectrometer (QMS422, Balzers). The optimum reduction temperature for different reducing gases (hydrogen or carbon monoxide or syn-gas) was specified in dynamic TGA studies. The oxygenate products obtained over the catalyst consists of essentially linear primary C1 to C6 alcohols. The formation of both alcohols and straight-chain hydrocarbons (n-paraffins) tends to follow regular trends with carbon number (Schulz-Flory distribution). The values of chain growth probabilities depend on activation procedure. The catalyst activated with CO produced more higher alcohols than that reduced with hydrogen.

Key words: higher alcohol synthesis, pre-treatment effect, thermogravimetry, heterogeneous catalysis, catalyst activation

1. INTRODUCTION

The synthesis of higher aliphatic alcohols (HAS) from synthesis gas (H_2 and CO) has been an area of active research for the last several decades. The mixture of alcohols is considered as an alternative additives to gasoline to increase the octane number, to lower the volatility of fuel and to reduce

environmental pollution. The presence of oxygen in the fuel allows for better combustion and decreasing the source of hydrocarbon emissions. An alcohol mixture from syngas could be also used to synthesized other octane improvers such as for example methyl tertiary butyl ether (MTBE).

Methanol and higher alcohols can be simultaneously produced from synthesis gas on many different types of catalysts. The catalysts can be roughly classified to two categories [1]:

- modified Fischer-Tropsch and Group VIII metal based catalysts,
- modified methanol synthesis catalysts.

The HAS catalysts have primarily evolved from modified zinc/chromium oxide high pressure methanol synthesis catalysts. With the progress in effective desulfurization techniques for the syngas, a new generation of copper/zinc oxide methanol synthesis catalysts operated at substantially lower temperatures was developed. In both cases, the addition of alkali to the catalyst resulted in the formation of higher (C_2+) alcohols.

The isomer distribution in the alcohol mixture involves linear primary, branched primary and secondary alcohols depending on the catalyst preparation. The reaction of HAS proceeds according to the following equation:



where n is the number of carbon atoms in the forming alcohol and most often takes values from 1 to 6. The modified methanol synthesis catalysts, has been shown to produce a significant amount of branched alcohols and the alcohol product do not obey so-called Anderson-Schulz-Flory (ASF) distributions, i.e. the rate of alcohols formation exponentially decreases as their carbon number increases. On the other hand the primarily linear alcohols synthesized over modified Fischer-Tropsch synthesis catalysts usually obey the ASF distribution.

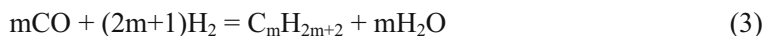
The most important side reaction occurring on the HAS catalysts is the water-gas shift (WGS) reaction, proceeding according to the following equation



The synthesis gas that is produced by modern coal gasifiers has a H_2/CO ratio in the range of 0.5 to 1 and it is advantageous to use catalysts that have some WGS activity since H_2 is the limiting reactant for alcohol synthesis at

this H₂/CO ratio. However, the considerable amount of unwanted CO₂ is produced at the same time. The WGS reaction causes another positive effects i.e. water, which is formed in reaction (1), is utilised.

Large quantities of straight chain hydrocarbons - mainly *n*-paraffins (reaction 3) and to a lesser extent 1-olefins (reaction 4) can be also produced on the certain types of HAS catalysts:



In the present study the effect of different pretreatment procedures on the Cs-doped Cu/ZnO catalyst was studied in a fixed bed micro-reactor. In addition to reactor tests, the reduction behavior of the catalyst was studied by thermogravimetric analysis. Our previous studies [2,3] showed that large quantities of unwanted hydrocarbons and CO₂ were produced in the reaction over the catalyst used in this study. The catalyst was provided by Institute of Chemical Engineering Polish Academy of Sciences, Gliwice, Poland. From the selectivity point of view, the catalyst is similar to modified Fischer-Tropsch catalysts, although it should have been modified methanol catalyst containing mainly CuO and ZnO. Presumably the addition of other metals, primarily iron (about 4 wt-% on oxide basis), has changed the catalyst properties considerably. It is interesting that similar catalyst containing the same oxides, but originated from different batch of preparation produced very small amount of hydrocarbons under similar process conditions [4].

Studies with several precipitated iron catalysts [5-8] have shown that pretreatment procedure may have a significant effect on subsequent catalyst performance during Fischer-Tropsch synthesis. Pretreatment conditions (nature of reducing gas, temperature, duration and gas flow rate) can be used to alter catalyst activity, product selectivity and/or to provide a long term stability.

The catalyst reduction is the process of oxygen removal from the catalyst which is bounded with metals in the form of oxides. In the case of reduction by hydrogen, the reaction proceeds according to the scheme:



whereas in the case of reduction by CO:



where MeO is the metal oxide (mainly Cu and Fe).

2. EXPERIMENTAL

The fixed-bed reactor system used in this study was constructed of 9 mm I.D. stainless steel tube with an effective bed volume of $1 \div 10 \text{ cm}^3$. The diagram of system process is shown in Fig. 1. The feed gases (CO, H₂, Ar or premixed mixture of them) before entering the reactor passed through the purification trap and pre-heater. The feed gas flow-rate and feed ratio were controlled using three calibrated mass flow controllers (premixed mixture of CO, H₂ and Ar). After pressure was released through a back pressure regulator, any condensable products could be collected in cold trap operating at ambient pressure and temperature close to 0°C. The flow rate of the exit gas was measured periodically using a soap film flowmeter.

About 1 g of grounded and sieved to $0.100 \div 0.125 \text{ mm}$ (30 to 60 mesh) catalyst was charged into the reactor. The catalyst was placed in between two layers of glass balls of particle size 0.080-0.100 mm. After drying in flowing nitrogen ($282 \text{ cm}^3 \cdot \text{min}^{-1}$) at 463 K for 2 h the catalyst was activated. Four sets of activation conditions were employed to evaluate the effect of activation parameters on the subsequent catalyst performance. All activations were conducted at a gas space velocity of $30 \text{ m}^3 \text{ kg}^{-1} \text{ h}^{-1}$ and at atmospheric pressure. Test identification and activation conditions are shown in Table 1.

Table 1. Activation conditions and test designation.

Test	conditions		
	temp., °C	reducant	duration, h
F-0102	180	H ₂ : N ₂ = 1:20	5
	220	H ₂ : N ₂ = 1:20	5
	220	H ₂ : N ₂ = 1:5	2
F-0201	220	H ₂ : N ₂ = 1:4	8
	250	H ₂ : N ₂ = 1:4	1
F-0202	280	H ₂ : N ₂ = 1:4	12
F-0203	280	CO : N ₂ = 1:4	12

After pretreatment, the catalyst was tested for 120-150 hours at 593 K and 5 MPa, the gas space velocity of $9.5 \text{ Nm}^3 \text{ h}^{-1} \text{ kg}^{-1}$ and feed gas ratio H₂/CO= 2/1. Syngas flow rate was fixed at the level that products remained in the area of non-condensing concentrations. Tail gas samples were analysed in a PERKIN ELMER gas chromatograph for H₂, CO, N₂, CO₂, C₁-C₆ alcohols and C₁-C₉ hydrocarbons. Oxygenates and hydrocarbons (paraffins and 1- and 2-olefins) concentrations were determined using SPB-1

60 m x 0.53 mm capillary column and a flame ionisation detector. Gases and lighter hydrocarbons (C_1 - C_2) were quantified using 18' x 1/8'' SS Silica Gel 60/80 GRADE 12 packed column and a TCD detector.

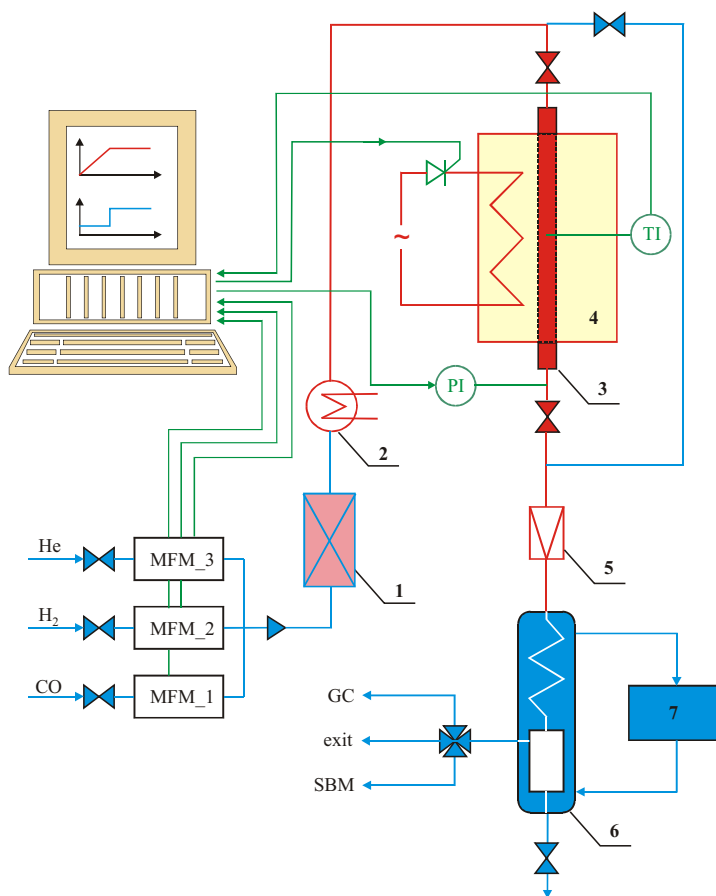


Figure 1. Experimental set-up (1- purification trap, 2 - preheated, 3 – fixed bed micro-reactor, 4 – furnace, 5 – back pressure regulator, 6 – cold trap, 7 – cryostat)

Prior to reduction and synthesis, in the microreactor the process of catalyst reduction was investigated in the thermobalance (TGA/SDTA851 LF, of Mettler-Toledo) coupled with the mass spectrometer (QMS422 from Balzers). The mass spectrometer was also used for on-line detection of water and/or carbon dioxide during the pre-treatment performed in the reactor. This enabled to determine the reduction degree, optimum temperature and time required to reduce the catalyst for a given type of

reduction gas. Extensive reduction studies were performed with pure copper oxide (CuO) that is the main component of the precursor of the catalyst used in this study.

3. RESULTS AND DISCUSSION

The optimum reduction temperature for different reducing gases was specified in dynamic TGA studies (constant temperature growth). As an optimum value such one was assumed for which the highest rate of the sample mass change was observed (DTG). Figure 2 shows the effect of the kind of reducing gases on the behaviour of Cs-Cu/ZnO catalyst in the TGA unit under dynamic conditions (constant temperature ramp).

As can be seen from Fig. 2, the reduction rate increases rapidly above 200°C and then gradually drops with further increase in temperature. The rate of mass loss above about 300°C is almost constant and rather slow. These results indicate that the reduction is not complete even at high temperatures.

This can be better seen from Fig. 3, where degree of reduction during the pre-treatment is presented. The degree of reduction was calculated from experimental weight loss, and the theoretical weight loss based on known composition of the catalyst sample. The observed increase in weight (Fig. 2) above 400°C suggests that the carbon deposition via Boudouard reaction ($2\text{CO} \rightarrow \text{CO}_2 + \text{C}$) becomes the dominant process even though the reduction was incomplete.

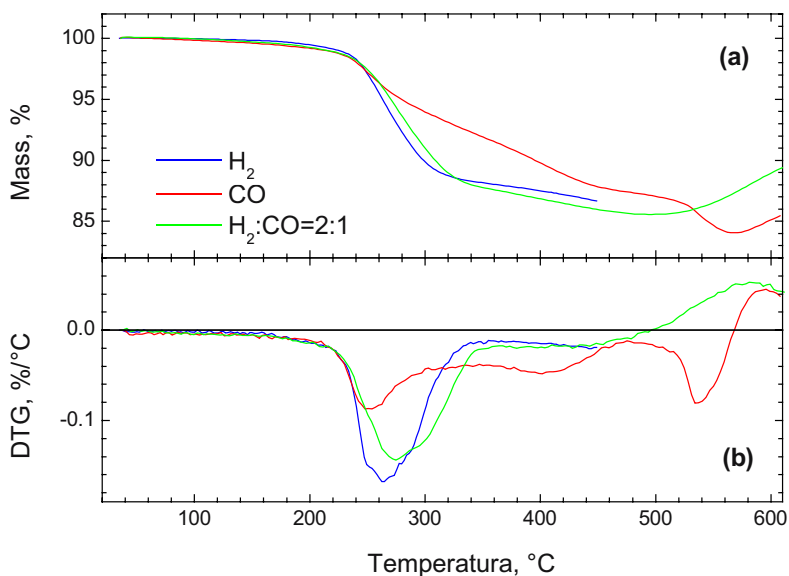


Figure 2. Changes of mass of the catalyst precursor in time (a) and the rate of this change (b) under non-isothermal conditions (linear increase of temperature) for different gases (heating rate $5^{\circ}\text{C}/\text{min}$, 40 % of reactive gas in inert, total gas flow rate $150\text{ cm}^3/\text{min}$)

In order to simulate the actual pre-treatment conditions followed during the HAS, isothermal reduction experiments were conducted in TGA unit. The catalyst sample was purged with Ar and the temperature was ramped at the rate of $5^{\circ}\text{C}/\text{min}$ from room temperature to a desired pre-treatment temperature. Then the argon flow was switched to reducing gas (hydrogen or carbon monoxide) and the temperature was maintained constant for a fixed period of time (up to 8 h). In Fig. 4 the rate of change in the catalyst mass as a function of time during reduction of the catalyst performed under isothermal conditions at 553K with $\text{CO}:\text{Ar} = 1:4$ is presented. The degree of reduction of the catalyst at these conditions was 57.5 % after 5 hours on stream. The oxygenate product obtained over the catalyst tested in a fixed-bed reactor consists of essentially linear primary alcohols, which distribute from C_1 to C_6 . Significant quantities of straight-chain hydrocarbons (mainly *n*-paraffins and to a lesser extent 1-olefins) and CO_2 were produced in the reaction.

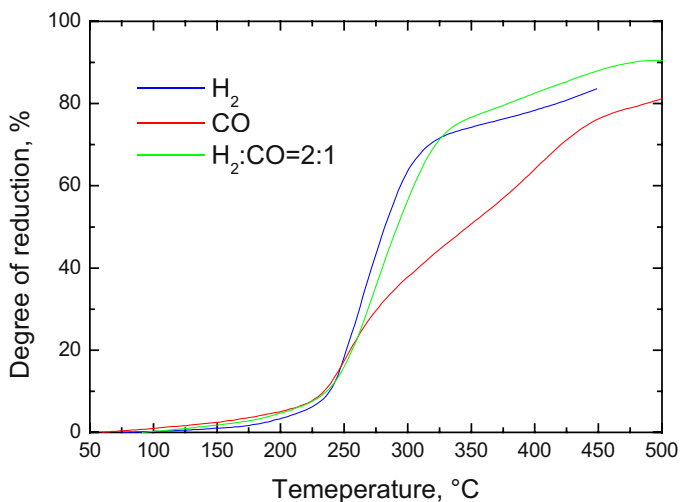


Figure 3. Effect of temperature on the reduction behaviour of Cs-Cu/ZnO catalyst in different gases under non-isothermal conditions in TGA apparatus (5 °C/min, 40 % of reactive gas in inert, total gas flow rate 150 cm³/min)

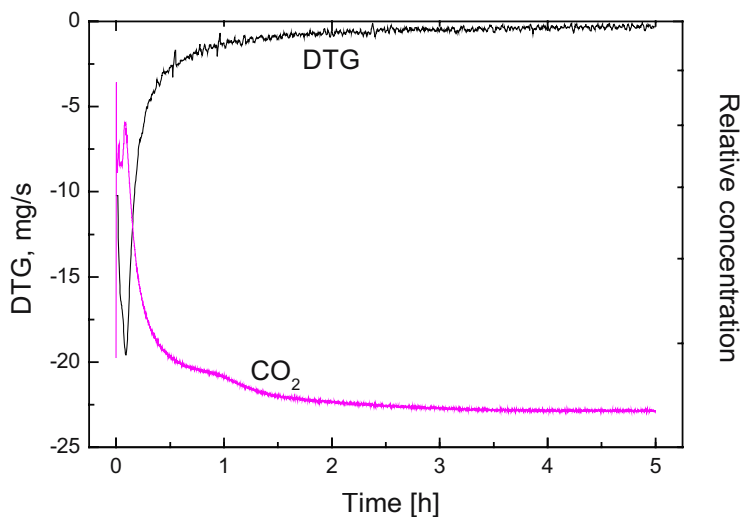


Figure 4. The rate of changes in the catalyst mass (DTG) and changes in the concentration of carbon dioxide vs. time during reduction of the catalyst Cs-Cu/ZnO under isothermal conditions at 553K with CO:Ar = 1:4.

Experimental data obtained in this study showed that formation of both alcohols and hydrocarbons tends to follow regular trends with carbon number. The carbon number distribution of the total product is often observed in Fischer-Tropsch synthesis [7]. If chain growth occurs by the addition of the single carbon monomer unit at a time, and the rates of chain termination and propagation are independent of carbon number, then the distribution of product is given by the Schulz-Flory equation:

$$y_i = (1 - \alpha)\alpha^{i-1} \quad (7)$$

where y_i indicates the mole fraction of all products containing i carbon atoms, and α is the chain growth probability, defined as the ratio of the rate of chain propagation to the total rate of chain propagation and termination ($0 \leq \alpha \leq 1$). According to this equation, the ASF plot of the $\log(y_i)$ versus i yields a straight line with a slope given by $\log(\alpha)$, and an intercept of $\log[(1 - \alpha)/\alpha]$.

Figure 5 illustrates the effect of activation procedure on product distribution for $C_1 \div C_6$ alcohols and hydrocarbons based on results obtained in runs F-0102 (H_2 reduction) and F-0203 (CO reduction). The chain growth probabilities for hydrocarbons and alcohols are 0.42 and 0.36 from data presented in Fig. 5a, and 0.48 and 0.51 from data in Fig. 5b. This shows that catalyst activated with CO produced more higher molecular weight alcohols and hydrocarbons than the catalyst reduced with hydrogen.

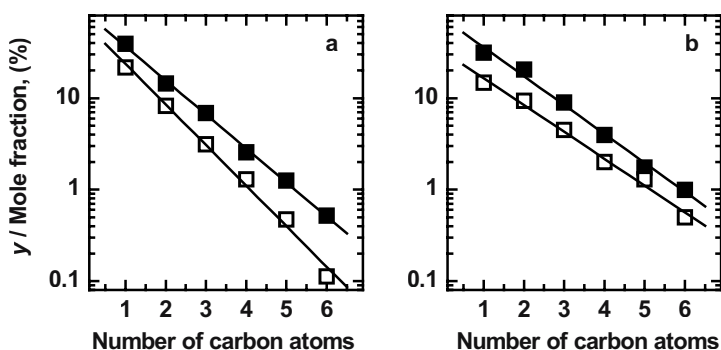


Figure 5. Anderson-Schulz-Florry carbon number product distribution for alcohols (□) and hydrocarbons (■) at 593 K, 5.0 MPa, $9.5 \text{ m}^3\text{h}^{-1}\text{kg}^{-1}$, feed ratio $H_2:CO = 2.2$. (a) Run F-0102; (b) Run F-0203.

The product distribution was a function of time-on-stream (TOS) as shown in Fig. 6 for the catalyst reduced in carbon monoxide. The catalyst reduced with CO achieved steady-state conditions (from the selectivity point of view) after about 60 hours, whereas for hydrogen reduced catalyst the initial period was shorter (about 20 hours).

The maximum values of the chain growth probabilities for hydrocarbons and alcohols (α_{HC} , α_{AL}) and maximum rate of hydrocarbon and alcohol production, respectively (R_{HC} , R_{AL}) obtained in individual tests are given in Table 2. The catalyst yield in the case of runs 1 and 3 is comparable and almost twice as high as in run 2. The catalyst revealed better selectivity for alcohols in runs 2 and 3.

Table 2. Cs-Cu/ZnO catalyst activity and selectivity

Run #	$R_{HC} / (\text{g kg}_{\text{cat}}^{-1} \text{h}^{-1})$	$R_{AL} / (\text{g kg}_{\text{cat}}^{-1} \text{h}^{-1})$	α_{HC}	α_{AL}
F-0102	110	90	0.42	0.36
F-0201	70	45	0.42	0.50
F-0203	120	100	0.48	0.51

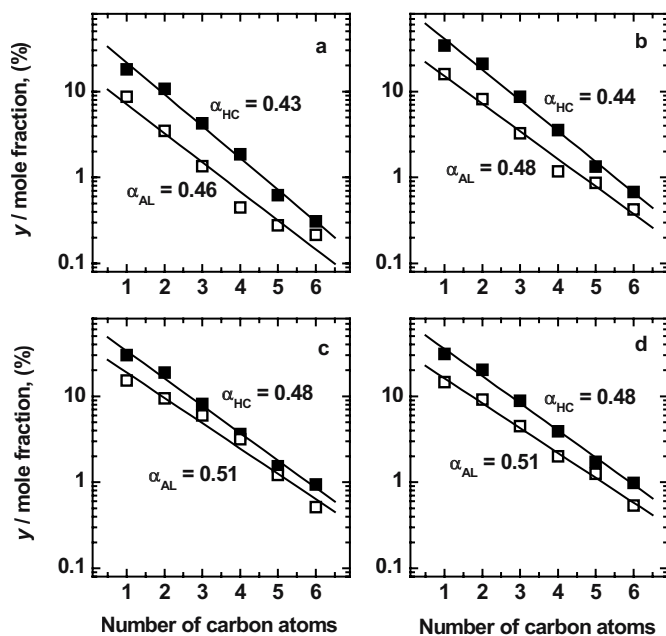


Figure 6. Effect of time-on-stream on Anderson-Schulz-Florry carbon number product distribution for alcohols (\square) and hydrocarbons (\blacksquare) at 593 K, 5.0 MPa, $9.5 \text{ m}^3 \text{ h}^{-1} \text{ kg}^{-1}$, feed ratio $\text{H}_2:\text{CO} = 2.2$. Run F-0203: (a) TOS = 6 h; (b) TOS = 27 h; (c) TOS = 57 h; (d) TOS = 80 h.

4. ACKNOWLEDGEMENT

The authors thank KBN (grant No. PBZ/KBN/14/T09/99/01b) for financial support

5. SYMBOLS

R	rate of production	$\text{g kg}_{\text{cat}}^{-1} \text{h}^{-1}$
α	the chain growth probabilities	-
SV	space velocity (at normal conditions)	$\text{m}^3 \text{h}^{-1} \text{kg}^{-1}$
y	mole fraction	-

Subscripts

AL	Reaction for alcohols
HC	Fischer-Tropsch reaction for hydrocarbons
WGS	water-gas-shift reaction
cat	Catalyst

6. REFERENCES

- [1] P. Forzatti, E. Tronconi, P. Italo, *Cat. Rev.-Sci. Eng.* 33(1&2), 109 (1991).
- [2] L. Nowicki, S. Ledakowicz, *Inz. Chem. Proc.* 19,195 (1998).
- [3] L. Nowicki, B. Klajnert, J. Łyżwa, *Przem. Chem.* 78, 54 (1999).
- [4] M. Kulawska, J. Skrzypek, *Chem. Eng. Proc.* 30, 33 (2001).
- [5] D.B. Bukur, D.B., L. Nowicki, R.K. Manne, X. Lang, X., *Appl. Catal. A: General*, 126, 85 (1995).
- [6] D.B. Bukur, D.B., L. Nowicki, R.K. Manne, X. Lang, X., *J. Catal.*, 155, 353 (1995)
- [7] R. B. Anderson, *The Fischer-Tropsch Synthesis*, Academic Press, New York, 1984.

Chapter 28

DEVELOPMENT OF HIGH TEMPERATURE CATALYTIC REACTORS FOR OXIDATIVE CONVERSION OF NATURAL GAS

S. Cimino^a, F. Donsi^a, R. Pirone^a, G. Russo^b

^a *Istituto Ricerche sulla Combustione, CNR – P. le Tecchio 80, 80125 – Napoli – ITALY*

^b *Dipartimento Ingegneria Chimica Università di Napoli “Federico II” – ITALY*

1. INTRODUCTION AND BACKGROUND

The catalytic oxidative conversion of natural gas and light hydrocarbons represents an attractive route for the production of both clean energy and synthetic fuels. Catalytic combustion can be regarded as an intrinsically clean and safe technology which allows a primary air pollution control, since energy is produced with high efficiency burning fuel/air mixtures also outside the flammability limits, at operating temperatures far lower than those of flame combustion and without the instability problems and pollutants (CO, NO_x, soot and unburned hydrocarbons) typical of the traditional processes [1-3].

On the other hand the production of synthesis gas from natural gas by catalytic partial oxidation (CPO) is considered a desirable alternative to highly endothermic steam reforming since it overcomes some of the problems related to high energy input, utility costs and polluting emissions [4]. Moreover, in the last years, the oxidative dehydrogenation of ethane (ODH) for ethylene production has received a renewed interest, due to the evidence that olefins can be efficiently produced with high yields, also if compared with those of the existing cracking processes, in catalytic reactors operated at high space velocity (short contact time reactors, SCTR) and temperatures in the range of 900–1000°C [5].

Typically, catalyst compositions for such processes have included precious metals (and/or rare earths) since Pt, Pd, Rh are commonly recognised among the most effective active components; nevertheless, their application in high temperature applications is strongly limited by problems of stability (PdO) and volatility (Pt) [3,5]. Moreover the large volumes of expensive catalysts needed, have placed those processes generally outside the limits of economic justification [4].

In recent years, a lot of research effort has been devoted to the study of alternative active phases such as perovskite-type oxides with general formula $A_{1-x}A'_x B_{1-y}B'_y O_{3\pm\delta}$ [6-7]. Indeed, such materials offer potential better features in terms of elevated chemical and thermal stability (up to 1100°C) and lower cost accompanied by a good specific activity which can be tailored through partial substitutions in the perovskite structure. The main drawback is related to their low porosity and strong tendency to sinter [6-7]. In order to increase their surface area and mechanical strength, perovskites have been dispersed onto high surface area refractory oxides (La/ γ -Al₂O₃, MgO and ZrO₂) and applied on suitable substrates (ceramic and metal honeycomb monoliths, foams) to obtain structured catalytic reactors [8-12]. Such novel monolithic catalysts have been profitably studied and tested in both autothermal methane combustion and ethane ODH at short contact times for ethylene production.

2. CATALYST PREPARATION AND TESTING

Commercial cordierite honeycombs (400 cpsi) were first washcoated with alumina by repeated dipping in a slurry of finely grounded γ -Al₂O₃ powder and pseudobohemite [8]. A similar procedure was employed also in the case of ceramic (mullite, α -alumina) foam substrates with different pore densities. La₂O₃ (7% w./w.) was added to the washcoat by impregnation, while LaMnO₃ active phase was dispersed on the monoliths using Deposition-Precipitation (DP) method through urea decomposition at 90°C [8], or by co-impregnation. Several cycles were needed to reach target perovskite loading (30% w./w.). After each cycle the monoliths were calcined at 800°C or 1100°C in air for 3 hours. Catalytic activity measurements for the different reactions were carried out directly on monolith catalysts to take advantage of their favourable heat and mass transfer properties both under pseudo-isothermal and auto-thermal conditions up to maximum temperatures of 1100°C [8-12].



Figure 1. Structured honeycomb and foam catalysts based on supported LaMnO_3 perovskite for high temperature oxidation processes.

3. CATALYTIC COMBUSTION

SEM inspection showed an homogeneous distribution of the active washcoat, characterised by a BET specific surface area as high as $127 \text{ m}^2/\text{g}$ [9] and which was still well anchored to the substrate after repeated ageing cycles at 1100°C . EDS microanalysis performed at different positions on several sections of the monolith confirmed that the preparation method allows a good and uniform dispersion of active metal species (Mn and La) along the reactor and inside the washcoat layer.

The catalytic activity in methane combustion is very promising, even higher than that measured on the corresponding catalyst powders with the same chemical composition. Isothermal catalytic activity measurements reveal that first ageing cycle slightly reduces the activity of fresh catalyst, while further repeated ageing treatments at 1100°C under reaction do not deactivate the monolithic reactor further [9]. In autothermal conditions, the monolithic catalyst is able to ignite a mixture of CH_4 (3% vol.) in air, at minimum inlet gas temperature of about 450°C , giving stable and complete methane conversion and negligible CO and NO_x emissions.

Transient ignition behaviour over monolithic reactors has been characterised and catalyst long term durability tested up to 120h under reaction conditions of interest for application in pre-mixed radiant burners (Fig. 2 A). After about 60 hours working time, ignition temperature levels off to a constant value, which is 370°C lower than that required on a nude cordierite monolith, keeping complete selectivity to CO_2 .

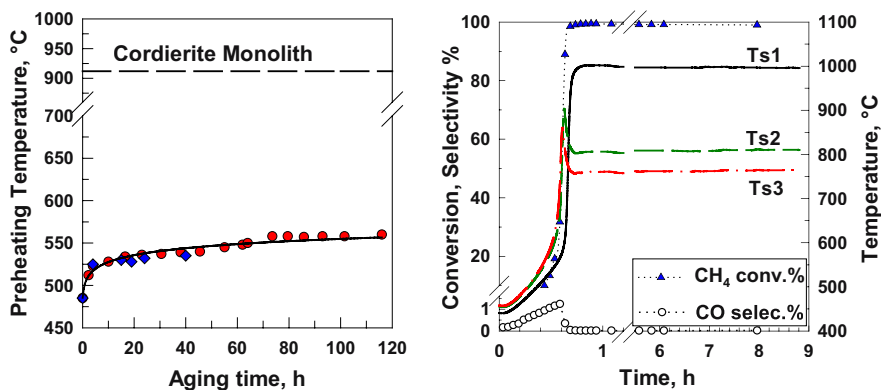


Figure 2. A) Minimum ignition temperature in methane combustion measured over $\text{LaMnO}_3/\text{La-}\gamma\text{Al}_2\text{O}_3$ monolithic catalysts of different length: (♦) 4.6 cm, (●) 2.3 cm.; Feed: CH_4 (3% vol.), O_2 (10% vol.); GHSV=44000 or 88000 h^{-1} . B) Typical catalyst axial temperature profile ($T_{s1}=0.5$, $T_{s2}=2.5$, $T_{s3}=3.4$, $L=4.6\text{cm}$), CH_4 conversion (▲) and CO selectivity (○) vs. time on stream. Inlet gas temperature: 580°C; GHSV=72000 h^{-1} .

As shown in Figure 2 B, an aged catalyst (after about 40 h in ignited conditions) ensured stable and almost complete conversion of methane during 9 h of continuous operation: in this case temperatures as high as 1000°C were constantly held at the reactor inlet (T_{s1}), indicating no appreciable deactivation of our LaMnO_3 -based monolith. Such results represent a clear improvement with respect to those reported under similar operating conditions by Arai and Machida [7] for $\text{La}_{1-x}\text{Sr}_x\text{MO}_3$ ($M=\text{Mn, Co}$) perovskites directly deposited over cordierite monoliths without the intermediate stabilised high surface area layer. Indeed, those authors found a fast and sudden deactivation of perovskitic catalysts, which became unable to sustain the reaction after only 20 minutes of operation, mainly because of drastic sintering phenomena.

4. ETHANE ODH

Until recently, it has been reported these processes are purely heterogeneous and can be regulated by the appropriate choice of the active component, support morphology and reaction mixture composition [13]. This seems to be true only at moderate temperatures, while above 800°C, it has been shown, both experimentally and theoretically [14], that the role of homogeneous reactions is crucial in ethylene production. As recently proposed [14], catalyst could be assumed to be active only for total

oxidation reactions, ethylene production reactions mainly occurring in the gas phase. In this case, use of very expensive noble-metal-based catalysts is not necessary. Nevertheless, even though different active phases have been studied, up to now only Pt-based catalysts showed to be reliable for the process in terms of thermal stability and performance. Use of Pt/Sn-based catalysts, which upon H_2 addition to the feed improved C_2H_4 selectivity [15], is limited by the volatility of Sn. Also non-noble-metal based catalysts, such as Cr_2O_3 and hexa-aluminates [16-17] showed respectively a limited lifetime and a quick coke deposition.

The novel $LaMnO_3$ -based catalysts, which did not show any sign of deactivation also in the ethane ODH at short contact times, were tested in comparison with Pt under the same configuration and experimental conditions, showing better performance under a large variety of conditions (Fig. 3A). In addition, the study of the effect of the main operating parameter, such as C_2H_6/O_2 feed ratio, total flow rate, preheating temperature and dilution, was addressed to tune up the process and optimise ethylene production [12].

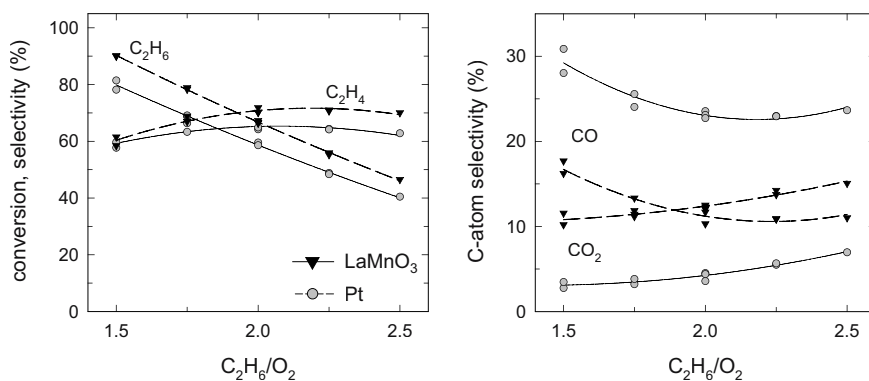


Figure 3. Ethane conversion and C-atom selectivity of C_2H_4 (a), of CO and CO_2 (b) on Pt (solid lines) and $LaMnO_3$ (dashed lines) in a honeycomb monolith reactor as a function of C_2H_6/O_2 ratio. Experimental conditions: GHSV = 24000 h^{-1} , N_2 = 30% vol.

The large ethylene yield observed on such catalyst, even higher than that reachable in a purely homogeneous process and different from Pt, called for additional investigations of the role of the catalyst. By means of numerical simulations we tried to clarify how the presence of the catalyst, which mainly drives the oxidation of ethane to CO_x and H_2O , interacts with the gas-phase kinetics for improving ethylene production. The results of our investigation demonstrate not only that (a) the short-contact-time concept successfully applies to the ODH of ethane on cheaper non-noble-metal

perovskite based honeycombed monoliths, but also that (b) better performance can be achieved on LaMnO_3 due to the more efficient oxidation of ethane to CO_2 than on Pt or in the gas phase (Fig. 3B), achieving a more efficient heat production and thus sacrificing less ethane.

5. CONCLUSIONS

Perovskites supported on high surface area refractory oxides have been proposed and tested as potential alternative to both noble metals (very active but not stable at high T and expensive) and hexa-aluminates (very stable at high T but scarcely active) for high temperature oxidative conversion of natural gas, in view of their intermediate properties of thermal resistance and good activity. Structured monolithic catalysts, prepared in a variety of shapes from such novel active phase, were originally developed for premixed methane combustion. These catalysts are characterised by an elevated specific oxidation activity, a thermal stability and durability markedly higher than corresponding bulk perovskite, which also make them suitable alternatives to Pt in short contact time reactors for ethane ODH.

6. REFERENCES

- [1] Pfefferle L., Pfefferle W., *Catal. Rev.-Sci. Eng.* 29 (1987) 219
- [2] Saint-Just J., der Kinderen J., *Catal. Today* 29 (1996) 387
- [3] Zwinkels, M.; Jaras, S.; Menon, P.; Griffin, T. (1993), *Catal. Rev.-Sci. Eng.*, 35, 319
- [4] Peña M. A., Gómez J. P., Fierro J. L. G., *App. Catal. A* 144 (1996) 7-57
- [5] Schmidt L., Huff M., *Catal. Today* 21 (1994) 443-454
- [6] Arai H., Yamada T., Eguchi K., Seyama T., *Appl. Catal.*, 26 (1986) 265
- [7] Arai H., Machida M. *Appl. Catal. A*, 138 (1996) 161
- [8] Cimino S., R. Pirone, L. Lisi, M. Turco, G. Russo, *Catal. Today*, 59 (2000) 19
- [9] Cimino S., R. Pirone, G. Russo, *Ind. Eng. Chem. Res.* 40 (2001) 80
- [10] Cimino S., R. Pirone, L. Lisi, *Appl. Catal. B* 35 (2002) 243
- [11] Cimino S., A. Di Benedetto, R. Pirone, G. Russo, *Catal. Today* 69 (2001) 95
- [12] Donsì F., Pirone R., Russo G., *J. Catal.* 209 (2002) 51.
- [13] Bodke A., Bharadwaj S., Schmidt L., *J. Catal.* 179 (1998) 138
- [14] Beretta A., Ranzi, E., and Forzatti, P., *Chem. Eng. Sci.* 56 (2001) 779
- [15] Bodke A., Henning D., Schmidt L., Bharadwaj S., Maj J., Siddall J., *J. Catal.* 191 (2000) 62.
- [16] Flick D., Huff M., *Appl. Catal. A* 187 (1999) 13
- [17] Beretta A., and Forzatti P., *J. Catal.* 200 (2001) 45

Chapter 29

THE EFFECT OF PROCESS CONDITIONS ON PRODUCT FORMATION IN FISCHER-TROPSCH SYNTHESIS

Sh. S. Itkulova

D.V. Sokolsky Institute of Organic Catalysis and Electrochemistry of the Ministry of Education and Science of the Republic of Kazakhstan; 142, Kunaev str., Almaty, 480100, Kazakhstan; Fax: (007) 3272 915722; e-mail: itkulova@nurast.kz

Abstract: Effect of conditions of the Fischer-Tropsch synthesis on the product formation has been studied over Co-containing catalysts. It has been established that the composition and yield of products are strongly depended on the process conditions (temperature, pressure, space velocity and CO/H₂ ratio). By regulation of the process conditions it is possible to produce certain hydrocarbon fractions over bimetallic Co-containing supported catalysts.

Keywords: Fischer-Tropsch Synthesis (FTS), synthesis-gas, Co-containing catalysts, hydrocarbons

1. INTRODUCTION

Syngas (CO+H₂) is recognised as an alternative and perspective raw material for the production of synthetic oil fractions. Syngas may be produced by a conversion of different carbon-containing sources. At present, the production of methanol and different hydrocarbons from syngas obtained by conversion of natural gas or coal are industrially used. The effectiveness of the Fischer-Tropsch synthesis, product distribution and their yield depends on catalyst activity and selectivity. The efficiency of catalysts on a base of cobalt or iron commonly used for this process may be increased by modification of their composition.

Earlier some results on bimetallic Co-containing catalysts studied in the FTS have been reported by authors [1-2]. This paper has dealings with studying the effect of the FTS process conditions on product composition and yield over Co-containing catalysts modified by iridium and supported on alumina.

2. EXPERIMENTAL

Bimetallic Co-containing catalysts were prepared by impregnation of alumina with a solution containing both the Co and the Ir compounds and following thermal treatment. The total metal concentration in the catalyst was 10 wt.%. Iridium content in bimetallic catalysts was varied from 0.5 to 10 wt.% from total metal content. Below Ir amount has been indicated as percentage by mass from all metal content (Co + Ir).

Physico-chemical properties of catalysts at different stages of their preparation and operation were studied by using: XRA, TEM and IR-spectroscopy. The degree of cobalt reduction was obtained from amount of hydrogen liberation, which was measured in a closed system and calculated as a ratio of number of cobalt atoms in zero-valence state to total calculated number of cobalt atoms in catalyst. The methods were described in [1-2].

The hydrogenation of CO was carried out in a flow reactor. The CO+ H₂ mixtures with different CO/ H₂ ratio (1/4-3/2) were prepared. The reaction was studied at varying conditions: pressure from 0.1 to 2.0 MPa, temperature from 423 to 553K, and space velocity (S.V.) from 100 to 3000 hr⁻¹. Experiment duration was 3-100 hours.

The stability of Co-Ir/Al₂O₃ was tested in pilot conditions with the commercial synthesis gas produced by conversion of natural gas. The duration of continuous exploitation was more than 2000 hours.

The reaction products were analysed by gas chromatography and fractional distillation. The physico-chemical properties of liquid and solid hydrocarbons were determined by standard methods.

3. RESULTS AND DISCUSSION

By TEM-analysis of 10% Co-Ir (9.5:0.5)/Al₂O₃-catalyst it has been observed that metal particles are high dispersed (size is 1.5-2.0 nm) and uniformly distributed. It has been shown that particle dispergation increases after catalyst reduction by hydrogen and during CO+ H₂ reaction.

The high thermostability of bimetallic nano-particles has been observed. The agglomeration of nano-particles controlled by TEM is started at T is about 1073K. Only high-dispersed X-ray amorphous phase has been found in catalyst tested in industrial conditions during more than 2000 hours. No graphite is observed over catalyst surface after its exploitation.

It is necessary to note that Co remains in zero-valence state in catalyst preliminary passivated in an inert atmosphere even after effect of air. The degree of Co reduction in Co-Ir (95:5)/Al₂O₃ freshly reduced is 64.5% and undergone air during 1 hour is 62.3%. Cobalt reduction degree is increased with Ir content.

Some results have been reported earlier [1-2]. It has been established that the addition of iridium to Co/Al₂O₃ causes:

- Decrease of reduction temperature of cobalt;
- Increase of dispersity of both metals;
- Saving the metallic state of Co and resistance to air influence;
- Increase of stability to influence of high T and P.

These results confirm the strong Ir influence on the composition, structure and adsorption properties of Co-containing catalysts. It has been supposed that the interaction between Co and iridium over alumina surface occurs with the formation of bimetallic nano-particles of cluster type. These nano-particles are characterised by high thermostability and activity in the FTS.

It has been observed that the process conditions are strongly affected on composition and yield of hydrocarbons.

For example, increase of temperature is accompanied with raising CO conversion and leads to a growth both of methane formation and carbon dioxide yield. The fraction of liquid hydrocarbons is completely disappeared at 473K and atmospheric pressure, when the 100% CO conversion is occurred (Table 1). This dependence is observed at high pressure too. In Table 2 the data obtained at P= 0.9 MPa are given. At conversion above 80% methanation is prevailed.

Pressure increase caused enhancing polymerization reaction. High-molecular hydrocarbons – ceresines (C₃₀⁺) are formed at P ~ 1.0 MPa. There is no ceresin formation at atmospheric pressure (Table 3). CO conversion is increased with pressure growth. Table 4 shows increasing CO conversion from 65.3 to 78.8% at increasing pressure from 0.5 to 1.5 MPa (H₂/CO=1/2, space velocity – 2000 hr⁻¹).

Varying CO/H₂ ratio results in a change of olefin/paraffin ratio in products. Due to decreasing hydrogen content the olefin formation is increased. It is shown in table 5.

Increase of space velocity leads to the formation of lighter hydrocarbons and prevailing olefins among reaction products (Table 6). Higher temperatures required to keep CO conversion at the same level at increasing space velocity cause the shortness of hydrocarbon length.

4. CONCLUSIONS

The process conditions have a very strong influence on the composition and yield of products in the Fischer-Tropsch synthesis over Co-containing supported catalysts. Thus,

- raising temperature leads to increasing CO conversion degree, shortening the carbon chain length, decreasing olefin yield and growth of methane formation;
- increase of pressure is accompanied with lengthening of carbon chain;
- increase of space velocity causes the formation of lighter hydrocarbon fraction and increase of olefin formation;
- increase of CO/H₂ ratio leads to growth of olefin yield.

The CO conversion degree should be certain for each hydrocarbon fraction produced.

Table 1. The effect of temperature on the product composition and yield in the Fischer-Tropsch synthesis over Co-Ir/Al₂O₃ (H₂/CO=2.2, S.V.=100 hr⁻¹) at P=0.1 MPa

T, K	K _{CO} , %	Selectivity by products, %			
		C ₁	C ₂ -C ₄	C ₅ ⁺	CO ₂
423	48.1	10.9	38.9	48.6	1.6
443	61.1	10.0	30.8	57.5	1.7
453	75.7	18.4	52.9	20.0	8.7
473	100.0	52.3	17.7	-	30.0

Table 2. The effect of temperature on the product composition and yield in the Fischer-Tropsch synthesis over Co-Ir/Al₂O₃ (H₂/CO=2.2, S.V.=100 hr⁻¹) at P=0.9 MPa

T, K	K _{CO} , %	Selectivity by products, %	
		C ₁	C ₁₀ ⁺
440	60	6.8	36.3
450	80	4.9	63.6
463	93	13.8	36.2
468	100	43.0	1.8

Table 3. The effect of pressure on the product composition and yield in the Fischer-Tropsch synthesis over Co-Ir/Al₂O₃ (H₂/CO=2.2, S.V.=100 hr⁻¹)

Pressure, MPa	T, K	K _{CO} , %	Selectivity by products, %		
			C ₅ ⁺	C ₁₀ ⁺	Ceresines (C ₃₀ ⁺)
0.1	453	75.7	52.9	20.0	-
1.0	453	78	76.3	72.9	17.9

Table 4. The effect of pressure on the product composition and yield in the Fischer-Tropsch synthesis over Co-Ir/Al₂O₃ (H₂/CO=2.2, S.V.=2000 hr⁻¹)

Pressure, MPa	T, K	K _{CO} , %	Selectivity by products, %	
			C ₅ ⁺	C ₁₀ -C ₂₄
0.5	513	65.3	73.4	68.5
1.0	513	79.9	85.2	76.3
1.5	513	78.8	87.3	83.5

Table 5. CO hydrogenation over 10%Co-Ir (9.5:0.5)/Al₂O₃ (1.0 MPa, S.V. =1000 hr⁻¹)

CO/ H ₂	T _{exp} , K*	K _{CO} , %	Yield of (C ₂₋₂₅), %	Content of olefins in C ₅ ⁺ , %	CO ₂ , %
1/ 4	473	82.1	95.9	5.0	0.3
1/ 2	498	87.1	93.8	10.0	2.0
2/3	523	86.3	86.1	20.0	10.0
1/1	528	66.4	80.4	50.0	16.5
3/2	543	55.0	67.6	59.0	29.8

* T_{exp} are optimum for given ratio of CO/H₂

Table 6. Influence of space velocity on the olefin yield at CO hydrogenation over 10% Co-Ir (9.5:0.5) /Al₂O₃ (P=1.0 MPa, CO/H₂=1/2)

S.V., Hr ⁻¹	T _{exp} , K *	K _{CO} , %	Yield of C ₂₊ , %	Content of C ₃₀ ⁺	Content of olefin in Fractions			
					C ₂	C ₃	C ₄	C ₅₊
100	453	75.7	87.5	17.9	traces	10.0	17.0	8.0
400	493	84.4	93.3	3.5	-	21.0	14.0	10.0
1000	498	87.1	93.8	-	-	30.0	21.0	10.0
1500	508	90.0	93.8	-	-	57.0	31.0	24.0
2000	523	87.3	94.0	-	-	64.0	43.0	31.0

* T_{exp} are optimum for given space velocity

5. REFERENCES

- [1] Itkulova Sh.S., Zakumbaeva G.D., *Eurasian ChemTechn. Journ.* 2000, 2, 75–80
- [2] Itkulova Sh.S., "The bimetallic Co-containing supported on alumina catalysts in the synthesis on the base of carbon oxides". in "Principles and method for accelerated catalyst design", E. Derouane *et al.* Eds., Kluwer Acad. Publisher, 2002, P.407-415

Chapter 30

MATHEMATICAL MODELING OF STEAM REFORMING TUBES WITH SHAPED PARTICLES

A.P. Kagyrmanova, I.A. Zolotarskii, N.V. Vernikovskaya, E.I. Smirnov, V.A. Kuzmin

Boriskov Institute of Catalysis SB RAS, Pr. Akad. Lavrentieva 5, Novosibirsk 630090, Russia. Tel.: +7-3832-341278; fax: +7-3832-341878. E-mail address: zudilina@catalysis.nsk.su

1. INTRODUCTION

The catalytic steam reforming of natural gas is the main way to the production of ammonia, methanol and hydrogen for over 50 years. The steam reformer of a modern ammonia or methanol plant is a most expensive item of the plant and its improvement is very important to decrease final product costs.

Last years application of shaped catalysts in steam reforming tubes became prevailing. It has placed emphasis on improving the efficiency and safety of steam reformer. Transition from regular catalysts to shaped ones allows to increase an apparent catalyst activity; to enhance heat transfer; to reduce a pressure drop along a tube. Recently developed theory for a prediction of radial heat transfer properties of beds packed by shaped particles [1, 2] allows to estimate and to compare performance of such catalysts.

Many studies on a mathematical modeling of steam reformers [4-6] use models of various levels of complexity. But most of these models are simplified, heat transfer parameters being not well defined, especially for shaped catalyst. In the present work modeling of steam reformer tubes is performed for different shaped catalysts based on an original two

dimensional pseudo homogeneous model. The model accounts for the following heat and mass transfer phenomena: heat transfer between the tube wall and catalyst bed, conductivity and diffusivity in the radial direction in the packed bed and intraparticle diffusion.

2. THE MATHEMATICAL MODEL

2.1 The catalyst pellet model

A gas stream in steam reforming of methane consists of six components, reaction rates depending on concentrations of five components taking part in the reactions. Due to considerable increase in gas volume caused by reaction stoichiometry, the individual mass flux cannot be expressed using a simple Fick's law, Therefore, a general dusty gas model is used in the work. A resulting mass balance of the i -th component in a catalyst pellet of slab geometry can be presented by the following equation:

$$\frac{\partial}{\partial r} (D_{ri}^* \frac{\partial C_i}{\partial r}) - \frac{RT}{P} \frac{\partial}{\partial r} (V_i^* C_i) = \sum_{j=1}^3 \gamma_{ij} \omega_j \quad , i = \overline{1,5} \quad (1)$$

where D_{ri}^* is a diffusivity of a component i through other components of the mixture, V_i^* is a hydrodynamic velocity of a component i .

Both D_{ri}^* and V_i^* depend on all concentrations and mass fluxes. The kinetic model of Xu and Froment [7] is used in this work.

Boundary conditions:

$$r = 0 : \frac{\partial C_i}{\partial r} = 0 , \quad i = \overline{1,5}$$

$$r = R_{grain} : C_i = C_i^{surface} \quad i = \overline{1,6}$$

2.2 The mathematical model of a reformer tube

The reactor model applied is referred to in literature as a 'two dimensional homogenous model without axial dispersion', in which the heat

and mass balance equations and corresponding boundary conditions are as follows:

$$\begin{aligned} & \frac{P_0}{RT_0} \frac{\partial(\overline{U_l y_i})}{\partial l} + \frac{1}{r} \frac{P_0}{RT_0} \frac{\partial}{\partial r} (r \overline{U_r y_i}) - \\ & - \frac{1}{r} \frac{\partial}{\partial r} \left(\frac{P D_r}{RT} \frac{\partial y_i}{\partial r} \right) = \sum_j (1 - \varepsilon) \gamma_{ij} \overline{\omega_j} \end{aligned} \quad (2)$$

$$\begin{aligned} & \frac{P_0}{RT_0} \overline{U_l} C_p \frac{\partial T}{\partial l} + \frac{P_0}{RT_0} \overline{U_r} C_p \frac{\partial T}{\partial r} - \sum_i C_{Pi} \left(\frac{\partial T}{\partial r} \right) \frac{P}{RT} D_r \frac{\partial y_i}{\partial r} - \\ & - \frac{1}{r} \frac{\partial}{\partial r} (r \lambda_r \frac{\partial T}{\partial r}) = -(1 - \varepsilon) \sum_j H_j \overline{\omega_j} \end{aligned} \quad (3)$$

Equations for axial and radial components of the gas velocity originated from reaction stoichiometry are defined as:

$$\frac{\partial \overline{U_l}}{\partial l} = \frac{2RT_0}{R^2_{tube} P_0} \int_0^{R_{tube}} \sum_i \sum_j r (1 - \varepsilon) \gamma_{ij} \overline{\omega_j} dr \quad (4)$$

$$r \overline{U_r} = - \frac{RT_0}{P_0 r} \int_r^{R_{tube}} (1 - \varepsilon) r \sum_i \sum_j \gamma_{ij} \overline{\omega_j} dr + \frac{1}{r} \frac{\partial \overline{U_l}}{\partial l} \left(\frac{R^2_{tube}}{2} - \frac{r^2}{2} \right) \quad (5)$$

The following boundary conditions were applied:

$$0 \leq r \leq R_{tube} \quad l = 0: \quad \overline{U_l}(0, r) = \overline{U_0} \quad r = 0: \quad \frac{\partial y_i(l, 0)}{\partial r} = 0$$

$$T(0, r) = T_{in} \quad \frac{\partial T(l, 0)}{\partial r} = 0$$

$$y_i(0, r) = y_{iin} \quad \overline{U_r} |_{r=0} = 0$$

$$0 \leq l \leq L, r = R_{tube} : \quad \frac{\partial y_i(l, R_{tube})}{\partial r} = 0 \quad \bar{U}_r(l, R_{tube}) = 0$$

$$\lambda_r \frac{\partial T}{\partial r} = \alpha(T_w - T) \quad (6)$$

For description of a heat transfer coefficient α the linear pre-wall model of convective radial thermal conductivity gives [1]:

$$\alpha = \frac{\lambda_r}{\delta[\ln(\lambda_r / \lambda_{r,g}) - 1]} \quad (7)$$

Original correlations for a radial conductivity of beds packed by shaped particles [2] are used. The pressure drop equation used in this work is based on the hydrodynamic model with accounting for a gas flow in particle holes [7].

3. RESULTS

Mathematical modeling of steam reformer tubes packed by shaped catalysts listed in the table below is presented in the work. The trilobed catalyst was developed by the Boreskov Institute of Catalysis recently [3]. Parameters of a typical methanol plant reformer were used in modeling. The table gives some characteristics of catalysts in these conditions. Intrinsic activity of all catalysts was assumed to be the same.

Catalyst type	Specific surface area (relative)	Pressure drop (relative)	Apparent heat transfer coefficient (relative)
Trilobed particle: outer diameter of each lobe: 9 mm, length: 20 mm, hole diameter: 5 mm	1	1	1
4-hole cylinder: outer diameter: 14 mm, length: 19 mm, hole diameter: 3,6 mm	0,95	0,98	0,68
10-hole cylinder: outer diameter: 19 mm, length: 16 mm, hole diameter: 2,5 mm	0,82	1,05	0,56

A verification of the suggested mathematical model was performed and presented in the work. Particularly, importance of radial viscous flow in the tube (\overline{U}_r) and within a pellet (V_i^*), different boundary conditions at a tube wall is discussed. Simulated performance of different catalysts is presented and compared. The advantage of trilobed particles to diminish wall tube temperature is shown.

4. NOMENCLATURE

$C_i, C_i^{surface}$ - mole fraction and surface mole fraction component i , $mole/m^3$

\overline{C}_0 - mole fraction under n.c., $mole/m^3$

C_{pi} - heat capacity component i , $J/mole \cdot K$

C_p - total heat capacity, $J/m^3 \cdot K$

D_r - effective radial diffusivity of the bed, m^2/s

H_j - enthalpy change of reaction j , $J/mole$

l, L - tube length coordinate, m

P - pressure, atm

R - gas constant, $atm \cdot m^3 / mole \cdot K$

R_{grain} - equivalent radius of catalyst pellet, m

R - tube radius coordinate, m

T, T_w - temperature and tube wall temperature, K

$\overline{U}_l, \overline{U}_r$ - axial and radial gas velocity under n.c., m/s

ω_j - effective catalyst pellet rate, $mole / m^3 \cdot s$

y_i - mole fraction component i

λ_r - effective radial thermal conductivity of the bed, $J / m \cdot s \cdot K$

$\lambda_{r,g}$ - gas thermal conductivity, $J / m \cdot s \cdot K$

γ_{ij} - stoichiometric coefficient component i in reaction j

ε - bed porosity

5. ACKNOWLEDGEMENTS

The authors would like to thank NATO's Scientific Affairs Division for the support (project SfP-972557).

6. REFERENCES

- [1] E.I. Smirnov, A.V. Muzykantov, V.A. Kuzmin, A.E. Kronberg, I.A. Zolotarskii, *Chem. Eng. Journal*, 91(2003) 243-248.
- [2] E.I. Smirnov, A.V. Muzykantov, V.A. Kuzmin, I.A. Zolotarsky, G.W. Koning, A.E. Kronberg. *Chemistry for Sustainable Development*, 11 (2003) 293-296.
- [3] A.S. Ivanova, I.I. Bobrova, I.A. Zolotarskii, E.I. Smirnov, V.A. Kuz'min, A.S. Noskov, V.N. V.N. Parmon, Catalysts and the way of syn-gas production by steam-reforming of hydrocarbons. Russian patent application: # 2001111600 of 26.04.01
- [4] S. Grevskott, T. Rusten, M. Hillestad, E. Edwin, O. Olsvik, *Chem. Eng. Science*, 56(2001) 597-603.
- [5] M.A. Soliman, S.S. Elnashaie, A. Al-Ubaid and A. Adris, *Chem. Eng. Science*, 8 (1988) 1801-1806.
- [6] M.E. Abashar, S.S. Elnashaie, *Math. Comput. Modelling*, 7 (1993) 85- 100.
- [7] J. Xu, G.F. Froment, *AIChE Journal*, 1 (1989) 88 – 96.
- [8] E.I. Smirnov, A.V. Muzykantov, V.A. Kuzmin, A.E. Kronberg, I.A. Zolotarsky, 1-st International School-Conference on Catalysis for Young Scientists. Abstracts, (2002) 272-274.

Chapter 31

APPLICATION OF NMR MICROIMAGING FOR THE INVESTIGATION OF THE HETEROGENEOUS CATALYTIC REACTIONS INSIDE CATALYST PELLETS AND FIXED CATALYST BED

A.A. Lysova^{1,2,3}, I.V. Koptyug¹, A.V. Kulikov², V.A. Kirillov²,
R.Z. Sagdeev¹, V.N. Parmon²

¹International Tomography Center, Institutskaya St. 3A, Novosibirsk 630090, Russia,

²Boreskov Institute of Catalysis, acad. Lavrentiev Pr. 5, Novosibirsk 630090, Russia,

³Novosibirsk State University, Pirogov St. 2, Novosibirsk 630090, Russia

Fax: +7 3832 331399, +7 3832 343269;

E-mails: lysova@tomo.ncs.ru, koptyug@tomo.ncs.ru, parmon@catalysis.nsk.su

1. INTRODUCTION

It has been shown in the last few years that NMR imaging can be used as a powerful non-destructive method for the investigation of material structure and properties and for the studying of the processes occurring inside these materials. This method allows, in particular, to get the data concerning the spatial distribution of the liquid phase inside the porous object impregnated with liquid with spatial resolution of some hundred or even some tens of microns and follow its redistribution directly in the course of the investigated process. The possibility to obtain at the same time the spatial and NMR spectroscopic information makes very promising the application of NMR imaging for the investigation of the multiphase catalytic processes including the multiphase processes of C₁-chemistry, e.g. of Fischer-Tropsch synthesis in slurry or organized structures like honeycombs which are very exothermic.

Multiphase processes in the reactors with the fixed catalyst bed and co-current liquid-gas flow are widely used in industry. Usually such reactors work at the stationary regime but under some conditions there occur critical phenomena such as local overheating of the catalyst bed, oscillations of the temperature and reacting phase composition, existence of the exothermic bypassing reactions. The interaction of the heat and mass transport processes with the catalytic reaction in the reactor can lead to the hot spot formation and even reactor runaway. It is necessary to investigate experimentally the critical phenomena in the catalyst bed as well as on an individual catalyst pellet under conditions of the occurrence of exothermic reaction. The distribution of the liquid phase inside the catalyst pellet at the different modes of the reactor operation is there especially of great importance.

2. RESULTS AND DISCUSSION

For the first time in the history of NMR imaging we have carried out the experiments under conditions when the reactor with the operating catalyst was placed directly inside the NMR imaging probe. Note that these investigations were carried out at relatively high temperatures of the gas flow (67 °C) and catalyst pellet (up to 185 °C). We studied by this method the formation and the propagation of the chemical waves in the fixed granular bed which mimics a catalyst bed. Some peculiarities of the highly exothermic three-phase reaction of hydrogen peroxide decomposition were also studied.

2.1 BELOUSOV-ZABOTINSKY REACTION

As far as we know the most studies of catalytic reactions by NMR imaging deal with the homogeneous catalytic Belousov-Zhabotinsky reaction. This reaction is the oxidation of some organic compounds by bromate anion catalyzed by transition metal ions. Under certain conditions in this reaction occur the oscillations of the reagent and intermediate concentrations and the formation of the space-time wave structures.

Fig. 1 shows the possibility to use NMR imaging for the detection and investigation of the peculiarities of the chemical waves propagation in the model granular bed imitating the bed of the catalyst pellets. The investigation of the influence of the medium inhomogeneity on the behavior of this typically homogeneous system is possible in principle to perform only by NMR imaging method because the granular bed is opaque and thus the processes that occur in the volume of the bed are inaccessible for the

studying by other methods. It was found that the transfer from the homogeneous to the heterogeneous medium assists the decreasing of the influence of the convective liquid flow on the propagation of the wave front and allows to detect directly *in situ* the spherical and planar waves propagating in the bed. It was shown that the wave activity in the bed is observed only when the size of the pores between the pellets in the bed is greater than the critical size determined by the velocity of the propagation of the plane chemical wave.

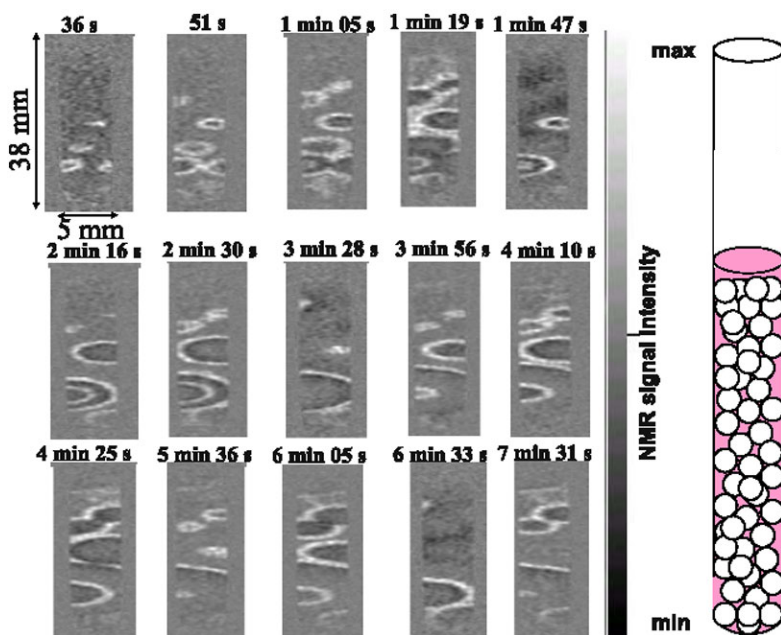


Figure 1. Typical 2D images of the tube filled with the glass particles of 0.5 mm in diameter and the Belousov-Zhabotinsky reaction solution. The spatial resolution was $(310 \times 230) \mu\text{m}^2$. The acquisition time of each 2D image was 14.3 s. The time corresponding to the middle of the acquisition period of image is shown in each image.

2.2 HYDROGEN PEROXIDE DECOMPOSITION

The next step that we have done – we turned to the really heterogeneous catalytic processes. We prepared a composite catalyst pellet consisted of an activated part and a non-activated part to establish the state of the catalyst

pellet in the course of hydrogen peroxide decomposition. The composite pellet was preliminary filled with water and then placed in the 3 M hydrogen peroxide solution. Since the relaxation time of nuclear spins in hydrogen peroxide solution differs from the relaxation time of pure water, we observed the decrease of the NMR signal intensity in the non-activated part of the pellet due to diffusion of hydrogen peroxide molecules into the pellet. In the activated part of the pellet such decrease of the NMR signal intensity was not observed. It means that hydrogen peroxide molecules do not diffuse into the catalyst pellet, and the decomposition process under low H_2O_2 concentrations and moderate activity of the used catalyst occurs not in the whole volume of the pellet, but in a thin surface layer.

2.3 AMS HYDROGENATION

We investigated the state of the catalyst pellet in the reactor with the co-current gas-liquid flow in the course of α -methylstyrene hydrogenation for which the three-phase mode of the catalytic process inside the pellet is typical. The fig.2 shows the redistribution of liquid phase inside the catalyst pellet under conditions of simultaneous supply of hydrogen and liquid AMS to the initially dry catalyst pellet. The change of the image intensity from the dark color to the bright color corresponds to the increase of the liquid phase content. In the areas of white color the level of the NMR signal is lower than the level of the noise. It is obvious that the liquid phase content in the pellet increases gradually. The maximal pellet overheating was observed during the 7th minute of the experiment (165 °C, image 2). Then the temperature of the pellet was gradually decreased as a result of the increase of the liquid phase content in the pellet. In the moment of the detection of the last image when the catalyst pellet is almost completely filled with liquid phase the temperature of the catalyst pellet (54 °C) is lower than the temperature of the gas flow (69 °C) due to an intensive endothermic evaporation of liquid on the pellet's surface. The lower NMR signal intensity in the periphery of the pellet and rugged front of the liquid phase propagation inside the pellet also point to the occurrence of evaporation and hydrogenation processes. The vapor produced reacts on the non-wetted part of the porous structure.

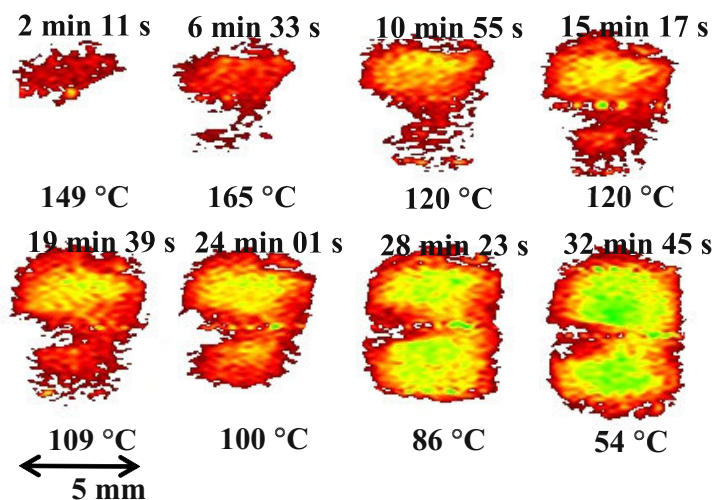


Figure 2. Typical 2D images of the liquid phase distribution inside the catalyst pellet of 15% Pt/Al₂O₃ in the process of AMS hydrogenation under conditions of simultaneous supply of hydrogen and liquid AMS to the top of the initially dry pellet. The spatial resolution was (230×140) μm²; the acquisition time of each image was 4 min 22 s.

Thus, *in situ* NMR imaging demonstrates that impregnation of the porous catalyst with a liquid reagent at the simultaneous occurrence of endothermic reagent evaporation and its exothermic hydrogenation leads to the formation, inside the catalyst pellet, of two domains with the strongly differing liquid phase content.

In the presented experiments the images of the NMR signal intensity of liquid phase were obtained without distinguishing the AMS and cumene contributions. It is difficult to establish the spatial distribution separately of the reagent and the product because the lines of the proton NMR spectra of liquid in the porous structure are much broadened in comparison to the bulk liquid. Nevertheless, it is possible in principal to use NMR imaging with spatial resolution for measuring the reagent and product quantity.

We have demonstrated the possibility to use NMR imaging for an independent investigation of the reagent and product distribution along the fixed catalyst bed worked at the stationary mode under conditions of the supply of hydrogen and liquid AMS to the bed. In particularly, we found that in the upper part of the catalyst bed to which the liquid reagent is permanently supplied, the bed is filled predominantly with the reagent; in the middle of the catalyst bed 30 mm long, the mixture of AMS and cumene in comparable quantities is present; at the outlet of the bed we observed the

NMR spectrum only of the product. The general tendency of an increase of the reagent/product ratio from top to bottom of the catalyst bed as well as a non-uniformity of conversion to radius of the catalyst bed was also observed in this experiment.

3. CONCLUSIONS

NMR imaging was used for the first time for the detection of chemical waves in the granular bed and for the *in situ* investigation of the heterogeneous catalytic reactions including the reaction at elevated temperatures. We achieved in our experiments the temperature interval of ca. 200°C which is just suitable for the Fischer-Tropsch synthesis.

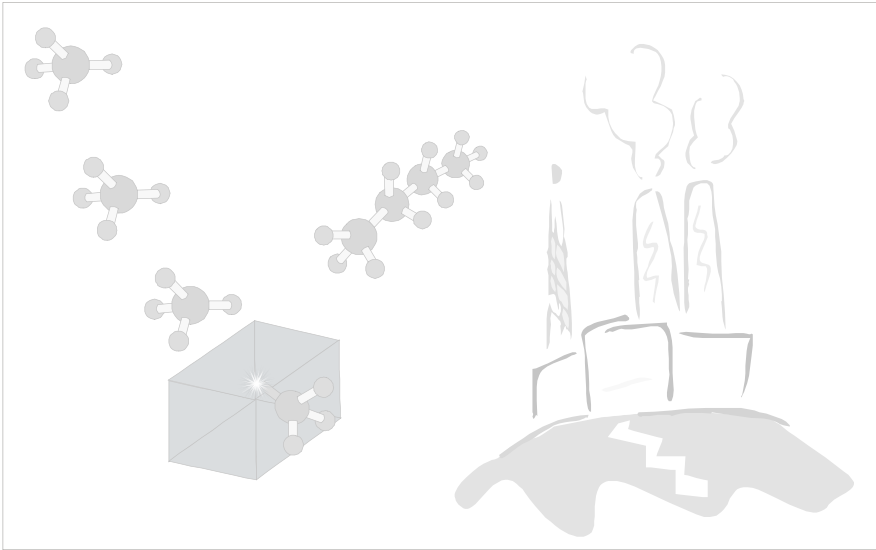
4. ACKNOWLEDGEMENT

The work was supported by the grant of the Russian Foundation for Basic Research (02-03-32770). A.A. Lysova is gratefully acknowledges a scholarship awarded by the Zamaraev International Charitable Scientific Foundation.

5. REFERENCES

- [1] I.V. Koptyug, A.V. Kulikov, A.A. Lysova, V.A. Kirillov, V.N. Parmon, R.Z. Sagdeev, *Journal of American Chemical Society*, 124, pp. 9684-9685, 2002.

SECTION 3



CONCLUSIONS

Chapter 32

NATURAL GAS AS FEEDSTOCK

Jacques C. Védrine

Laboratoire de Physico-Chimie des Surfaces, ENSCP, 11, rue P. & M. Curie, F- 75005 Paris, France

Abstract: Natural gas is a very cheap and abundant raw material but its main components, methane, ethane and propane, are rather chemically inactive compounds, which makes their upgrading to more valuable products quite difficult. Moreover the natural resources are often quite far from consumers, which makes their commercialisation even more difficult. However, in the last thirty years, natural gas has seen its importance growing tremendously due to the increase in price of oil and its expected and inexorable shortage in a more or less far future.

The actual challenge is then to use natural gas as an important feedstock and to transform it to more valuable compounds. There are two ways:

1 - The industrially applied processes based on partial oxidation to syngas ($\text{CO}+\text{H}_2$) and its further transformation to synfuel or methanol;

2 - All chemical transformation to other compounds such as direct partial oxidation to methanol or formaldehyde, or direct conversion to aromatics or a variety of hydrocarbons, etc.

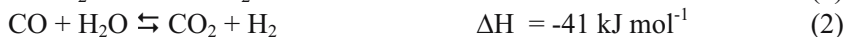
In this paper we are considering the actual state of the art in industrial processes and summarising all ideas expressed during a workshop held at a NATO-ASI in July 2003 in Vilamura, Portugal, as possibilities for the future.

Key words: Natural Gas, Feedstock, challenges, running processes, new reactions of methane and new products

1. INTRODUCTION

Natural gas as feedstock is a real challenge since it involves all bottlenecks met in conversion of light alkanes. Depending on the source of natural gas, it contains various and non negligible amounts of methane (major), ethane, propane and other alkanes and its price depends mainly on its geographical location, since its resources are rarely located in areas with high population. Therefore, natural gas price reflects it. For chemical industries the main application, at present, consists in partial oxidation to syngas ($\text{CO} + \text{H}_2$).

Such syngas technology dates from the beginning of the last century, with deployment of the so-called Haber-Bosch process in 1917, developed in Germany. The process comprises endothermic reaction of steam reacting with coke producing hydrogen according to [1] followed by the slightly exothermic water gas shift reaction WGS [2] and Boudouard reaction [3]:



The gas obtained is rich in hydrogen and was used in the Haber process for ammonia production by adding nitrogen and in the Fischer-Tropsch process for the conversion of coal to liquid fuels.

The concept of activating methane via analogous reactions of steam reforming was investigated in Germany at about the same time. In the 1950s it appeared that naphtha could be steam reformed economically to provide a cheap source of hydrogen. Many plants were then constructed, when methane sources were too remote or not easily available. In the past 25 years, natural gas was increasingly available as the main feedstock for steam reforming. Two applications of syngas are becoming of increasing importance:

- Manufacture of liquid fuel from remote or marginal natural gas resources (Fischer-Tropsch route being major);
- Generation of hydrogen for fuel cells

The sources of natural gas remaining in 2003 amount to ca. 180 trillions m^3 , corresponding to 70 years of production at 2001 level [1]. The Middle East has the greatest remaining resources with 40%, followed by former Soviet Union. Production equaled 3 trillions m^3 per year in 2000 with 92% sold and the 8% remaining being re-injected or flared. At present the largest producer is North America (33%), followed by Middle East (26%), Western

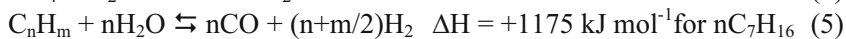
Europe, and former Soviet Union (11.5%), Africa (11.2%), Asia & Oceania (8.9%), etc. “fire ice”-methane hydrates on ocean bottoms may be estimated as 8,000 trillions cubic metres.

The conversion of natural gas to methanol via $\text{CO} + \text{H}_2$ or to syngas is the most widely practiced actual route to added value. The first step is the conversion of natural gas to syngas, which in turn is converted to syngas, with 65% of cost associated with the production of syngas. Several routes to syngas are possible and different processes giving different CO/H_2 ratio values, as schematized in the reactions given below in part 2. Syngas does represent the best route for hydrogen (as source for NH_3 , etc.), H_2 -CO (methanol, for MTO, MTP, MTG processes), for H_2 -CO (FT products, waxes, lubricants, etc.). The MTO (methanol to olefines, mainly ethylene and propylene) process has recently overcome the exploratory phase with two technologies, the methanol to olefines by Hydro/UOP on SAPO-34 zeolitic material and the methanol to propylene on proprietary zeolite catalyst by Lurgi/Statoil. The old MTG process from Mobil on ZSM-5 zeolite was only developed industrially in New Zealand and produces currently mainly methanol. The production of hydrogen in syngas process will be increasingly important, for instance for solid oxide fuel cell (SOFC) or for all hydrotreating catalytic reactions. The objective in fuel cell is to convert methane or hydrogen or other fuel directly to electricity as expressed by the Nernst equation ($E^0 = n\Delta G^0$), i.e. ideal efficiency is expressed by $\Delta G^0/\Delta H^0$ for the overall combustion reaction.

2. PROCESSES OF INDUSTRIAL APPLICATIONS

The choice of the syngas technology is dictated by the need for high conversion, the requirements for syngas composition and the scale of operation. Lets us consider several of these reactions:

2.1 Steam reforming:



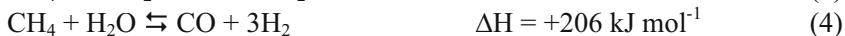
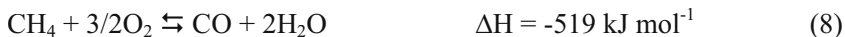
2.2 CO₂ “Dry” Reforming:



2.3 Catalytic partial oxidation (CPO):



2.4 Autothermal reforming (ATR)



2.5 Total Oxidation



Steam and CO₂ reforming reactions are strongly endothermic and, hence, the manufacture of syngas requires a high temperature to achieve high methane conversion. The overall heat of reaction becomes negative, which implies that heat should be supplied to the system. Note that dry reforming is not yet practiced industrially, although its CO/H₂ ratio is more suitable for FT reaction process than steam reforming reaction. It was studied in the 50s on Ni catalyst by M. Prettre *et al.* [2].

Classic Fischer-Tropsch (FT) reaction on Co or Fe based catalysts converts syngas to synfuel, i.e to mixtures of hydrocarbons, particularly waxes. The main products are n-paraffins for more than 90% together with olefines and alcohols. The molecular weight distribution follows the Schultz-Flory model.

Methane is firstly converted to syngas, which may then be processed to give alcohols and hydrocarbons [3-8]:



The production of methanol is an important industrial reaction with high yield on Cu/ZnO-Al₂O₃ type-catalysts as in the process developed by ICI long time ago. The production of synfuel via the Fisher-Tropsch process [7] is economically less attractive and is used in only few places. However, the expected ineluctable shortage of crude oil has led to serious consideration of wider applications of methane sources.

3. PROCESSES NOT YET INDUSTRIALLY APPLICABLE

The obvious attraction of the direct processing of natural gas to obtain more valuable products has led to the study of oxidation (oxidative coupling in the 70s), NO catalysed oxidation and direct oxidation to formaldehyde or methanol on MoO₃/SiO₂ catalyst, of reactions with halides or sulfates and of pyrolysis based reactions. Only high temperature pyrolysis has been exploited industrially, the other processes based on these reactions were more or less abandoned for economical reasons. Many studies were performed in the 70s by industry and 80s in academia of oxidative coupling of methane at high temperature (>650°C) on basic complex oxides (e.g. MgO, doped with rare earth-based oxides [9]) with formation of ethane/ethylene. This tentative failed for economical reasons, as a 20% maximum yield in C₂ hydrocarbons was reached.

It therefore appears that alternative routes to syngas for C₁ utilisation remains a major challenge. This implies:

- New reactions for commodities, fine chemicals and functional chemicals;
- Revisiting our concept and ideas about energy, electricity, re-injection and flaring issues;
- Implication on sustainable strategy (CO₂, environment, etc.);
- Financial aspects, costs and profits;
- Careful analysis of ΔT parameter, which is an important parameter of the analysis, as described by J Rostrup-Nielsen in his paper [1]. It corresponds to the price of product minus that of the feedstock minus investment minus profit minus process running and minus energy spent;
- Great efforts in improving reactors efficiency by new chemical engineering studies and processes should be emphasised. The use of

membranes as gas distributors or removal of products or water may be of importance for the future, if diffusivity problems are solved physically (flow rates rapid enough to avoid huge reactors, resistance to membrane deterioration during reactions, etc.) and economically speaking.

The most obvious idea to think about any possibility is to look at methane dissociation or insertion of elements such as oxygen, according to the following schemes:

3.1 CH₄ decomposition:



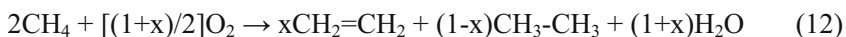
3.2 Direct oxygen insertion (oxidation)

One may then think about the following reactions:

- $\text{CH}_4 + \frac{1}{2} \text{O}_2 \rightarrow \text{CH}_3\text{OH}$ on H_2SO_4 (oleum)
- $\text{CH}_4 + \text{O} \cdot \rightarrow \text{CH}_3\text{OH}$
- CH_4 thermal decomposition on Ni or Ni alloy into H_2 and carbon tubes as pioneered by R.T. Baker from Exxon in the 70s;
- Photochemical dissociation of dioxygen into reactive O \cdot (TiO_2 solar)

Recent possibilities have been proposed as alternatives

- Oxidative coupling, which consists of converting methane to CH_3° radicals in the presence of oxygen and a basic doped oxide catalyst [9] at ca. 700°C, see supra. The CH_3° radicals couple to form ethane, which thermally dehydrogenates to ethene under reaction conditions, according to:



The process developed by ARCO could provide 16% yield at 20% conversion and 80% selectivity, but was not economically attractive and then abandoned;

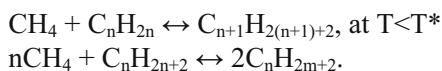
- Oxidative esterification by two major routes, one to CH_3Cl and the other one to $\text{CH}_3\text{OSO}_3\text{H}$. The first route consists in converting methane with O_2 and HCl over oxychlorination catalyst with a yield of 30%, much higher than the 2% for direct oxidation. For the second route the methyl group can be protected to further oxidation by an

electronegative group, such as HSO_4^- . Methane is then oxidised to methylbisulfate with 80% yield per pass, using SO_3 as oxidant according to:



In a second step, methylbisulfate is hydrolysed to methanol and, then, SO_2 is oxidised to SO_3 . Note that traces of water are to be avoided, since SO_3 gives then H_2SO_4 , which imposes drastic dried conditions, while corrosive sulfuric acid limits application.

- Direct partial oxidation of methane to methanol at high pressure or formaldehyde at low pressure. Many catalysts have been proposed, but the reactions can occur, even without any catalyst. The yield rarely exceeds 2% and is then not economically attractive;
- Non oxidative routes. Several routes have been proposed to convert methane to olefines or aromatics without the use of oxidants:
- High temperature thermal pyrolysis to methane and ethyne [10]
- High temperature methane aromatisation, mainly to benzene and naphthalene, at high temperature ($>700^\circ\text{C}$) using Mo/ZSM-5 catalyst [11, 12] and assigned to MoC_2 formed in ZSM-5 material during pre-activation or reaction.
- Low temperature methane coupling via surface carbides [13].
- These processes necessitate swing-type reactors and are highly energy consuming, at least for the first two, which limits their applicability.
- A rather recent and surprising finding is the observation that methane can react with other reactants such as C_nH_m giving products, as given in the following examples:
 - Method for production of aromatics from methane, called “Bicyclar” process such as $\text{CH}_4 + n[\text{C}_2\text{-C}_4] \rightarrow \text{aromatics} + 6\text{H}_2$, e.g. $\text{CH}_4 + 2 \text{C}_3\text{H}_8 \rightarrow \text{C}_6\text{H}_5\text{CH}_3 + 6\text{H}_2$ $T^* = 600^\circ\text{C}$ on Zn, Ga/ZSM-5 catalyst with $\text{CH}_4/[\text{C}_2\text{-C}_4] > 4$. This process corresponds to a Russian patent assigned to the Boreskov Institute of Catalysis, Novosibirsk, RU [14];
 - Method for production of components for motor fuels, called “Bi-reforming” process, such as $\text{CH}_4 + \text{C}_5$ giving benzene + 4H_2 at $T^* \sim 725^\circ\text{C}$ on Pt/ Al_2O_3 catalyst. E.g. $[\text{C}_1\text{-C}_4] + \text{C}_n$ giving bilateral chain benzenes + 4H_2 . This process corresponds to a Russian patent assigned to the Boreskov Institute of Catalysis, Novosibirsk, RU [15].



Another challenge, obviously not limited to natural gas is to deal with sustainability, which is a major concern of this NATO, Advanced Study

Institute. Let us ask some questions and make suggestions, although not often realistic, but which express our present abnormal human behaviour.

- What is sustainability? Certainly we cannot meet sustainability with everything nor do- with the exception of photocatalysis. Obviously we need better selectivity resulting in less consumption/loss for the same effect;
 - What we should be doing is to minimise problems, energy consumption and raw material consumption by using catalysis, which is a key technology;
 - Why not to limit American cars to 2L engines, increase the price of fuel significantly and plant trees, extensively!
 - We should focus on:
 - Increased selectivity;
 - Avoidance of obvious problems, such as halides or sulfates;
 - Regard sustainability as a real objective, not a word associated with a successful grant application;
 - Accept that people will not readily change their way of life, but work to make it more sustainable;
 - How can we avoid natural gas, which is flared in the NG fields, and succeed in its transformation in liquid or commodities fuel? ;
 - How natural gas from biomass can be exploitable? ;
 - How to exploit oil fields and natural resources at best, i.e. with limited loss: including heavy oils, tar sands, oil shale? ;
 - CO₂ minimisation and heat thermal pollution remain a major issue and any progress is hardly expected and should be looked for in research plans. This is the next “hot topic”, after the sulfur and VOCs issues have been solved in a satisfactory manner;
 - Development of renewable fuels against fossil fuels;
 - Move to 100% selectivity in carbon to products transformation;
 - Sustainability measured by financial, environmental and social impacts;
 - Syngas to further conversion, as the process is not at maximum efficiency.

4. CONCLUSIONS

Necessity for natural gas as a feedstock has become increasingly important and economic policy has changed in the five last years and

remains a great challenge for the future, due to the increase in price of oil and its expected and inexorable shortage in a more or less far future. At the present time, the main industrial process in operation consists in methane partial oxidation to syngas, followed by its transformation to methanol or synfuel. Two applications of syngas are becoming of increasing importance:

- Manufacture of liquid fuel from remote or marginal natural gas resources (Fisher-Tropsch route being major);
- Generation of hydrogen for fuel cells.

Reforming for fuel cell hydrogen has been proposed as an alternative, comprising generally a mix of partial oxidation of methane, autothermal reforming and compact reforming.

Alternative routes have been proposed, particularly for direct conversion of methane and are still not commercially interesting. Therefore, a large place remains for further researches in the field, which should absolutely associate catalyst makers, chemical engineering and economics. Some trends have been proposed to activate directly methane by reactant as oxygen, chlorine, oleum, and, even, other hydrocarbons (e.g., bicyclar or bi-reforming processes).

5. REFERENCES

- [1] J.R. Rostrup-Nielsen, in “*Sustainable strategies for the upgrading of natural gas: fundamentals, challenges and opportunities*”, E.G. Derouane et al. (ed.), Kluwer Academic Press, Dordrecht, 2004, this book;
- [2] M. Prettre et al., C.R. Acad. Sci., Paris, 1953;
- [3] L. Guzzi and Kiricsi, Appl. Catal. A: Gen., 186 (1999) 375;
- [4] G.E. Keller and M.M. Bhasin, J. Catal., 73 (1982) 9;
- [5] Z. Yan, C.X. Xiao, and Y. Kou, Catal. Letters, 85 (2003) 378;
- [6] D. Keene, C.F. Cullis and D. Trimm, J. Catal. 19 (1970) 378;
- [7] J.R. Anderson, Appl. Catal., 47 (1989) 177;
- [8] D. Trimm, in “*Sustainable strategies for the upgrading of natural gas: fundamentals, challenges and opportunities*”, E.G. Derouane et al. (ed.), Kluwer Academic Press, Dordrecht, 2004, this book;
- [9] D. Filkova, D. Wolf, G. Gayko, M. Baerns, L. Petrov, Appl. Catal. A: Gen. 159 (1997) 33;
- [10] J. Well, F. Chevron, C. Raimbault, R. Genier, G. Renesme, L. Capogna and Y. Muller, Rev. Inst. Fr. du Pétrole, 47 (1992) 255;
- [11] L. Wang, L. Tao, J. Huang and D. Wang, Catal. Lett., 21 (1993) 35;
- [12] Y. Xu, L. Wang, M. Xie and X. Gou, Catal. Lett., 30 (1995) 135;
- [13] E. Mielezarski, S. Monteverdi, S. Amariglio and H. Amariglio, Appl. Catal. A: Gen., 104 (1993) 215;
- [14] Russian patent, assigned to the Borekov Institute of Catalysis, Novosibirsk, RU, No.2188225, issued on 27.08.2002;

- [15] Russian patent, assigned to the Boreskov Institute of Catalysis, Novosibirsk, RU, No.2144942, issued 10.01.2000.

Chapter 33

SUSTAINABLE STRATEGIES FOR THE UPGRADING OF NATURAL GAS

Conclusions of the Nato Advanced Study Institute

Eric G. Derouane

Center for Organic, Synthetic, and Catalytic Research, Universidade do Algarve, Campus de Gambelas, Faculdade de Ciências e Tecnologia, Department of Chemistry, 8000-117 Faro, Portugal.

Abstract: The NATO Advanced Study Institute aimed at presenting an integrated and coherent view of recent developments and prospects for the use of natural gas as a fuel or as a feed for the production of liquid fuels and higher value chemicals. Catalysis plays a key role in the conversion of natural gas to chemical products and is increasingly involved in the use of natural gas for the energy sector. In addition to the chemical challenges that need to be met to upgrade natural gas, methane in particular, chemical engineering issues also have to be considered and resolved and economic considerations cannot be ignored. The interplay between all the above factors was discussed in great detail by lecturers from both Industry and Academia.

Key words: Natural gas, catalysis, economy, engineering, liquid fuels, chemicals.

1. INTRODUCTION

1.1 Objectives

The objectives of the NATO Advanced Study Institute were to provide an integrated and coherent view, considering chemical, chemical engineering, and economy factors, of sustainable strategies directed at the upgrading of natural gas and to report in a tutorial manner on challenges and prospects for the utilization of natural gas as a source of chemicals and liquid fuels.

These objectives were reached by a comprehensive set of lectures delivered by scientists from Industry and Academia, two workshops on “Natural Gas as a Feedstock” and “Bottlenecks for the Conversion of Light Alkanes”, respectively, and recent research reports presented by the participants.

1.2 The scene

The proven reserves of natural gas increase at a greater rate than those of crude oil. The realization that supplies of crude oil are finite and that several of the remaining large reserves are located in politically sensitive locations has focused attention on the use of natural gas as a source of alternate fuels and valuable chemicals. Upgrading natural gas for those purposes relies extensively on catalytic science.

The composition of natural gas varies broadly depending on its origin. Natural gas in Western Europe and North America is rich (85+%) in methane and poor in C₂-C₄ hydrocarbons whereas in the Middle East natural gas can contain as little as 55% methane. In general terms, the composition of natural gas can be defined as 60-98% methane, 1-20% ethane, 1-10% propane, 1-4% butanes, 1-10% nitrogen and helium, 1-5% H₂S, and 1-10% CO₂. *Two questions arise from this observation. Should the C₂-C₄ hydrocarbons be separated from methane before processing of natural gas? How can natural gas purification be best performed?*

Another important consideration is the so-called “ΔP factor”, i.e., the expected profit margin underpinning the possible implementation of a new technology. When natural gas is only available at a price comparable to the fuel market, due either to production costs or transportation costs (as liquefied natural gas, LNG) from remote areas, it will be used as a fuel, i.e., as a direct energy source. This is mostly the case in the Western World. In remote areas, the price of natural gas is low and sometime even negative in locations where flaring is prohibited. *Therefore, although the technologies will likely be developed mainly in the Western World, new processes and plants for the upgrading of natural gas will most likely to be located in geographical areas that have little use for natural gas as a fuel. Such processes can be the production of liquid fuels or valuable chemicals, either as intermediates or final products.*

External factors also affect the supply-demand equilibrium (market and use) of natural gas. World stability and foreign government policies may dictate supply as well as consequences of legislations from public agencies (national or international), and sometime unfortunately decisions of politicians reacting too swiftly to proven or unproven causes amplified by the media and thereafter supported by public opinion.

Other factors that also need to be considered are the future discovery of new natural gas fields and likely changes in the operation and output of crude oil refineries.

Overall, a simplified picture is that natural gas will be used as a fuel and an energy source in energy demanding areas and as a source of chemicals in others, with most new technologies being implemented in remote areas and/or developing countries.

1.3 Where to?

Chemistry, chemical engineering, and economy and monetization factors will govern the development and implementation of new technologies for the upgrading of natural gas to liquid fuels and valuable chemicals.

With respect to chemistry, considering the inherent inertness of light alkanes, alkane activation and upgrading processes are generally operated at high temperature. Several undesired by-products will most often be formed simultaneously to the desired one(s) when converting natural gas, one exception being the production of methanol through a sequence of steps (reforming, shift, and synthesis). In general, separation costs will be relatively high. By-products formation must be reduced or a use for those must be found.

Another important consideration also impacting on the economy of such processes will be their overall energy efficiency. As much as energy can be supplied in various ways, energy losses also occur via several routes. An obvious one is the production of CO_2 . Another one is the production of water that lowers the amount of valuable hydrogen in the products and uses rather expensive oxygen. Finally, waste heat can also be produced. The latter can however be reduced if the water generated in oxidative processes is present as high pressure steam at a reasonable temperature.

Economy of scale and integration will play an increasingly important role. Natural gas or methanol “refineries” leading to a variety of products, operated as megaplants in the same manner as crude oil refineries, are currently being built and more being considered. Costs and market demand will be the main factors driving the development of new processes as well as their implementation and localization.

Most often, a delicate balance between all of the above factors will have to be achieved to ensure the success of forthcoming natural gas upgrading technologies

2. ACTIVATING LIGHT ALKANES

2.1 Why is the selective activation and functionalisation of light alkanes difficult?

Light alkanes are inherently inert molecules. They possess no “pi” electrons that provide the catalyst with a “handle” to “grab” the molecule. Single bonds are resistant to chemical attack. In the specific case of methane, activating the first C-H bond requires more energy than activating the second one in the primary functionalized product, which obviously renders difficult the direct selective oxidation of methane to methanol. The problem is slightly less severe for C₂-C₄ alkanes, although in this case one should also consider the possibility to activate the C-C bond. Two exceptions are (1) the selective oxidation of n-butane to maleic anhydride where a high selectivity can be reached because of the high electronic and conformational stability of the product, and the oxidation of isobutane to t-butyl hydroperoxide as the tertiary C-H bond of isobutane has unique reactivity.

2.2 Options for the conversion of light alkanes

Catalytica developed in the late 90's catalytic systems able to selectively oxidize methane to methanol in a single one-pass high yield. The best catalysts were platinum-based complexes and the oxidant 102% sulfuric acid. Keys to yields in methanol exceeding 70% were (1) the development of novel organometallic catalysts enabling C-H bond activation below 250°C and (2) the use of “product protection” to stabilize the desired product from over-oxidation, i.e., as methyl sulfate. Hydrolysis of the later liberates methanol and sulfuric acid. The major problem that prevented the further development of this technology was the dilution of sulfuric acid by water produced in the oxidation step and the necessary need for an associated sulfuric acid regeneration plant. In any case, the “product protection” concept is a most interesting one that should be kept in mind.

The non-oxidative conversion of light alkanes to higher hydrocarbons and hydrogen is possible using bifunctional catalysts, typically acid zeolites (e.g., H-MFI) also containing a dehydrogenating function. Well-known and now commercialized is the UOP-BP Cyclar process that converts propane to aromatic hydrocarbons, hydrogen, and light off-gas at 525-550°C using a Ga-modified H-MFI zeolite catalyst. More recently, it has been reported that methane can be converted to aromatic hydrocarbons and hydrogen on Mo-modified H-MFI catalysts operated at 700°C as reviewed and discussed in

the present volume. Conversion (ca. 12%) and selectivity to aromatics (ca. 70%) are limited by thermodynamics and catalyst lifetime is a major problem. Nevertheless this approach deserves more attention as it offers a natural gas “chemical separation” process enabling the conversion of the C₂-C₄ fraction to aromatics and hydrogen, leaving behind a methane stream that is more suitable as feed for classical steam-reforming.

As discussed in several lectures, it is however most likely that the preferred route for the upgrading of light alkanes will continue to be based on natural gas reforming to produce syngas, followed by shift, and various “synthesis” processes (methanol, Fischer-Tropsch, etc.), including the development and implementation of new technologies and megaplants. A revival of the chemistry of acetylene, a most versatile building block, and innovations in the chemistry of formaldehyde and acetic acid should also be considered.

3. ISSUES AND OPPORTUNITIES

3.1 The bandwagon syndrome

As mention earlier, there is increasing interest in the upgrading/conversion of natural gas and therefore, research in this field is expanding rapidly both in Industry and in Academia.

As far as Industry is concerned, it is obvious that any overcapacity of intermediate feeds or products will ultimately result in lower returns unless market demand increases and/or new downstream uses are identified.

With respect to Academia, it is important to note that fundamental research in this field, although necessary and certainly to be encouraged, should not be guided only by the necessity of immediate funding, the real and long term value of fundamental research being the intellectual property it generates.

There is complementarity between academic and industrial research that needs to be promoted in this field through a closer collaboration between these two communities, with industry playing a substantial role in defining the key challenges to be targeted by basic academic research.

3.2 Criteria for new products and/or new conversion pathways

Profitability will dictate new developments. Natural gas as a feed or intermediates derived from natural gas will have to be readily accessible or

be available at a reasonably low price from remote locations. Equally important will be the need for a favorable demand: either an existing market or a market that can be “educated”. Profitability evaluations should include capital and operating expenses as well as costs projections on feed and products values, activity of competitors, and else. Obviously, some of these factors can and will be affected by government policies and world stability.

The potential for diversification will be an important element in the development of new technologies. Obviously, the captive use of intermediates and/or products is an incentive to develop a new technology but the possibility of other applications and merchandizing options is equally important should market demand change.

Last but not least, the nature of the underpinning chemical and technological know-how will play a major role. Are they proven chemical or engineering approaches that will necessitate limited additional research and that are likely to be implemented in a acceptable timescale, or are they new chemistry and engineering approaches that will require substantial R&D investment and time?

3.3 Decreasing costs

As costs related to the upgrading of light alkanes will usually be rather high due to the high energy input needed to activate rather inert molecules, controlling costs is an important issue.

Minimising energy losses implies achieving maximum carbon efficiency, i.e., minimal CO₂ production, as well as optimizing the use of oxygen (an expensive reactant when used, e.g., partial oxidation of methane) by avoiding the production of low pressure/low temperature steam whose energy content cannot be recovered.

A variety of oxidants can be used for the reforming of alkanes. Although rather expensive, oxygen is the most efficient oxidant. Obviously, alternate routes less expensive than cryogenic separation should be searched for to separate oxygen from air. The direct use of air may appear attractive at first sight as it avoids the necessity for an oxygen plant. However, it implies that large volumes of nitrogen have to be dealt with, which prevents operation with recycle (building up of nitrogen in the recycle loop) and increases downstream costs (compressing, heating, separation). In addition, for reactions operated at high temperatures and in particular when hydrogen is also present the possible formation of toxic CN-group containing compounds (small amounts of HCN included) should not be overlooked. N₂O has also been considered as an efficient oxidant. However, it is expensive and not readily available. Therefore, it is only suitable for small scale applications. Cl₂ and Br₂ are other oxidants that have been looked into

for the activation of methane, with chloro- and bromo-methanes being thereafter converted to liquid products. The major drawback in the latter case is the production of HCl or HBr that need to be captured or recycled as Cl_2 or Br_2 . The latter is not practical when large amounts of HCl or HBr have to be treated as an equivalent amount water (contaminated with Cl_2 and Br_2) is produced simultaneously and has to be disposed of.

Increasing attention is being paid to process integration. An example is the combination of endothermic steam reforming with exothermic catalytic partial oxidation, in the case of methane, to achieve the desired syngas H_2/CO ratio and heat balance. Improving separation and integrating by-products utilization are also being actively looked at. Last but not least, similar to the operation of oil refineries that integrate several different processes to achieve the maximum conversion of intermediates to desired products, natural gas and methanol “refineries” are being considered, “Gas-to-Liquids” (GTL) processes evolving into “Gas-to-Products” processes (GTP) and methanol being used on-site as an intermediate to higher value chemicals. Methanol and acetic acid megaplants are likely to deliver in the future large amounts of base chemicals suitable for diversification.

4. CHALLENGES

4.1 Innovative chemistry

There are plenty of opportunities for innovative chemistry using C_1 or C_1 -derived building blocks such as methanol, formaldehyde, methylformate, and dimethyl ether. In particular, one should note the potential offered by dimethoxy methane (DMM) and poly-dimethoxy methane (PDMM) as liquid fuels. One should not overlook either new developments in the chemistry of ketenes (derived from acetic acid) and acetylene (from the high temperature pyrolysis of methane) that are known to be efficient building blocks.

Effective CO_2 utilization is still a challenge as well as some other specific reactions. Among those are the direct selective conversion of methane to methanol, the terminal oxidation of light alkanes, the use of methane as a co-reactant in the upgrading of higher hydrocarbons, and new routes for the conversion of C_2 - C_4 alkanes (ethane to ethanol, propane to isopropanol, etc.).

In the general field of Fischer-Tropsch chemistry, narrowing or controlling directly the Schulz-Flory distribution is still the major challenge.

Alternate routes to the current syngas chemistry used for methane utilization will continue to be considered further. In addition to those already mentioned above, it is worth considering the “Bicyclar” and “Biforming” conversions currently being researched at the Boreskov Institute of Catalysis in Novosibirsk as well as the novel organometallic chemistry being developed by the group of J.M. Basset in Lyon.

4.2 Innovative chemical engineering

In addition to the trends mentioned above, opportunities exist for the development of compact reactors for the local production of syngas, hydrogen, methanol, etc... as precursors to chemicals or fuels.

New technologies for slurry, fluid bed, and fixed bed reactors, as well as membrane reactors, are likely to appear.

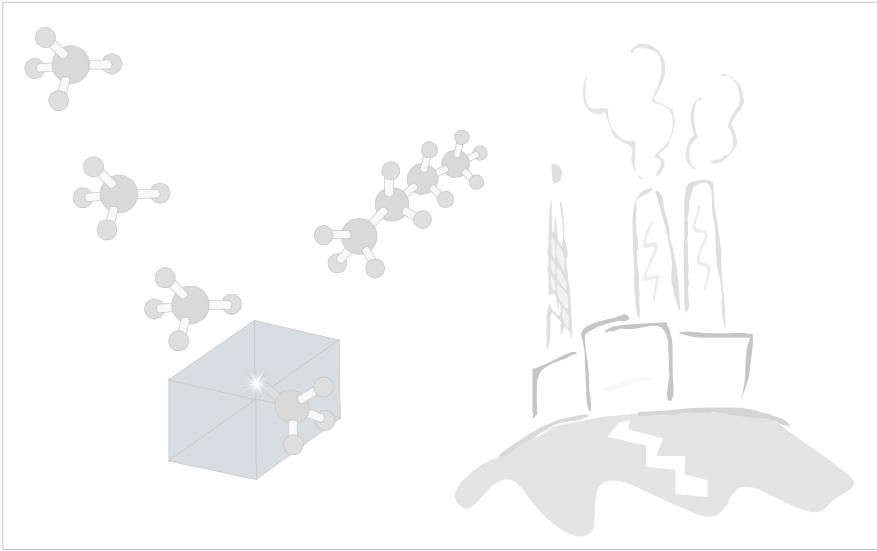
Active research will continue to grow in the general field of membrane reactors, with specific attention being paid to the purification and distribution of the reactants, the type of catalyst used and whether it is incorporated in the membrane, and the removal of products. The practical implementation of membrane reactors in commercial units depends on the achievement of adequate fluxes through the membrane and minimizing the presence of pinholes reducing selectivity, in particular for non-metallic membranes.

5. CONCLUSIONS

Upgrading of natural gas to liquid fuels and chemicals is a research field of increasing importance, where both fundamental chemistry as well as innovative engineering have an important role to play.

In most cases, economic considerations will drive the choices with natural gas being used directly as an energy source in locations where there is a market for natural gas as a fuel or for power generation. Upgrading of natural gas will occur in remote locations or when cheap natural gas is available.

Carbon yield, economy of scale, megaplants, and natural gas based “refineries” are key words that will guide or describe future developments.



PARTICIPANTS

PARTICIPANTS

Directors:

- ✓ Prof. Eric Derouane
Universidade do Algarve
Faculdade de Ciências e Tecnologia - Química
Campus de Gambelas
P-8000-117 Faro
Portugal
- ✓ Prof. Valentin N. Parmon
Boreskov Institute of Catalysis
Prospekt Akademika Lavrentieva, 5
Novosibirsk 630090
Russia
- ✓ Prof. Francisco Lemos
Instituto Superior Técnico
Departamento de Engenharia Química
Av. Rovisco Pais 1
1096 Lisboa Codex
Portugal
- ✓ Prof. Fernando Ramôa Ribeiro
Instituto Superior Técnico
Departamento de Engenharia Química
Av. Rovisco Pais 1
1096 Lisboa Codex
Portugal

Organising Committee:

- ✓ Pedro Borges
Instituto Superior Técnico
Departamento de Engenharia Química
Av. Rovisco Pais 1
1049-001 Lisboa
Portugal
- ✓ Hugo Carabineiro
Instituto Superior Técnico
Departamento de Engenharia Química
Av. Rovisco Pais 1
1049-001 Lisboa
Portugal
- ✓ Isabel Fonseca
Universidade Nova de Lisboa
Departamento de Química
Quinta da Torre
2825-114 Caparica
Portugal
- ✓ Filipe Freire
Instituto Superior Técnico
Departamento de Engenharia Química
Av. Rovisco Pais 1
1049-001 Lisboa
Portugal
- ✓ Maria Amélia Lemos
Instituto Superior Técnico
Departamento de Engenharia Química
Av. Rovisco Pais 1
1049-001 Lisboa
Portugal
- ✓ José Manuel Lopes
Instituto Superior Técnico
Departamento de Engenharia Química
Av. Rovisco Pais 1
1049-001 Lisboa
Portugal

- ✓ Carla Pinheiro
Instituto Superior Técnico
Departamento de Engenharia Química
Av. Rovisco Pais 1
1049-001 Lisboa
Portugal
- ✓ Ricardo Ramos Pinto
Instituto Superior Técnico
Departamento de Engenharia Química
Av. Rovisco Pais 1
1049-001 Lisboa
Portugal

Lecturers:

- ✓ Martin Atkins
BP Chemicals
Bd B
Chertsey Road
Sunbury-on-Thames
Middx TW15 2QU
United Kingdom
- ✓ Jean-Marie Basset
CPE Lyon - Laboratory COMS
Domaine Scientifique de la Doua
BP 2077
43, boulevard du 11 novembre 1918
69100 Villeurbanne
France
- ✓ Theo Fleisch
BP America
501 Westlake Park Blvd
PO Box 3092
Houston TX 77253
USA

- ✓ Alexander A. Khassin
Boreskov Institute of Catalysis
Prospekt Akademika Lavrentieva
5, Novosibirsk 630090
Russia
- ✓ Jean-Paul Lange
Shell Research & Technology Centre
Badhuisweg 3
Amsterdam 1031 CM
The Netherlands
- ✓ Albert L. Lapidus
Zelinskii Institute of Organic Chemistry
Leninski Prospekt, 47
117913 Moscow
Russia
- ✓ Miguel Menendez
University of Zaragoza
Department of Chemical Engineering
50009 Zaragoza
Spain
- ✓ Jens Rostrup-Nielsen
Haldor Topsøe A/S
Nymøllevej 55
DK-2800 Lyngby
Denmark
- ✓ Domenico Sanfilippo
Snamprogetti
Viale DeGasperi, 16
20097 - S. Donato Milanese
Italy
- ✓ Frigyes Solymosi
Institute of Solid State and Radiochemistry
University of Szeged
Dóm tér 7
6701-Szeged
Hungary

- ✓ Hugh Stitt
Johnson Matthey Catalysts
PO Box 1
Billingham
Cleveland TS23 1LB
United Kingdom
- ✓ David Trimm
CSIRO Petroleum
PO Box 3000
Glen Waverley
Vic - 3150
Australia
- ✓ Malgorzata Witko
Polish Academy of Sciences
Institute of Catalysis and Surface Chemistry
ul. Niezapominajek 8
30 239 Cracow
Poland

Workshop Coordinators:

- ✓ Claude Naccache
CNRS
Institut de Recherches Sur la Catalyse
Villeurbanne
France
- ✓ Jacques Védrine
Ecole Nationale Supérieure de Chimie de Paris
Laboratoire de Physico-Chimie des Surfaces
ENSCP
11 rue P. & M. Curie
F, 75005 Paris
France

Participants:

- ✓ Paulo Araújo
Quimigal
Quinta da Indústria
Beduído
3860-680 Estarreja
Portugal
- ✓ Süheyda Atalay
Ege University
Faculty of Engineering
Department of Chemical Engineering
Bornova-Izmir 35100
Turkey
- ✓ Akila Barama
Faculté de Chimie- USTHB
Laboratoire de Chimie du Gaz Naturel
PB 32 El Alia
16111 Bab Ezzouar
Alger
Algeria
- ✓ María Guío Carrión
Inst. Catalysis and Petroleum Chemistry.
C/ Marie Curie s/n
Cantoblanco
28049 Madrid
Spain
- ✓ Stefano Cimino
Istituto Ricerche sulla Combustione - CNR
P.le Tecchio 80
80125 Napoli
Italy
- ✓ Gabriele Clarizia
Research Institute on Membrane Technology
ITM-CNR
via P. Bucci, c/o University of Calabria Cubo 17/C
87036 Arcavacata di Rende (CS)
Italy

- ✓ Bob Colman
Stylacats
United Kingdom
- ✓ Vicente Cortes
C.S.I.C. - Insitiuto de Catalisis y Petroleoquímica
Campus Cantoblanco
28049 Madrid
Spain
- ✓ Carlos López Cruz
Instituto de Tecnología Química (UPV-CISC)
Rubén Darío nº 22
46021 Valencia
Spain
- ✓ Mirosław Derewinski
Institute of Catalysis and Surface Chemistry
Polish Academy of Sciences
Niezapominajek 8
PL 30-239 Kraków
Poland
- ✓ François Fajula
Laboratoire de Matériaux Catalytiques et Catalyse en Chimie Organique
UMR 5618 -ENSCM-CNRS
8 rue de l'Ecole Normale
34296 Montpellier Cedex 5
France
- ✓ Diana Filkova
Institute of Catalysis
Bulgarian Academy of Sciences
Acad. G. Bonchev Str.
Bl. 11
1113 Sofia
Bulgaria
- ✓ Vidar Frøseth
NTNU (Norwegian University of Technology and Science)
Department of Chemical Engineering
7591 Trondheim
Norway

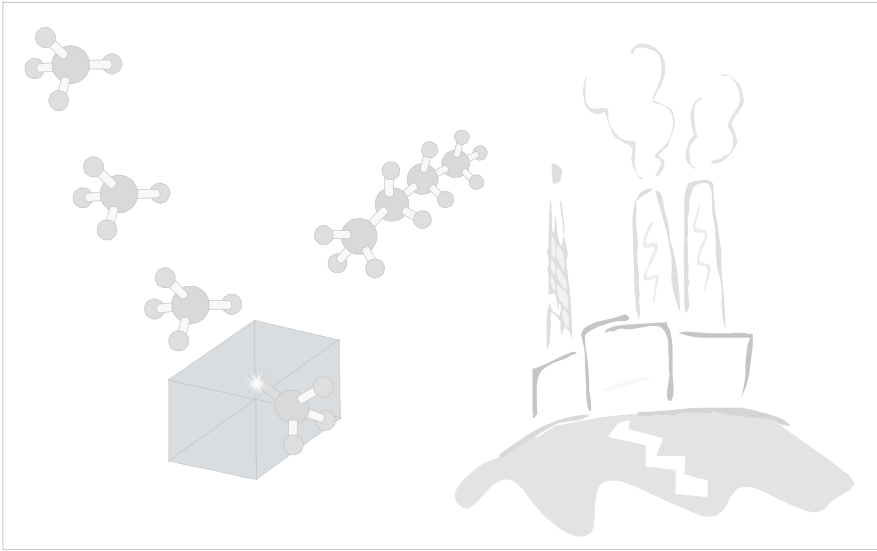
- ✓ Isabelle Gener
Université de Poitiers - UFR Sciences
URA CNRS 350
40, Av. Du Recteur Pineau
86022 Poitiers Cedex
France
- ✓ Grzegorz Giecko
University of Maria Curie-Skłodowska
Faculty of Chemistry
Department of Chemical Technology
3 M. Curie-Skłodowska Sq.
20-031 Lublin
Poland
- ✓ Jean-Pierre Gilson
Total - Raffinage & Marketing
51, Esplanade du Général de Gaulle
92907 Paris La Défense Cedex
France
- ✓ Sholpan Itkulova
Institute of Organic Catalysis and Electrochemistry
142, Kunaev str. Almaty 480100
Kazakhstan
- ✓ Irina Ivanova
Moscow State University
Chemistry Department
Leninskie Gory
119892 Moscow
Russia
- ✓ Jean-Francois Jolly
Institut Français du Pétrole
BP 3- 69390 Vernaison
France
- ✓ Aygana P. Kagyrmanova
Boreskov Institute of Catalysis
Pr. Akad. Lavrentieva 5
Novosibirsk 630090
Russia

- ✓ Beata Kilos
Adam Mickiewicz University
Grunwaldzka 6
60-780 Poznań
Poland
- ✓ Mathieu Lardeux
Total
CSTJF
Office CA156
Avenue Larribau
64000 Pau
France
- ✓ Stanislaw Ledakowicz
Technical University of Lodz
Faculty of Process & Environmental Engineering
Wolczanska 213/215
93005 Lodz
Poland
- ✓ Robin van Leerdam
Wageningen University
Subdepartment of Environmental Technology
Bomenweg 2
6703 HD Wageningen
The Netherlands
- ✓ Anna Lysova
Boreskov Institute of Catalysis
Lavrent'ev Pr. 5
630090 Novosibirsk
Russia
- ✓ Luísa Martins
Instituto Superior de Engenharia de Lisboa
Rua Conselheiro Emídio Navarro, 1
1950-062 Lisboa
Portugal

- ✓ Beatrice de Menorval
Université de Poitiers - UFR Sciences
URA CNRS 350
40, Av. Du Recteur Pineau
86022 Poitiers Cedex
France
- ✓ Piotr Michorczyk
Cracow University of Technology
Institute of Organic Chemistry and Technology
Warszawska 24
31-155 Kraków
Poland
- ✓ Claude Naccache
CNRS
Institut de Recherches Sur la Catalyse
Villeurbanne
France
- ✓ Izabela Nowak
A. Mickiewicz University
Faculty of Chemistry
Grunwaldzka 6
PL-60-780 Poznan
Poland
- ✓ Gianni Pederzani
Enitecnologie - Catalyst and Process Technology Research Center
F. Maritano 26
20097 San Donato Milanese (Milano)
Italy
- ✓ Barbara Pietruszka
Institute of Low Temperature Plasma Physics (INP) Greifswald
Friedrich-Ludwig-Jahn-Strasse 19
17489 Greifswald
Germany
- ✓ Witold Piskorz
Jagiellonian University
Faculty of Chemistry
ul. Ingardena 3
Poland

- ✓ Andrey Popov
Moscow State University
Chemistry Department
Leninskie Gory
119892 Moscow
Russia
- ✓ José Relvas
Instituto Superior Técnico
Departamento de Engenharia Química
Av. Rovisco Pais 1
1049-001 Lisboa
Portugal
- ✓ Zenon Sarbak
Adam Mickiewicz University
Faculty of Chemistry
Grunwaldzka 6
60-780 Poznań
Poland
- ✓ Albert Schweizer
The Dow Chemical Company
1776 Building
Midland MI 48674
USA
- ✓ Jean Thivolle-Cazat
CPE Lyon - Laboratory COMS
Domaine Scientifique de la Doua
BP 2077
43, boulevard du 11 novembre 1918
69100 Villeurbanne
France
- ✓ Svetlana Tungatarova
Institute of Organic Catalysis and Electrochemistry
142, D.Kunaev str.
480100 Almaty
Kazakhstan

- ✓ Ayse Hilal Yilmaz
Ege University
Faculty of Engineering
Department of Chemical Engineering
Bornova-Izmir 35100
Turkey



SUBJECT INDEX

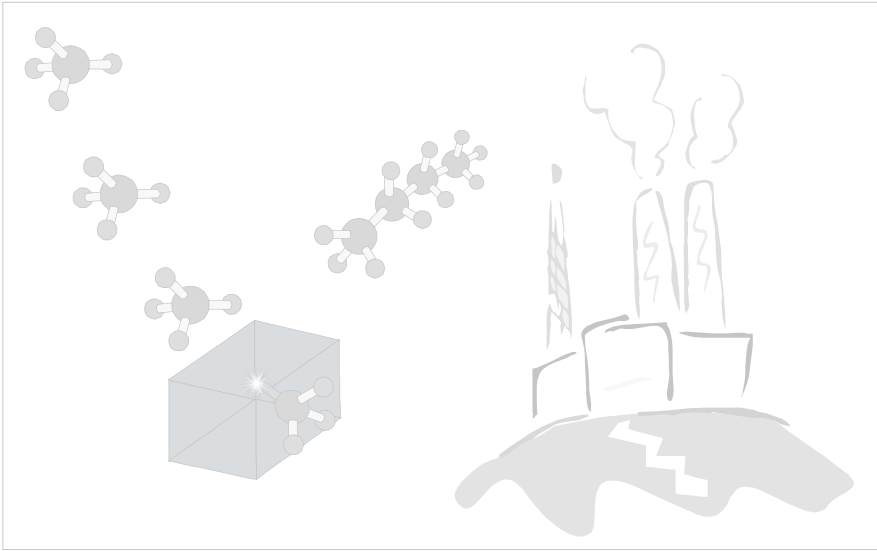
SUBJECT INDEX

- ^{13}C Mas Nmr.....325, 326, 327, 329
Acidity293, 313
 Lewis46, 346
Alkylation12, 65, 221, 227, 236, 293, 300
Arrhenius321
Batch Reactor116, 274
Binding Energy.....92, 99, 303
Brönsted.....29, 46, 48, 49, 141, 144, 320, 343, 344, 345,
 348
Catalyst
 Activity141, 193, 234, 245, 248, 359, 366, 375, 381
 Deactivation.....150
 Life10, 170, 235, 344, 409
 Preparation.....358
Catalytic Reaction40, 85, 88, 105, 107, 117, 147, 180, 221,
 320, 388, 392, 397
Clusters87, 90, 91, 93, 96, 101, 141, 309, 310, 311
Coke.....64, 74, 133, 141, 142, 145, 148, 150, 154,
 161, 165, 179, 214, 216, 218, 222, 224, 225,
 226, 227, 228, 230, 233, 275, 297, 298, 299,
 331, 334, 335, 351, 352, 353, 354, 355, 373,
 396
Coking129, 144, 155, 168, 178
Combinatorial
 Catalysis314
Cordierite.....370, 371, 372
Cracking10, 13, 38, 40, 43, 65, 75, 76, 130, 178, 211,
 214, 216, 217, 218, 219, 220, 221, 222, 227,
 238, 249, 294, 313, 317, 318, 321, 322, 327,
 331, 369
Cyclization.....85, 144, 145
Deactivation.....144
 Coke Deposition224
 Fouling.....219, 227, 238
 Poisoning33, 175, 177, 179
Dehydrogenation30, 32, 37, 38, 43, 45, 46, 74, 75, 76, 77, 88,
 97, 142, 147, 150, 151, 152, 154, 157, 159,
 160, 161, 164, 165, 166, 167, 168, 181, 211,

	215, 216, 218, 223, 227, 229, 230, 231, 233, 242, 325, 327, 328, 329, 330, 331, 332, 333, 334, 335, 338, 344, 351, 369
Density Of States	88, 90, 92
Diffusion.....	5, 6, 102, 157, 241, 244, 245, 246, 247, 250, 257, 258, 259, 260, 340, 382, 390
Limitations.....	245, 258
Dimerization	48, 85, 226, 236, 237, 238
Effectiveness Factor	257
Ethylbenzene	133, 212
Exafs	110, 111, 112
Fisher-Tropsch.....	396, 399, 403
Fixed-Bed Reactors	209
Flow Pattern.....	199, 204
Fluidized-Bed	170, 178
Fouling.....	219, 227, 238
FTIR	37, 47, 295
Genetic Algorithm	321
Heat Transfer Coefficient	203, 384
Homogeneous Catalysis	107
Hydrocracking	13, 131, 132
Hydrogenation	48, 64, 74, 140, 143, 168, 171, 173, 175, 184, 186, 219, 220, 224, 242, 244, 250, 258, 259, 260, 376, 379, 390, 391
Hydrogenolysis.....	108, 249, 325, 328, 330
Hydrothermal Synthesis	286
Hydrotreating.....	13, 219, 397
In Situ Techniques	
MAS NMR	325, 326
NMR	391
Ir Spectroscopy	294, 343, 344, 345
Lewis	46, 48, 49, 177, 294, 343, 344, 345, 348
Monolith	189, 241, 250, 252, 370, 371, 372, 373
Reactor.....	373
Mulliken Population	90, 91, 94, 311
Natural Gas.....	3, 4, 5, 7, 8, 10, 12, 13, 14, 15, 16, 17, 20, 22, 52, 55, 60, 66, 75, 125, 126, 127, 128, 129, 130, 133, 134, 137, 138, 139, 140, 142, 143, 145, 149, 177, 178, 179, 180, 183, 185, 186, 207, 211, 214, 265, 266, 267, 269, 270, 271, 273, 275, 279, 280, 283, 301, 319, 337,

	343, 351, 369, 374, 375, 376, 381, 395, 396, 397, 399, 402, 403, 405, 406, 407, 409, 411, 412
NMR.....	109, 110, 111, 114, 326, 328, 329, 387, 388, 390, 391, 392
Poisoning.....	177
Polymerization.....	169, 170, 171, 173, 174, 175, 177, 220, 223, 226, 238, 377
Reaction	
Mechanisms.....	339, 340
Rate.....	6, 156, 196, 223, 227, 235, 236, 243, 245, 250, 259, 315, 382
Reactor	
Batch.....	116, 274
Monolith.....	373
Slurry.....	132, 247, 250, 256
Stirred Tank.....	233
Trickle-Bed.....	238
Reforming.....	6, 7, 8, 10, 11, 14, 17, 19, 20, 21, 66, 67, 68, 69, 74, 79, 80, 128, 129, 130, 155, 165, 179, 180, 181, 182, 183, 184, 185, 186, 187, 188, 189, 190, 191, 192, 193, 194, 195, 196, 198, 199, 200, 202, 203, 204, 206, 207, 227, 230, 369, 381, 382, 386, 396, 397, 398, 401, 403, 407, 409, 410, 411
Regeneration.....	46, 70, 115, 165, 168, 178, 191, 221, 224, 225, 227, 228, 229, 230, 408
Relaxation Time.....	390
Silicoaluminophosphates.....	224, 397
Simulation Techniques	
DFT.....	105
Hartree-Fock.....	87
Slurry.....	69, 70, 132, 178, 247, 249, 250, 256, 257, 258, 260, 261, 370, 387, 412
Syngas.....	3, 7, 10, 12, 13, 15, 16, 17, 20, 21, 51, 60, 63, 64, 66, 68, 69, 70, 72, 74, 126, 127, 128, 129, 130, 131, 132, 134, 137, 167, 179, 180, 181, 182, 183, 184, 185, 186, 187, 188, 189, 191, 192, 193, 194, 195, 205, 206, 207, 242, 248, 249, 256, 358, 375, 395, 396, 397, 398, 399, 403, 409, 411, 412

Temperature Gradient.....	198, 203, 216
Temperature Programmed Desorption	27, 37, 173, 174, 313, 314, 315
Thiele Moduli	245
Thiele Modulus.....	245
Trickle-Bed Reactor	238
Volatile Organic Compounds	402
Vpo Catalyst	159
Wetting	260
Xrd.....	286, 287, 288, 289, 294, 302, 303
Yield	10, 13, 15, 16, 22, 26, 28, 30, 58, 64, 65, 71, 72, 73, 77, 99, 138, 140, 142, 150, 160, 166, 167, 169, 173, 174, 175, 176, 192, 216, 217, 223, 224, 226, 242, 247, 260, 261, 297, 298, 301, 305, 332, 335, 347, 366, 373, 375, 376, 377, 378, 379, 399, 400, 401, 408, 412
Zeolite.....	27, 141, 156, 167, 249, 290, 293, 295, 300, 356
ZSM-5.....	26, 27, 29, 30, 33, 37, 40, 41, 42, 43, 45, 46, 49, 73, 141, 142, 144, 156, 178, 221, 223, 248, 249, 313, 314, 315, 319, 320, 322, 324, 325, 330, 397, 401



AUTHOR INDEX

AUTHOR INDEX

	Chapter	Page
F.S. Atalay	24	345
S. Atalay	24	345
P. Ayrault	16	301
O.V. Barsukov	25	351
J.M. Basset	5	107
T. Bedyk	27	365
J.C. Bordado	16	301
P. Borges	20	321
E. Broclawik	19	317
H. Carabineiro	21	327
S. Cimino	28	377
G. Clarizia	14	287
C. Coperet	5	107
D. Crisan	18	309
E.G. Derouane	20, 22, 25, 33	321, 333, 351, 413
M. Derewinski	25	351
F. Donsi	28	377
N. Dragan	18	309
E. Drioli	14	287
R. Edreva-Kardjieva	18	309
F. Fajula	22, 25	333, 351
D. Filkova	18	309
J. Gascon	8	149
I. Gener	16	301
M. Di Girolamo	11	217
N.S. Gnep	17	305
R. Gryboś	4	85
M. Guisnet	16, 17	301, 305
Javier Herguido	8	149
Sh.S. Itkulova	29	383

	Chapter	Page
I.I. Ivanova	22, 25	333, 351
A.P. Kagyrmanova	30	389
A.A. Khassin	12	249
B. Kilos	15	293
V.A. Kirillov	31	395
Yu.G. Kolyagin	22	333
I.V. Koptyug	31	395
J. Krysciak	25	351
A.V. Kulikov	31	395
V. A. Kuzmin	30	389
J.-P. Lange	3	51
A.L. Lapidus	9	173
S. Ledakowicz	27	365
M.A.N.D.A. Lemos	20, 21	321, 327
F. Lemos	20, 21, 25	321, 327, 351
J.M. Lopes	16	301
A.A. Lysova	31	395
J.P. Marques	16	301
Miguel Menendez	8	149
B. De Menorval	17	305
P. Michorczyk	23	339
I. Miracca	11	217
I. Nowak	15	293
L. Nowicki	27	365
J. Ogonowski	23	339
T. Olewski	27	365
V.N. Parmon	13, 31	273, 395
L. Petrov	18	309
R. Pirone	28	377
W. Piskorz	19	317
A.G. Popov	25	351
J. Quartararo	22	333
D. Ralowicz	23	339
R. Ramos Pinto	20	321
F. Ramôa Ribeiro	16, 20, 21	301, 321, 337

	Chapter	Page
J.R. Rostrup-Nielsen	1	3
G. Russo	28	377
R.Z. Sagdeev	31	395
D. Sanfilippo	11	217
Z. Sarbak	26	359
A.V. Smirnov	25	351
E.I. Smirnov	30	389
S. Soignier	5	107
F. Solymosi	2	25
E H Stitt	10	185
M. Taoufik	5	107
Carlos Tellez	8	147
J. Thivolle-Cazat	5	107
R. Tokarz-Sobieraj	4	85
D. Trimm	6,7	125, 137
J. Védrine	20, 32	321, 403
N.V. Vernikovskaya	30	389
J.C. Volta	15	293
X. Wang	21	327
M. Witko	4	85
A.H. Yilmaz	24	345
M. Ziolek	15	293
I.A. Zolotarskii	30	389